ANALYSIS AND SIMULATION OF THE HIGH-SPEED TORQUE PERFORMANCE OF BRUSHLESS D.C. MOTOR DRIVES

by

Sabah Kati Safi, M.Sc.

A Thesis submitted in partial fulfilment
of the requirements for the degree of
Doctor of Philosophy

Department of Electrical and Electronic Engineering

The University of Newcastle upon Tyne
1994

This Thesis is dedicated to

my parents, my wife and my childern

Declaration

I confirm that no part of the material offered has previously been submitted by me for a degree in this or any other University.

Copyright

ACKNOWLEDGEMENTS

I would like, first of all, to express my many thanks and sincere gratitude to my supervisor, Dr Paul P. Acarnley for his guidance and enthusiam during this work.

Similarly, thanks are due to Professor A. Jack of the department of Electrical and Electronic Engineering for making available the facilities in the department. Particular, thanks are due to members of the Electric Drives and Machines Group for their co-oporation. Thanks are also due to members of the electronic and mechanical work shops and also to the members of the general office for their assistance and services and in general all of those who have contributed directly or indirectly towards this work.

This work also brings to mind people whose attitudes and efforts has contributed to my educational pursuit: my parents who convinced me of the value of education, my wife and later on my children Emmel and Hanna who patiently endured my many hours of study.

ABSTRACT

The work presented in this thesis is concerned with the analysis, modelling, simulation and control of a surface mounted permanent magnet motor supply by a voltage controlled Pulse-Width Modulation (PWM) inverter.

In Chapter 1 an overall description of the design and construction of individual components of the brushless dc drive system is presented along with a review of the general concept of the drive system. This type of machine is compared with other types of machine and the potential advantages of this new concept, both technical and economic, outlined.

In Chapter 2 the operation and the control aspects of the brushless dc motor are described, with particular emphasis placed on the basic requirements for the operation, torque production, performance characteristic and control. The high-speed torque control methods are also described and their merits are reviewed. In addition the effects of different parameters of machine design on the torque-speed characteristics are discussed.

Chapter 3 elaborates on the analysis and simulation work by presenting a comprehensive analysis which aims to show that direct three-phase representation can be used as an effective tool for performance assessement of brushless dc drive systems operating over a wide speed range.

In Chapter 4 the performance of the brushless dc motor supplied by a PWM inverter with a view to improving the high-speed torque performance is investigated. Simulation and analysis of the brushless dc motor is presented in which the actual parameters of the experimental machine are used. The aim of the analysis is to simulate a brushless d.c. drive system operating in closed-loop control modes, which use high speed torque control techniques in conjunction with a PWM control technique.

A detailed analytical model which makes possible the use of machine

theory for representing the performance of the brushless dc motor is presented in Chapter 5. The method utilizes the phasor diagram, where machine performance in terms of the main control variables such as voltage and phase advance angle is demonstrated. Chapter 5 also presents an analytical expression for the phase-advance angle which yields maximum torque at a given motor speed.

An analytical study concerning the optimum phase advance is developed in Chapter 6. In this work two analytical approaches to the problem of obtaining an optimum phase advance angle are presented. Chapter 6 presents a detailed analysis of the shape of the current and back-emf waveforms in a trapezoidal brushless dc motor drive and their effects on the torque/speed performance.

Chapter 7 presents the implementation of a microprocessor based system, which can set the phase advance angle to its optimum value at any motor speed. This implementation is done in real time on the protortype drive using a TMS320C30 digital signal processor. Features of the method proposed in this thesis include the estimation algorithms for predicting the time advance. Experimental results on a drive system demonstrate the satisfactory performance of both the hardware and software of the control scheme.

CONTENTS

Symbols

ac	alternating current	
B	flux density	(T)
B_r	rotor flux density	(T)
B_s	stator flux density	(T)
dc	direct current	
e	phase back-emf	(V)
E	electro-motive force	(V)
E_{pk}	peak value of back-emf	(V)
f_r	friction coefficient	
i	phase current	(A)
I	current	(A)
J	moment of inertia	(Kgm^2)
J_M	moment of inertia of the motor	(Kgm^2)
J_L	moment of inertia of the load	(Kgm^2)
k_e	back-emf voltage constant	
k_t	torque constant	(Nm/A)
L	self-phase inductance	(H)
M	mutual inductance	(H)
p	number of pole pairs	
p	derivative operator	
PWM	pulse width modulation	
R	resistance	(Ω)
t	time	(s)
Δt	step length time	(s)
T_e	motor torque generated	(Nm)
T_L	load torque	(Nm)

T_F	friction torque	(Nm)
v	phase voltage	(V)
V	voltage	(V)
V_{dc}	dc link voltage	(V)
ω_r	angular velocity	(rad/s)
θ	electrical angular position of the rotor	(degree)
$\Delta\theta$	motor position increment per step	
α	phase advance angle	(degree)
ψ	torque angle	
ψ	flux linkage	
σ	conduction angle	(degree)

subscripts

a	phase a
b	phase b
c	phase a
k	time interval pulses

CHAPTER 1

INTRODUCTION

1.1 General

Many industrial, commercial, and domestic applications require variable-speed motor drives. Traditionally, dc machines have dominated this application area. Although the machine is more expensive than the rival induction motor, the control principles and the power inverter required are somewhat simpler in dc brushed drives because, generally, armature current is approximately proportional to torque and armature voltage is approximately proportional to speed. However, the main disadvantages are its commutators and brushes because, d.c. motors operate by virtue of an electro-mechanical commutator, which is a major source of unreliability. In practice d.c. motors require frequent maintenance to ensure trouble free commutation. Furthermore, the sparking associated with the action of a commutator makes a d.c. motor drive unsuitable for use in certain industrial locations, since the sparks can cause radio interference or ignite flammable gases. In addition, the relative orientation of brushes and commutator bars are fixed and can not be changed during operation.

The requirement from industry for reliable, low-maintenance, controlled drives has therefore led to considerable work in recent years on various "brush-less" drive systems. This controlled drive achieves the desired performance, by a combination of a machine and power electronics.

The thesis is concerned with work on controlled drives of brushless d.c. motor type. The object of the work described in this thesis is to develop first, the general background, through analysis, modelling and simulation, necessary for controlling permanent magnet brushless dc motor, second, to assess the

influences of control on the important performance parameters of brushless dc motor drives and third to present control techniques for improved high-speed performance of brushless dc motor drives.

1.2 Classification of Permanent Magnet Machines

Basically two types of three-phase permanent magnet machine have been designed and constructed. They both comprise four components: a power supply, a power converter (such as a voltage source inverter), a motor and a rotor position sensor, as shown in figure 1.1. The motor is a three-phase type with the "armature" winding carried on the stator. A permanent magnet is mounted on the rotor to provide the working flux. The stator windings are energised by the power converter, which is itself controlled by the rotor position sensor. The motor torque arises from the misalignment of the stator and rotor magnetic axes, and the position sensor ensures that the torque angle remains essentially constant as the rotor turns. Hence continuous unidirectional torque is generated by the motor, at any speed. However there are important details, both in the design and operation, which require careful attention.

1.2.1 Brushless Sinusoidal Permanent Motor Drive

The brushless sinusoidal permanent magnet drive uses continuous rotor position feed back. The motor is supplied with sinusoidal voltages and currents by pulse width modulation of the dc supply voltage. The ideal motor back emf is sinusoidal, so that the interaction with sinusoidal currents produces constant torque with very low ripple. The motor is designed for a sinusoidal supply, with a three phase distributed stator winding and the rotor mounted magnets shaped so as to give sinusoidal air-gap flux distribution and hence a sinusoidally alternating back-emf pattern is produced. This type of motor is known as a sinusoidal brushless dc drive.

1.2.2 Brushless Trapezoidal Permanent Motor Drive

The second category of permanent-magnet motor drive is referred to as the brushless trapezoidal permanent motor. In this type of drive the position feedback is not continuous, but is obtained at fixed positions, usually every 60° electrical in the three-phase machine, or alternatively the voltage may be fed in blocks of 120°, with a simple limit to ensure that the current does not exceed the motor or power-switching capability. The ideal back emf is trapezoidal with the constant part of the waveform timed to coincide with the intervals of constant phase current, leading to the production of a constant total torque from the three phase machine. In this drive, the motor is designed for a rectangular current supply, with a three phase concentrated stator winding and the rotor mounted magnets shaped so as to give a trapezoidal air-gap flux distribution in order to provide the ideal trapezoidal induced back-emf and thus the ideal trapezoidal torque.

1.3 Power Switching Circuit

1.3.1 Inverter Configuration

In both the sinusoidal and trapezoidal drive types, control of current in the motor windings is accomplished by a three-phase bridge arrangement, as shown in figure 1.2, in which each of the star-connected machine windings can be connected to either of the dc supply rails. As a consequence of this reason, six devices are used allowing two phases of the motor to be conducting at a given time, with consequent improvement in power/volume ratio. It should be noted it is also possible to operate the motor with unipolar currents using three switching devices. Copper utilisation is poor since only one coil can be excited at a time, but the simple design offers cost advantages.

The dc supply itself may be derived from a battery, in an automotive application for example, or in the case of an industrial drive may originate in a controlled rectifier connected to the machine ac supply. The inverter operates on a fixed d.c. link voltage, which makes it possible to use a common d.c. bus. The use of the d.c. bus minimises the need for cabling and main connection devices. Since it is often necessary to return stored energy from the machine to the dc supply it is necessary in either case that a large storage capacitor should be connected to the supply so that surplus energy can be absorbed.

In addition the constant d.c. link voltage allows the combination of several inverters with separate controls to a common power supply. This is an important advantage for servo drives, because in most servo drives applications more than one servo drive is needed. The number of devices thus installed will be substantially reduced compared to inverters with separate d.c. supplies.

In the trapezoidal machine drive the power switching bridge acts as an electronic commutator, switching dc current between windings according to the instantaneous rotor position. The current waveforms characteristic of this type of drive are obtained by switching on one device of the three in the upper and lower rows of the bridge. The d.c. supply voltage is then connected across the series combination of two windings, with one winding carrying positive and the other negative current. During this time the third winding is left unconnected to either supply rail, unless it is carrying current from a previous excitation interval, in which case this current decays through a path formed by freewheeling diodes.

It is also possible to use the power switching bridge to control the level of the current in the machine windings. Two separate approaches are in common use. The first method is the so-called current chopper in

which the conducting devices are switched on or off according to whether the instantaneous current in the machine is too low or high. The alternative method, which is usually used, is a closed-loop current control system with the average voltage applied to the machine winding being dependent on the difference between the actual and demanded current. Pulse width modulation (PWM) is used to control the average winding voltage, the mark:space ratio for conduction of the power switching devices being varied according to the voltage required. This implies a need for fast power switching devices. A variety of switching devices are currently used in a PWM voltage inverters for brushless motor drives, including bipolar transistors, gate-turn-off thyristors (GTOs) and various types of field-effect transistors, as well as hybrid (bipolar/field-effect-IGBT) types. With new switching devices continually being introduced, and with the move to integrate all the base or gate drive and protection circuitry within the main device package (the so called 'Smart-Power' approach), it will be some time before an industry standard emerges.

Selection of appropriate devices is dictated by switching frequency, power handling capability and cost-including that of the ancillary circuitry needed to operate the devices. The former two characteristics are compared for different devices in figure 1.3.

1.3.2 The Operation of the Inverter

To illustrate the commutation of the inverter, which is driving the three phase motor, a standard operation mode using 120° conduction angle is considered in figure 1.2 in which two switching devices are conducting at any time. In figure 1.4 signals 1, 2 and 3 drive the three upper switching devices of the inverter bridge while signals 1, 5 and 6 drive the three lower switching devices. Note that in the same inverter leg, the signals that drive the upper and lower transistors are never on at the same time.

A complete electrical cycle starts turning on switching devices S1 and S6 and then the corresponding motor terminal of phases a and c are connected to the dc supply. Thus the current flows through phase a and phase c. When the torque production capability from phase c is exhausted, switches S6 is turned off and S5 is turned on which energises phase a and b. Next phase a loses its ability to produce torque and has to be commutated. Switching devices S1 is turned off and S3 is turned on, which energises phases c and b. This completes one half of the electrical cycle. In the second half of the cycle, the permanent magnet polarity on the rotor as viewed by the stator is reversed. This requires that the current in the stator windings also be reversed in order to continue generating torque in the same direction. Thus in the second half of the cycle, to provide torque in the same direction, the on state switching device sequences must be (3,4) and (2,6). Table 1.1 shows the switching device sequence required for forward and reverse sequence of the inverter operation.

According to the scheme explained above, six commutations occur in one electrical cycle. For a six pole motor, which is the case in this work, three electrical cycles are required per mechanical revolution. Thus, each commutation occurs every 60° electrical or 20° mechanical. In general for a p pole machine using the above commutation scheme, 3p commutations are required per mechanical revolution.

To illustrate the mechanism of how the inductive energy stored in the winding is returned to the source or circulated in the motor windings during the 60° intervals, the combination motor-inverter shown in figure 1.4 is used. In this figure at the conclusion of the (1,6) commutation sequence, the phase c and switch S6 are turned-off, thus, the current path to ground via S6 is interrupted and replaced by free-wheeling diode D3 and switch S1, and the path is complete through phases a and c. The effect is that

a and c windings are momentarily short circuit through the diode and the transistor. Both the diode and switching device have small voltage drops. In the next commutation sequence initially involving the (S1,S5) combination S1 and winding a are turned off. In this case, the short circuit is through switch S5 and diode D4.

An interval of 60° is available to release the energy stored in a winding after a commutation. When the motor current drops to zero during this interval, the motor winding is disconnected from the source voltage and it is free to assume any voltage level between the two inverter bus potentials, depending upon the internal motor drops.

1.4 Permanent Magnet Motor Design

1.4.1 The Rotor Configuration

The rotor magnetic field excitation, in the brushless dc motor, is provided by a permanent magnet instead of a discrete winding carrying dc current. It is desirable in many applications for the rotor inertia to be as low as possible so as to allow high-acceleration and hence a fast responding drive. For these reasons as well as to reduce cost, the rotor configuration is very simple.

There are many possible rotor configurations for the permanent magnet brushless dc motor. The issues here saliency or not, flux concentration or not, high armature reaction or not and mechanical integrity. It is also, how to place the magnet and non-magnetic sections into a cross section of the rotor. The non-magnetic sections are usually air, but can be also be epoxy non-magnetic steel or resin when a high strength material is needed, for example in the shaft of the machine.

For the conventional inner rotor, radial-field machine there are three

rotor structures, as shown in figure 1.5. The surface-mounted magnet machine where magnets are mounted on the rotor surface (figure 1.5a), and the buried or interior permanent magnet machine where magnets are mounted inside the rotor body (figure 1.5b and 1.5c).

A surface magnet design is perhaps the simplest. This consist simply of magnets generally arc shaped but sometimes with flat inner surfaces which are usually simpled glued to the surface of the rotor core. The rotor core is usually laminated to avoid the action of ripple field and is keyed to the solid shaft. However, the surface-mounted magnet machine is essentially nonsalient with a large air-gap and is commonly used. Because of the large airgap, the armature reaction effect on pole flux is insignificant. Therefore, the variation of airgap flux under stator current change is minimised.

The interior (or buried) magnet machine has salient pole structure. The effective airgap is narrow and the armature reaction effect is significant and dominant and therefore control in the constant torque and the constant power region (flux weakening) is possible. In interior permanent magnet machines, usually, the basic difference in the rotor is in the orientation of the magnets. It is either the magnetic axis of the magnets oriented radially or circumferential direction.

A further configuration is the so-called disc machine in which the active portion of the flux is axial and the winding current is radial. To get the most from a disc layout the machine has to be large in diameter and short in axial length and its benefits from being multiple pole. Because the active length of the armature conductors is short and the velocity of the armature conductors varies sharply along their length. The inner part of the conductors is less and less useful becaues the rate of cutting flux at a fixed speed is reducing with radius. There are circumstance in which such a shape is advantageous for instance in robotics.

1.4.2 Selection of Rotor Magnet

Since permanent magnet brushless dc motor performance depends mainly on the airgap flux, the configuration of the rotor using different magnets will vary widely as well. Unlike electromagnets the excitation is flux dependent and therefore non-explicit. As can be seen from the following discussion some magnets operate at very low flux density and may require flux guiding. Hence permanent magnet motors need to be individually designed unlike conventional motors which can be easily standardised.

Associated with the configuration, it is necessary to choose the appropriate permanent magnet material. The difference in magnet material properties results in different optimal dimensions and thus a different volumetric ratio between iron and magnet.

A variety of magnet materials are available which vary greatly in characteristic and cost. The design criteria for a permanent magnet providing the field excitation in a brushless dc motor are (i) high coercivity to resist demagnetisation, as the magnets are positioned directly next to the airgap and the stator currents, they must able to withstand the full demagnetising effect of stator winding, (ii) high energy product to give minimum magnet volume, (iii) low temperature coefficient to give stable performance under all conditions and to resist demagnetisation, (iv) low cost, (v) ease of machining into desirable shapes. There is in general a trade-off between (i) to (iii) and (iv) and (v). Comparison is further complicated by the need to redesign the machine for each different material.

The characteristics of most interest when considering permanent magnet material are described by the intrinsic magnetisation curve (B-H_c) and demagnetisation curve (B-H). These characteristics are shown in figure 1.6 for most common classes of permanent magnet which are currently used in

permanent magnet rotor. The typical parameters of the material constituting the magnets are (i) residual induction (B), in Tesla (ii) demagnetising force (H), in Am^{-1} (iii) energy product (BH_{max}), in Joules.

The cast permanent magnets of Alnico type are alloys composed of aluminum, nickel, cobalt, titanium, and iron in different proportions. They do produce good remanent flux densities but have low corecive forces, and so they are easily demagnetised. In addition they are not readily available in anything but very standard shapes and care is required to machine them. As they are conductive, eddy currents can be induced in them.

Ceramic ferrite magnets are obtained through high-temperature synthese and being very hard and fragile, also cannot be processed with conventional machine tools. They usually consist of alloys of iron oxide or barium oxide. They exhibit improved linear B-H characteristics at the price of a lower magnetic induction value compared to Alnico. The energy product of ceramic magnets is slightly less than Alnico but, due to their higher demagnetisation force, do not demagnetise on open circuit.

Rare earth magnets, of which samarium cobalt ($SmCo_5$) has become the most popular, have the most linear B-H characteristics. However, they exhibit low magnetic induction values compared to Alnico magnets. Rare earth magnets have very high energy products but on average cost 20 times more than the Alnico or ceramic varieties for comparable performance. They do offer one advantage to the motor designer in that the magnetic material can be magnetised prior to assembly. In other words, the rare-earth magnet has high coercivity making it extremely resistant to demagnetisation. This eliminates the need for keeper rings during assembly and disassembly of frameless motors and nullifies the possibility of demagnetisation during motor operation. Less material is required for a given application compared with Alnico or other materials.

The high coercivity of these materials influences the design of motors and significant performance improvements have been made possible. Because the magnets are shorter in the direction of magnetisation they may be oriented radially instead of circumferentially. This has the effect of lowering winding inductance, thus the amount of energy which must be exchanged from one winding to the next during commutation is reduced. The commutation system operates under less load with better reliability.

The Alnico magnets have non-linear B-H characteristics which is a particular problem which needs special consideration if this material is to be used. Since the material is easily magnetised, it is usual to supply it in the unmagnetised state, allowing it to be machined before assembly into the motor. Only at this stage is the material magnetised, using either the armature windings or a purpose-built magnetising structure. Note that subsequent dismantling of the motor is likely to cause a loss of magnetisation. Alnico magnets are usually supplied in a range of rectangular block or cylindrical shapes, though it is possible to obtain rotors cast in these materials.

Alnico magnets, and rare earth are relatively expensive and their use is restricted to high-performance machines where the power/volume ratio must be maximised. However, ceramic ferrite magnet is inexpensive but limited by its low maximum energy product, due to the lower values of residual flux density. Zimmerman, [1982] has shown that the ferrite magnet is much cheaper than the Alnico and samarium cobalt for machines of similar power. A comparison of ferrite and samarium cobalt magnet fitted motors has been reported by Demeradash et al [1983]. Their works show that the performances of both materials are virtually identical but the ferrite magnet motor is twice as heavy, of twice the volume and five times the inertia of the samarium cobalt motor. It is however concluded that cost overides these disadvantages in favour of the ferrite magnets in all but the most demanding applications.

Neodymium iron magnets were introuced in the mid 1980's with the expection that their cost would be less than samarium cobalt, because of the high iron content, and their magnetic performance superior. So far both of these expectations are unfulfilled. Commercial forces have caused costs to remain comparable to samarium coblat. As far as magnetic performnce is concerned the material has a very high residual flux density combined with high coercivity, but it suffers from a large loss of effect with temperature and a low maximum temperature above which the remnant field in the magnet is lost permanently. However neodymium iron boron does have good mechanical properties, and is finding a growing number of electrical machine applications.

In addition, a comparison between those permanent magnets deemed suitable for permanent machines use is given in table 1.2.

1.4.3 Stator Design

Brushed dc motors have distributed armature windings and the interconnections between the windings and the commutator is arranged so that only those coils under the influence of the field at a given moment are carrying current. Similarly small brushless dc motors have a concentrated one slot per pole per phase armature winding, for example eighteen slots for a three phase six pole machine, as shown in figure 1.7. The slots are often skewed to avoid tooth ripple effects. Careful air gap design, particular the shaping of the magnets results in a trapezoidal back-emf, as explained earlier in the previous section. The one slot per pole per phase winding arrangement is a very inefficient use of the stator bore. Machines designed for sinusoidal feed are equipped with a distributed winding as for a conventional ac machine.

1.5 Position Detection

Rotor position sensing on a brushless dc motor is usually required for two distinct purposes (i) for commutation control (ii) for voltage control

or speed control. The latter is usually omitted on low cost appliance type drives. This section is devoted to commutation control.

The purpose of the commutation sensor is to provide rotor information to control the flow of current in the machine windings. It thus needs only to be a relatively crude device giving the instant at which each commutation should be occur. However, although only a few outputs per revolution are required the instants at which these outputs appear are critical to the efficient running and dynamic performance of the drive since the commutation must occur at the most torque-efficient point.

1.5.1 Commutation Methods

In commutation control, the brushless dc motor must incorporate some means of detecting the position of the rotor poles in relation to the stator phases, so that the phase currents are accurately commutated and therefore, that the desired operating characteristics of the motor are obtained.

The current conduction pattern in the brushless dc motor, as shown in figure 1.8, is that each phase conducts, alternately for 120° and then remains no-conducting for 60°, also only two phases conduct at any given time. Current transitions, from one phase to the other, occur every 60° and due to the flat top of the back-emf in each phase a flat top current is required to produce a constant torque. Therefore rotor position sensors are needed only to detect the transition points which occur every 60°.

The permanent magnet sinusoidal brushless motor requires sinusoidal currents, the magnitude of which depends on the instantaneous rotor position. All three phases conduct simultaneously and continuous rotor position feedback is needed.

The encoder is usually installed within the motor and the resulting position signals are fed back to the commutation control circuit. However,

there are various types position sensors available for commutation control. The most reliable position sensor techniques do not involve contact between stationary and moving parts; i.e. they are brushless. Practical contactless position sensors which satisfy the constraint of cost, reliability, and accuracy, include:

(a) Optical Encoder

When signals are provided solely for commutation rather than for accurate positional measurement the optical encoder takes the following form. The rotor is fitted with a perforated metal or plastic disc. This passes through a housing (mounted on the stator core or case) which contains one light emitting diode (LED)/phototransistor pair per phase. The phototransistors are turned on when a perforation in the disc permits light from the LED to pass through. The performance of LEDs degrades above 75° C and this limitation demands careful location of the sensor. The position of the disc on the shaft and of the LED/phototransistors pair is critical to efficient operation and leads to an increase in the complexity of manufacture and hence an increase in the cost.

Advantages of the optical sensor method include the fact that the signals from the LED/phototransistors rise and fall quite abruptly and so the switching points are well defined. Also, the signals are d.c. and so do not require rectification or filtering. In addition, the LED/phototransistor signal is usually very low power and so may require amplification before it can be used for control purpose.

(b) Hall Effect Sensors

Hall effect devices are available for brushless dc motor commutation control and give a digital output [Carvajal, et al, 1985] in response to a

magnetic field. They are usually mounted around either the permanent magnet rotor or a separate magnet assembly attached to the motor shaft, the individual elements activated either by the main magnetic flux or end leakage flux.

One device per phase is required for commutation. As mentioned above, these devices must also be mounted in the precisely defined positions for accurate commutation leading to increased production cost.

Recent developments have enabled Schmitt Triggers to be built into the devices thus resulting in a rise and fall time of less than nanoseconds permitting very high-switching rates.

(c) Back-EMF Sensors

Sensing of back emf has been employed for commutation mainly in low cost drives or in high inertia constant speed applications. Several authors have described commutation strategies for the so-called sensorless brushless machine [Paraskeva, 1984], [Iizuka, al et, 1985], [Le-Huy, 1982], [Grandpierre, al et, 1984]. In these schemes the switching of the inverter devices is usually determined by monitoring the zero crossing points in each motor emf waveform during the time when no current is being fed into that phase winding. In order to start the motor from standstill, the windings are initially driven synchronously by signals generated in the control processor for the machine.

An analogue comparator circuit is used to detect when back emf has reached a predetermined level. At starting and low speeds the method does not function since no back-emf or only a small back-emf is induced and the motor is usually run-up open loop until a speed is reached where sufficient back-emf is available for commutation. It will be apparent that such a system is not suitable for the drives which need to achieve a good low speed performance. Also there is often a great deal of spurious noise on

the signals due to the switching action on the phase winding and this can make accurate detection impossible.

The advantage of the technique is that the shaft-mounted sensor is eliminated, resulting in increased system ruggedness and reduced cost. However, this method has been implemented successfully to constant voltage drive used for motors less than 1 KW power rating [Iizuka, al et, 1982]

(d) Current Sensors

The rate of change in the phase current is dictated by the incremental inductance of the phase circuit. The incremental inductance is, in turn, a function of the rotor position and the phase current. The rotor position can be deduced from a knowledge of phase current and its rate of change [Acarnley, et al, 1985].

The latter two methods require some electronic processing circuitry. and, in addition, the variation of phase advance angle and excitation conduction angle is complicated. They do not, however, require the parts to be mounted on the shaft as is the case of an optical encoder. One application of the latter methods is when environmental conditions hinder the mounting of extra devices on the motor shaft.

1.5.2 Speed Sensing Methods

Some devices available for speed and positional feedback control are reviewed briefly in this section. The most desirable place for mounting a transducer is in close proximity to the driven load (reducing the effect of wear and backlash in the drive) so the feed back loop of the whole system needs to incorporate drive components such as gearboxes and leadscrews. However, as mentioned earlier in the preceding section, drives are commonly provided with an integrally mounted tachogenerator, encoder or resolver which facilitates the marketing of the drive package but can result in degraded system performance.

(a) Tachogenerator

This is available in brush and brushless types. The use of a brushed tachogenerator with a brushless dc motor negates many of the advantages of the motor, so brushless tachogenerators are normally employed. A tachogenerator is a small precision made electrical machine and the signal available for feedback is a generated back emf at its terminals. Its performance as a sensor is thus poor at low speeds and it is suitable for "speed control" only. Brushless tachogenerators give pulses from a series of stator mounted coils, which are decoded to give a speed signal. By using a frequency to voltage converter integrated circuit, an analogue signal can be provided for controllers.

(b) Resolver

Resolvers are ac devices giving sinusoidal outputs which can be decoded for speed information. The outputs can be used in analogue form or converted to digital signals using commercially available resolver to digital converter integrated circuits. The sinusoidal output signals make the device most suited to speed feedback control applications with a sinusoidal brushless dc motor.

(c) Other Sensor Possibilities

Precision encoders suitable for servo use are more sophisticated versions of the optical encoder devices which were described earlier. Outputs are available with particular code patterns (e.g. Gray code or binary coded decimal), thus giving an absolute indication of position at any point and reducing the need for further signal processing. Encoders of this type are known as 'absolute' encoders. Incremental encoders simply give out a number of pulses per revolution which are counted and averaged for speed measurement or for positional information.

An index pulse channel, giving one output per revolution, may be provided to allow the position count to be reset, reducing the possibility of

cumulative errors. Most encoders give out two pulse trains which are in quadrature. Encoders are available with very large numbers of output pulses per revolution, giving a positional resolution of small fractions of a degree.

1.6 Brushless DC Drive Control Configuration

Details of brushless dc motor control will be discussed in the following chapter and this section is limited to the general configuration of the drive control.

A cascade control structure is usually adopted for brushless d.c. motor drive applications (figure 1.9). This consists of an outer speed loop that compares the speed demand with the measured speed to produce an error signal. The error signal is required to indicate whether the motor is running at the desired speed and if it is not then it would indicate the direction and magnitude of the error. The PID speed controller then performs a proportional, integral and differential operation upon the error between the two signals. The terms in the PID controller may be varied, so the dynamic response of the speed controller can be modified to suit different load and operating conditions.

The speed controller output sets the current demand and is responsible for the torque which in turn reduces the error. The main purpose of the current controller is to reduce the error signal to zero by varying the torque of the motor by adjusting the current. According to this principle, and by referring to figure 1.9, the inner current loop compares the current demand with actual motor current and produces a current error signal which is fed to the pulse width modulation (PWM) control circuit. This produces signals which are fed to the commutation control circuit which activates the correct motor phases. The use of a single current loop greatly simplifies the control system, and maintains a control strategy close to that of a brushed dc

motor. It is worth noting that although the analogy with brushed dc motor performance holds in that speed is linearly proportional to supply dc voltage, speed reversal (or the direction of operation of the motor) is achieved by reversing the phase sequence of the switching waveforms provided by the converter rather than by reversing the supply polarity.

In order to control the speed via the torque, it is necessary to devise a method of controlling the supply voltage. The most suitable method is a switched power supply using a pulse width modulation (PWM) switching strategy. The strategy usually used is to modulated the dc supply voltage across the motor windings. The reference voltage for the PWM is produced by a closed loop current controller.

The brushless dc motor drive used in this work employs the complementary PWM switching strategy. This method is characterised by comparing the current reference voltage, together with its inverse, with a triangular carrier waveform of a fixed frequency. This comparison produces the two switching signals C1 and C2 (figure 1.10), where C1 and C2 switch the top and bottom halves of the inverter bridge respectively. The two switching pulse trains are then distributed across both halves of the bridge so that the desired output currents to the motor windings are achieved.

1.7 Microprocessor-Based Brushless DC System Control

Traditionally the electronic control of the power inverter of a brushless dc motor drive has been implemented with analogue components like resistors, capacitors and op-amps (operational amplifiers), however, this approach suffers from several major disadvantages; particularly component value changes due temperature variations, susceptibility to electrical noise, and lack of flexibility due to the hardwired nature of the system. These problems have provided the motivation of applying digital technology to the control of brushless dc

motors. Digital circuits overcome the first two problems mentioned above, however, they still suffer from lack of flexibility and can become very complex if sophisticated control is attempted. The arrival of the microprocessor in the early 1970's has now allowed the possibility of implementing the control algorithms with software rather than hardware. With powerful instruction sets of these devices, different task and control algorithms are now practical.

The control of the speed and torque of electrical machines, which had already considerably evolved with the adoption of power inverters, is now undergoing an even more fundamental change towards less expensive, though increasingly sophisticated systems, owing to the introduction of microprocessors for the implementation of the internal loops of the control system. A microprocessor based control system for industrial drives promises several distinct advantages. One of the most important is flexibility as the control procedure is implemented in the software. Therefore, to change the control procedure in order to obtain different desired characteristics, only the software needs to be modified with minimum or no change in hardware. The microprocessor control can be completely digitised, which will decrease its sensitivity to external influences. Discrete components and wiring can be reduced or eliminated, a factor which should improve reliability. Also as prices of microprocessor and associated peripherals continue to fall, the microprocessor-based control will become cost competitive. Continued developments in microprocessor technology leading to increase processing speeds will provide improved performance in speed, regulation, response time and resolution. Implementation of new control techniques, such as field-weakening control and field orientation, in real time have been made possible by the microprocessor.

In order to exploit all the advantages offered by the introduction of microprocessors in control systems, one aim of the project described in this thesis is to describe the application of a microprocessor in a wide-range speed

control system for a brushless dc motor drive using field weakening based on the phase advance control algorithms.

1.8 General Properties of Brushless DC Motor

Brushless permanent magnet motor drive systems present inherent advantages over ac and dc machine drives and have design features which make them suitable for high-performance industrial drive applications such as machine tools and robots. They are preferred to the induction and synchronous machines in the majority of high performance applications because of their high power/weight ratio and relative ease of control.

The stator core and stator windings of a three phase induction motor are the same as those of a synchronous machine used in permanent magnet synchronous and brushless dc drives. The only difference in construction between the two machines is in the rotor. An induction motor with a squirrel cage rotor is one of the lowest cost machines to manufacture as it eliminates all brushes, resulting in an exceedingly simple and rugged construction. There is no insulated winding on the rotor and an excitation power supply is not required.

The brushless dc motor drive is inherently smaller than the induction drives given the same load condition, Brawn [1982]. The induction servo motor is mechanically and electrically rugged and is low in cost. It produces torque by the interaction of the stator magnetic field with the rotor field induced by the stator field. Consequently torque control requires the measurement or calculation of the relationship between these two coupled fields. The disadvantages of inductions motors are complex control techniques and losses in both the stator and rotor. In a brushless dc motor torque is produced by the interaction of the stator magnetic field with rotor flux, which are decoupled. Heat dissipation from windings occurs only on the stator. Control

simplicity and low losses for the brushless dc motor are counter-balanced by the additional material cost of the motor.

In addition, further features of brushless dc servomotors include no-maintenance design (bearing lubricated for life), totally enclosed non-ventilated specification with thermal ratings for a continuous full-load stall, and low inertia for high acceleration.

As the cost of power and control electronic components as a proportion of the total drive cost continues to decrease and as users become more familiar with brushless dc motor drives, it seems likely these drives will replace brushed dc systems in a large number of applications. Savings can be made in the cost of the driven equipment, because the need to make the motor accessible for brush maintenace has been removed.

1.9 Review of Literature

During the last two decades, considerable work has been reported on the subject of brushless dc drives. This has resulted in increasing sophistication of these drives, in both machine design and control design aspects.

Little analysis has been done on the variable frequency operation of the machine prior to the development of semiconductor inverters capable of producing variable frequency voltage supplies. In published literature several authors have described some of the methods applicable for the simulation of brushless dc motor systems. The most common methods are based on one of three types of approach: (i) d-q axis model Krause, et al [1984, 1987], Williamson, et al, [1978], Sebastian and Slemon [1987], Slemon and Gumaste [1983], Bowes and Clare [1988], Bowes and Clements [1983], Chalmers and Hamed [1985] (ii) direct solution method Demerdash, et al, [1980, 1982, 1985] Piriou and Razek [1986], Piriou, et at, [1986] Braun and Creer [1986], Semail, et at, [1987], (iii) Fourier series, Bolton and Ashen, [1984], Le-Huy, et al,

[1986].

Most of these studies reported in the literature consider the performance of the brushless dc machine with sinusoidal supply voltages. However this condition may not always be applicable. As the types of control strategy, supply condition and back-emf are quite diverse in trapezoidal brushless dc motors, a suitable model is needed to analysis and to simulate this type of drive. However little work seems to have been done on the development of a model suitable for this type of drive. It is one purpose of the present work to investigate this area further.

The modelling of brushless dc motors and drives is not a subject that has been well and systematically covered in the literature. However, the machine has often been designed using finite element techniques, but only a number of a specific examples [Fouad and Nehi, 1981][Davat et al, 1985][Boules, 1983][Eid and Mouillet, 1984], rather than a general metholodogy have been reported.

There is a large body of literature devoted to the design and application of brushless dc motor drives. Most of the works in this area tend to state that the complete brushless dc drive can be assumed identically equivalent to brushed dc servo drives. It is apparent that some machine design work is based on the technique used for brushed dc motors. Woodbury [1974] presents curves giving losses and other parameters for given torques and speeds, as well as discussing overall drive design. Tripathi, et al [1980] shows the design of a very crude form of drive.

Servo control in most brushless dc motor uses standard techniques and most drives have analogue 'proportional and integral' controller, combined with current control discussed by some authors [Zimmerman, 1982][Murty, 1984], [Nashiki, 1982]. Oudet and Ettelman [1985] describe a control method, whereby a brushless dc motor is run open loop as stepper motor or closed

loop as a brushless dc motor depending on which characteristic is best suited to the operating conditions obtaining at a particular time. Jack, et al, [1988] discuss the design of small brushless dc drives in which high speeds are coupled with the requirement of precise speed stability.

A number of applications of novel controls have been implemented in the brushless dc motor drives. Ogasawa et al [1986] have proposed a current method which continuously checks for imbalance of back-emf. Stone and Buckley [1985] describe a current control method that lies outside the commutation loop, its demands being switched into the various phases as commutation occurs. Rise time of currents in the phase winding being switched in are carefully matched to current decay times in the phase being switched out to minimise torque ripples due to the current disturbance. Baron [1983] uses a look-up table and fast current to compensate for torque due to the motor design in order to minimise torque ripple.

A good deal of interest has been shown in recent years in flux-weakening control method of brushless dc motors. However, in a brushed dc machine, the field and armature currents can be controlled independently and, owing to the action of the commutator, are always held at 90° electrical to one another. Flux weakening control techniques emulate this ideal situation for the brushless dc drive. A number of applications of this technique have been reported in the literature [Snesyer, et al, 1985], [Sebastian, and Slemon, 1987], [Jahans, 1987], [Bose, 1988], [Ogasawara. et al, 1986], [Brosnan and Brown, 1984], [Vagati and Villata, 1983], [Vagati and Villata, 1985], [Husels, 1984]. Pfaff et al [1984] discuss a technique which combine hysteresis comparator current control with vector control methods. All this work has been done for a motor excited by sinusoidal voltage source. Meshkat and Persson [1984] and Persson and Meshkat [1985] have applied the technique to a trapezoidal brushless dc motor for torque ripple by using current waveforms of special

shape store in the memeory (ROM) of the microprocessor. The results of this work show that the technique expands the operational torque-speed range by a factor two.

The major advances in dc drives have been made in the control area with the introduction of the microprocessor. It is now possible to perform tasks such as storing constants, solving special algorithms, and solving special relay logic, at relatively little cost and effort to the customer. Drive designs using the microprocessor have provided low component counts and interconnection.

The microprocessor can be used for multiple applications in power electronics. These applications include variable-speed drives and power converter control. Papers in the literature on the application of the microprocessor have not concentrated mainly on the brushless dc motor but they are worth referencing to illustrate the capabilities of the microprocessor. El-Sharkawi and Coleman, [1986], have reported on the microcomputer control of a brushless dc motor. Walter, [1987] has reported on a brushless dc motor controlled by a microprocessor. Patrick and Chales, [1985] have reported on the pulse width modulation control of brushless dc motors. Acarnley, et al [1982] has reported on the prediction and realisation of optimum switching angle of a stepping motor. Bose, et al, [1986] has reported on the microcomputer control of the switched reluctance motor. The microprocessor controlled the power inverter as well as the speed and torque feedback loops. Kenjo and Takahshi [1980] have published detail on the microprocessor controlled self-optimisation drive of a step motor.

In spite of all this work on permanent magnet brushless dc motor drives, there remain very significant areas where a clear understanding is lacking. A broad understanding of the behaviour of the brushless dc motor drive therefore needs to be achieved, which can only be done by modelling and simulation of the drive. Also an assessement of control variables on

the behaviour of the drive is needed to provide the necessary back-ground for controlling the brushless dc motor drive, particularly the idea of having the microprocessor improve the performance of brushless dc drive systems at high-speed operation using microprocessor algorithms is worth investigating. These are the main objectives of the work presented in this thesis.

1.10 Thesis Contributions

The work presented in this thesis has been modelling, simulation and detailed analysis of the operation characteristics of a surface mounted permanent magnet motor switched by a PWM inverter. Particular consideration has been given to a three phase motor with trapezoidal back-emf.

The major contribution lies in the prediction of the behaviour of the PWM inverter-fed brushless dc motor through modelling and simulation and assessment of the effects of phase advance and conduction angle controls on the overall performance of the drive system.

A mathematical method for the modelling of brushless dc drives is developed. The basic approach of the method is to incorporate the operation of the inverter by using sets of differential equations which describe the switching state of the inverter devices in the combined drive system.

A computer simulation approach for brushless dc motors is also presented. The simulation approach is presented for steady state and transient conditions of operation of the drive system. The drive system is operated with a closed-loop strategy which uses the phase advance control technique in conjunction with PWM control technique. Using this approach the high-speed torque performance of a brushless dc motor is investigated. This study has dealt with different control methods. Their differences are assessed and discussed. From the simulation, conclusions are drawn about the merit and demerits of these control methods. The results, due to different machine

parameters, on the performance of the motor drive are investigated, particularly at high-speed operation.

Analytical approaches to the determination of the optimum phase advance angle of the permanent magnet brushless dc motor are developed, and a computation study is presented.

This thesis proposes an original microprocessor closed-loop system using estimation algorithm methods of time advance for brushless motor drives to improve the high-speed performance of the drives. Features of the algorithms proposed include the estimation of phase advance at a real time point. Also the features of the microprocessor based time advance estimation are described, focussing on application of a TMS320C30 digital signal processor in a wide range speed control system.

1.11 Thesis presentation

This thesis consists of eight chapters. The following chapter presents operation, control and performance characteristics of permanent magnet machines for brushless dc drive applications. The operation and requirements of the drive are discussed. A method of analysis is used in order to investigate the control requirements of the drive system. Different control methods are presented. The effect of some parameters on machine performance is also discussed.

Chapter Three presents a mathematical model for the brushless dc drive. This model uses a unified equivalent circuit simulation which models both the inverter switching states and motor equivalent circuit as one complete system. Also a computer simulation approach to predict the performance characteristic of brushless dc motor drive is presented.

In the next chapter a simulation and detailed analysis of the performance of brushless dc motors switched by a PWM inverter is is presented.

This investigation has dealt with the quantitative effect of both 120° and 180° conduction angles of inverter operation and various machine parameters, on the torque-speed characteristic.

Chapter Five presents an analytical model which describes the high-speed torque performance of the brushless dc motor in terms of phase advance angle, using two-axis machine theory.

In the next chapter two simplified analytical approaches for obtaining the optimum phase advance angle in the high speed range are presented. The merits of these methods, compared with trail-and-error based on simulation, are described.

Chapter Eight covers the experimental brushless dc motor drive system and practical realisation of the phase advance algorithms in conjunction with PWM voltage control using a TMS320C30 digital signal processor.

In the final chapter general conclusions are drawn and suggestions are made for future work.

Table 1.1 Forward and reverse rotation sequence of inverter operation

Rotation Sequence	Switching-on					
Forward	1,6	1,5	3,5	3,4	2,4	2,6
Reverse	1,6	2,6	2,4	3,4	3,5	1,5

Table 1.2 Typical Characteristics of the most Widely used Types of Permanent Magnet Materials

Property	symbols	Materials					Unit
		Alnico	Sintered $SmCo_5$	Bonded $SmCo_5$	Ferrite	Nd-Fe-B	
Remanence	B_r	0.95	1.12	0.55	0.38	1.19	T
Intrinsic coercivity	IH_c	410	1100	620	260	1200	kA/m
Normal coercivity	BH_c	90	670	410	220	850	kA/m
Max energy	$BH_{(max}$	35	150	50	25	210	kJ/m^3
Recoil permeability	μ_r	3.0	1.05	1.1	1.1	-	-
Curie temperature	T	820	720	-	450	310	$°C$
Density	ρ	7300	8300	5100	4800	7400	kg/m^3
Resistivity	R_s	0.5	0.6	10^5	10^{10}	1.45	$\mu\Omega m$

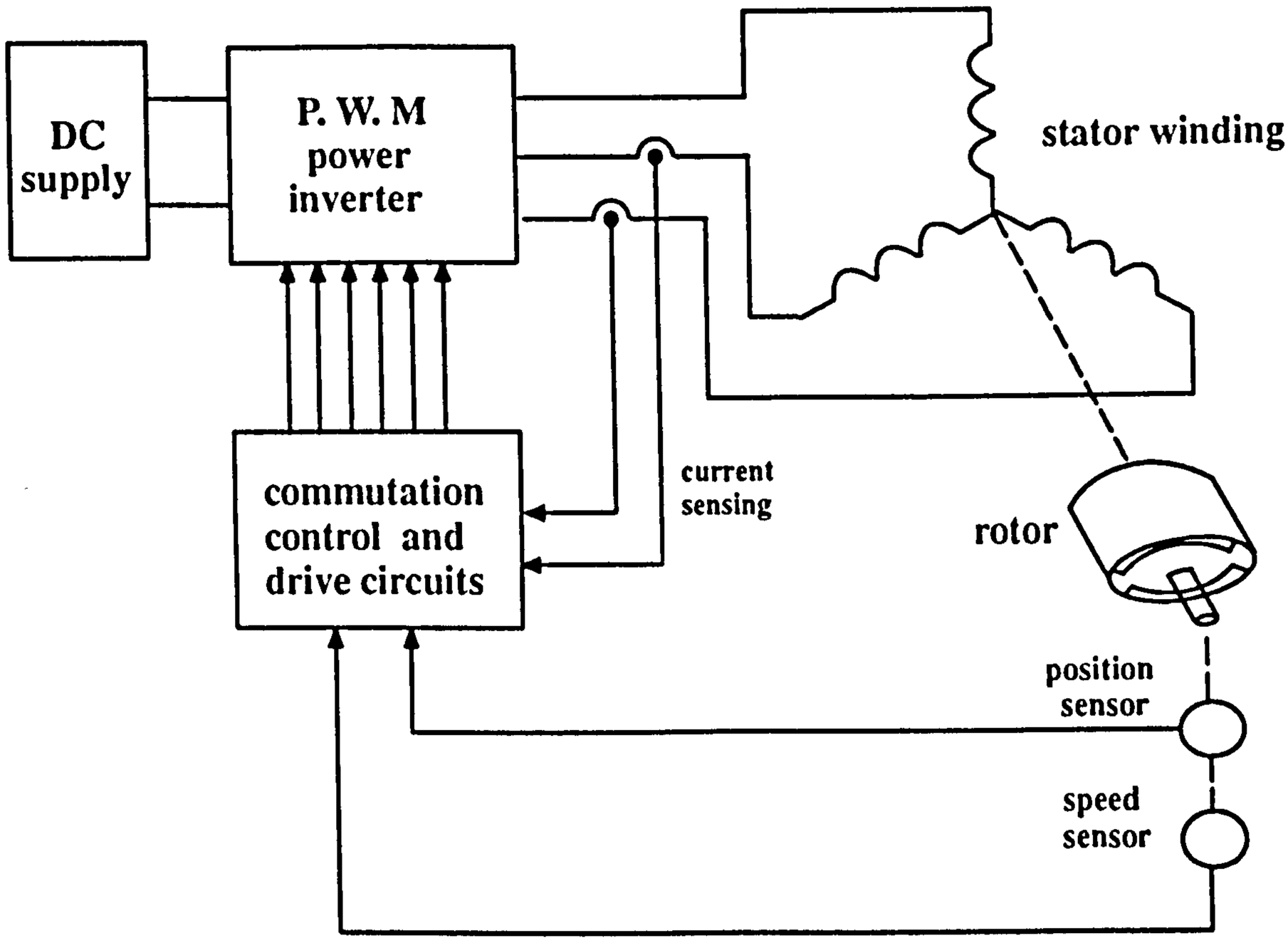

Figure 1.1 Brushless dc motor configuration

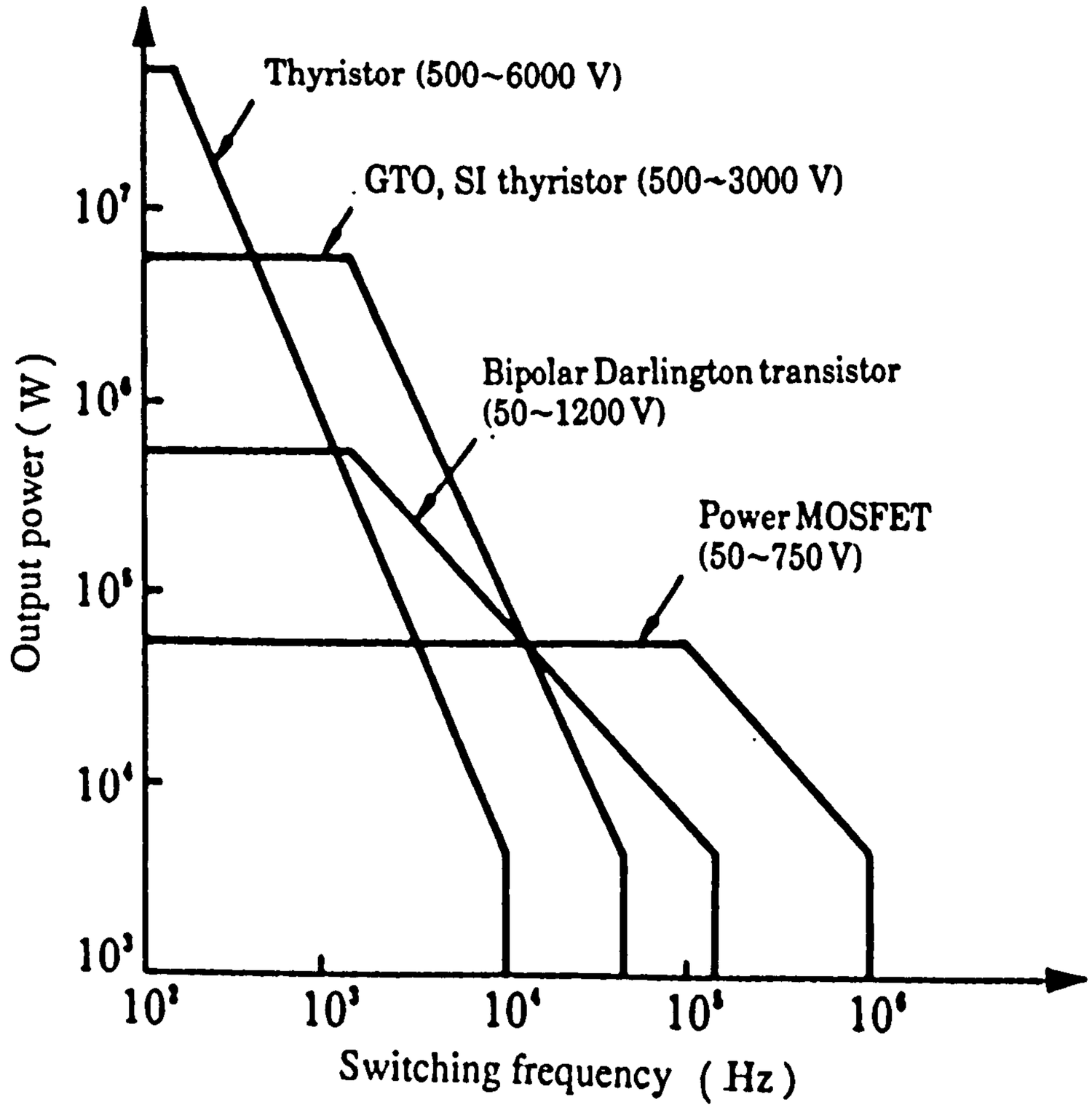

Figure 1.3 Switching frequency / power output

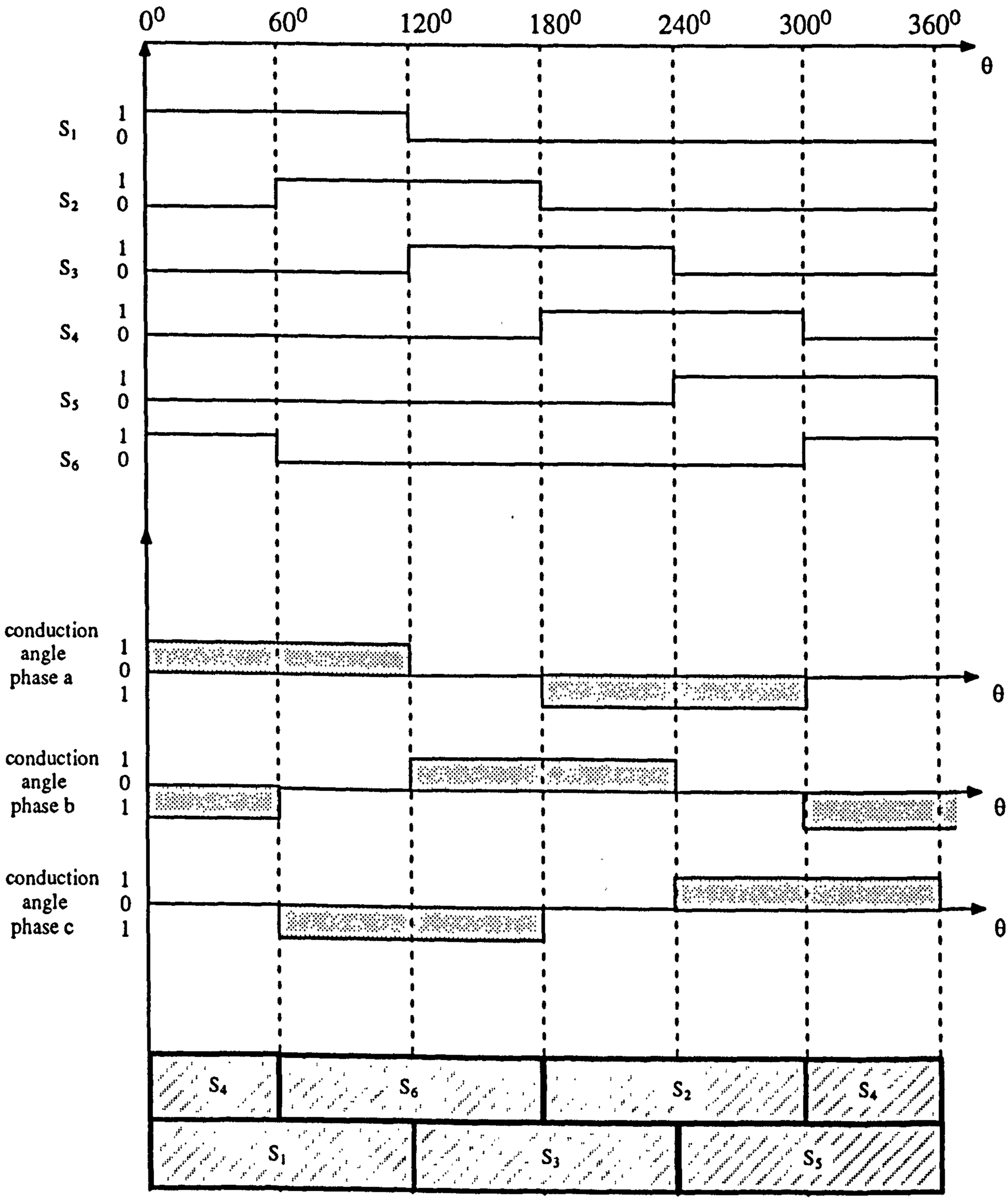

Figure 1.4 Switching timing of the power inverter

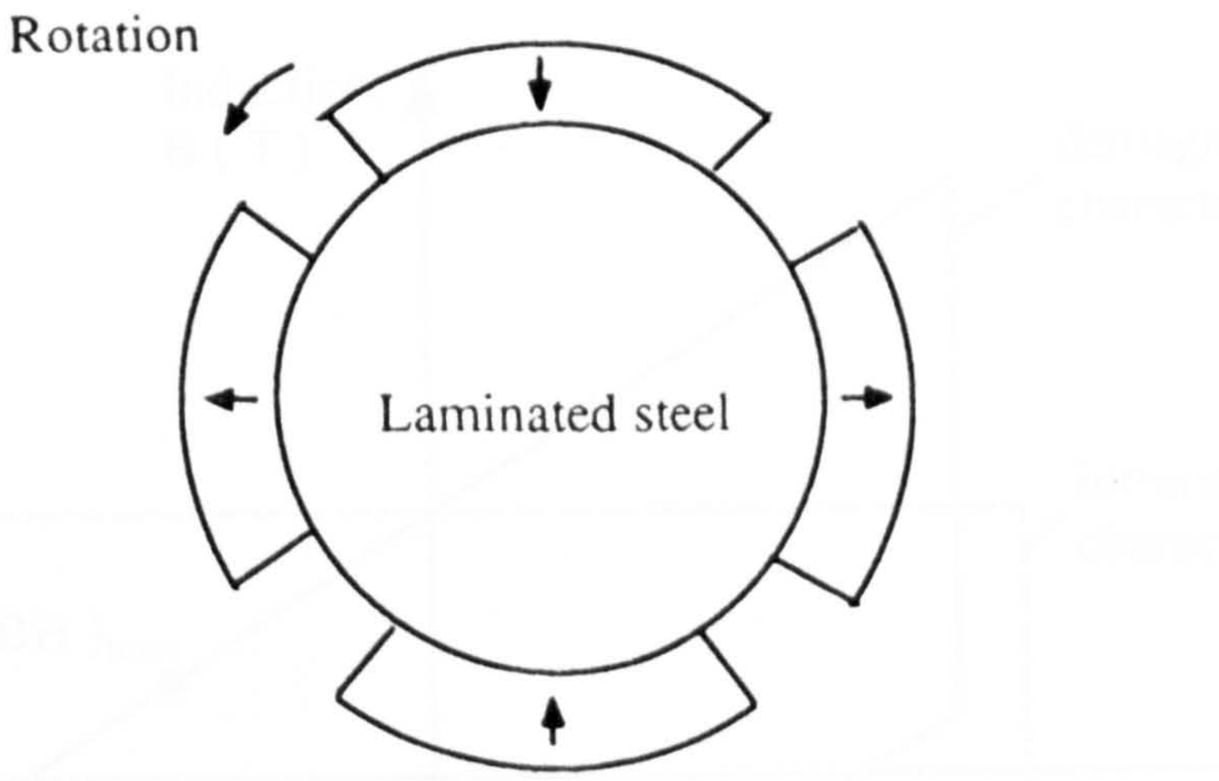

(a) Four pole rotor with surface–mounted magnets

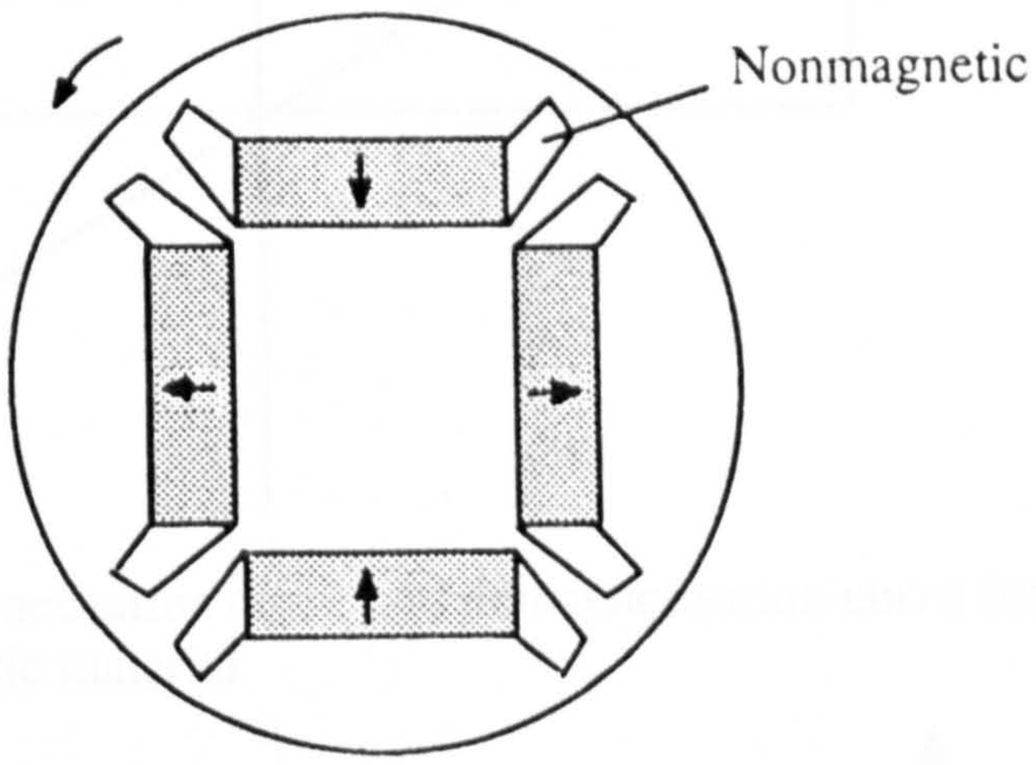

(i) interior magnets rotor

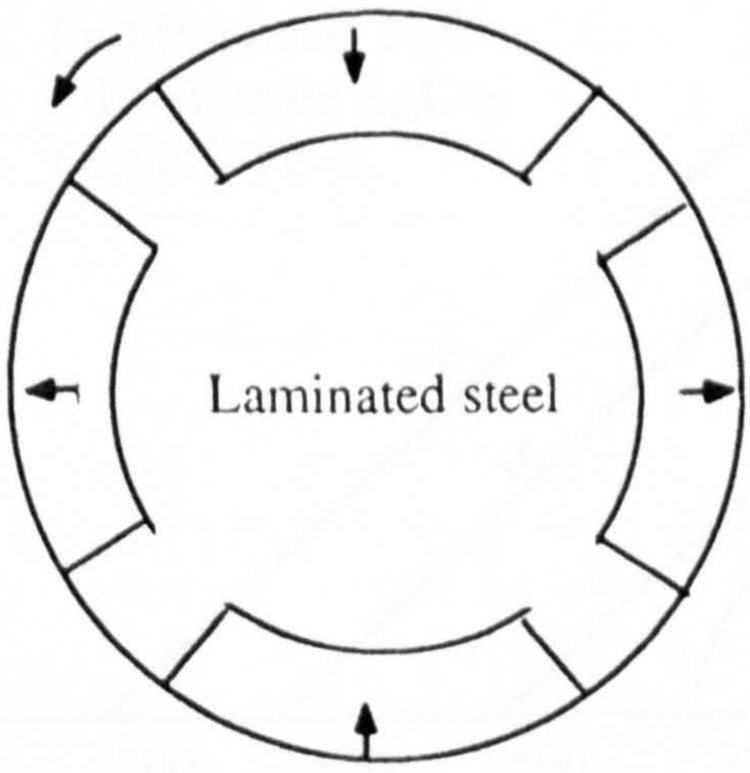

(ii) Buried magnets rotor

(b) Four pole permanent magnet rotor with salient poles

Figure 1.5 Permanent magnet rotor configuration

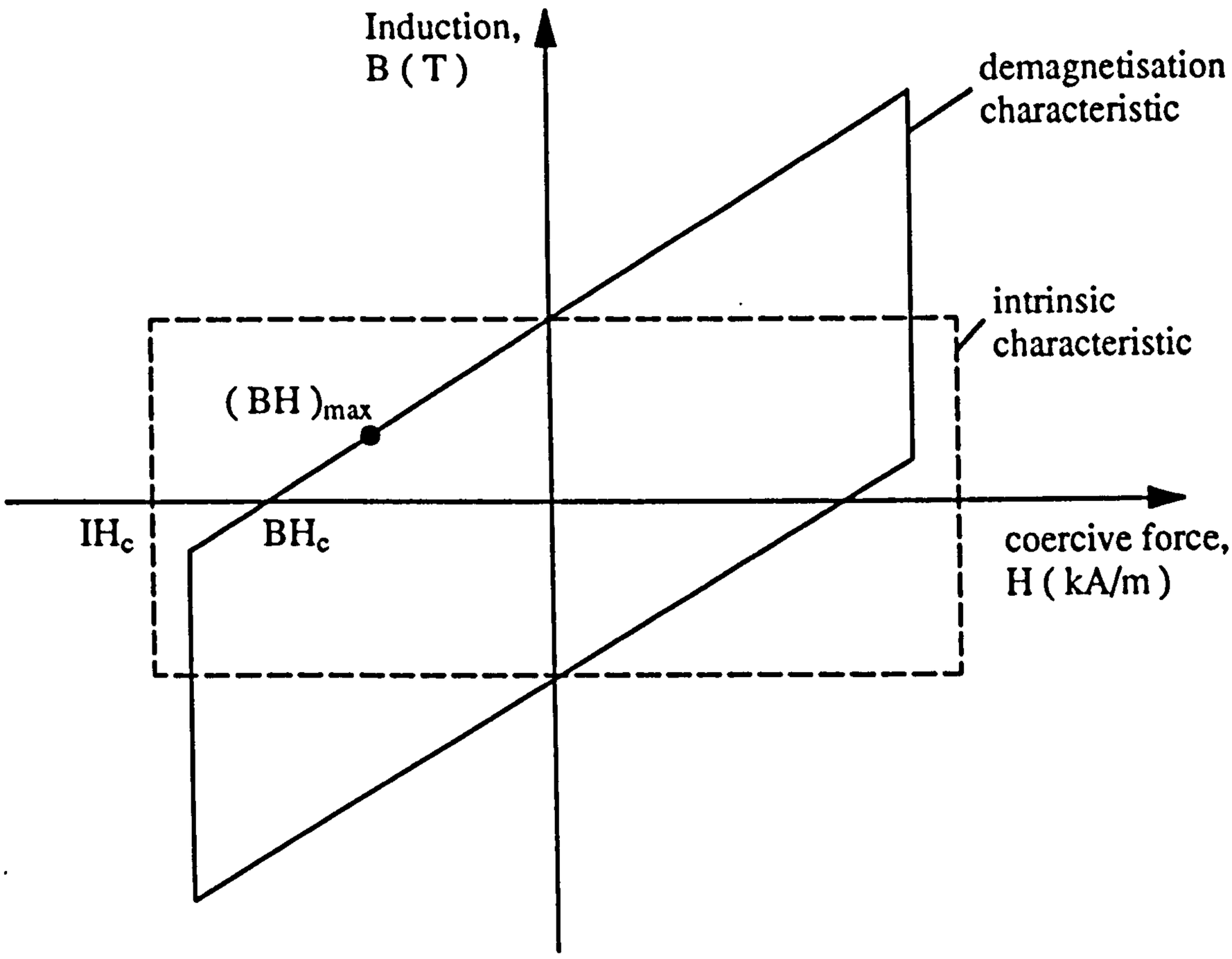

(a) Intrinsic magnetisation curve and demagnetisation curve for hard magnetic material

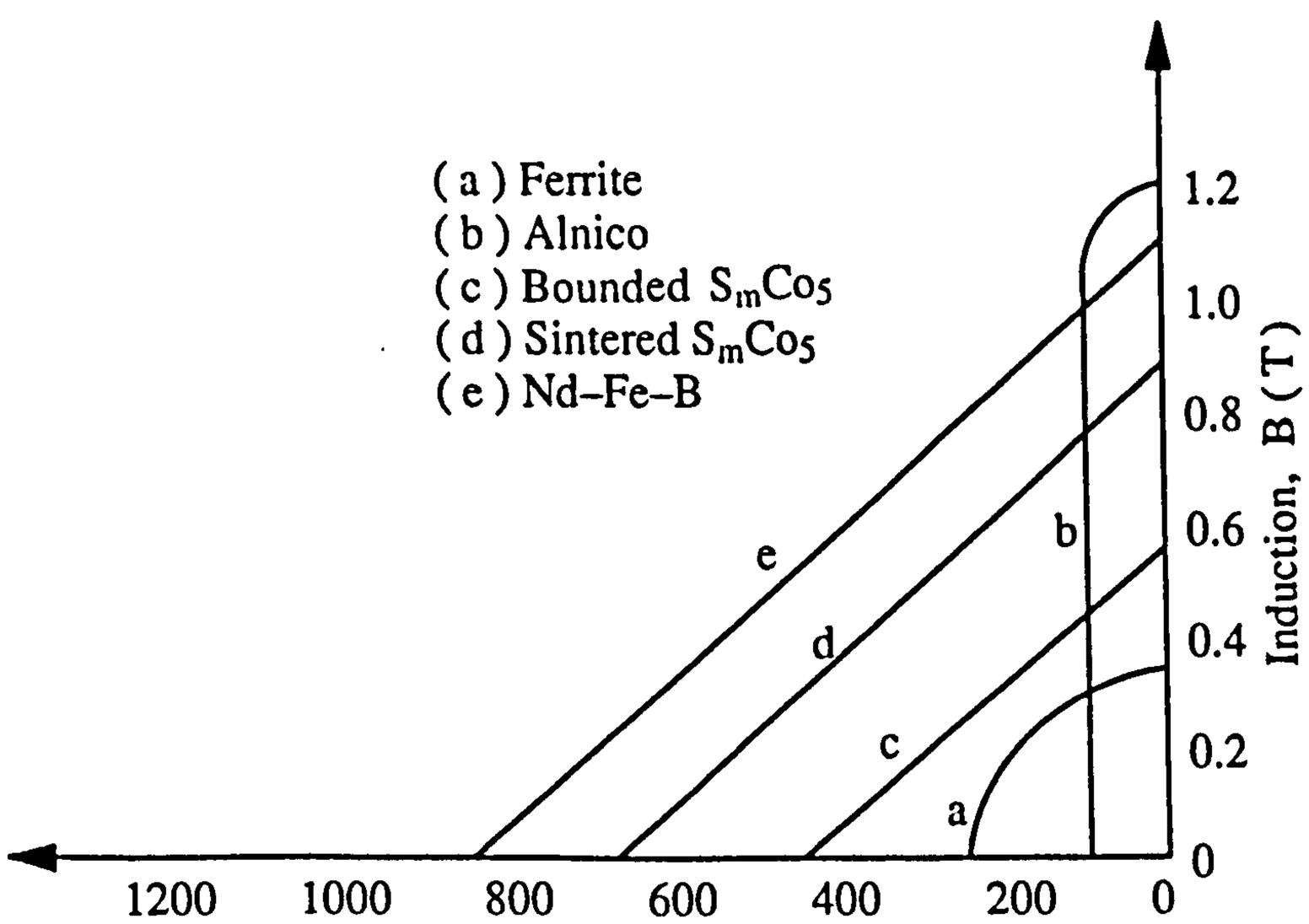

Figure 1.6 B–H characteristics for most common permanent magnet materials

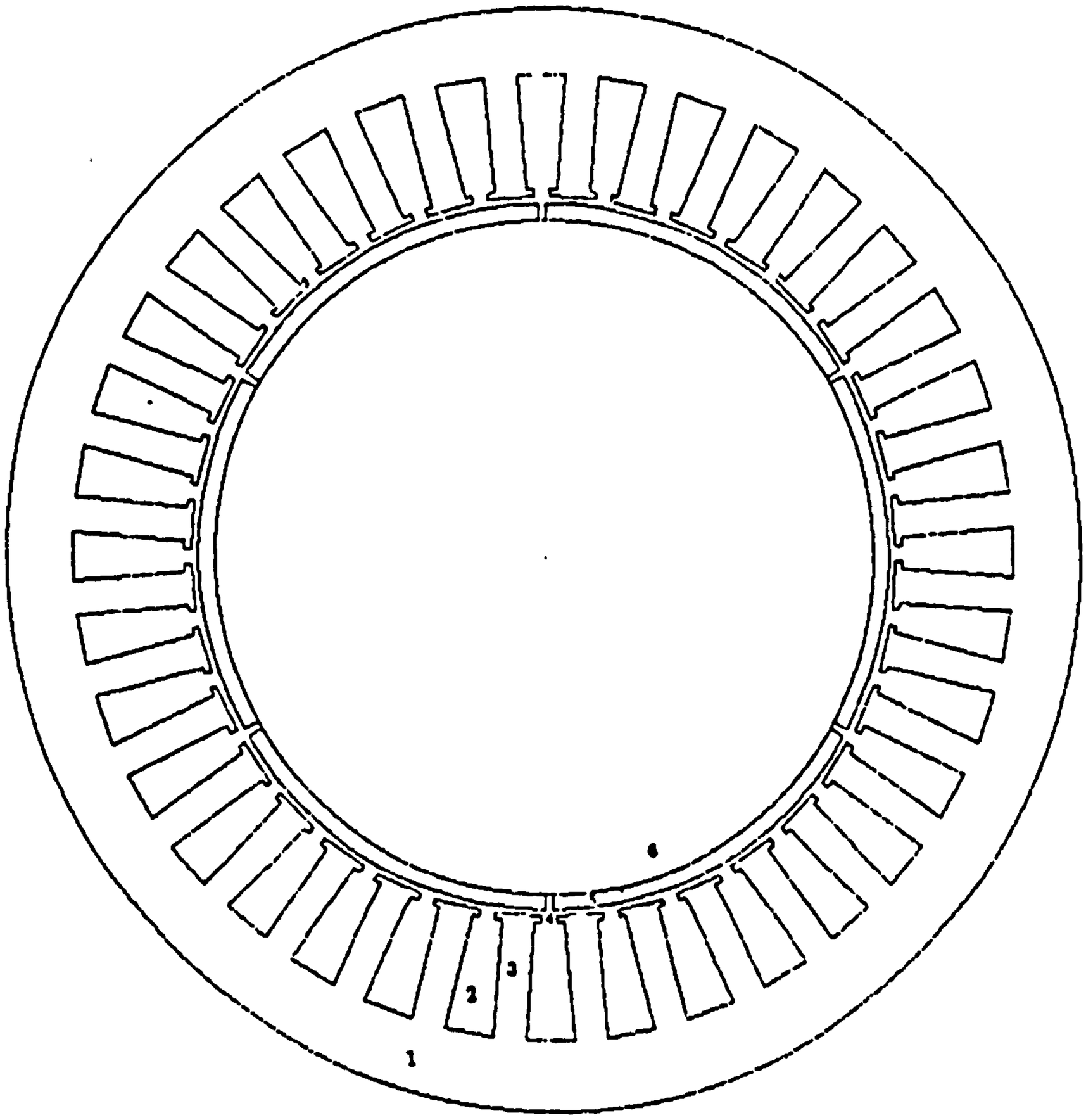

Figure 1.7 Cross section of prototype motor.

1 stator lamination
2 slot
3 slot tooth
4 air gap
5 rotor pole
6 rotor shaft

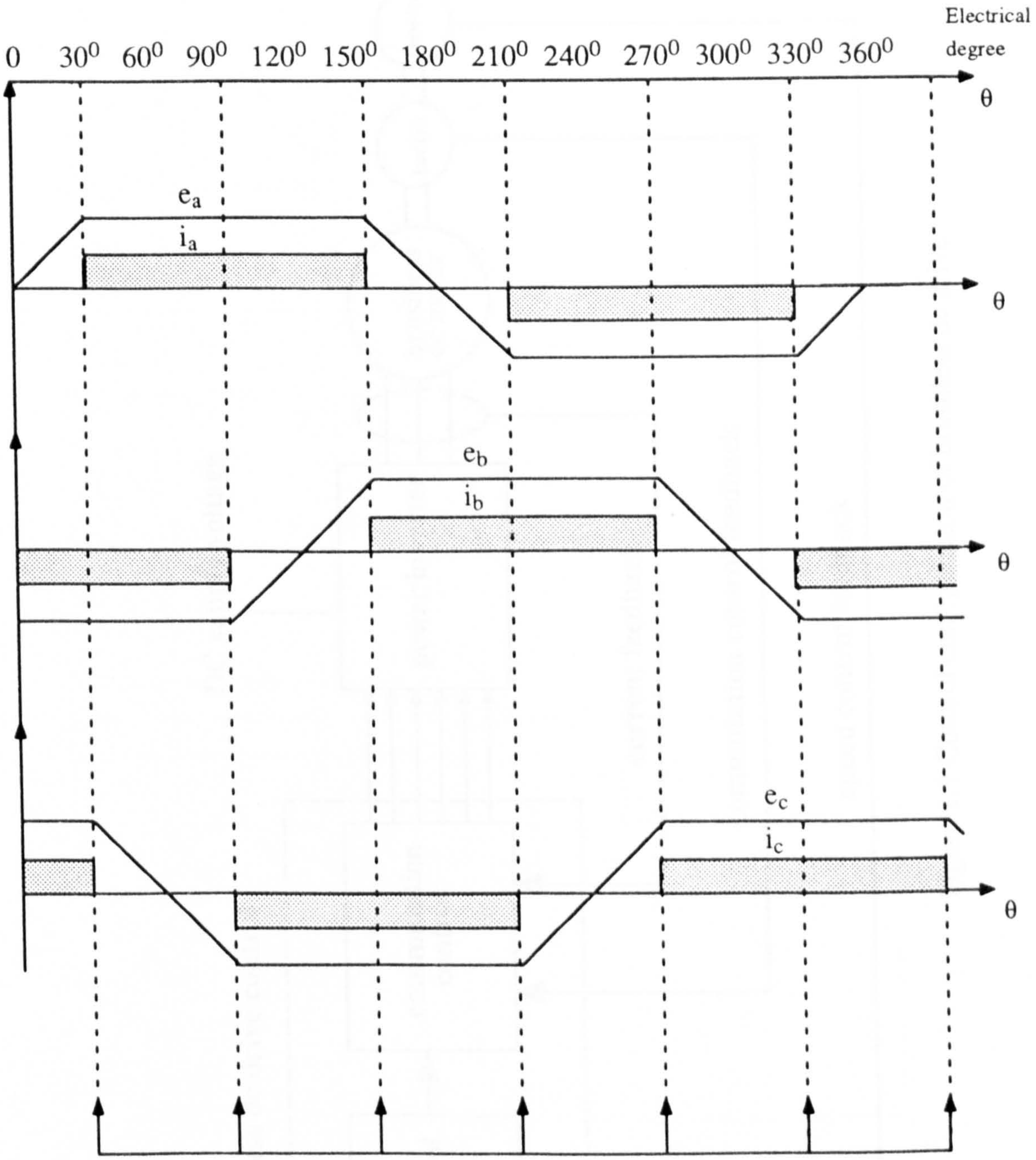

commutation points for
the position encoder

Figure 1.8 Position detection for current commutation

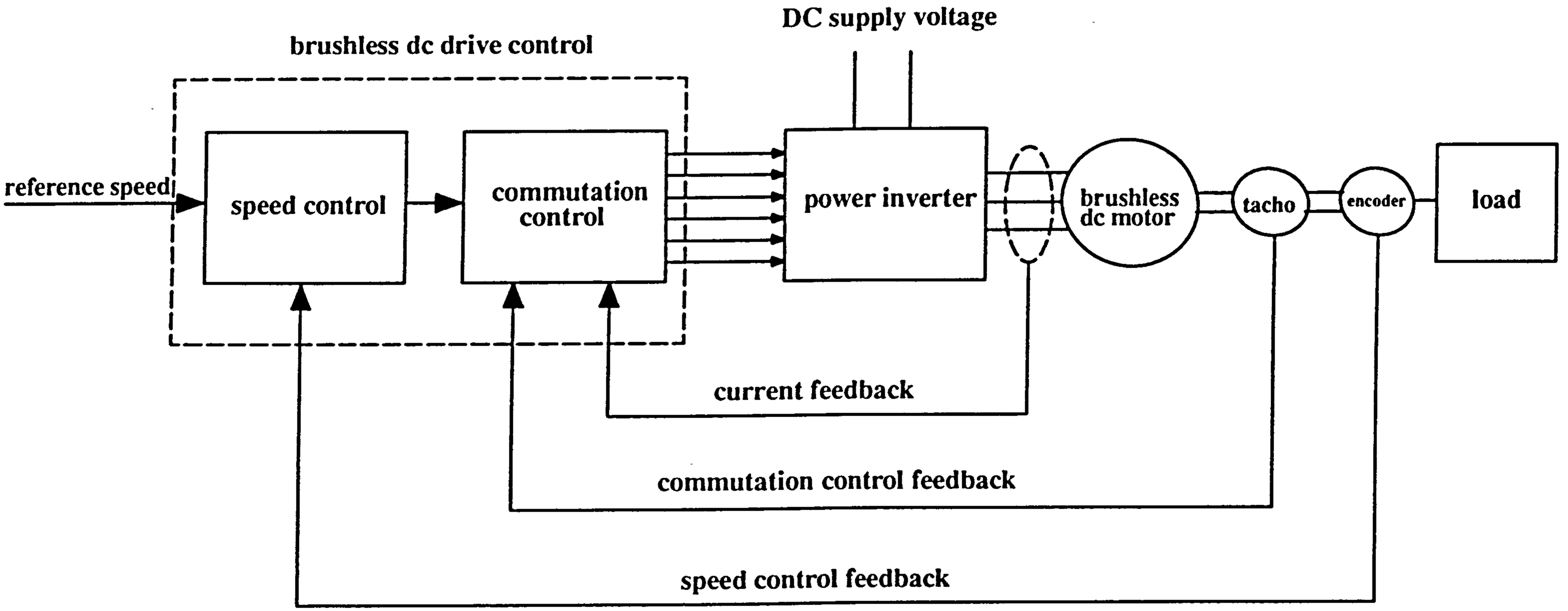

Figure 1.9 Control configuration of brushless dc drive

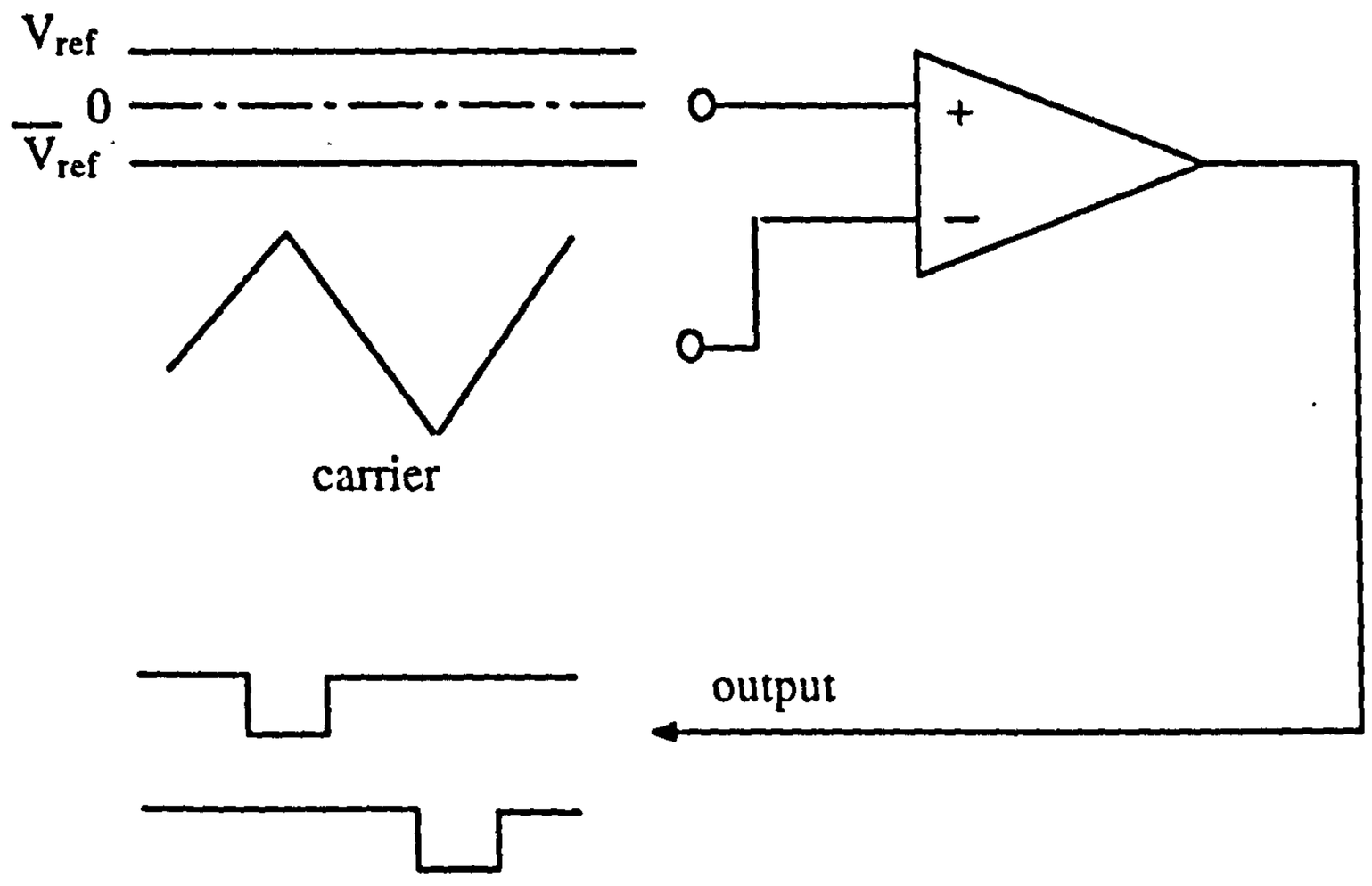

(a) $V_{ref} \geq 0$

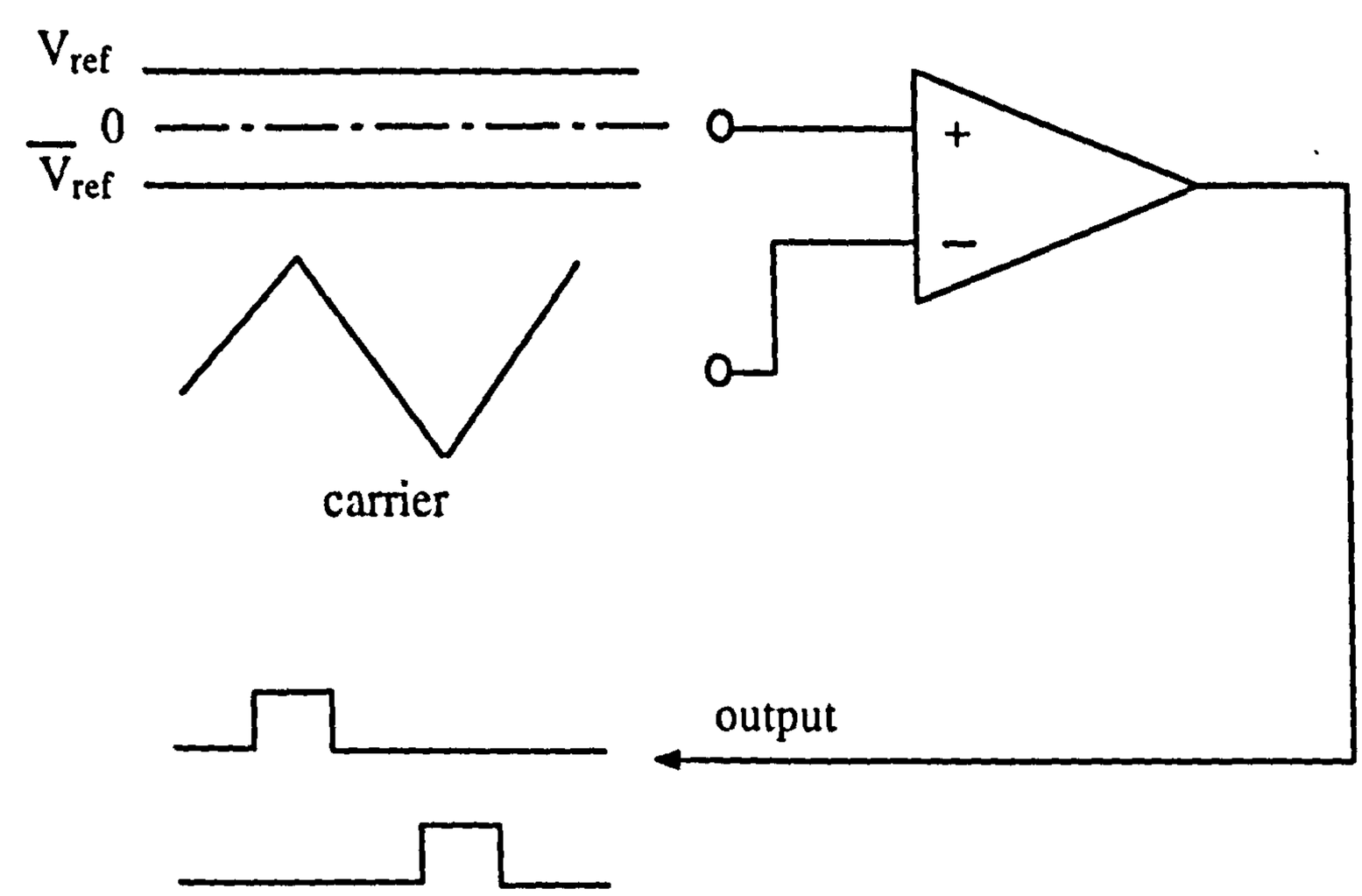

(a) $V_{ref} \leq 0$

Figure 1.10 Generation of PWM drive signal

CHAPTER 2

OPERATION, CONTROL AND PERFORMANCE CHARACTERISTICS OF PERMANENT MAGNET BRUSHLESS DC MOTOR DRIVES

2.1 Introduction

This chapter describes the operation and control of a brushless d.c. motor drive, in which a voltage source inverter is used to drive a three phase machine. In Section 2.2 a more detail investigation of the operation of a brushless d.c. motor is given and torque production in the permanent magnet brushless dc motor with rectangular excitation is also discussed. Section 2.3 describes different control aspects of the brushless d.c. motor, particularly the investigation of the high-speed torque performance when both the phase advance angle and extended conduction angle methods are used. The final part of the chapter presents the principle parameters which effect the high-speed torque performance.

2.2 Operation and Torque Production of Brushless DC Motors

2.2.1 Operational Requirements

The general form of current waveform produced by a voltage source inverter is shown in figure 1.4. In order to match a brushless motor to such a supply current waveform, it is necessary to design the motor so that the back-emf of each phase winding has a shape as close as possible to that of the current supply. In both conduction angles of inverter operation, resulting phase current depends on the relative magnitudes of resistance and

inductance in the phase winding (or L/R). Typical load current waveforms for 180° conduction angle are shown in figure 2.1, for one phase only, for resistance dominated, slightly inductance dominated, or heavily inductance dominated to demonstrate the change in waveform for different L/R load ratios. It can be seen that the current wave shape and conduction time is a function of L/R.

Also it can be seen that in the case of a resistance dominated winding, the phase current is constant during the on period and is in phase with phase back-emf. The constant square phase current is useful because it results in a greater torque output from the motor and allows the supply/inverter VA to minimised. Further the current in each phase is voltage forced and so it is important to minimise the effect of the inductance to allow rapid current rise times.

A trapezoidal back-emf of the form shown in figure 2.2 can be generated in a phase winding by arranging the rate of flux linkage to be constant when a back-emf is required and to be zero during the desired zero volt back-emf periods (i.e. the flux linkage is constant during these times). This can be achieved by using a rotor which has a constant flux density, B, across each pole face (i.e. a square wave of flux across each pole phase arc) in combination with an unskewed, concentrated phase winding (one slot per pole per phase). The necessary flux density distribution across each rotor pole pair and the relation between flux distribution, flux linkage and back-emf is shown in figure 2.2. When the rotor is moving at a constant speed the back-emf generated in the phase winding is constant during the time that a pole face passes underneath the coil. The induced voltage in phase windings are equal to the rate of change of flux linkages

$$e_k = \frac{\partial \lambda_k}{\partial t}, \qquad k = a, b, c \tag{2.1}$$

where

$$\lambda = N\phi \tag{2.2}$$

where

λ is the magnetic flux linkage of corresponding coil k,

N is number of turn of the coil,

ϕ is magnetic flux of the coil.

If the winding is distributed rather than concentrated, or the stator is skewed, there is a tendency for the resultant generated back-emf to be sinusoidal. This is because various parts of the winding meet the leading and trailing edge of the pole flux at different times and so the vector sum of the individual emfs is by no means constant with time and it may result in a large cogging torque for the machine. In other words, cogging torque is caused by interaction between the rotor magnet flux and the stator teeth.

In order to limit the ripples in the airgap flux density caused by slot openings, semi-closed or closed slots can be used in the stator. However, the requirement for a low inductance stator winding places a restriction on the form of the slot that can be used. Often semi-closed or closed slots provide a good path for leakage flux and so increase the stator inductance. An open slot may be used even though this results in a large ripple component in the airgap flux density.

In practice one way of minimising cogging torque is to choose carefully the relative widths of the slot opening, rotor pole arc, and slot pitch. An

alternative way of minimising the tooth ripple though skewing of either the stator teeth or the rotor magnets. However, skewing increases the complexity of motor construction. Also tooth ripple can be effectively eliminated by using an airgap winding [Jack, et al, 1988].

Finally, it can be seen in figure 2.2a that the magnet pole arc does not cover 180° electrical. The interpole regions are necessary to avoid excessive pole to pole leakage flux.

2.2.2 Operational Limits

The stator current must normally be limited to a maximum value due to stator heating. This value may be somewhat dependent on the speed because of its effect on stator cooling rate, iron losses, and skin effect, but may be considered constant as a first approximation.

The stator flux linkage, λ, must normally be limited to a maximum value to limit the stator iron loss and the saturation in the machine. The flux linkage, λ, may be considered constant or may decrease with increased speed due to the increased iron losses. Accordingly the stator voltage must be made proportional to speed to maintain maximum flux. The maximum speed is determined by mechanical considerations.

Having explained the basic requirements and limitations of a brushless dc motor operation, the mode of operation can now be described.

2.2.3 Principle Operation of a Brushless dc Motor

When a multiphase sinusoidally distributed synchronous motor is driven from a sinusoidal voltage supply, the airgap flux generated by the stator winding travels around the airgap at a constant rate which is directly proportional to the supply frequency. However, if the stator windings are driven from a rectangular current supply, the stator mmf (magnetomotive

force) moves around the airgap in a series of discrete moves. In a permanent magnet brushless d.c. motor this mmf stepping occurs every 60° electrical. The instants at which the stator field moves from one location to the next are determined by a rotor position sensor, which directly controls the stator voltage waveforms produced by the inverter.

It is, however, clear that when alternating current flows in the machine windings, a rotating magnetic field is created that causes the rotor to revolve. Therefore it is appropriate to examine how a rotating magnetic field can be created by a combination of a d.c. power supply and manual switches or power transistor in the brushless dc motor drive.

Figure 2.3 shows how the currents are distributed in the windings and how the magnetic field is located in the motor when the U and V terminals are connected to the positive terminal of the battery and the W to the negative terminal. It is seen that two magnetic poles, the north and south poles are created in the winding arrangement. The field distribution can be represented by a vector, illustrated in the centre of the rotor, as shown in figure 2.4.

Figure 2.4 also illustrates the relationship between six different switching states and the magnetic field vector. There are other possible switching states but these six can be used in sequence to rotate the field; when the switching is carried-out downwards, the field rotate clockwise (CW); with switching sequence upwards, the field will rotate counter-clockwise (CCW). In either sequence, one switching action makes the field travel through 60°, and hence six sequential operations make a full rotation. In other words during each current cycle there are six switching states and thus stator current in the stator phase windings. Therefore, a two pole machine rotates by 360° for every six excitation changes. This establishes six possible stator mmfs acting along the axes of the windings. The stator field moves in a discrete step of

60° electrical each time switching takes place from one current state to the next.

At the beginning of each state, the stator flux, due the stator mmf, leads the rotor flux by 120° electrical in the direction of the rotation. This angle decreases at the end of the same state due to rotor motion and the fact that the stator flux, due to the stator mmf, remains stationary during the state. At the end of the state the rotor position sensor signals the power inverter to initiate the next current state. This produces a 60° electrical forward step of stator flux in the direction of the rotation. At this point, the two fluxes are again separated by 120° electrical. This process is repeated six times over each current cycle.

These repetitive discrete stator mmf steps lead to a machine operation which is analogous to a conventional synchronous machine operating with variable torque angle that fluctuates between 120° and 60° six times in one complete cycle.

At this point it should be mentioned that the process of commutation and conduction occurs at low speed. Because at this speed there is no or little back-emf and the ideal current states are dictated entirely by the supply voltages. As the speed increases so do the back-emfs of the motor, the excitation pattern requirement is not easily to fulfill, as will be seen later in this work.

When the three voltage waveforms are used to drive a star connected motor, at any one instant in time, only two phases are conducting and one commutating . For example, phase a is commutating and phases b and c are carrying currents which can react with rotor flux to produce torque. Since the windings are in series, the current depends on the sum of the back-emfs within both phase windings. The stator flux at any time is the resultant of fluxes produced by the two energised phase windings.

2.2.3 Operation Methods of a Power Inverter

As explained previously, the fundamental principle of obtaining three phase a.c. currents to be supplied to a brushless dc motor, in which power switches are used for conduction of the supply from the dc source to the stator windings in the proper sequence. A number of sequences for operating the inverter switches are possible, but there are two fundamental methods that complete one cycle with six switchings; one is known as the 120° conduction angle and the other the 180° conduction angle type. Detail of these methods and their effects on the drive performance will be discussed in the following chapters, but this subsection is limited to the general description and configuration of these methods.

120° *Conduction Angle*

This method of switching sequence is determined by following the rule that one of the three switches is connected to the positive terminal, another to the negative terminal, and the last kept open. An example is shown in figure 2.5. In this figure the current distribution and resultant magnetic field are illustrated to show how a magnetic field rotates in a motor. A rotor placed in this magnetic field is caused to revolve in the same direction. If the sequence is reversed, the magnetic field and hence the rotor will rotate in the opposite direction.

180° *Conduction Angle*

Switching for this method is implemented with-out an off period; that is, each switch is always on either the positive or negative terminal, but the situation to be avoided is to have all three on the positive or negative terminal at the same time. The sequence for clockwise rotation is shown in figure 2.6. In this figure, the arrangement of the terminal U, V, and W has been rotated 180°.

In either the 120° or 180° conduction angle type, the magnetic field rotates at 60° intervals. But differences can be seen in the voltage waveforms. The comparison of these methods will be more discussed and presented in the following chapters.

2.2.5 Torque Production

Torque is produced by the motor whenever the axis of the rotor flux is not aligned with the axis of the stator flux, due to the stator mmf. Continuous rotation of the rotor can be achieved by arranging the rotor position sensor so that the stator flux, ϕ_s, always steps on a head of rotor flux, ϕ_f, as the motor moves towards the alignment axis.

The developed torque is proportional in magnitude to the product of two flux amplitudes and the trigonometric angle displacement between the two flux peaks. The torque angles between the stator and rotor fluxes are depicted at the beginning and end of a switching state. The rotor is forced into a rotational motion in a direction which tends to decrease the angular displacement between the two flux peaks. This continues until the next switching instant, at which time the stator flux, due to its mmf, moves forward in discrete stepping fashion, as described above. This in turn maximises the angular displacement between the two fluxes, and increases the torque, and the process of rotor motion is repeated to diminish this angular displacement.

It is, however, clear that the torque produced by the motor is basically a function of the stator flux (due to the stator mmf), the rotor flux and the angle displacement between the axes of these two fluxes. If the fluxes are sinusoidal distributed, the electromagnetic torque, T_e, produced by the motor is given by

$$T_e = k \times \phi_s \times \phi_f \times sin\psi \tag{2.3}$$

where

k is arbitrary constant, and,

ψ is the torque angle.

For the purpose of this discussion it is convenient to use equation (2.3) even though in general a voltage source inverter fed machine may not have sinusoidally distributed fluxes. It can be seen in equation (2.3) that the maximum machine torque for a given stator current is achieved when the torque is 90°. Unfortunately it is not possible to maintain a torque angle of 90° throughout a step because stator flux ϕ_s, due to the stator mmf, only exists along six fixed axes whereas rotor flux, ϕ_f, continuously rotates. However, it is possible to arrange the switching points of ϕ_s so that an average torque angle of 90° is achieved.

The stator flux, ϕ_s, saturation effects apart, is directly proportional to the phase currents. Therefore, if the phase currents flow in phase with the applied voltages, the stator mmf and thus the stator flux , ϕ_s, can be precisely controlled by the instant commutation of phase currents. This enables the average torque angle to be held at a value of 90° and so the torque per volt is maximised. The voltages must be switched onto the appropriate phase winding when the axis of ϕ_f is 120° behind the axis of ϕ_s, and then they remain connected until the axes of ϕ_f and ϕ_s are 60° apart. The average torque angle over the step is then 90°. At the end of the step the phase voltages are switched so that ϕ_s steps on by a further 60°.

A phase current will only flow in phase with the applied phase voltage if the phase winding impedance is resistive. This is only true either in a

motor which has negligible stator inductance or at low switching frequencies when any inductive reactance is small. Therefore, in a typical motor operating at a reasonable speed, the inductive reactance of the phase windings results in a significant time constant for the current. If the phase voltages are applied when $\psi = 120°$ there is a finite delay before the phase currents and stator flux, ϕ_s, reach their maximum values. Similarly, when the phase voltages are removed, the phase currents and ϕ_s do not disappear immediately but decay away exponentially via the inverter freewheel paths. This situation becomes worse when the back-emf reaches its maximum value at high-speed operation. This leads to poor utilisation of the torque producing capability of the motor predicted by equation (2.3) for two reasons. Firstly, the delay in ϕ_s rising and decaying means that the average value of ψ over the step is less than 90°. Secondly, the average value of ϕ_s is reduced over the step period because the phase currents do not attain their maximum values or decrease to zero as quickly as possible.

As will be shown in detail in the following sections, to limit these problems it is necessary to apply the phase voltages earlier than the $\psi = 120°$ position and also remove the voltages before the $\psi = 60°$ position. By advancing the voltages in time, it is possible to make the phase currents and hence ϕ_s occur over approximately the required period and with correct average spatial displacement from the axis of ϕ_f. The advance needed is similar to the brush shift required for good commutation in d.c. brushed (commutator) machines. The amount by which the phase voltages must be advanced depends on the speed of the motor.

In practice the control of the phase advance angle to maximise the motor torque over a speed range is generally easier than the control of the torque angle. This is because the position of e is directly related to the rotor direct axis (the axis of ϕ_f) and it is the position of this axis that is

monitored by the rotor position sensor. Therefore, the information needed for phase advance angle is readily available. In contrast, torque control requires a knowledge of the relative positions of both ϕ_f and ϕ_s, in addition to the need for a rotor position sensor to monitor the axis of ϕ_f, it is also necessary to monitor the phase currents in order to control the axis of ϕ_s.

Having explained the operation of a brushless dc machine, the basic requirement and implications of the drive control can now be described.

2.3 Control and Performance Characteristics of Brushless DC Motors

Before describing the implications of control methods of brushless dc motor drives, it is appropriate, at this stage, to analyse and review the more important functional control requirements associated with the drive system, and to assess these in terms of the inherent characteristics, i.e those which occur under the desired operating conditions.

2.3.1 Performance Analysis

According to the analogy between the brushless dc motor and brushed dc motor, the principle of this analysis is conducted. As in the brushed dc motor, the brushless dc motor performance can be predicted by using the same basic laws. From these laws, expressions have been derived relating the various principle parameters so that the functional requirements of the motor can be defined and assessed.

If the commutation is perfect and the current waveform is rectangular in shape, and if the converter is supplied from an ideal direct voltage source, V_{dc}, then terminal voltage of two phases is given by

$$V_{dc} = e_s + R_s i_s \tag{2.4}$$

where R_s is the sum of two phases resistance in series and e_s is the sum of two phases back-emfs in series. Equation (2.4) is exactly the same as that of the brushed (commutator) dc motor. The voltage drops across two converter switches in series are omitted, but they correspond exactly to brush voltage drops in series in brushed motor.

e_s is back-emf which is induced in the windings and it is proportional to both the motor speed, ω_r and flux, ϕ, i.e.,

$$e_s = k_b \phi_s \omega_r \tag{2.5}$$

where k_b is motor voltage (or emf) constant which has unit volt/rpm. In turn equation (2.4) can also be used to specify the phase current from

$$i_s = \frac{V_{dc} - e_s}{R_s} \tag{2.6}$$

substituting equations (2.5) into (2.6) yields:

$$i_s = \frac{1}{R_s}\left[V_{dc} - k_1 R_s \phi_s \omega_r\right] \tag{2.7}$$

The gross torque produced by the phase windings to overcome the load torque and mechanical losses, T_e, is given by:

$$T_e = k_t \phi_s i_s \tag{2.8}$$

where k_t is a torque constant which has unit Nm/A. The torque is a simple function of the current and the reason for such a simple relation is that the magnetic flux needed to generated torque, which is referred to as 'field flux'

is provided by a permanent magnet. One can assume that this flux level does not vary with speed.

Substituting equation (2.8) into (2.7) yields the following relationship between torque-speed characteristic:

$$V_{dc} = k_1 \phi_s \omega_r + \frac{R_s T_e}{k_2 \phi_s} \tag{2.9}$$

also after re-arrangement, equation (2.9) can be written in the following form:

$$\omega_r = \frac{V_{dc}}{\phi_s k_1}\left[1 - \frac{R_s T_e}{V_{dc} k_2 \phi_s}\right] \tag{2.10}$$

If k_1, k_2 are numerically equal, then the speed torque relation is given in the following;

$$\omega_r = \frac{V_{dc}}{\phi_s k}\left[1 - \frac{R_s T_e}{V_{dc} k \phi_s}\right] \tag{2.11}$$

When the motor is running light, so that the only mechanical resistance is that due its own friction, only a small driving torque is needed to keep the motor running. Since the motor torque is proportional to current, the no-load current will also be small. Hence under no-load (zero torque) condition,

$$\omega_{ro} = \frac{V_{dc}}{k \phi_s} \tag{2.12}$$

If the motor is operating under stalled conditions, i.e., $\omega_r = 0$, the following relations are obtained

$$T_{eo} = k \phi i_{so} \tag{2.13}$$

and

$$i_{eo} = \frac{V_{dc}}{R_s} \tag{2.14}$$

substituting equation (2.12) and (2.13) into (2.11) yields the following relationship between torque-speed characteristic

$$T_e = T_{eo}\left(1 - \frac{\omega_r}{\omega_{ro}}\right) \tag{2.15}$$

$$\omega_r = \omega_{ro}\left(1 - \frac{T_e}{T_{eo}}\right) \tag{2.16}$$

and for no-load torque

$$T_{eo} = \frac{T_e \omega_{ro}}{\omega_{ro} - \omega_r} \tag{2.17}$$

Equation (2.17) shows that for constant machine parameters, the noload speed is directly proportional the supply dc voltage.

From equation (2.4) it is also clear that

$$V_{dc} i_s = e_s i_s + R_s i_s^2 \tag{2.18}$$

which is interpreted as

$$P_i = P_o + P_{loss} \tag{2.19}$$

where P_i is electrical input power, P_o is rotational power (mechanical output power) and P_{loss} is power dissipated (copper losses) as heat in stator winding

resistance. The output power, P_o, is related to the speed and instantaneous electromagnetic torque by the relationship:

$$P_o = e_s i_s = \omega_r T_e \tag{2.20}$$

The equation that govern the load and the motor is given by

$$\frac{\partial \omega_r}{\partial t} = k\frac{T_e}{J} \tag{2.21}$$

In order to clarify the dependence of the motor behaviour on these equations, two important observations follow. Firstly the speed drop with load is very small. This is very desirable for most applications, since all we have to do to maintain almost constant speed is to set the appropriate stator voltage and keep it constant. Secondly, a delicate balance between V and e is revealed. The current is in fact proportional to the difference between V and e, so that quite small changes in either V or e give rise to disproportionately large changes in the current and this is the situation when the the drive is running at constant speed. For transient speed, the difference between V and e (V-e) must be limited in order to avoid excessive currents.

In a power inverter-fed drive it is vital that the current is kept within safe bounds, otherwise the power switches, which have very limited overcurrent capacity, will be damaged, and it follows from equation (2.4) that it should not allow V and e to differ by more than $i_s R_s$. It would be unacceptable, for example, to attempt to bring a motor up to speed simply on rated voltage. At standstill the back-emf is zero so when the phase voltage is suddenly applied to the phase winding, the initial current will rise immediately to $\frac{V}{R}$, and the value of this current would be very large.

In a such situation, it is quite impractical to change the speed in

that way, except for very small changes, because of the low value of winding resistance. For higher power drives the sudden change of phase voltage would cause many times rated current to flow. The phase current is extremely sensitive to changes in the voltage and some form of current-limiting feedback circuit must be used to prevent excessive current. In this approach the current is sensed, and the voltage V is automatically adjusted so that rated current is either never exceeds its rated value. The feedback current control will be discussed in the following section.

The speed of a motor cannot be changed instantaneously because of the energy stored in its mechanical moment of inertia. The rate of acceleration depends upon the net torque acting on the inertia, as shown in equation (2.21). If the short armature time constant is neglected, when the phase voltage is suddenly applied to the phase winding, the current will rise immediately to $\frac{V}{R}$ and the motor will accelerate so that the speed rises exponentially, proportional to the winding resistance and the moment of inertia.

2.3.2 Control Characteristics

The control strategy for the brushless dc drive system is designed to optimise the overall drive system with the following main aims (i) proper matching between various elements of the system including operation of the inverter and the motor and to ensure these will work near their maximum power limits simultaneously (ii) providing maximum-available torque at the given motor and inverter rating.

In the system design, matching between inverter rating and motor rating is of prime concern. For the inverter the current is the most critical factor, while for the brushless motor, the power rating and thermal rating play the main roles. Under these conditions of rated power and torque the

armature voltage and magnetic flux are at their maximum values and the phase current is at its maximum continuous value. The value of phase currents is limited by allowable temperature rise of the windings and will normally be chosen against steady state thermal limits. Under the inverter rating, the armature dc voltage is maximum because there are voltage limitations on the power switching devices. The speed corresponding to rated voltage and current (and flux) is defined as 'base speed'.

By referring to equation (2.11), the two basic modes of speed control are immediately apparent from this equation. No load speed is seen to be proportional to supply dc voltage and inversely proportional to flux.

Assume that the motor is running at base speed (or around rated speed). Firstly the speed can be reduced to zero by reducing dc supply voltage, V_{dc}, because ϕ is limited by magnetic saturation, see section 2.2.2. If the winding current remains at its maximum during this process the torque will also remain constant at its rated value. Secondly the speed cannot be raised by increasing the supply dc voltage V_{dc} because this is already maximum. Instead, the airgap flux must be reduced by adjusting the phase advance angle between the rotor flux and airgap resultant flux, as will be discussed later in this chapter. These two control characteristics are the so called 'constant torque operation' and 'constant power operation' as shown in figure 2.7. These regions of operations will be described below.

(i) Constant current operation (Controlled-current region)

For speeds below the based speed (ω_{rb}), the power inverter switching angle is kept at a constant value that maximise the motor torque with minimum ripple. The motor average torque is controlled by regulating the motor phase currents. In a brushless dc motor, the motor phases are sequentially energised so that only two phases are acting at any time. To operate in torque control mode, the current in active phases must be controlled

by a current regulator and thus only two current sensors are used in a system.

As will be described later in this section, the function of the current regulator is to compare the measured current, i_m, with the reference current, i_{ref}. The error is processed by a PID controller that provides the control signal for a PWM voltage controller. The latter generates the required switching frequency that maintains the current equal to the reference value.

(ii) Constant voltage operation (field weakening region)

For speeds above base speed, ω_{rb}, the current regulator is no longer effective because the back-emf is high and the forcing voltage is insufficient to maintain constant current. The PWM duty cycle is then at its maximum value. The motor speed can be increased by using the commutation control variables such as the advance and phase commutation as a function of the speed so as to obtain the product $T\omega_r$ equal to a constant.

The voltage is usually kept constant at its rated value, limited by the inverter. The current is limited by the rating of the machine. However, for the sake of comparison with brushed dc machines, this mode of operation is often considered as a constant power region or "field weakening region".

The interpretation of figure 2.7 is not always understood but is important in the control aspects. It means that any torque up to the full rated value can be obtained at any speed up to the base speed and any power up to rated power above base speed. The maximum speed depends upon mechanical and stability limitations of the motor design. Most brushless dc motor drives will operate up to twice the base speed.

Clearly the characteristic of figure 2.7 is fundamental to the drive selection. It is wasteful, involving a larger power supply and motor, to specify machine voltage control over the whole speed range if the application only requires full torque up to a fraction of this speed and power equal to or less

than rated power at higher speeds. A good example of the use of a wide constant power speed range is in machine tool drives. Field weakening control is therefore used over this range, where the machine back-emf is approximately equal to the dc supply voltage and dc supply voltage is applied directly across the armature phase winding. This control will be discussed in detail in the following section.

It must also be emphasised that the discussion has been conducted in terms of continuous rating limits. It may be that the duty cycle of a particular application can permit the phase current to rise to an overload value of, say, twice continuously rated current for short periods, in which case the upper limits to the areas in figure 2.7 will be defined by this peak current, but the peak current is limited by inverter device rating.

The following section presents a theoretical performance analysis of several control methods for brushless dc motor drives which are being fed from a PWM current controlled inverter. The three main control strategies which improve the high-speed torque performance of the machine, have been investigated.

2.4 Control Methods of Brushless DC Motors

In many applications the brushless dc motor is required only to travel at a single speed, with a specific load torque and specific supply voltage. In variable speed applications it is necessary to provide some means to vary the motor speed. Also when a variable output torque is needed a method has to be provided to control the input power to the motor.

Methods of controlling the brushless dc motor include basically two functions; magnitude control and commutation control. Magnitude control is the process of adjusting the current level in the phase windings in order to produce the required level of torque. Commutation control can be used

as a control variable to improve the motor speed-torque characteristics, by advancing the instant of commutation or by extending the commutation angle.

The object of the work presented in the following sections is to introduce the aspects of the different control methods and strategies of the brushless dc motor to allow speed torque variation.

2.4.1 Voltage Control

The expression for the speed, ω_r, of a brushless dc motor, which is given by (2.11), shows that the motor speed is essentially controlled by adjusting the stator supply voltage. This gives control up to base speed (corresponding to full armature voltage and full flux)) and the motor can operate at any speed up to base speed, and any torque (current) up to rated value by appropriate choice of armature voltage, as describe in the preceding section.

Speed control using voltage control for a brushless dc motor can be achieved by adjusting the dc voltage supply, either in an open loop system or in a more advance control based on the feedback control techniques. The voltage-controlled brushless dc drive has very poor speed regulation with open-loop control. To obtain the necessary speed accuracy, closed loop control is usually necessary. Closed loop systems generally have the advantages of greater accuracy, improved dynamic response and reduced effect of disturbances such as loading.

The closed-loop control basically compares demanded and measured speed then varies the motor torque according to some control procedure. In some controllers for example, if the motor speed is higher than that set by the command signal then the error voltage is used to reduce the value of the maximum allowable inverter current and, hence, motor driving torque. As the motor decelerates, the error voltage falls until the required speed is obtained.

In this particular implementation the motor speed error is minimised but never zero. The precise implementation of speed control is dependent on the power circuit and controller used.

A simplified block diagram of a speed closed-loop control system is shown in Figure 2.8a. The reference speed is given by V_{ref} and it is compared with measured speed $V_m = k\omega_r$. The angular ω_r is regulated so as to minimise the difference of V_{ref} and V_m. Note that k is a constant of the transducer which converts the rotational speed into voltage level and $G_v(s)$ is the transfer function of the motor when voltage is considered as the input variable.

In block diagram 2.8a, G indicate the gain of the amplifier which amplifies the error $(V_{ref} - V_m)$. The input voltage to the motor is therefore;

$$V_{dc} = G(V_{ref} - V_m) \tag{2.22}$$

V_{ref} is larger than V_m the voltage V_{dc} is large and positive and therefore causes the motor speed to be higher than that set by the V_{ref}. When V_m is slightly lower than V_{ref} a constant speed specified by V_{ref} will be maintained while the motor receives an appropriate voltage.

This error is then processed through PID controller which operates on it with proportional, integral and differential (PID) action in order to optimise the closed loop response and also to obtain the current demand. Each of the three operators is scaled independently, (figure 2.8b).

Because torque is the direct result of motor current, (as shown in section 2.3.2), in many applications it is the current that is the most important parameter to control. Furthermore, it has already been explained in section 2.3.2 that even a relatively small, rapid increase in the applied phase voltage will drive a very large current through the motor winding. This cannot be allowed to happen, because even a relatively small over-current will damage

the transistors of the inverter. The fundamental requirement of brushless dc motor control is therefore to protect the inverter transistor switches from damaging current during transients, and to limit peak currents, which could cause damage to motor windings. This is always done by closed loop control of the motor current as shown in figure 2.8c.

In the closed loop current controller, the instantaneous measure current i_m in the motor winding is detected by the current sensor, which provides the feedback signal for current control loop. This signal is compared with the current command, i_{ref}, which is obtained by a PID speed controller, and a current error Δi is generated. Upon this error the current regulator is activated to maintain the current level within adjustable limits.

The action of the regulator is to switch the dc supply voltage across pairs of machine lines in either sense. This can be done effectively through pulse width modulation of the voltage. The PWM scheme is often used in the current loop to maintain the current in the phase windings equal to the commanded current. In the PWM, the control voltage is achieved by comparing the current servo amplifier output with a constant frequency triangular waveform. The result is a square wave of fixed frequency with a variable mark/space ratio which determines the input voltage and subsequently the speed of the motor. Full torque can be maintained over a wide range of speed, and the maximum speed is determined by the voltage available from the controller. Since the motor back-emf is proportional to speed, this limit tends to be a sharp one, and occurs as soon as the PWM duty cycle reaches 100%.

It is clear that current control operation provides effective torque control and inherent protection. However, current regulation is no longer effective at higher speeds. At these speeds the voltage reaches its full value, and control at higher speeds cannot be achieved since the voltage cannot

be increased further. In such a situation, the commutation control offers two further important control parameters: the phase advance angle and extended conduction angle. Phase advance angle represents the rotor angle at which a given phase is turn-on, and extended conduction angle represents the commutation angle at which a given phase is turn-off. In general stepper motor terminology, the phase advance angle is referred to as switching angle or lead angle, that is the rotor angle at which driving voltage is applied to a given phase in advance of the detent position for that phase.

However, control of these angles makes available a very wide range of performance characteristics and control possibilities. In the following section these high-speed torque methods are discussed in detail.

2.5 High-Speed Torque Control Methods

In many application the machine must produce torque in proportion to its winding current level. As discussed earlier, the machine usually operates with a closed-loop current controller and the machine's electromagnetic torque is proportional to the winding currents. Therefore the most important type of motor control is torque regulation, since the torque (current) controller forms the essential inner loop for most speed controllers.

In high speed operation the torque speed range over which current can be regulated is limited by the dc voltage source of the inverter. In such operation, the terminal voltage approaches the maximum that can be supplied by the inverter causing a transition from PWM to sine-wave operation (as will be shown later). In this transition region the PWM-controller is unable to regulate the phase currents resulting in a rapid deterioration in torque-speed performance.

In order to improve current controller operation and to maximise the available output torque in this higher speed-operation, the commutation control can be used to improve the motor torque in the trapezoidal brushless drive. There are three ways in which the commutation control can influence the output torque of the machine. These are (i) phase advance (ii) extended conduction angle (iii) supply current. The relative merits of each control method are described in the following section.

2.5.1 Field Weakening Control Method

As shown earlier, it is not possible for the drive to operate 'above speed' where the dc supply voltage and the induced back-emf are equal. In a conventional brushed dc machine with a separate field winding this problem is overcome by reducing the field current and thereby the field flux in the machine, hence the use of the term 'field-weakening'. This solution is not easily applicable in brushless dc motors where the source of field flux is a permanent-magnet. However, operation into the field-weakening region of a brushless dc drive is possible by appropriate reduction of the resultant airgap flux according to the load or rotor speed by controlling the space phase angle.

To achieve this principle the applied voltage directly determines the spatial position of the resultant of airgap flux. The spatial position of rotor flux is determined by the rotor axis. The position of the rotor axis is detected by the position sensor and the resulting signals are used to control the applied voltage, V. The stator flux direction with respect to the rotor flux can be "oriented" by adjusting the instant of current switching in the stator winding as a function of the rotor position. In this case when the current is commutated earlier, the direction of stator flux makes an angle greater than the normal operating angle of 90° with the rotor flux axis and thus the resultant airgap flux is reduced to some minimum value. The amount by which the phase voltage must be advanced depends on the speed of the

motor. The process of advancing the applied phase voltage with respect to the back-emf in order to maximise the torque per voltage is equivalent to increasing the load angle of the sinusoidal brushless dc motor.

According to the above considerations, the phase advance angle, α, is a measure of the space phase angle between the resultant air-gap flux and the rotor flux or the time phase angle between the voltage and back-emf. The angle may be adjusted by advancing or delaying in time the signals from the shaft position sensor. This form of control can be obtained by adjusting the commutation (or phase) angle in respect to the position in order to maintain adequate stator current. At the same time, the stator flux occur over approximately the required period, so that the stator flux has the correct average spatial displacement from the axis of the rotor flux allowing the machine to operate in a mode equivalent to field-weakening. It is this strategy which is described in the following section.

2.5.1.1 A Basic Concept of Phase Advance Control

At low speeds when the excitation period for each phase is much greater than the phase circuit time constant. The waveforms of the winding rectangular currents will flow in phase with applied voltage. The phase advance angle of 0° is most advantageous in producing the maximum torque, as will be shown in the following chapter.

At higher speeds, the inductive reactance of the windings results in a significant time constant and as a consequence, the time taken for currents to rise and decay after switching becomes an increasingly significant proportion of each winding excitation interval. In a such situation if phase voltages are applied, there is a finite delay before the phase currents and stator flux reach their maximum values. Similarly when the phase voltages are removed, the phase currents and stator flux do not dispear immediately by decay away exponentially. This situation have two effects (i) the delay in phase current

rising and decaying mean that the average value of the normal operating angle is less than 90° (ii) the current is phase shifted relative to the back-emf. Consequently the torque ouput is reduced and the torque ripple is very significant. Improvement in performance are obtained by advancing the applied phase voltage relative to the back-emf as speed increases.

To understand the nature of the phase advance angle variation, consider the back-emf, e, waveform for a typical machine, as shown in figure 2.9. With zero phase advance the winding begins conducting at 30° after the corresponding back-emf has crossed its zero value and continues for the conduction angle ($\sigma = 120°$). An advance of α means that the phase is made to conduct at an angle α earlier ($\theta = 30° - \alpha$) and as a consequence of this process a large potential difference between V and e which causes the current waveform to rise and ecay more quickly, as shown infigure 2.10.

From the discussion of this section it is obviously important that a brushless dc drive incorporating both PWM voltage and field weaking (using phase advance) control should employed. The former gives control up to base speed, whereas the latter gives control above base speed.

2.5.1.2 Implementation of Phase Advance Control

Further discussions and investigations on the problems concerning the phase advance control are the subject of the following chapters. The investigations of these chapters address the following problems (i) what are the optimum phase advance angles and how may they best be calculated or found experimentally ? (ii) the implementation of the microprocessor based phase advance in a practical closed-loop system.

It was shown that the phase advance angles affect the performance of the motor drive and they are not constant. For maximum high-speed torque production they need to be varied as a function of speed, magnitude of

current and load. The first approach is to drive a mathematical relationship between torque, speed, and phase advance angle, to predict the optimum angles in accordance with this criteria and to compare the predicted with that obtained experimentally. The second approach was to develop flexible algorithms suitable for the microprocessor which allows evaluation of the influence of this control variable on the drive system.

It is the initial aim of the following chapters to present numerical simulation and analytical methods to use them to obtain the required phase advance angle and to compare the predicted trajectory with that experimental tested by the microprocessor using a trail-and-error method and then to store the table of angles (or time intervals) in the memory for a closed-loop microprocessor implementation. Chapter 7 will describe the software and hardware implementation of new phase advance algorithms developed for the microprocessor implementation in a high-speed control system using phase advance controller.

2.5.2 Extended Conduction Angle Control Method

The normal mode of operation for three-phase trapezoidal brushless d.c. drives involves each winding carrying positive current for intervals of 120° electrical and negative current for intervals of 120° electrical during the excitation cycle. These current intervals are timed to coincide with the corresponding polarity of back emf. When designing the motor an attempt is made to ensure that the back emf is constant for 120° electrical intervals so that the product of constant current and back emf leads to constant torque.

Although this idealised performance can be approximated closely at low speeds, distortion of the current waveform at high speed causes a reduction in maximum torque output and an increase in torque ripple. The potential advantages of earlier current turn-on have been discussed in the previous

section. One penalty to be paid for the use of the phase advance procedure is that each winding is switched-off before the corresponding back emf has fallen to zero. Therefore it would appear to be advantageous to extend the interval for which the winding is excited.

A particularly convenient method is to use winding excitation intervals of 180° since the requirement for rotor position signals is unchanged; excitation changes still occur at 60° intervals. With this excitation pattern all three phases carry current at any time instant, with one phase being connected in series with the parallel combination of the other phases. Thus current in each winding has two 60° intervals per cycle when the current magnitude is at the demanded level and four intervals when the current is at half of the demanded current, as shown in figure 2.11.

2.5.3 DC Chopper Control Method

The d.c. supply voltage has to be large enough to ensure that rated current can be circulated against the induced back-emf in the motor windings at rated speed. During acceleration from rest the induced back-emf is initially negligible and the winding currents would then be many times rated if no current control is used. For low speed operation, where the back-emf is low, the d.c. bus voltage is not critical, but as the back emf is increased, a point is reached where a current controller is not able to command the desired current.

Ideally therefore, a power switching circuit is needed which will keep the current constant through-out the on period regardless of back emf. A current chopper allows the use of a high d.c. supply voltage so that the actual currents flowing into the machine are maintained as closely as possible to the references during constant torque operation. As a consequence of this, the d.c. chopper is capable of controlling the drive operation over a

wide torque/speed range. The chopper control method has the advantage of fast transient response, as it is possible to change torque levels during a winding excitation interval. Also torque ripple can be reduced, at the expense of increased switching losses, by ensuring that the excursions of current associated with chopping action are very small.

Nevertheless, the operating speed limit in a drive with current chopping is still dependent on the comparative magnitudes of d.c. supply voltage and back emf. The action of the current chopper, in this context, may be viewed as facilitating the application of enhanced supply voltage by preventing excessive winding currents at low speed.

2.6 Factors Affecting Machine Performance at High-Speed

2.6.1 Effect of Winding Inductance

As explained previously it is important that the phase currents of a brushless dc motor be increased to its desired value or decreased to zero as quickly as possible in order to achieve best utilisation of the torque-producing capacity of the motor. Unfortunately, the presence of the motor phase inductance prevents the current from changing instantaneously. The situation becomes worse when the phase back-emf reaches its maximum value at high-speed operation.

In such an operation, the rise time of the current depends on the voltage differential between the d.c. supply voltage and the induced back-emf and the time constant of the stator winding which is given by the ratio of the stator leakage inductance to resistance (L/R). However, the electrical time constant determines how fast the current will reach its full value after a winding has been switched-on. The higher this ratio, the longer is the current to reach its full value and the greater the deviation from the idealised

value and shape. The lower the time constant, the faster is the current to reach its value and this leads to faster response of the drive and therefore the better performance. In other words the machine winding inductances must be low enough for a given back emf so that the current can build up to the required values at higher speeds of operation, under the d.c. supply voltage constraint. This can be accomplished in a number of ways such as operating the core at higher flux densities, reducing the slot and end leakage inductance. Alternatively, it should be possible to compensate the effect of higher winding inductance by adjusting the phase advance angle.

2.6.2 The Combined Effects of the Machine Inductance and Phase Advance Angle

The previous section's discussion of the mechanism by which phase advance can benefit high-speed performance concentrated on the need to ensure that current and back-emf are coincident in time. At speeds approaching the base speed, where available dc supply voltage and the back-emf are comparable in magnitude, this argument becomes more difficult to apply, as it becomes increasingly difficult to force current into windings.

For an explanation of operation at higher speeds it is necessary to consider energy flow in the drive. The power switching circuit supplies electrical energy to the motor and this energy is converted either to mechanical energy which is the motor output or stored as magnetic energy. When the switching transistor is turned-off the associated stored magnetic energy is either returned to the d.c. supply (through the freewheeling paths) or is converted to mechanical output energy, if the decaying winding current flows against back emf.

By employing the phase advance procedure, phase current is allowed to build-up in the motor winding before the back emf reaches any significant level. Thus during the early part of the winding excitation interval, electrical

energy is being taken from the supply and stored as magnetic energy as the winding current attains its initial high value. When the back emf does reach its maximum level, mechanical output energy is obtained by conversion of both the electrical energy input from the supply and the previously stored magnetic energy from the windings. In terms of the voltage balance in the windings, current is being forced to flow against the back emf by the d.c. supply and the voltage caused by decaying current in the winding inductance.

2.7 Summary and Conclusion

The operation and the control aspects of the brushless dc motor are described, with particular emphasis placed on the basic requirements for the operation, torque production, performance characteristic and control. The high-speed torque control methods are also described and their merits are reviewed. In addition the effects of different parameters of machine design on the torque-speed characteristics is discussed.

In the next chapter a mathematical model of the brushless dc motor will be introduced. Also the simulation procedure, which has simplified further the mathematical model, is described. However this procedure is used to investigate in detail the high-speed torque control methods as well as the effect of the machine parameters.

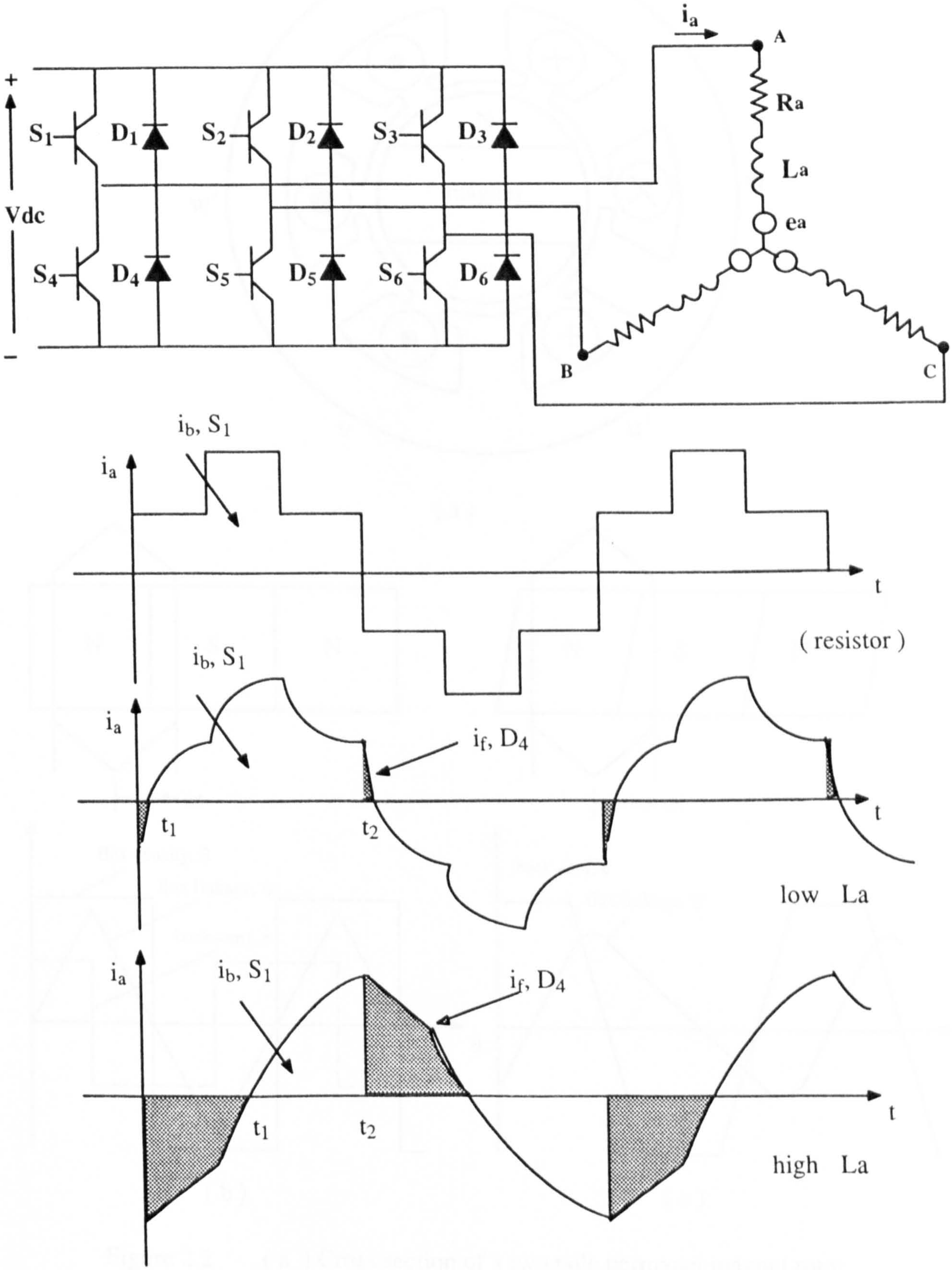

Figure 2.1 Phase currents

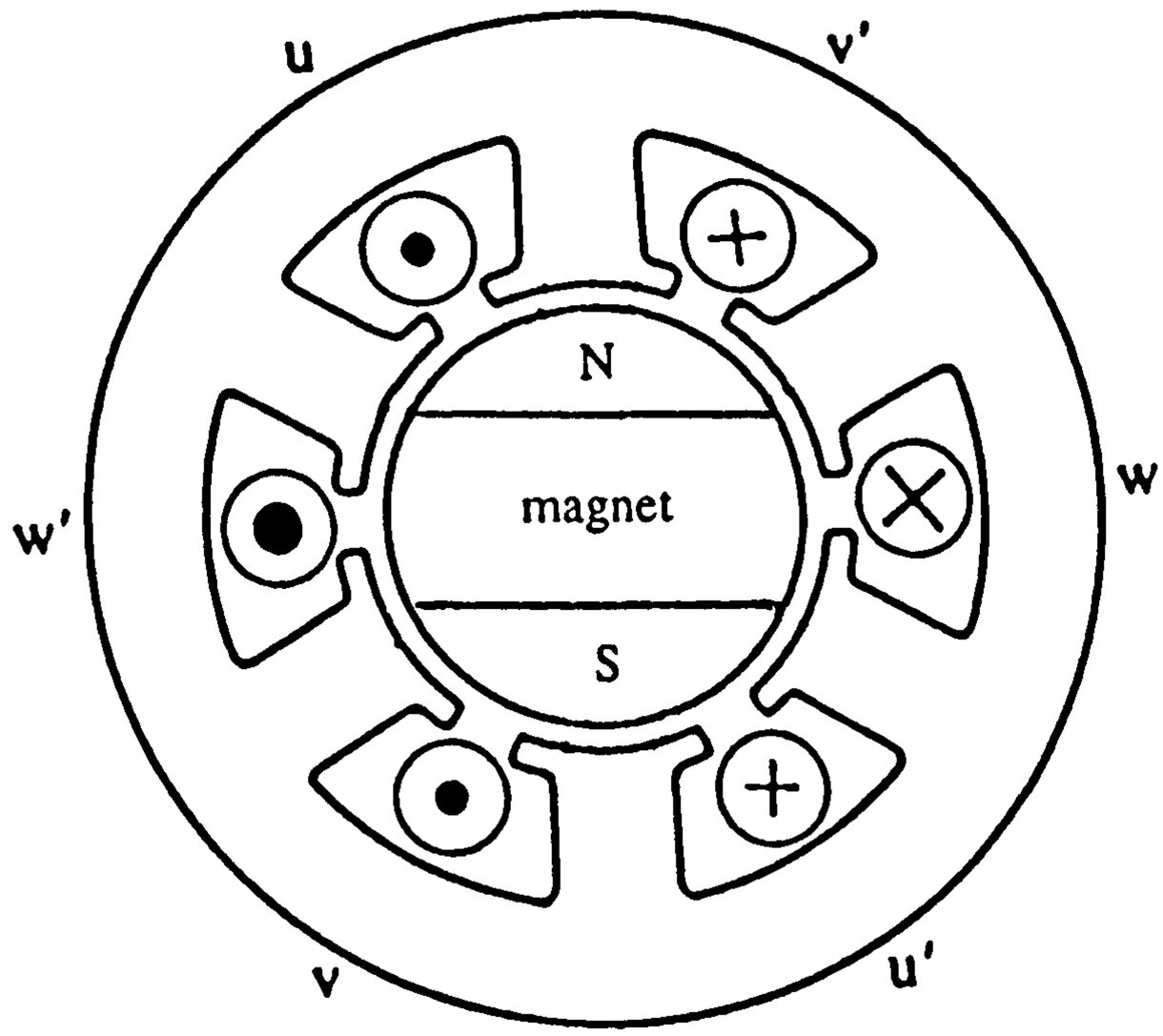

(a)

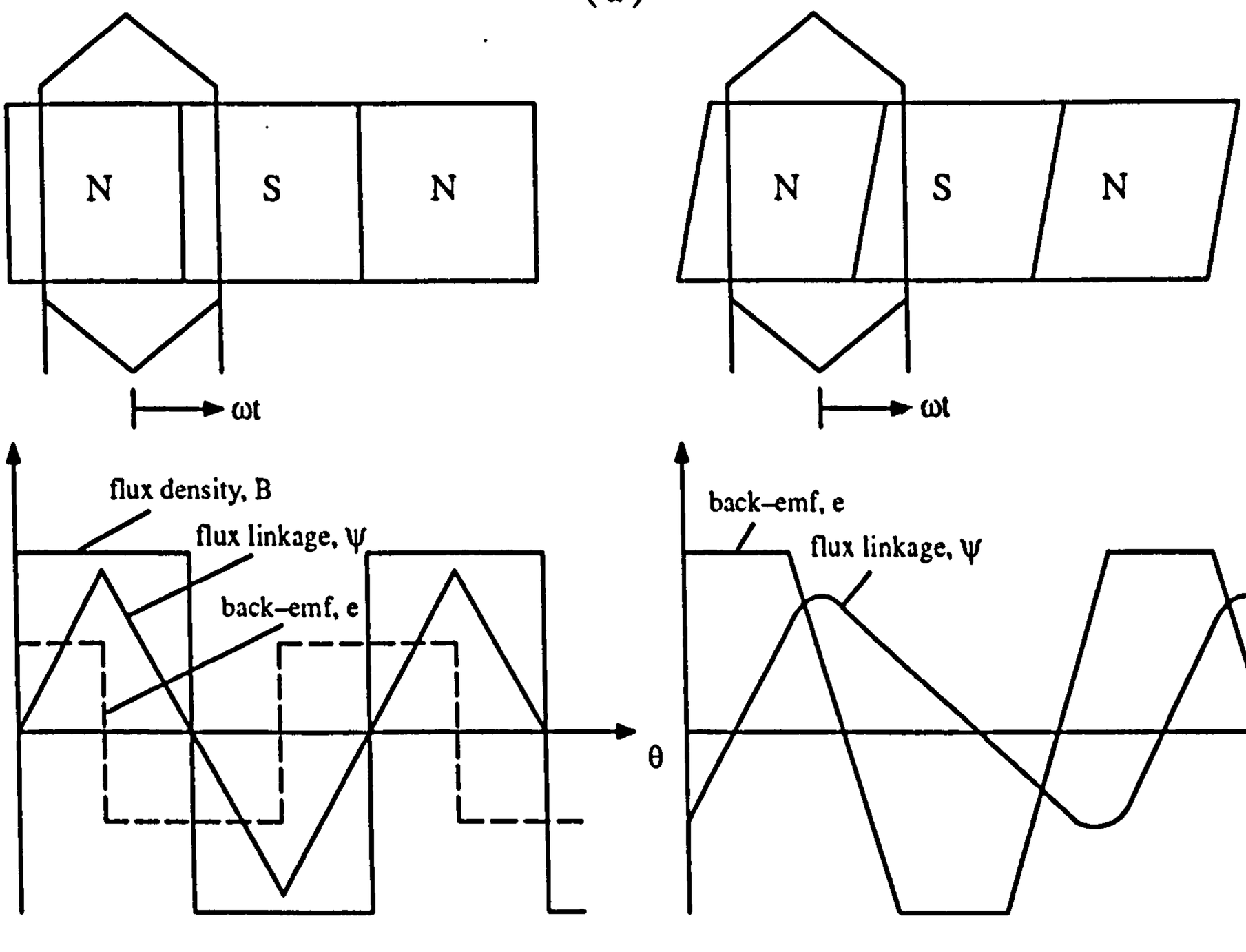

(b) (c)

Figure 2.2 (a) Cross section of a two pole permanet magnet rotor
(b) Relation between flux distribution, flux linkage and induced back–emf
(c) Flux linkage ψ and induced back–emf, e with a rotor magnetisation skewed by one slotsegment

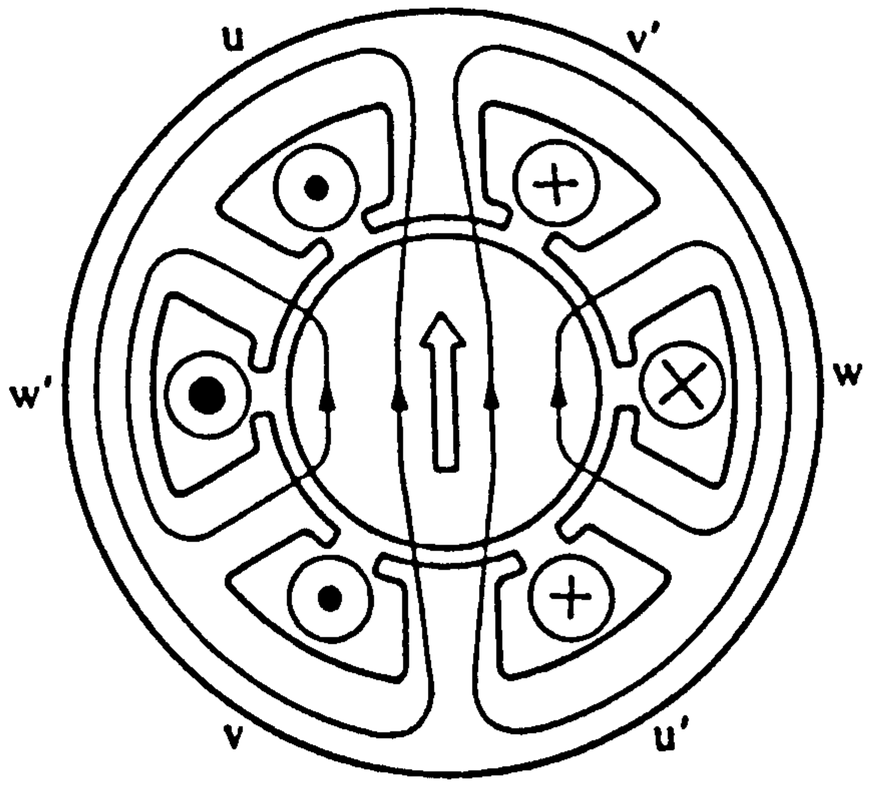

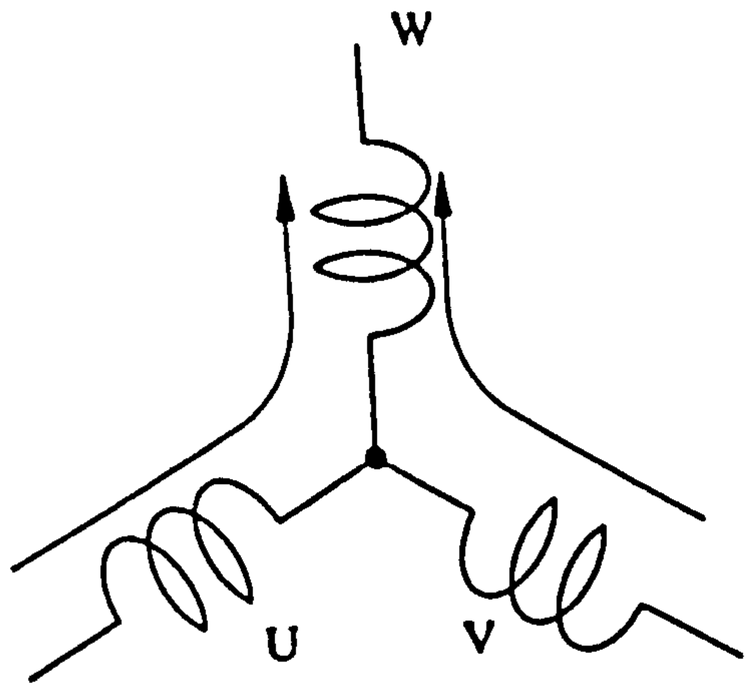

Figure 2.3 current and flux distribution

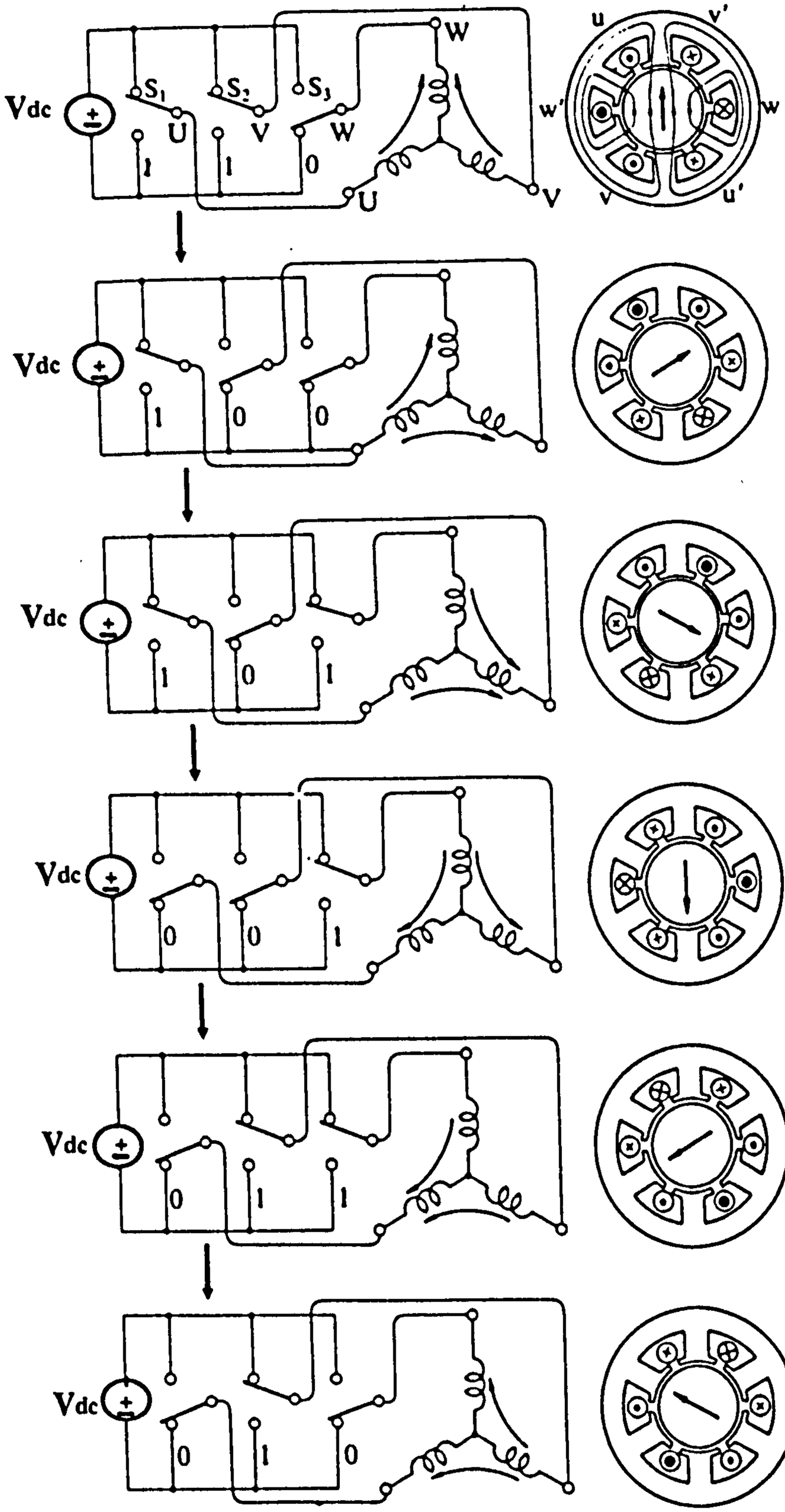

Figure 2.4 Relation between six different switching states

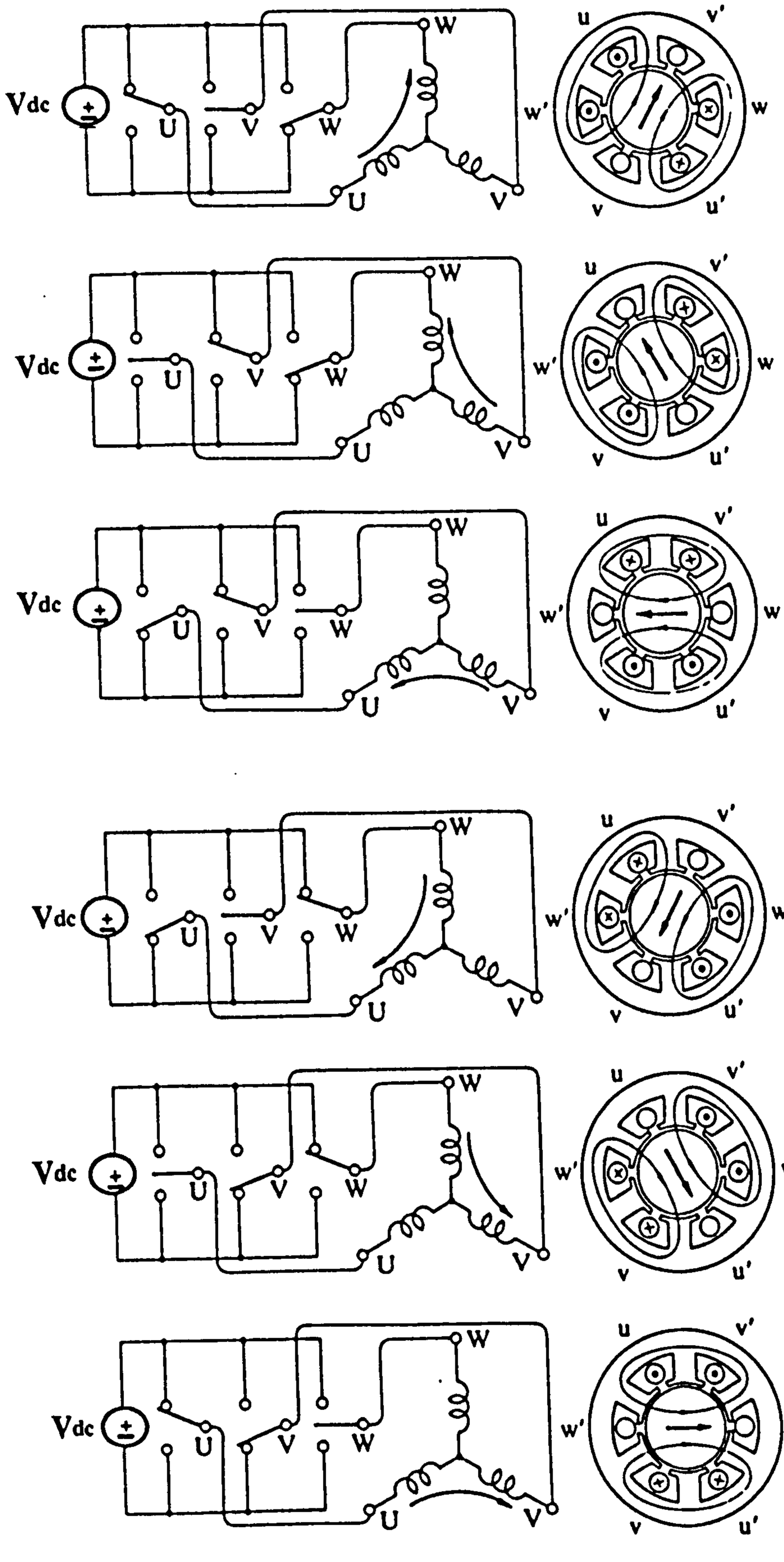

Figure 2.5 Switching sequence for 120° conduction angle

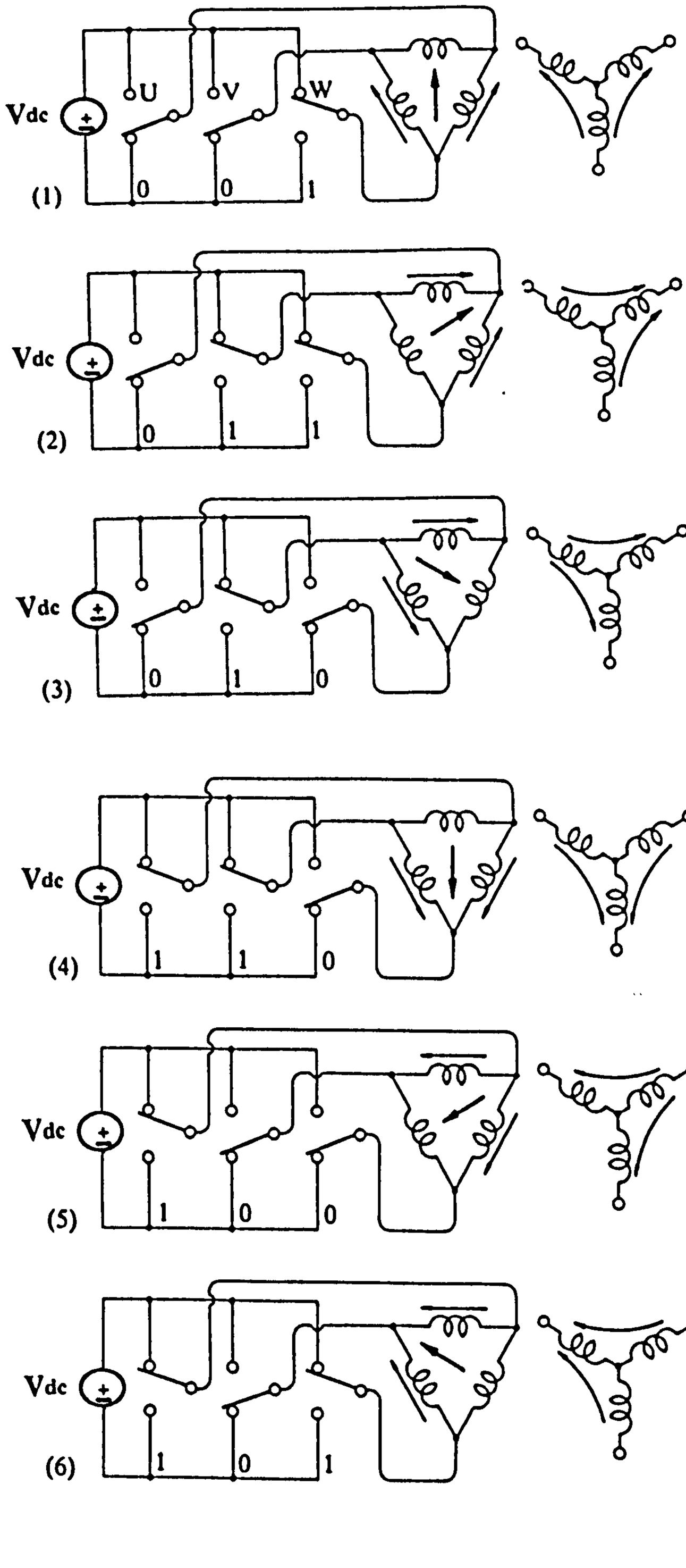

Figure 2.6 Switching sequence for 180° conduction angle

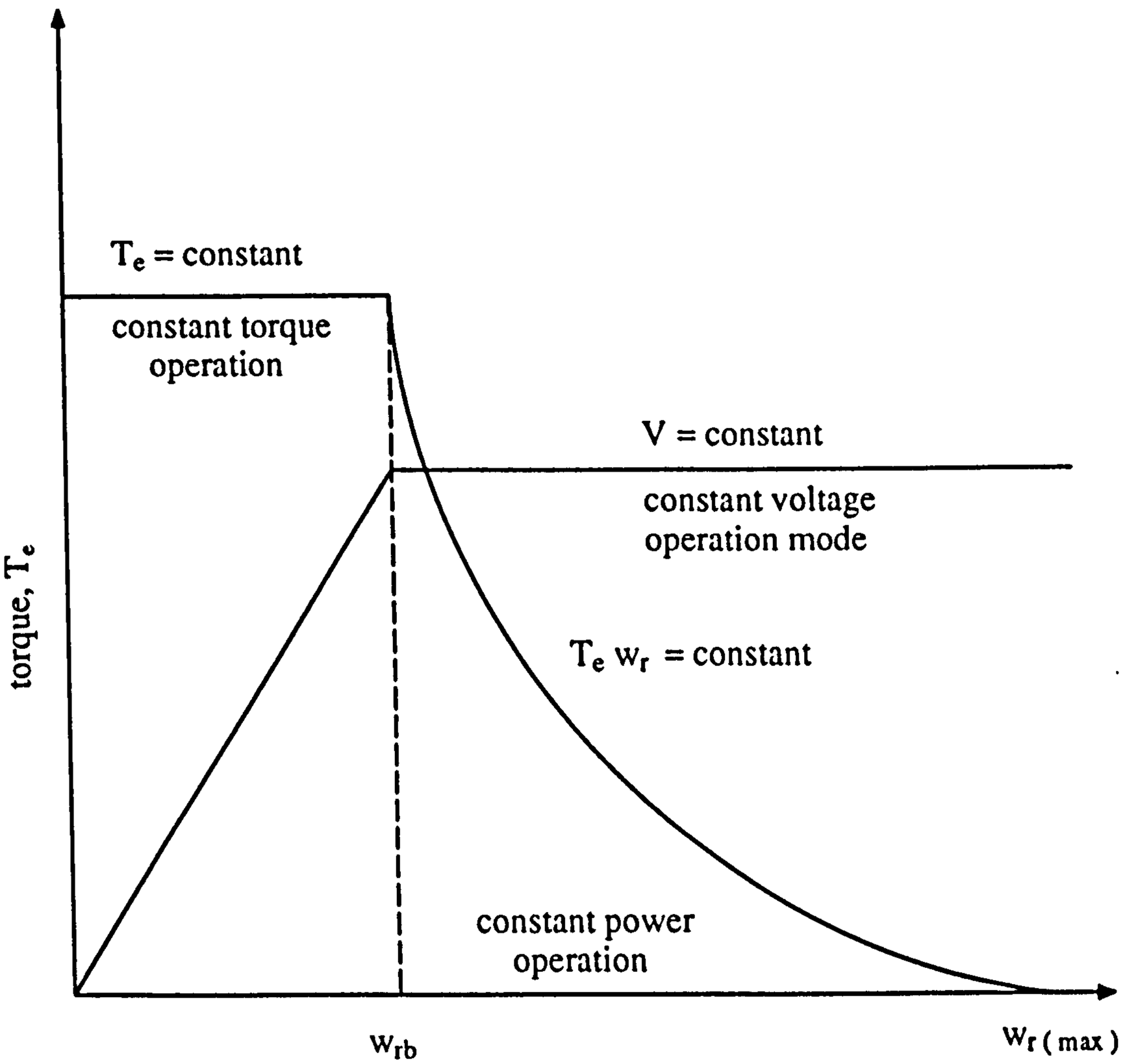

Figure 2.7 Speed–torque characteristic of drive system

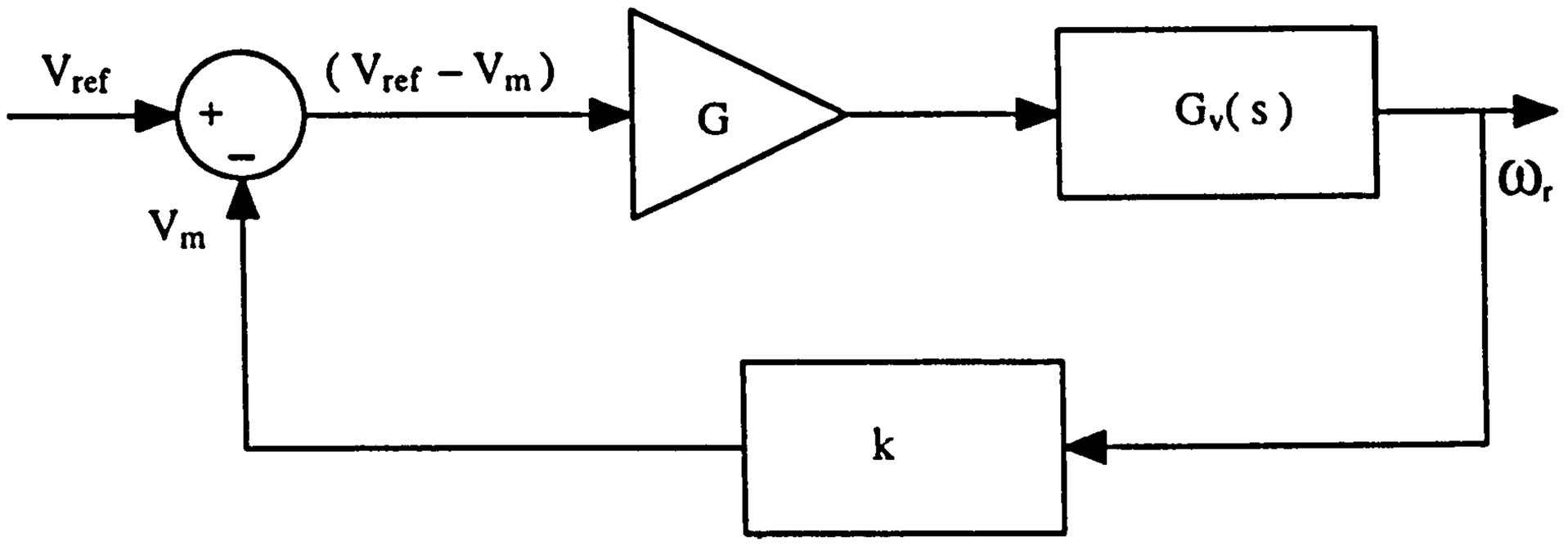

(a) without current feedback

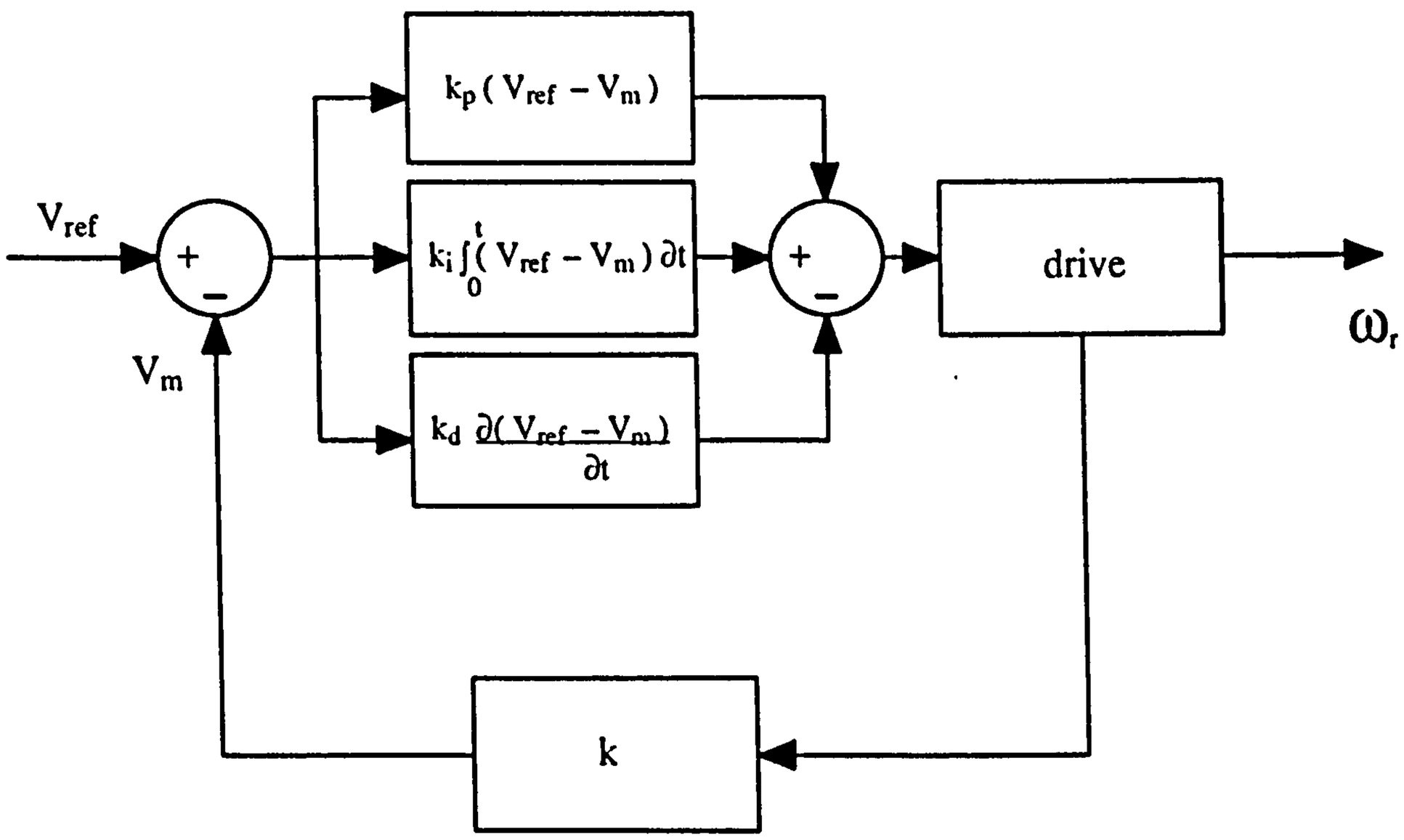

(b) PID controller

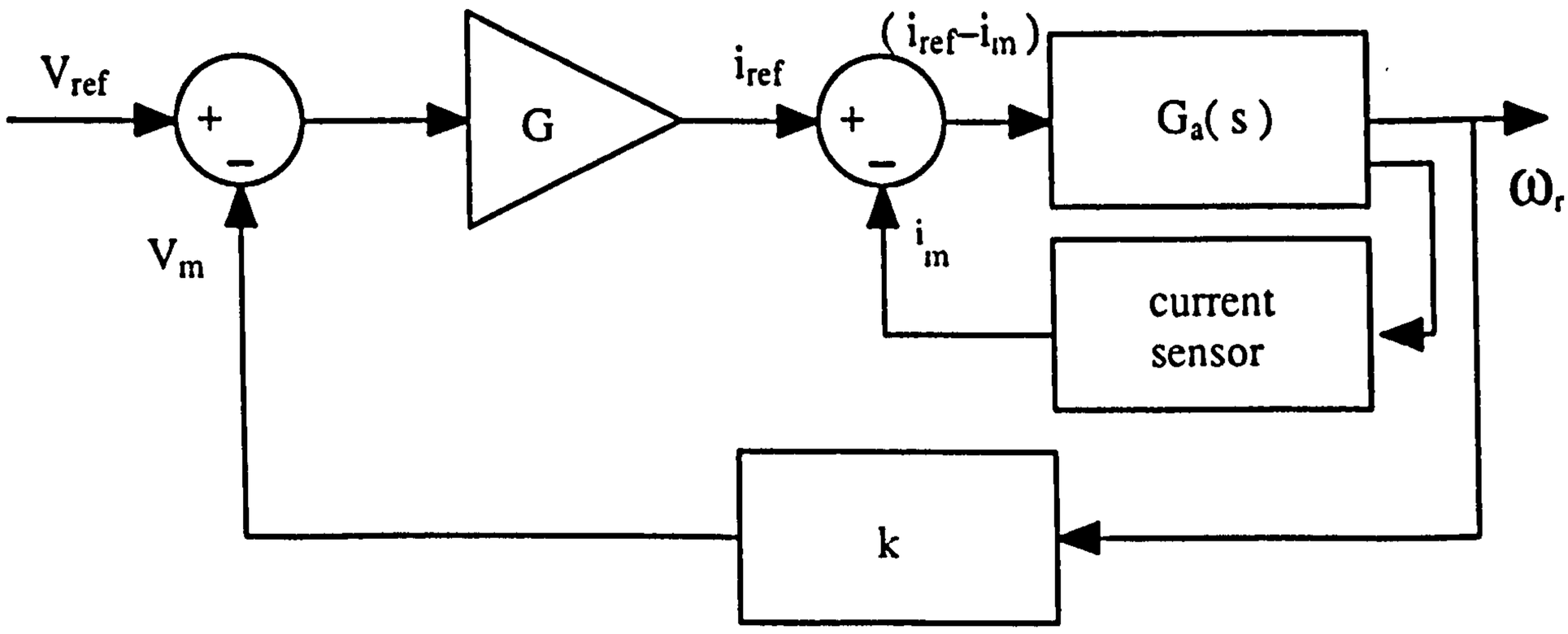

(c) with current feedback

Figure 2.8 Voltage control

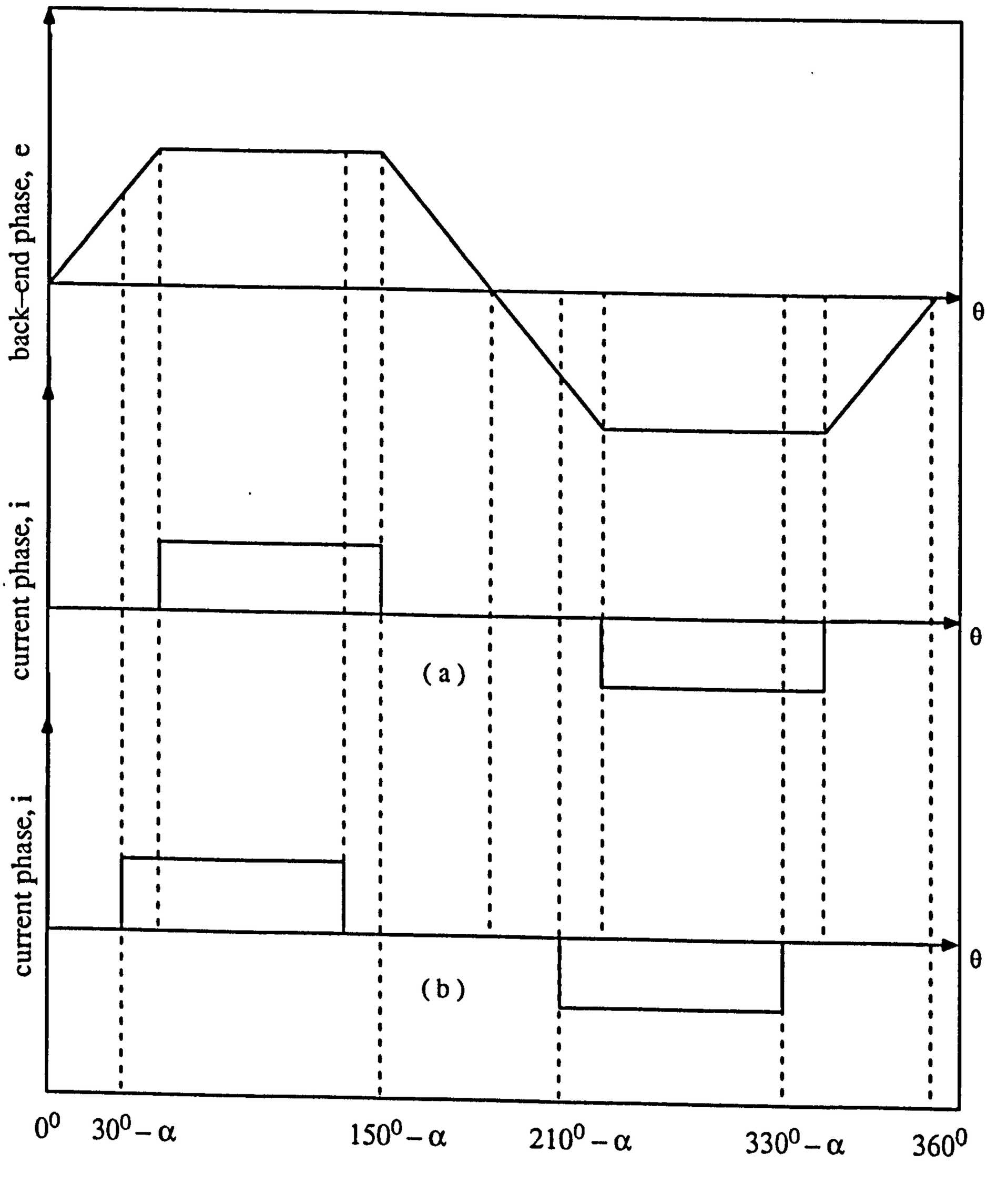

Figure 2.9 Phase advance control
(a) without phase advance
(b) with phase advance

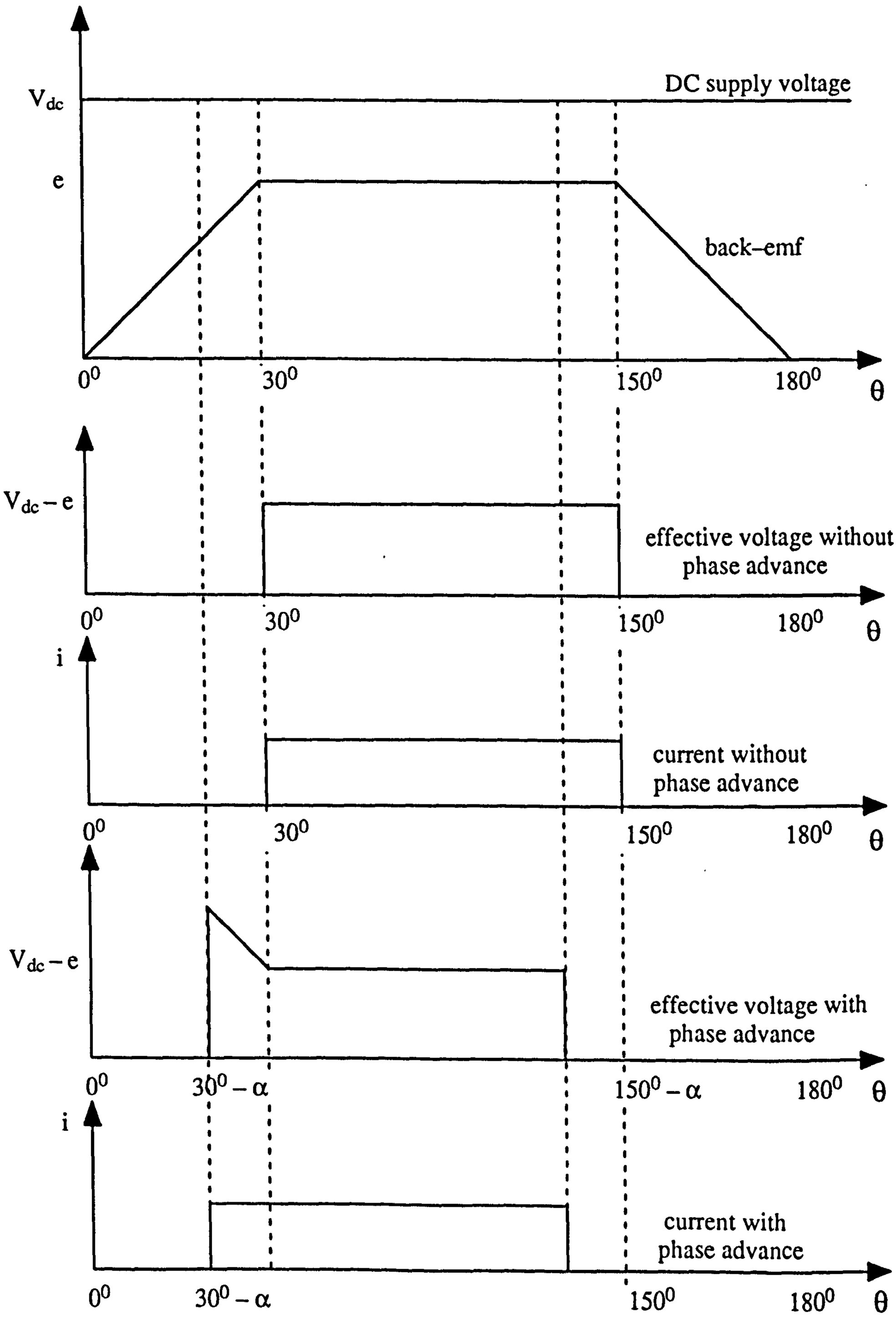

Figure 2.10 Phase advance control

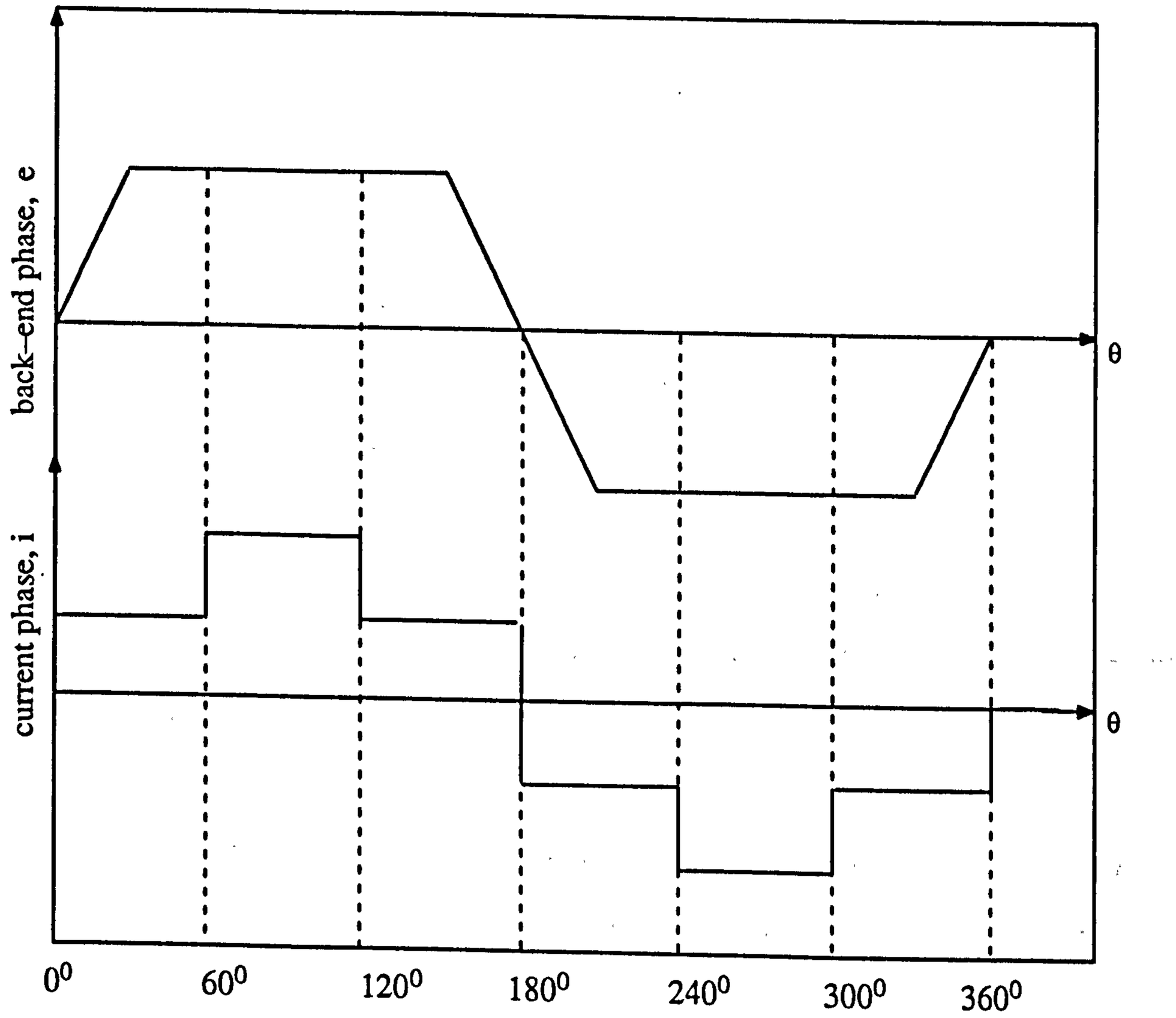

Figure 2.11 Extended conduction angle method

CHAPTER 3

MODELLING AND DYNAMIC ANALYSIS OF BRUSHLESS PERMANENT MAGNETIC MOTOR DRIVES

3.1 Introduction

In order to aid an understanding of the interaction between the brushless dc motor and power converter as well as the basic principles for the development of the torque improvement methods, modelling and analysis is very important. The design of a trapezoidal-emf, permanent magnet drive often necessitates analysis, to establish its performance and dynamic behaviour.

A brushless dc drive system operating from a power inverter is subjected to variable frequency nonsinusoidal input voltage or currents. The behaviour of a brushless dc motor with nonsinusoidal input voltage or current differs significantly from its behaviour to sinusoidal inputs in both transient and steady state conditions. Although conventional methods of analysis give useful information, they are based on this simplification concerning the current and voltage waveforms, so that the finer points of the performance are overlooked at different operating conditions. Therefore improved techniques are needed for analysing the performance of the motors in order to give accurate results under such operating conditions. For accurate prediction of machine electrical quantities and to improve the drive's performance, digital simulation with numerical techniques is necessary.

With advent of modern digital computers, numerical methods can be employed efficiently for solving differential equations. In such a case, a three-phase model can be used for exact study of the brushless dc motor. Direct solution of the three phase untransformed voltage equations permits a wider class of operating conditions, particularly transient performance to

be studied more conveniently. It also helps the design modification for the machine as well as the power inverter or control element since the actual quantities are used in the simulation.

This chapter elaborates on this approach by presenting a comprehensive analysis which aims to show that direct three-phase representation can be used as an effective tool for performance assessement of brushless dc drive systems operating over a wide speed range. A mathematical model of the complete drive system, based on the direct representation approach, is presented. The model system includes representation of the motor, power inverter, feedback transducers and controller for a pulse width modulation (PWM) voltage controller. The model incorporates a time stepping numerical technique for solving the sets of differential equations which are used to describe the drive under all its operating conditions and permit the neutral point to float.

The simulation technique has been tested on the drive under consideration. The predicted and experimental results have been compared and presented. In this chapter, a mathematical model for the brushless dc motor and inverter is presented first. Then after developing the mathematical model, a concept of a general simulation package used here is introduced and tested on the system drive under consideration.

3.2 Relation Between Present Analysis Methods and Previously Published Analysis

The increasing use of brushless dc motor drives has led to new analyses being published. Work has been published on the subject of sinusoidal brushless motors fed from variable frequency sinusoidal voltage supplies. In the published work several authors have described some of the methods applicable for the simulation of brushless dc motor systems. The methods reported fall mostly into one of two categories; either the solution of a transformed representation of the motor equivalent circuit using a 'reference

frame' technique or 'direct' solution of the equivalent circuit network.

Most of the analyses which express the equivalent circuit in a transformed state use Park [Park, 1979] or a similar transformation in order to define two independent axes of the motor. Chalmers, et al. [1975], Kaufman and Plunkett [1984], Krause, et al [1984, 1987], Williamson, et al [1978], Sebastian and Slemon [1987], Slemon and Gumaste [1983], Bowes and Clare [1988], Bowes and Clements [1983] have derived the d-q axis equivalent circuits for the motor. Other authors have also considered applications with highly salient rotor configurations, such as interior magnet rotor structures [Chalmers and Hamed, 1985]. For the simplest solution using this method it is necessary to assume only sinusoidal variation of the winding and flux density distributions.

Usually the solution of the combined motor-inverter circuit is base on the two-axis d-q models which lead to easy solution for operation under balance signal-frequency operating conditions; but, for unbalanced operating conditions including nonsinsoidal supply, the direct solution of the three phase performance equations seems much more convenient [Wallace and Spee, 1987], [Nyamusa and Demerdash, 1987]. The normal transformation to two-axis coordinates replaces both the rotor and the stator physical variables with new sets of transformed variables. The process of translating this information into the transformed coordinate system becomes difficult and must be approached differently in each specific problem, particularly if the terminal constraints are mixed.

Thus the direct method becomes the better method of solution because: (i) the functional dependence of the system parameters on the operating conditions may be represented accurately and conveniently if the nature of variation of these parameters has been established (ii) space harmonic may be included in the analysis (iii) the three phase system with nonsinusoidal supply can be analysed much more conveniently (iv) the variable involved are

measurable, 'real' quantities which appear in the experimental motor circuits and they are not transformed to any other reference frame for solution. Moreover, the method is quite general and may readily be modified to predict the performance of the system under various operating conditions by incorporating the proper terminal constraints. Thus motor performance under fault operating conditions, like inverter commutation failure, etc., may be studied.

Several authors have used the direct simulation method for the analysis of brushless dc drives. During these investigations the value of this model has been demonstrated for simulation of nonideal drives Demerdash, et al, [1980, 1982, 1985] Spee and Wallace [1988], Pillay and Krishnan [1988] Piriou and Razek [1986], Piriou, et at, [1986].

The authors note that for drives of this type, it is the combined action of the motor and the controller which is one of the most important features: Acarnley and Hughes [1988], Acarnley, et al, [1988], Funabiki and Himei [1985], Bolton and Ashen [1984], Lipo and Turnball [1979]. For the simulated solution, which is one of the most useful methods of analysis, it is necessary to derive an accurate model of both components. Any current, or load, dependence of the equivalent circuit components is especially significant for systems operating at low voltages where the relative effect of such load dependence may be quite large.

A full representation of the combined motor-inverter circuit is difficult due the fact that different parts of the system respond to events over a wide range of time scales and where PWM inverter and non-sinusoidal motor back-emfs interact.

Although this is theoretically possible using proprietary circuit simulators such as SPICE, in practice they are invariably found to be difficult to implement and relatively slow to solve. An alternative technique is a general simulation package which has been developed by the Electric Drives and

Machines Group in the University of Newcastle. This package is developed to solve the equivalent circuit directly. It has been found convenient and flexible to use, and allows all interactions between the various elements of the variable-speed drives to be considered within the frame work of the drive system.

In the present study the simulation package is adopted. This has the advantage that the simulation method can be expanded with a degree of reasonable accuracy required by the model and that it is a close representation of the physical system under consideration. The technique has the flexibility for simulating quite diverse supply conditions, including PWM or current mode, the back-emf waveforms, as well as alternative control strategies. The motor voltages and impedances are determined from representation of the airgap flux density and stator winding distribution which are stored explicity in the program data. This is a more flexible approach than that where only the electrical equivalent circuit impedances and emfs are used and hence, using this approach, any changes in the motor design are modelled directly. The action of the inverter is represented by the development of a set of differential equations which describe its operation under normal operation and also under transient and fault condition.

The method of solution used is a time-stepping solution of electrical and mechanical equivalent circuit equations of the combined system. The method has proved to be quick to develop and operate on a mainframe computer system.

The majority of simulation methods recently published [Demerdash, et al, 1980] , Pillay and Krishnan [1988] represent each phase as an independent winding with end grounded and other supplied from either a positive or negative supply depending on which power devices are switched on at a particular instant. In reality for a star connected motor, the three phases are connected together at the neutral point and, in most systems, the neutral

point is left to float, the only defined voltages being those between lines. Thus a formulation in phase voltage terms is inappropriate to this system and line voltage expressions should be used. In the present work an improved mathematical model has been presented which is formulated in line voltage terms to allow the neutral point to float.

The improved model explicity represents two modes of inverter operation. These modes are (i) commutation mode, when all of the currents are not zero (ii) and conduction mode, when two coils are conducting and one is open. The representation is done by incorporating additional switching states into the model. This provides a model which accurately represents the drive at every instant; this contrasts with the representation used in published work Liu, et al. [1989], where artificial time constants are introduced to represent current flow through the diode devices. The commutation and conduction of the inverter are represented by adopting different systems of equations to represent the motor under different operating conditions.

This analysis method has brought a more comprehensive understanding of the behaviour of the drive, and constitutes a departure from the conventional methods used in simulating the brushless dc drives. The system differential equations and subsequent numerical solutions are a very useful means in predicting and updating of the state of the model every computing step. In this chapter the different aspects of modelling and analysis such as performance equations and representation of inverter operation, method of analysis, and method of solution are developed and presented.

In the subsequent sections, the mathematical analysis model for the brushless dc motor and inverter is presented first. Then the simulation procedure used in the general simulation package is outlined.

3.3 Mathematical Model of Brushless DC Drive System

3.3.1 Modelling and Method of Analysis

The analysis of the system consists of two parts

(a) analysis of the motor

(b) analysis of the power inverter.

To carry out the analysis it is necessary to obtain proper model for the motor and the power inverter. These models are then properly combined to obtain the full analysis of the system. Figure 3.1 shows the basic elements of a three phase, brushless dc system drive. By combining models for each element, viz the motor and its load, the power switching circuit and the commutation control circuit, a mathematical model of the complete system can be derived.

3.3.2 Assumptions

The analysis of such a system is complicated by the interactions between the machine itself and the power electronic circuits used to provide the appropriate voltage and current waveforms. Consequently in order to make the analysis simpler, it is common practice to make a number of assumptions in the derivation of system equations, namely:

(i) the power converter supply voltage dc rail is constant,

(ii) the devices (switches and diodes) in the power switching circuit are ideal,

(iii) eddy current and hysteresis effects in the machine's magnetic materials have negligible influence on the winding current,

(vi) motor armature saturation effects are neglected,

(v) there is no saliency and therefore the self and mutual inductances are constant and independent of rotor position.

3.3.4 Model for Motor Analysis

The motor is modelled using the equivalent circuit representation of a three phase brushless dc motor which is given in figure 3.2. By taking into account the positional difference of the phases, each phase of the motor is represented by a resistance, an inductance and a back emf which is a function of both speed and instantaneous rotor position. The torque exerted on the shaft by each phase is computed independently and the instantaneous values for three phases are summed to yield a total electromagnetic torque. This is then fed to a mechanical model to yield speed and integrated to obtain position. The commutation circuit is modelled by controlling those windings carrying current as a function of the rotor position and the whole of the drive is modelled in a voltage closed-loop mode. The average voltages applied to the machine are controlled by pulse width modulation (PWM) of the dc supply voltage and a controller simulation allows different controllers to be examined.

Assuming linearity by neglecting saturation effects, the flux-linkage of the winding may be expressed as the sum of the flux linkages due to each of the three phase stator windings resulting in a trapezoidal induced back-emf phase shifted by 120° electrical.

The back-emf waveform is modelled as a piecewise linear approximation. This approach is more amenable to change should different motors need to be investigated than the more obvious method of storing a table of data of emf versus rotor position. The calculation therefore relates the voltage as a function of angle to the peak values and the result is used simply as multiplying factor of speed in calculations of back-emf, as shown figure 3.3. The analytical formulation of the back-emf waveforms which are shown in figure 3.3 can also be calculated by equations (3.1a)-(3.1c). The motor may be operated such that only the flat portions of the induced back-emf waveforms can be used

$$
\left.
\begin{aligned}
e_a &= e_{pk} && for && 0 \le \theta \le \frac{2\pi}{3} \\
e_a &= e_{pk}\frac{\left(\frac{5\pi}{6} - \theta\right)}{\frac{\pi}{6}} && for && \frac{2\pi}{3} \le \theta \le \pi \\
e_a &= -e_{pk} && for && \pi \le \theta \le \frac{5\pi}{3} \\
e_a &= e_{pk}\frac{\left(\theta - \frac{11\pi}{6}\right)}{\frac{\pi}{6}} && for && \frac{5\pi}{3} \le \theta \le 2\pi
\end{aligned}
\right\} \qquad (3.1a)
$$

For phase b and phase c

$$
\left.
\begin{aligned}
e_b(\theta) &= e_a\left(\theta + \frac{2\pi}{3}\right) \\
e_c(\theta) &= e_a\left(\theta + \frac{4\pi}{3}\right)
\end{aligned}
\right\} \qquad (3.1b)
$$

where

$$
e_{pk} = k_b \omega_r \qquad (3.1c)
$$

where

θ = rotor angle in mechanical radians;

e_{pk} = maximum value of back-emf, radian$^{-1}s^{-1}$;

e_a =instantaneous value of back-emf, radian$^{-1}s^{-1}$;

k_b =voltage (or back-emf) constant, volt/rpm.

In the simulation package used here, the motor is operated such that the back-emf is calculated at 1000 rpm by direct spatial differentiation of the phase flux distribution, the back-emf at other speeds is calculated by simple scaling. The results are calculated and stored over one cycle at intervals of one electrical degree.

The model uses the phase equivalent circuits to calculate the contributions to the instantaneous torque made by each phase. Speed is derived using a very simple mechanical model incorporating inertia and viscous damping. The inertia relevant to the model is the total inertia of the rotating system.

3.3.5 Formulation of Motor Equations

The equations of the motor model are derived as follows:

$$\begin{pmatrix} v_a \\ v_b \\ v_c \end{pmatrix} = \begin{pmatrix} R & 0 & 0 \\ 0 & R & 0 \\ 0 & 0 & R \end{pmatrix} \begin{pmatrix} i_a \\ i_b \\ i_c \end{pmatrix} + p \begin{pmatrix} L_{aa} & L_{ab} & L_{ac} \\ L_{ab} & L_{bb} & L_{bc} \\ L_{ca} & L_{cb} & L_{cc} \end{pmatrix} \begin{pmatrix} i_a \\ i_b \\ i_c \end{pmatrix} + \begin{pmatrix} e_a \\ e_b \\ e_c \end{pmatrix} \qquad (3.2)$$

In a machine with wide pole arc surface-mounted magnets there is a little change in the machine inductances with angle, and it is possible to simplify equation (3.2) by making the assumptions that:

$$\left.\begin{aligned} R_a = R_b = R_c = R \\ L_{aa} = L_{bb} = L_{cc} = L \\ L_{ab} = L_{ac} = L_{ba} = L_{bc} = L_{ca} = L_{cb} = M \end{aligned}\right\}$$

so equation (3.2) becomes

$$\begin{pmatrix} v_a \\ v_b \\ v_c \end{pmatrix} = \begin{pmatrix} R & 0 & 0 \\ 0 & R & 0 \\ 0 & 0 & R \end{pmatrix} \begin{pmatrix} i_a \\ i_b \\ i_c \end{pmatrix} + p \begin{pmatrix} L & M & M \\ M & L & M \\ M & M & L \end{pmatrix} \begin{pmatrix} i_a \\ i_b \\ i_c \end{pmatrix} + \begin{pmatrix} e_a \\ e_b \\ e_c \end{pmatrix} \qquad (3.3)$$

where the stator winding is star connected with the star-point isolated, the three phase currents are related:

$$i_a + i_b + i_c = 0 \qquad (3.4)$$

and

$$pi_a + pi_a + pi_c = 0 \qquad (3.5)$$

and therefore:

$$Mi_a + Mi_b + Mi_c = 0 \tag{3.6}$$

Using this relation in equation (3.3) gives the simplified form:

$$\begin{pmatrix} v_a \\ v_b \\ v_c \end{pmatrix} = \begin{pmatrix} R & 0 & 0 \\ 0 & R & 0 \\ 0 & 0 & R \end{pmatrix} \begin{pmatrix} i_a \\ i_b \\ i_c \end{pmatrix} + p \begin{pmatrix} L-M & 0 & 0 \\ 0 & L-M & 0 \\ 0 & 0 & L-M \end{pmatrix} \begin{pmatrix} i_a \\ i_b \\ i_c \end{pmatrix} + \begin{pmatrix} e_a \\ e_b \\ e_c \end{pmatrix} \tag{3.7}$$

The per phase currents, voltages and back-emfs can not be obtained by direct measurement since the star point is not available. Usually the star connected motor model represents each phase as an independent winding with one end grounded and the other supplied from either a positive or negative supply depending on which power devices are switched on at a particular instant. In reality for a star connected motor, the three phases are connected together at the neutral point and, in most systems, the neutral point is left to float, the only defined voltages being those between phases (i.e., the line voltages). Thus a formulation in phase voltage terms is inappropriate to this system and line voltage expression should be used instead. The approach, which is presented in this section, is formulated in line voltage terms to allow the neutral point to float.

The machine line voltage equations can be derived from the phase voltage equation, using equation (3.7) and by referring to figure 3.1. The phase voltage equations of equivalent circuit are derived as follows

$$v_a = Ri_a + \frac{d}{dt}\left(Li_a + Mi_b + Mi_c\right) + e_a \tag{3.8a}$$

$$v_b = Ri_b + \frac{d}{dt}\left(Li_b + Mi_c + Mi_a\right) + e_b \tag{3.8b}$$

$$v_c = Ri_c + \frac{d}{dt}\left(Li_c + Mi_a + Mi_b\right) + e_c \tag{3.8c}$$

From the line voltages which are related to the phase voltage by the relations;

$$\left.\begin{aligned} v_{ab} &= v_a - v_b \\ v_{bc} &= v_b - v_c \\ v_{ca} &= v_c - v_a \end{aligned}\right\} \tag{3.9}$$

equation (3.8) can be rewritten as

$$v_{ab} = Ri_a - Ri_b + (L - M)\frac{di_a}{dt} + (M - L)\frac{di_b}{dt} + (e_a - e_b) \tag{3.10a}$$

$$v_{bc} = Ri_b - Ri_c + (L - M)\frac{\partial i_b}{\partial t} + (M - L)\frac{di_c}{dt} + (e_b - e_c) \tag{3.10b}$$

$$v_{ca} = Ri_c - Ri_a + (L - M)\frac{di_c}{dt} + (M - L)\frac{di_a}{dt} + (e_c - e_a) \tag{3.10c}$$

thus, the electrical equations of the motor can be written as follows:

$$\begin{pmatrix} v_{ab} \\ v_{bc} \\ v_{ca} \end{pmatrix} = \begin{pmatrix} R & -R & 0 \\ 0 & R & -R \\ -R & 0 & R \end{pmatrix} \begin{pmatrix} i_a \\ i_b \\ i_c \end{pmatrix} + \begin{pmatrix} L-M & M-L & 0 \\ 0 & L-M & M-L \\ M-L & 0 & L-M \end{pmatrix} p \begin{pmatrix} i_a \\ i_b \\ i_c \end{pmatrix} + \begin{pmatrix} e_{ab} \\ e_{bc} \\ e_{ca} \end{pmatrix} \tag{3.11}$$

where

$$\begin{pmatrix} e_{ab} \\ e_{bc} \\ e_{ca} \end{pmatrix} = \begin{pmatrix} e_a - e_b \\ e_b - e_c \\ e_c - e_a \end{pmatrix} \tag{3.12}$$

With three phase star connected, there is no neutral. Thus the motor is constrained because the sum of the three currents must be zero at all instants, i.e.

$$i_a + i_b + i_c = 0, \tag{3.13}$$

thus only two independent currents exist, by considering currents i_a and i_b as independent quantities, with i_c related by equation (3.14). With this respect, if it is known that one phase carries no current at a particular time then only one independent current exists. However, the currents which need to be modelled will change depending on operating conditions-hence although the equations are fairly simple, careful switching between sets of equations is required.

3.3.6 Torque and Mechanical Motor equations

General Torque Equation

For the system under consideration, the instantaneous electromagnetic torque, T_e, produced at an instantaneous speed, ω_r, can be written down by inspection as

$$T_e = \frac{1}{\omega_r}\left[e_a i_a + e_b i_b + e_c i_c\right] \tag{3.14}$$

Torque During Commutation and Conduction

Since there are only one or two independent currents (section 3.3.1) the torque equations need to be formulated in terms of the current(s) that is (are) the state variable(s) at a particular instant, for example if i_a and i_b are the state variables then

$$i_c = -i_a - i_b \tag{3.15}$$

so the general expression of torque, given in (3.14), becomes for this condition

$$T_e = \frac{i_a(e_a - e_c) + i_b(e_b - e_c)}{\omega_r} \tag{3.16}$$

or if i_a is the state variable and $i_c = 0$, then $i_b = -i_a$ and

$$T_e = \frac{i_a(e_a - e_b)}{\omega_r} \tag{3.17}$$

Mechanical Equations

The load presented to the machine may be expressed in general terms by

$$Jp\omega_r + D\omega_r + T_L = T_e \tag{3.18}$$

where J is the moment of inertia, D is damping torque coefficient, T_L is the load torque applied to the machine, and T_e is defined in equations (3.15) and (3.16).

The mechanical system equations will always have two states of speed and position since the back-emf is a function of the rotor position. Thus overall the motor can be represented by equations of order three or four.

3.4 Modelling and Operating Conditions of the Power Inverter

3.4.1 Power Inverter Model

A three-phase bridge inverter is used to drive the brushless dc machine described above. In general, either bipolar transistor or F.E.T. devices can be used but, for the system described here, the usual arrangement with bipolar devices and free-wheeling diodes is used. The action of the power inverter is to connect the dc supply voltage between pairs of the machine lines.

The power inverter model is shown in figure 3.4. The switching devices are represented by switches S1 to S6 and the freewheeling paths by diodes D1 to D6. The switching information for active devices is provided from rotor position sensors. The power inverter is assumed to function in the following manner. If a switch is closed, the appropriate voltage rail is connected to the relevant phase winding. When the switch opens, the current flowing in the phase causes the freewheeling diode to connect the phase to the opposite voltage rail until the current falls to zero, at which point the phase is disconnected. Voltage drops in the transistors and diodes are ignored.

Logic circuitry within the power circuit of the system is used to decode the rotor position information from the position sensor output signals into the the base drive commands for inverter devices. However the positioning of the devices and appropriate decode logic ensures that the voltages in each stator winding, and hence that average torque developed by the motor is maximised.

3.4.2 Inverter Operating Conditions

The operation of the power inverter is based on stages that are used to determine the performance of the motor. The first one determines the phase sequence and the moment of current commutations from one phase to the following one. This stage is determined from a rotor position sensor. The second stage the time for which the inverter switches are turned-on. However, the direction of the operation of the motor is determined by the sequence of the switching waveforms provided by the power inverter. An additional

logic input to the commutation circuit is used to specify forward or backward operation of the motor. A more detail representation of the power inverter operation modes (i.e., its switching states and the conditions which determine the switching instants) is required in order to model and simulate the inverter circuit behaviour. Thus, a detailed representation of these operation modes is described below.

The operation of the power inverter with three phase brushless dc machines is based on the six conduction regions, each of 60° electrical. During each interval one switch in the top half of an inverter leg and another switch in the bottom half of a different inverter leg, are conducting. The third inverter leg is off and so current can not flow through switches of that leg but is able to flow through the freewheeling diodes of the inverter leg in the usual way.

As a consequence of this the electromagnetic states of the machine (see Chapter 2) are repeated every 60° electrical of rotor travel, and that two distinct operation intervals occur within each 60° region. The conduction interval of the motor current is defined as that interval during which only two stator phases carrying current as the rotor advances according to the device switching sequence of the commutation control circuit. During this interval no freewheeling diodes are conducting and the dc supply voltage is applied across the two conducting phases. The voltage on the third phase is undefined (it is not necessarily zero) and no reference is made to it in the equations describing this particular interval.

After successive phase commutated off, current can also flow through the free-wheeling diodes of each inverter leg, due to the energy stored in the armature inductance of each winding after successive phase commutated off. Specifically, in the winding recently switched off, then the inverter diode carrying that current unclamps, i.e., current continuity in the phase just turned off is maintained by the freewheeling diode connected to the opposite

supply rail from the one previously supplying the current. For example, in figure 3.5, if switch S1 is turned off current continuity is maintained by the diode in parallel with switch S2. The situation will continue until the current in this phase decays to zero at which time the diode stops conducting.

The prediction of the inverter operation permits the subdivision of the each 60° electrical region of the excitation cycle of the inverter into two distinct modes. For example, referring to figure 3.5, consider the case when switches S1 and S4 are conducting. If switch S6 is turned on and switch S4 off at a commutation, the freewheeling diode in parallel with switch S3 will be active. There are thus six conduction conditions associated with freewheeling diodes for each rotational direction; combining these with the six conditions when freewheeling diodes are inactive yields a total of eighteen conduction states to be modelled.

The current controller of the power inverter uses either pulse width modulation (PWM) or fixed off-time strategies to limit device current at low motor speeds. If a PWM switching strategy is included in the simulation model, each PWM cycle would require further switching states since there are conditions when all six switches are turned off and current flows entirely through the freewheeling diodes. However, computer implementation of this would be reasonably straightforward as there are many similarities between the states.

The mode of operation and thus the switching state of the inverter is not only dependent on the rotor position and rotation direction, but also depends on the flow of regenerative or freewheeling currents through any of the diodes in each inverter leg. These effects are as described below: for a given rotor position a given pair of devices is switched on. The rotational direction determines both the pair of devices to be switched on at the next commutation and freewheeling diode that will come into circuit when the commutation occurs. The current zero condition is used to implement the

change from a diode in circuit to a diode out of the circuit condition for a particular pair of devices turned on. These constraints considerably simplify the task of state selection which is defined by the following rules, assuming that initially two devices are on and no freewheeling diodes are conducting:

(1). Rotor position defines the devices to be switched on at commutation.

(2). At a commutation the state changes to one which includes a freewheeling diode. The freewheeling diode in circuit is defined by the position and by which devices are previously on.

(3). The next change of state will be when the diode current reduces to zero in which case the change of state following this will be a commutation.

Six conduction conditions associated with freewheeling diodes occur for each rotational direction and six conditions when only two phase winding are conducting, can be identified. The transition between these modes depend purely on the circuit currents.

For each of the six conduction intervals and two modes of operation the action of the inverter is completely defined. It is therefore necessary to represent the operation of the inverter in a systematic way before any solution of the whole system is possible. The governing equations for the different intervals (or modes) in an excitation cycle will be analysed and presented below.

3.4.3 General Solution for Power Inverter

In this subsection the general solution of the power inverter are derived to simulate its switching states imposed by operating conditions described above. As was noted, the switching operation of the inverter is divided into six switching states for the conduction interval and six switching states for commutation interval over the 360° of an excitation cycle. These operating switching states of both intervals will be modelled by means of the machine line voltages.

3.4.3.1 Analysis of Conduction Circuit

In this mode consider when both devices are on and two phases are carrying current, the dc supply voltage is applied to machine lines. The equivalent circuit of the motor during the conduction state is shown in figure 3.5. The solution for this circuit can obtained by applying Kirchoff's voltage law

$$\begin{pmatrix} v_a \\ v_b \\ v_c \end{pmatrix} = \begin{pmatrix} R & 0 & 0 \\ 0 & R & 0 \\ 0 & 0 & R \end{pmatrix} \begin{pmatrix} i_a \\ i_b \\ i_c \end{pmatrix} + p \begin{pmatrix} L-M & 0 & 0 \\ 0 & L-M & 0 \\ 0 & 0 & L-M \end{pmatrix} \begin{pmatrix} i_a \\ i_b \\ i_c \end{pmatrix} + \begin{pmatrix} e_a \\ e_b \\ e_c \end{pmatrix} \tag{3.20}$$

The analytical equations for six switching states can now expressed in the following way using above equation:

State 1: Consider the case when switches S1 and S4 (or S2 and S3) are conducting and the current flows in phases a and b only, then the following conditions apply:

$$\begin{pmatrix} i_a \\ i_b \\ i_c \end{pmatrix} = \begin{pmatrix} i_a \\ -i_a \\ 0 \end{pmatrix} \tag{3.21}$$

substituting equation (3.21) into equation (3.20) yields

$$\begin{pmatrix} v_a \\ v_b \\ v_c \end{pmatrix} = \begin{pmatrix} R & 0 & 0 \\ 0 & R & 0 \\ 0 & 0 & R \end{pmatrix} \begin{pmatrix} i_a \\ -i_a \\ 0 \end{pmatrix} + p \begin{pmatrix} L-M & 0 & 0 \\ 0 & L-M & 0 \\ 0 & 0 & L-M \end{pmatrix} \begin{pmatrix} i_a \\ -i_a \\ 0 \end{pmatrix} + \begin{pmatrix} e_a \\ e_b \\ e_c \end{pmatrix} \tag{3.22}$$

and according to the relation of $v_{ab} = v_a - v_b = V_{dc}$ and $e_{a_b} = e_a - e_b$, equation (3.22) is re-written in the following simplified form

$$v_{ab} = 2Ri_a + 2(L-M)\frac{di_a}{dt} + e_{ab} \tag{3.23}$$

and this expression may also be written in the following form

$$\frac{di_a}{dt} = -\frac{R}{(L-M)}i_a + \frac{1}{2(L-M)}\left(v_{ab} - e_a + e_b\right) \tag{3.24}$$

State 2: In this case consider switches S1 and S6 (or S2 and S5) are conducting and current flows in phases a and b only. Then the same procedure can be applied to the condition when phases a and c are conducting and phase b carries zero current. For this case, $i_c = -i_a$, or

$$\begin{pmatrix} i_a \\ i_b \\ i_c \end{pmatrix} = \begin{pmatrix} i_a \\ 0 \\ -i_b \end{pmatrix} \tag{3.25}$$

thus

$$v_{ca} = -2Ri_a + 2(M-L)\frac{di_a}{dt} + e_{ac} \tag{3.26}$$

which may also be written for this state in the following form

$$\frac{di_a}{dt} = -\frac{R}{(L-M)}i_a + \frac{1}{2(L-M)}\left(v_{ca} - e_c + e_a\right) \tag{3.27}$$

where $v_{ca} = v_c - v_a = V_{dc}$ and $e_{ab} = e_a - e_c$.

State 3: Consider the case when switches S3 and S6 (or S4 and S5) are conducting. In this case phases b and c conduct and phase a carries no current the state variable of current has no change from i_a to i_b or i_c. Using i_b as a state variable and taking $i_c = -i_b$ gives the following condition

$$\begin{pmatrix} i_a \\ i_b \\ i_c \end{pmatrix} = \begin{pmatrix} 0 \\ i_b \\ -i_b \end{pmatrix} \tag{3.28}$$

thus, the solution of equation with this switching state is

$$v_{bc} = 2Ri_b + 2(L - M)\frac{di_a}{dt} + e_{bc} \tag{3.29}$$

which may also be written for this state in the following form

$$\frac{di_b}{dt} = -\frac{R}{(L - M)}i_b + \frac{1}{2(L - M)}\left(v_{bc} - e_b + e_c\right) \tag{3.30}$$

where of $v_{bc} = v_b - v_c = V_{dc}$ and $e_{ab} = e_b - e_c$. Equations (3.24), (3.27) and (3.30) are required to cover the six switching states during the conduction period. Conduction expressions for other combinations of excited phases could be derived by transposition of winding and device numbering.

3.4.3.2 Analysis of Commutation Circuit

During the excitation cycle, a state occurs (which is called switching transition state) when all three phases are carrying current conducting or carrying currents. An equivalent circuit for the commutation is shown in figure 3.6.

The commutation circuit can be analysed by assuming that all three currents are not zero and there are two independent currents with the third current related by, $i_a + i_b + i_c = 0$. Thus, two independent currents must be calculated so the appropriate voltage polarity must be applied to the phase until the current decays to zero.

This means that the commutation is included in the analysis model by modifying the ideal forcing function v_{ab}, v_{bc} and v_{ca}. The star of the commutation period is represented by one of the voltages being forced to zero. The process continues, depending on the state of the drive system. This process is simplified the model because only the same two voltages are used for all conditions.

In addition, it is possible to use three system equations, one set each for the possible commutations of non-zero line voltages. These equations which are governing the commutation period are found below.

Circuit Commutation Equations

To derive the system equation of the commutation circuit, three possible situations are considered:

Case I: By considering the case where line voltages v_{ab} and v_{bc} are included, the first electrical equation can be derived as follows:

$$v_{ab} = Ri_a - 2Ri_b + (L-M)\frac{di_a}{dt} + (M-L)\frac{di_b}{dt} + e_{ab} \tag{3.31}$$

and

$$v_{ac} = Ri_a + 2Ri_b + (L-M)\frac{di_a}{dt} + 2(L-M)\frac{\partial i_b}{\partial t} + e_{bc} \tag{3.32}$$

which can be represented by the following matrix;

$$\begin{pmatrix} v_{ab} \\ v_{ba} \end{pmatrix} = \begin{pmatrix} R & -R \\ -R & -2R \end{pmatrix} \begin{pmatrix} i_a \\ i_b \end{pmatrix} + \begin{pmatrix} L-M & M-L \\ L-M & 2(M-L) \end{pmatrix} p \begin{pmatrix} i_a \\ i_b \end{pmatrix} + \begin{pmatrix} e_{ab} \\ e_{bc} \end{pmatrix} \tag{3.33}$$

which can be arranged;

$$\begin{pmatrix} L-M & M-L \\ L-M & 2(M-L) \end{pmatrix} p \begin{pmatrix} i_a \\ i_b \end{pmatrix} = \begin{pmatrix} R & R \\ -R & -2R \end{pmatrix} \begin{pmatrix} i_a \\ i_b \end{pmatrix} + \begin{pmatrix} v_{ab} - e_{ab} \\ v_{bc} - e_{bc} \end{pmatrix} \tag{3.34}$$

and this equation can be simplified further to obtain the following form;

$$p \begin{pmatrix} i_a \\ i_b \end{pmatrix} = \frac{1}{(L-M)} \begin{pmatrix} R & R \\ -R & -2R \end{pmatrix} \begin{pmatrix} i_a \\ i_b \end{pmatrix} + \frac{1}{3(L-M)} \begin{pmatrix} (2v_{ab} + v_{bc} - (2v_{ab} + e_{bc}) \\ (v_{bc} - v_{ab}) - (e_{bc} - e_{ab}) \end{pmatrix} \tag{3.35}$$

This is a simple system electrical equation of two independent variables, i_a and i_b which represent the commutation model in terms of line voltages and

back-emfs. If the two stator currents in (3.35), position and the mechanical equation are grouped together, then the machine can be described by a fourth order matrix equation.

The same procedure can be repeated to find the second and third system equations, where machine line voltages v_{ab} and v_{ca} for case II are used and where the line voltages v_{bc} and v_{ca} for case III are used.

3.5 Commutation Control

The position encoder feedback gives an output which changes six times every one electrical revolution. This is usually converted directly into signals to switch on appropriate phase windings. The positioning of the sensors and appropriate decode logic ensures that the voltage applied to the motor are maintained in phase with voltages induced in each stator winding. The model is designed so that errors in placement of one or more sensors (so that commutation becomes advanced or retarded) can be simulated. This is potentially an important feature since accurate placement of the sensors is a costly manufacturing process and a simulation of the effect of less accurate placement on the performance could give pointers to ways in which designs could be changed to allow less accurate placement.

3.6 PWM Voltage Control

Operation of the drive under closed loop system conditions can be incorporated into the simulation. The voltage is simulated using the PWM switching strategy, which is employed to modulate the dc supply voltage. This simulation strategy is based on the comparison of the voltage reference signal and its inverse. The reference voltage for modulation, however, is produced by a closed loop current controller. In this controller, the current calculated at each interval is compared to the demand and an error current is generated. After proportional, integral and differential controlling actions the

scaled error current is compared to a triangular waveform, and as a result of this comparison, device switching signals appropriate to the instantaneous rotor position are produced.

This control procedure can be summarised in the following steps;

$i_{error} = i_{ref} - i_m$,

$i_{int} = i_{new}\Delta t + i_{old}$,

$i_{dif} = \frac{i_{new} - i_{old}}{\Delta t}$,

$V_{amp} = i_{gain}(k_p i_{new} + k_i i_{int} + k_d i_{dif})$,

$V_{ref} = k_{pwm} V_{amp}$.

Where i_m is measured current, i_{ref} is referenced (or demanded) current and voltage demand (or reference), V_{ref}, is PWM voltage. The controller model is arranged to be as flexible as possible to allow the development of control algorithms. In other words the principle advantages of this method of representation is that it is not limited to one particular controller or control strategy. For example the difference between a PWM and a fixed-off time controller may be implemented by a change in the algorithm which determines the transition between the various modes of operation of the controller.

3.7 Formulation of the Problem for Computer Simulation Package

The solution method used in the computer program uses similar phase equivalent circuits as the previous section. This system model includes the PWM switching strategy and thus it has switching states which operate on six modes for the commutation interval and six modes for the conduction interval over the 360° of an excitation cycle. The effective circuit configurations in these modes is summarised and is shown in figure 3.13.

For these modes, it is not possible to calculate the current for each phase in isolation when current is flowing in all three phases. In this case the winding currents are calculated in terms of the line voltages. For example,

by considering the case when the current flows in phase a and b during the conduction (figure 3.5) and by neglecting the effect of the mutual inductance M, the line voltage equation is given; (see the previous section):

$$V_{dc} = 2Ri_{ab} + 2L\frac{di_{ab}}{dt} + e_{ab} \tag{3.36}$$

This equation can be solved using numerical integration to find i_{ab} and hence the winding currents i_a and i_b. Conduction equations for other combinations of excited phases can be derived by transposition of winding and devices numbering. During commutation (figure 3.6), the independent currents must be calculated, so a second equation is generated by considering the operating condition of $V_{dc} = v_a - v_c$, $i_{ac} = i_a = -i_c$, $e_{ac} = e_a - e_c$ and by neglecting the mutual inductance;

$$V_{dc} = 2Ri_{ac} + 2L\frac{di_{ac}}{dt} + e_{ac} \tag{3.37}$$

However, the differential equations are solved to find the independent winding currents in terms of series connected windings. Since the star point is unconnected, $i_a + i_b + i_c = 0$, using this relation and the definitions of i_{ab} and i_{ac} it is possible to express the actual winding currents in terms of i_{ab} and i_{ac}:

$$\left.\begin{aligned} i_a &= \frac{i_{ab} + i_{ac}}{3} \\ i_b &= \frac{i_{ab} - 2i_{ac}}{3} \\ i_c &= \frac{i_{ac} - 2i_{ab}}{3} \end{aligned}\right\} \tag{3.38}$$

so given the solution for i_{ab} and i_{ac} it is possible to calculate the winding current. The solutions of the circuits equations for modes III-VI (figure 3.7d-3.7f) are carried-out as in modes I and II.

In this simulation procedure, the phase voltages, v_a, v_b and v_c are selected according to the operating condition of the inverter. In order to illustrate the solution, a typical 120° interval is chosen for the discussion. Over this interval, there are four operating conditions to be considered with different v_a, v_b, v_c in each condition;

(1). At the start of the interval it is assumed that phase a is connected to the positive supply rail ($V_{dc} = v_a$), phase b is connected to the ground rail, and phase c is switched off following a period of positive current conduction causing freewheeling current to flow from the ground rail.

(2). When the current in phase c decays to zero it is forced to remain at zero until a further change in excitation occurs. Only windings a and b are now excited and by virtue of the series connection $i_a = -i_b$. During this time region, therefore, equation (3.36) is used.

(3). The third operating state starts with a change in the pattern of excited windings at a time defined by the load angle. The excitation change has the effect of turning off phase b and turning on phase c in the negative sense, while phase a remains excited in the positive sense. The (negative) current in phase b decays over this region by flowing against the positive supply voltage. Hence all three phases are excited. Subject to these constraints, equations (3.36) and (3.37) are solved for i_{ab} and i_{ac} and the actual winding currents calculated from equation (3.38).

(4). The final operating state starts when the current in phase b decays to zero. Only phase a and c are now excited and by virtue of the series connection $i_a = -i_c$. During this time region, therefore, equation (3.37) is used.

Having computed the solution for one 60° interval, the remaining five intervals and consequently for all time are easily obtained by using the same procedure because the inverter is triggered symmetrically.

Once these currents are obtained, the calculation of average torque, efficiency

and torque ripple can proceed. As the mechanical output is produced by the product of induced back-emf e_a, e_b, e_c and currents i_a, i_b, i_c, the torque is given by

$$T_e = \frac{1}{\omega_r}[i]^T[e] \tag{3.39}$$

3.8 Numerical Solution of the System Equations

The solution of the system equations is obtained by a step-by-step method, with sufficiently small step length. The system equations of performance are thus solved by some method available for the solution of a system of ordinary differential equations. Although a choice between these methods tends to be difficult to make, the general considerations in selecting an algorithm, apart from the nature of the problem to be solved, are numerical stability, simplicity of the algorithm in terms of its implementation on the computer, the solution time and memory requirements. Two of the most commonly used numerical methods for a computer solution are the predictor-corrector method and the Runge-Kutta method. In both methods, accuracy is dependent on the integration step used. However most of the formulas used are truncated series. Therefore, the truncation error has to be continually checked and appropriate adjustment on the time step implemented. This takes more computation time.

The Predictor-Corrector method is commonly used. Among these methods the Euler-Predictor-Corrector method appears to give better results than other predictor corrector methods and has the largest stable region. As these methods require more than one-point to calculate the next point, they are not self-starting. This is the main disadvantage of these methods.

On the other hand, all the Runge-Kutta methods require just one point to calculate the next point, and therefore they are self-starting and require an initial solution. If the initial steady-state vector is known, direct

evaluation of the steady-state performance of the drive can be implemented without having to go through the transient solution. This saves computer time. The evaluation of the steady-state performance directly without going through the initial transient has been successfully applied to the induction machines controlled by the power inverter [Novotny, et al, 1968], [Lipo, 1971]. However, the technique proposed in these references is only applicable to the case where the excitation consists of alternate periods of a normal sine wave and periods of open circuit operation. In the case of the brushless dc motor, the excitation is not sinusoidal. Further, the waveforms of the states can not be explicitly defined because many intermediate variables are dependent on the operating conditions. Hence, numerical integration may be used to solve the system of equations.

A fourth-order Runge-Kutta method has employed in solving the system differential equations which are described the models described in the previous sections. As compared to lower order Runge-Kutta methods, the Fourth-order Runge-Kutta method, which is described below, has the advantage of higher accuracy and therefore greater stability. However, it involves a greater number of calculation for each step, and therefore takes more computation time.

A description of this method is briefly given here. Estimation of truncation error in each step is made by comparing the results with normal and half the normal step lengths.

For digital computation it is convenient to rearrange the equation of instantaneous motor phase currents equation in matrix notation as follows

$$i = f(i,t) = [L]^{-1}(v - i[R] - e) \tag{3.40}$$

which contains terms which may vary depending on the operating conditions (voltages). A Runge-Kutta representation of this equation give the following algorithm for time step.

$$i_{k+1} = i_k + \frac{t}{6}\left(a + 2b + 2c + d\right) \tag{3.41}$$

where

$$a = hf(i_k, t)$$

$$b = hf(i_k + \tfrac{1}{2}a, t_k + \tfrac{1}{2}h)$$

$$c = hf(i_k + \tfrac{1}{2}b, t_k + \tfrac{1}{2}h)$$

$$d = hf(i_k + c, t_k + h)$$

h=step size

The above algorithm is used as a procedure to calculate the instantaneous motor phase current vector i_{new} using the previously calculated value of motor phase current vector i_{old} and the function $f(i,t)$ defined in equation (3.40).

The motor dynamic equation is used to calculate the new instantaneous speed, $\Delta\omega_r$ after the instantaneous torque is calculated at each time step. The speed ω_r is the rate of change of position with respect to time. Friction torque, T_f, load torque, T_L, damping factor D, motor and load inertia, J_M, J_L, respectively are input parameters to the simulation approach.

$$T_e = (J_M + J_L)\Delta\omega_r + D\omega_r + T_f + T_L \tag{3.42}$$

Rewriting equation (3.42) in the following form

$$\Delta\omega_r = \frac{\left(T_e - D\omega_r - T_f - T_L\right)}{(J_M + J_L)} \tag{3.43}$$

3.9 Solution of the System Equations

3.9.1 Current Calculation

To accomodate the square-wave phase voltages, it is necessary to calculate the instantaneous phase currents at discrete points in time. The derivatives of the phase currents are then represented by

$$\frac{di}{dt} \approx \frac{i_{new} - i_{old}}{\Delta t} \tag{3.44}$$

where i_{new} is the value of the current at the end of the time-step Δt, and i_{old} is the value of the current at the start of the time step. If the time intervals between calculations is small, equation (3.44) is a reasonable approximation, since the maximum rate of change of current is V/L, the validity of the approximation is ensured by evaluating the change in current over a time interval (Δt) which is sufficiently short that $V\Delta t/L$ is small. The current waveforms are calculated by applying a Runge-Kutta algorithm for step by step integration.

A Runge-Kutta algorithm for step by step integration is written as a procedure to calculate the new value of instantaneous motor phase current vector i_{new} using the previous calculated value of motor phase current vector used to solve the differential equation over each time step. In this case, an artificial transient procedure has to be followed. Starting with arbitrary initial conditions, an excitation cycle (commutation and conduction) is studied; the conditions at the end of the cycle are taken as initial conditions for a second cycle and a third and so on until steady cycles are achieved.

3.9.2 Phase Advance Angle Calculation

The phase shift, α, is dependent on the instant of switching the voltage in the phase winding and the start of the flat top of the back-emf in that phase. Therefore, in the simulation the back-emfs are delayed by angle α and the currents are commutated at the same instant as if no phase advance is applied.

3.9.3 Solution Procedure for 180° Conduction Angle

When the inverter operates with a 180° conduction angle, three switching transistors are always turned-on at any instant of time; therefore this type of switching assures continuous flow of current in the motor phases. In this case the stator lines are not subject to open circuit conditions, and solution must proceed via the calculation of two independent currents (e.g. i_{ab} and i_{ac} in mode I).

3.10 Validation of the Model

To test the model described in previous sections, the solution for the drive with 120° conduction angle obtained from simulation analysis was compared to the tested results of the experimental system. The machine was run at 1100 rpm for a dc supply voltage of 120 V. Results are given of comparison of the simulation prediction and the experimental current waveforms for different phase advance angles. Figures 3.8 and 3.9 show the comparison of the simulation results and the experimental current waveforms for 0° and 15° phase advance angles respectively. One can note a good agreement between the prediction and the practical measurement.

The experimental verification was obtained for a 20 KW industrial machine tool drive. The detail parameters of this drive are shown in Appendix 1.

3.11 Summary and Conclusions

This chapter describes the analysis work that was carried out on a trapezoidal brushless d.c motor. The aim of the analysis is to model a brushless d.c. motor drive operating in closed-loop modes. A generalised approach and computer simulation method for comprehensive analysis of a brushless dc motor drive has be developed and presented. The analysis takes into account all possible modes of operation of the inverter including commutation and conduction.

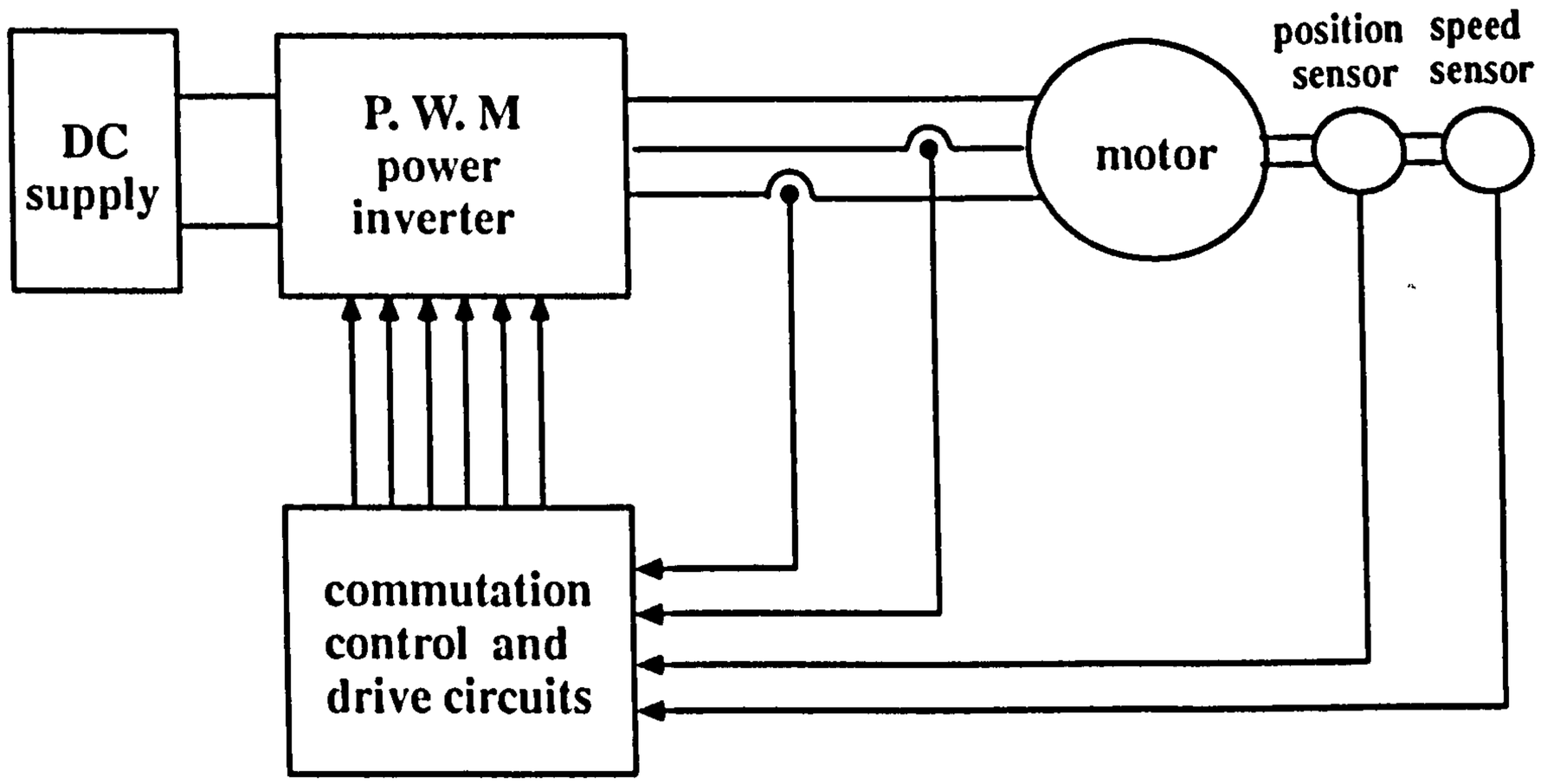

Figure 3.1 Schematic of brushless dc drive

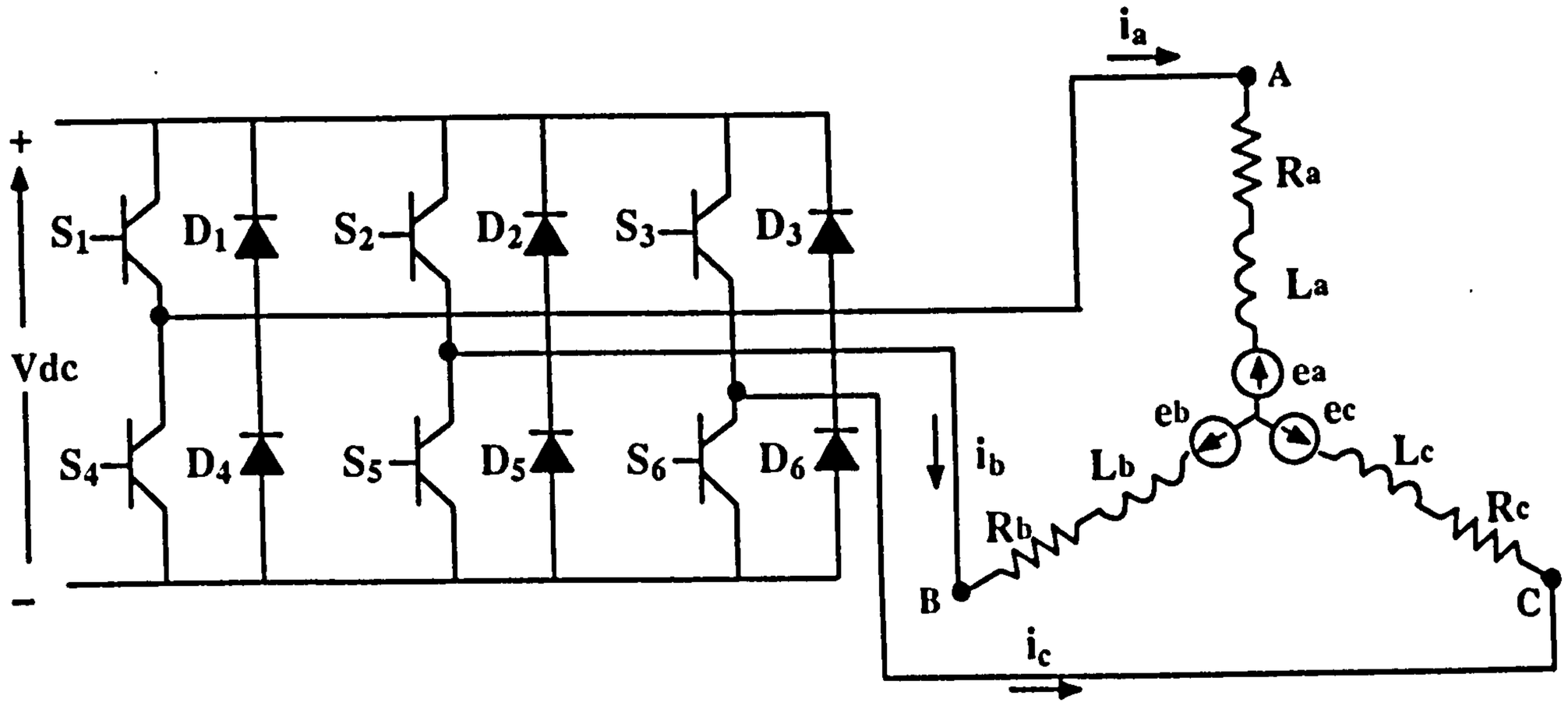

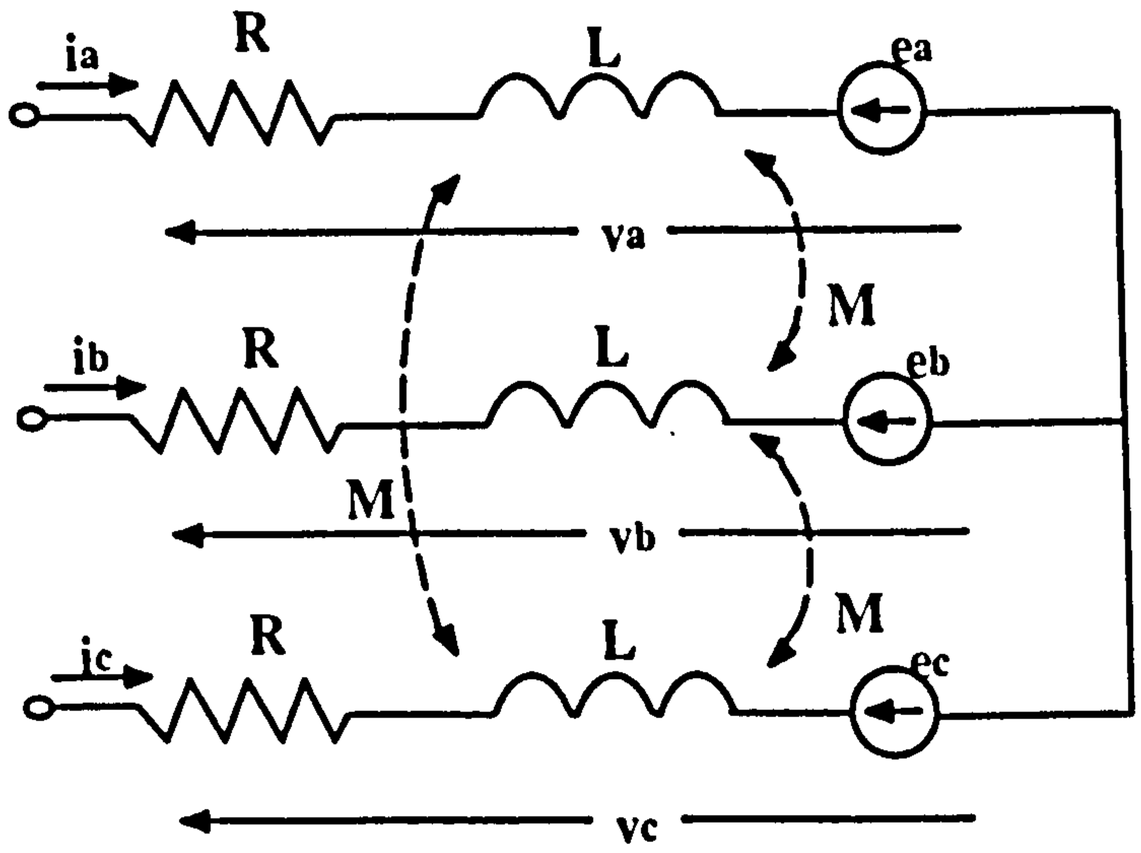

Figure 3.2 System model and conversion

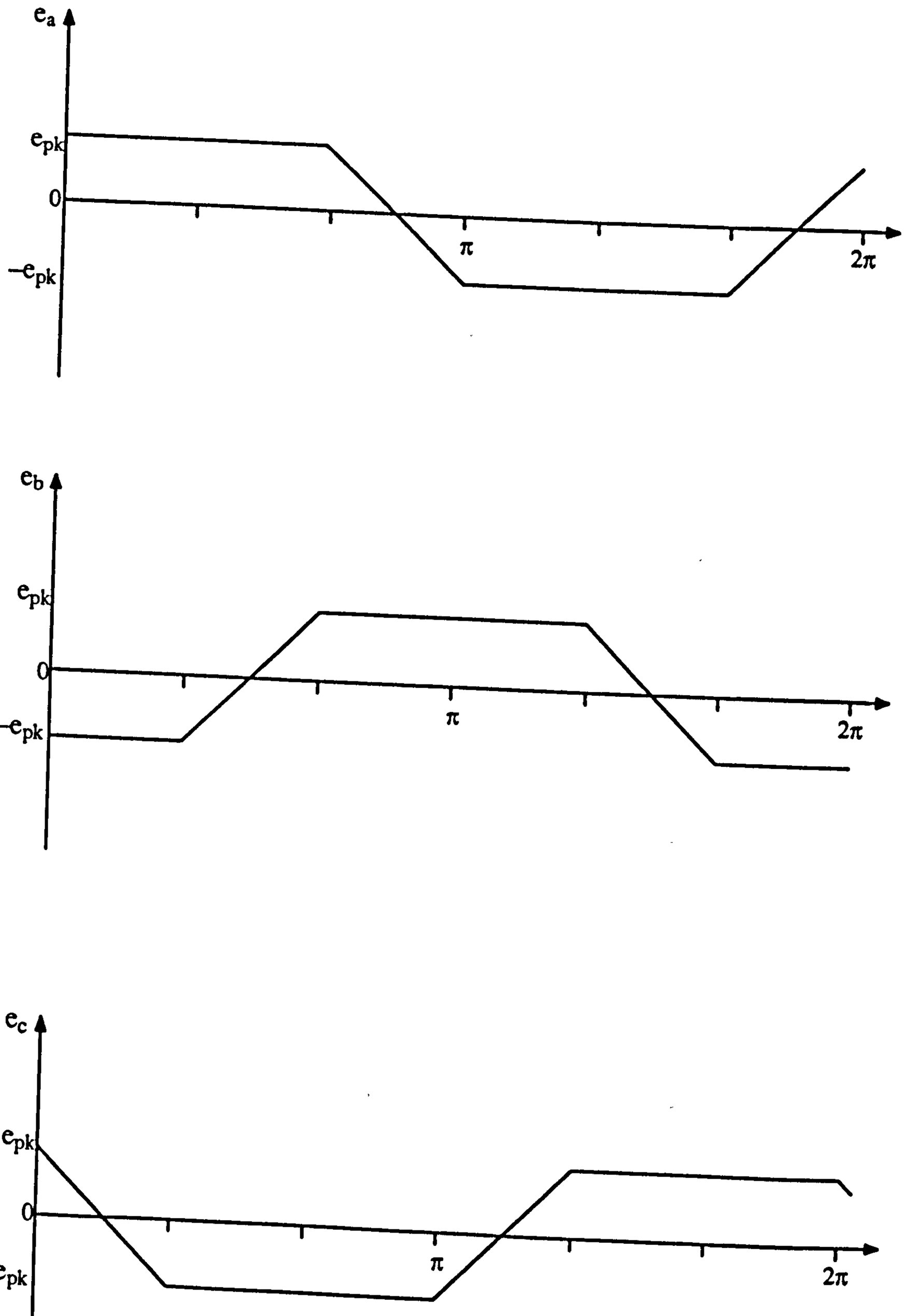

Figure 3.3 Machine back–emf

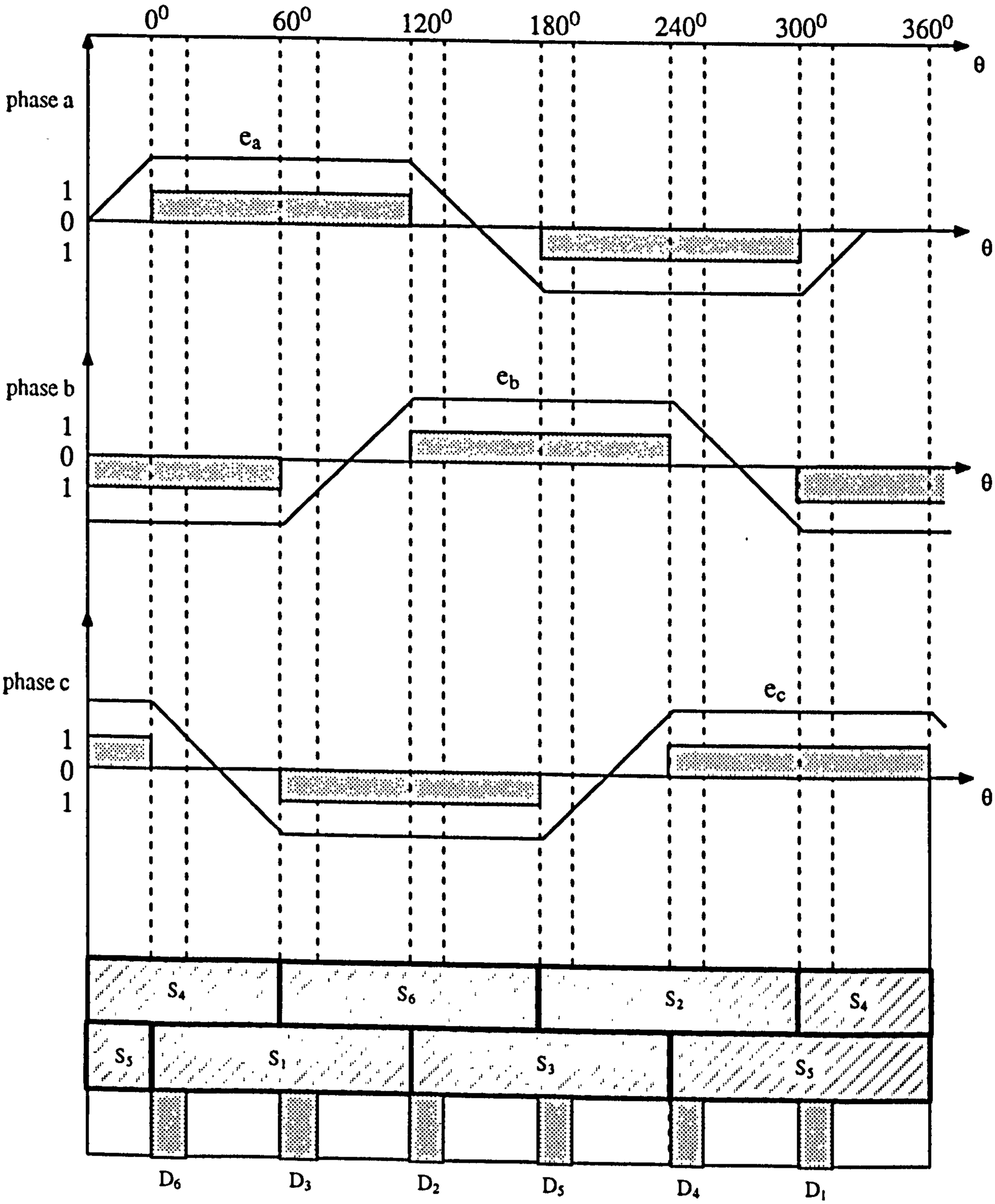

Figure 3.4 Power inverter model

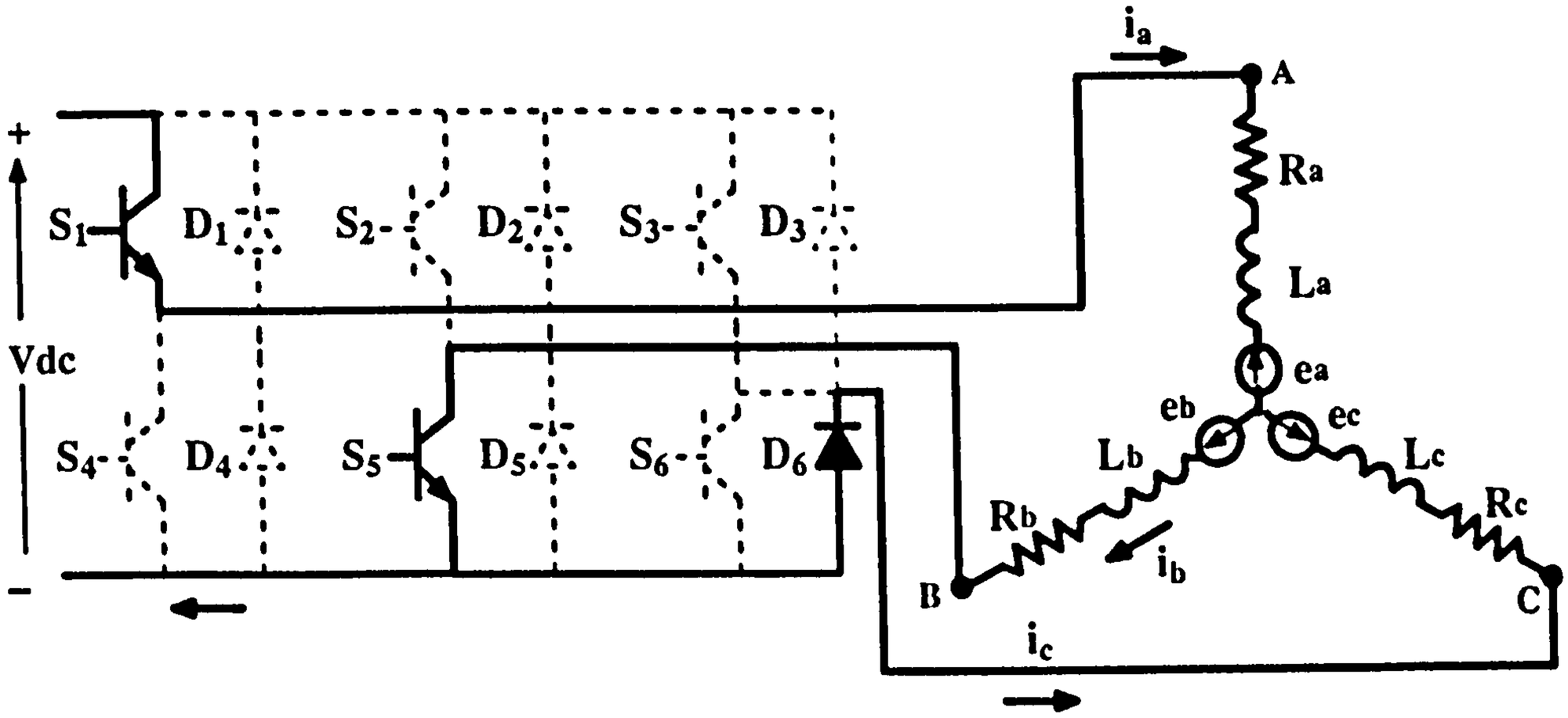

A

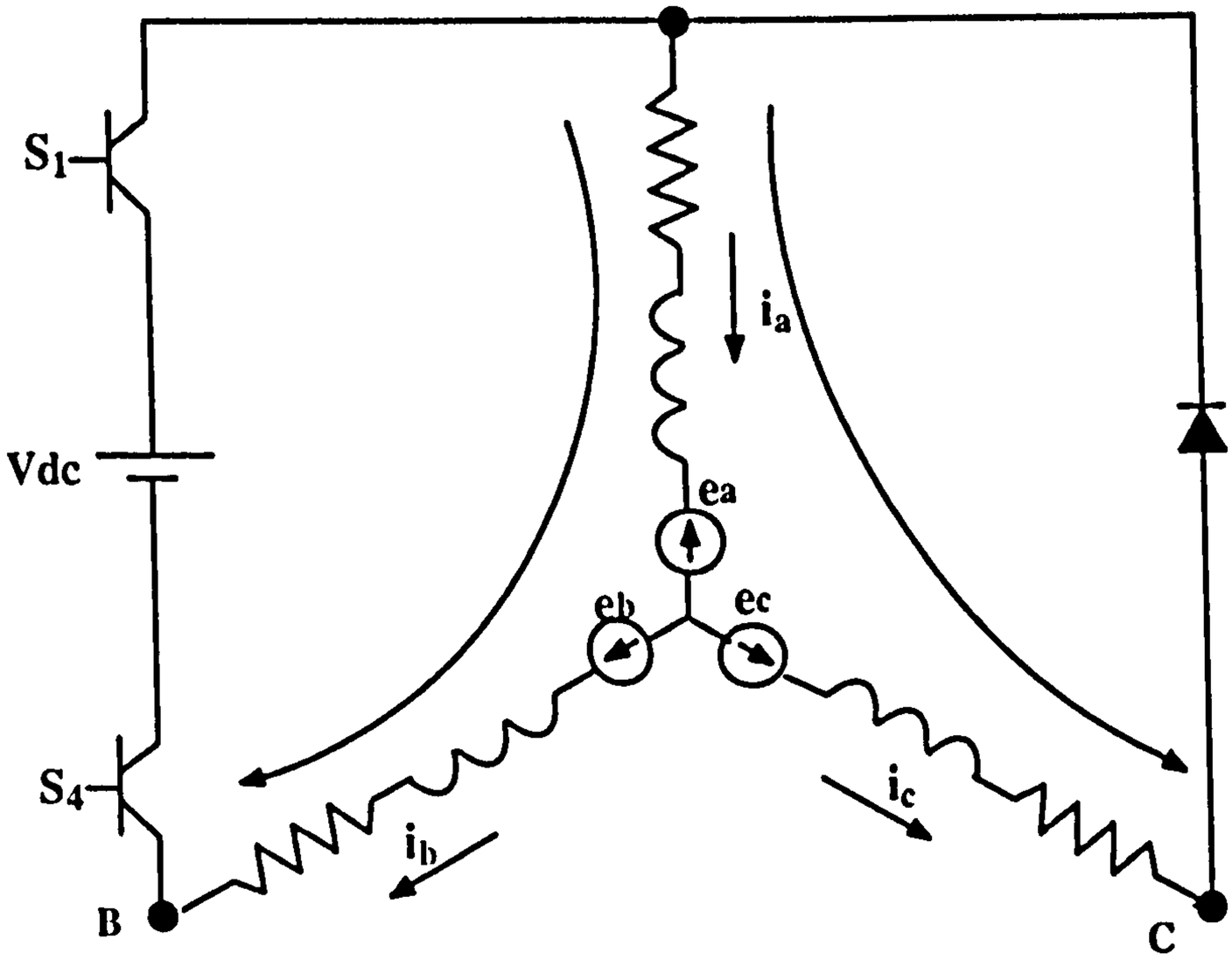

Figure 3.6 Commutation mode of the inverter

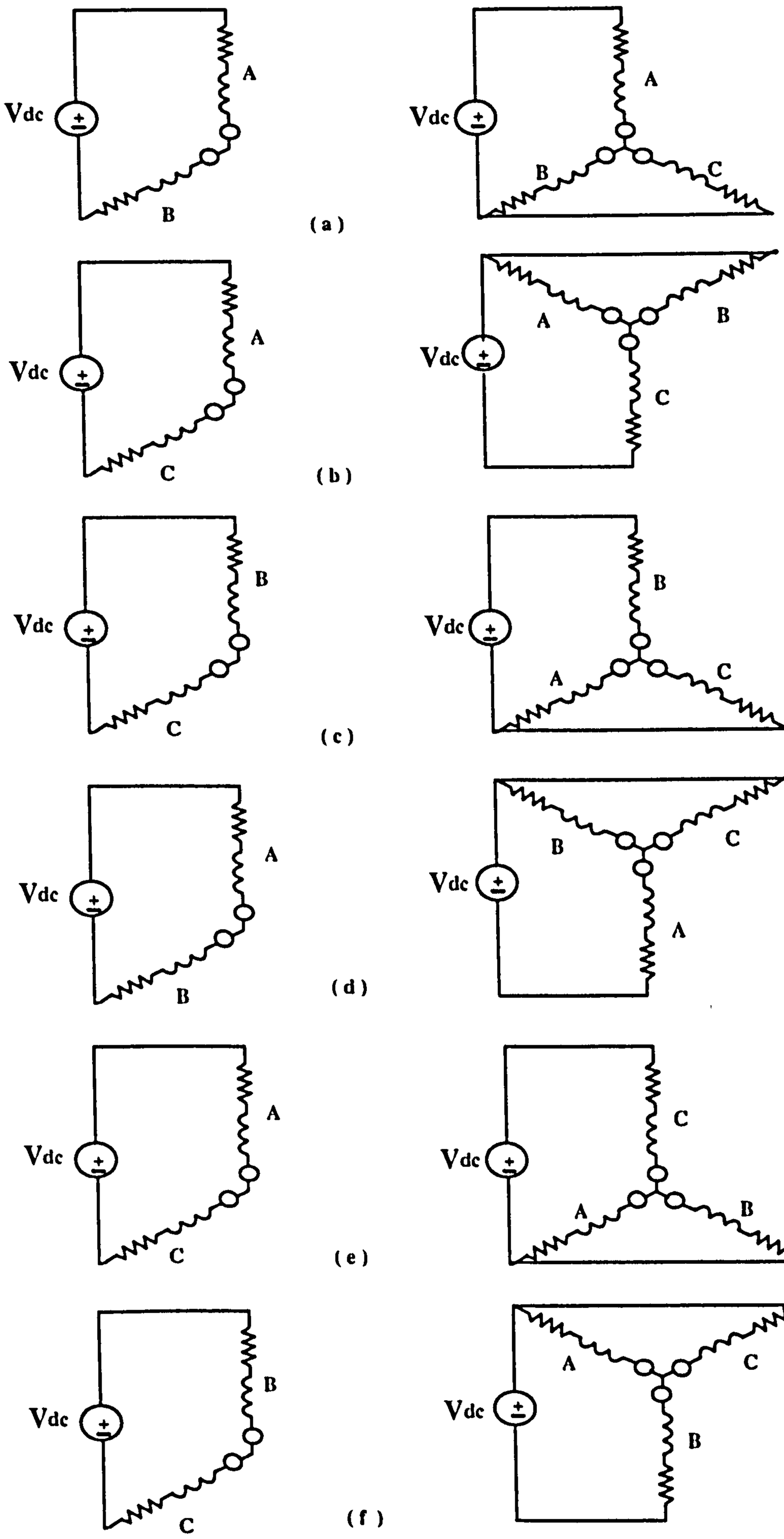

Figure 3.7 Operating modes (a) mode I (b) mode II (c) mode III (d) mode IV (e) mode V (f) VI

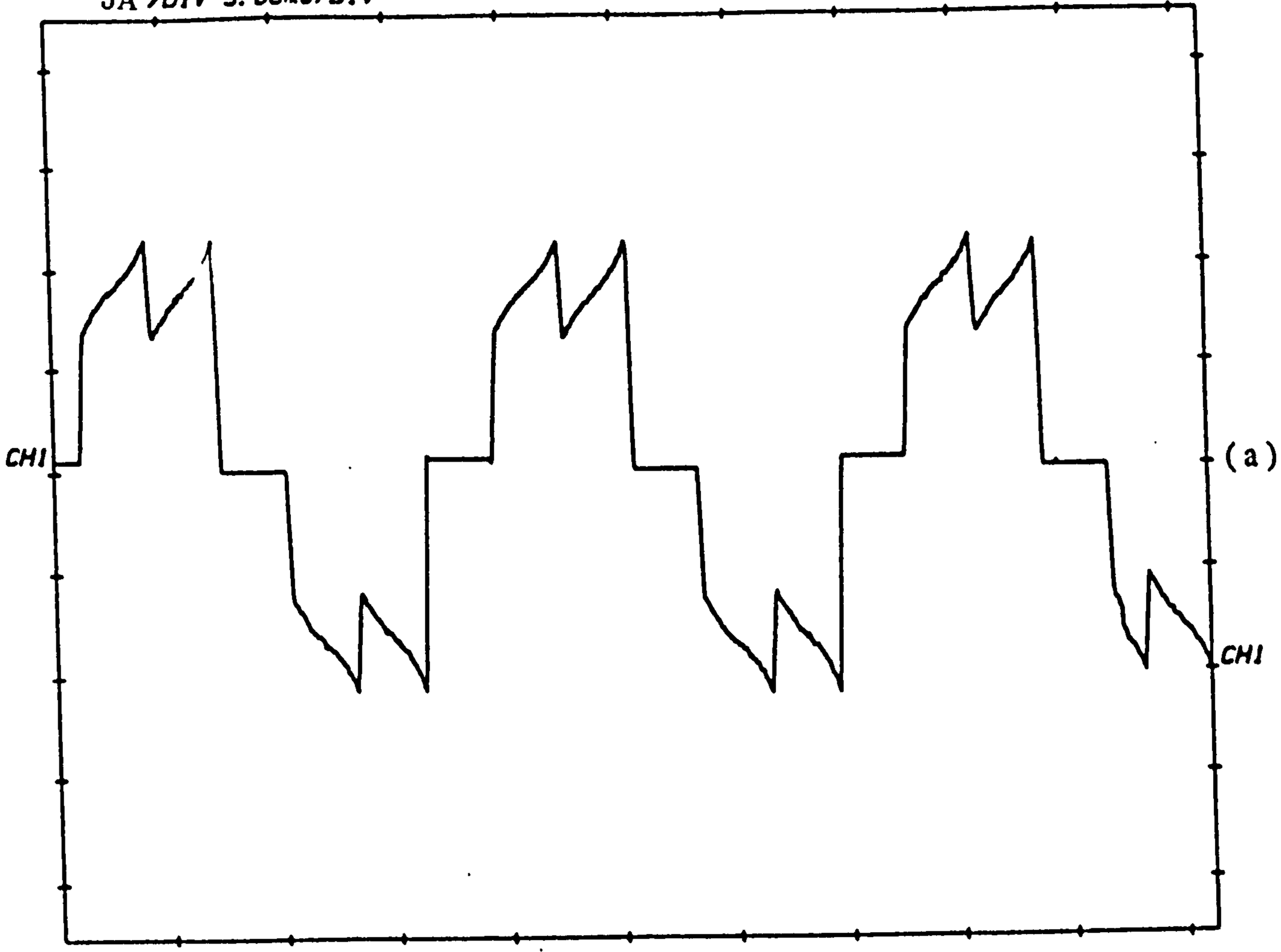

Figure 3.8 Measured phase current for 120° conduction angle
(a) No phase advance,
(b) 15° electical phase advance

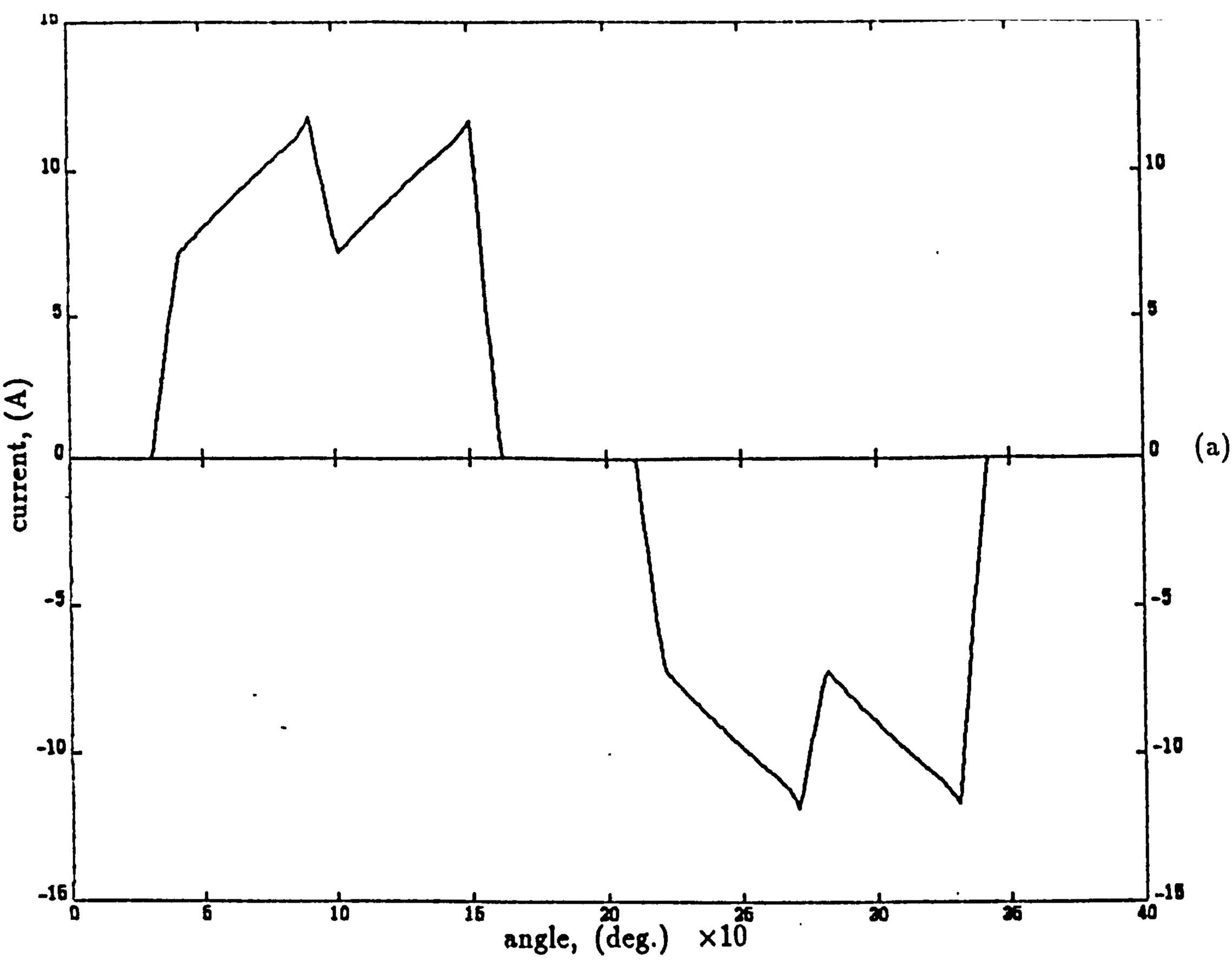

Figure 3.9 Predicted phase current for 120° conduction angle.
(a) No phase advance
(b) 15° electical phase advance

CHAPTER 4

SIMULATION AND ANALYSIS OF A PERMANENT MAGNETIC BRUSHLESS DC MOTOR DRIVE

4.1 Introduction

Simulation of a permanent magnet brushless motor drive prior to its hardware implementation is desirable in order to study in detail the drive system, particularly at the design and testing stage of suitable drive control strategies. In this chapter simulation and analysis for the operation of the brushless dc motor is presented in which the actual parameters of the experimental machine are used.

The aim of the analysis is to simulate a brushless d.c. motor drive operating in closed-loop control modes, which uses phase advance control techniques in conjunction with a PWM control technique and also an investigation of this control on the dynamic behaviour of the system when account is taken of the load's mechanical dynamics. The investigation has included both 120° and 180° conduction angles of inverter operation, with provisions to select the phase advance angle for commutation. The effect of variation of parameters such as the inductance on the high-speed torque performance of the drive has also been included in the study.

The simulation method described in the previous chapter is first used to demonstrate the versatility of the direct three-phase model and secondly to investigate the detail behaviour of the system under investigation under the high-speed torque control methods which have been discussed in detailed in Chapter 2. During this investigation performance characteristics, such as torque/speed, rms current, efficiency, current ripple, and torque ripple are obtained and compared for these control methods. Also the combined

effects of the machine inductance and phase advance angle on the machine performance are assessed for conduction angles of 120° and 180°.

In addition, numerical and analytical investigations of the operating range of the phase advance angle are presented. During this investigation a theoretical approach to demonstrate the operating range of the phase advance angle in permanent magnet brushless dc motors has been presented.

4.2 Steady-State Performance Analysis of PWM Current-Controlled Inverter-Fed Brushless DC Motor

The following sections investigate the high-speed torque control methods, such as phase angle control and extended conduction angle. The drive system, including its controller is simulated on the computer, using the simulation package described in the preceding chapter. The performance characteristics, such as torque/speed, r.m.s. current, % torque ripple and % efficiency are examined for these control schemes and the effect of variation of parameters such as the machine inductance on the high-speed torque performance is also examined.

4.2.1 Performance Characteristics

In order to evaluate the overall performance of the drive under different control schemes, the following performance quantities are considered.

Torque-Speed Characteristics

It shows the variation of speed with torque and indicates both steady-state and transient performances.

Current and Torque Ripples

There are important performance quantities as far as the low speed operation of the motor is concerned. The torque and current ripple factors can be defined as

$$T_{e_{ripple}} = \frac{T_{e_{max}} - T_{e_{min}}}{2T_{e_{ave}}} \times 100\% \tag{4.1}$$

and

$$i_{ripple} = \frac{i_{max} - i_{min}}{2i_{ave}} \times 100\% \tag{4.2}$$

Efficiency

It is widely recognised as an important characteristic of the machine. As an aid to understanding motor efficiency it is sometimes more helpful to consider the motor losses rather than efficiency. The determination of efficiency requires that the losses of motor components be determined as a function of the machine operating variables such as current and frequency. An evaluation of these losses will indicate the most efficient way to operate the system over the speed range. The losses are identified as the copper loss, I^2R, in the stator conductor and the core loss in the stator iron that is adjusted for the operating conditions over the speed range. However, the efficiency is defined as the ratio of the power output, P_o, divided by the power input, $P_i(= P_o + machine \quad losses)$, and is calculated as follows;

$$\eta = \frac{P_o}{P_o + machine \quad losses} \times 100\% \tag{4.3a}$$

$$\eta = \frac{\left(T_{e_{ave}} \times \omega_r\right)}{\left(T_{e_{ave}} \times \omega_r\right) + 3I_{ave}^2 R + iron \quad loss} \times 100\% \tag{4.3b}$$

where $T_{e_{ave}}$ is the average torque which indicates the ripple content in the motor torque and $I_{ave}^2 R$ is the average winding copper loss. The iron loss is dependent on the motor speed, peak backing iron flux density and stator core material. The iron loss values are stored as straight lines on logarithmic axis for B_{peak} and loss density. To cope with different frequencies a number of

lines at different frequencies are stored. Intermediate frequencies are obtained by linear interpolation. However, the frequency is obtained by

$$f = \frac{np}{120} \tag{4.4}$$

where f is the frequency of the current, p is the magnet pole number on the rotor. n is the motor speed in rpm.

Descriptions of high-speed torque control schemes studied in this chapter as well as the definition of other parameters have been presented in Chapters 2 and 3.

4.2.2 Simulation System

The results presented in this work were obtained for a 20 KW industrial machine tool drive. The drive system consists of a six pole brushless dc motor with rare earth magnets and has a general geometry typical of servo motors. The details of the brushless dc drive system used for the investigation are given in Appendix 1.

In the following sections of this chapter the tests in the equations are steady-state tests with the machine driving a dynamometer load at various speeds. In this mode the drive is operating with a current loop but without a speed loop. The current loop's transfer function has proportional, integral and differential components but differential action is intended to eliminate high frequency signals and is not significant to the response of the drive.

Performance predictions were made for a current demand of 60 A. Although this current is approximately three times the motor continuous rated current of 23 A which constitutes the steady-state thermal limit for the machine, such current levels can occur as a result of rapid changes in speed demand. Although a brushless dc motor is magnetically saturated at rated current, larger current can still improve the motor's torque.

4.3 Low Speed Performance for 120° and 180° Conduction Angles

The simulation results presented in this section are for low-speed operation. The low speed region is defined here as that region over which the current is maintained constant by the PWM-switching action of the inverter and thus full torque is available.

4.3.1 Conduction Angle of 120°

Figure 4.1 is used as a basis for comparing aspects (e.g. voltage, current, average torque and torque ripple) of the machine performance at low speed (100 rpm). The phase current is still approximately rectangular in shape. Also from this figure the switching action of the inverter can be clearly seen, and the currents are controlled by the controller.

Consequently the phase current easily reaches the current demand of 60 A, since there is a large margin in available voltage. At this speed the current ripple factor and torque ripple factor of the corresponding waveforms are low.

There is no reduction in torque production at low speed and under this condition the drive requires zero phase advance angle. Also it should be noted that the opposite polarity spikes at the centre of the current waveform are caused by the stator currents commutating from one phase to another.

4.3.2 Conduction Angle of 180°

To demonstrate the effect of this method at low speeds figure 4.2 shows that winding current waveform is near quasi-square in shape and easily reaches the demanded current of 60 A. As can be seen from this figure the current in each phase winding has two 60° intervals per cycle when the current magnitude is at the demanded value and four intervals when the current is a half of the demanded.

As a consequence of this the torque is reduced. This is because the current waveform does not match the induced voltage waveform. Also the current ripple factor and torque ripple factor of the corresponding waveforms increases, since the windings are excited at rotor positions where the induced emf is not constant.

4.4 High-Speed Torque Performance for 120° and 180° Conduction Angles

When considering the characteristics of a drive at high-speed, two main operating speed ranges are distinguished- the high speed region below the base speed (below 3000 rpm in this case) and the extended speed range above the base speed (above 3000 rpm). In such an operation, current changes are forced by the voltage difference of the supply voltage available and the back-emf.

4.4.1 Conduction Angle of 120°

To examine the drive performance at high speed, speeds of 1000, 2000, and 3000 rpm and a current demand of 60 A are considered. The overall shape of the characteristics and details of the results for these cases are shown in figures 4.3-4.5. It is clear from these figures that a reduction in output torque is observed up to around 2000 rpm, is due to the increasing size of the switch-on times constant relative to an electrical cycle. At higher speeds the machine runs of voltage and/or time to force the input current up to the demanded level and the reducing difference between dc supply voltage and back-emf, $(V_{dc} - e)$, now dictates the output. In other words, the supply voltage is insufficiently large to maintain the required value of input current to the motor against the increased values of induced back-emf.

As can be seen from figure 4.4 when the motor is running at a speed of 2000 rpm the motor phase current is still switched by the controller, but the shape of the waveform is determined by the difference between the

applied voltage and motor back-emf and the motor's effective inductance and resistance. This prediction can clearly be seen from figure 4.5 when the motor is running at speed of 3000 rpm. At this speed the motor phase current only just reaches the demand maximum value of the current and so only starts to chop at the tail of the period. In addition, it is interesting to note from figure 4.5 that in the high-speed region the current waveform becomes near sinusoidal in shape.

As will be seen in the following section, it is very helpful if the phase advance technique is used to keep the current in phase with respect to the emf.

4.4.2 Conduction Angle of 180°

At high speeds an extended conduction angle has a different effect on the torque, resulting from winding inductance and high-speed limitations. The results of these constraints may be explained by referring to the current waveforms which are shown in figures 4.6-4.8. These figures show the current, back-emf and torque at various speeds with zero phase advance. It can be seen from these figures that an increase of the rotor speed causes the current to change shape considerably. Also it should be noted that as speed increases, the distortion of current effectively delays the waveform and increases the shift between the current and back-emf. As a consequence of this the predicted current and torque waveshapes have considerably deteriorated.

It is important to note that, with 180° conduction, when positive excitation is started, there is a large negative current in the phase winding, which must decay to zero before positive current can be established. At high speeds the decay time of the initial negative occupies a considerable part of the excitation interval and the negative torque produced by the negative current reduces the average torque. As the conduction angle increases the initial negative current becomes larger and requires a longer time to decay to zero.

4.5 Effect of High-Speed Torque Control Methods on the Machine Performance Characteristics

4.5.1 Conduction Angle of 120°

The effect of phase advance on the machine characteristics is demonstrated in figures 4.9-4.10 which show rms current and average torque characteristics of the machine as a function of speed with phase advance angle of $\alpha = 0°$, 15°, 30°, 45°, and 60°. Torque-speed curves of figure 4.10 provide a useful summary of the motor's capacity to operate under closed-loop control, over the whole range of load conditions. The curves of this figure show, that, as the speed increases, the torque produced at any phase advance angle will reach a maximum before falling to zero, and with large phase advance angles, a positive torque is not produced at low speeds. The envelope of the torque/speed curves defines the maximum torque the motor can produce at each speed. This torque decreases at high-speeds, as it becomes increasingly difficult to establish the rated phase currents in the motor winding. As can be seen in Fig. 4.10 the torque improvement in the high-speed region is increased as more phase advance is introduced until an optimum is reached for that particular speed.

Figures 4.11-4.13 illustrate how this improvement in performance is obtained by employing the phase advance procedure at three operating speeds. The waveforms of figures 4.11-4.13 also show that with the correct value of phase advance angle for a particular operating speed, the current is nearly in phase with the back emf and thus there is a large improvement in the values of torque obtained at speeds between 2000 and 3000 rpm. Although the improvement in torque output for phase advance angle used for a speed of 1000 rpm is small, the phase advance angle is a useful aid in achieving a better waveshape phase current over such a range of operating speed.

Although torque ripple is of less concern at high speeds, due to the low-pass filtering effect of the combined motor and load inertias, it is worth

comparing the torque waveforms in figures 4.3-4.5 and figures 4.11-4.13. These show that phase advance leads not only to higher levels of average torque, but also to lower levels of torque ripple.

4.5.2 Extended Conduction Angle of 180°

Similar trends are observed in the case of the extended conduction angle method with varying phase advance angle. Figures 4.14-15 summaries the drive performance with extended conduction angle. Improvements in performance are obtained by advancing the winding excitation relative to the induced emf as speed increases. Figures 4.16-4.18 illustrate how these improvements in performance are obtained by using the phase advance procedure at three operating speeds. As an example, the results of figure 4.18 shows that when the phase advance angle=45°, the average torque at speed of 3000 rpm is typically 1.5 times the maximum torque when the phase advance angle=0°.

4.5.3 Performance Comparison Between 120° and 180° Angles

It is of interest to compare the difference in machine performance when operating with the two conduction angles. Figure 4.19 is used as a basis for comparing the torque-speed characteristics of a brushless d.c. motor drive with 120° and 180° conduction angles. For both conduction angles the phase advance method is effective in improving torque at high speeds, in the range 4000-6000 rpm.

As can be noted from the results of these figures the benefits of an extended conduction angle with phase advance are most pronounced at very high speed. For this particular case, the greatest torque improvement appears in the range 4000-6000 rpm.

4.6 The Combined Effect of Winding Inductance and Phase Advance Angle

To further examine the combined effects of both phase advance angles and winding inductances on machine performance, figure 4.20 shows how torque and rms current vary with winding inductance for different values of phase advance at a typical speed of 2000 rpm. The phase inductance of the actual motor is 3.1 mH and it can be seen from the torque against inductance characteristic that this is a near-optimal value if there is no phase advance. However if the total phase inductance is doubled, to a value of 6.2 mH, torque production is improved from 38 Nm to 52 Nm at 2000 rpm and from 24 Nm to 46 Nm at 3000 rpm. To realise these higher levels of torque it is essential to apply the phase advance method, with more phase advance being required for higher phase inductances.

At high speeds, figures 4.21-4.22 show the deterioration of motor current and torque waveform with an increase in phase inductance at speed of 3000 rpm. However, The benefits of higher inductance are evident from a comparison of figures 4.21-4.22 and figures 4.23-4.24 which refer to operation speeds of 2000-3000 rpm, where the back emf of round 200 V and 250 V are a significant proportion of the available dc supply voltage (550).

The results in Table 4.1 reinforce the important points of the above discussion. This table is very instructive in obtaining an insight into the way the rms current, machine torque, % torque ripple and % efficiency depend on the total phase winding inductance and phase advance. As can be seen from the results of Table 4.1 there is large improvement in the values of torque from the variation of phase advance angles at speeds between 2000 and 3000 rpm. For the case of 2000 rpm, the output torque at different phase advance angles can be compared with the torque obtained when the motor is running with zero advance angle. When $\alpha = 30°$ an average torque improvement of 12.5% is obtained.

4.7 Transient Performance Analysis of PWM Current-Controlled Inverter-Fed Brushless DC Motor

For transient conditions of operation the motor mechanical system must be included in the simulation model described in the previous chapter. The transient analysis of a brushless dc motor with torque control schemes is simulated on the computer and the simulation package described in Chapter 3. The results of the armature current, the electromagnetic torque and the speed for a steady-state operating point are taken as a reference in determining the electromagnetic characteristics of the drive system under transient conditions.

4.7.1 Transient Performance Prediction

One of the most difficult conditions to model is that of acceleration of the motor from standstill to a steady state operating point (i.e. speed changes, $\Delta\omega_r$, following the switching operation). Since the machine will be accelerating during the transient period, the dynamic equation

$$\Delta\omega_r = \frac{T_e - D\omega_r - T_L}{J_M}\Delta t \tag{4.5}$$

shows that the predicted acceleration of the motor for constant acceleration torque is inversely proportional to the motor inertia, J_M, and proportional to the accelerating torque $(T_e - T_L)$. For this transient condition the initial values of motor current and rotor speed required for the solution of the equivalent circuit must be known.

For the operation of the motor under steady-state conditions described in Chapter 3, the sample rotor position step angle and the time step interval, Δt between successive steps of rotor position, $\Delta\theta$, are fixed by constant speed of the motor, ω_r and these are related by the following relation;

$$\Delta\theta = \omega_r \Delta t \tag{4.6}$$

As the speed of the motor is constant, rotor position is always defined for any time and so the motor open circuit emfs and position sensor information used to define the condition zone of the inverter are always known. For transient operation the motor speed is not constant and so the time taken for the motor to move through any fixed angle, $\Delta\theta$, can vary. As the drive is position commutated rather than time commutated, it is more appropriate to fix the position increment between successive sampled steps and then allow the time taken for that position movement to be set by the motor speed of equation (4.6). In present work the transient performance is accomplished using the following equations

$$v = [R][i] + [L][pi] \tag{4.7a}$$

$$T_e = \frac{1}{\omega_r}[e][i]^T \tag{4.7b}$$

$$\Delta\omega_r = \frac{T_e - B\omega_r - T_L}{(J_M + J_L)}\Delta t \tag{4.7c}$$

The equation for torque includes second order differential of angles. To reduce these to first order the change in speed is introduced $\Delta\omega_r$ in equation (4.7c) as auxilarly variable. The speed, n, is then calculated as follows

$$n = \frac{60\omega_r}{2\pi} \tag{4.8}$$

Then the calculated value of the speed n compared with the speed demand and a speed error is generated. This error is then processed through PID controller which operates on it with proportional, integral and differential (PID) action in order to optimise the closed loop response and also to obtain the speed demand.

4.7.2 Predicted Results of the Transient Characteristics

In this section, the simulation model was used to predict the closed-loop response of the system to an acceleration from standstill for both 120° and 180° conduction angles. For the present system used here the load torque applied to the motor was a purely frictional one and the inertia of the total system was the active inertia of the motor. The motor inertia, J_m, used in these studies was 0.0095 kgm^2. In each case of study the motor is allowed to accelerate from standstill for 0.6 second.

The dynamic simulation tests for two conditions are presented. Both are for conduction angles of 120° and 180° conduction angles with phase advance values of 0° and 30°. These tests were performed when the motor is switched on at standstill for 0.6 second without torque load ($T_L = 0$), and running under its own inertia (load inertia $J_L = 0$). This is because the steady-state load torque is so small, that it can not be recognised in the current during the operation with constant speed.

Figures 4.25-4.26 show the transient acceleration for 120° and for phase advance values of 0° and 30° respectively. In these figures the phase current, torque developed by the motor and the speed of the motor without load inertia are shown. From these figures it can be seen that with a large phase advance value of 30°, a positive torque is not produced for this particular speed operation and thus the phase advance control is not effective, as described earlier in section 4.4. Also small ripples in speed can be seen due to the torque ripples.

Under the same conditions figures 4.27-4.28 show the transient acceleration for 180° and for phase advance values of 0° and 30°. In these figures the phase current, torque and the speed are shown. The transient speed responses show the same trend as that of 120°. The transient speed decreases with phase advance control.

For an investigation of the performance of the machine under transient

conditions it is also useful to consider a low power and thus low voltage inverter in order that the effect of the control methods on the performance can be studied. The differences of transition times due to the control schemes are more evident, if the inverter has less power. Results for both 120° and 180° with phase advance values of 0° and 30° are presented in figures 4.29-4.32. For these figures the power of the inverter was lowered to 80% by reducing the dc supply voltage V_{dc}. For the two different types of set values the current, torque and speed wave forms are shown. Near the highest speed (in this case 530rpm) the current has a higher frequency and an amplitude of 60 A (figure 4.30). The current becomes more trapezoidal and gets a phase delay by itself. The transition time of speed is 0.3 second. The best results come out, if the phase advance control method is applied at low dc supply voltage, as shown in figures 4.30 and 4.32.

In such tests the voltage of the inverter is not now sufficient to constrain the current in such speed operations. The transition times are 0.3 second for 120° and 0.4 second for 180°. So it is clear that with 180° conduction transition times are within reach, for which in the case of 120° feeding a bigger inverter is necessary.

For deceleration the different conduction angles are equivalent due to the fact, that the supply voltage is sufficient at any moment.

It is clear from the above tests that with 120° conduction angle the torque is always larger resulting in a faster start-up. For steady-state operations it was shown that at any given speed there is a specific phase advance angle which maximises the torque developed by the motor. In order to get the benefit of full torque producing capability of the motor to achieve high acceleration it is possible to have a speed dependent phase advance angle during start-up so that the developed torque lies on the torque/speed characteristics envelope. As the motor speeds up a phase advance angle is adjusted for maximum torque production.

4.8 Numerical Investigation of the Effective Operating Range of the Phase Advance Angle

4.8.1 General Consideration

It has been shown in the preceding sections if the motor is to operate over a wide speed range and deliver the maximum possible torque at all times, it is essential to have some form of phase advance angle control. The phase advance angle should be zero at low speeds and increase toward some maximum value as the speed increases.

It was explained earlier in Chapter 2 that the phase advance angle, α, represents a shift in the switching points from the ideal. Due to the practical manufacturing limitations, it is not possible to guarantee perfect positioning of the phase commutation sensors. The effect of this limitation can be assessed by observing the effect of adjusting the operating range of the phase advance angle on the drive characteristics.

The operating range for the phase advance angle, α, will be determined in practice by the limitations of the machine performance characteristics. Specifically the choice of maximum value for the phase advance angle will be determined by the operating speed, by the actual shape of the machine back-emf waveform, and by the reduction of the resultant airgap flux density and is a compromise between the machine performance characteristics (i.e. to maximise average torque, to minimise torque ripple, to maximise efficiency or to minimise current).

4.8.2 Predicted Results of the Effective Operating Range of the Phase Advance Angle

Useful guidance about the limitations of the maximum phase advance angle is best described by the simulation results which are presented in Tables 4.1 and 4.2. Owing to the low and high speed characteristics, which are

described in the preceding sections, the instant of current switching can only be advanced effectively within the range $0 \leq \alpha \leq 60$. For all operating speeds if the phase advance is more than the required range, the machine will produce more negative torque and so lead to higher torque ripple.

As was shown earlier if the drive operates at low speeds, the excitation period for each phase is much greater than the phase circuit time constant and, as a consequence, the waveforms of the winding rectangular currents will flow in phase with applied voltage. Owing to the shape of the back emf waveform, if the phase advance is more than the value of α_p (i.e. $\alpha \geq \alpha_p$), the machine will produce more negative torque and so lead to a higher torque ripple, as shown in figure 4.33. Therefore, for low speed operations the phase advance angle of 0° is most advantageous in producing the required torque.

At high speed the test results of Tables 4.1 and 4.2 suggest that the drive can only be operated with phase advance which is a working compromise between the level of torque ripple that can be tolerated, and the maximum allowable phase advance angle to produce further improvements in high-speed torque performance. It can be seen that at speeds upto the base speed an increase in the phase advance angle to a maximum value of 45° increases the average torque of the machine. As can be noted, for this case, machine performance is considerably improved and it is easy to see why it is necessary to use a maximum phase advance angle of 45° from the analysis in the preceding section.

It can also be noted that at speeds exceeding the base speed an increase in the phase advance value of 60° increases the machine's torque, at the expense of an increase in the torque ripple, but this may reasonably be regarded as acceptable for high speed applications.

Although the average torque of the machine has improved slightly when the maximum phase advance angle of 90° is used, an unacceptably large increase in torque ripple of about 100% results. Also it is interesting to note

that the average torque starts to decrease when the drive operates at a phase advance angle above 90° and therefore it is necessary to impose limits on the phase advance angle when it is used.

From the above investigation it can be concluded that the phase advance angle can be varied over a wide range up to 60° without detracting from overall machine performance. Also when priority is given to a large average torque, whilst the torque ripple is not very important the effective point of phase advance value can be selected to meet these application requirements.

4.9 Analytical Investigation of the Effective Operating Range of the Phase Advance Angle

Further consideration of the relationship between the stator and the resultant fluxes, adds additional insight into the nature of the effective operating range of the phase advance angle that could be used in the brushless dc motor. It has been explained in Chapter 2 that the resultant airgap flux density is mainly determined by the stator and rotor flux densities. Also the stator current basically determines the nature of stator flux and the magnitude of this flux is directly proportional to the magnitude of the current.

This section presents a theoretical approach to assess the operating range of the phase advance angle in permanent magnet brushless dc motors in which the phase advance angle of the phase current is determined by the effect of stator flux density in the air-gap on the resultant flux density.

4.9.1 Theoretical Approach to the the Maximum Operating Range of the Phase Advance Angle

The basic approach described here is to derive a mathematical relation between resultant flux density of the machine, applied phase current in terms of phase advance angle and stator flux density distribution and using this relation

to assess the effect of maximum phase advance angle on the resultant flux density. This analysis requires information about the stator mmf waveform, stator flux density distribution, stator phase current and rotor flux density distribution. These parameters can be represented by Fourier series analysis. This method of analysis is one of the most convenient ways of satisfactorily describing the variation of these quantities. This method assumes linear superposition is possible and hence that the magnetic circuit of the machine is linear and does not saturate. However, this analytical method provides useful insight into the range of phase advance angle and its effect on the weakening of the resultant airgap flux density of the machine.

4.9.2 Field Analysis by Fourier Series

4.9.2.1 Applied Phase Current

For the system described here the stator current in the motor phase winding is a controlled a rectangular waveform. For 120° conduction angles, the applied phase current in kth phase winding can be described by the Fourier series as follows

$$i_k(t,\alpha) = \hat{I}cos(\omega_r t - 2(k-1)\frac{\pi}{3} + \alpha) \tag{4.9}$$

and hence the phase one current is

$$i(t,\alpha) = \hat{I}cos(\omega_r t + \alpha) \tag{4.10}$$

If the motor is runing at speed, ω_r, the instant of current commutation may be determined in respect to the angular position, θ_e, where $\theta_e = \omega_r t$. If commutating current into phase winding, a, at $\theta_e = -60°$, corresponds to zero phase advance, the maximum phase current is reached at $\theta_e = 0$, thus a maximum flux density is produced by the phase winding and rotor flux density.

If applied phase current is to be commutated into the phase earlier than $\theta_e = -60°$, then phase advance can be included in expression (4.10);

$$i(t, \alpha) = \hat{I} cos(\omega_r t + \alpha) \tag{4.11}$$

4.9.2.2 Airgap Flux Density Distribution

The resultant airgap flux density can be thought of as composed of stator flux density set up by the current in the stator winding, and the flux density which is generated by the rotor. The resultant airgap flux density, B_r, is equal to spatial superposition of rotor and stator flux densities.

Assuming the rotor flux density and stator mmf which is generated the flux density have trapezoidal distributions. The spatial distribution of airgap flux density for a pair of poles can be represented by a Fourier series, when referred to some point in the airgap of the machine, is given by expression;

$$B_r(\theta, t, \alpha) = \hat{B}_f cos(\theta - \omega_r t - \beta) + \hat{B}_s cos(\theta - \gamma) i(t, \alpha) \tag{4.12}$$

where

B_f is the fundamental component of the rotor flux density,

B_s is the fundamental component of the stator flux density,

β is the angle of the rotor axis with respect to fixed reference,

γ is the angle of the axis of the winding (a) with respect to the reference axis.

Expression (4.12) shows that the minimum (or maximum) airgap flux density of the motor may be determined by the stator current and phase advance angle. It should be noted that (90°-α) electrical is the torque angle, ψ. For maximum flux density and thus torque production this angle is set to zero. ($\alpha = 0$ corresponds to the condition of torque angle, $\psi = 90°$ used in the sinusoidal machine type). Thus for this condition the fundamental component

of stator ampere-conductor wave and the rotor flux density distribution are coincidental. Clearly deviation from the condition of maximum airgap flux density may be achieved by advancing (or delaying) the instants of current commutation. Thus the advance of the instants of current commutation provides a measure of control over the resultant airgap flux density. In practice, for the system under consideration, the phase advance angle, α, is set by the rotor position sensors which are used to provide the switching signals for inverter devices which deliver current from the supply to the motor phase windings (see Chapter 2).

It is clear from the above analysis that at zero phase advance the stator flux density is leading the rotor flux density by 90°. When the phase current is advanced by an amount α then the stator flux density produced by this current makes an angle greater than 90° with rotor flux density and the resultant airgap flux density will be reduced at this position. The resultant airgap flux density can be reduced somewhat with rated stator current by increasing the phase advance angle, α, over some range.

For the system described here, the maximum phase advance angle range that can be applied is 60° electrical. At this position the resultant airgap flux density reaches its minimum and as a consequence of this the back-emf will also be reduced, since it is proportional to the resultant airgap flux density.

From the above analysis it can be concluded that for the system under consideration, to provide a significant improvement in high-speed torque performance, the phase advance should be within the range between 0° and 60°. A phase advance angle should be 0° for starting, the maximum value of 45° upto the base speed and a maximum value of 60° for speeds exceeding the base speed.

4.10 Summary and Conclusion

This study has demonstrated the versatility of the direct three-phase model. Both transient and steady-state characteristics are evaluated using the simulation procedure described in Chapter 3 which utilises the actual phase variable of the machine.

During this study the performance of brushless d.c. motors switched by a PWM inverter is investigated, with a view to improving the high-speed torque performance. The investigation has included both 120° and 180° conduction angles of inverter operation, with provisions to select the phase advance angle for commutation. The influence of winding inductance on torque at high speeds has also been included in the study.

The results of analysis has clearly shown that the high-speed torque characteristics of the brushless d.c. motor can be considerably improved simply by adjusting the chosen setting of the phase advance angle.

The results of analysis has clearly shown that the high-speed torque characteristics of the brushless d.c. motor can be considerably improved simply by adjusting the chosen setting of the phase advance angle and using appropriate conduction angles. It has been shown that the torque available from a commercial drive at high speeds (i.e., 2000 rpm and 3000 rpm) can be improved by 12.5% using phase advance. The results have also shown that high speed torque performance can be improved by phase advance, combined with modest increases in winding inductance.

The results of the numerical and analytical analyses have shown that the phase advance should be within the range between 0° and 60° in order to provide a significant improvement in high-speed torque performance. A phase advance angle should be 0° for starting, the maximum value of 45° upto the base speed and a maximum value of 60° for speeds exceeding the base speed.

The results has also shown that in high-speed region the current waveform becomes effectively sinusoidal in shape because the current control

capability of the drive is severely limited. Therefore, in order to predict the high-speed performance of the machine in term of the optimum phase advance angle quite reasonably, the sinusoidal analysis must be used. The determination of this optimum angle in an analytical manner is approached by simplifying the representation of the motor to an approximate case of balanced symmetrical windings having constant inductances (both self and mutuals) and sinusoidal supply voltages. An analytical approach for obtaining the optimum phase advance angle in the high and extended speed ranges is presented in the following chapter.

Table 4.1a Machine parameters and their influence on machine performance

Winding Inductance (mH)	Advance Angle (Degree)	R.M.S Current (A)	Average Torque (Nm)	Torque ripple (%)	Efficiency (%)
1.55	0.0	48.47	54.19	19.4	75.5
3.1	0.0	47.83	53.40	19.5	75.7
6.2	0.0	46.51	50.65	24.7	75.8
9.3	0.0	45.08	46.56	29.3	75.4
12.4	0.0	45.26	41.33	16.1	75.0
1.55	15.0	48.54	53.47	22.1	75.2
3.1	15.0	47.98	54.07	16.8	75.9
6.2	15.0	46.61	53.68	15.8	76.8
9.3	15.0	45.34	51.84	17.4	77.1
12.4	15.0	44.80	49.12	15.4	76.6
1.55	30.0	48.49	48.85	48.5	73.6
3.1	30.0	48.02	50.38	36.2	74.5
6.2	30.0	46.87	52.22	21.6	76.1
9.3	30.0	45.53	52.61	14.8	77.3
12.4	30.0	44.49	51.81	09.6	77.5
1.55	45.0	48.54	41.44	83.3	70.2
3.1	45.0	48.12	43.51	66.9	71.6
6.2	45.0	46.91	46.90	43.1	74.1
9.3	45.0	45.85	49.18	28.0	75.8
12.4	45.0	44.70	50.16	20.6	77.1
1.55	60.0	48.53	31.13	130.1	63.9
3.1	60.0	48.12	33.84	103.6	66.3
6.2	60.0	46.98	38.48	70.3	70.0
9.3	60.0	44.23	42.54	56.8	74.4
12.4	60.0	44.84	44.81	31.0	74.9

$I_{demand} = 60$ A, $n = 1000$ rpm.

Table 4.1b Machine parameters and their influence on machine performance

Winding Inductance (mH)	Advance Angle (Degree)	R.M.S Current (A)	Average Torque (Nm)	Torque ripple (%)	Efficiency (%)
1.55	0.0	47.93	53.70	19.8	86.1
3.1	0.0	46.39	51.08	27.5	86.3
6.2	0.0	44.86	38.61	41.5	83.6
9.3	0.0	31.02	25.13	82.0	87.2
12.4	0.0	23.28	18.64	94.0	89.8
1.55	15.0	48.05	53.82	19.8	86.1
3.1	15.0	46.84	53.97	15.3	86.7
6.2	15.0	44.68	50.17	15.4	87.0
9.3	15.0	33.80	34.97	53.4	88.9
12.4	15.0	25.38	26.10	60.4	91.3
1.55	30.0	48.08	49.74	39.8	85.1
3.1	30.0	46.97	51.75	28.1	86.2
6.2	30.0	43.20	52.71	17.0	88.2
9.3	30.0	37.18	42.36	37.1	89.0
12.4	30.0	27.93	31.73	42.3	90.0
1.55	45.0	48.09	42.62	75.0	83.1
3.1	45.0	47.03	45.80	55.1	84.6
6.2	45.0	44.75	49.70	26.1	86.8
9.3	45.0	40.79	46.96	32.0	88.2
12.4	45.0	30.64	35.24	44.6	90.8
1.55	60.0	48.01	32.37	119.6	78.9
3.1	60.0	47.05	36.86	87.9	81.6
6.2	60.0	45.21	43.09	39.7	84.9
9.3	60.0	44.39	48.40	27.6	86.7
12.4	60.0	33.31	36.34	54.1	89.6

$I_{demand} = 60A$, $n = 2000$ rpm.

Table 4.1c. Machine parameters and their influence on machine performance

Winding Inductance (mH)	Advance Angle (Degree)	R.M.S Current (A)	Average Torque (Nm)	Torque ripple (%)	Efficiency (%)
1.55	0.0	47.53	52.92	22.5	90.3
3.1	0.0	45.11	47.82	31.6	90.3
6.2	0.0	26.20	24.53	48.5	93.2
9.3	0.0	17.51	16.19	58.8	94.9
12.4	0.0	13.16	12.08	61.2	95.8
1.55	15.0	47.61	53.72	20.3	90.4
3.1	15.0	46.46	53.12	21.2	90.7
6.2	15.0	30.98	34.51	24.9	93.3
9.3	15.0	20.70	22.92	29.5	95.2
12.4	15.0	15.55	17.16	32.3	96.1
1.55	30.0	47.85	50.23	37.1	89.7
3.1	30.0	46.81	52.29	23.4	90.4
6.2	30.0	36.36	42.08	10.5	92.6
9.3	30.0	24.25	28.05	13.9	94.7
12.4	30.0	18.20	21.04	16.3	95.8
1.55	45.0	47.82	43.30	69.8	88.3
3.1	45.0	46.83	46.90	46.1	89.4
6.2	45.0	41.74	46.72	18.8	91.4
9.3	45.0	27.85	31.27	22.5	93.9
12.4	45.0	20.91	23.50	24.1	95.2
1.55	60.0	47.80	33.36	112.6	85.3
3.1	60.0	46.80	38.30	72.5	87.4
6.2	60.0	44.62	44.69	23.7	89.9
9.3	60.0	31.30	32.30	34.1	92.7
12.4	60.0	23.50	24.33	35.7	94.3

$I_{demand} = 60A$, $n = 3000$rpm.

Table 4.2a Torque/speed/phase advance angle characteristics for 120°

Speed (rpm)	Advance Angle (Degree)	R.M.S Current (A)	Average Torque (Nm)	Torque ripple (%)	Efficiency (%)
1000	0.0	47.83	53.40	19.5	75.7
	15.0	47.98	54.07	16.8	75.9
	30.0	48.02	50.38	36.2	74.5
	45.0	48.12	43.51	66.9	71.6
	60.0	48.12	33.84	103.6	66.3
	75.0	48.01	21.55	176.1	55.6
	90.0	48.01	8.14	523	32.1
2000	0.0	46.39	51.08	27.5	86.3
	15.0	46.84	53.97	15.3	86.7
	30.0	46.97	51.75	28.1	86.2
	45.0	47.03	45.80	55.1	84.6
	60.0	47.05	36.86	87.9	81.6
	75.0	47.10	25.36	124.1	75.3
	90.0	47.09	12.52	305.9	60.1
3000	0.0	45.11	47.82	31.6	90.3
	15.0	46.46	53.12	21.2	90.7
	30.0	46.81	52.29	23.4	90.4
	45.0	46.83	46.90	46.1	89.4
	60.0	46.80	38.30	72.5	87.4
	75.0	46.81	27.10	100.9	83.1
	90.0	46.45	14.88	212.9	73.2

Table 4.2b Torque/speed/phase advance angle characteristics for 120°

Speed (rpm)	Advance Angle (Degree)	R.M.S Current (A)	Average Torque (Nm)	Torque ripple (%)	Efficiency (%)
4000	0.0	28.70	30.67	28.1	94.9
	15.0	31.67	36.18	25.9	94.8
	30.0	39.21	43.88	23.8	93.7
	45.0	46.29	47.80	40.4	92.1
	60.0	46.87	39.73	61.8	90.4
	75.0	46.62	28.91	81.5	87.4
	90.0	46.67	16.85	145.5	80.2
5000	0.0	9.36	20.26	44.0	97.6
	15.0	12.72	14.17	46.3	97.5
	30.0	20.17	21.46	48.0	97.7
	45.0	31.20	30.60	54.6	95.1
	60.0	45.83	39.87	53.8	92.5
	75.0	46.34	29.72	73.9	89.9
	90.0	46.09	17.76	122.0	84.4
6000	0.0	2.641	-2.87	-122.9	00.0
	15.0	1.106	0.612	336.3	81.2
	30.0	7.95	7.973	75.9	97.3
	45.0	18.57	17.05	77.9	96.8
	60.0	32.77	26.54	76.6	94.8
	75.0	45.64	30.65	67.2	91.9
	90.0	46.31	19.00	106.7	87.2

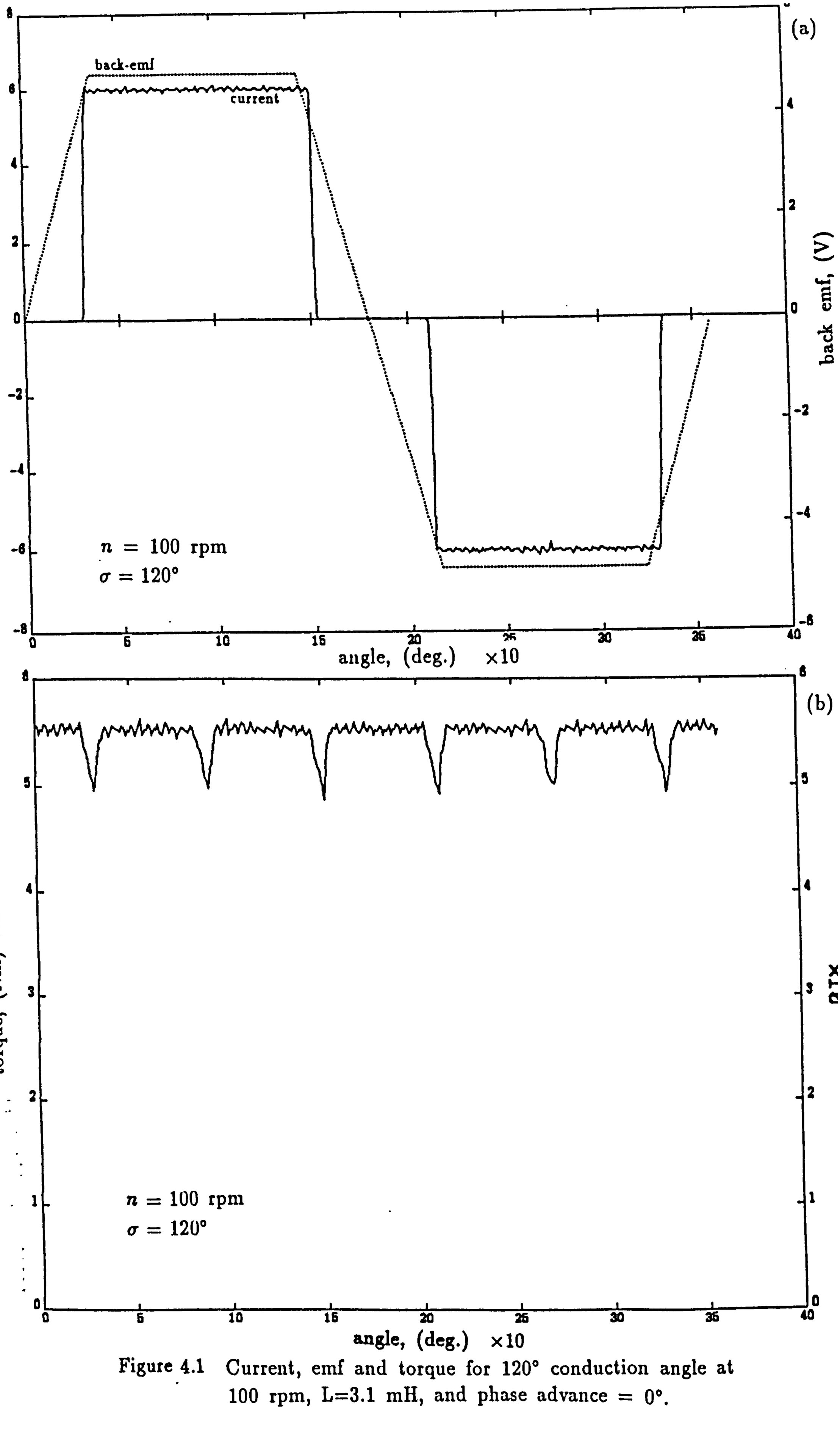

Figure 4.1 Current, emf and torque for 120° conduction angle at 100 rpm, L=3.1 mH, and phase advance = 0°.

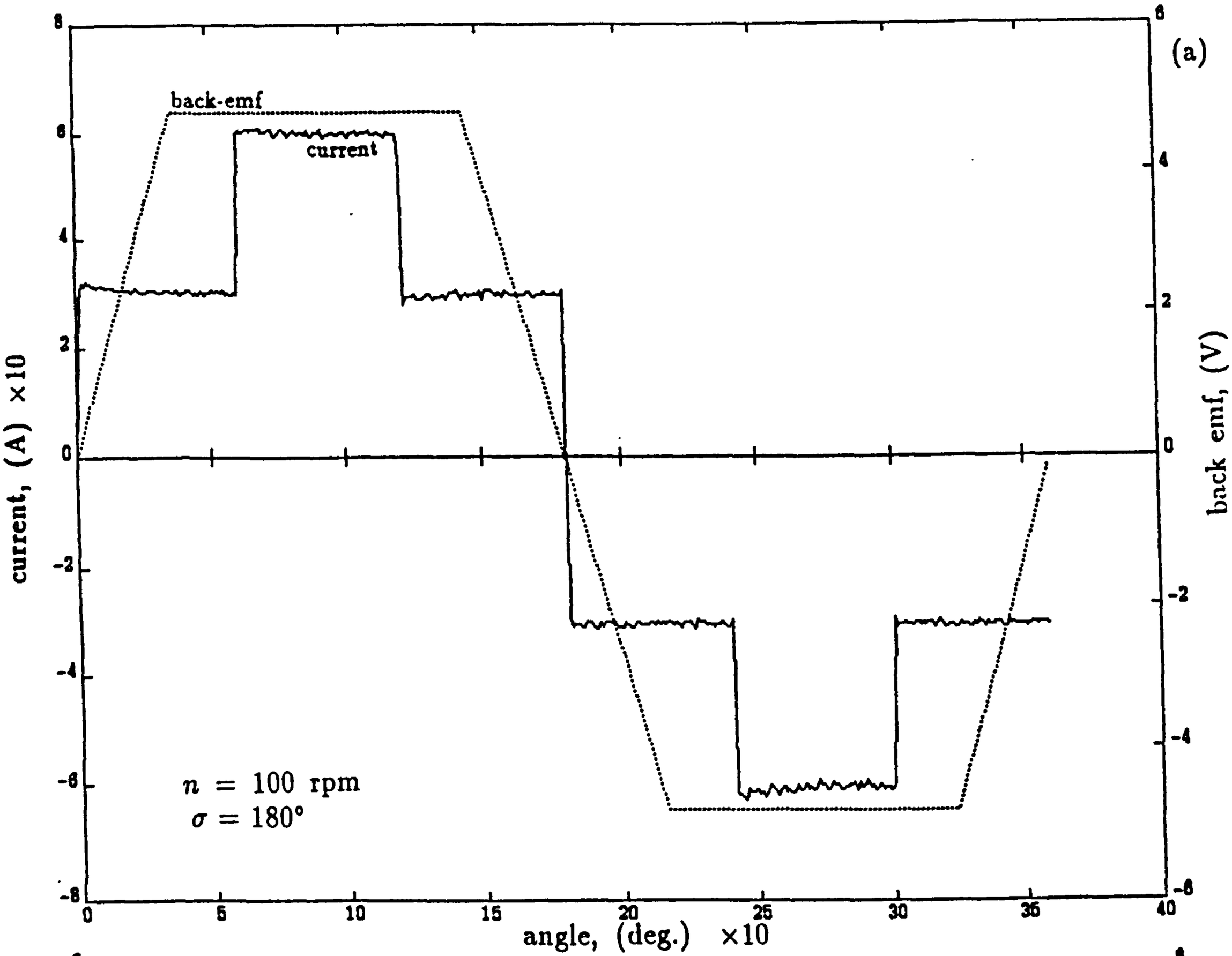

Figure 4.2 Current, emf and torque for 180° conduction angle at 100 rpm, L=3.1 mH, and phase advance = 0°.

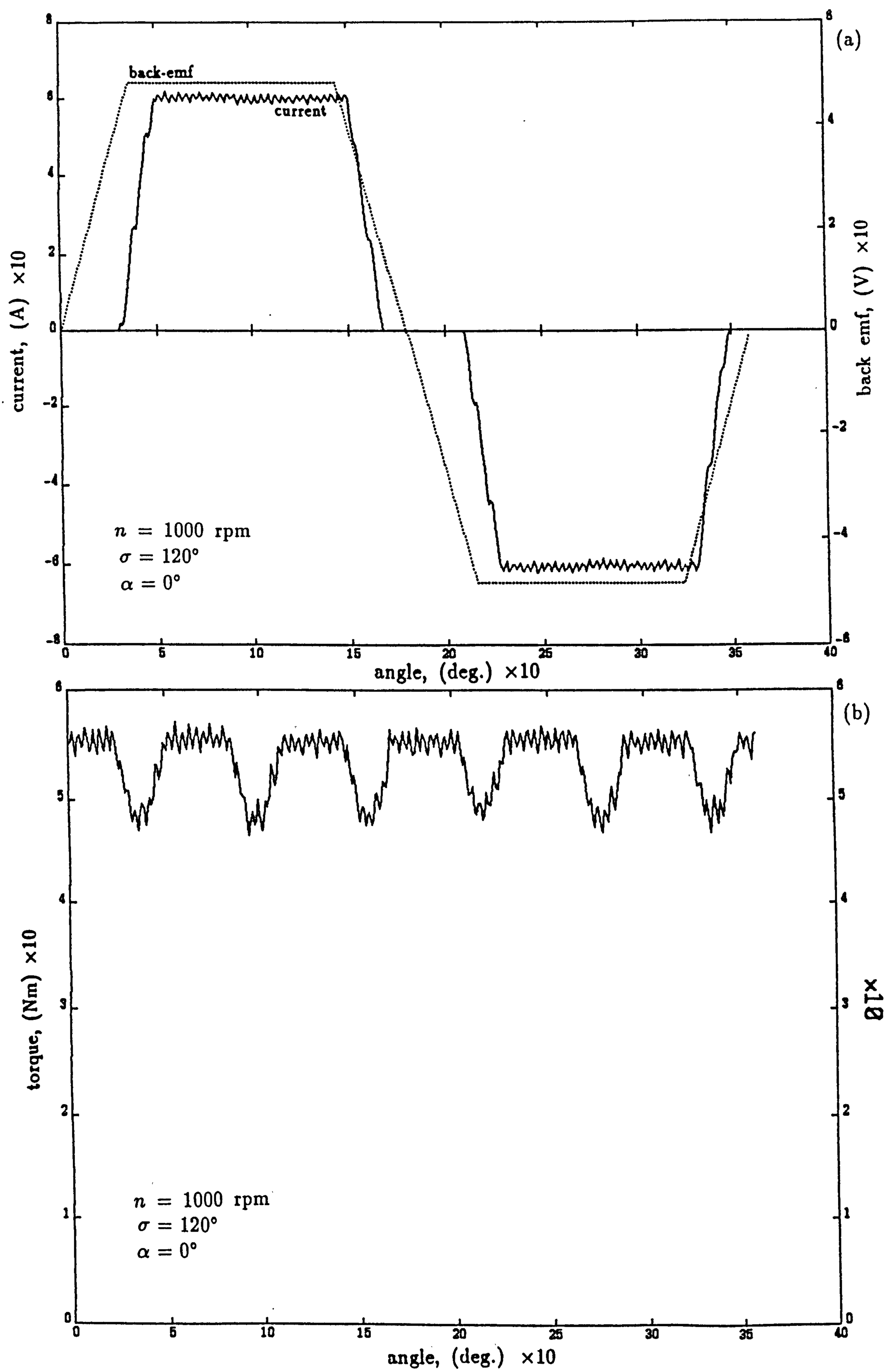

Figure 4.3 Current, emf and torque for 120° conduction angle at 1000 rpm, L=3.1 mH, and phase advance = 0°.

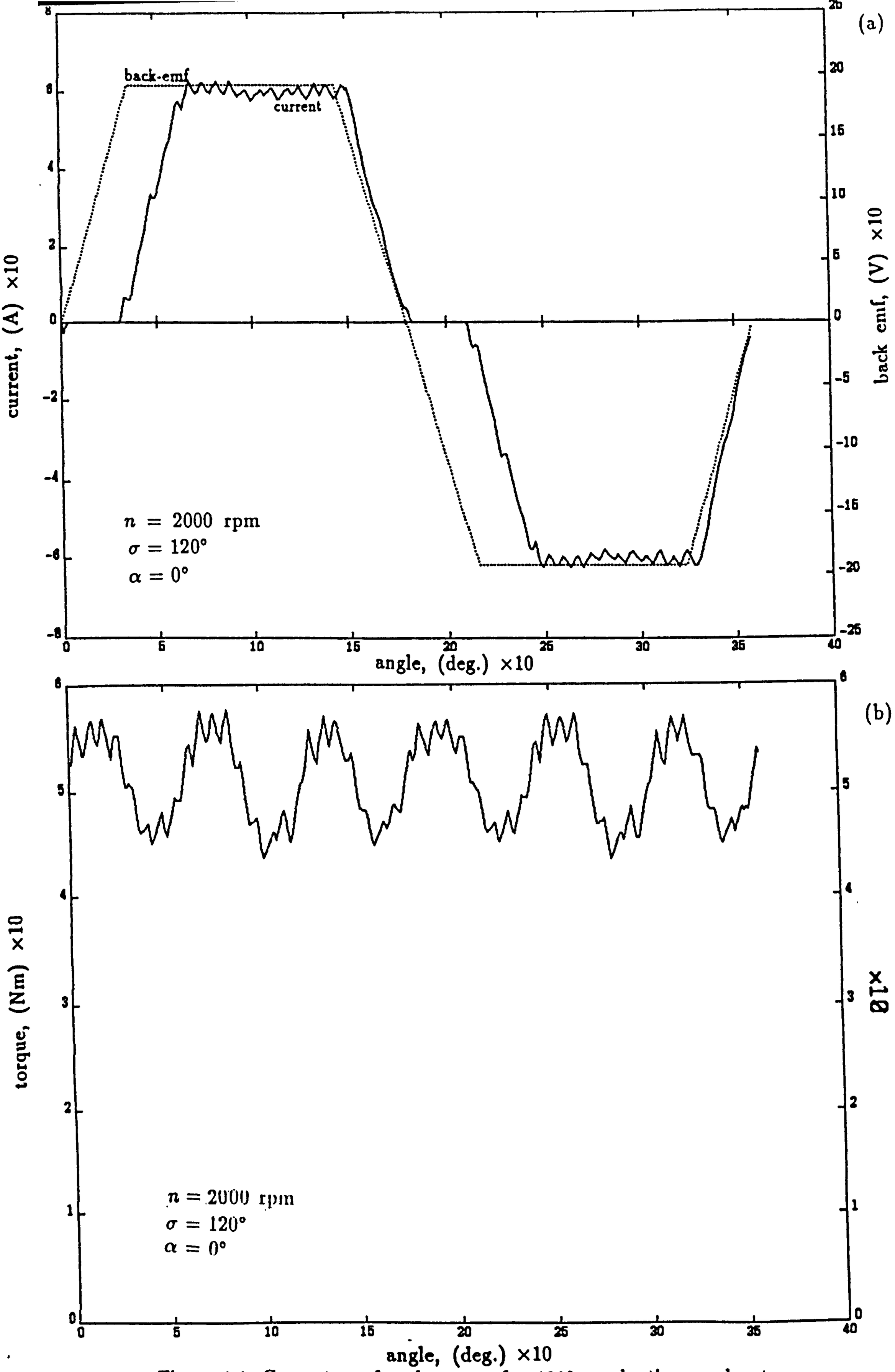

Figure 4.4 Current, emf and torque for 120° conduction angle at 2000 rpm, L=3.1 mH, and phase advance = 0°.

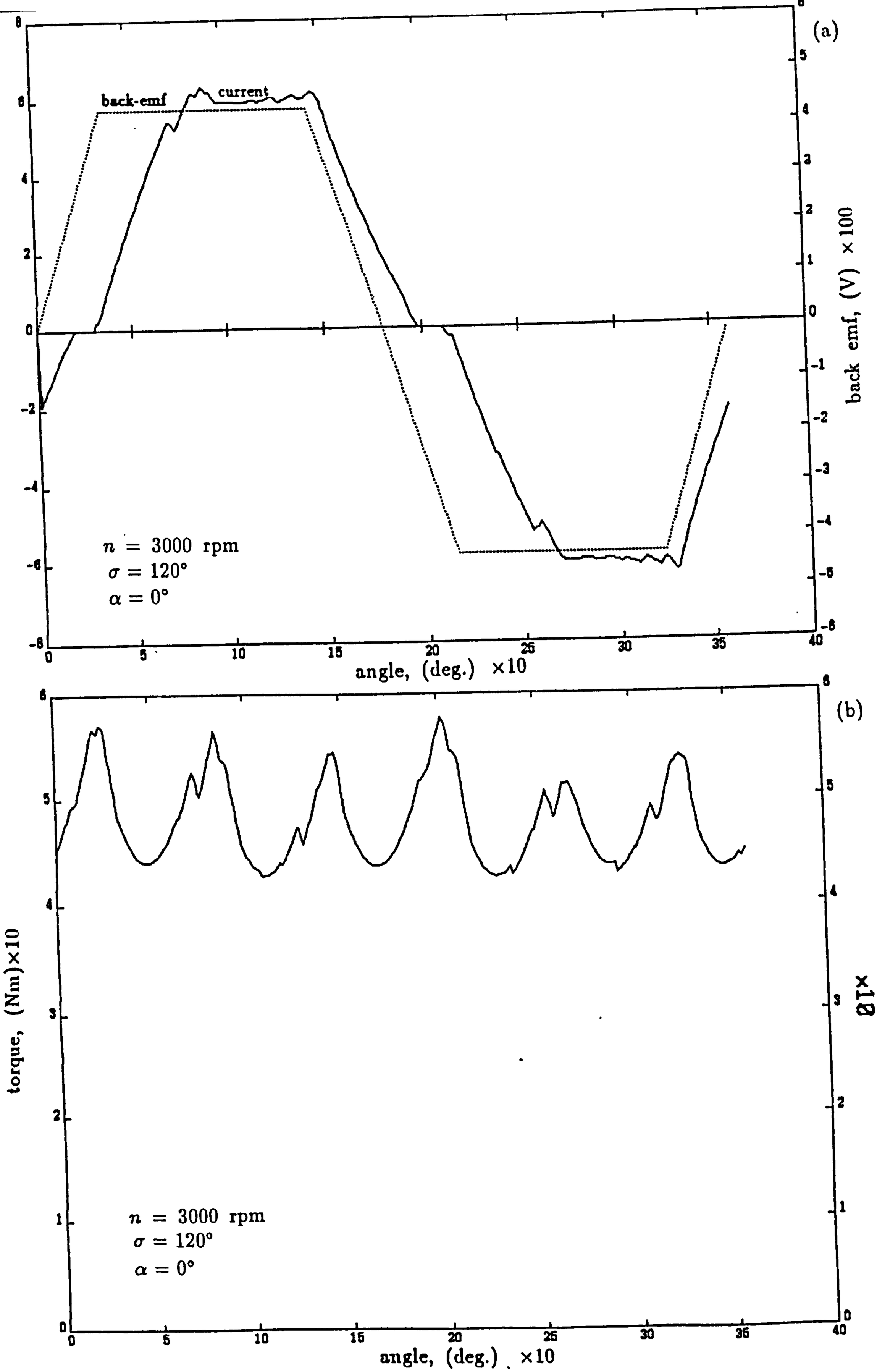

Figure 4.5 Current, emf and torque for 120° conduction angle at 3000 rpm, L=3.1 mH, and phase advance = 0°.

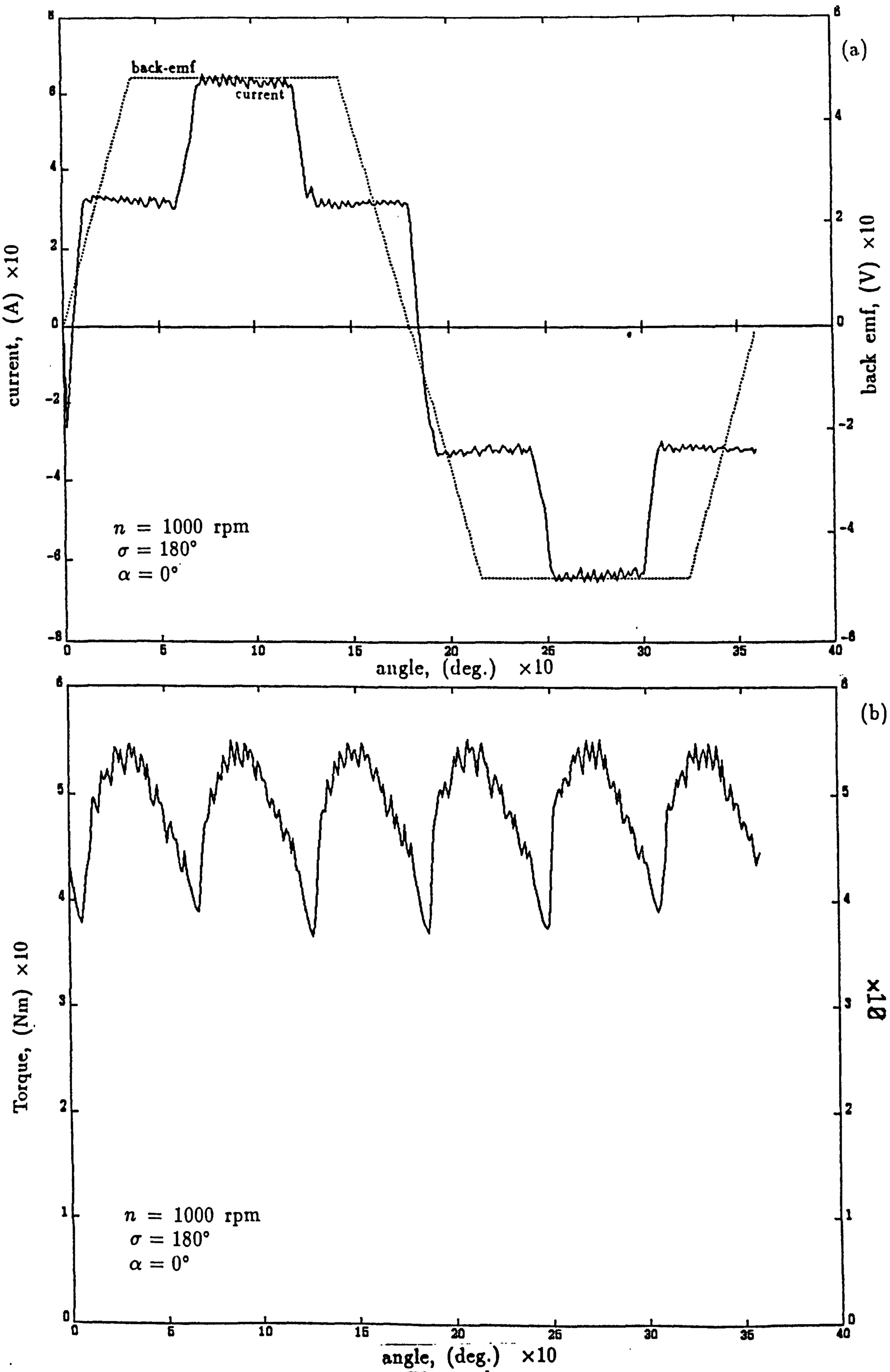

Figure 4.6 Current, emf and torque for 180° conduction angle at 1000 rpm, L=3.1 mH, and phase advance = 0°.

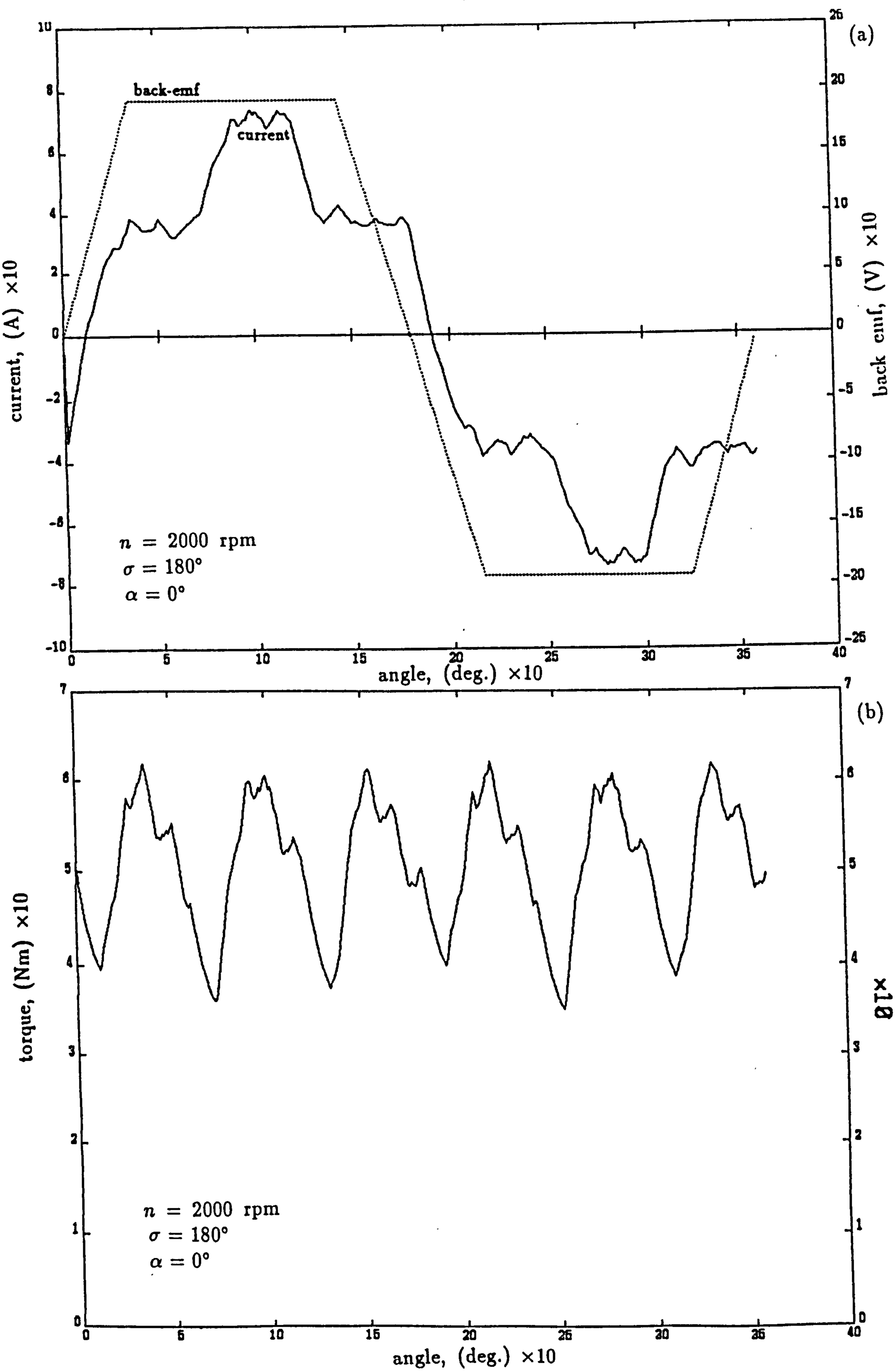

Figure 4.7 Current, emf and torque for 180° conduction angle at 2000 rpm, L=3.1 mH, and phase advance = 0°.

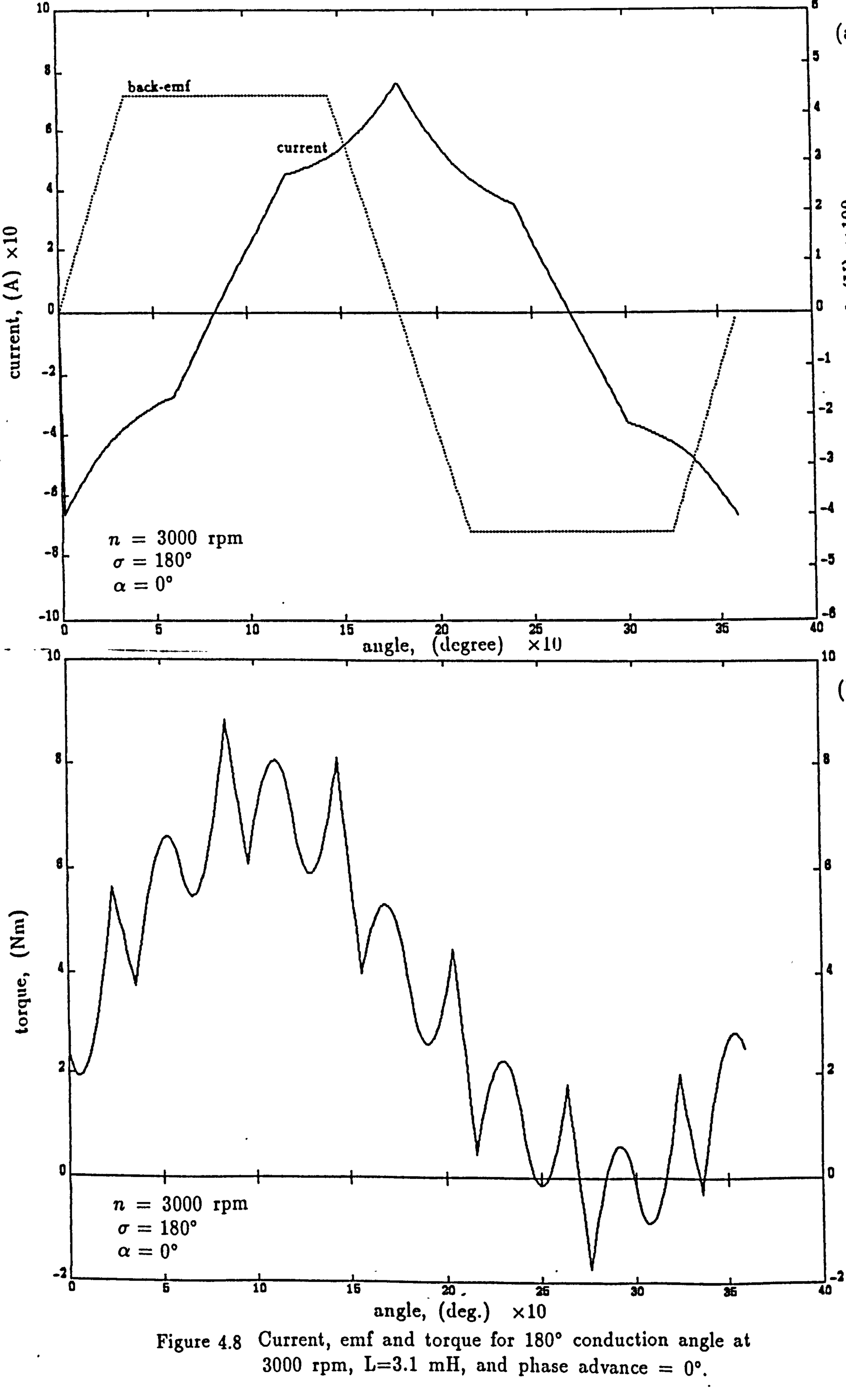

Figure 4.8 Current, emf and torque for 180° conduction angle at 3000 rpm, L=3.1 mH, and phase advance = 0°.

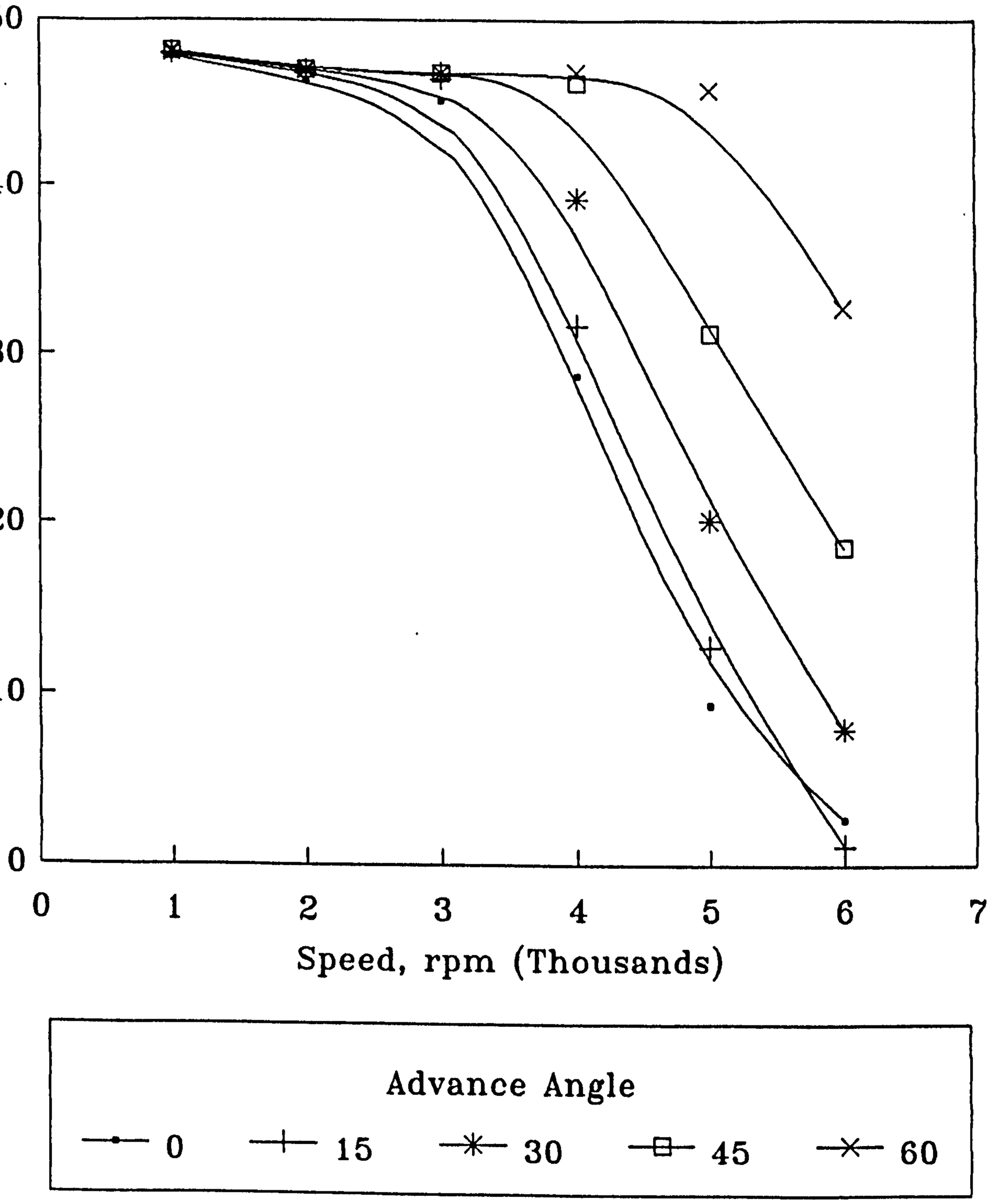

Figure 4.9 current/speed characteristics for various phase advance angles using 120° conduction angle

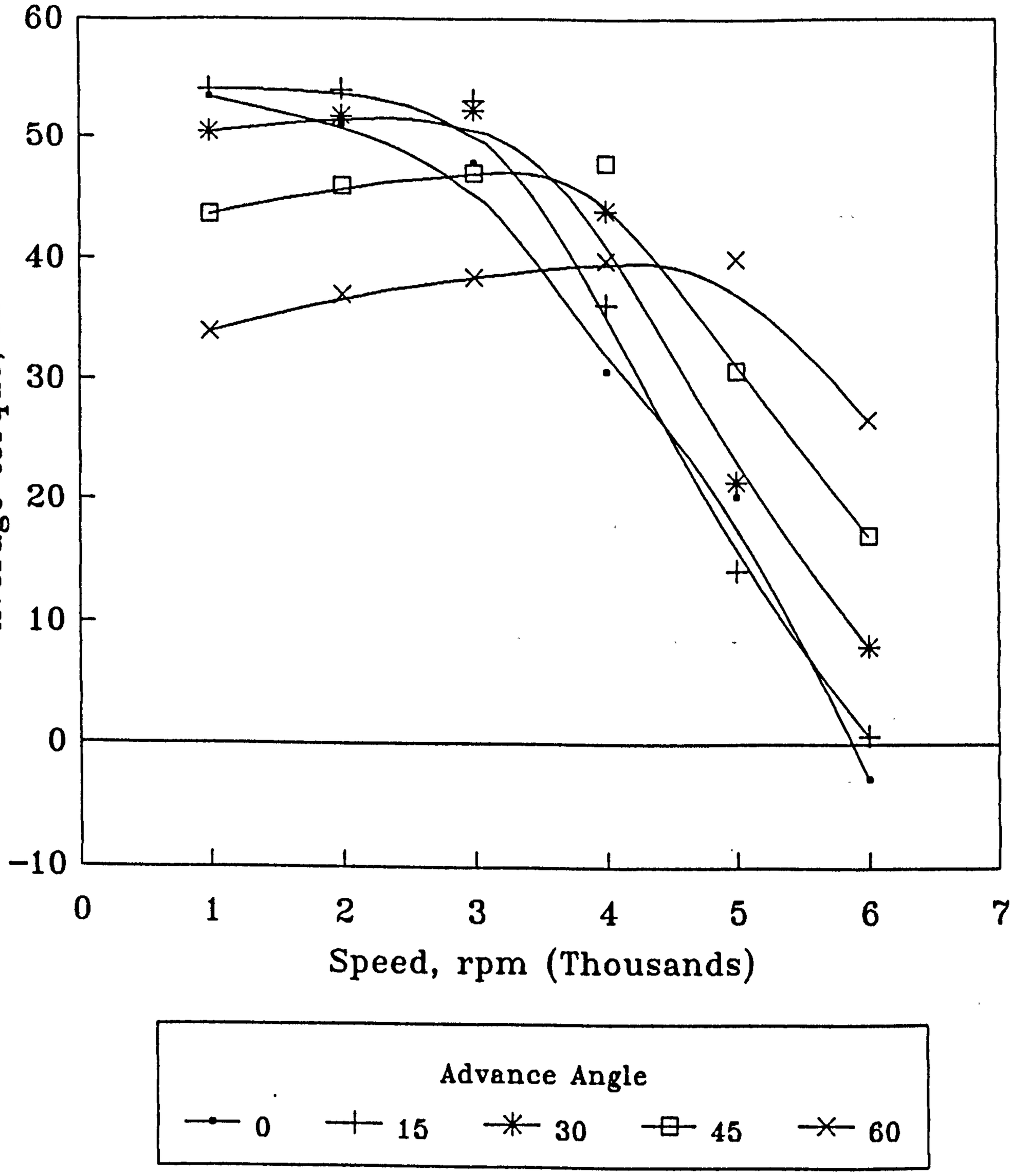

Figure 4.10 Torque/speed characteristics for various phase advance angles using 120° conduction angle

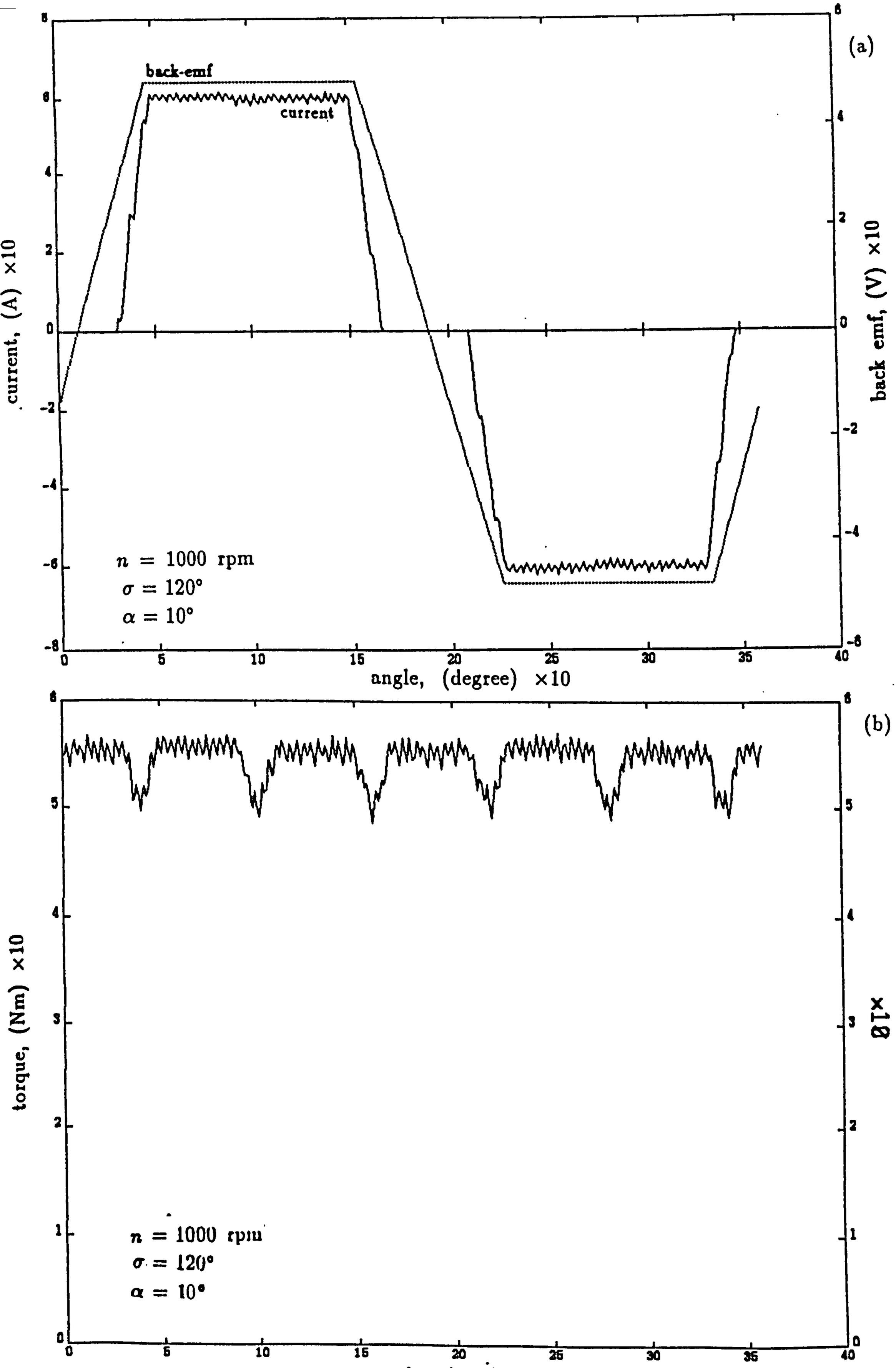

Figure 4.11 Current, emf and torque for 120° conduction angle at 1000 rpm, L=3.1 mH, and phase advance = 10°.

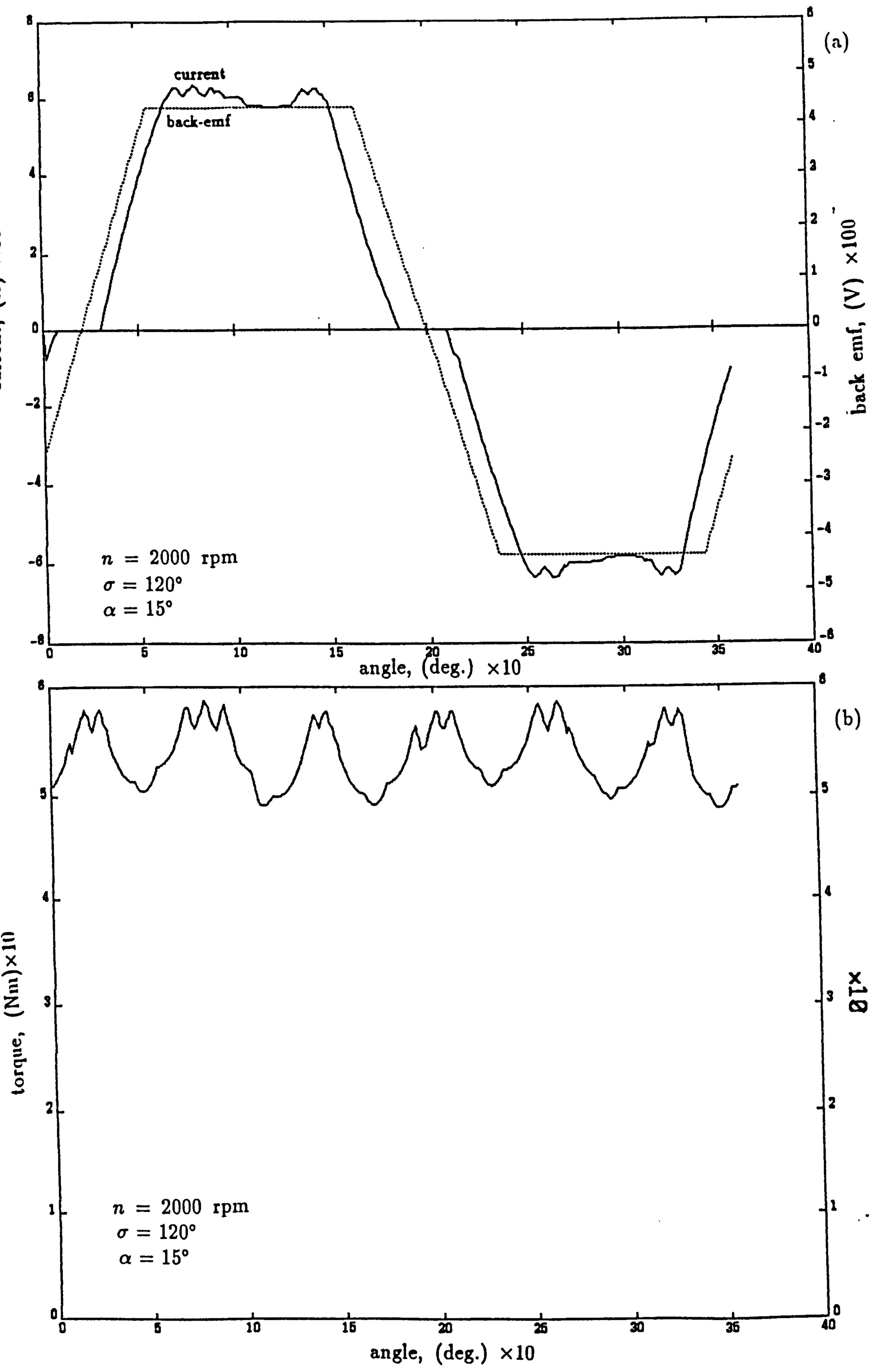

Figure 4.12 Current, emf and torque for 120° conduction angle at 2000 rpm, L=3.1 mH, and phase advance = 15°.

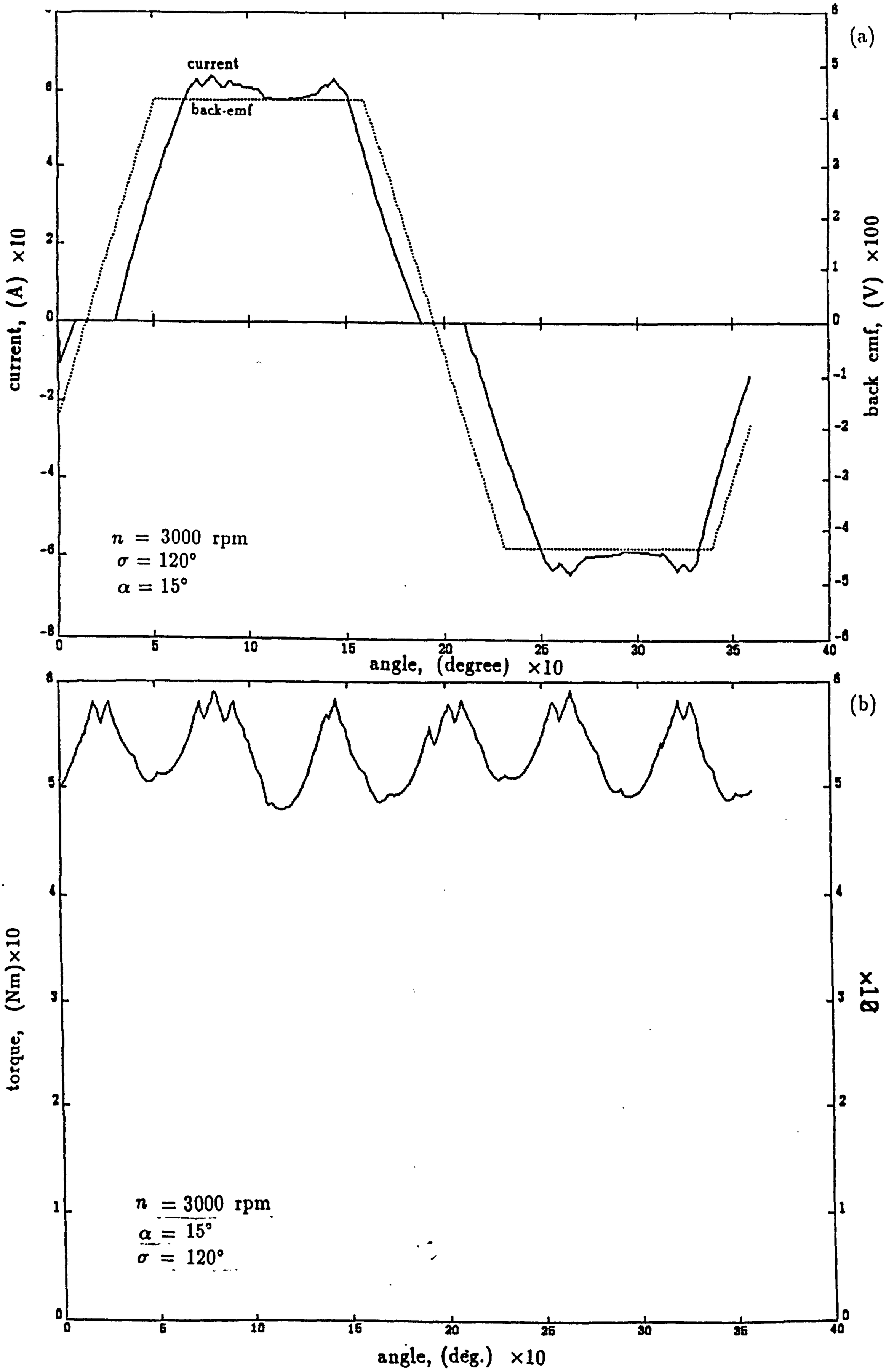

Figure 4.13 Current, emf and torque for 120° conduction angle at 3000 rpm, L= 3.1 mH, and phase advance = 15°

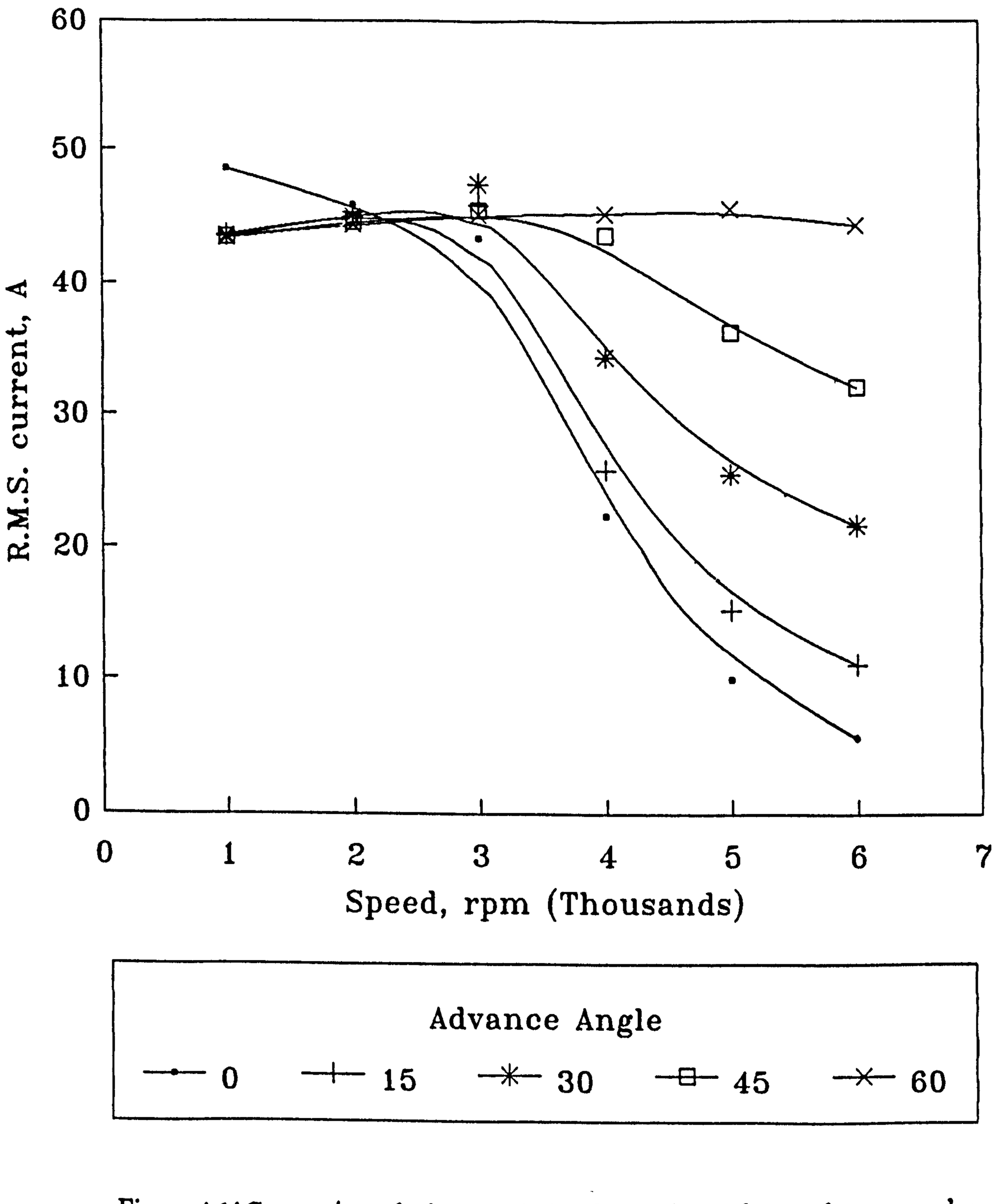

Figure 4.14 Current/speed characteristics for various phase advance angles using 180° conduction angle

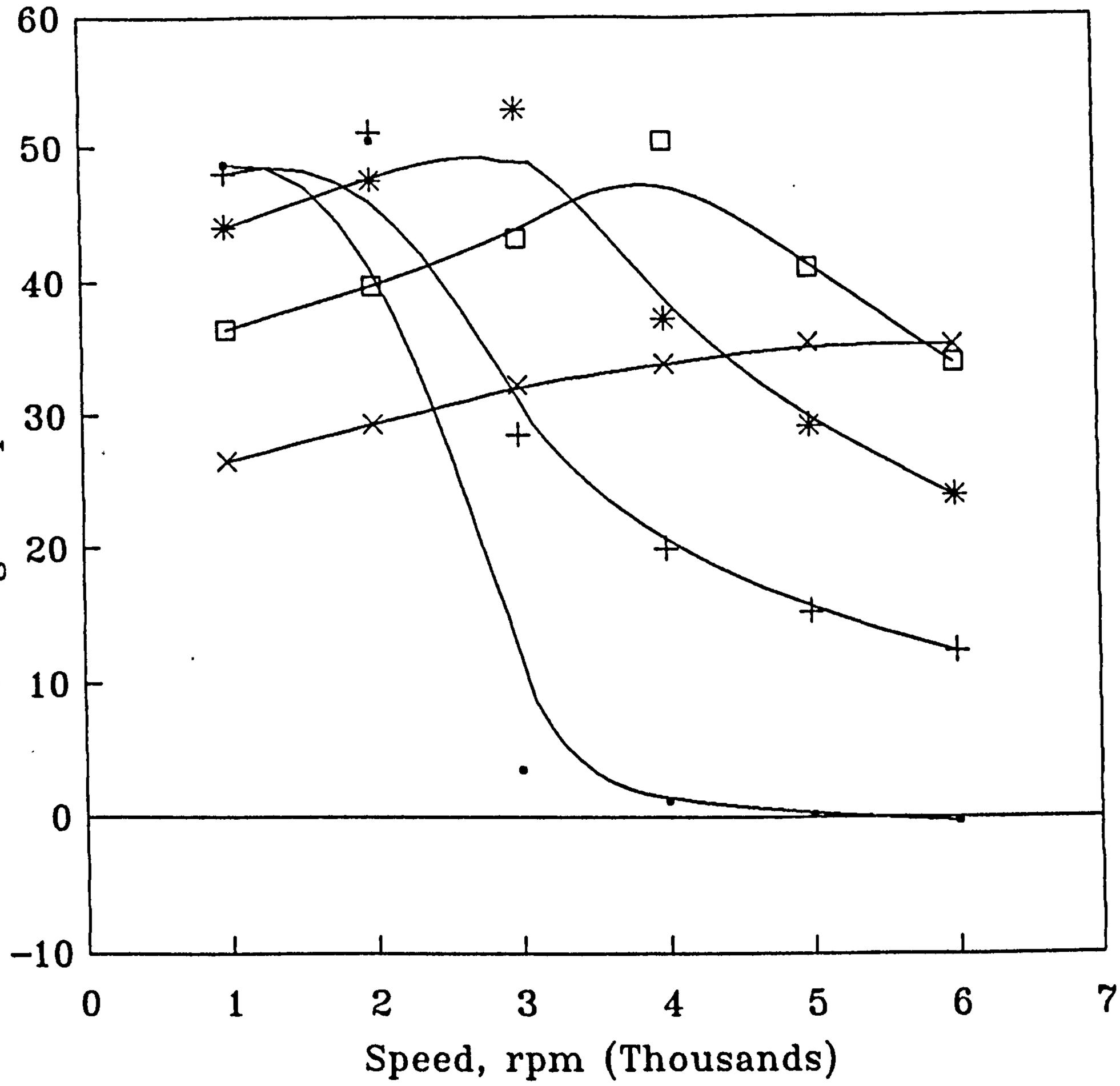

Figure 4.15 Torque/speed characteristics for various phase advance angles using 180° conduction angle

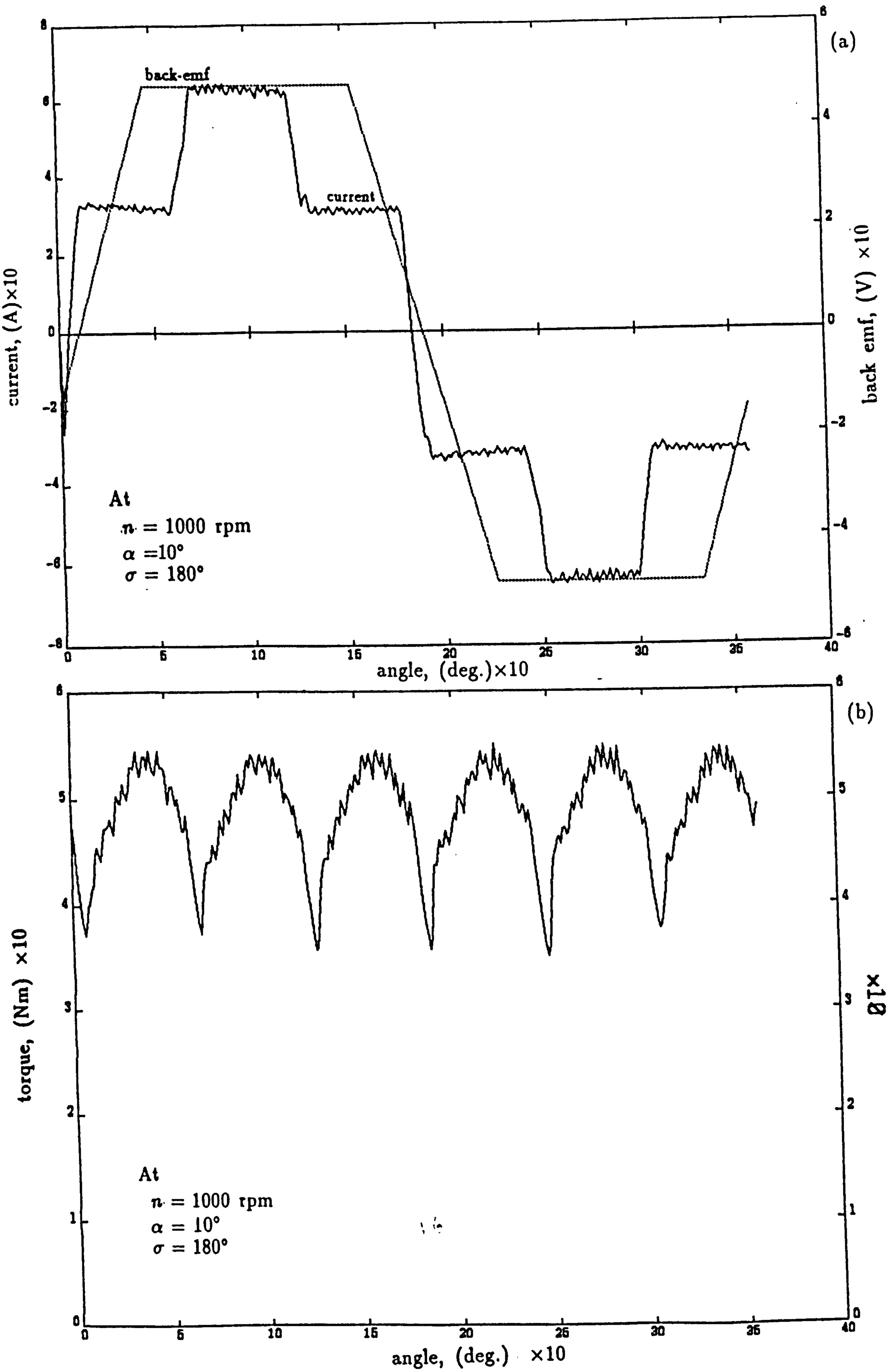

Figure 4.16 Current, emf and torque for 180° conduction angle at 1000 rpm, L=3.1 mH, and phase advance = 10°.

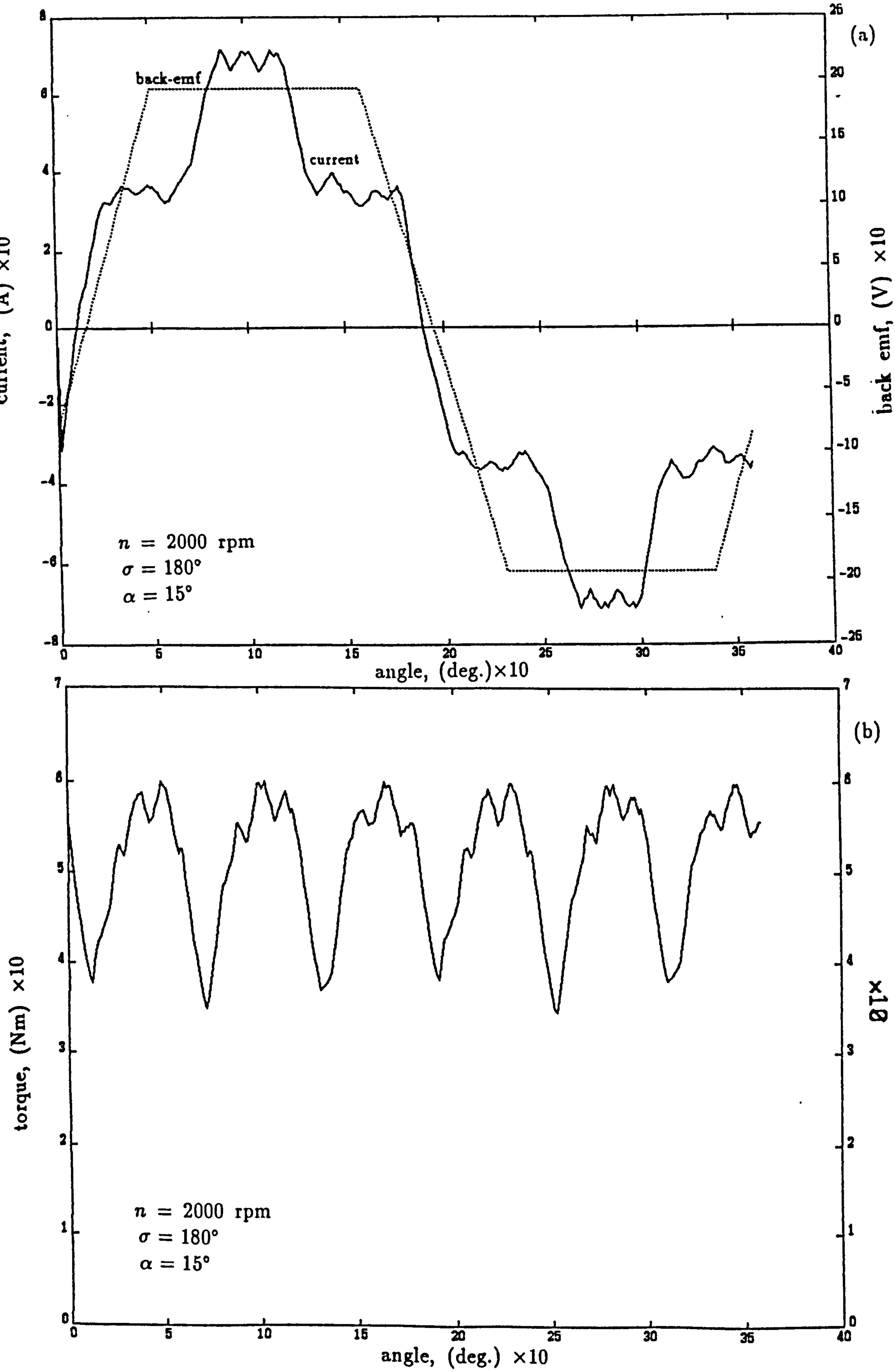

Figure 4.17 Current, emf and torque for 180° conduction angle at 2000 rpm, L=3.1 mH, and phase advance = 15°.

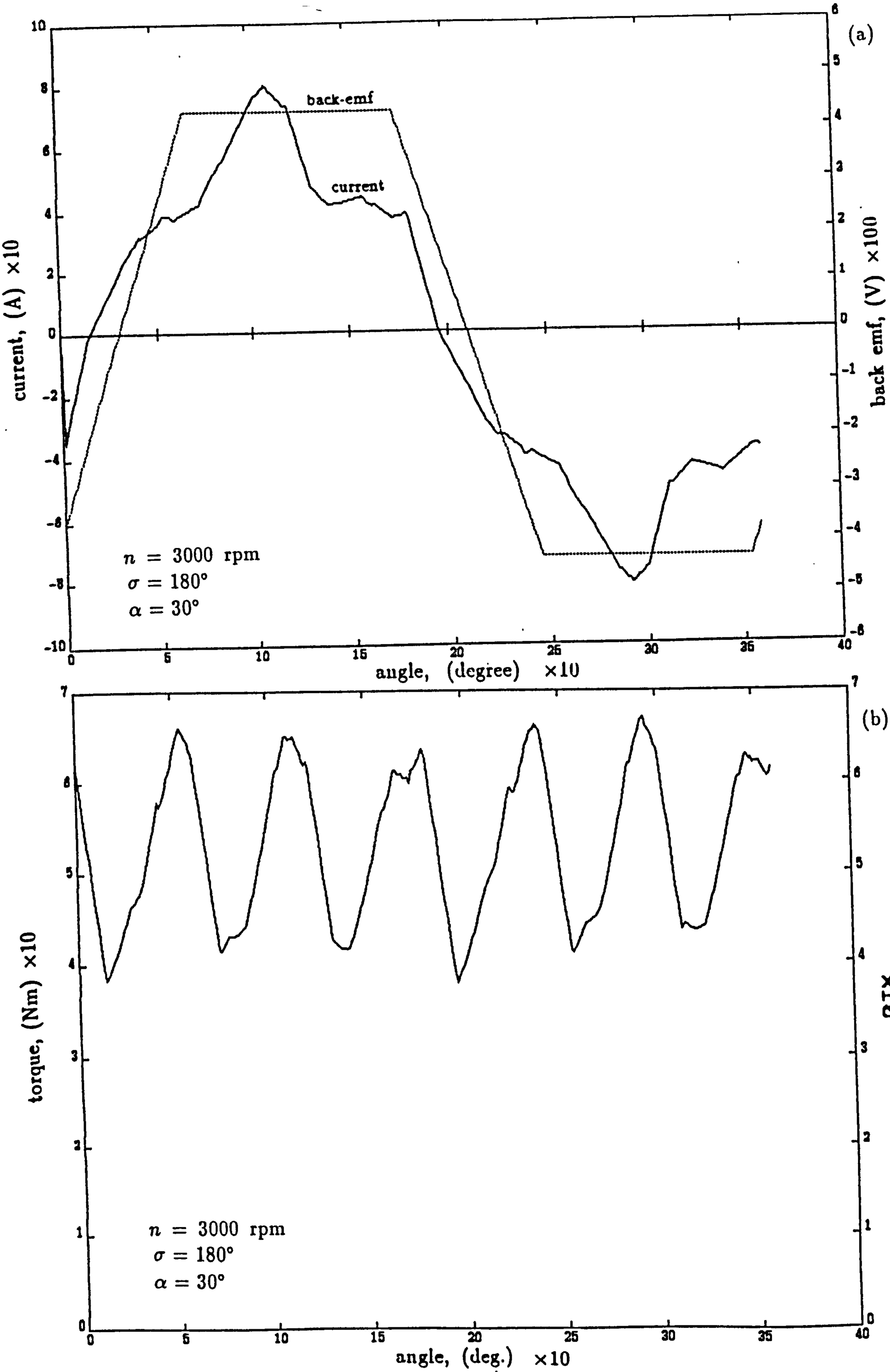

Figure 4.18 Current, emf and torque for 180° conduction angle at 3000 rpm, L=3.1 mH, and phase advance = 30°.

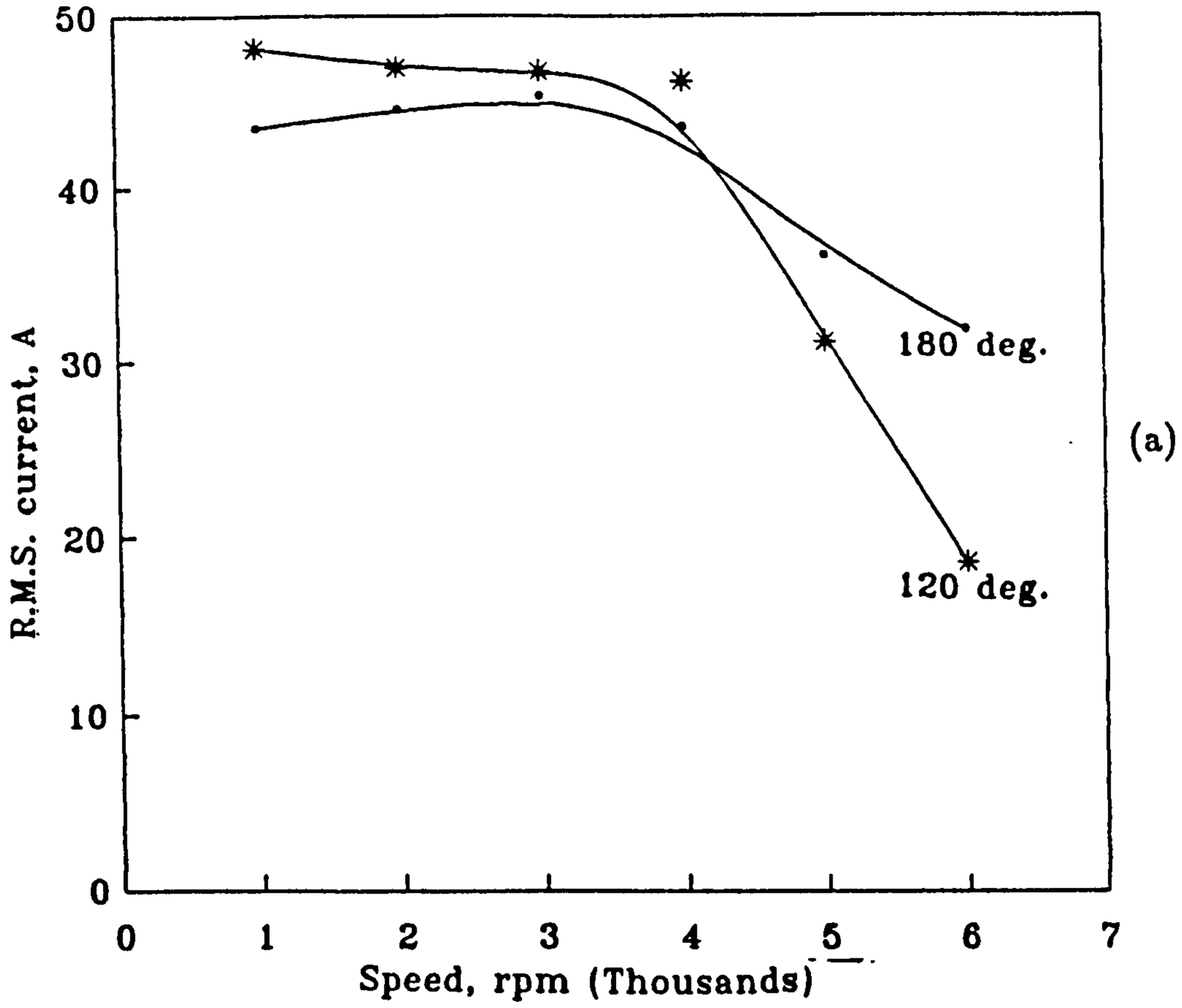

(a)

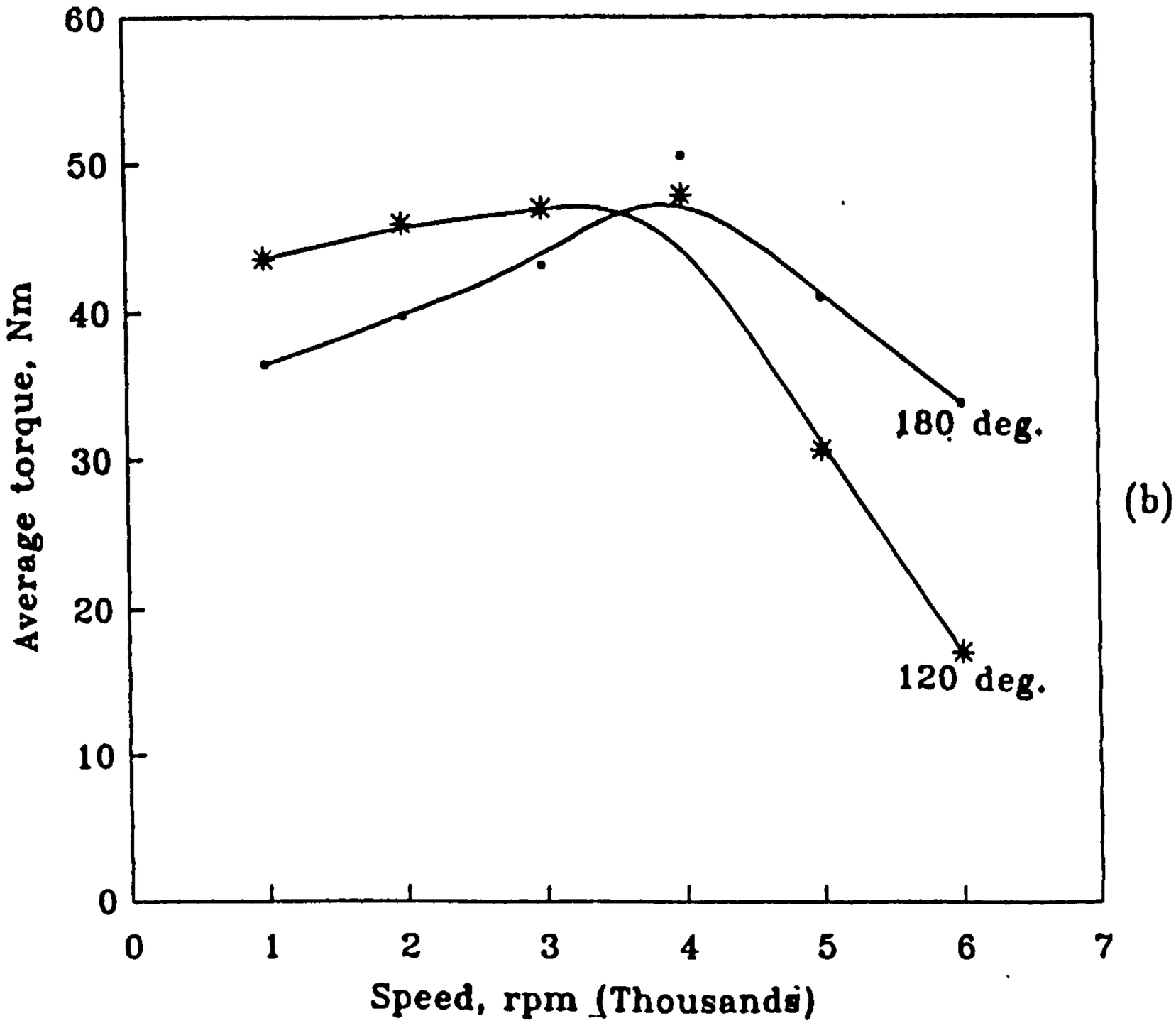

(b)

Figure 4.19 Comparison performance between 120° and 180°
(a) rms current-speed performance
(b) torque-speed performance.

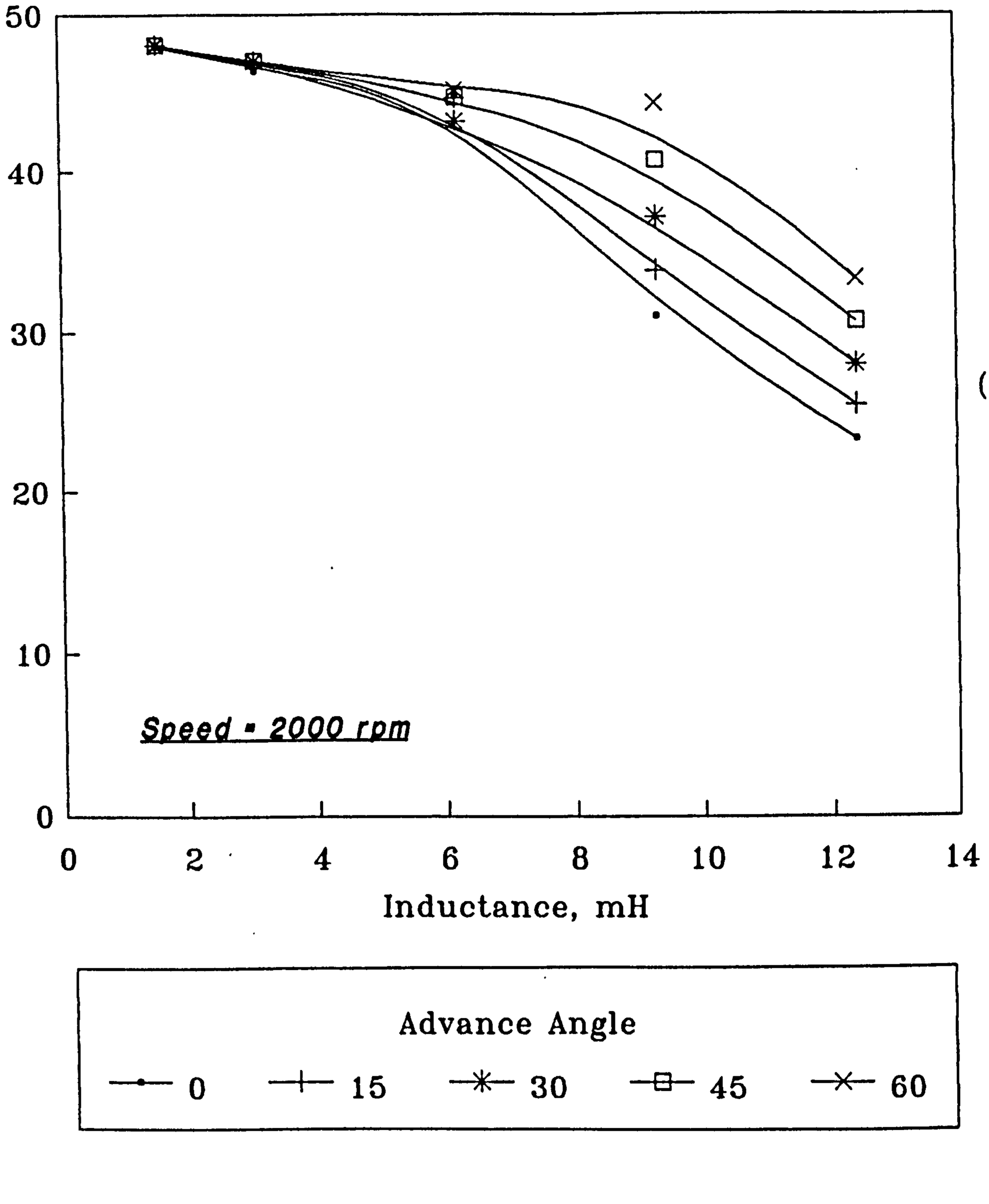

Figure 4.20a Rms current vs inductance characteristics with various values of phase advance using 120° conduction angle

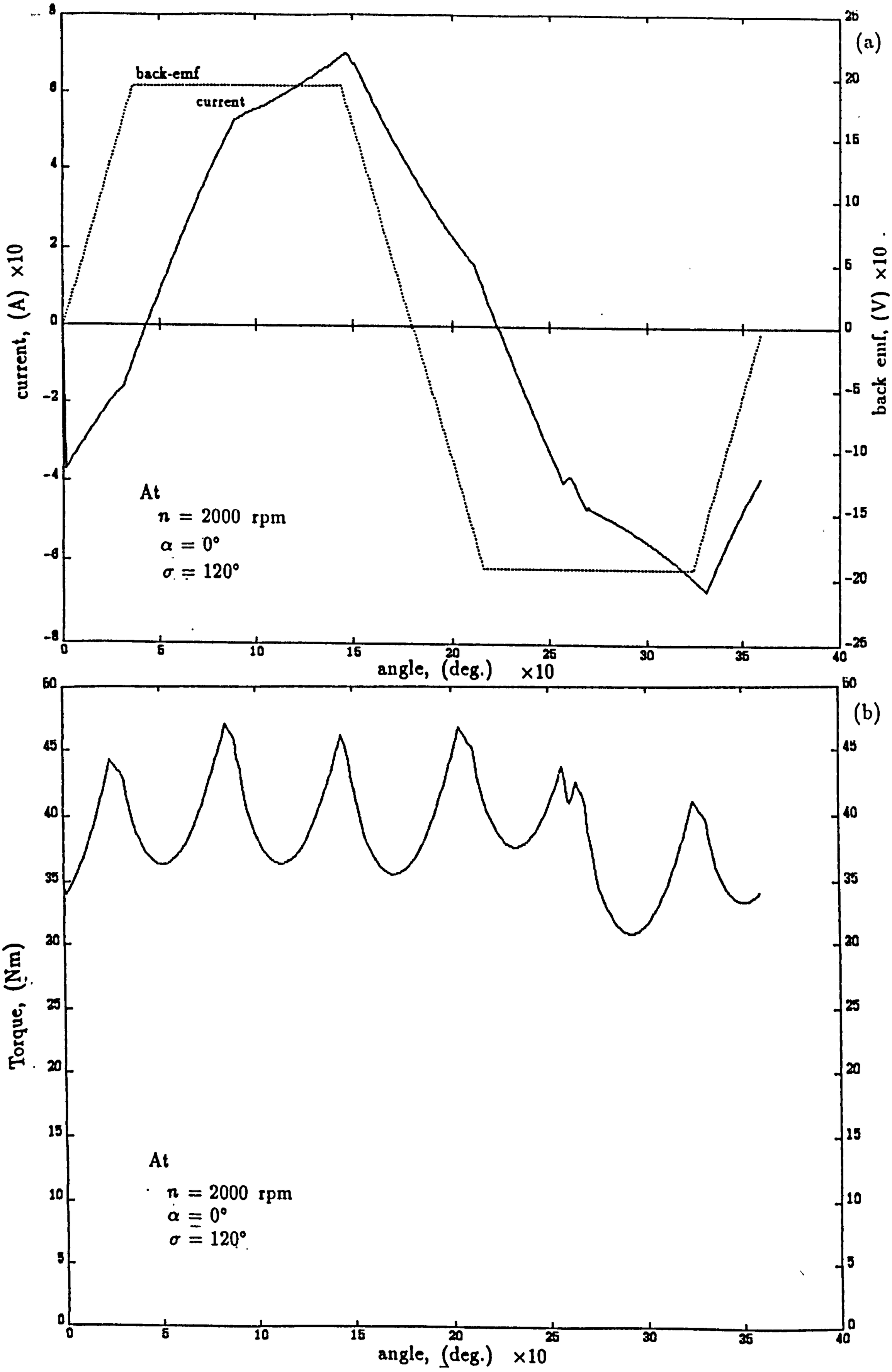

Figure 4.21 Current, emf and torque for 120° conduction angle at 2000 rpm, L=6.2 mH, and phase advance = 0°.

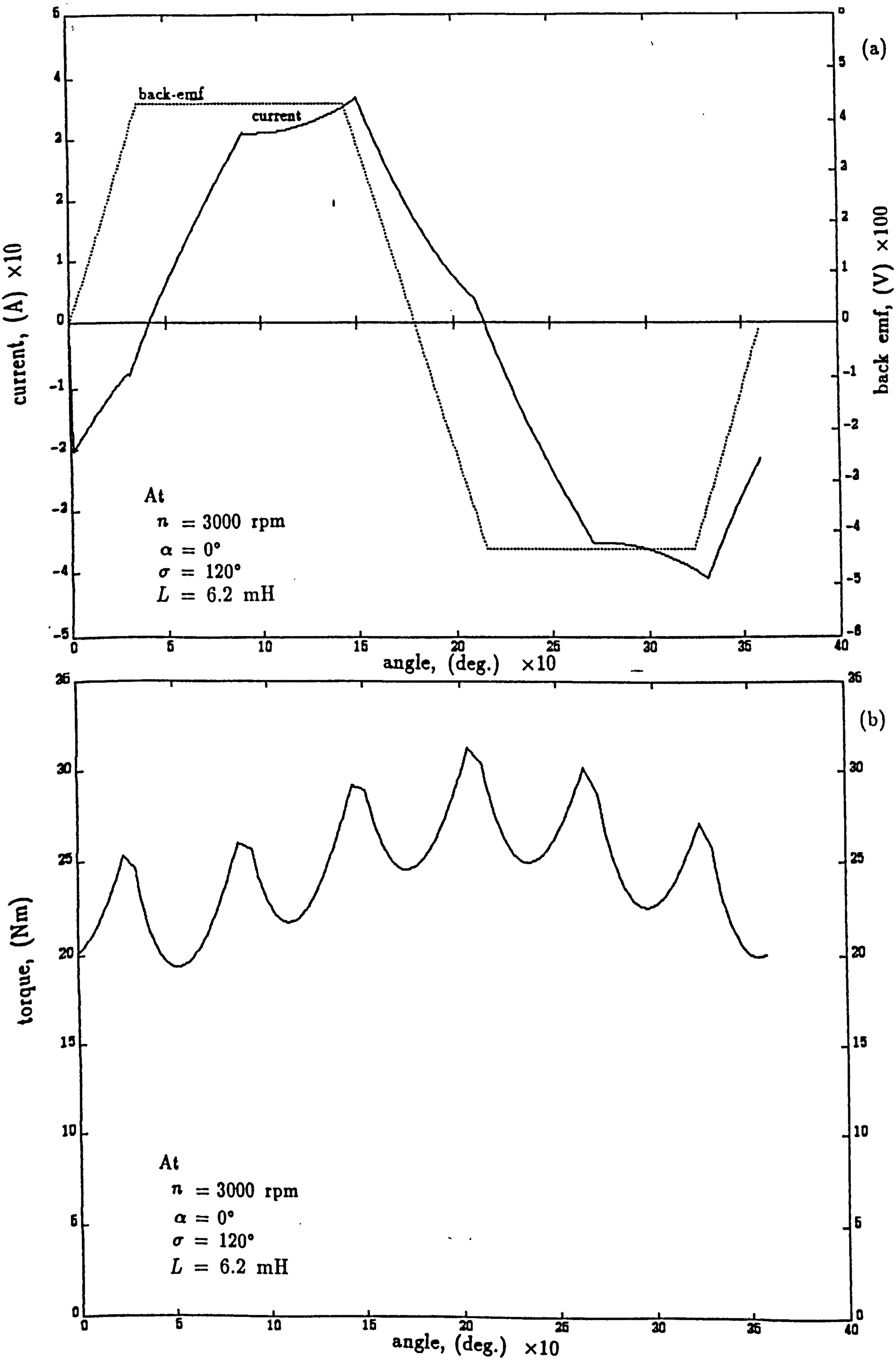

Figure 4.22 Current, emf and torque for 120° conduction angle at 3000 rpm, L=6.2 mH, and phase advance = 0°

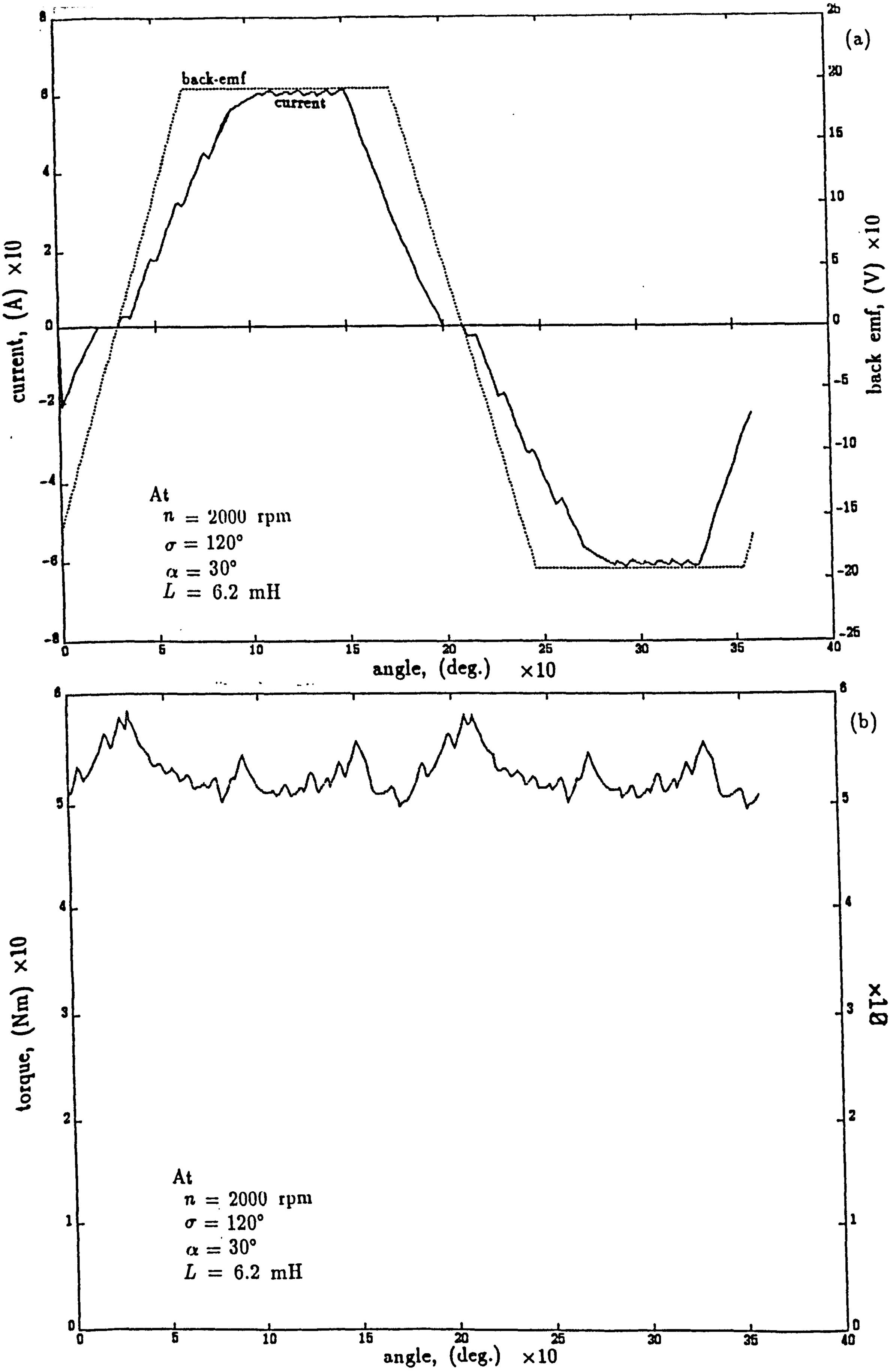

Figure 4.23 Current, emf and torque for 120° conduction angle at 2000 rpm, L=6.2 mH, and phase advance = 30°.

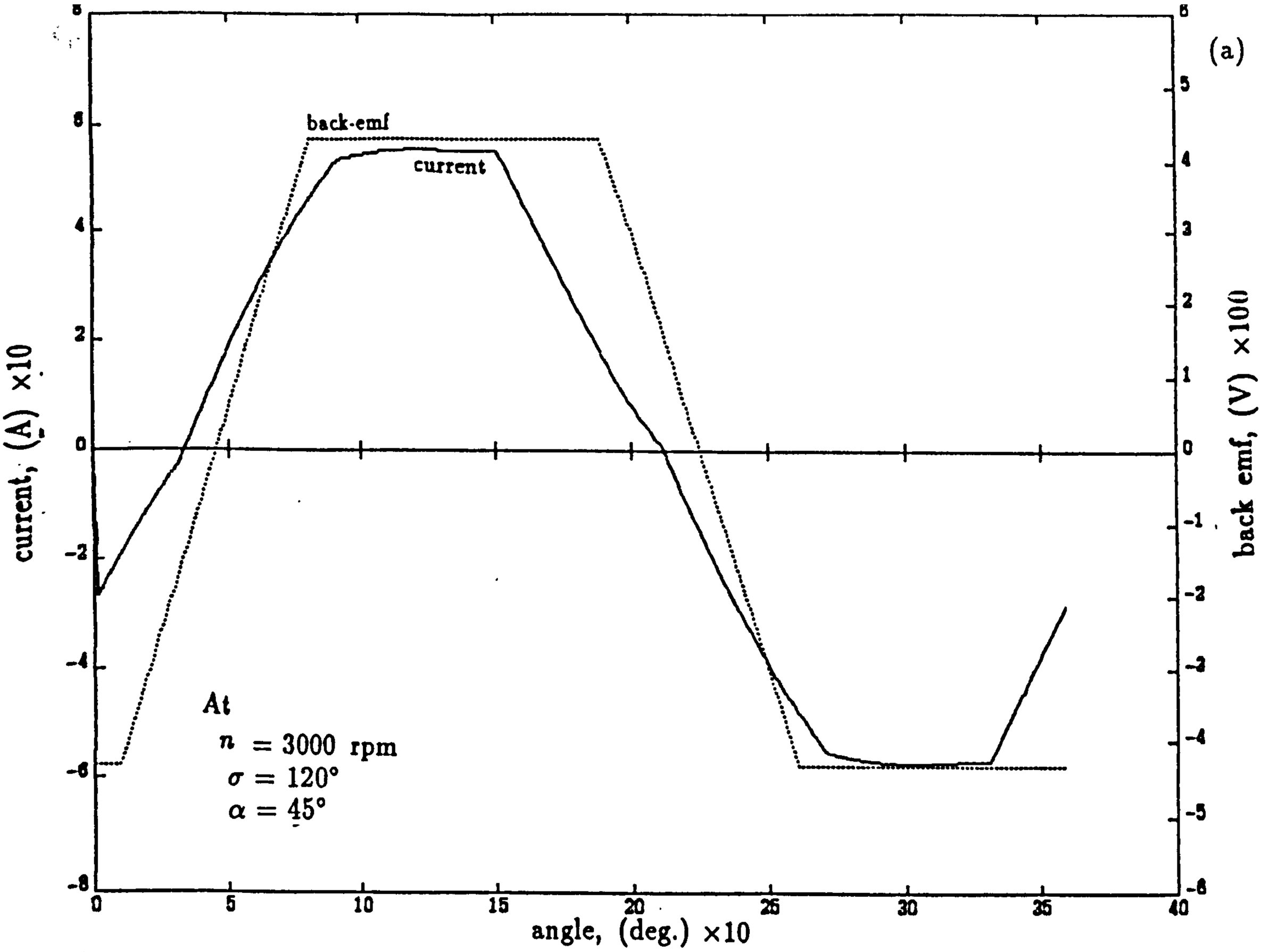

Figure 4.24 Current, emf and torque for 120° conduction angle at 3000 rpm, L=6.2 mH, and phase advance = 45°.

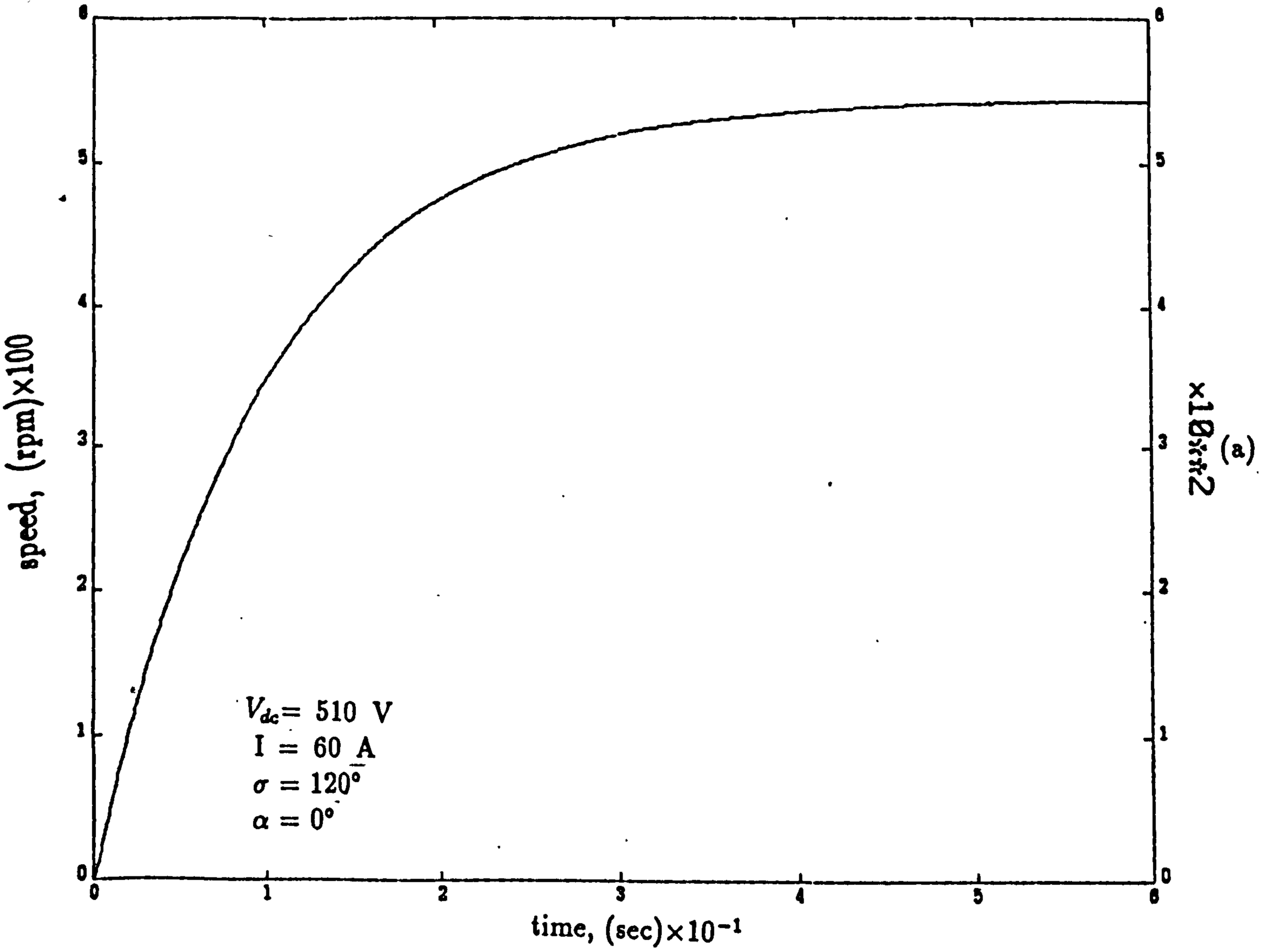
speed, (rpm)×100
V_{dc}= 510 V
I = 60 A
σ = 120°
α = 0°
time, (sec)×10⁻¹
(a)

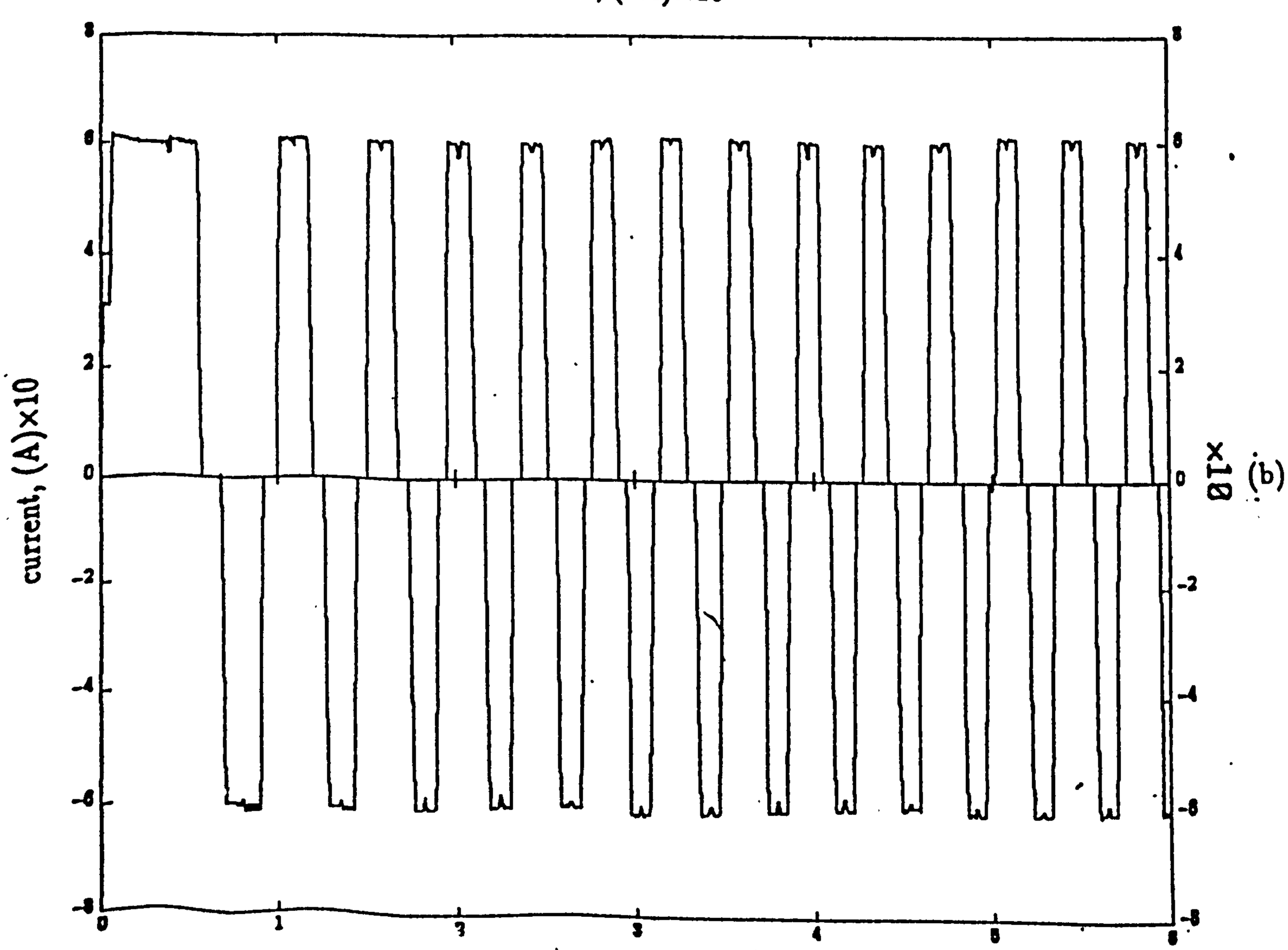
current, (A)×10
time, (sec)×10⁻¹
(b)

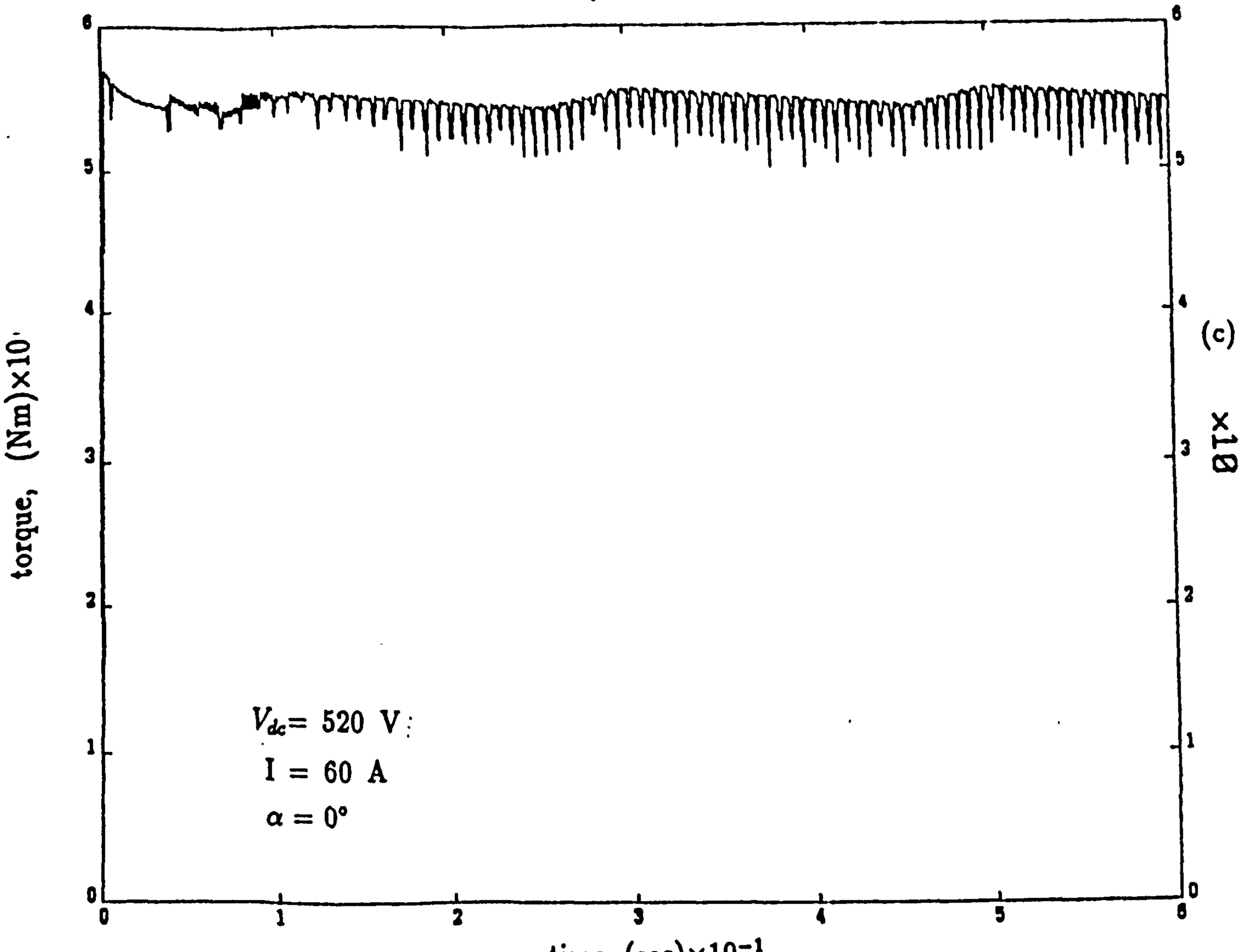

Figure 4.25 Speed, current and torque waveforms for 120° during acceleration.

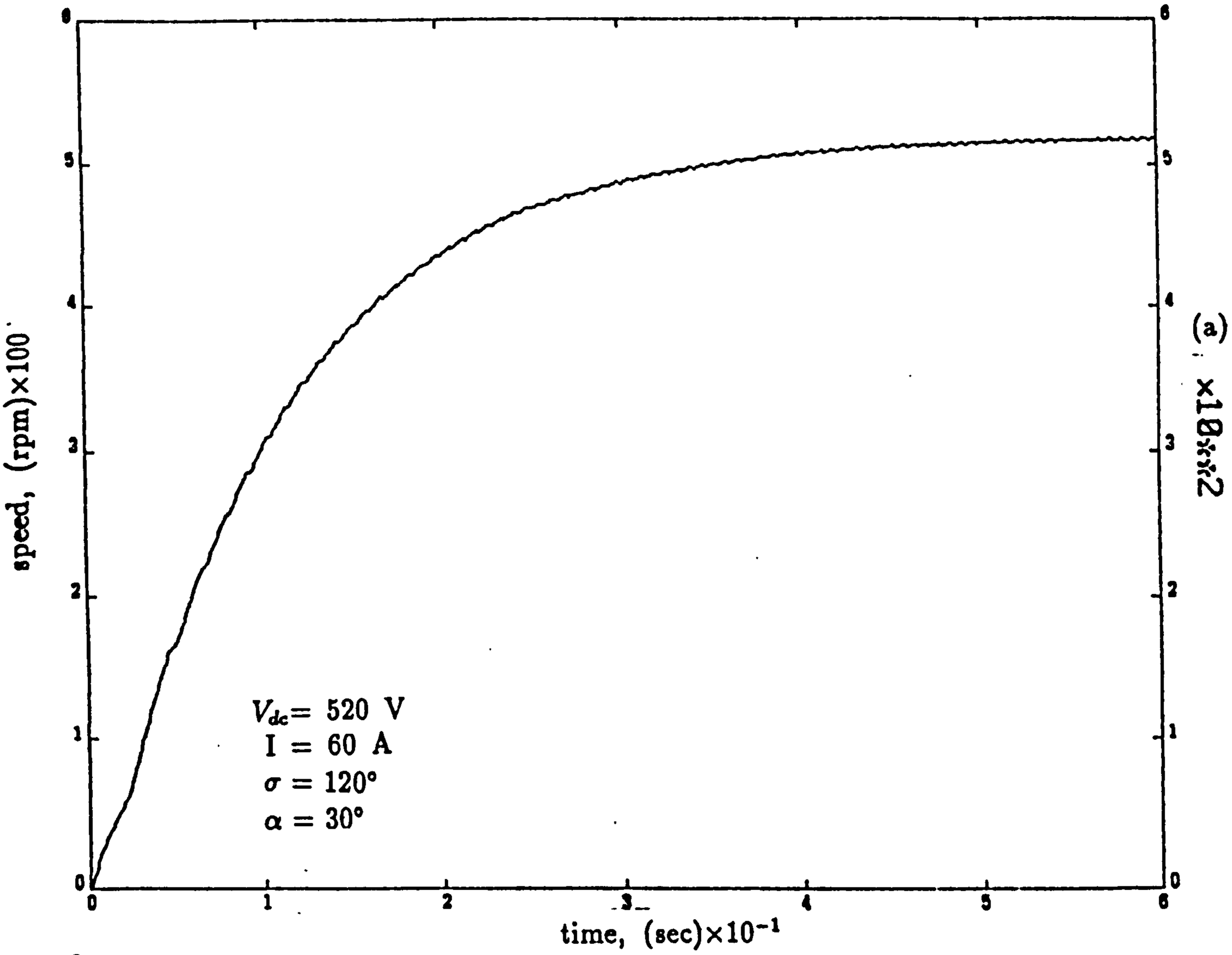
speed, (rpm)×100
time, (sec)×10⁻¹
V_{dc}= 520 V
I = 60 A
σ = 120°
α = 30°
(a)
×10×2

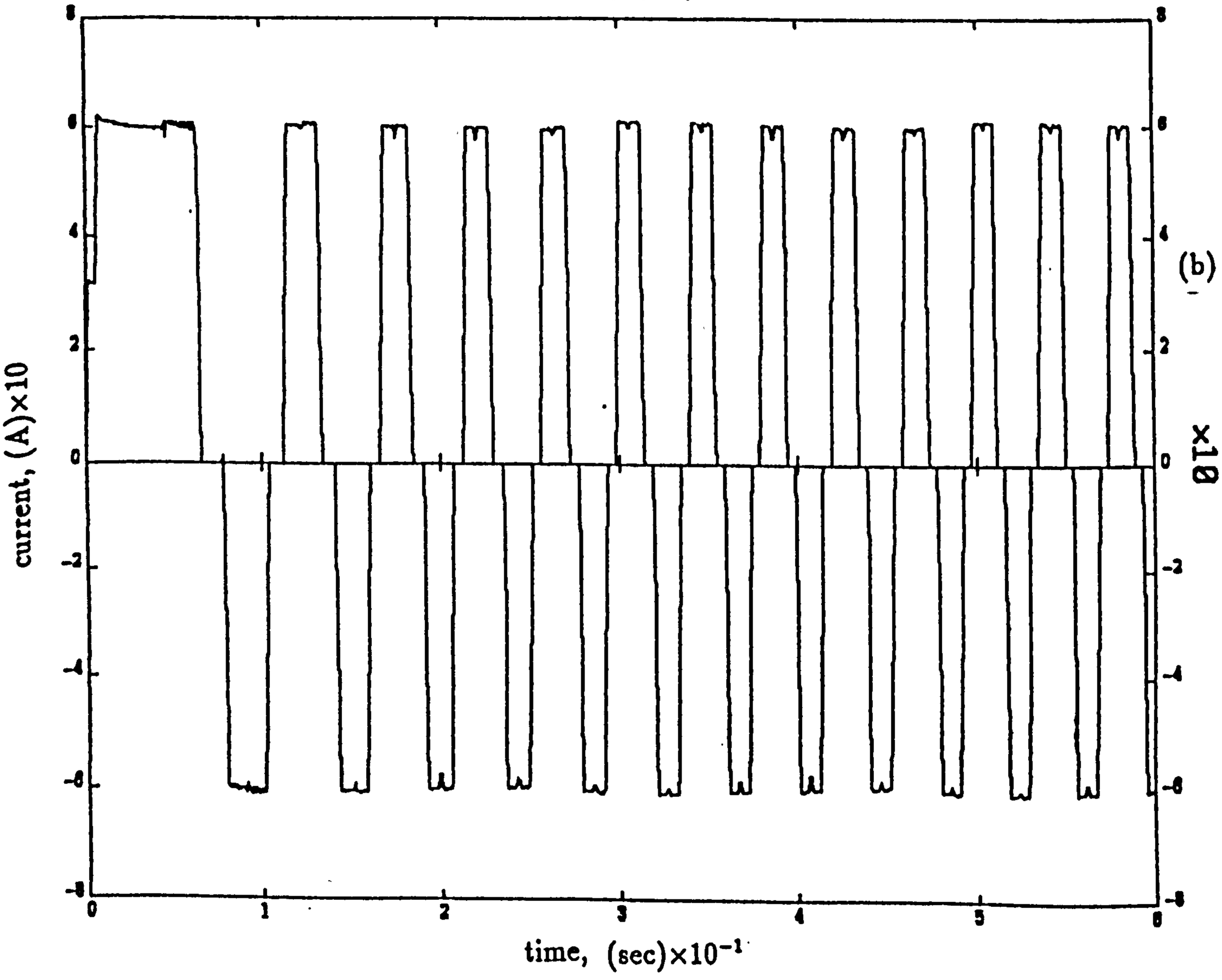
current, (A)×10
time, (sec)×10⁻¹
(b)
×10

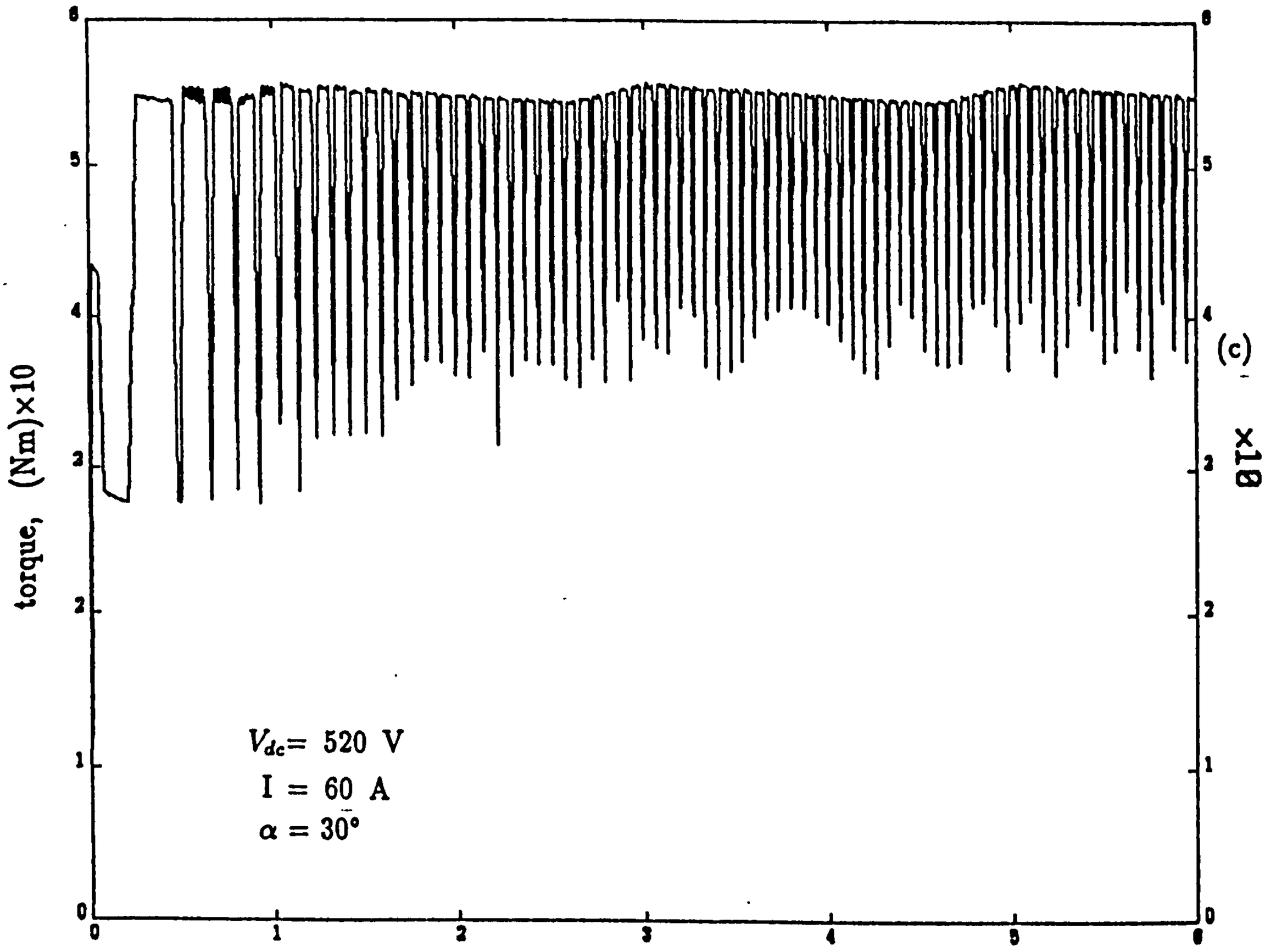

Figure 4.26 Speed, current and torque waveforms for 120° during acceleration.

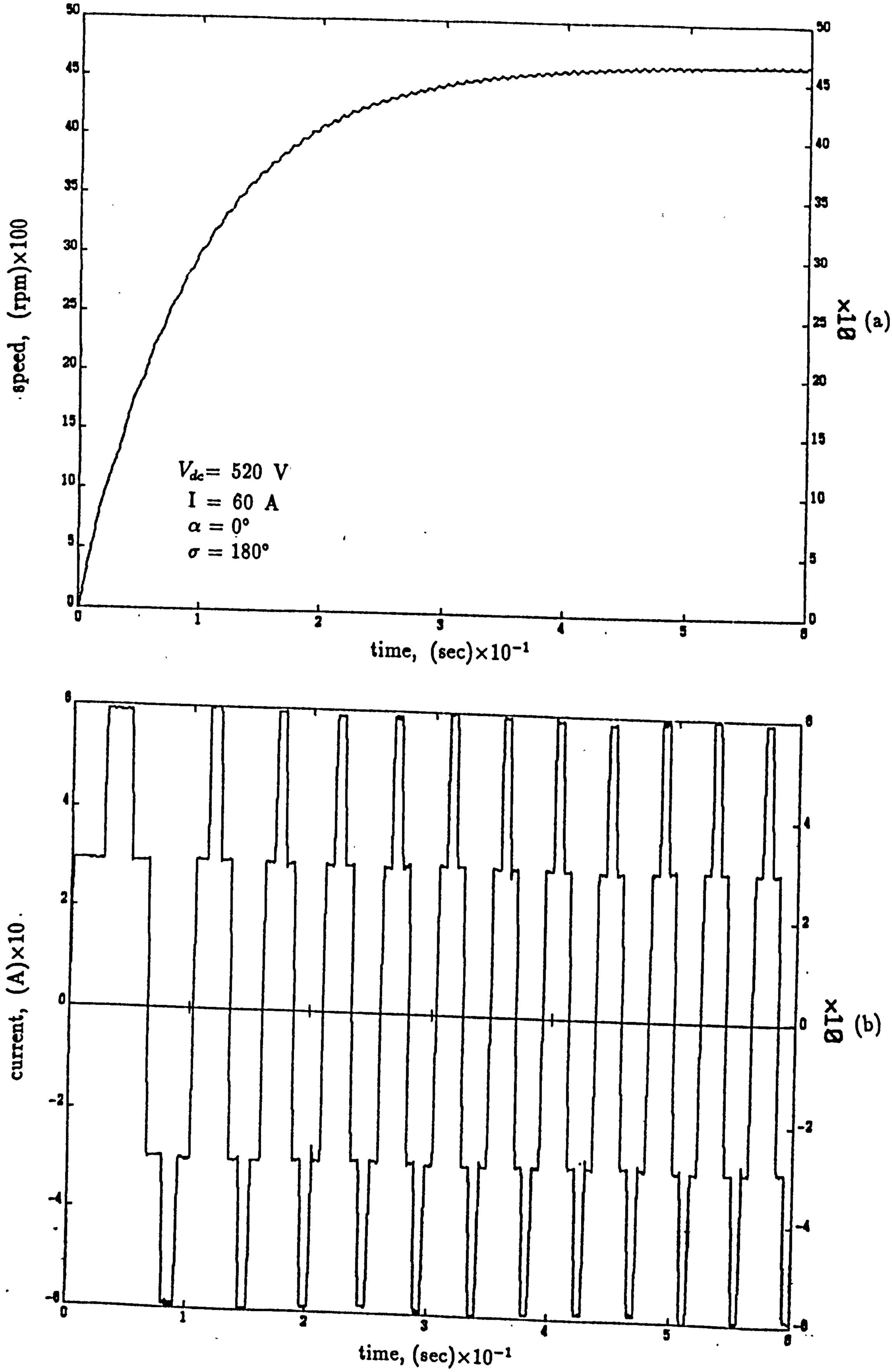
speed, (rpm)×100
50
45
40
35
30
25
20
15
10
5
0
0
1
2
3
4
5
6
time, (sec)×10⁻¹
V_{dc}= 520 V
I = 60 A
$\alpha = 0°$
$\sigma = 180°$
(a)
current, (A)×10
8
4
2
0
-2
-4
-6
(b)

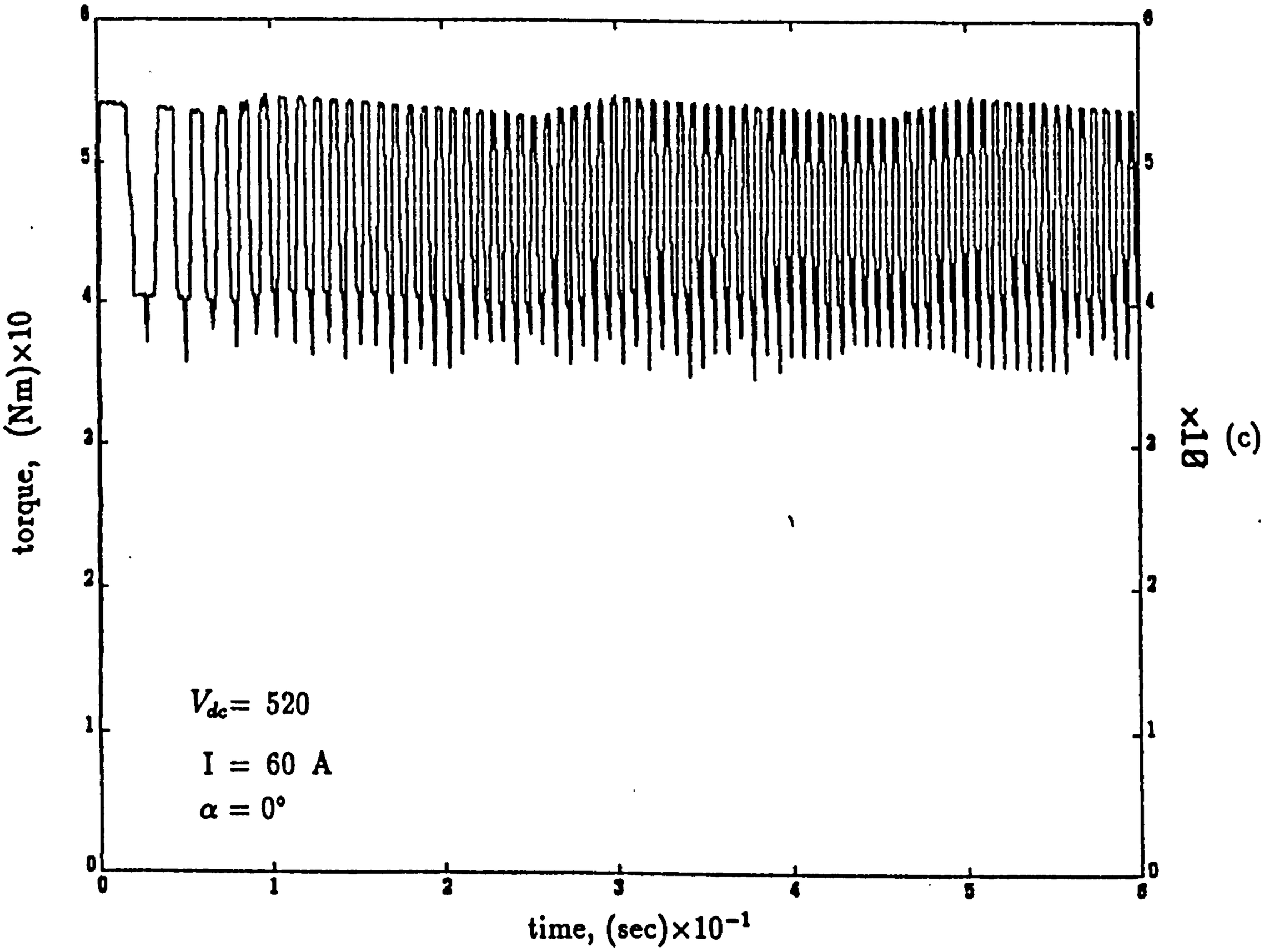

Figure 4.27 Speed, current and torque waveforms for 180° during acceleration.

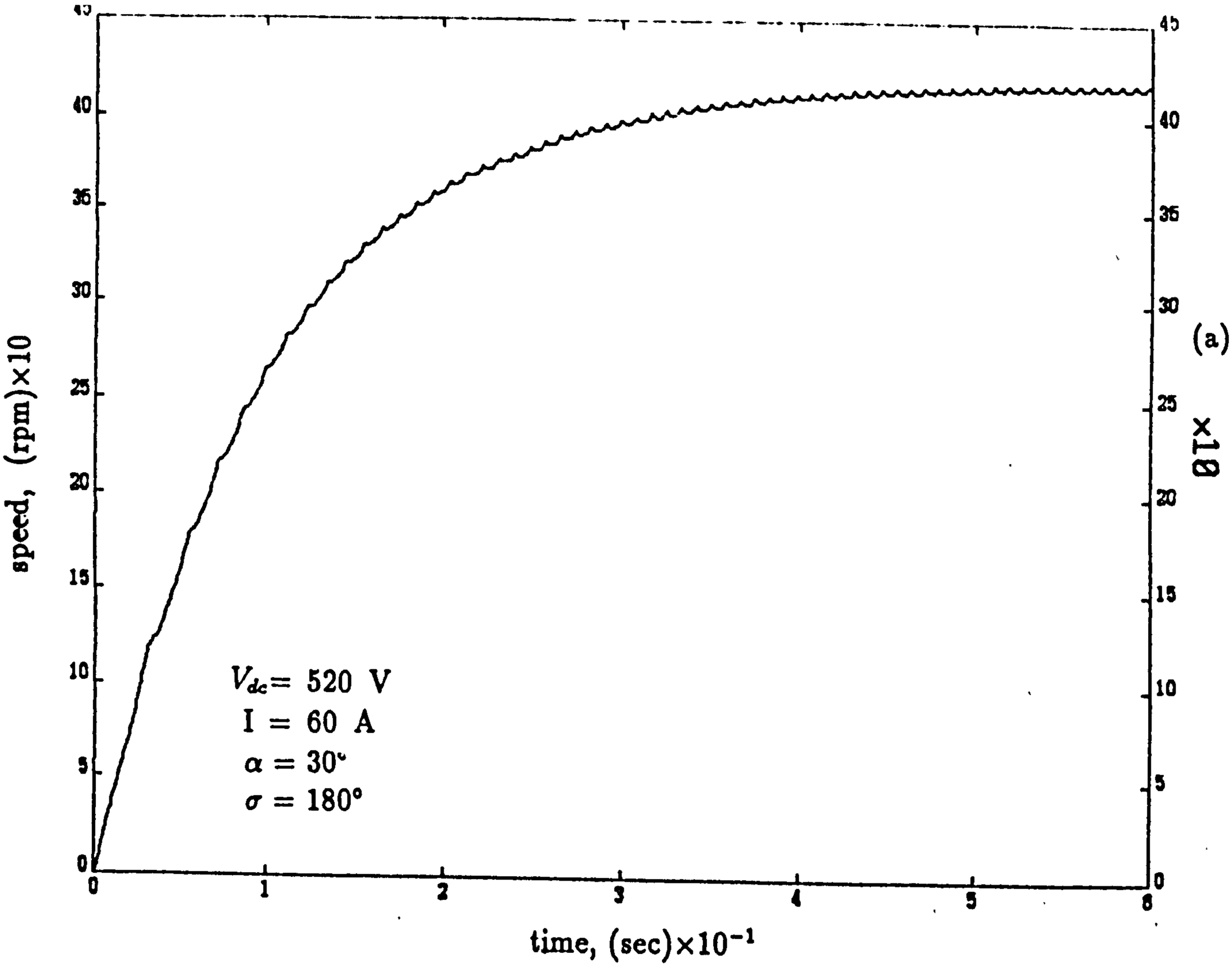
speed, (rpm)×10
0
5
10
15
20
25
30
35
40
45
V_{dc}= 520 V
I = 60 A
$\alpha = 30°$
$\sigma = 180°$
0
1
2
3
4
5
6
time, (sec)×10⁻¹
(a)
θ1×10

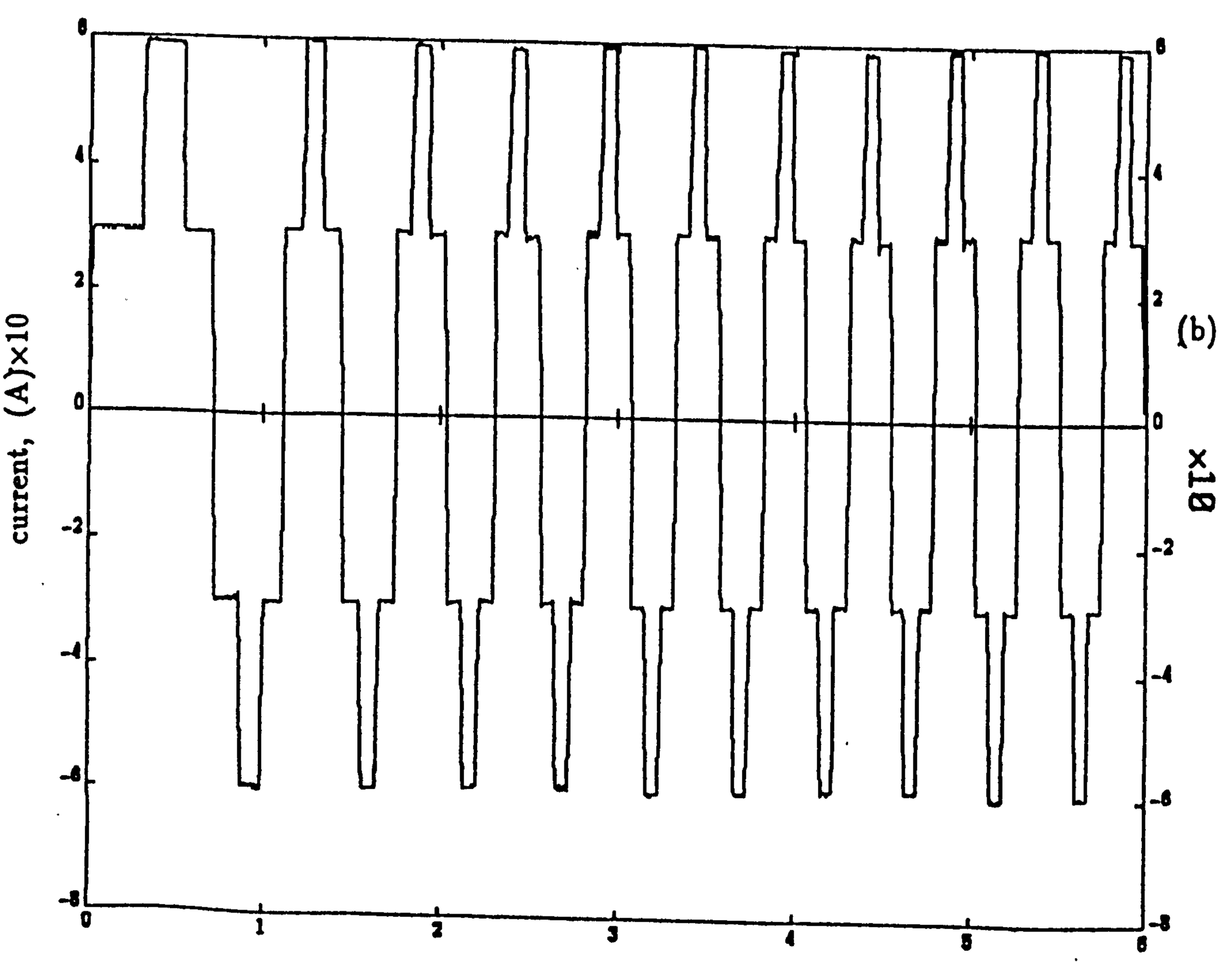
current, (A)×10
6
4
2
0
-2
-4
-6
-8
0
1
2
3
4
5
6
time, (sec)×10⁻¹
(b)
θ1×10

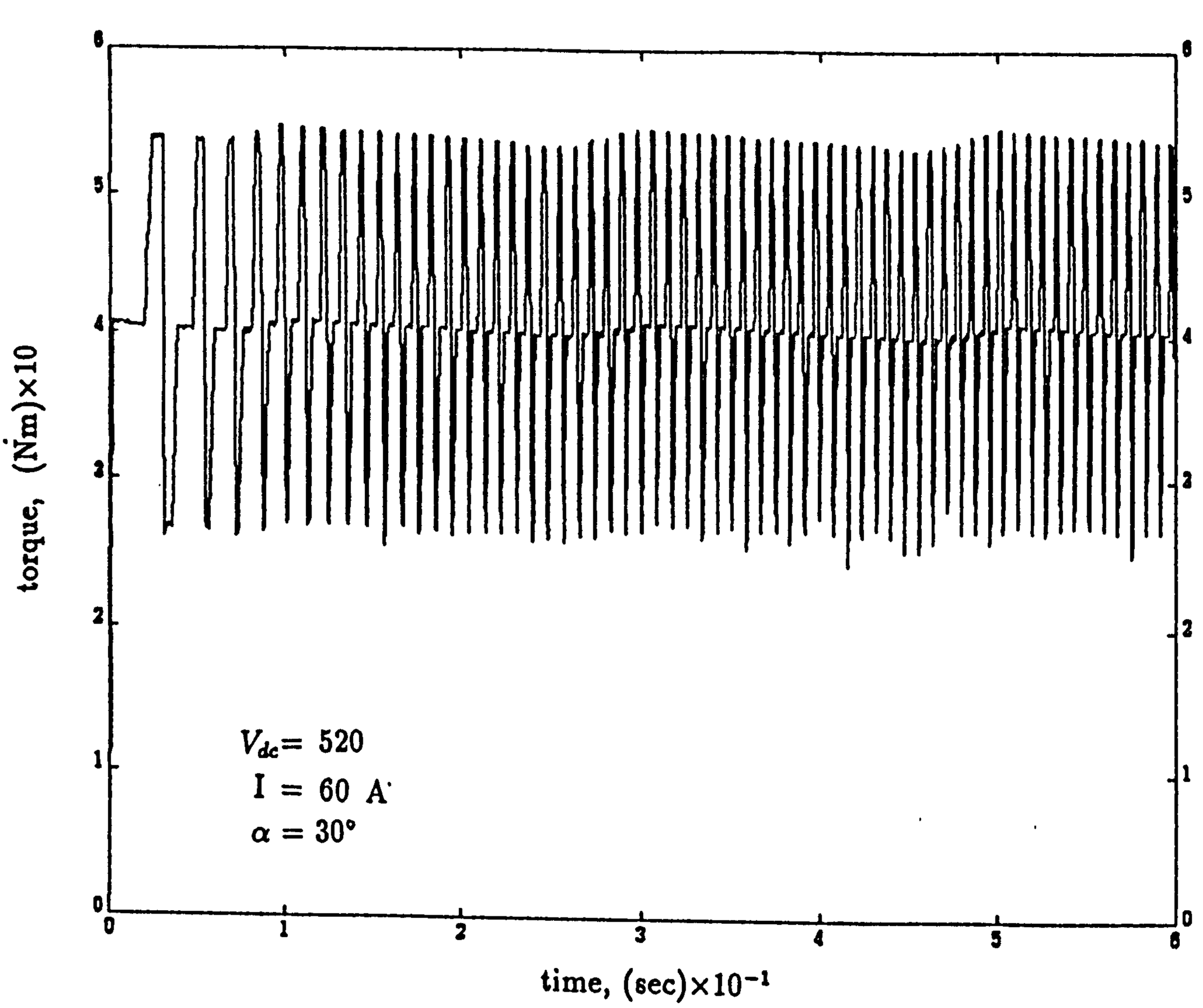

Figure 4.28 Speed, current and torque waveforms for 180° during acceleration.

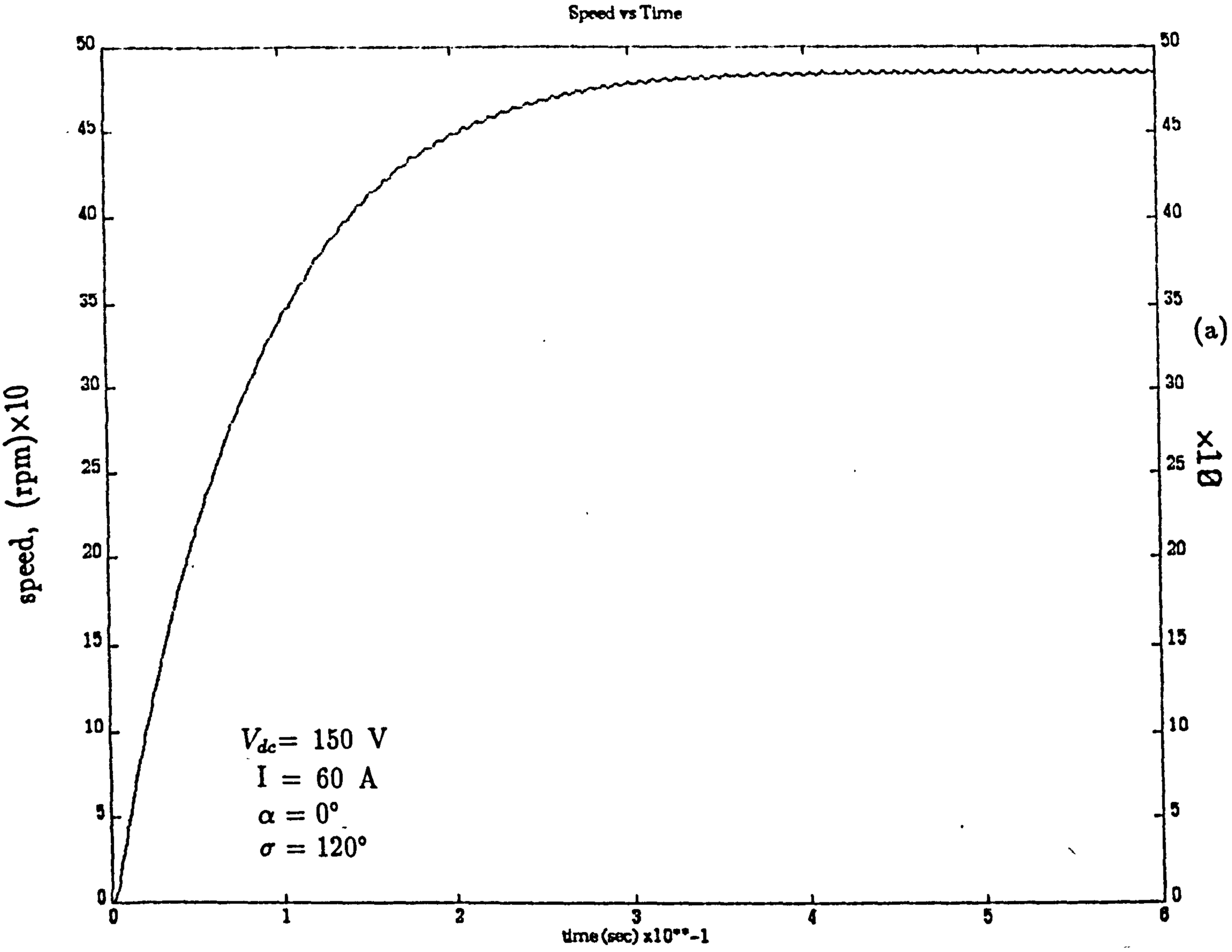
Speed vs Time
speed, (rpm)×10
50
45
40
35
30
25
20
15
10
5
0
0
1
2
3
4
5
6
time (sec) x10**-1
V_{dc}= 150 V
I = 60 A
α = 0°
σ = 120°
(a)

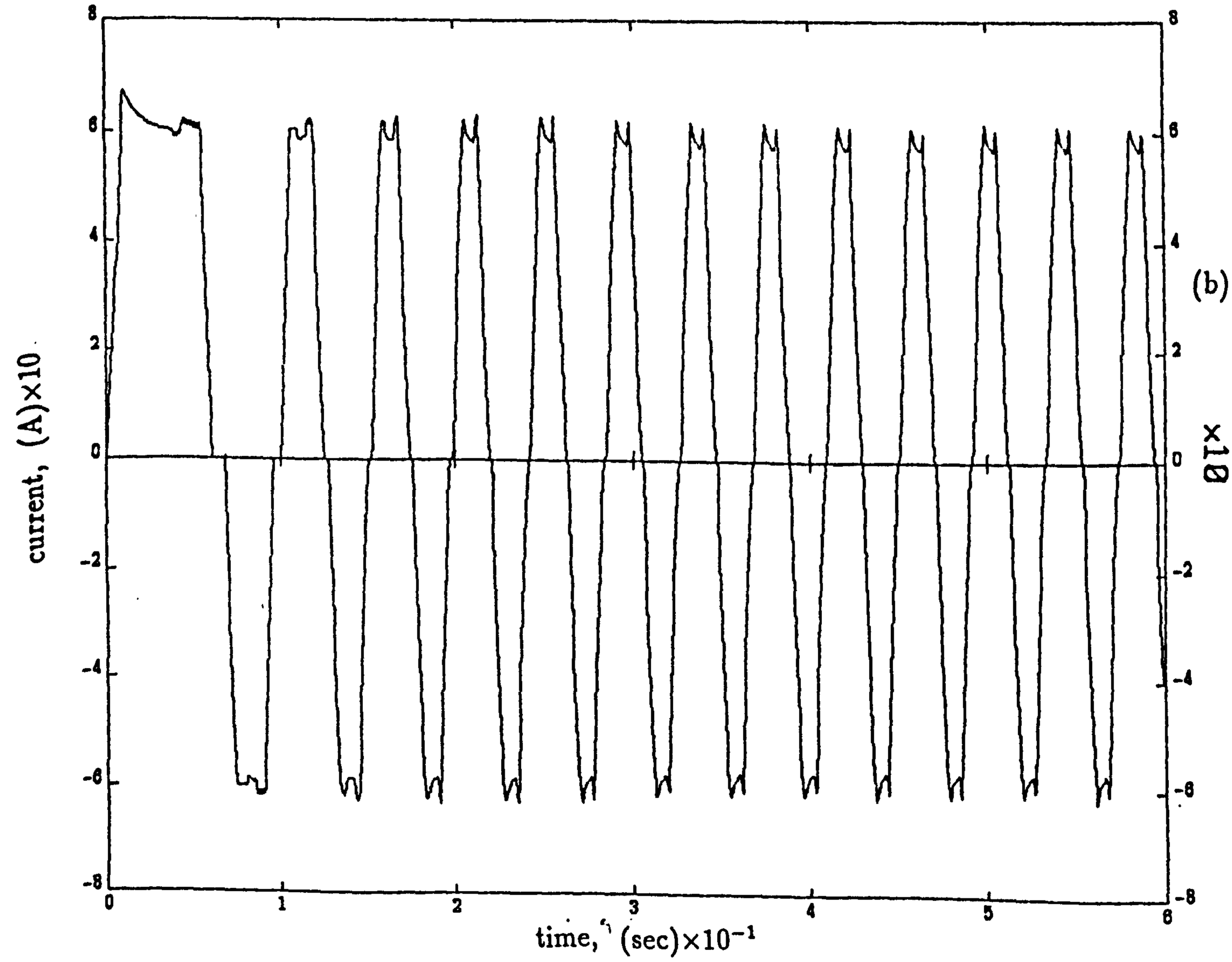
Current vs Time
current, (A)×10
8
6
4
2
0
-2
-4
-6
-8
0
1
2
3
4
5
6
time, (sec)×10⁻¹
(b)

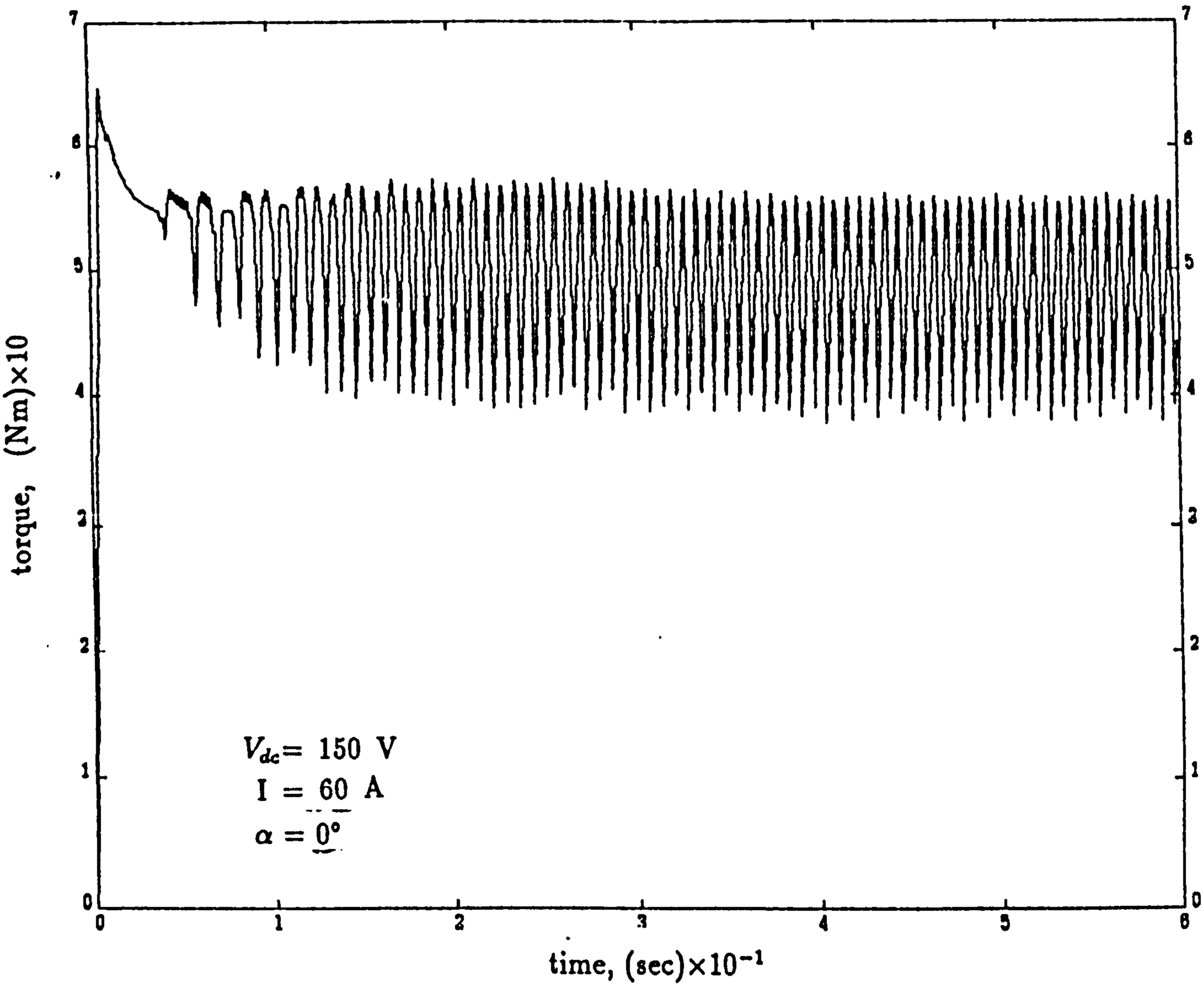

Figure 4.29 Speed, current and torque waveforms for 120° during accele r ation.

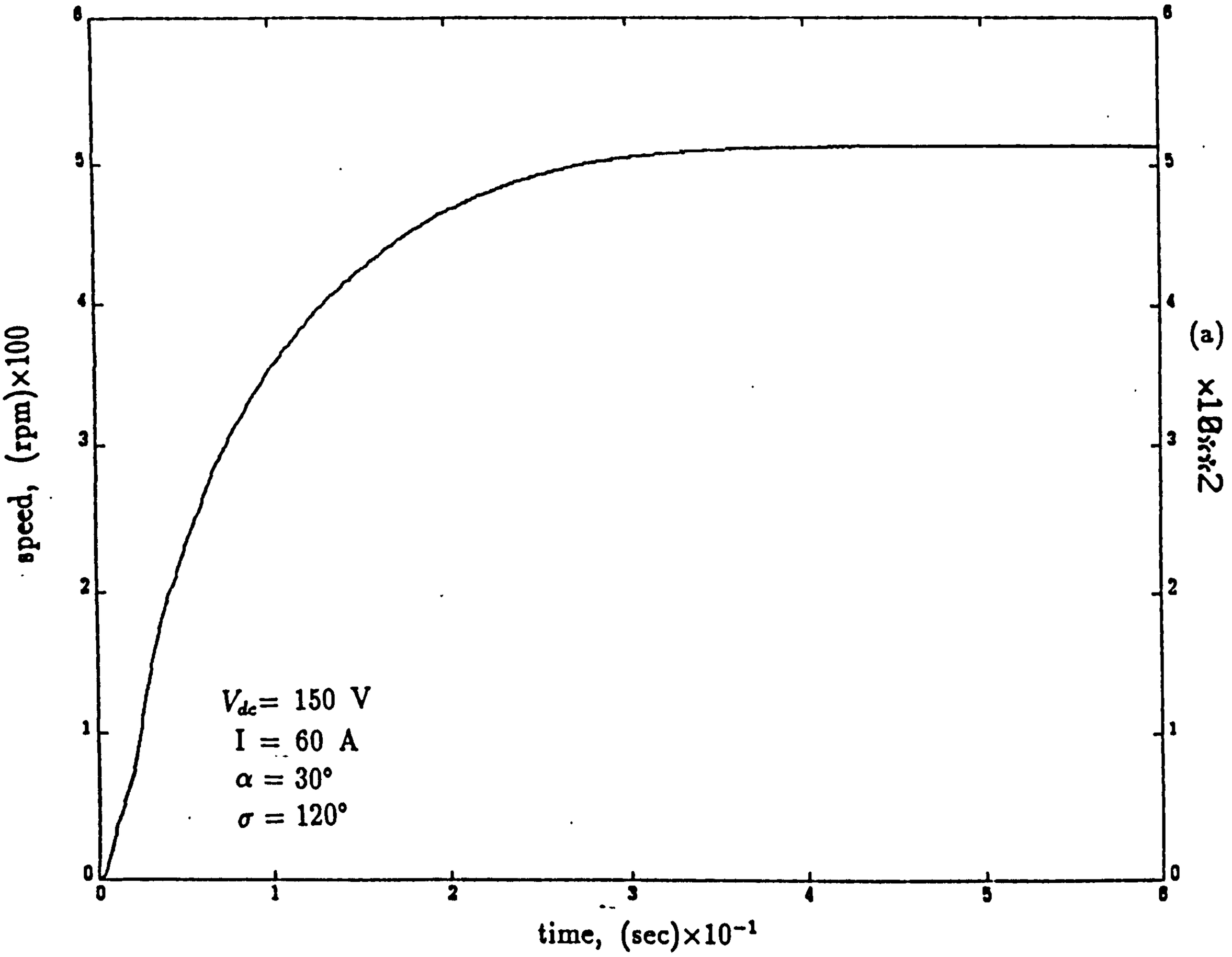
speed, (rpm)×100
time, (sec)×10⁻¹
(a)
V_{dc}= 150 V
I = 60 A
α = 30°
σ = 120°

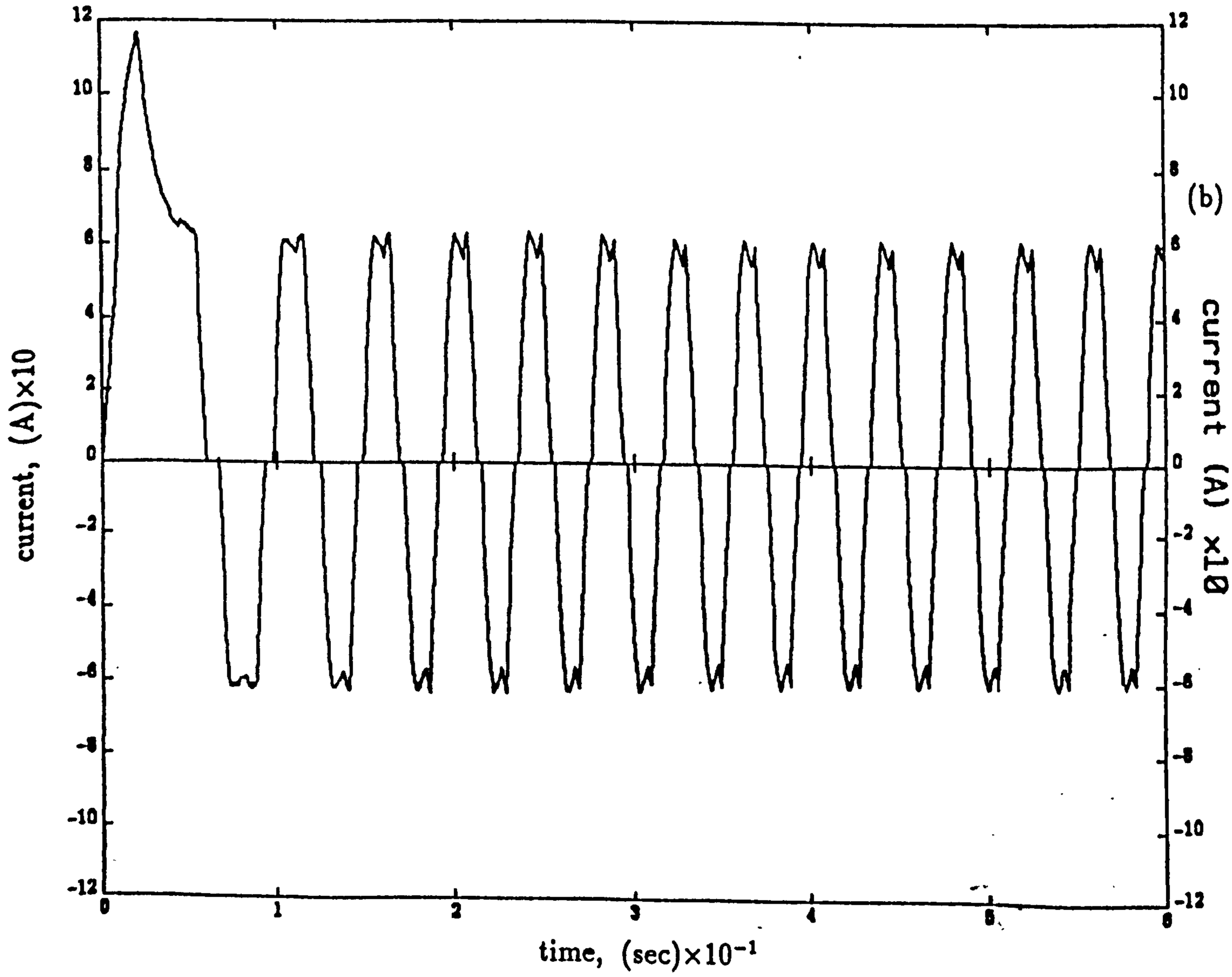
current, (A)×10
time, (sec)×10⁻¹
(b)
current (A) ×10

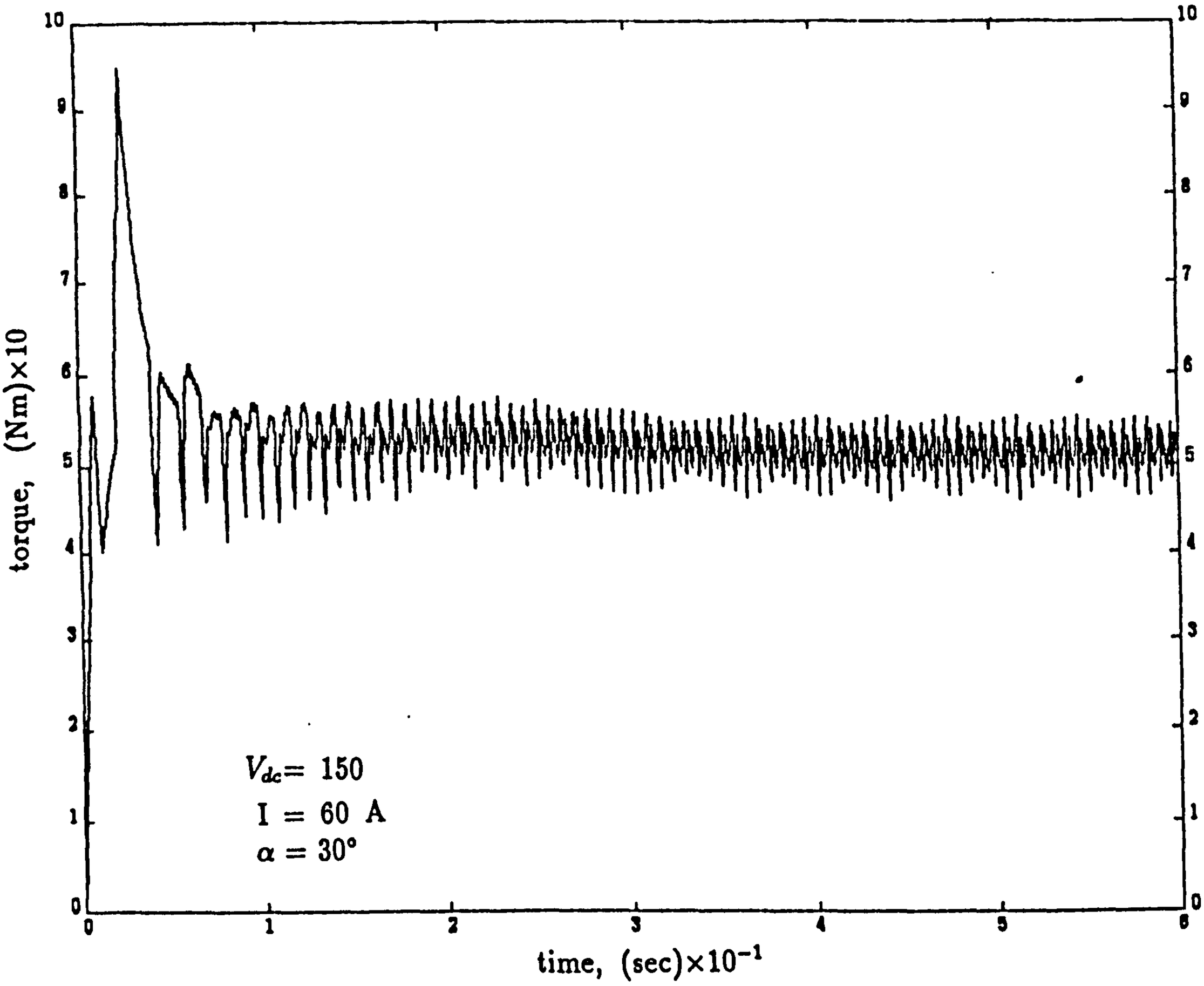

Figure 4.30 Speed, current and torque waveforms for 120° during acceleration..

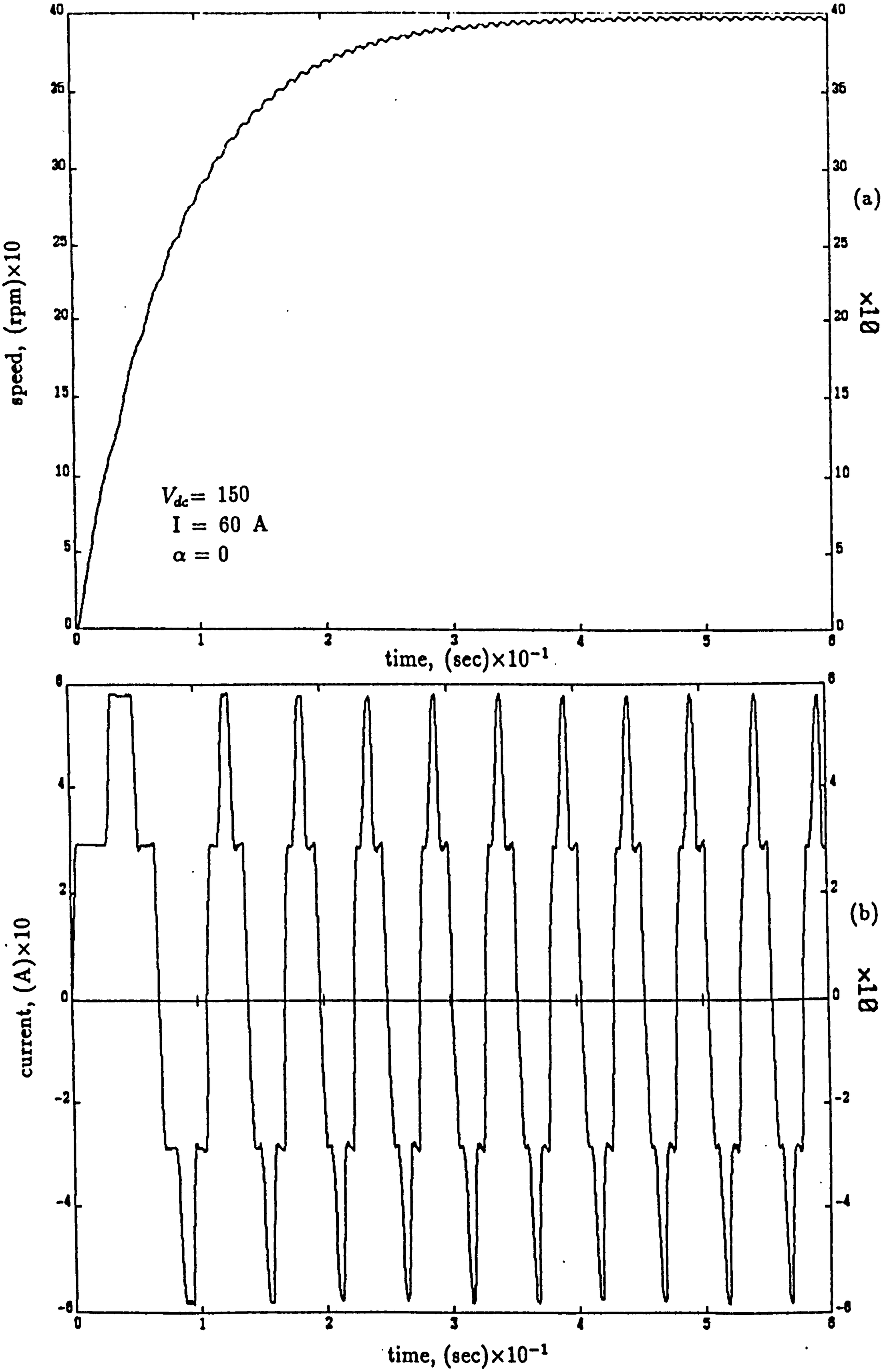
speed, (rpm)×10
V_{dc}= 150
I = 60 A
α = 0
time, (sec)×10⁻¹
(a)
current, (A)×10
time, (sec)×10⁻¹
(b)

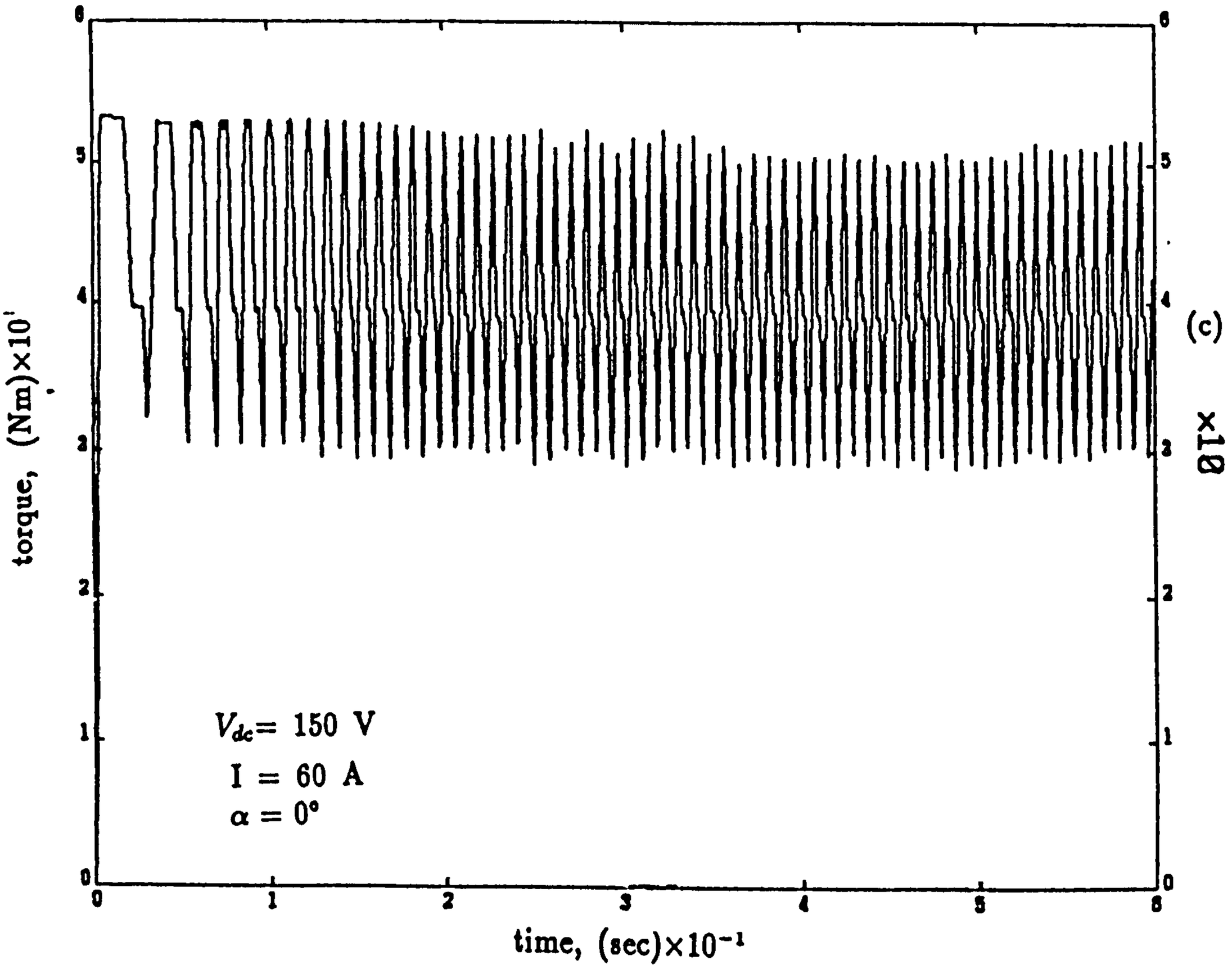

Figure 4.31 Speed, current and torque waveforms for 180° during acceleration.

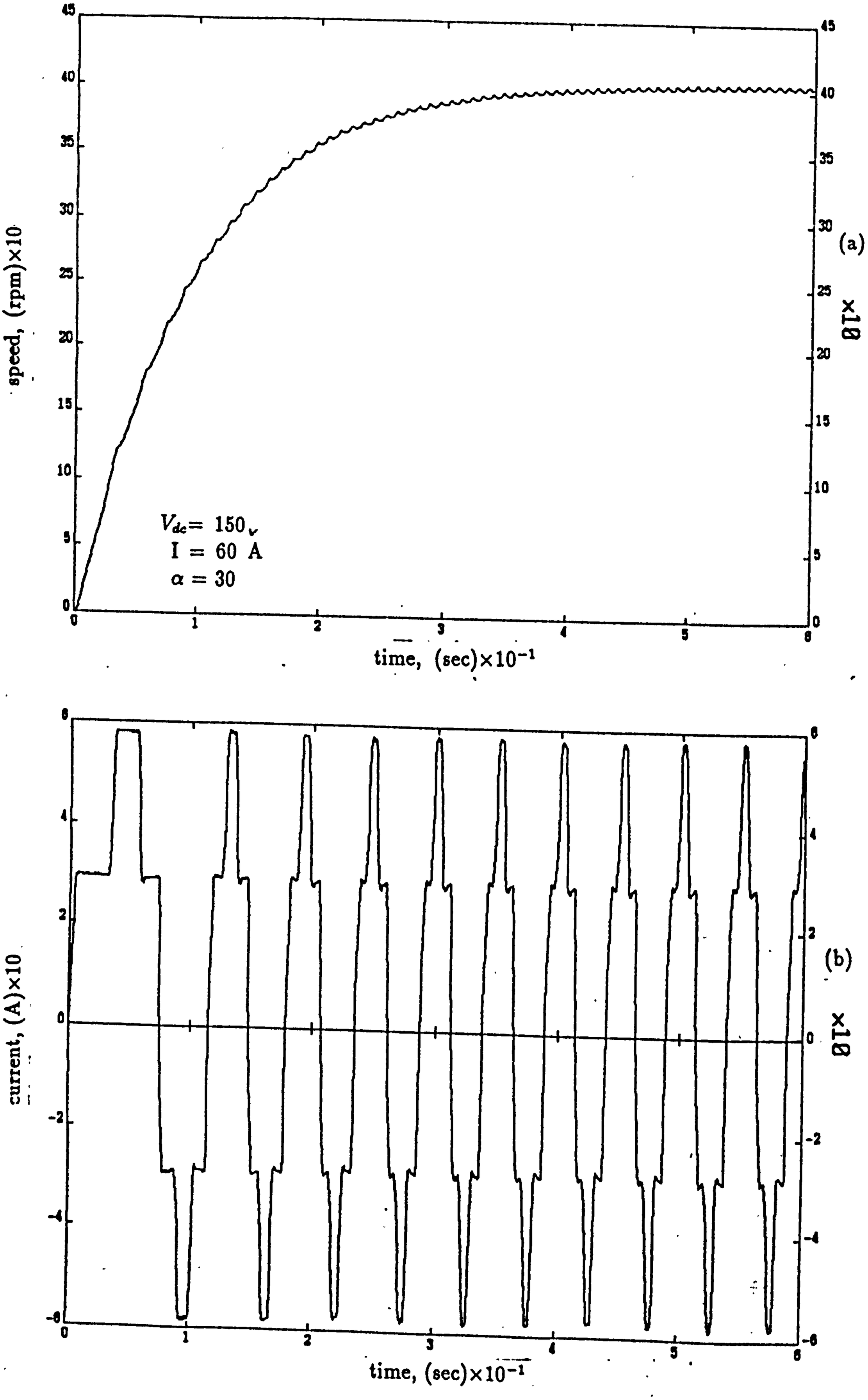
speed, (rpm)×10
45
40
35
30
25
20
15
10
5
0
0
1
2
3
4
5
6
time, (sec)×10⁻¹
V_{dc}= 150 v
I = 60 A
α = 30
(a)
current, (A)×10
6
4
2
0
-2
-4
-6
(b)

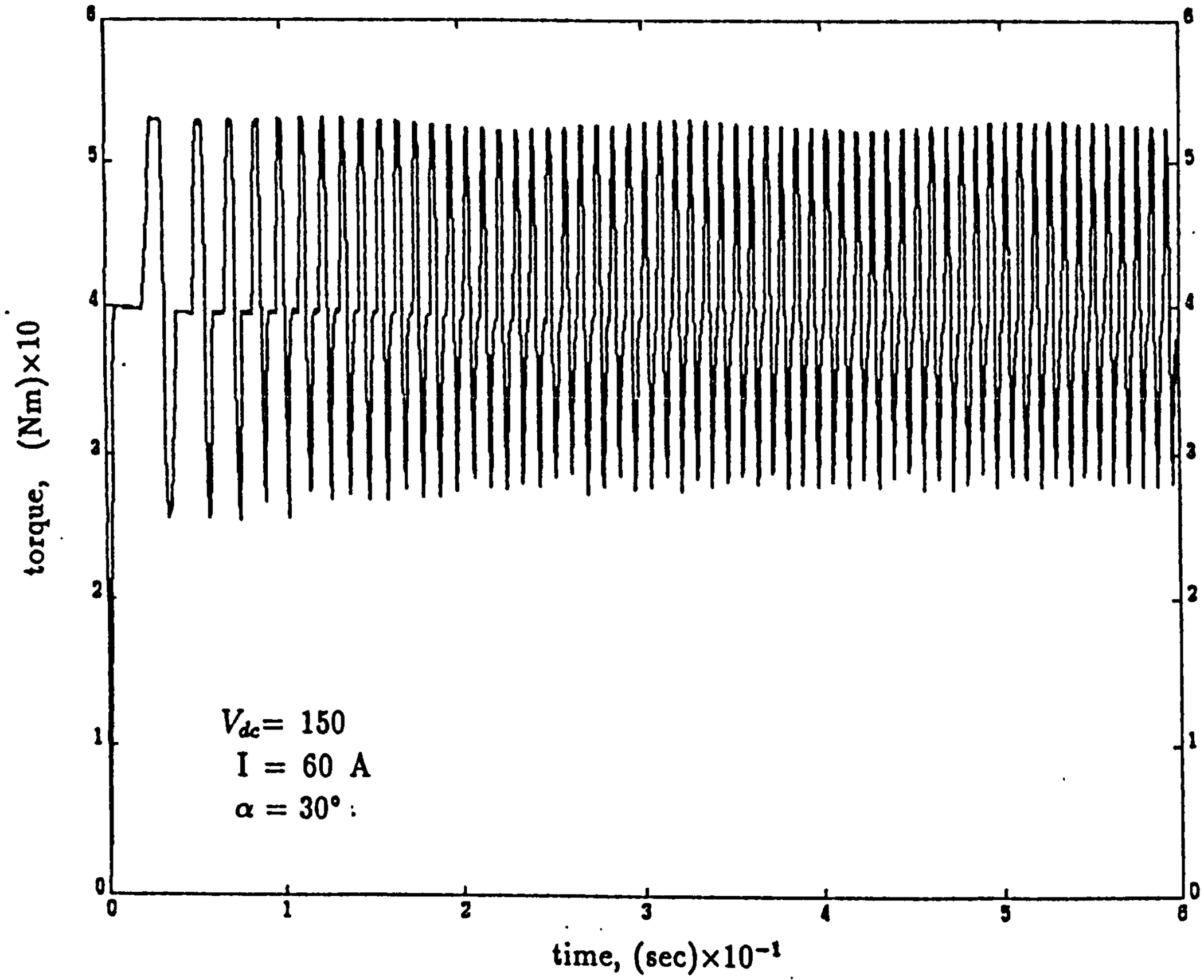

Figure 4.32 Speed, current and torque waveforms for 180° during acceleration.

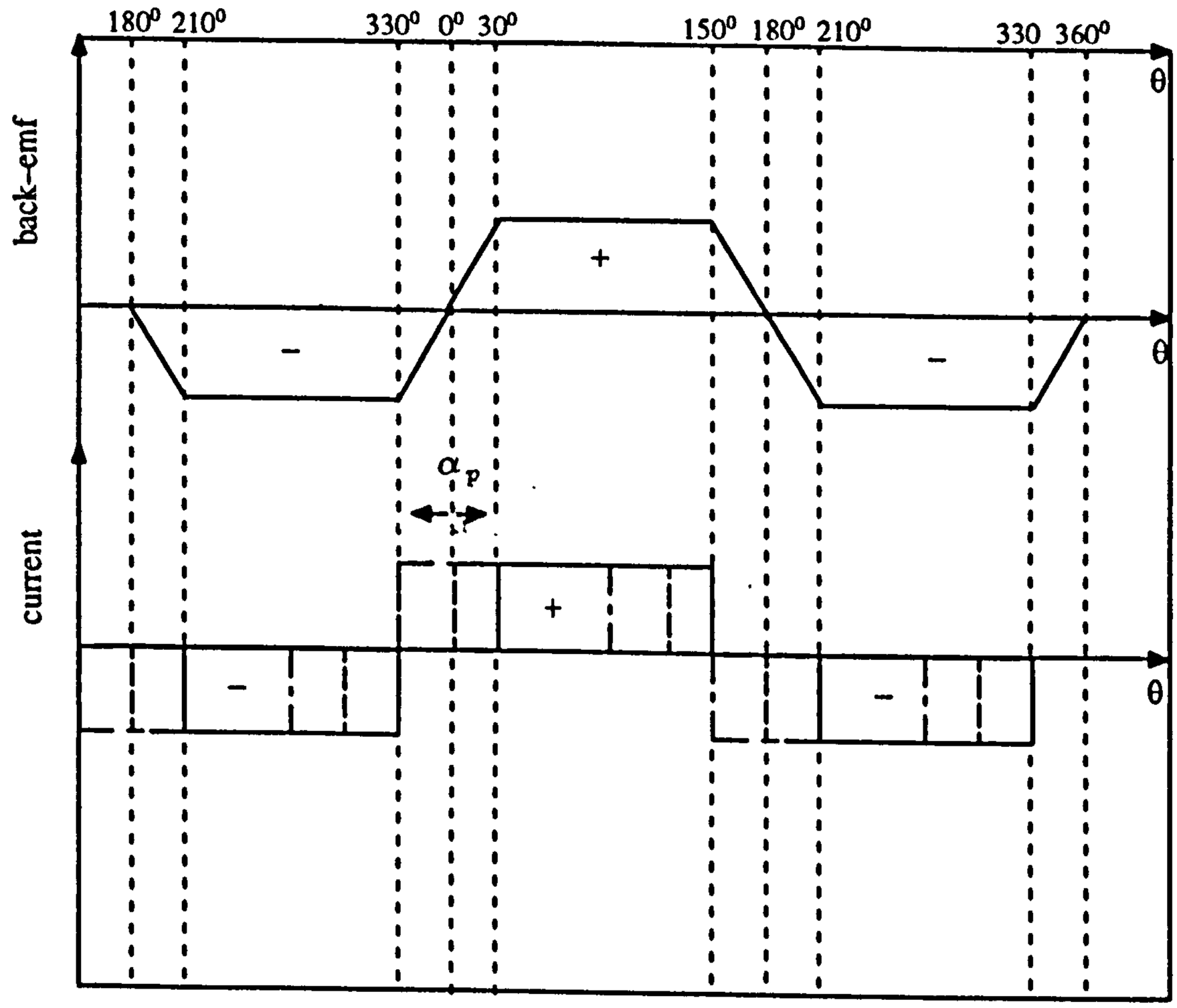

Figure 4.33 Relationship in time between back–emf and current with various phase advance

CHAPTER 5

ANALYTIC APPROACH
TO THE PERFORMANCE CHARACTERISTICS OF BRUSHLESS MOTORS

5.1 Introduction

In the previous chapter, the analysis demonstrates that accurate phase advance angle selection is important if the optimum performance is to be obtained from a brushless dc drive. If the speed of the motor is kept constant, there is an optimum phase advance angle at which maximum torque occurs. The choice of $\alpha = \alpha_{opt}$ yields maximum torque and substantially improves the torque/speed characteristic above the rated speed.

The analysis has also shown that when the machine operates at high-speed the limits of the PWM current controller are reached, so the current limit is not controlled. As a result the current waveshape becomes more sinusoidal and thus sinusoidal inputs can be assumed in a such an operation.

In addition, the approach has generally been to derive a mathematical relation between torque, speed and phase advance angle, to predict the optimum angles in accordance with the above criteria.

For the above reasons, sinusoidal analysis (machine theory) can be used to give a useful insight into the typical torque/speed curves that can be expected at high-speed operations.

As in any inverter drive, a complete analysis requires relating the dc side inverter variables and ac side machine variables. With voltage inverters the machine voltage is directly related to the inverter voltage. Since the dc side impedance is always small in a voltage inverter, it is often quite acceptable to neglect its effects and the machine then can be considered

as being supplied from an ideal voltage source. Since this is also the case in most machine applications utilising a conventional fixed frequency, machine performance with a voltage inverter supply is often very similar to the conventional operation of the machine. However, the methods employed have been such that the relationship to conventional steady-state machine theory (equivalent circuits, phasor diagram) has not been used to predict the high-speed torque performance of brushless dc motor when it is fed from a PWM voltage inverter.

This chapter presents the application of these concepts to the brushless dc motor drive. The resulting overall equivalent circuits provide a simple means for understanding and predicting the machine characteristics, particularly at high speeds. A detailed analytical model which makes possible the use of machine theory for representing the performance of the brushless dc motor has been presented. This model is used to derive the equations which describe the steady state characteristics of a drive system consisting of a permanent magnet machine supplied from a PWM voltage inverter operating in both 120° and 180° conduction angle modes and with provision to shift the phase of the stator voltages relative to the rotor position. The method utilizes the phasor diagram, where machine performance in terms of the main control variables (i.e. voltage and phase advance angle) is demonstrated.

In addition, an analytical expression for the phase-advance angle which yields maximum torque at a given motor speed, is also derived. This expression is a very useful contribution for obtaining the machine performance in terms of optimum phase advance angle in higher speed operation.

The quantitative effect of the phase advance angle on the torque/speed curve at high speed operation using sinusoidal analysis is also presented.

5.2 Circuit Model

A three phase, permanent magnet brushless machine is depicted in Fig. 5.1. The star-connected stator windings are assumed to be identical, sinusoidally distributed windings displaced 120°. The three sensors shown in Fig. 5.1 are rotor position sensors. In most applications the stator is supplied from an inverter which is switched at a frequency corresponding to the rotor speed.

5.3 Analysis and Model Development

One of the convenient ways of dealing with analysis of the permanent magnet motor is to consider the buried permanent magnet brushless dc motor performance first and then deduce the torque equations for surface mounted magnet brushless dc motor.

The analysis is based on two axis representation developed from generalised machine theory. Such a representation is well documented [Adkins, 1957], [Kelly and Simmons, 1968], [Krause, 1974].

5.4 Assumptions

Several assumptions are required in order to use this relatively elegant representation and the determination of the machine performance in terms of the phase advance angle in an analytical manner is approached by (i) simplifying the representation of the motor to an approximate case of balanced windings having sinusoidal induced voltages and (ii) simplifying the excitation by considering only the fundamental component of the applied voltage (iii) leakage inductance, mutual inductance, magnetic circuit saturation and losses such as eddy currents and hysteresis are neglected. Generally these assumptions do not present many restrictions while they simplify the model.

5.5 Analytical Method for Interior Permanent-Magnet Brushless DC Motor

5.5.1 Equivalent Circuit

The simplified equivalent circuit of figure 5.2 forms the basis of machine analysis and solution. Each winding of the brushless dc machine is modelled using the equivalent circuit, in which a supply phase voltage, V, is applied to a series connection of a resistance, R, inductance, L, and a back-emf voltage source, E, as shown in figure 5.2. All of the voltages and currents in this circuit are rms per phase values. Calculation of the developed torque is a matter of calculating the power input and accounting for the copper losses. Thus the power input of the equivalent circuit, which corresponds to the m phase windings is estimated by

$$P_i = mVIcos\phi \tag{5.1}$$

The total mechanical output power, P_o, is given by

$$P_o = mT_e\omega_r \tag{5.2}$$

The copper loss of m phases (or the ohmic losses), P_c, is given by

$$P_c = mI^2R \tag{5.3}$$

The power output of the equivalent circuit, which corresponds to the mechanical power output of the motor, neglecting the effect of eddy current and hystresis losses, is

$$P_o = P_i - P_c = T_e\omega_r = mVIcos\phi - I^2R \tag{5.4}$$

or as

$$T_e = \frac{m}{\omega_r}(VIcos\phi - I^2R) \qquad (Nm) \tag{5.5}$$

The current, I, and power factor, $cos\phi$, can be eliminated from equation (5.5) by using the phasor diagram, as shown in the following section.

5.5.2 Phasor Diagram

If a permanent magnet brushless dc motor is represented by the phasor diagram in figure 5.3, a set of equations can be obtained which describes the performance of the machine in terms of the phase advance angle, α. The d-axis and the q-axis are used as reference axes. By reference to the phasor diagram, the rms axis currents I_d and I_q are found by projecting the voltage, V, on the d and q axes. Thus the phase current, I is resolved into two component parts, the direct axis current, I_d, and the quadrature axis current, I_q;

$$Icos\phi = I_q cos\alpha - I_d sin\alpha \tag{5.6}$$

which are related by the following equation

$$I = \sqrt{I_d^2 + I_q^2} \tag{5.7}$$

Where:

α is the phase difference between phase voltage, V, and phase back-emf, E, which is called the phase advance angle

ϕ is the phase difference between V and I, which is called the power factor angle.

substitution of (5.7) into (5.5) yields

$$T_e = \frac{m}{\omega_r}[V\left(I_q cos\alpha - I_d sin\alpha\right) - \left(I_d^2 + I_q^2\right)R] \tag{5.8}$$

Having eliminated the current phase, I, and power factor, $\cos\phi$, the analysis can be continued to remove I_d and I_q from the equation.

Again with reference to the phasor diagram, the axis currents I_d and I_q are found by projecting or resolving the voltage, V, on the d and q-axis thus obtaining

$$\left.\begin{aligned} V_d = V sin\alpha = \omega_r L_q I_q - R I_d \\ V_q = V cos\alpha = R I_q + \omega_r L_d I_d + E \end{aligned}\right\} \tag{5.9}$$

the d- and q-axis current components obtained from equation (5.9) are

$$\left.\begin{aligned} I_d = \frac{V\omega_r L_q cos\alpha - RV sin\alpha - E\omega_r L_q}{(R^2 + \omega_r^2 L_d L_q)} \\ I_q = \frac{V\omega_r L_d sin\alpha + RV cos\alpha - ER}{(R^2 + \omega_r^2 L_d L_q)} \end{aligned}\right\} \tag{5.10}$$

but

$$E = k_b \omega_r \tag{5.11}$$

allows equation (5.10) to be re-written as

$$\left.\begin{aligned} I_d = \frac{V\omega_r L_q cos\alpha - RV sin\alpha - k_b\omega_r^2 L_q}{(\omega_r^2 L_d L_q + R^2)} \\ I_q = \frac{V\omega_r L_d sin\alpha + RV cos\alpha - k_b\omega_r R}{(\omega_r^2 L_d L_q + R^2)} \end{aligned}\right\} \tag{5.12}$$

substituting equation (5.12) into equation (5.8), the electromagnetic torque, T_e, for the buried magnet machine can be expressed in terms of the rotor reference frame variables

$$T_e = \frac{m}{\omega_r}\Big(\frac{Vcos\alpha(V[\omega L_d sin\alpha + Rcos\alpha] - k_b\omega_r R)}{(R^2 + \omega_r^2 L_d L_q)} - \frac{Vsin\alpha(V[\omega_r L_q cos\alpha + Rsin\alpha] - k_b\omega^2 L_q)}{(R^2 + \omega_r^2 L_d L_q)} - \Big(\frac{V(\omega L_q cos\alpha - Rsin\alpha) - k_b\omega_r^2 L_q}{(R^2 + \omega_r^2 L_d L_q)}\Big)^2 R - \Big(\frac{V(\omega_r L_q sin\alpha + Rcos\alpha) - k_b\omega_r R}{(R^2 + \omega_r^2 L_d L_q)}\Big)^2 R\Big) \quad (5.13)$$

Since the winding resistance has little effect upon the machine performance except at very low speeds, it is often quite acceptable to neglect its effect (i.e., $R = 0$). In terms of stator voltages and the angle α, the machine torque of equation (5.13), with stator resistance neglected, is

$$T_e = \frac{m}{\omega_r^2}\Big((\frac{VE}{L_d})sin\alpha + \frac{1}{2}[V^2(\frac{1}{L_q} - \frac{1}{L_d})sin2\alpha]\Big) \quad (5.14)$$

As can be seen that the first term of this equation can readily be recognised as the magnet torque term and the second term represents the contribution of the reluctance torque caused by saliency.

5.6 Analytical Method for Machines with Surface Mounted Magnets

Although the analysis is carried-out without neglecting saliency, the assumption that a brushless d.c. motor is a magnetically round rotor device simplifies the analysis while preserving the basic steady-state operating characteristics of the inverter-machine combination. The direct and quadrature axis inductances of the surface mounted machines are approximately equal. This is because the length of the air gap is equal to that of the magnet which has a permeability approximately that of air. This results in the direct and quadrature axis inductances of a surface mounted machine being

approximately equal, i.e.,:

$$L_d = L_q = L \tag{5.15}$$

substitution of equation (5.15) into the torque expression (5.13) gives the torque equation for a machine with surface mounted magnets. The equation is long and complicated but can be simplified by substitution of equation (5.15) and the following:

$$X = \omega_r L \tag{5.16}$$

and

$$Z = \sqrt{R^2 + \omega_r^2 L^2} \tag{5.17}$$

Where:

X is the phase winding reactance,

Z is the phase winding impedance.

and thus the torque equation (5.13) becomes

$$T_e = \frac{mE}{\omega_r Z^2}[VX sin\alpha + VR cos\alpha - ER] \tag{5.18}$$

by substituting equations (5.11) and (5.18) into (5.14), the output torque of the surface mounted machine can obtained in the following general form

$$T_e = \frac{mk_b}{Z^2}[VX sin\alpha + VR cos\alpha - ER] \tag{5.19}$$

For the machine in which R is negligible at reasonable values of angular velocity, ω_r, equation (5.19) reduces to:

$$T_e = \frac{mk_b}{X^2}[VX]sin\alpha \tag{5.20}$$

i.e.;

$$T_e = \frac{m}{\omega_r}[\frac{EV}{X}]sin\alpha \tag{5.21}$$

when comparing this equation with equation (5.14) it is clear that reluctance torque is approximately zero for a machine with surface mounted magnets. The total motor torque is equal to the electromagnetic torque only, the maximum of which is produced at $\alpha = 90°$; i.e. when stator flux is perpendicular to the rotor flux at standstill.

As can be seen from equation (5.14), the opposite is true in the buried permanent machine. The reluctance variation between the d and q axes can be significant with the d axis reluctance usually being larger than that of the q axis. This is because whereas in the magnetic circuit on the q axis, there is only iron, a part of the magnetic circuit on the d axis consists of the magnet which has a permeability approximately that of air. This increases the d-axis reluctance, hence reducing its inductance. This means that in addition to the electromagnetic torque, a reluctance torque exists in buried machines, as can be seen in the second term of equation (5.14), this additional component arises from the presence of saliency. However, this reluctance can be used to increase the torque rating of the machine.

In summary, the derivation given in this section shows that a machine with surface mounted magnets is merely a special case of a buried machine in which the direct and quadrature axes inductances are equal.

5.7 Controlled-Torque-Phase Advance Angle Permanent-Magnet Brushless DC Motor

5.7.1 Characteristic of the Drive at Low Speeds

Equation (5.19) shows that the torque of a brushless dc motor is dependent on the applied phase voltage, V, the back-emf voltage, E, and the phase advance angle between the two voltages, α. To achieve maximum torque, it is evident from equation (5.19) that the phase advance angle should be zero. At low speed operations the phase reactance, $\omega_r L$, is very small compared to the resistance ($R \geq \omega_r L$) and may, therefore, be neglected. Thus making $Z = R$ and for these conditions of phase advance angle and operating speed the equation (5.19) simplifies further, i.e;

$$T_e = \left(\frac{mk_b}{R}\right)[V - k_b\omega_r] \tag{5.22}$$

5.7.2 Characteristic of the Drive at High-Speeds

Expression (5.19) shows that torque will be maximised if the phase advance angle, α at a specified value of $\alpha = 90°$. If the α is $\alpha = 90°$, then equation (5.19) becomes

$$T_e = \left(\frac{mk_bR}{Z^2}\right)[VX - ER] \tag{5.23}$$

or as

$$T_e = \left(\frac{mk_bR\omega_r}{Z^2}\right)[VL - k_bR] \tag{5.24}$$

It should be noted the torque that the motor developed at standstill is zero if $\omega_r = 0$. Therefore at low operating speeds the optimum phase advance angle to maximise motor torque, is zero degrees.

For high-speed operation, the phase resistance, R, is very small compared to the reactance ($R \leq \omega_r L$) and may, therefore, be neglected. Thus making $Z = X$ and for these conditions of phase advance angle and operating speed the equation (5.24) simplifies further, i.e;

$$T_e = \frac{m}{\omega_r}\left(\frac{k_b V}{L}\right) \tag{5.25}$$

A machine with surface mounted magnets operated with position feedback can therefore be started at low speeds with $\alpha = 0°$, and as the speed rises the phase advance angle can be increased up to 90° giving a series motor characteristic. Although equation (5.19) is valid for any speed, positive values of ω_r and $T_e(0 \leq \alpha \leq 90°)$ are of primary interest.

It is interesting to point-out the well known similarities between the operating characteristic of the inverter-fed permanent magnet motor combination and d.c. machines. By examining equations (5.22) and (5.25) and with $\alpha = 0$, the brushless dc motor can produce either the shunt (constant field current independent of line current) or series (field current proportional to line current) characteristic.

5.8 The Optimum Phase Advance Angle for Maximum Torque at a Given Speed

It is clear from the above analysis that the phase advance angle is the main control parameters and good design practice of brushless dc motors is very much concerned with the optimum choice of this angle for a given voltage and speed. This section presents a derivation of an analytical expression for optimum phase advance angle.

There is a phase advance angle which results in the maximum torque being developed for a given speed, ω_r, and applied voltage, V. The value of the phase advance angle, α, at which a maximum or minimum electromagnetic

torque occurs for a given rotor speed may be obtained by taking the first derivative of T_e, given by equation (5.19), with respect to α and setting the result equal to zero ($\frac{\partial T_e}{\partial \alpha} = 0$).

$$\frac{\partial T_e}{\partial \alpha} = \left(\frac{mk_b}{Z^2}\right)[VXsin\alpha + VRcos\alpha] = 0 \tag{5.26}$$

Solving this relation for α yields the value of α for maximum or minimum steady-state torque at a given motor speed.

$$tan\alpha_{opt} = \frac{X}{R} \tag{5.27}$$

or as

$$\alpha_{opt} = arctan\left(\frac{\omega_r L}{R}\right) \tag{5.28}$$

This result shows that the angle α_{opt} is a function of the machine time constant and operating speed, and the closure of the phase advance control would need the knowledge of the relationship between α_{opt} and these parameters, in particular to the speed of the motor. However, this phase advance angle, α_{opt}, for maximum or minimum torque is the angle of the impedance of the machine. That is, since the machine works with shaft position sensors, the fundamental frequency of the inverter output voltage and thus current is always the same as the rotor speed. In other words, $\omega_e = \omega_r$, $\tau_s\omega_r = \frac{\omega_e L_e}{R}$. Where τ_s is stator time constant which is analogous to the armature circuit time constant of a dc machine. The maximum or minimum steady-state electromagnetic torque at a given motor speed may be determined by substituting equation (5.28) into equation (3.19).

The motor speed n (in rpm) can be substituted into equation (5.28) by using the following equation:

$$\omega_r = \frac{2\pi n}{60} \tag{5.29}$$

allows equation (5.28) to give

$$\alpha_{opt} = arctan\left(\frac{2\pi}{60}\right)\left(\frac{nL}{R}\right) \tag{5.30}$$

Equation (5.19) is a condition for obtaining the required electromagnetic torque for a given speed, and equation (5.30) is for the operation to maximise the output torque of the machine. Specifically at a given speed, optimum torque is produced if the phase advance angle is set to the optimum of the phase advance angle value (α_{0pt}) at that speed.

Then, the optimum control method which maximises the torque capability of the machine is realised to control the phase advance angle and voltage to satisfy equations (5.19) and (5.30) at the same time.

However, at zero speed, the optimum phase advance angle is therefore zero degrees as deduced from the simplified equations (5.22) and (5.24). As the speed increases towards infinity, the optimum phase advance angle settles at a maximum value of 90°. The drive has then series d.c. motor characteristics as shown earlier by equation (5.25).

As explained in Chapter 2, phase advance angle, α_{opt}, is set up based on the signals from position sensors as a control variable and the optimum torque would be the parameter determined incidentally. Speed control of the inverter-permanent magnet motor combination is typically achieved by pulse width modulation. It is now clear that high speed torque control may also be achieved by shifting the phase of applied voltages. Hence the combination of pulse width modulation and phase advancing may be used to advantage in most high-speed applications.

Finally the expression (5.30) is a useful contribution to the study the optimum phase advance angle and gives a qualitative idea of the optimum operating conditions, particularly at high speed. Although Acarnley and Gibbons, [1982] do consider the rate of change of torque with respect to the load angle in order to derive an expression for the torque in a stepping motor, the derivation of this expression for the brushless dc motor provides a simple means for understanding and predicting the optimum machine performance in terms of phase advance angle.

5.9 Calculations of Motor Variables

5.9.1 Phase current

Often the fundamental phase current, I, is of interested. It can be obtained from the phasor diagram shown in figure 5.4. A short trigonometric analysis leads to the result

$$V_z^2 = V^2 + E^2 - 2VE\cos\alpha \tag{5.31}$$

where

$$V_z = IZ \tag{5.32}$$

where ZI is the voltage across the winding impedance Z. In turn equation (5.33) can be used to specify the machine current from

$$I = \sqrt{\left(\frac{V^2 + E^2 - 2VE\cos\alpha}{Z^2}\right)} \tag{5.33}$$

5.9.2 Power factor

This is an important performance quantity which decides the KVA requirement for the motor drive system. The general definition of power factor, PF, is

$$PF = \frac{P_i}{VA} = \frac{3VIcos\theta}{3VI} \tag{5.34}$$

where VA is the product of the rms voltage and rms current.

$$PF = .cos\theta \tag{5.35}$$

the power factor, PF, is derived from the phasor diagram of 5.4, as follows:

$$PF = cos\frac{\pi}{2} - (\beta + \gamma) \tag{5.36}$$

where

$$\gamma = \frac{\pi}{2} - arctan(\frac{X}{R}) \tag{5.37}$$

and

$$\beta = arccos\left(\frac{V - Ecos\alpha}{IZ}\right) \tag{5.38}$$

5.9.3 Efficiency

If the iron loss is neglected, the efficiency of the motor is calculated by:

$$\eta\% = \frac{P_o}{P_i} \tag{5.39}$$

where

$$P_o = \frac{T_e n\pi}{30} \tag{5.40}$$

and

$$P_i = 3VI\cos\theta \tag{5.41}$$

5.10 Rotor Position/Speed and Phase Advance Angle Relationship

The relationship between position/speed and phase advance angle will now be demonstrated. For simplicity, only a two pole machine will be considered. For this machine, one complete cycle of phase excitation corresponding to one complete revolution of the rotor (i.e. one cycle of excitation corresponds to rotation through two rotor pole pitches). Therefore the relationship between rotor position, θ_r, and angular speed of phase excitation, ω_r, is found in the following manner.

The distance taken by the rotor to rotate one revolution is given by

$$d_r = \frac{2\pi}{p} \tag{5.42}$$

The time taken to rotate one revolution is given by

$$t_r = \frac{2\pi}{p\omega_r} \tag{5.43}$$

The motor speed over one revolution or one supply cycle is

$$\left.\begin{aligned} \frac{\partial\theta_r}{\partial t} &= \frac{d_r}{t_r} \\ \frac{\partial\theta_r}{\partial t} &= \frac{(\frac{2\pi}{p})}{(\frac{2\pi}{\omega_r})} \end{aligned}\right\} \tag{5.44}$$

therefore

$$\frac{\partial\theta_r}{\partial t} = \frac{\omega_r}{p} \tag{5.45}$$

Integrating equation (5.45) with respect to time gives the variation of rotor position with the time

$$p\theta_r = \omega_r t - \alpha$$

or as

$$\alpha = \omega_r t - p\theta_r \tag{5.46}$$

The line-to-neutral voltages of the machine supplied from a voltage source inverter, with provision for phase control, may be expressed in a Fourier series expansion:

$$V = \frac{2V_{dc}}{\pi}[cos\theta_e + \frac{1}{5}cos5\theta_e + \frac{1}{7}cos7\theta_e + ...] \tag{5.47}$$

where

$$\theta_e = \int_0^t \omega_e + \theta_e(0) \tag{5.48}$$

5.11 Analysis of Inverter-machine operation

As pointed out earlier, the state of the sensors shown in Fig. 5.1 provides information regarding the position of the rotor poles and, thus, the position of the q and d axes. This information can be used to determine the switching of the inverter, which may be a voltage source or a current source. However, this work is primarily concerned with a voltage source inverter. When the machine is supplied from this inverter, the fundamental component of the stator applied voltages may be expressed as

$$V = 2V_s cos\theta_e \tag{5.49}$$

where the amplitude V_s may be a function of time and thus

$$\theta_e = \int_0^t \omega_e + \theta_e(0) \tag{5.50}$$

where $\theta_e(0)$ is the time zero position of the applied voltages, which will play an important role in the operation of the brushless dc. motor since it can be controlled by delaying or advancing the switching of the source inverter relative to the measured rotor position.

The voltage V_{dc} is the voltage applied to the inverter and $\theta_e(0)$ is the time zero angle of the applied voltages. It is important to note both V_{dc} and $\theta_e(0)$ are controllable variables and may be varied as a function of time. Since the machine is equipped with shaft position sensors, the fundamental frequency of the inverter output voltage is always the same as the motor speed. In other words, $\omega_e = \omega_r$ and $\theta_e(0)$ may adjusted by appropriate switching of the transistors in the inverter. For the purposes of compactness, it is convenient to define

$$\alpha = \theta_e(0) - \theta_r(0) \tag{5.51}$$

Although V_{dc} may be varied if the inverter is supplied from a controlled rectifier, the inverter is often supplied from a d.c. source such as a battery. In this case, the effective value of stator phase voltages is varied by pulse width modulation (PWM). Pulse width modulation may be taken into account, in this analysis, by multiplying the stator voltages by a pulse train which becomes a controllable multiplier of V_{dc} if the harmonics due to pulse width modulation are neglected as is often done.

5.12 Results and Discussion

5.12.1 Performance Prediction

The brushless dc motor used for this work is a 20 KW industrial machine tool drive. The simulation results are based on a dc link voltage of 550 V, a phase resistance 0.26 Ω, and a phase inductance of 3.1 mH. The data of the drive is shown in Appendix 1.

A program is written to calculate various motor parameters, including torque and phase current over a wide speed range for particular phase advance angle and inductance.

5.12.2 Torque/Speed and Phase Advance Angle Characteristics

The torque produced at any phase advance angle can be found by evaluating equation (5.19) with corresponding phase advance angle. For example, a typical set of torque/speed/phase advance angle characteristics for the Bosch drive operated with the supply voltage of 520 volts are shown in figure 5.4a and figure 5.4b shows in more detail the variation of the torque at high-speeds (between 1000 and 6000 rpm). However, these are the torque/speed curves for the trapezoidal brushless motor operated on a sinusoidal voltage supply.

The torque speed characteristics for phase advance angles of 0°, 15°, 30°, 45°, 60°, 75° and 90° at a supply dc voltage of 520 volts are shown in figure 5.4. It can be seen that a phase advance angle of 0° results in a torque/speed characteristic with a high starting torque, but the torque falls rapidly to zero as the speed increases. Advance angle of 90° results in zero starting torque, but there is much more torque produced at high-speeds. This enables the motor to run faster on the same phase voltage than it can with a 0° phase advance angle. Phase advance angles between 0° and 90° result in torque-speed characteristics that come within the bounds set by the 0°

and 90° characteristics. The four curves in figure 5.4 suggest that there is an optimum phase advance angle that can be selected at a given speed in order to maximise the available motor torque.

5.12.3 Machine Characteristics with Optimum Phase Advance

(i) Torque/Optimum Phase Advance Angle Characteristic

Figure 5.5 illustrates the optimum phase advance angle versus speed curve as calculated by means of equation (5.30). It can be seen that there is a certain value of phase advance angle which maximises the output torque of the machine. The higher the speed is, the larger phase advance angle is required to produced the maximum torque. In conclusion, therefore, the optimum torque producing capability of the drive can be achieved by selecting a speed dependent phase advance angle.

(i) Torque/Optimum Phase Advance Angle Characteristic

The maximum torque T_{eo} is also plotted along with the optimum phase advance angle, α_{opt}, which yields maximum torque. It is clear from this figure that for $\omega_r \geq 0$ maximum torque will occur between $\alpha = 0$ and 90°.

These are the optimum torque/speed curves for the drive operated on a sinusoidal voltage supply. The curves of figure 5.6 reveal that a significantly larger torque can be achieved if the angle α is maintained at the value to produce maximum torque, α_{opt}.

Nevertheless the analysis and the computation results in this section illustrate the fact that in a brushless permanent-magnet motor, the phase advance angle must be carefully adjusted to optimise the performance at a given speed.

5.12.4 Effect of Machine Parameters on Torque/Speed Characteristics

The computation analysis also includes a set of curves for different phase advance angles at phase inductances of 6.0, 9.0 and 12 mH. Figures 5.7, 5.10 and 5.13 show the family of curves obtained for phase advance angles of 0°, 15°, 30°, 45°, 60°, 75° and 90° respectively. These results show that the phase inductance affects the magnitude of the torque/speed curve and it does change the shape of the curve significantly in the high speed range. The phase inductance is therefore the important parameter that fixes the torque/speed characteristic of a given motor.

To examine further the effect of the phase inductance on the other parameters, figure 5.8, 5.9, 5.11, 5.12, 5.14 and 5.15 display a series of graphs which show how the phase advance angle and the optimum torque vary with phase inductance.

The other motor quantities such as phase current and efficiency have not been plotted since the main point to be made at this stage is the importance of the phase advance angle control in the brushless d.c. motor, if it is to operate effectively over a wide speed range.

5.13 Summary and Conclusion

The brushless d.c. motor supplied from an inverter with phase advance angle control, has been analysed using sinusoidal theory. The voltage, current and torque equations derived are valid for the steady state operating condition. Whilst many brushless permanent magnet motor systems use voltage source inverters, it is nevertheless valuable to use sinusoidal analysis to predict the probable performance characteristics. The advantages of the sinusoidal equations are that they are simple to understand and easy to use.

The main contribution of this chapter is the formulation, based on the machine theory approach, of the equations describing the machine performance in terms of the main control parameters. In the course of developing these equations, a better understanding of the interaction of the machine elements is obtained.

The results of analysis verify that the high speed torque characteristics of the brushless dc drive system are markedly influenced by controlling the phase advance angle.

In addition, the high speed torque characteristics of a specific machine, due to advancing the phase of the stator applied voltages, may be ascertained from the time constant and rotor speed and these quantities are readily available. Phase advancing also provides a means of high-speed torque control which could be used in conjunction with pulse width modulation PWM control technique.

Moreover, the brushless d.c. motor possesses a trapezoidal back-emf and a square wave current which are a major obstacle to any analysis based on sinusoidal assumptions. However, sinusoidal analysis of the brushless d.c. motor system gives a useful insight into the typical torque/speed curves that can be expected, particularly at high speed operations. Whilst the predictions are not necessarily quantitatively accurate, they do give a qualitatives idea of the optimum operating conditions.

The equations presented in this chapter will be used further to investigate the optimum phase advance angle for high speed operations in the following chapter.

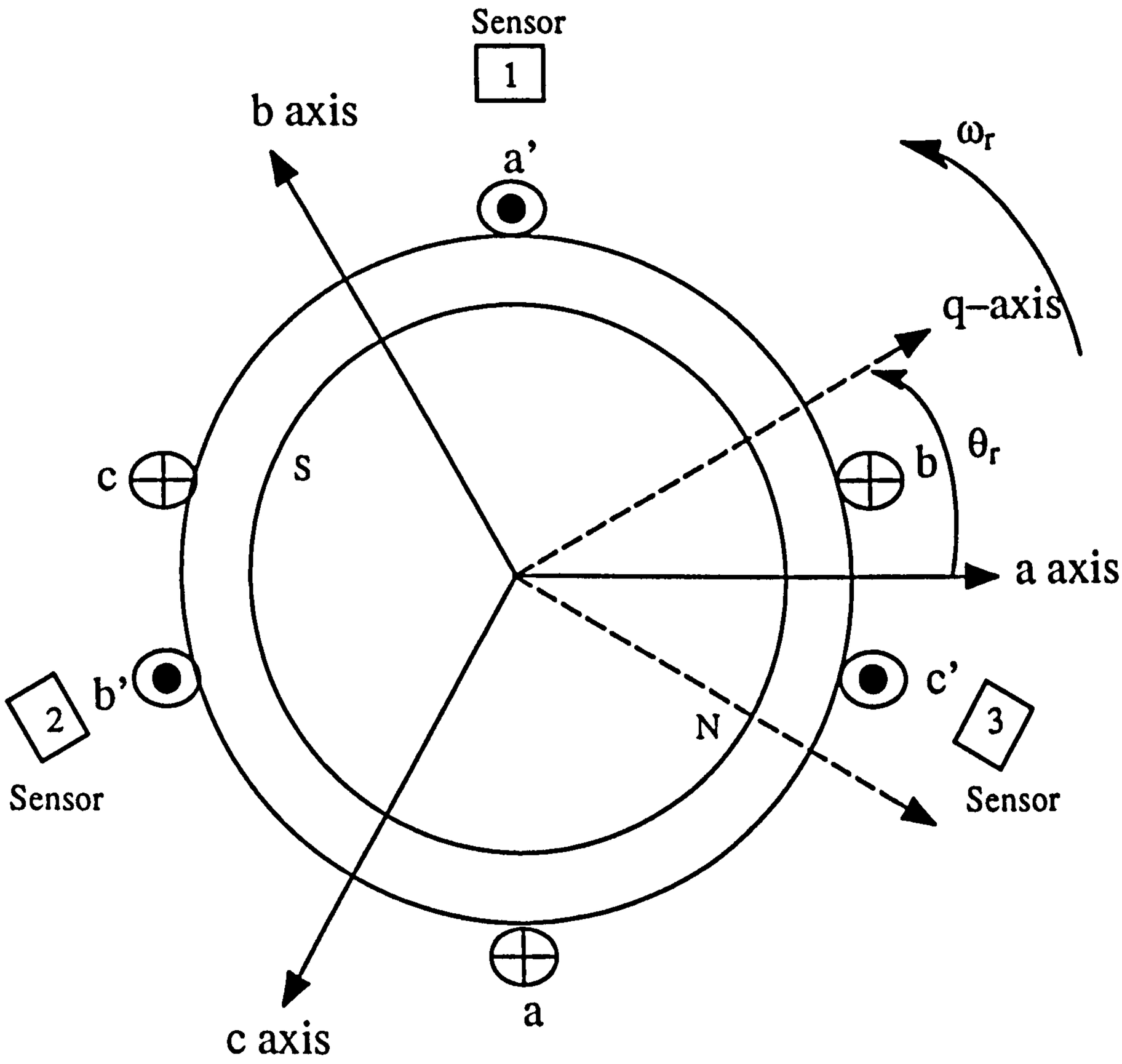

Figure 5.1 Two pole three phase machine

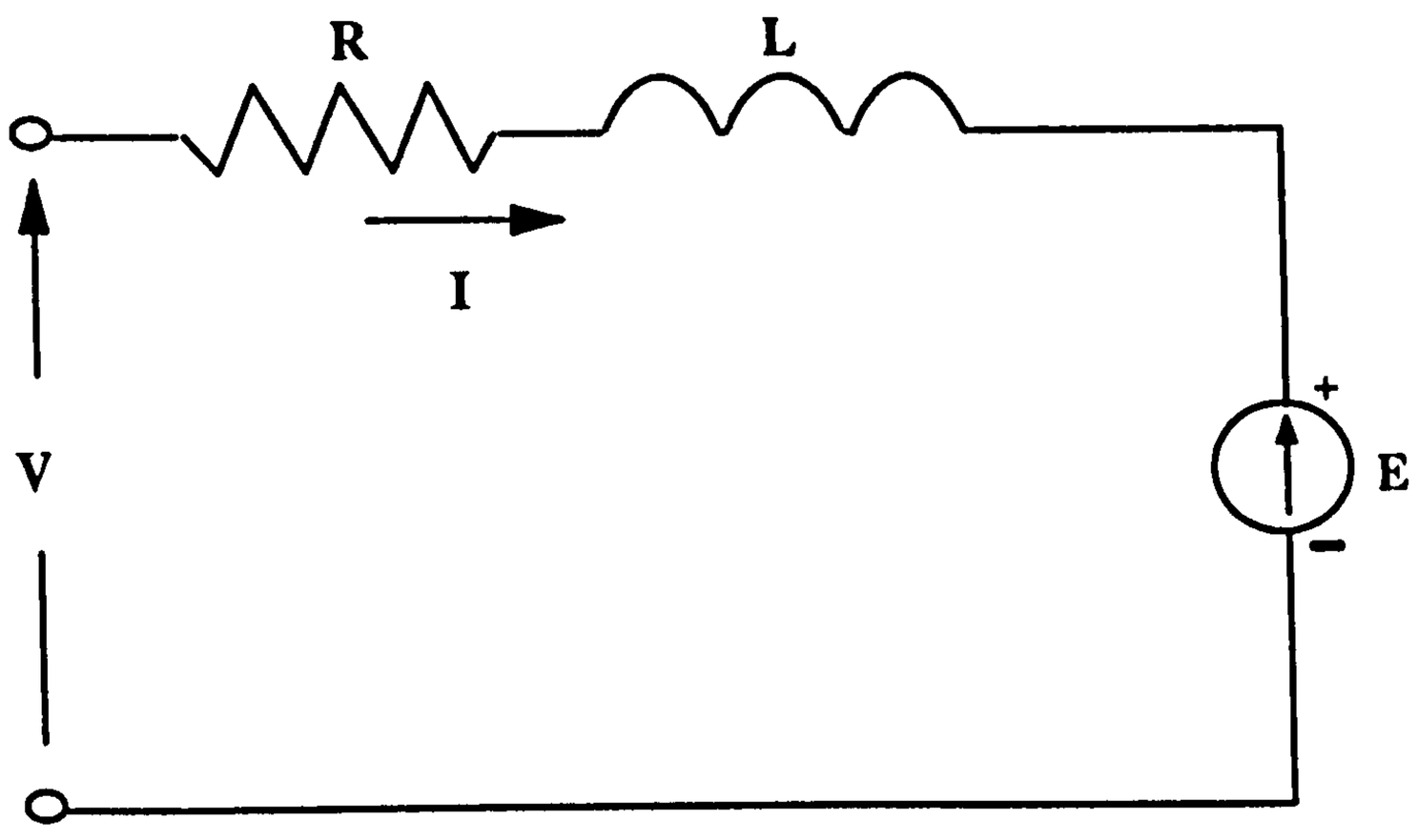

Figure 5.2 Equivalent circuit of the machine

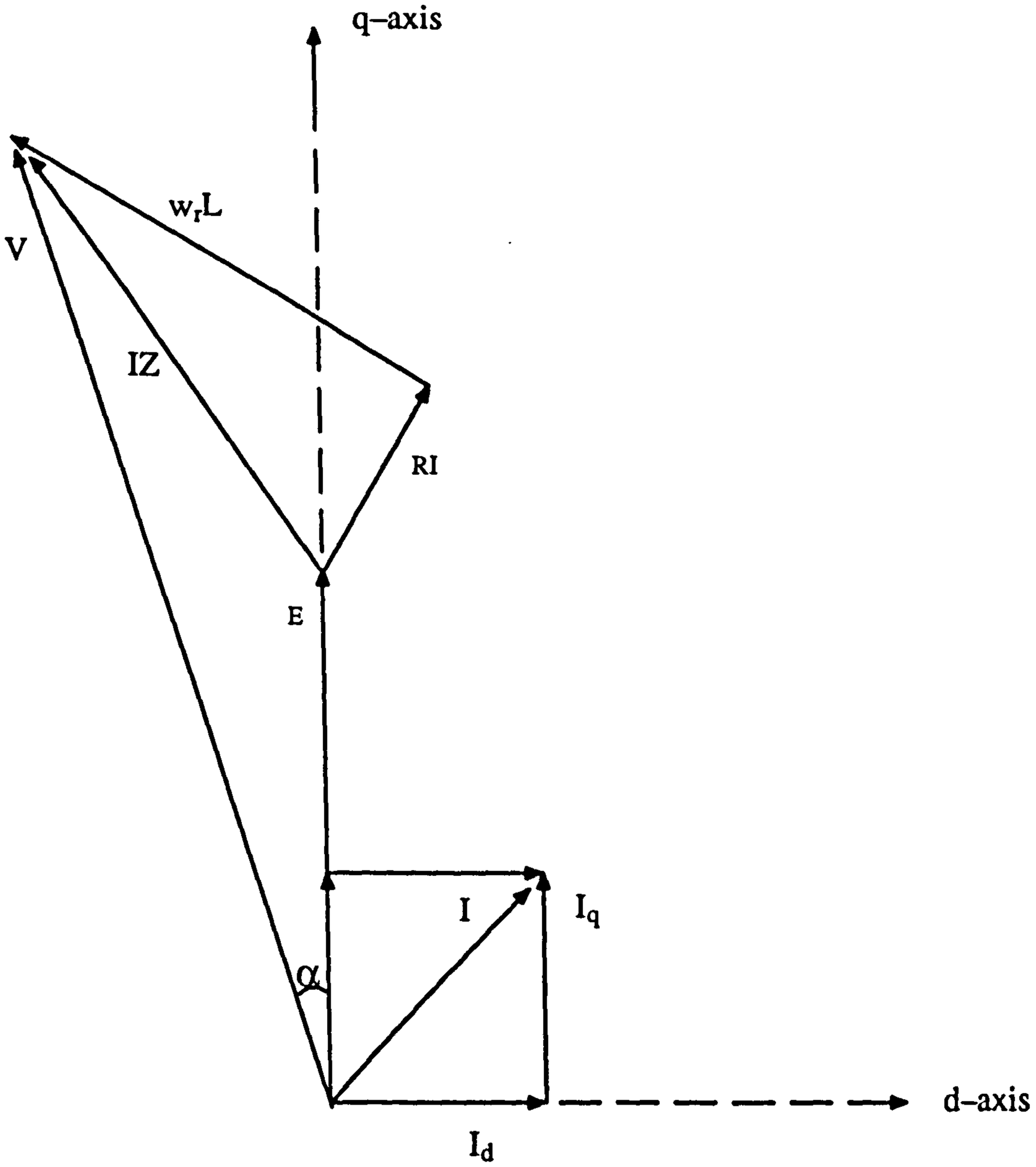

Figure 5.3 Phasor diagram for the brushless dc motor

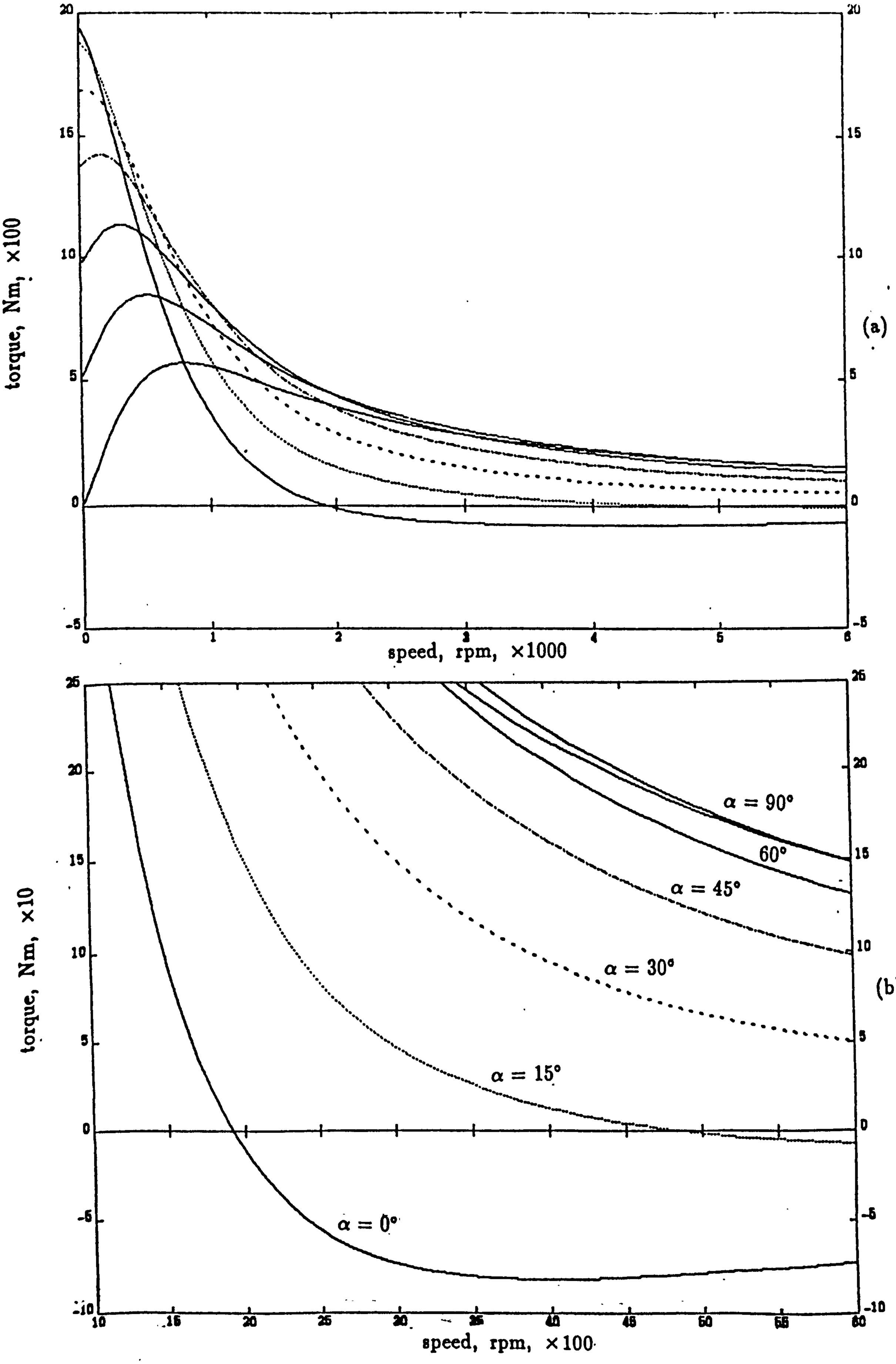

Figure 5.4 Torque/speed characteristics for various phase advance angles.

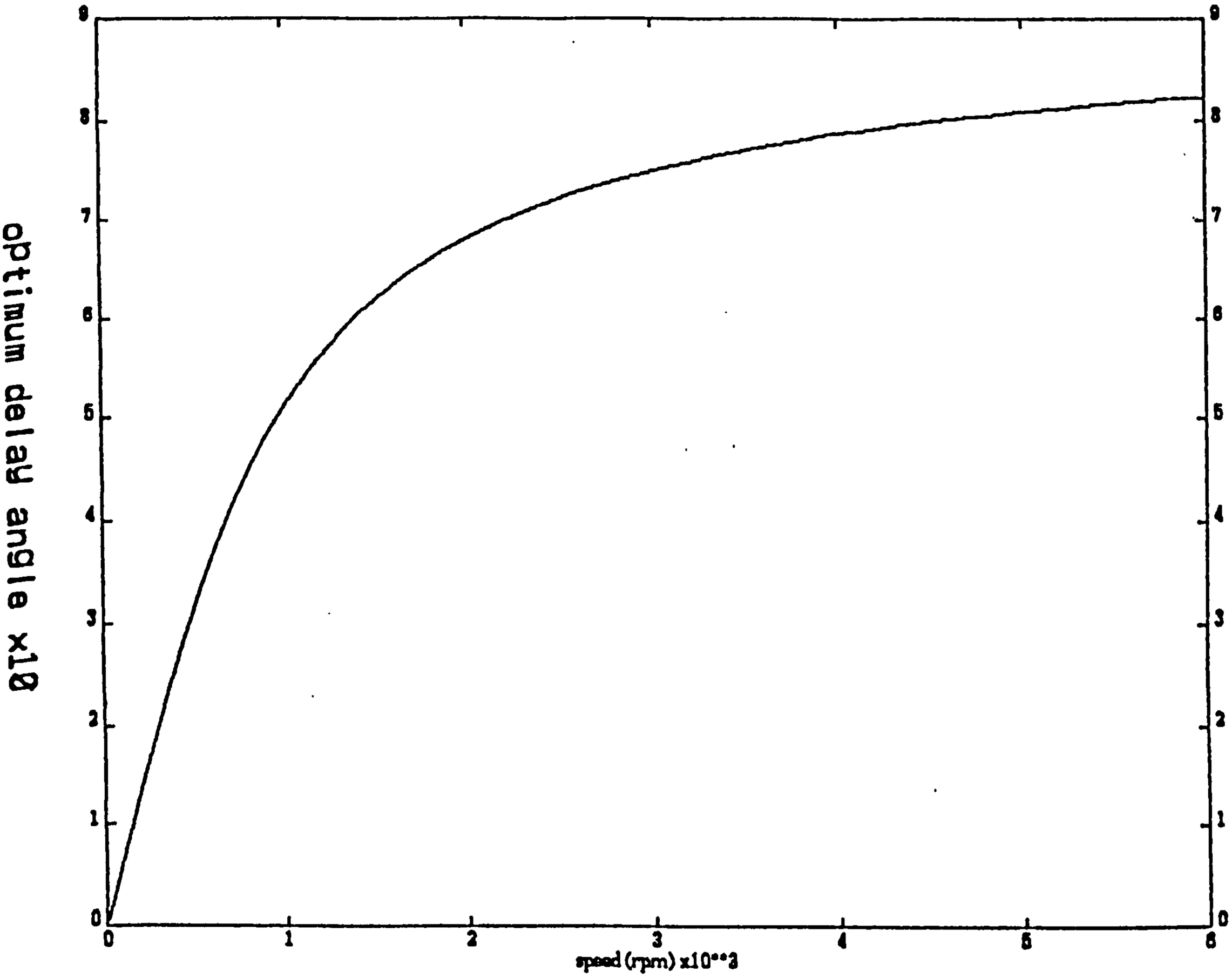

Figure 5.5 Optimum phase advance angle/speed characteristics.

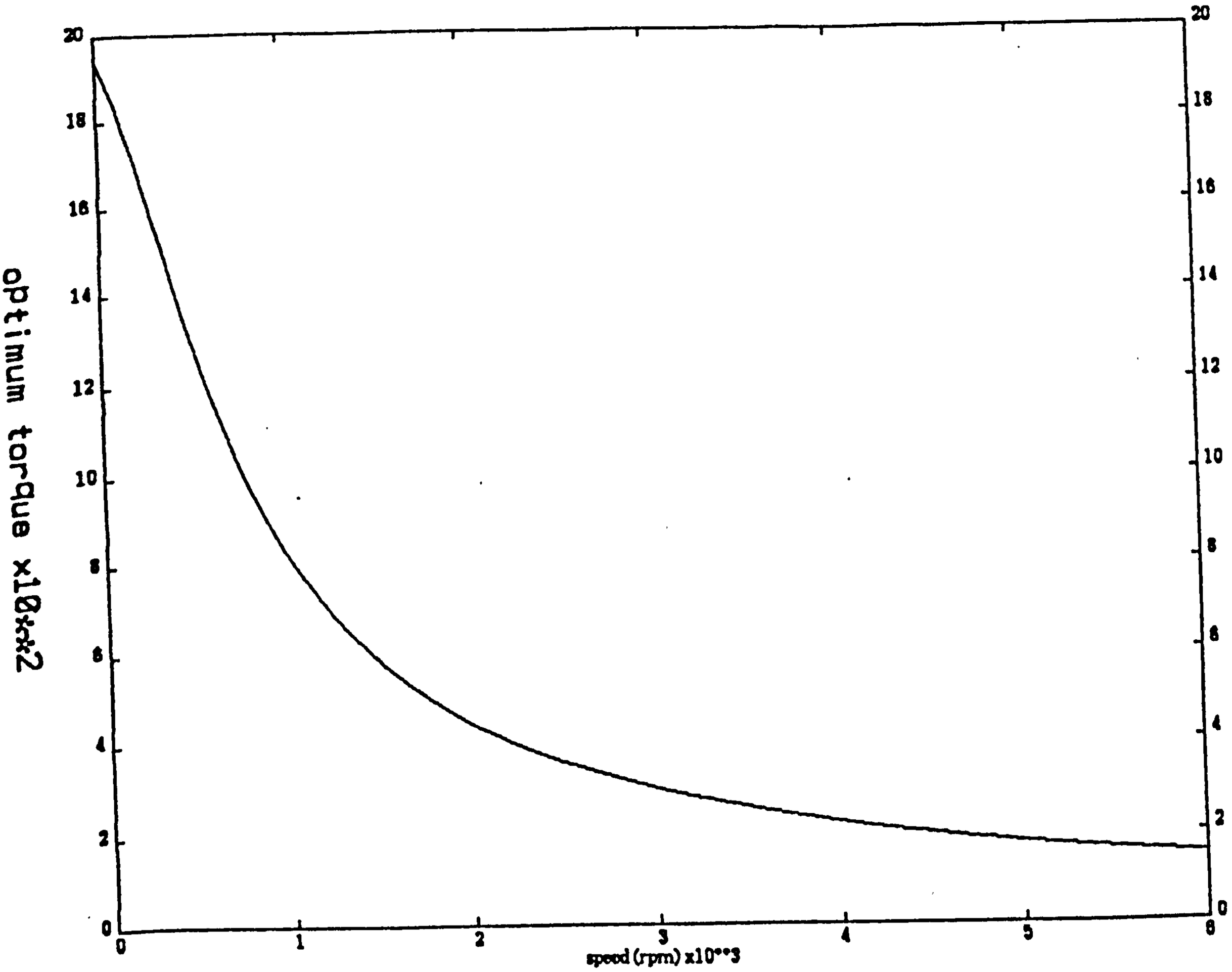

Figure 5.6 Torque/speed characteristics for optimum phase advance angle.

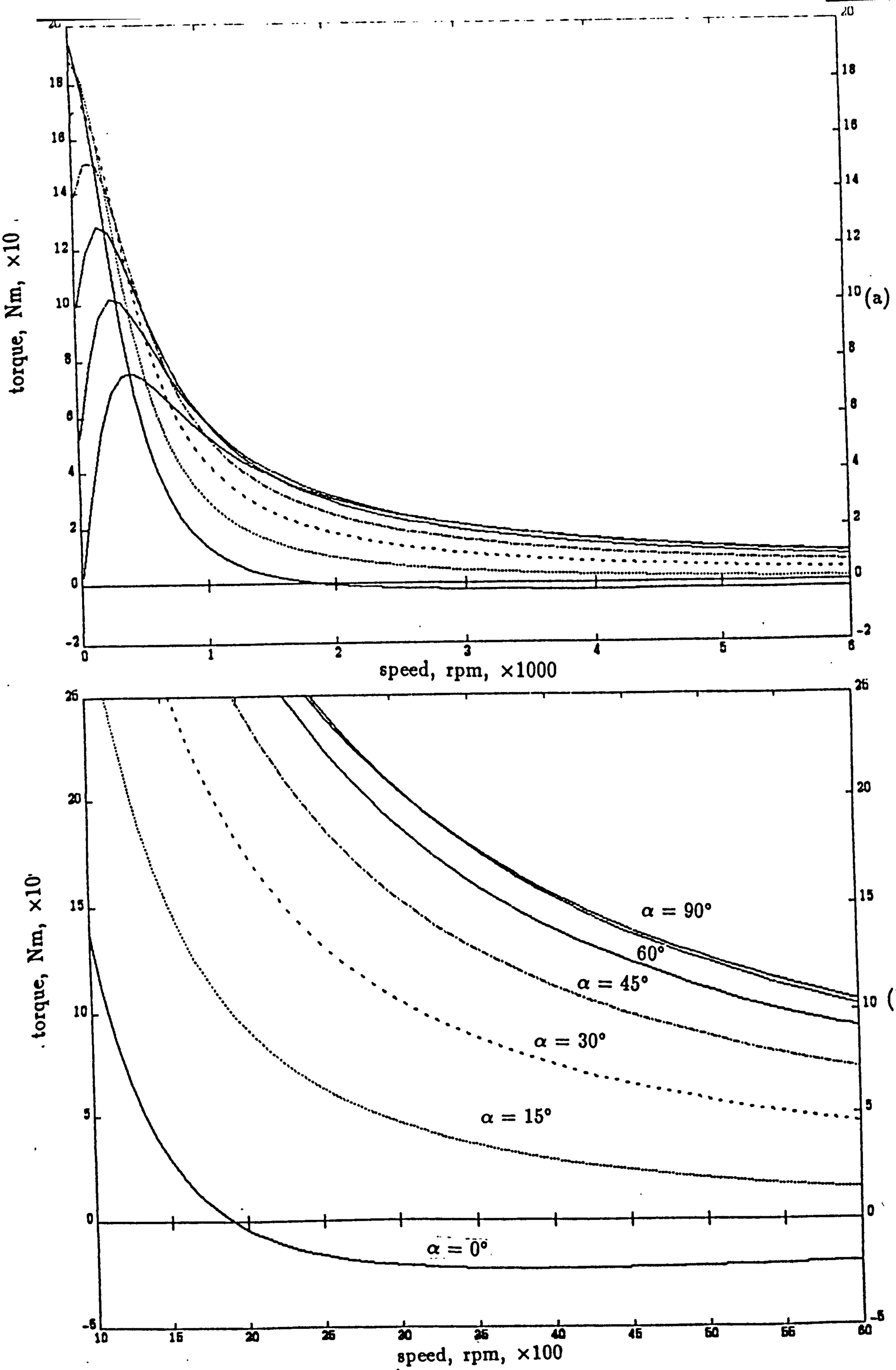

Figure 5.7 Torque/speed characteristics for various phase advance angles, for phase inductance of 6.0 mH.

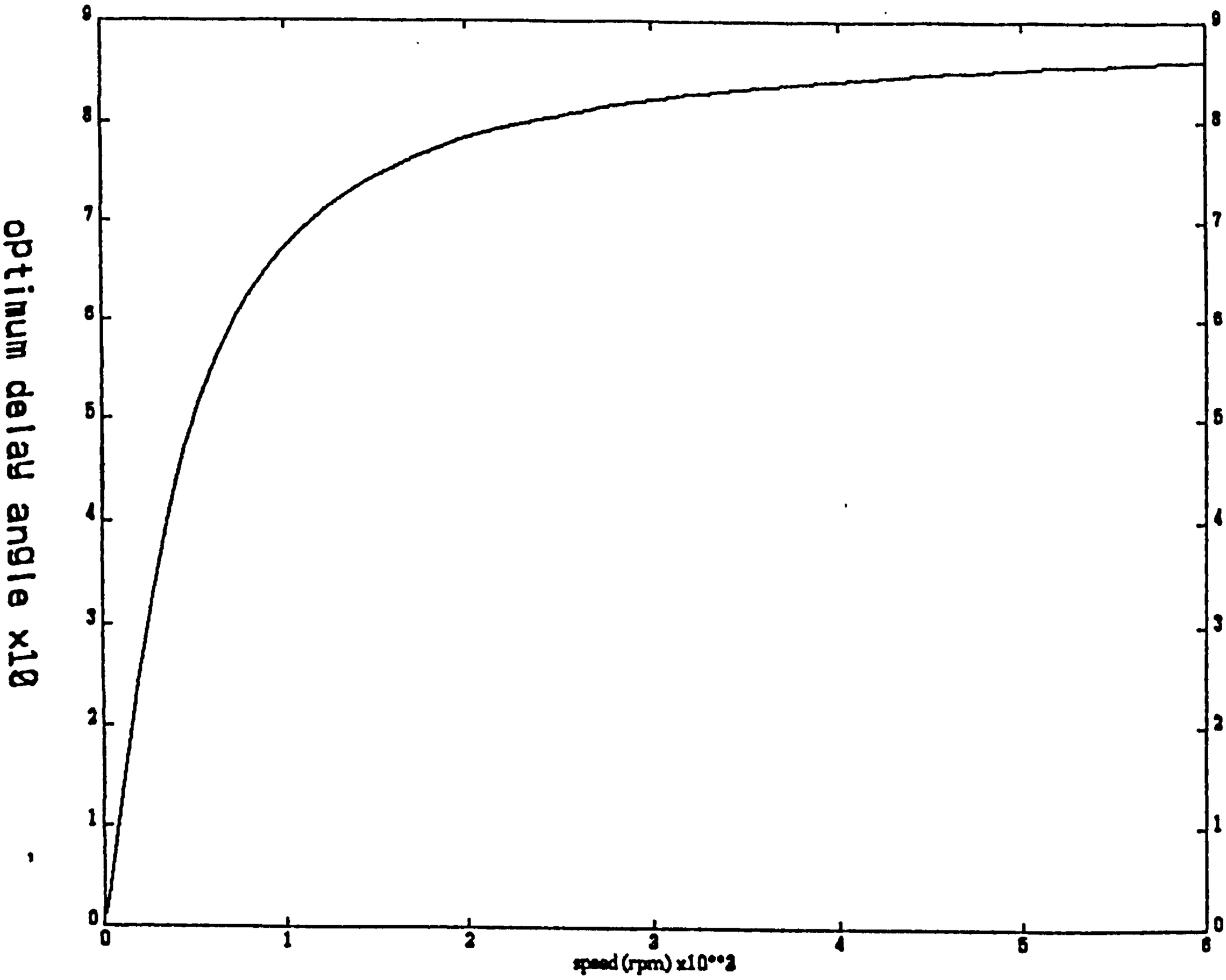

Figure 5.8 Optimum phase advance angle/speed characteristics, for phase inductance of 6.0 mH.

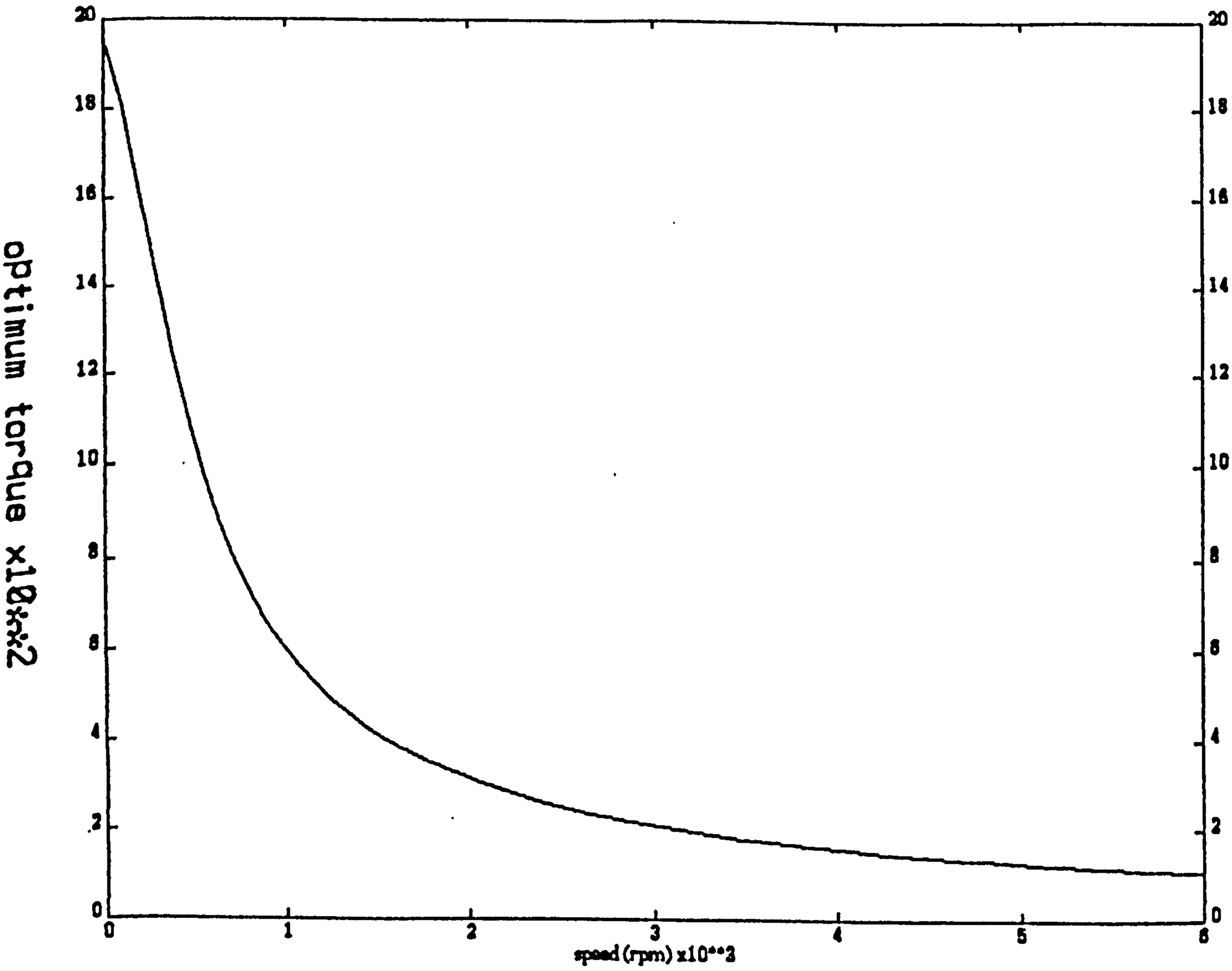

Figure 5.9 Torque/speed characteristics for optimum phase advance angle, for phase inductance of 6.0 mH.

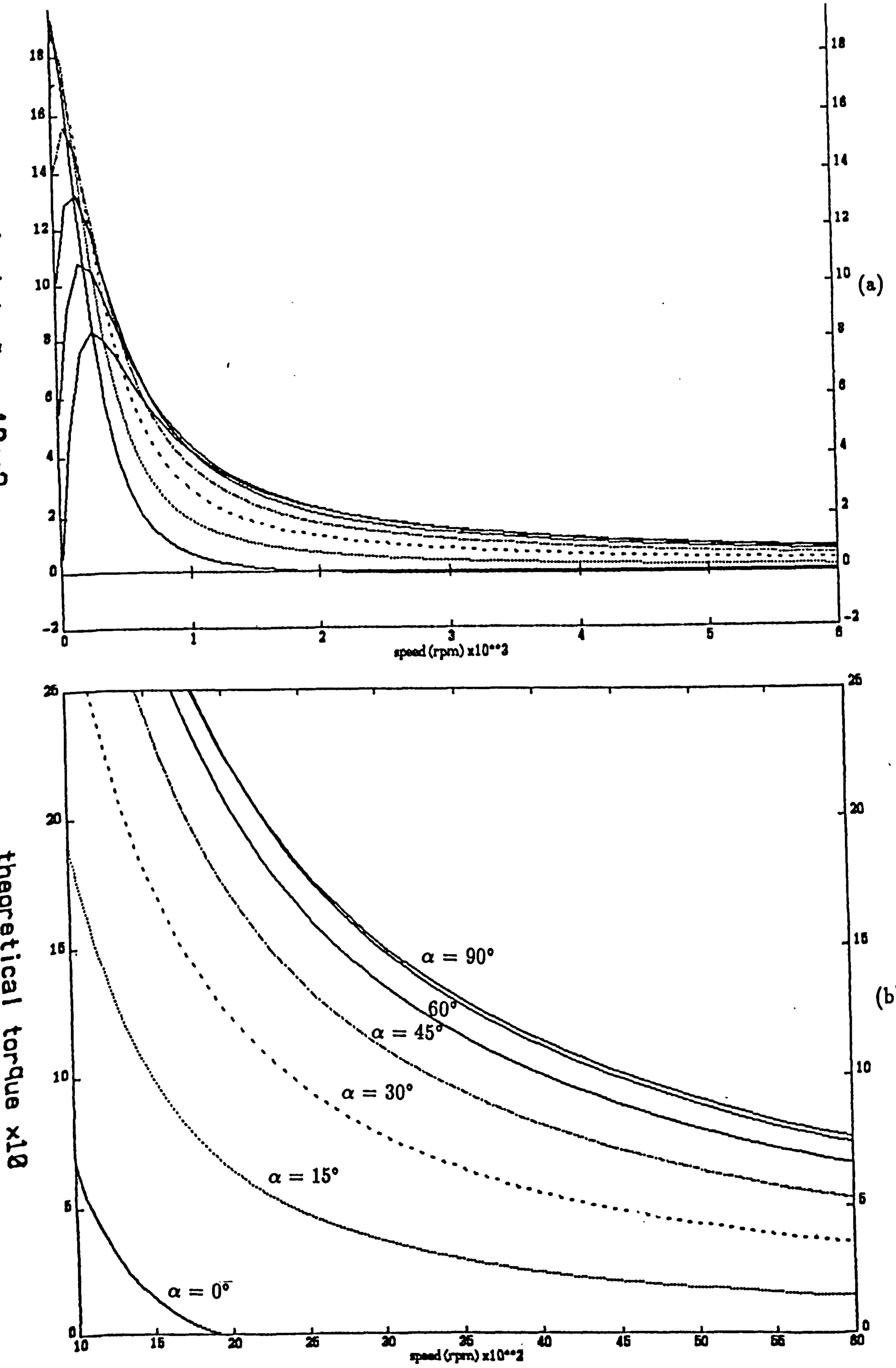

Figure 5.10 Torque/speed characteristics for various phase advance angles, for phase inductance of 9.0 mH.

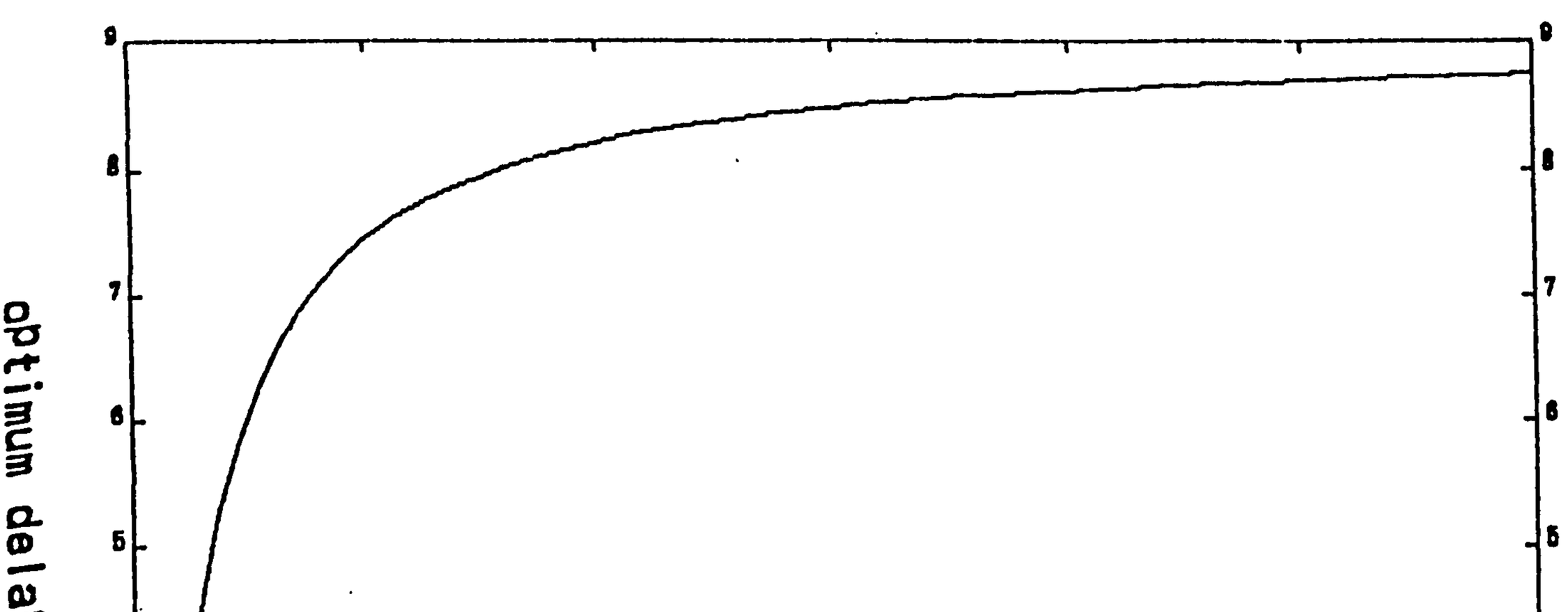

Figure 5.11 Optimum phase advance angle/speed characteristics, for phase inductance of 9.0 mH.

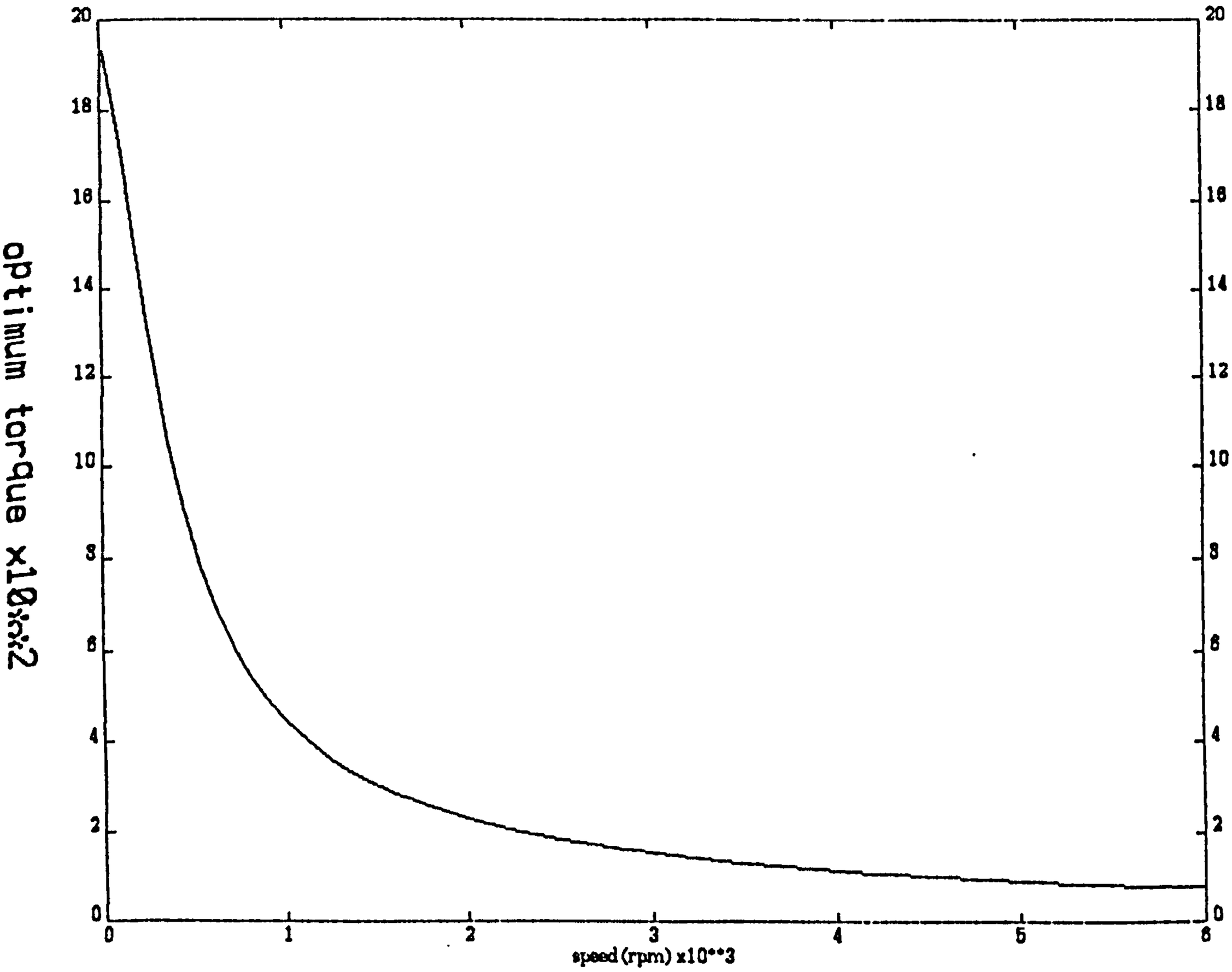

Figure 5.12 Torque/speed characteristic for optimum phase advance angle, for phase inductance of 9.0 mH.

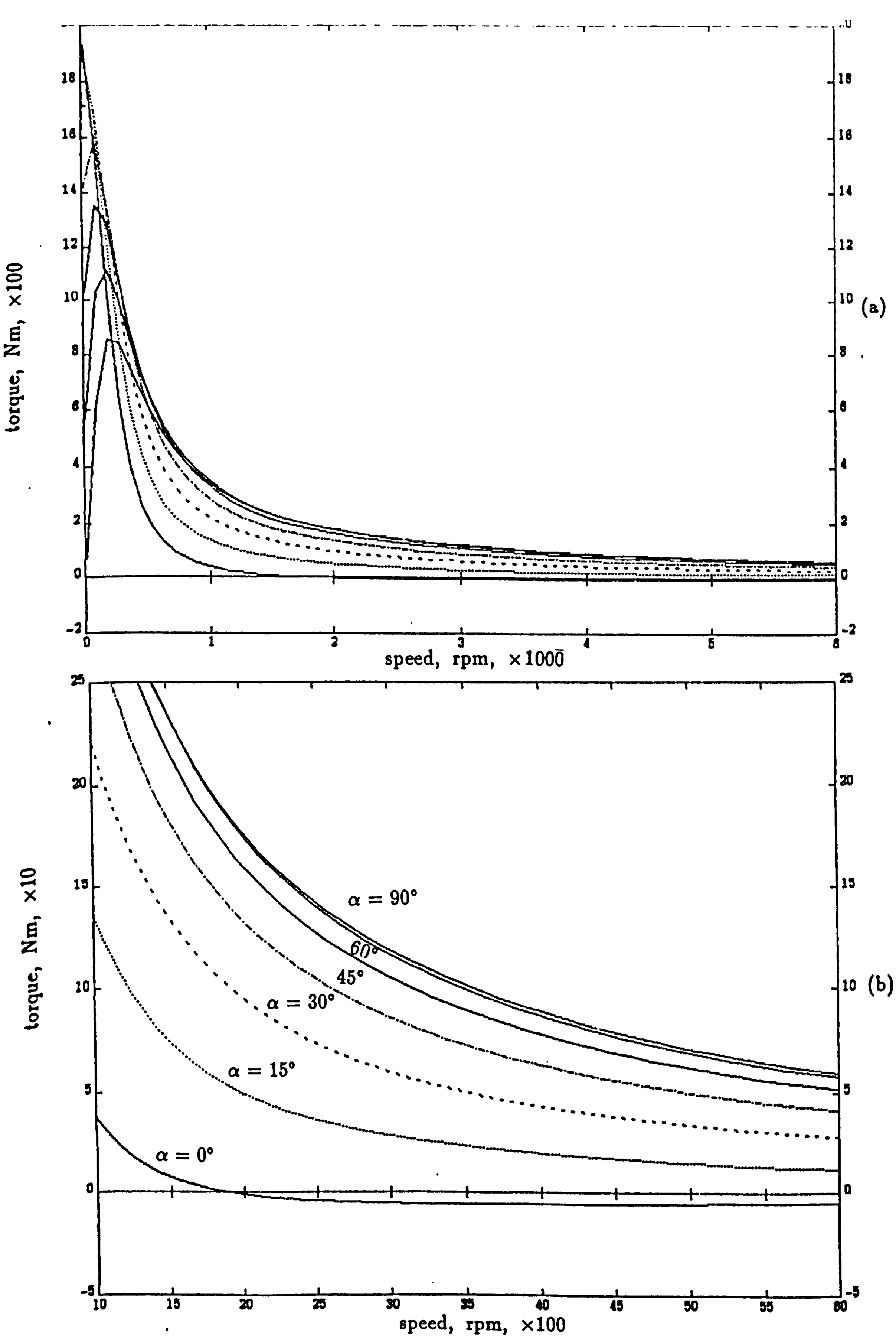

Figure 5.13 Torque/speed characteristics for various phase advance angles, for phase inductance of 12.0 mH.

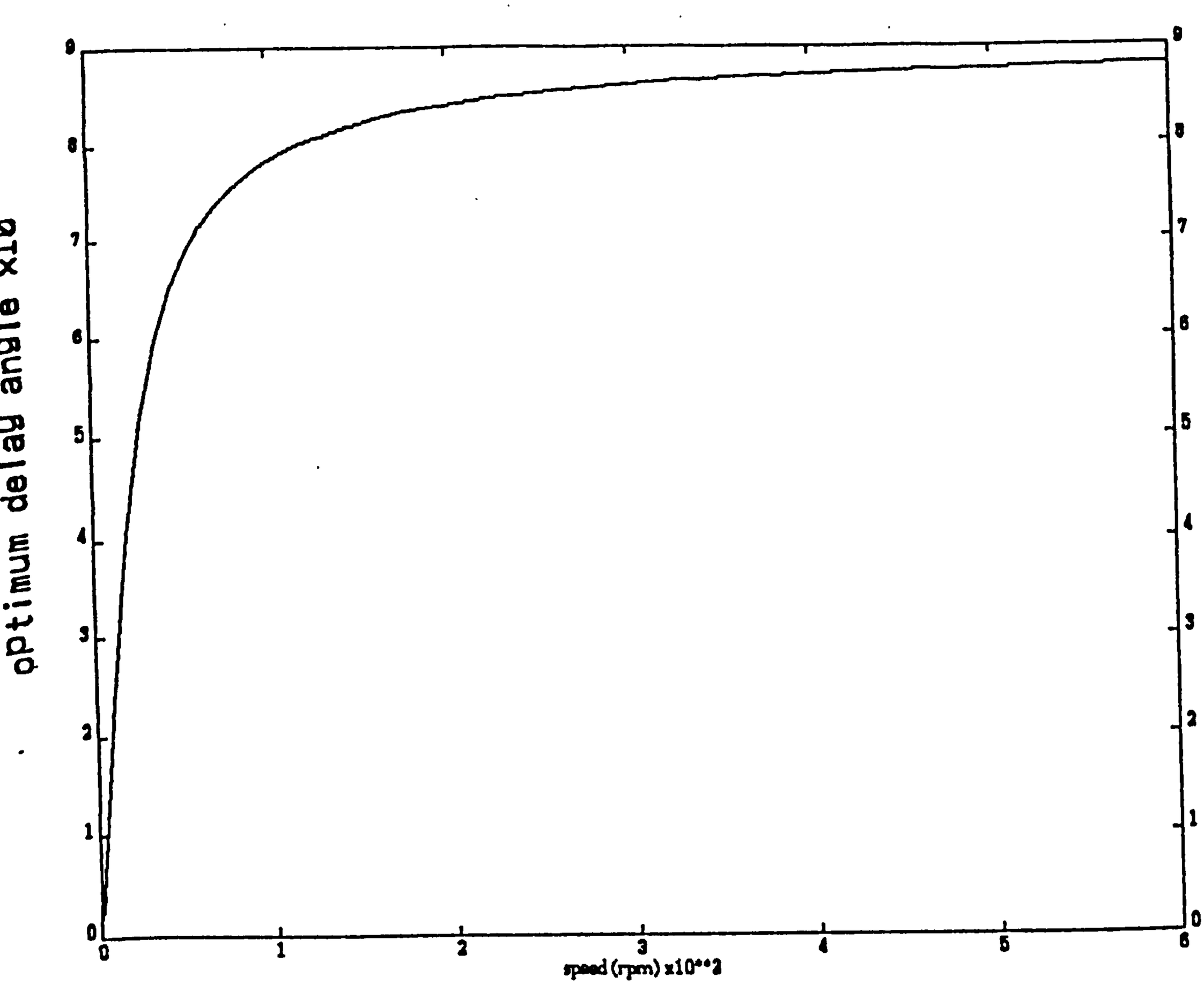

Figure 5.14 Optimum phase advance angle/speed characteristics, for phase inductance of 12.0 mH.

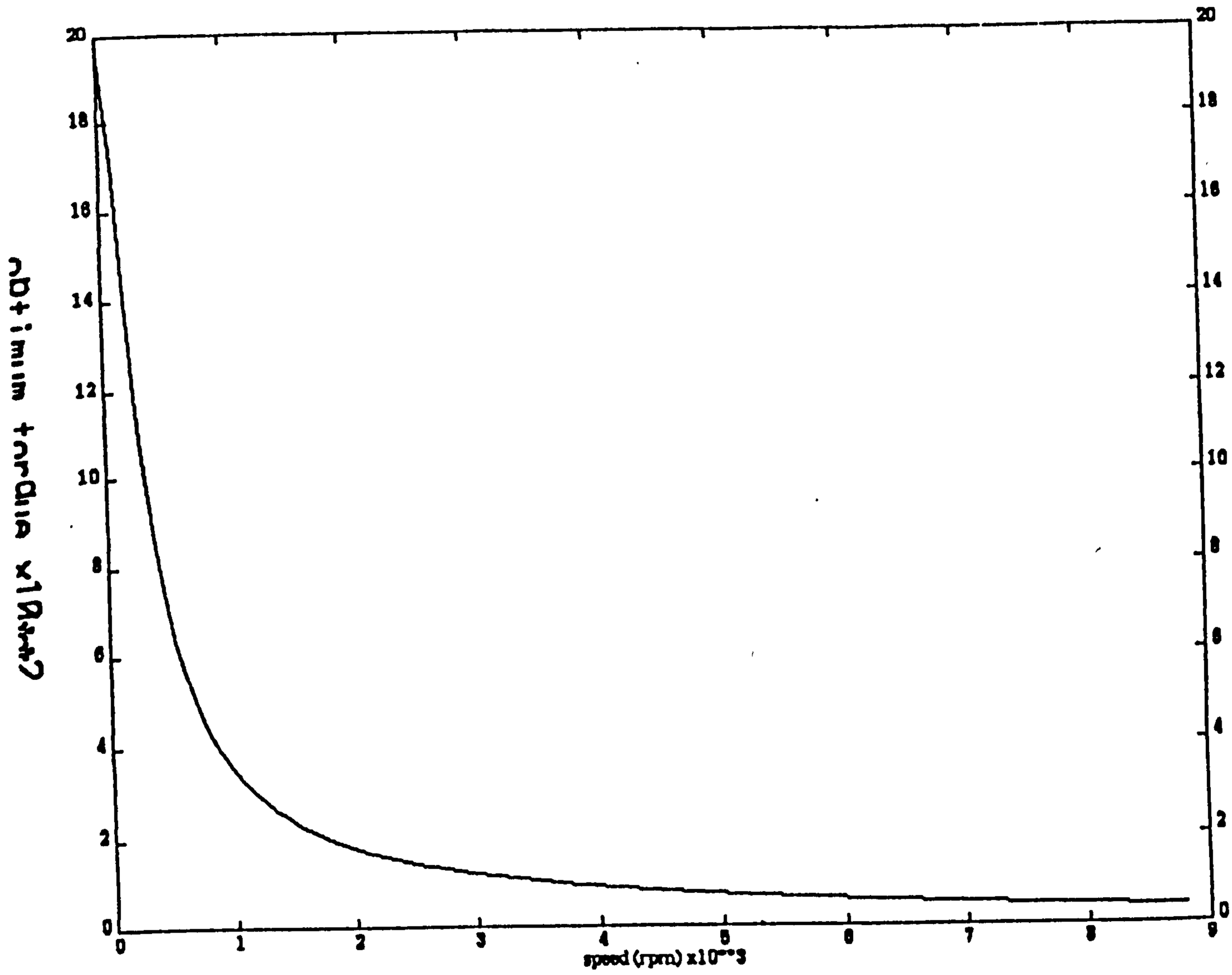

Figure 5.15 Torque/speed characteristics for optimum phase advance angle, for phase inductance of 12.0 mH.

CHAPTER 6

ANALYTICAL INVESTIGATION OF THE OPTIMUM HIGH-SPEED TORQUE PERFORMANCE

6.1 General

The critical importance of the phase advance angle in the successful high-speed operation of the brushless dc machine drive makes an analytical approach especially valuable since time spent on trail-and-error setting up in the laboratory is eliminated.

Although it would be possible to implement trail-and-error using the simulation, this approach, which is presented in Chapter 4, is involved and requires a substantial amount of computation time to establish best steady state operating points. It is therefore desirable to establish simplified analytical representations which yield a more direct means of finding the optimum phase advance angle when the system operating limits in the high and extended speed ranges.

In this chapter, an analytical study concerning the optimum phase advance is developed. In this study two analytical approaches to the problem of obtaining an optimum phase advance angle are presented. The first method is based on the controlled current waveform, where the phase current is effectively limited and therefore it assumes that the current must rise before back-emf in order that the current has attained the desired value at the start of the on-period. The second is based on sinusoidal analysis where the stator current is effectively sinusoidal at high-speed operation.

This chapter also presents a detailed analysis of the shape of the current and back-emf waveforms in a brushless dc motor drive and their effects on the torque/speed performance. From this analysis, it has been shown that the current and back-emf waveform shapes have a direct effect on the constant torque operation as well as the maximum torque that the brushless dc motor can deliver. During this investigation, a detailed analytical method for obtaining the required relationship between motor parameters in order to predict the desired shape of the current waveform is presented.

6.2 Analysis and Control of Current Waveform

6.2.1 General Control Considerations

It was apparent during the motor test-simulation, that the shape of the phase current was dependent to some extent on both the speed of the motor and the magnitude of the phase current. When the motor operates at high speeds, the current in the machine winding does not reach the demand current and then, it is no longer controlled. This limit depends on the value of the current and on the speed. This situation has direct effect on the maximum torque that the brushless dc motor can deliver. As was noted in the chapter 4 it is very helpful if the phase advance control is used to keep the current in phase with respect to the phase back-emf.

However, there is no feedback in the system to ensure that the phase advance angle has an optimum value at any torque load or speed. The approach of this problem, when the current limit is considered, is to derive a mathematical relationship between torque, speed and phase advance angle, to compute the optimum angles in order to maximise the torque output of the machine and to compare the predicted results with that obtained experimentally. It is the aim of this section to develop an analytical method which can be used to predict the phase advance angle. The method derived in

this section is believed to be a useful contribution to quantifying the effect of phase advance control on the trapezoidal brushless motor system performance, particularly when the current limit is considered.

Before describing the development of the new method, it is appropriate to summarise the drive conditions for the motor in relation to speed and to give an indication of the form of current waveforms which can be expected over the whole speed range.

6.2.2 Control Mechanism of the Current Waveform

The motor current and hence torque, is controlled by turning off one of the conducting inverter switches for a fixed period of time when the motor/inverter input current reaches a preset limit. The switch is turned on, and the voltage is reapplied to the motor, at the end of a fixed interval. As such it is one of simplest current control procedures available. Other inverter controllers developed subsequently have introduced much more advanced control switching strategies, such as PWM current control, as described in the previous chapter.

Current is driven from the supply rail via two active switch devices into two of the motor phase windings. The equivalent circuit of the system has been discussed in the previous chapters but can be for convenience given simply by equation (6.1) below, where the resistance of the motor phase windings and the conduction voltages of the inverter active switches have been neglected.

$$V_{dc} = L_s \frac{\partial i}{\partial t} + e_s(wt) \tag{6.1}$$

where

L_s is the total inductance of the two phase windings

i_s is the current in the active windings

$e_s(wt)$ is the line voltage of the active motor windings

For constant torque operation, the line voltage at the terminals, e, is constant over a 60° conduction period before the current, i, is switched to another of the motor line pairs. Assuming that the dc supply voltage, V_{dc}, is greater than the motor line voltage, the rate of rise current of the motor current is given by:

$$\frac{\partial i}{\partial t} = \frac{1}{L_s}(V_{dc} - e) \tag{6.2}$$

During the current chopping mode of operation, the input current is turned-off and the motor phase current, maintained by the inductances of the windings, continues to flow. Again neglecting the motor winding resistance and inverter device voltage drops

$$0 = L_s\frac{\partial i}{\partial t} + e_s(wt) \tag{6.3}$$

or if the induced back emf is constant during this interval, the machine current falls linearly

$$\frac{\partial i}{\partial t} = -\frac{e}{L_s} \tag{6.4}$$

The linearly rising and falling motor phase current, described by equations (6.2) and (6.4), can be considered for two different motor speeds within the constant torque region of operation.

At low speeds the motor phase current will only fall by a small amount during the fixed off time defined by the equation (6.4), as the motor line voltages which drive the current are much smaller at low speeds. However, due to the large difference between the dc supply voltage, V_{dc}, and motor line voltage, e, may be very short indeed. At these lower speeds the effective switching frequency of the power inverter switches becomes quite high, but the duty factor of the switching devices will be reduced.

At higher speeds the comparatively high value of motor back emf produces a large fall in motor phase current within fixed off time. Consequently the motor current delivered to the motor may be considerably less than the maximum specified value. The time taken for the current to return to its specified maximum value before current control is subsequently initiated will be comparatively long as, at higher speeds, the difference between the applied dc voltage, V_{dc}, and the motor back-emf, e, will be small. The duty factor of the converter switching devices will be large.

6.2.3 Current Waveform Characteristic for the Operating Speeds

Having analysed and studied all the available phase current waveforms at different operating speeds from the simulation test presented in Chapter 4, it was concluded that the drive system, in which the stator current is regulated by a voltage source PWM inverter, has two main control regions (a) region 1: the PWM action regulates the level of stator current to a limit value and the drive is said to be operating in the constant current mode (b) region 2: the current limiting using the PWM action becomes ineffective and is practically non-existent so the drive is said to be operating in constant voltage mode. In this second region the electrical time constant of the winding is relatively large in comparison to the excitation interval of each phase. Therefore the higher frequency components of excitation are heavily filtered and the major

current component is at the fundamental frequency. As a consequence of this the current waveform becomes sinusoidal in shape. Hence under this operating condition it is appropriate to derive an analytical expression for the optimum phase advance angle based on the sinusoidal analysis.

To demonstrate all this, figure 6.1 illustrates the drive conditions for the motor in relation to speed. Figure 6.1 shows also the amplitude and form of current waveforms which can be expected over the speed range. A wide variation of the form factor is evident. As is clear from examination of this figure the shape of the phase current, which is indicated by the point a in figure 6.1, is dependent on both load and the speed of the motor. As can be seen when the motor is running at low speed the phase current is still switched by the PWM current controller and can easily reach the required value because the applied voltage is sufficiently large to maintain this value. When the motor is running at a speed which is indicated by point b on the figure 6.1 the waveform shape is determined by the difference between the applied voltage and back-emf and also by both resistance and inductance of the winding. When the motor is running around point c in figure 6.1 the speed is still set by the maximum voltage, but the current is always below the demanded maximum value and starts to become sinusoidal in shape because it is determined by the time constant of the winding, as explained earlier. At point d both the voltage and current have their full rated values, so this voltage is insufficient to maintain the required value of current to the motor against the increased values of induced back-emf, as it was at point c. At this point the electrical time constant of the winding is relatively large in comparison to the excitation interval of each phase. As a consequence of this the current waveform becomes sinusoidal in shape.

6.3 Analytical Procedure to Determine the Optimum Phase Advance Angle

6.3.1 Controlled-Current Method

At higher speeds the increased back-emf in the stator phase windings is such that the motor input current never reaches the demand (or preset) maximum value required to initiate the current, or torque, control mechanism. The motor input current and output torque fall off with increasing speed as the input voltage to the system becomes insufficient to drive the rated current of the machine against the increased emf in the motor phase winding. As a consequence of this, the limited rate of change of phase current causes a phase delay of current with respect to the phase back-emf.

To ensure a reasonably square current waveform and to operate effectively over a wide speed range in a drive operating with current control, the switches must be closed in advance of the rising back-emf region, as shown in figure 6.2, so as to allow time, t_r for the current to build-up. During this switch-on angle, the current is considered to reach the desired level, I and is given by

$$I = \frac{\partial i}{\partial t} t_r \tag{6.5}$$

which shows during this t_r the current is allowed to build-up linearly up to its on value of I before the induced emf reaches any significant level. The time t_r can be related to the period of the current frequency, T by the following relation;

$$t_r = \gamma \frac{T}{2} \tag{6.6}$$

where γ can be chosen to give the required time advance of current waveform in one cycle and T is a period of current frequency and can be expressed in

terms of an angular velocity of the motor by the following relation

$$T = \frac{1}{f} \tag{6.7}$$

the frequency of the current, f, and the motor speed, ω_r are related as follows

$$f = \frac{p\omega_r}{2\pi} \tag{6.8a}$$

and the motor speed can also be expressed in revolutions per minute (rpm) as follows

$$\omega_r = \frac{2\pi n}{60} \tag{6.8b}$$

The rate of rise of current in the phase winding can be approximately calculated by

$$\frac{\partial i}{\partial t} = \frac{V_{dc} - e}{L} \tag{6.9}$$

If the rise current is advanced by γ in order to obtain the desired current level, I has to be controlled as follows by combining equations (6.5), (6.6), (6.7) and (6.8)

$$\gamma = \frac{pILn}{30V} \qquad (deg.) \tag{6.10}$$

since γ is a fraction of the half cycle period (or the time per cycle), it can also be expressed in terms of an angular distance, α, and thus this time in terms of electrical degrees is given by

$$\alpha = 360^{\circ}\gamma \qquad (deg.) \tag{6.11}$$

combining equations (6.10) and (6.11) yields

$$\alpha = \frac{6pILn}{V_{dc}} \tag{6.12}$$

which shows that the phase current is turned on at an advance angle, α, and it rises linearly from its zero value to value I. It should be noted that the effective applied phase voltage is actually the inverter output voltage and not the motor terminal phase voltage.

At speeds typically below a few revolutions-per-minute defined as the start-up mode, full torque is available. The PWM mode, which extends up to a base speed of ω_b, essentially defines the constant torque region when the current is controlled by chopping (PWM) operation. Beyond the PWM operation mode the curve enters into the constant power region where the high-speed torque is controlled only by the α angle. Above the critical speed, the limiting α angle is reached.

Looking at the machine from the point of view of the current-torque relationship, the torque developed by two phase windings, as shown in equation (6.15), shows a linear proportionality with supply current, i_s;

$$T_e = 2\frac{E}{\omega_r} i_s \tag{6.13}$$

where

$$E = k_b \omega_r \tag{6.14}$$

and equation (6.13) becomes

$$T_e = 2k_b i_s \tag{6.15}$$

where k_b is an arbitrary constant. Now the phase advance angle can be written in terms of the motor torque, peak phase current, speed, phase inductance, phase voltage

$$\alpha = \frac{6pT_eLn}{V_{dc}k_b} \tag{6.16}$$

6.3.2 Method for Constant Voltage Mode

It has been pointed out earlier that a current-controlled voltage-source inverter is a good compromise for the problem of feeding a brushless dc motor because current control operation provides effective torque control. However, current regulation is not effective at high speeds so that the inverter operates in the voltage-source mode. In other words, the torque/speed range over which current can be regulated is limited by the dc voltage source of the inverter. The terminal voltage approaches the maximum that can be supplied by the inverter causing a transition from PWM to constant voltage operation. In order to maximise the available output torque through out the region of constant voltage control, it is appropriate to use sinusoidal analysis to predict the optimum phase advance angle in the extended speed range.

A detailed analytical model for high speed operation has been presented in Chapter 5, using two-axis machine theory. In this analysis, the developed torque of the motor is found by the following equation

$$T_e = \left(\frac{mE}{\omega_r Z^2}\right)[VXsin\alpha + VRcos\alpha - ER] \tag{6.17}$$

this torque can be maximised at a motor speed n when the phase advance angle is set to its optimum value

$$\alpha_{opt} = arctan\left(\frac{2\pi}{60}\right)\left(\frac{nL}{R}\right) \tag{6.18}$$

This is because the optimum position of the instant commutation of the phase

current was found in the proceeding chapter as

$$\theta_{opt} = 90° - arctan\left(\frac{2\pi}{60}\right)\left(\frac{nL}{R}\right) \tag{6.19}$$

and this equation shows that if the speed of the motor $n = 0$ the phase advance angle, α_{opt}, equals 0°. As the speed increases, the instant of the current commutation should be advanced by a position $arctan\left(\frac{2\pi}{60}\right)\left(\frac{nL}{R}\right)$. However, the variation of the phase advance angle with motor speed is described in detail in Chapter 5 and the results of this investigation shows that at all speeds the voltage applied to the winding must advance in phase to compensate for the increasing phase lag between current and applied voltage. As a consequence of this, the current in a winding is in phase with the corresponding back-emf and hence the optimum torque production can be obtained.

6.4 Comparison of Optimum Phase Advance Angle Calculated by Analytical and Simulation Methods

In order to investigate the validity of both analytical methods set forth in the previous sections, their results are verified by comparison with results obtained by the simulation approach.

Figure 6.3 shows the phase advance angle versus speed using controlled-current, constant voltage mode and and simulation methods. It is seen that the results of the controlled-current method are in close agreement with those of the simulation method at high-speeds and differ widely from the constant voltage method which gives satisfactory results only in the extended speed range. This should be expected as the controlled-current method has been developed for a drive operating with the current mode whereas the constant voltage mode was developed for a drive operating in constant power mode (field weakening).

6.5 Transition Between Constant Current Region and Constant Voltage Region Using a Simple Algorithm

6.5.1 General Control Considerations

As explained earlier, the speed/ torque characteristic of the brushless dc motor drive has different regions of operation: the first region is the constant current region. In this region, torque is controlled by current amplitude using PWM controller and by advancing the commutation angle. The second region is the constant voltage (or field weakening) region and current and torque can only be controlled by advancing the commutation angle.

The transition point from the constant current control region to the constant voltage control region is reached, when the dc supply voltage, V_{dc}, of the motor is equal to the motor back-emf. The current demand, I_{demand}, at this point depends on the transition speed which can be termed the base speed (or corner speed). If the speed control loop requires a current higher than the value at the base speed the drive system operates in the constant voltage region and thus the PWM current controller runs out. The analysis that the combination of the control region methods and the base speed is given by the following simple algorithm.

6.5.2 Transition Control Algorithm

In order to combine the control region methods, which are derived in the preceding section, in the whole speed range a transition factor, $K(w)$, is introduced which specifies a relation between the transition speed, ω_T, (i.e., base speed) and speed regions, ω. In the case of a $K(\omega) = 1$, the drive operates in the constant current control region. But for a transition factor $K(\omega) = 0$, the drive operates in the constant voltage region. If the transition factor $K(\omega) = \frac{1}{2}$, the drive operates at base speed region.

The general effect on the phase advance angle/speed curve taking account of control regions is shown in figure 6.3. The analysis that the combination of control regions due to the transition factor is given by the following expression [Safi, et al, 1993];

$$\alpha_T = K(\omega)\alpha_i + (1 - K(\omega))\alpha_v \tag{6.20}$$

where

α_i is phase advance angle for the constant current control region and is given by equation (6.12).

α_v is phase advance angle for the constant current control region and is given by equation (6.19).

and

$$K(\omega) = \frac{1}{(1 + \frac{\omega}{\omega_T})} \tag{6.21}$$

It is clear from the above analysis that the transition between control regions are governed by a transition factor that determines when transition takes place. Expression (6.20) can be used effectively in the whole speed range and also will easily determine the base speed at which the current controller runs-out. The result of expression (6.20) is verified by comparison with analytical and simulation methods. It can be seen from figure 6.4 that the results of the combined algorithm is in close agreement with that of the simulation method.

6.6 Torque Improvement Methods by Waveform Shaping

The current and back-emf waveform shapes have a direct effect on the constant torque operation as well as the maximum torque that the brushless dc motor can deliver. This section presents a detailed analysis of the shapes of the current and back-emf waveforms in a brushless dc motor drive and their effects on the torque/speed performance.

6.6.1 Conditions for Constant Torque Operation

In Chapter 2 the basic operation of the brushless dc motor is presented. The method of torque production is described by a frequently used method where the idealised motor phase current and motor phase voltage waveforms were multiplied together to find the contribution to the total motor torque made by each motor phase. The shape of the resultant torque waveform is determined by the motor back-emf waveshape. This method assumes that all armature reaction fluxes are negligible and that the motor phase currents can be established and discontinued instantaneously. These assumptions are usually considered in an analysis of a brushless dc machine.

Figure 6.5 shows the characteristics of trapezoidal back-emf drive. As can be seen from this figure, if each of phase current and voltage is either constant or zero, then the total torque developed by the motor is also constant. The shape of the back-emf waveform outside the two 120° conduction zones where current is supplied to each phase from the dc supply does not affect the shape or amplitude of the resultant torque waveform. Thus the trapezoidal back-emf waveshape gives torque ripple-free operation when driven by three phase quasi-square currents.

The constant torque production mechanism of the motor can be readily understood by noting that, under idealised conditions, at any time there is only one current path in the star connected motor circuit. This current, assumed to be constant, is supplied via the power inverter devices through two phases of the motor. The current flows for a complete 60° interval until

one of the power inverter devices switches; the current then flows through a different combination of motor windings. Therefore for each 60° interval of the total excitation cycle, constant current is driven across successive lines of the motor to give continuous motor operation.

Therefore for constant torque production in a system drive with 120° winding conduction, it is essential that the interval of constant back-emf should also span at least 120° conduction angle. For this system a back-emf waveform of this type is most easily obtained using magnets with a wide-arc and full-pitched concentrated windings. However in a larger machine better thermal performance is obtained with a distributed winding, which is more easily assembled and has more compact end windings if the coils are short-pitched. Inevitably there must be a compromise between the conflicting requirements and this may lead to a less than ideal induced emf waveform.

In contrast, there are some other alternative ideal back-emf waveforms which give constant power conversion when driven by quasi-square currents. These back-emfs are of particular interest; they have a composite trapezoidal emf shape and different top intervals but they give constant power conversion. The noteworthy features of these particular waveshapes are discussed later in this section.

In principle it should be possible to compensate for imperfections in the back-emf waveform by optimising the phase winding currents so that torque delivered by the motor remains constant. One approach of the the problem is to derive a simplified analytical representation which yields a more direct means of finding the desired shape of the phase current at the system operating limits in the high and extended speed ranges. This method is discussed in the following section.

6.6.2 Torque Improvement by Means of Back-EMF Waveform Shaping for 120° and 180° Conduction Angles

The choice between possible motor designs which have different back-emf waveforms is usually determined from a consideration of the mean power converted by each alternative design. This is proportional to the mean value of induced emf over the top 60° span of the motor voltage, which is the power converting region. Consequently those phase voltage waveshapes which are constant over the power converting region give the preferred solution of maximum torque production. The trapezoidal back-emf is a practical design which gives maximum torque production with low torque ripple (constant torque operation) and hence is the most widely used type of motor for drives of this type. However in practice the back-emf waveshape of the motor is affected by leakage and other effects in the airgap of the machine which means that these ideal waveforms can not always be achieved in a particular machine design.

It is interesting to examine the effect of back-emf waveform shaping which minimises the torque ripple and thus satisfies the condition for constant torque operation discussed above. Clearly the choice of a particular stator winding determines the shape of the motor back-emf waveforms for a particular airgap flux distribution.

For constant torque operation, (or torque ripple-free operation), there is a set of trapezoidal back-emf waveforms with suitable constant flat intervals which will result in the constant torque condition being achieved for the drive system under consideration.

In this section, the simulation package was used to predict the effect of a back-emf waveform on the constant torque operation of the drive at low speed with various values of top constant emf intervals. The tests for two conditions are presented. Both are for conduction angles of 120° and 180° conduction angles with constant flat intervals of 90°, 105°, 120° and 135°.

6.6.2.1 Conduction Angle of 120°

To demonstrate the effect of a back-emf waveform shaping at low speed operation with various values of constant top interval. Figures 6.6-6.9 show the results for 120°, and constant top regions of 90°, 105°, 120° and 135°. In these figures the phase current and torque developed by the motor at 100 rpm is shown.

From these figures it can be seen that with a large constant top interval, the torque ripple of the motor is reduced. In both cases of 120° and 135° top flat intervals the torque constant operation can be achieved with minimum torque ripple.

6.6.2.2 Conduction Angle of 180°

Under the same conditions figures 6.10-6.13 show the effect of a back-emf waveform shaping at low speed operation with various values of constant top interval for 180° conduction. These figures show sets of waveforms for constant top intervals of 90°, 105°, 120° and 135°. Also in these figures phase current, torque developed by the motor are shown.

The results of these figures demonstrate an interesting point concerning the torque ripple. The torque ripple is increased by increasing the top region of the back-emf. This is because the current in each winding has two 60° interval per cycle when the current magnitude is at the demanded level and four intervals when the current is at half of the demanded current. As a result, the mismatch in the 60° interval of the current demanded with a larger back-emf's top interval can result in large torque ripple. Therefore in order to minimise the torque ripple it is necessary to choose a small back-emf top interval when the extended conduction angle method is used.

6.6.3 Torque Improvement by Means of Current Waveform Shaping for 120° and 180° Conduction Angles

As stated above, in machines with trapezoidal back-emf a rectangular current waveform is needed to produce constant torque operation and to maximize the torque production. These operations are relatively difficult because of the highly inductive nature of the motor and high energy involved as well as the back-emf which becomes large at high speed.

Also it was apparent during motor tests (Chapter 4), that the shape of the phase current was dependent to some extent on both the speed of the motor and magnitude of the phase current. However it was usually possible to keep the current waveform reasonably close to the desired shape by selecting an appropriate phase advance angle, as show in the earlier section. An alternative way is to limit the current magnitude with respect to operating conditions, as will be presented in this section.

In high speed operation, the winding current becomes trapezoidal rather than the desired rectangular shape due to the finite rise and fall times. It is these rise and fall times of current waveform that determine its shape when the torque load or speed of the motor varies. On the other hand, in the high-speed range the effect of the limited steepness of current becomes important because both the phase advance of current with respect to the emf and torque ripple amplitudes increase as speed increases. For such speeds the torque of the machine can be improved, if the current waveforms of the phase currents are constrained, as explained below.

If the current rise and fall times are the same, the effect of rising current in the winding could be compensated by decaying current in the previous excited winding during the commutation, thus leading to constant torque operation. But normally the current fall is faster than current rise so commutation torque ripples are produced and consequently maximum torque is reduced. The constant torque operation can be achieved by keeping the

current waveforms as close to rectangular in shape as possible.

With the brushless dc drive system, there is no feedback to ensure that the current waveform has desirable shape at any speed or torque load. Therefore it is of interest to determine a mathematical relation which can be used to predict the range over which the speed and phase current magnitudes can vary without there being any significant resultant distortion to the desired current waveform shape. This distortion of the current waveform is a result of combination of the design and control. It is shown in Chapter 4 that this distortion depends on the relative magnitude of the inductance and also on the frequency at which the phase winding is operating (i.e; at higher frequency there is a short time per cycle in which to force current to rise and to fall as desired). Therefore to ensure a reasonably square wave current waveform in a motor operating in a wide-range speed the phase current must be limited.

The method of current magnitude limiting is based on the rise time as a fraction of its time period (see figure 6.15). This type of limiting determines the magnitude of the current waveform relative to the speed range and if this is greater than some permitted limit the desired shape is only permitted to change by that limit value. This is a reasonable constraint for such a case, as explained later in the following analysis.

6.6.3.1 Analysis of the Shape of the Current Waveform

Before attempting the detailed analytical procedure to derive the required expression for optimum shape of the current waveform, it is useful to explain the main regions of current waveform, including the rise and fall times since the method of analysis is based on these regions and more background information is given to provide a sufficient explanation and an understanding of the analytical procedure.

The waveshapes shown in figure 6.14 cover a complete motor period, T, of 360° electrical degrees. The idealised motor current, i_a, i_b, i_c shown

(dashed line) is a three-phase rectangular current with 120° lag between phases. The actual current shown in full line is different due to the effect of inductance and induced voltage in the motor windings (see Chapter 3). The motor current shown is typical for low speeds and changes appreciably as motor speed increases.

To help in understanding the analysis of the current waveform, consider the voltage equations that show the currents in each phase are governed electromagnetically and electrically. In such an equation, for instance, the phases are coupled electromagentically via the mutual inductances and electrically by the condition that currents at the star point must sum to zero. It is important to understand the relative significance of various terms in this equation at rise and fall times and this can be aided by considering the single phase case which is governed by

$$V_{dc} = \Big(R + pL\Big)i + e \tag{6.22}$$

or

$$i = \frac{V_{dc} - e}{\Big(R + pL\Big)} \tag{6.23}$$

V_{dc} is the inverter output voltage which the effective phase voltage and L is the phase inductance. It is worth seeing what can be understood from these equations because, as noted earlier, this simple set-up encapsulates some of the essential features of actual winding current behaviour.

If the back-emf e is less that the applied voltage V_{dc}, the effective voltage will be positive and large. On the other hand if the applied voltage, V_{dc} is approximately equal to e, the effects of the phase current will be highly significant. A further point if the mutual inductance terms are included in the above equation, i.e.;

$$L\frac{di_a}{dt} = (V - e_b - i_a R_a) - M_{ab}\frac{di_b}{dt} - M_{ac}\frac{di_c}{dt} \tag{6.24}$$

the mutual will dominate when $(V_{dc} - e - i_a R_a)$ term is close to zero. By referring to equation (6.23), at switch-on V_{dc} is the output voltage of the inverter and back emf e is smaller than V_{dc} and of the same sign as V_{dc}, thus the current is driven by the voltage of $(V_{dc} - e)$ which will be large in comparison with any contribution from the mutual inductance terms. The current will thus increase at a rate determined by the self inductance and resistance of the winding and the change in $(V_{dc} - e)$ caused by the increase in e with speed and time. With load the torque demanded from the motor results in the current reaching large levels, causing the iR term to become significant toward the end of the rise time (since phase current, i has increased and $V_{dc} - e$ has reduced).

When the phase winding is commutated off, current continuity is maintained via the diode connected to the opposite side of the bus, thus reversing the sign of V_{dc}. This result in $(V_{dc} - e - i_a R_a)$ becoming a very large negative quantity which thus forces a small fall time. The change in sign of V_{dc} is the primary reason why the rise time is always considerably greater than the fall time.

A noteworthy conclusion from this analysis is that the rise and fall times of the current waveform determine their shape. In particular it appears from the above analysis that the rise time region is the major reason why the current waveform shape changes as the motor speed is increased. To keep the current waveform desirable at high speeds, the current magnitude should be limited and this may be realised by limiting the rise time region. In effect, this requires maintaining the rise time of this current waveform as a fraction of its period. The following section presents a simple analytical method for obtaining the required relationship which can be used to predict the range over which the speed and phase current magnitudes can be varied without there being any significant resultant distortion to the current waveshape.

6.6.3.2 Analytical Procedure to Determine the Optimum Shape of the Current Waveform

Figure 6.15 illustrates the method for phase current determination. Where the regions of rise and fall times are defined by times, t_r and t_f respectively and cycle of current period is defined by time, T.

In this analysis the rise time, t_r is calculated under the assumption that the phase current rises linearly upto its switch-on value of I in seconds and this current must have the desired level at the end of t_r seconds. The winding resistance is assumed to be neglected. The rise current under these assumptions is calculated by

$$I = \frac{\partial i}{\partial t} t_r \tag{6.25}$$

In order to avoid the distortion of the current, the rise time, t_r, is defined by

$$t_r = \xi T \tag{6.26}$$

where ξ is limited factor of the the maximum current and will be termed here the "limiting" current factor. It must be chosen to give the desired shape of current waveform in high speed operation. T is the period of current excitation and can be expressed in terms of an angular velocity of the motor

$$T = \frac{2\pi}{\omega_r} \tag{6.27}$$

and angular velocity of the motor can also be expressed in revolutions per minute (rpm)

$$n = \frac{T}{30} \tag{6.28}$$

The rate of rise of current in the phase winding can be approximately calculated by

$$\frac{\partial i}{\partial t} = \frac{V_{dc} - e}{L} \tag{6.29}$$

combining equations (6.25), (6.26), (6.27), (6.28) and (6.29) yields

$$\xi \leq \frac{ILn}{30\left(V_{dc} - e\right)} \tag{6.30}$$

Thus, if the t_r is limited by ξ in order to avoid the current distortion at high-speeds, I has to be controlled as follows from equation (6.30);

$$I \leq 30\xi\left(\frac{V_{dc} - e}{nL}\right) \tag{6.31}$$

There are a number of interesting points that can be made in relation to expression (6.31);

(i) The shape of the current waveform depends on the phase current magnitude and the motor speed when the values of V_{dc} and L are specified and will usually be fixed by the choice of the motor.

(ii) The shape of the current waveform is related directly to the required amplitude of the phase current, and this current is directly related to the load torque imposed on the motor. Since the current waveform distortion that occurs as the motor is loaded from zero to the full load torque, can be minimised by limiting the phase current magnitude that is required at full-load.

(iii) The choice of a particular ξ determines the shape of the desired current waveform shape since this factor is a fraction of the excitation period. However, the choice of a particular ξ is a consideration which is directly under the control of the designer.

In addition, the shape of current waveforms are dependent on having the knowledge of the limiting current factor, ξ because if the value of ξ is known accurately the prediction of the desired current magnitude can then be improved. Therefore a good estimation of ξ is required. The question then arises as to how accurately this factor must be known and optimum performance under all operating speed ranges can be obtained, as will be described below.

Estimation of limiting current Factor

Table 6.1 shows a number of results generated by the expression (6.29). The columns in this table are the limiting current factor, ξ, the motor speed and the current magnitude. The result was generated for a machine with the following parameters; $V_{dc} = 550V$, $L = 6.2mH$ and $e(wt) = 50V/1000rpm$.

Analytical Prediction for Current Limited Method

Speed	ξ	$30\xi\frac{V_{dc}-e}{L}$
(rpm)		(A)
1000	0.10	108.0
	0.15	97.0
	0.07	77.0
2000	0.10	42.3
	0.15	63.4
	0.07	29.1
3000	0.10	20.1
	0.15	30.2
	0.07	14.1

The results of table 6.1 shows that a value of 0.15 for ξ is capable of reaching the maximum obtainable current value at any speed and at the same time allows the phase current limit value to be obtained for desirable shape of its waveform.

To summarise the above analysis it will be emphasized that if the limiting current factor, ξ, is chosen to be high in order to give short rise time and the current wave is prevented from significant distortion, the controller may generate a desirable current waveform. The above analysis demonstrated how the factor, ξ, was chosen according to the motor speed range in order to give a rise time that is attainable for the desired shape of approximately $\xi = 0.15$.

Finally equation (6.30) can be considered as a constraint on the design of a brushless dc motor in order to improve the torque/speed performance for the system described here.

6.7 Summary and Conclusion

In this chapter analytical approaches for obtaining the optimum phase advance angle in the high and extended speed ranges have been developed. The merit of these methods, compared with trail-and-error based on simulation, is described.

This chapter presents also a detailed analysis of the shapes of the current and back-emf waveforms in a brushless dc motor drive and their effects on the torque/speed performance. From this analysis, it has been shown that the current and back-emf waveform shapes have a direct effect on the constant torque operation as well as the maximum torque that the brushless dc motor can deliver. A detailed analysis of the shapes of the current and back-emf waveforms in a brushless dc motor drive and their effects on the torque/speed performance has been presented. During this investigation, a detailed analytical method for obtaining the required relationship between

motor parameters, which can be used to predict the range over which the speed and phase current magnitudes can be varied without there being any significant resultant distortion to the current waveform shape, has been presented.

It has been shown that the principle benefit of analytical solutions is that they make it much easier to predict the optimum phase advance angle and the shape of the current waveform and to see how the various motor and drive parameters affect the system performance.

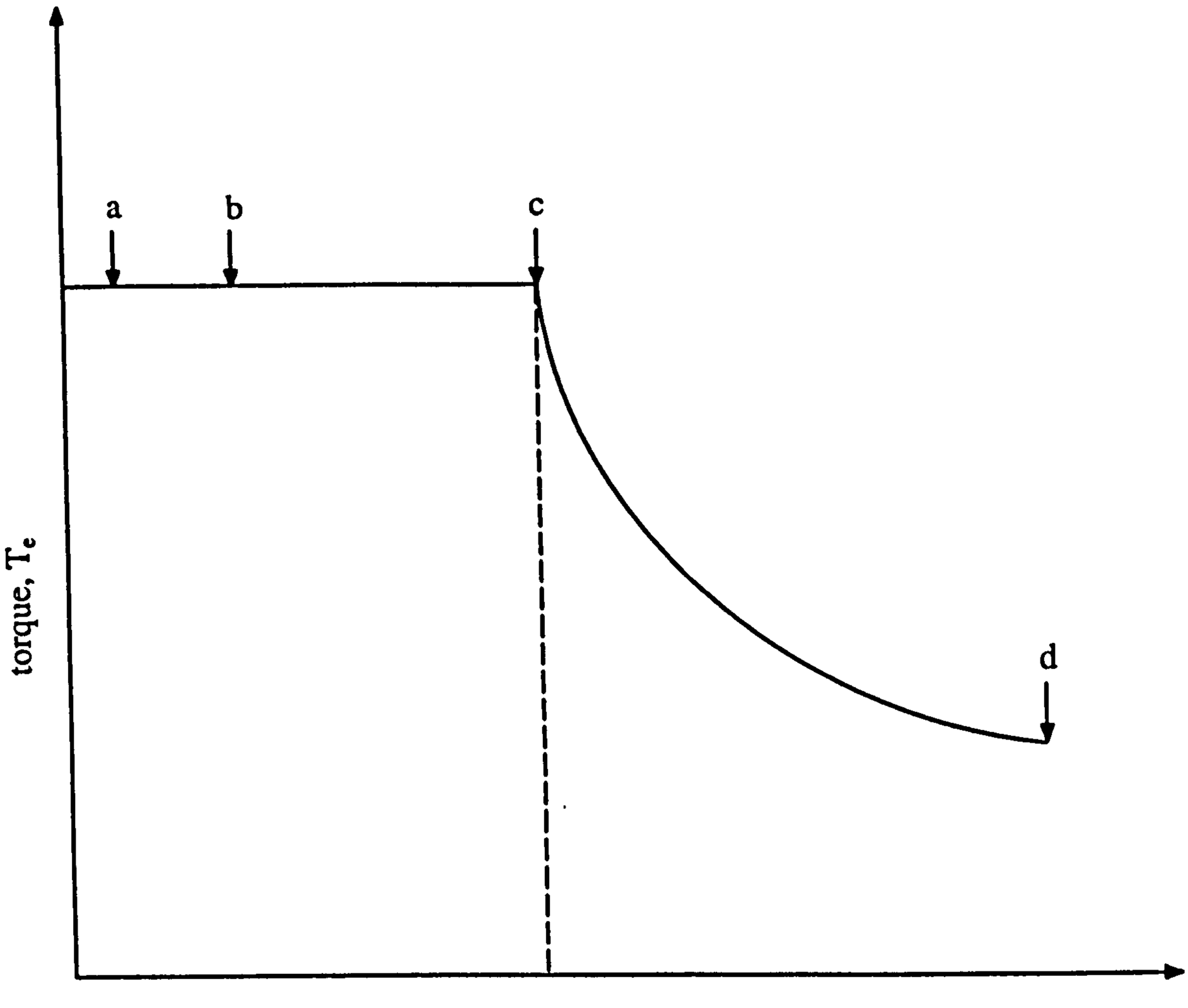

Figure 6.1a Torque/speed characteristics

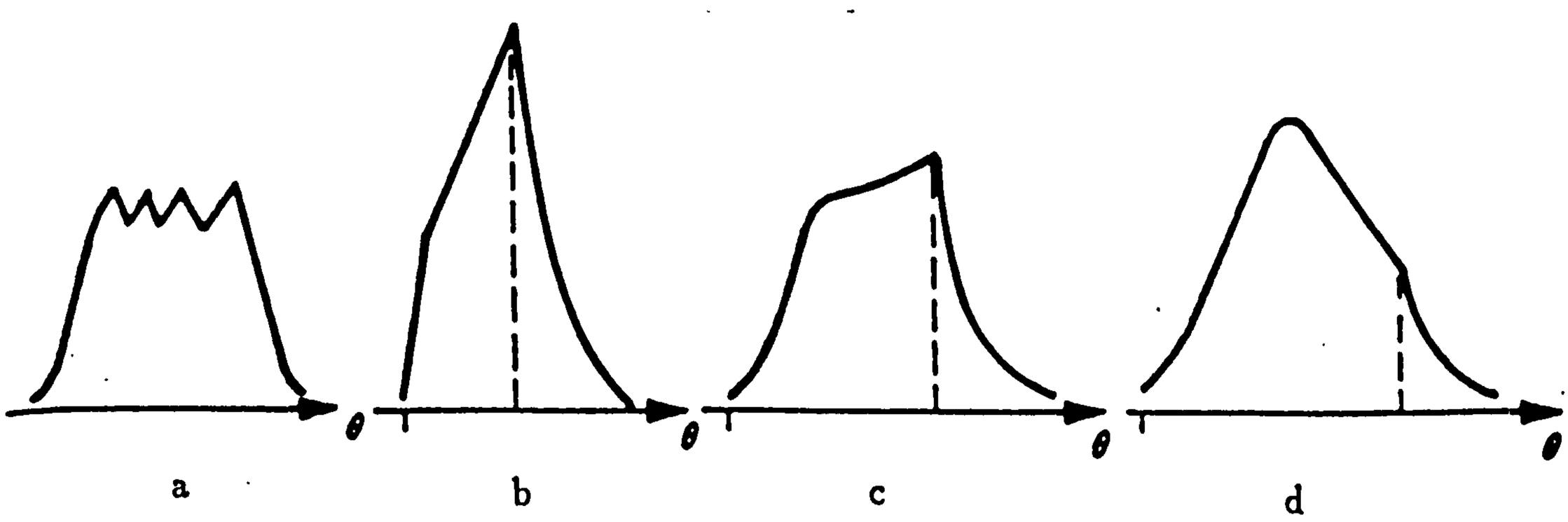

Figure 6.1b The shape of the current waveforms corresponding to the speeds of the motor

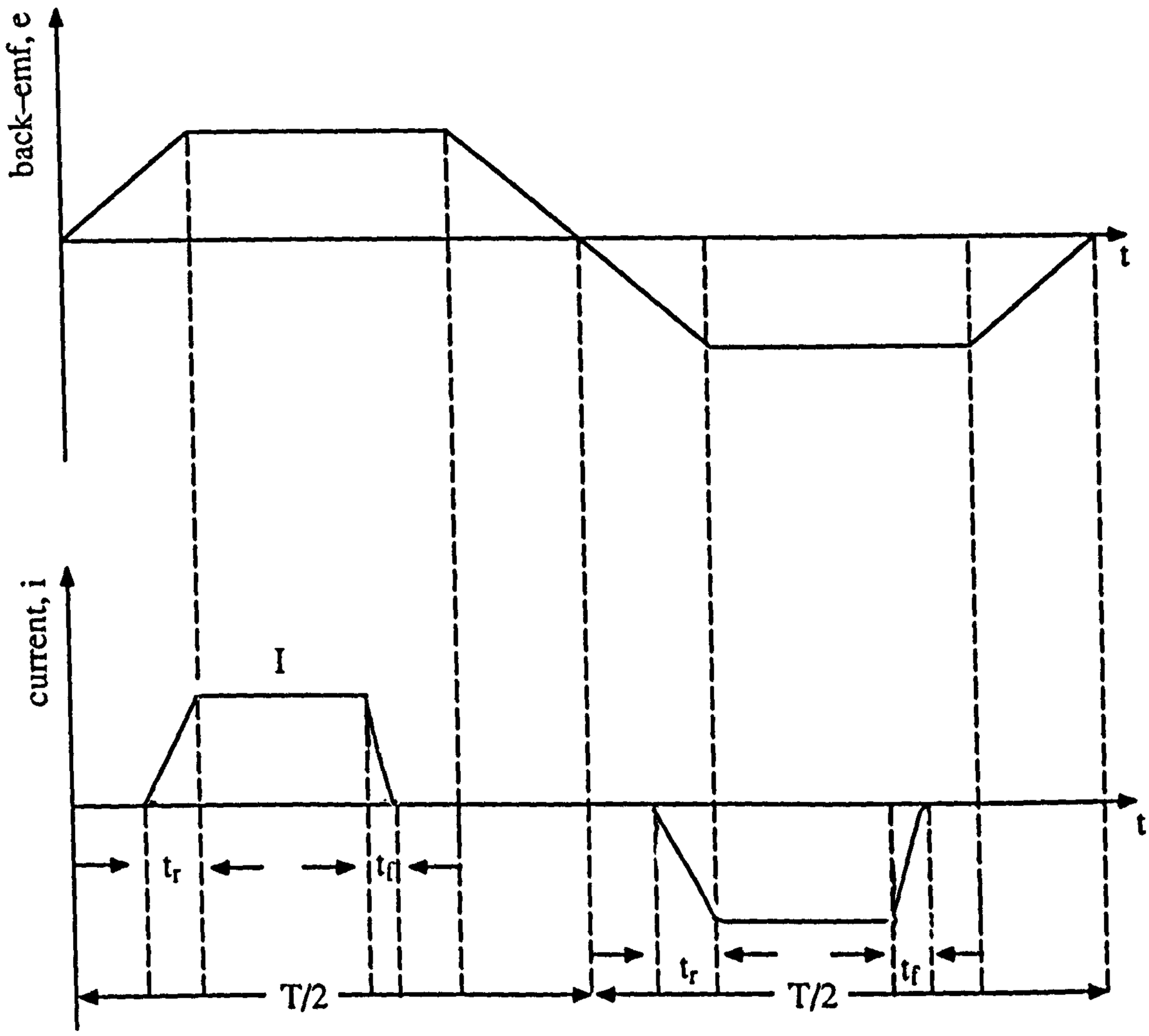

Figure 6.2 Analytical model for the phase advance

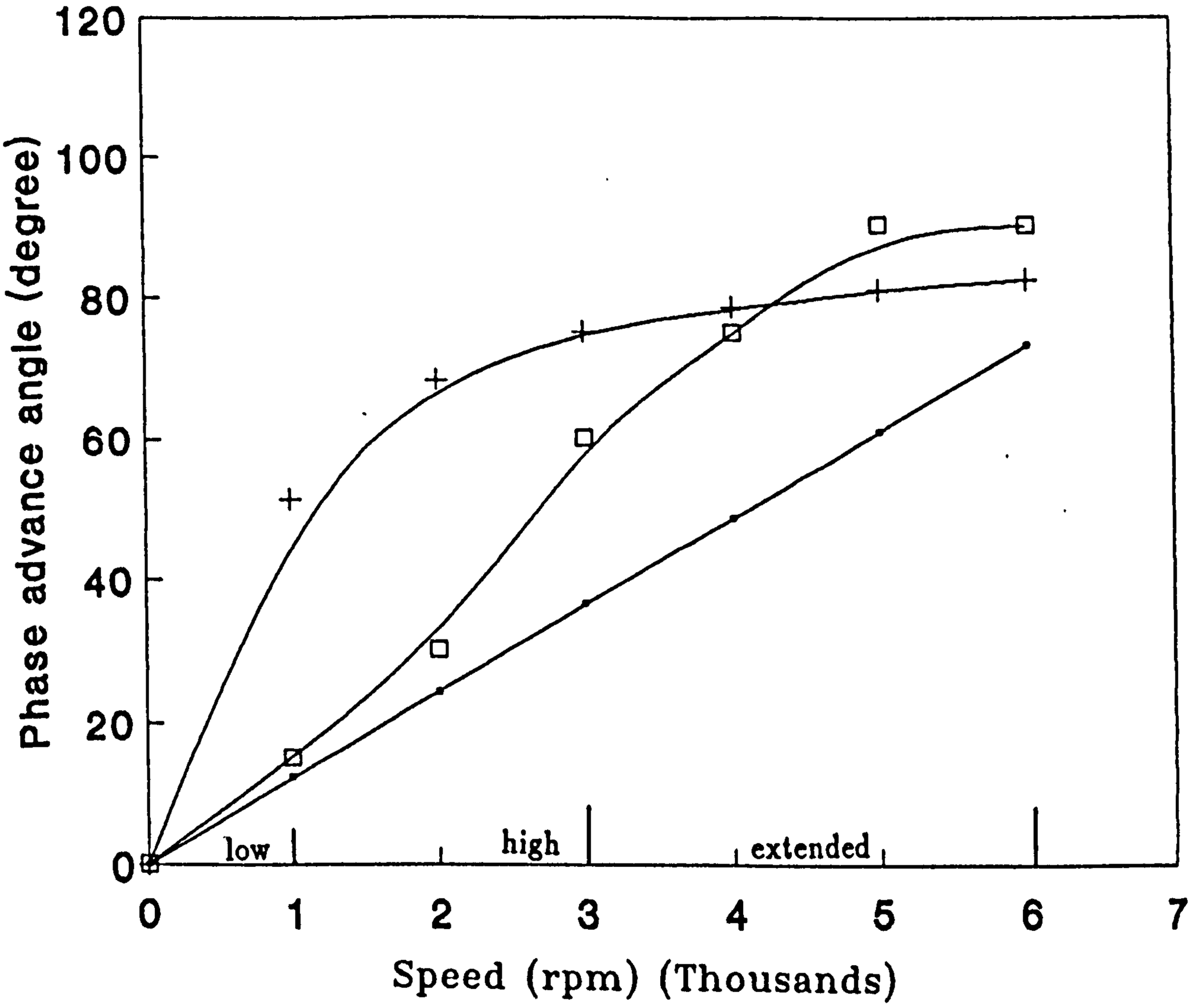

Figure 6.3 Comparison of phase advance angle calculated by analytical and simulation methods.

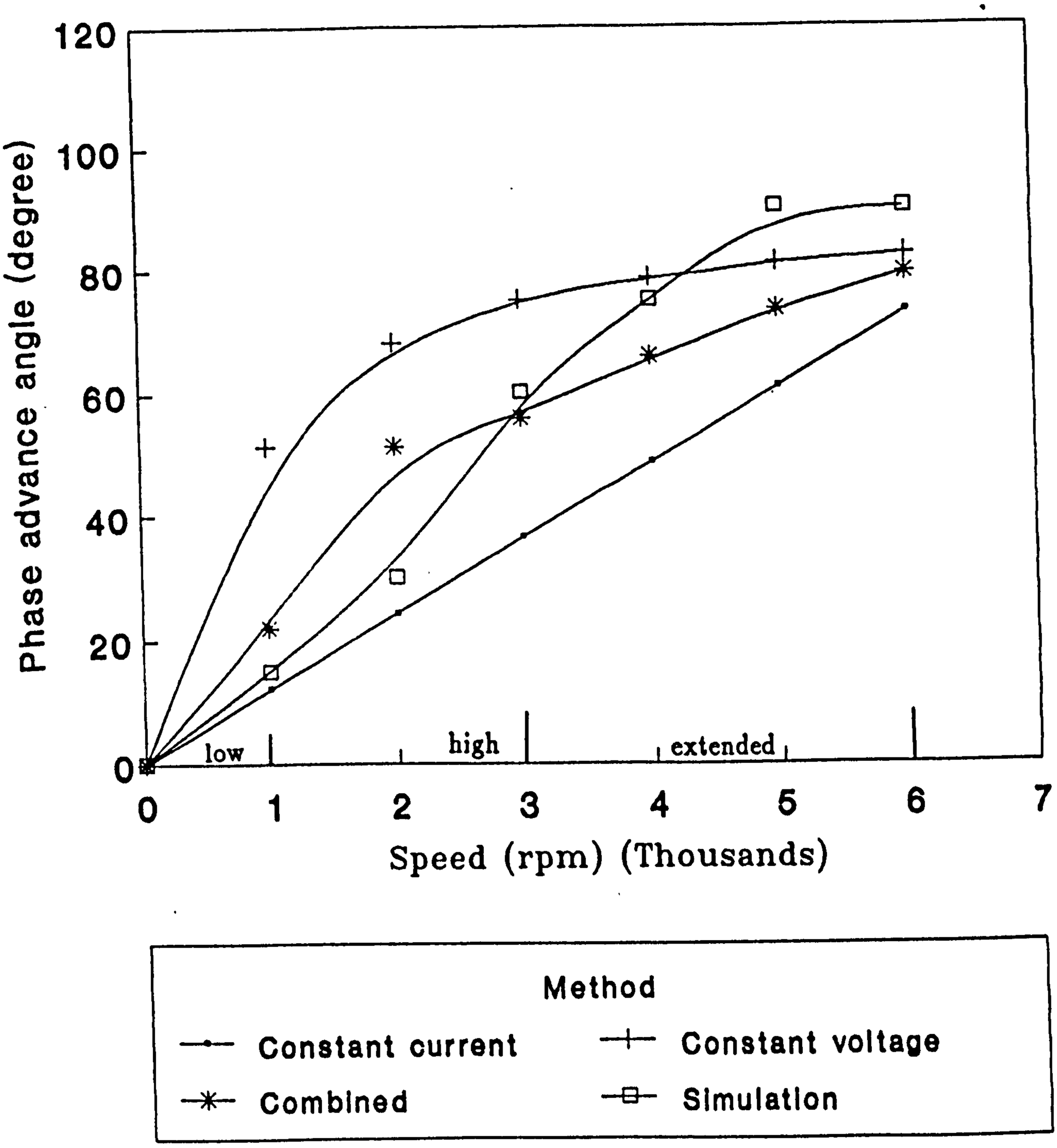

Figure 6.4 Comparison of phase advance angle calculated by analytical, combined and simulation methods.

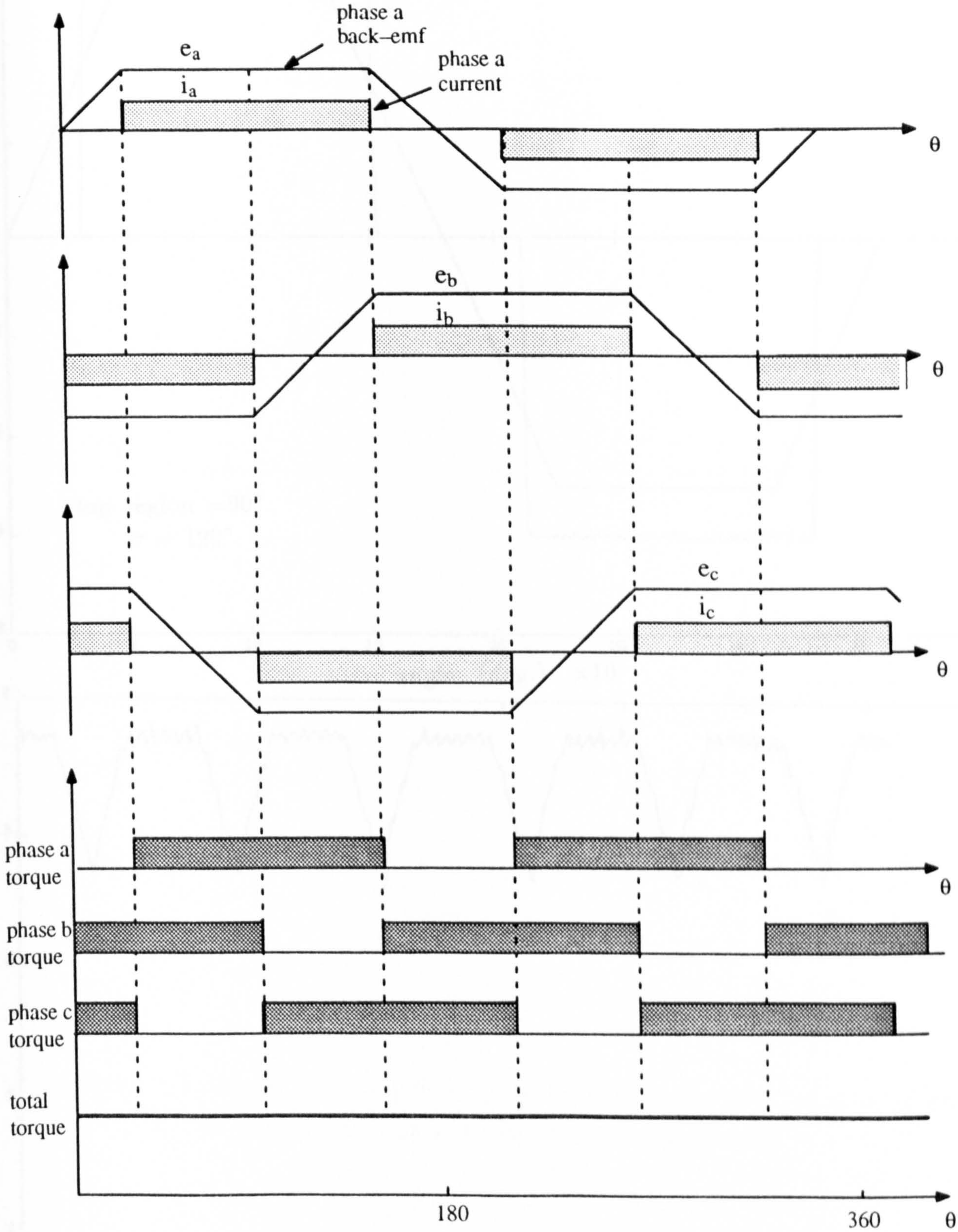

Figure 6.5 Torque production in trapzoidal emf motor

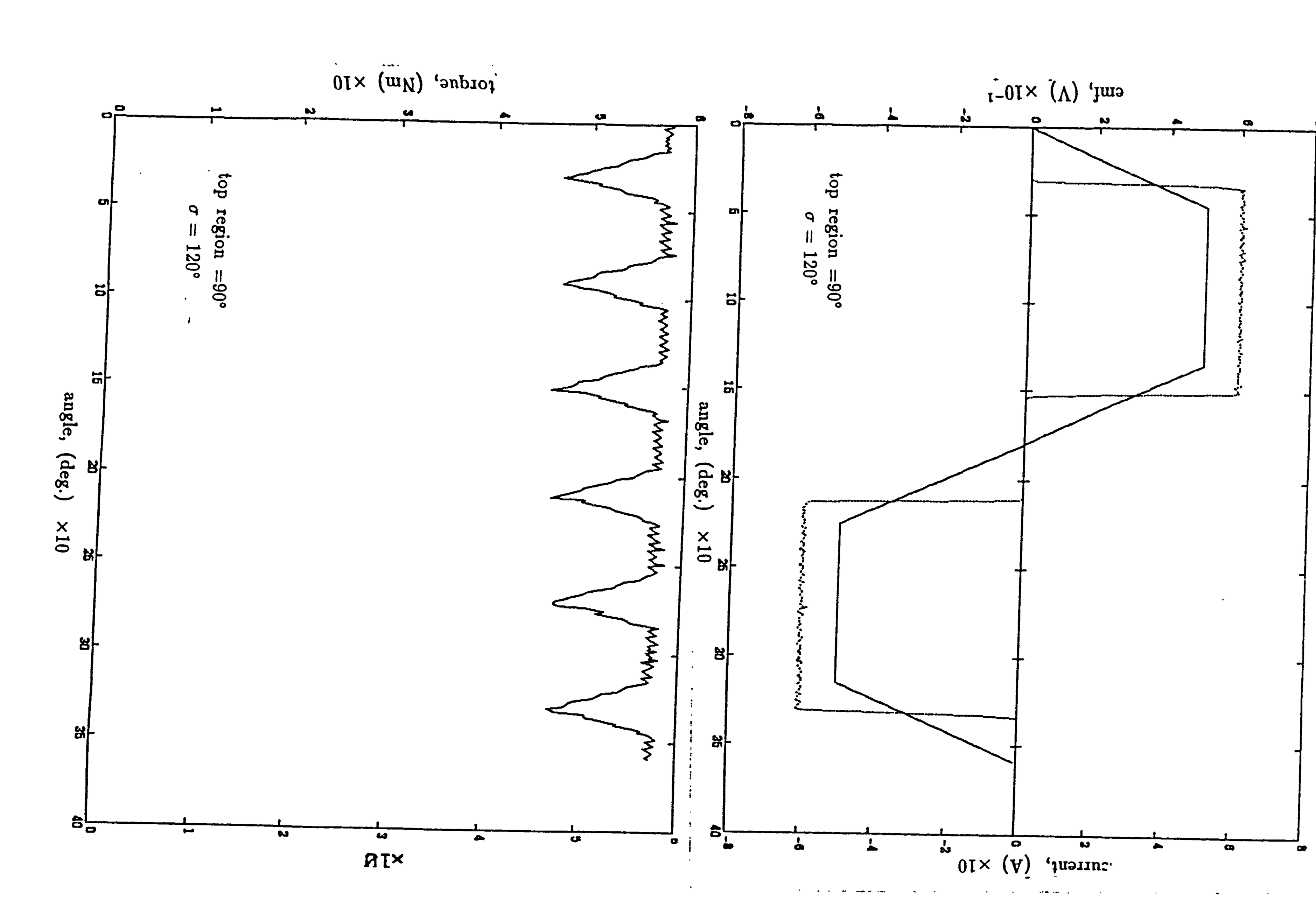
emf, (V) ×10⁻¹
top region =90°
σ = 120°
angle, (deg.) ×10
current, (A) ×10
torque, (Nm) ×10
top region =90°
σ = 120°
angle, (deg.) ×10
×10

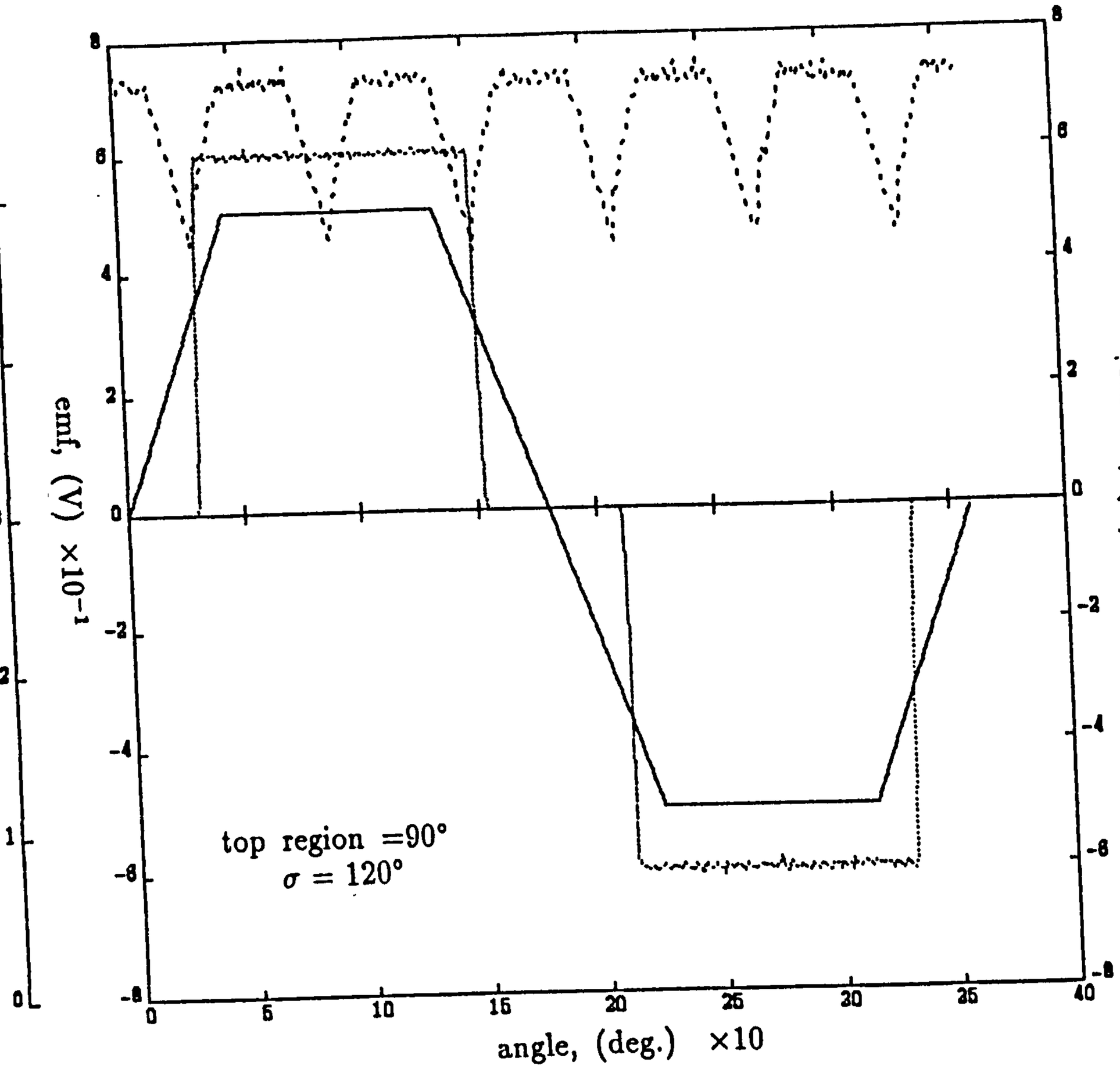

Figure 6.6 current, back-emf and torque waveforms for 120° conduction angle at speed=100 rpm and constant top region=90°.

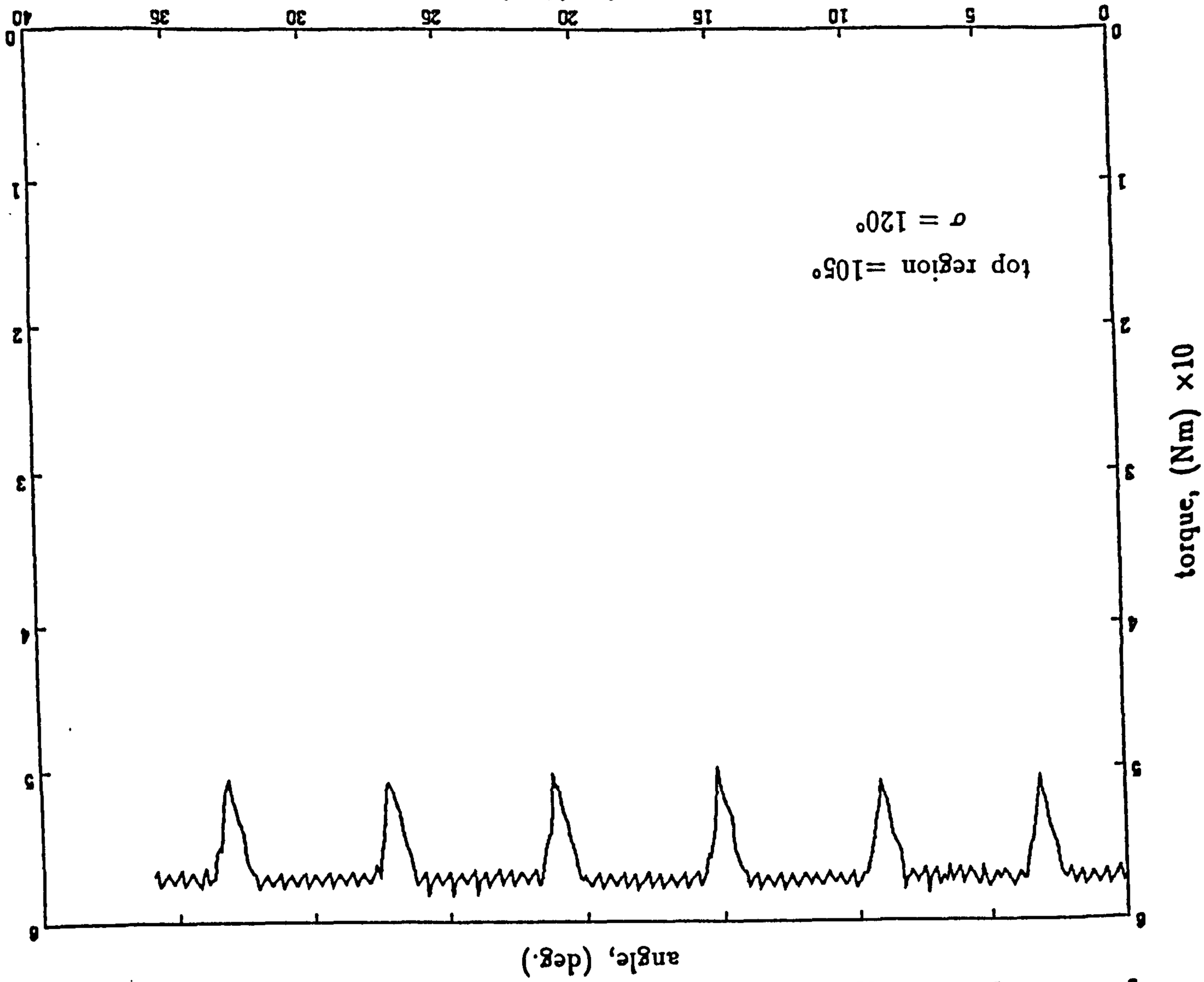
top region =105°
σ = 120°
torque, (Nm) x10
angle, (deg.)
top region =105°
σ = 120°
back emf, (V)
current, (A) x10
angle, (deg.)

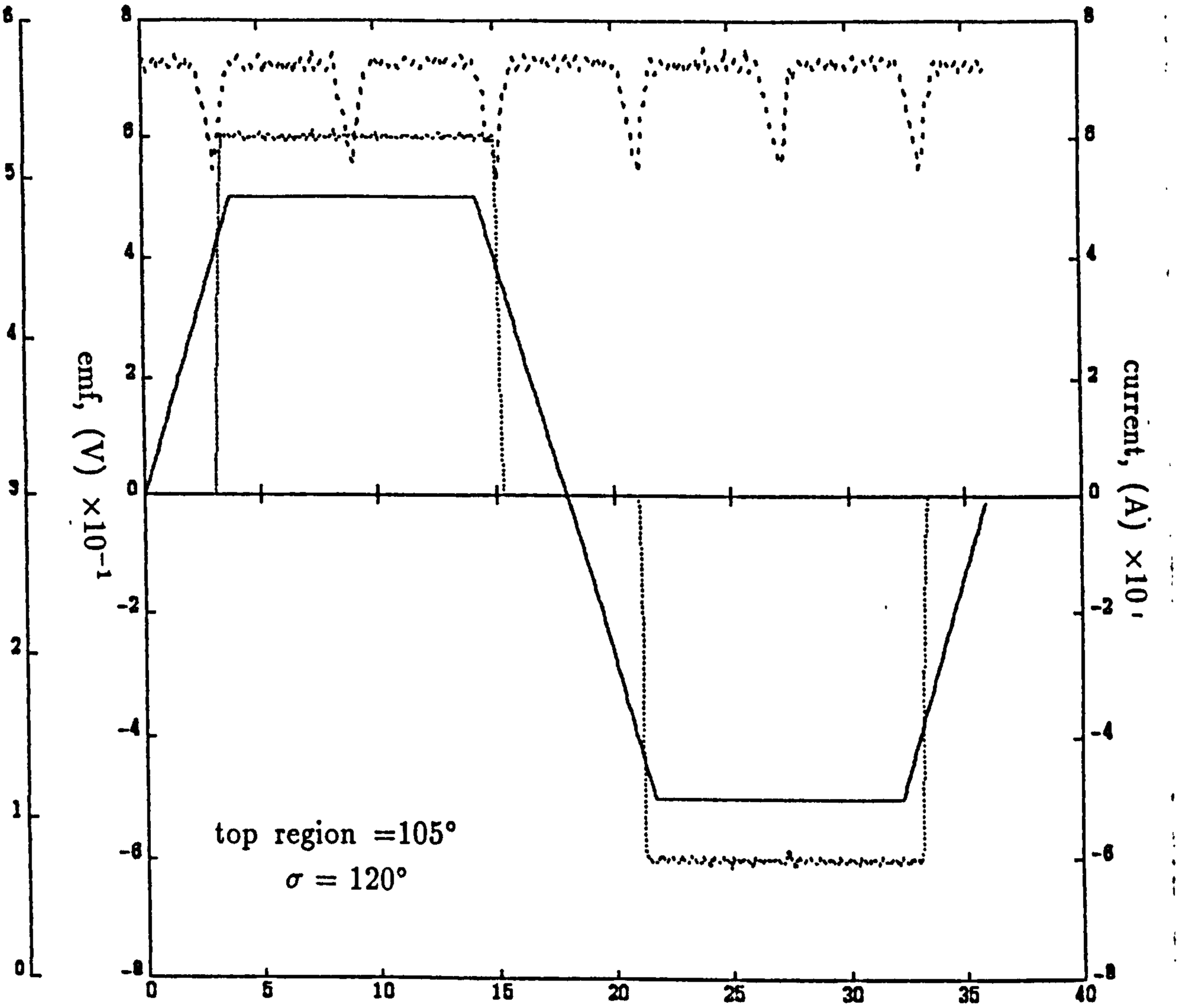

Figure 6.7 Current, back-emf and torque waveforms for 120° conduction angle at speed=100 rpm and constant top region=105°.

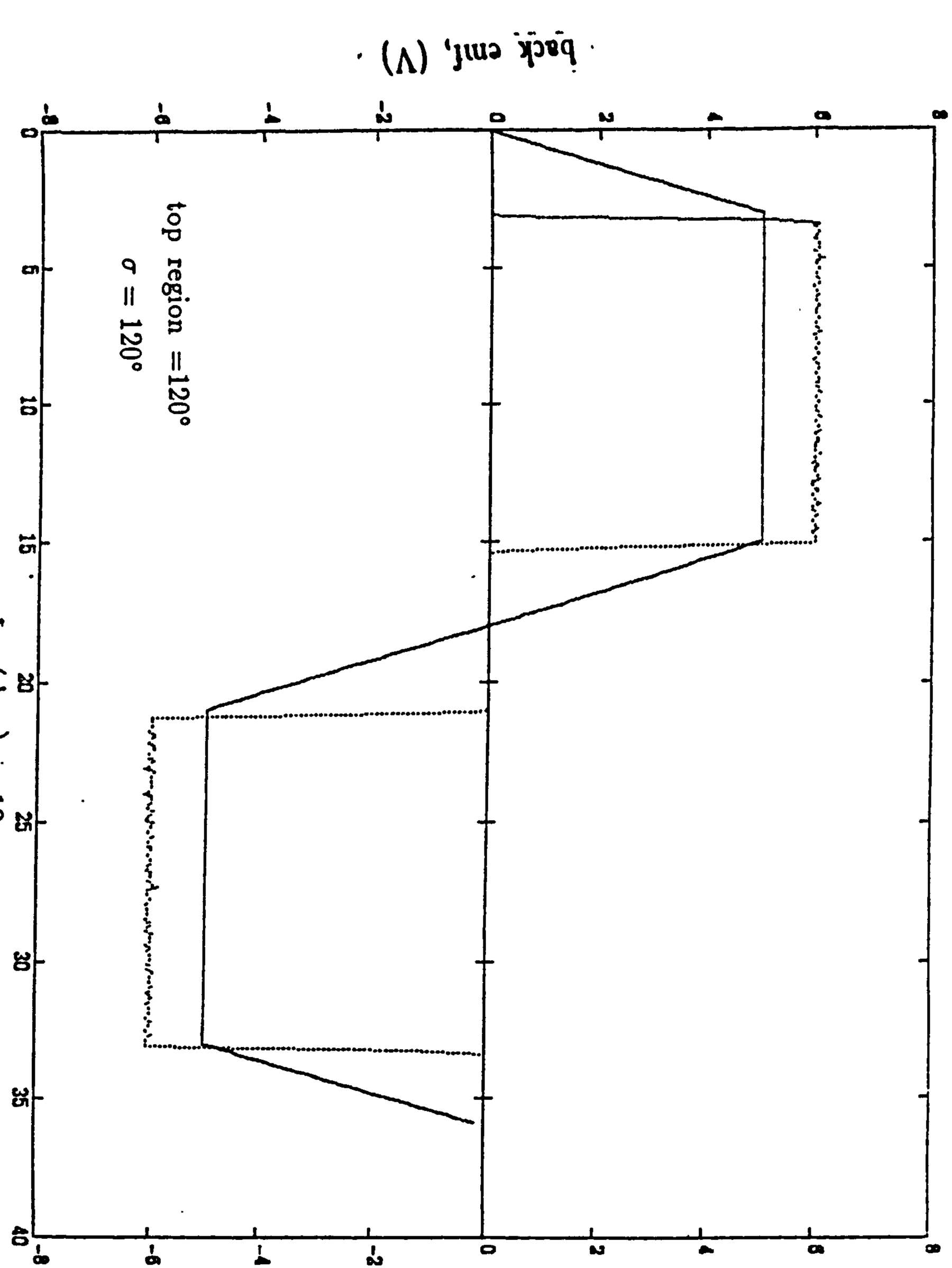
back emf, (V)
top region =120°
σ = 120°
angle, (deg.) ×10
current, (A) ×10

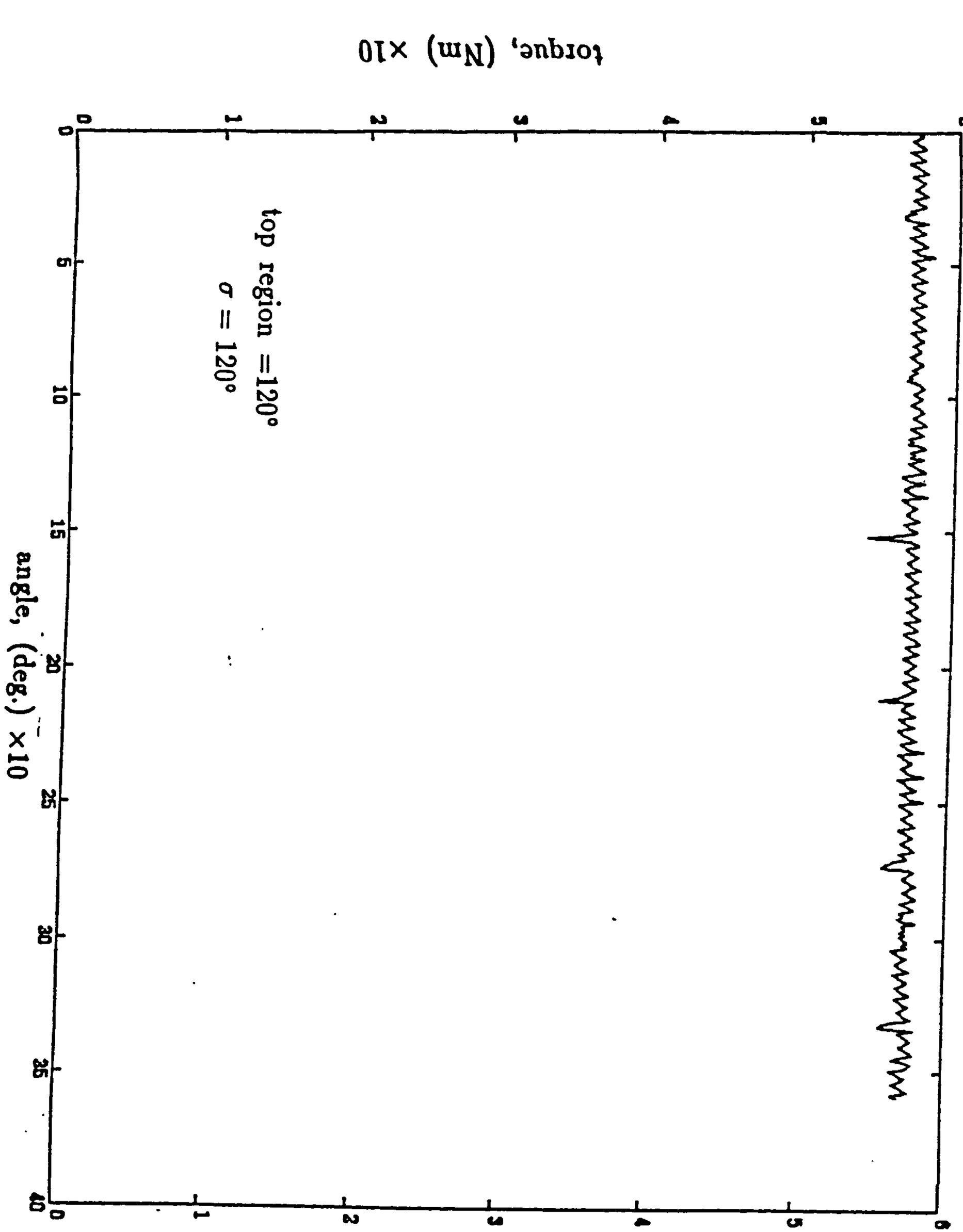
torque, (Nm) ×10
top region =120°
σ = 120°
angle, (deg.) ×10

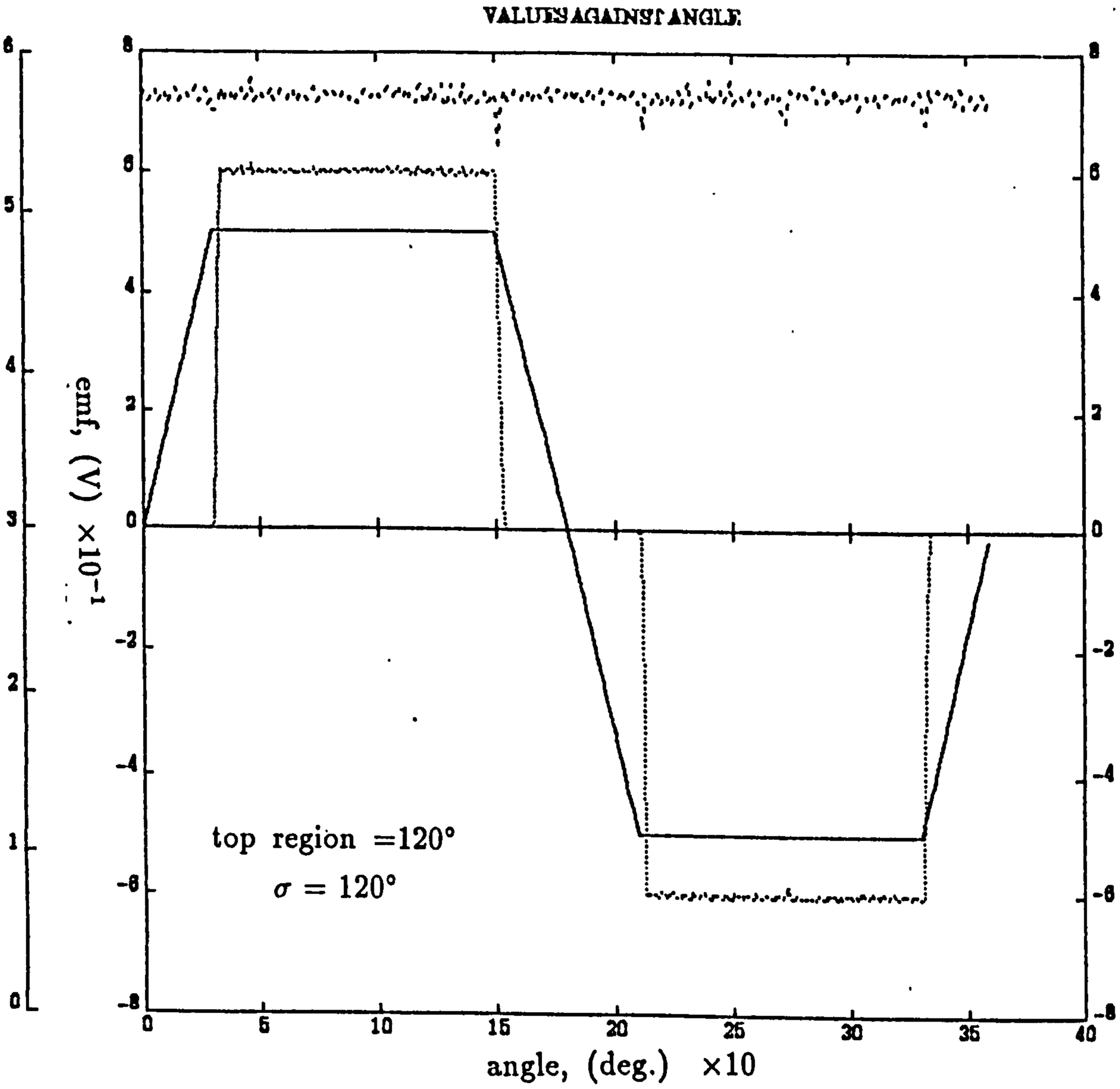

Figure 6.8 Current, back-emf and torque waveforms for 120° conduction angle at speed=100 rpm and constant top region=120°.

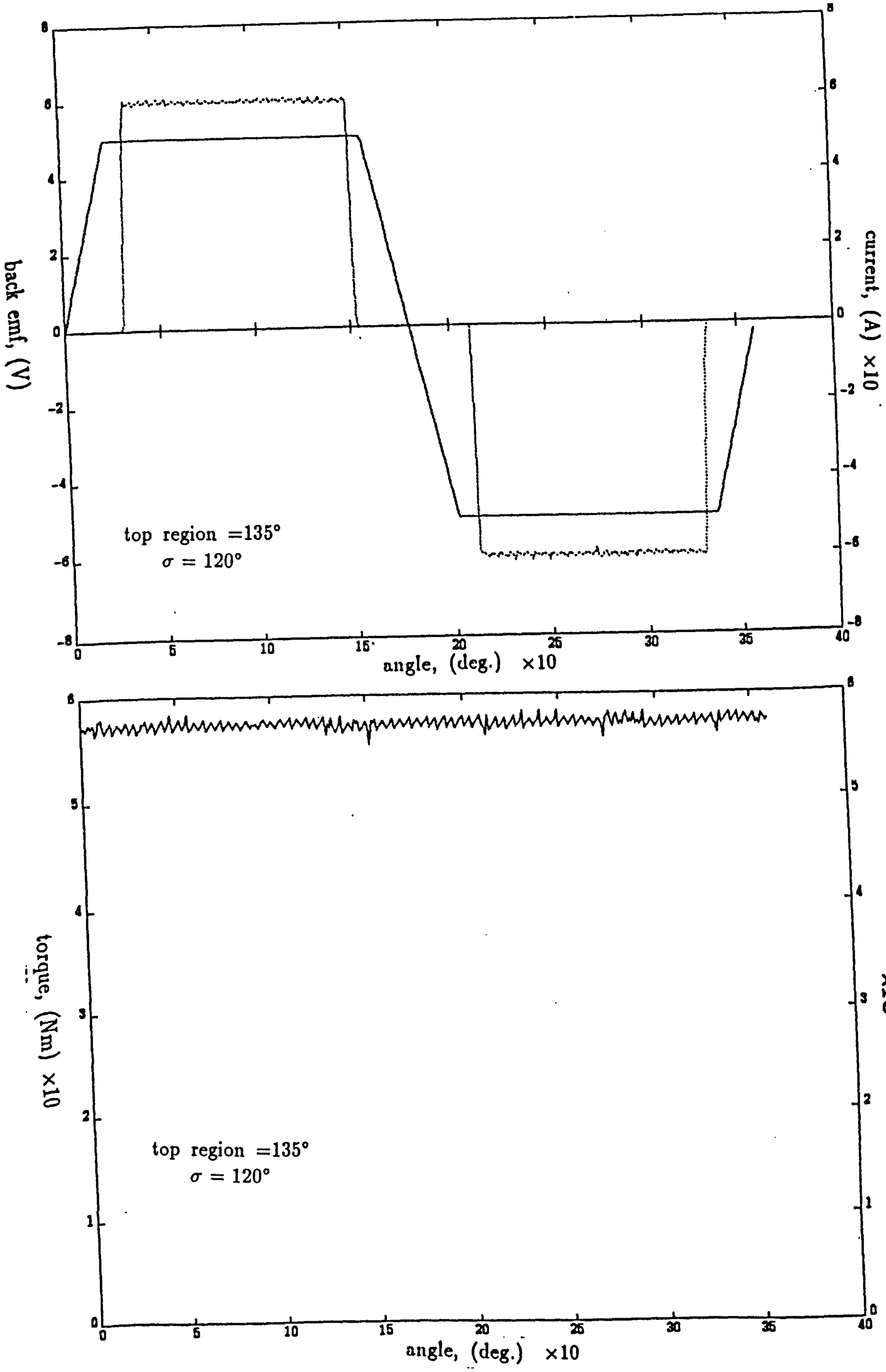
back emf, (V)
current, (A) ×10
top region =135°
σ = 120°
angle, (deg.) ×10
torque, (Nm) ×10
top region =135°
σ = 120°
angle, (deg.) ×10

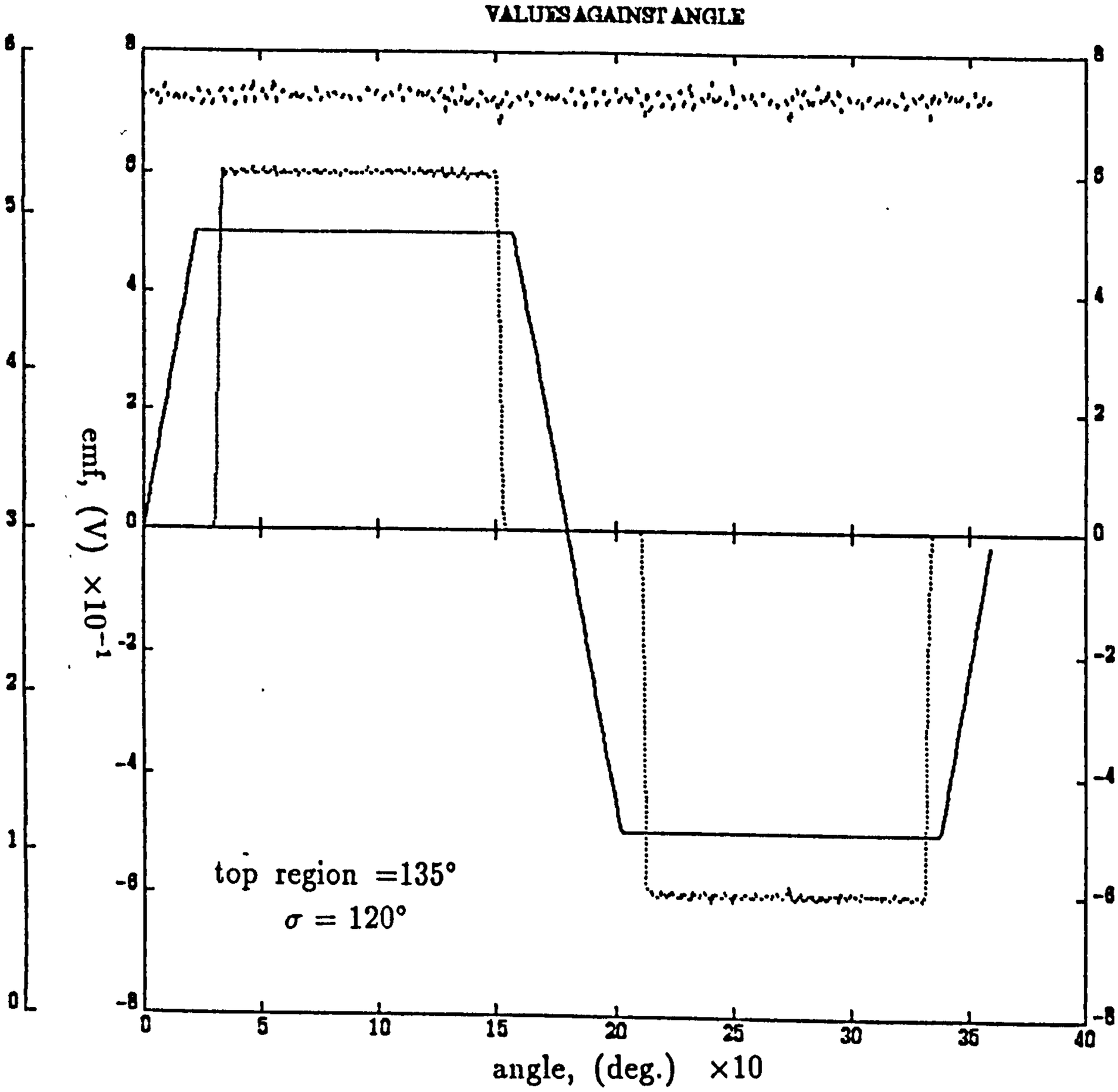

Figure 6.9 Current, back-emf and torque waveforms for 120° conduction angle at speed=100 rpm and constant top region=135°.

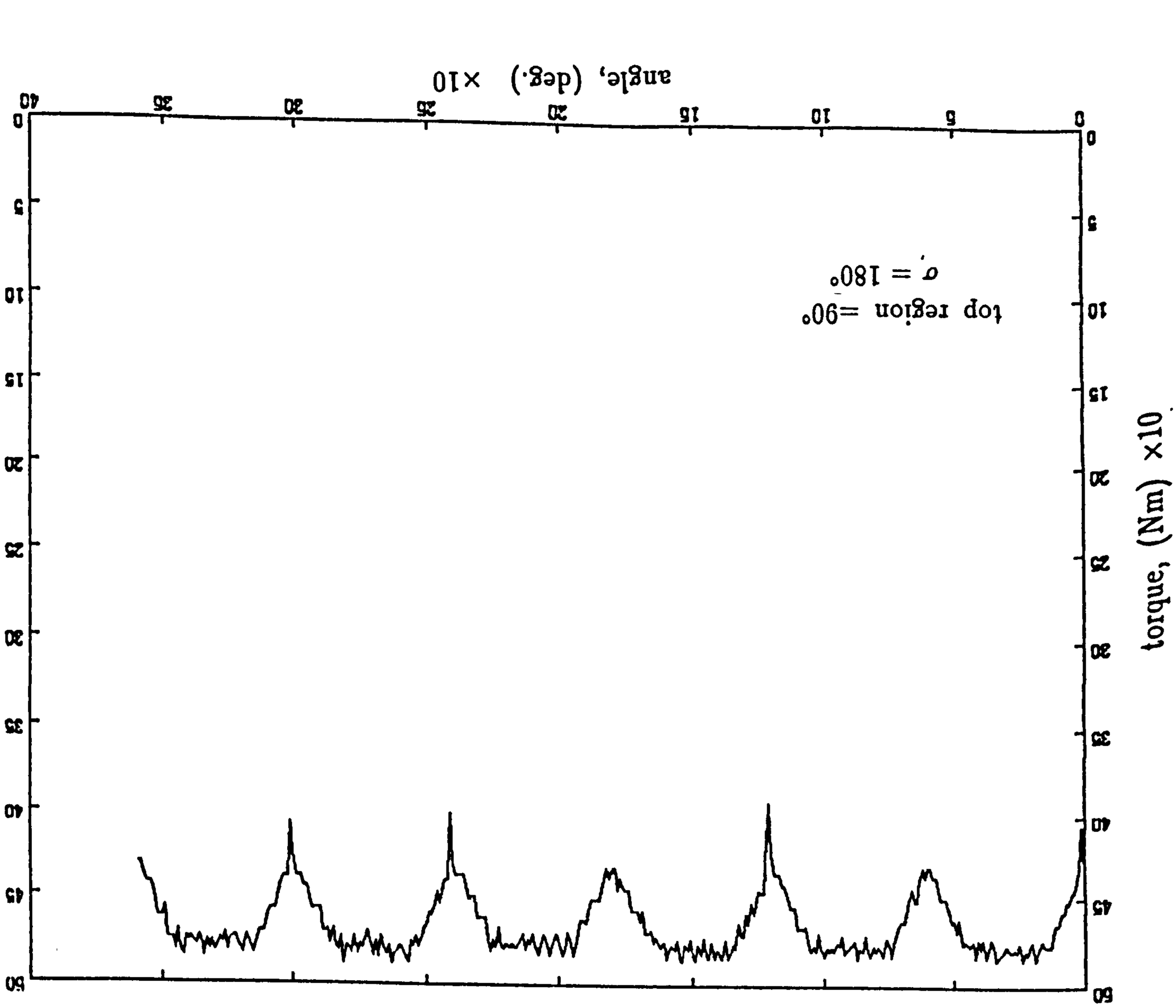
top region =90°
σ = 180°
torque, (Nm) ×10
angle, (deg.) ×10
0
5
10
15
20
25
30
35
40
45
50

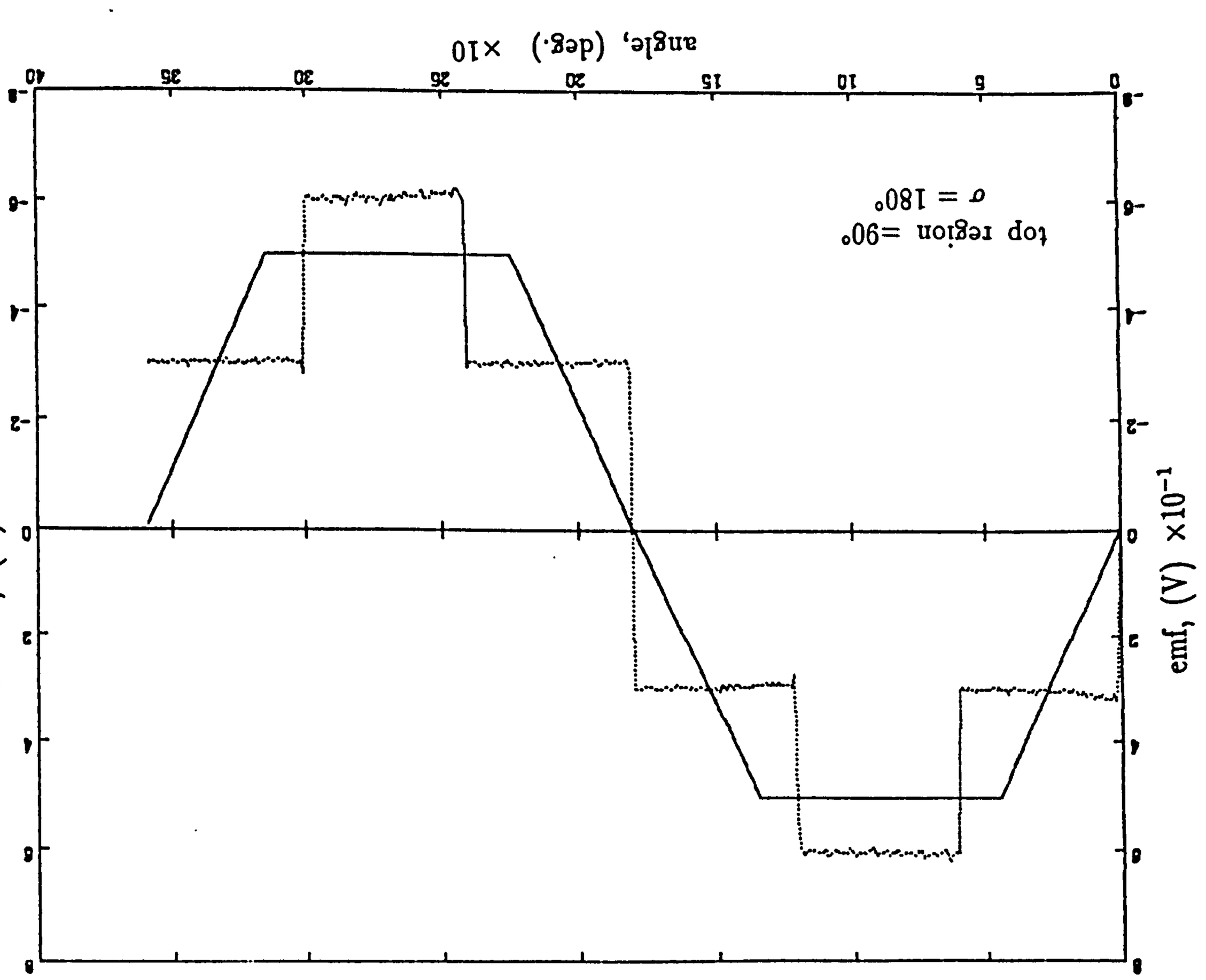
top region =90°
σ = 180°
current, (A) ×10
emf, (V) ×10⁻¹
angle, (deg.) ×10
0
5
10
15
20
25
30
35
40
-8
-6
-4
-2
0
2
4
6
8

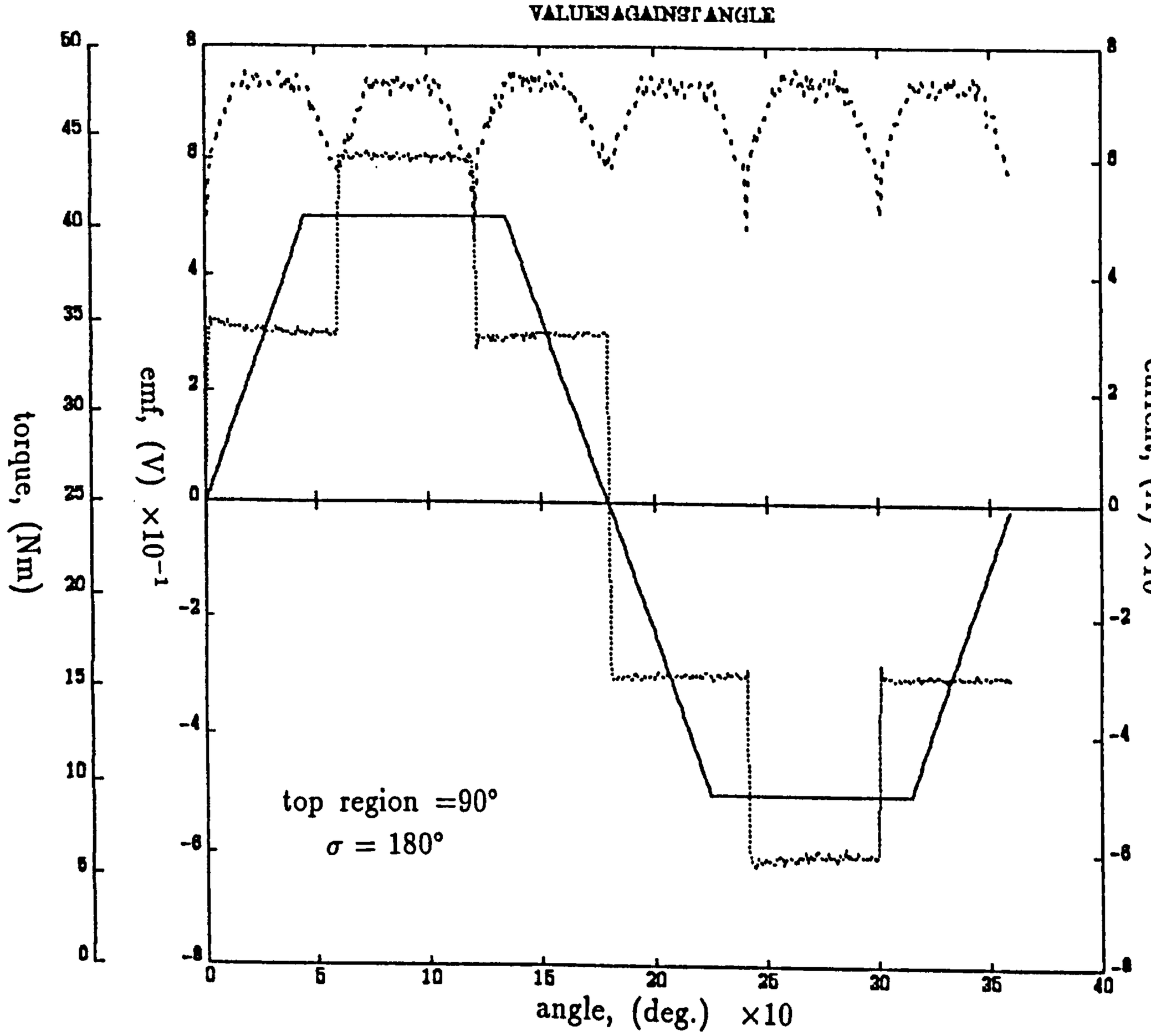

Figure 6.10 Current, back-emf and torque waveforms for 180° conduction angle at speed=100 rpm and constant top region=90°.

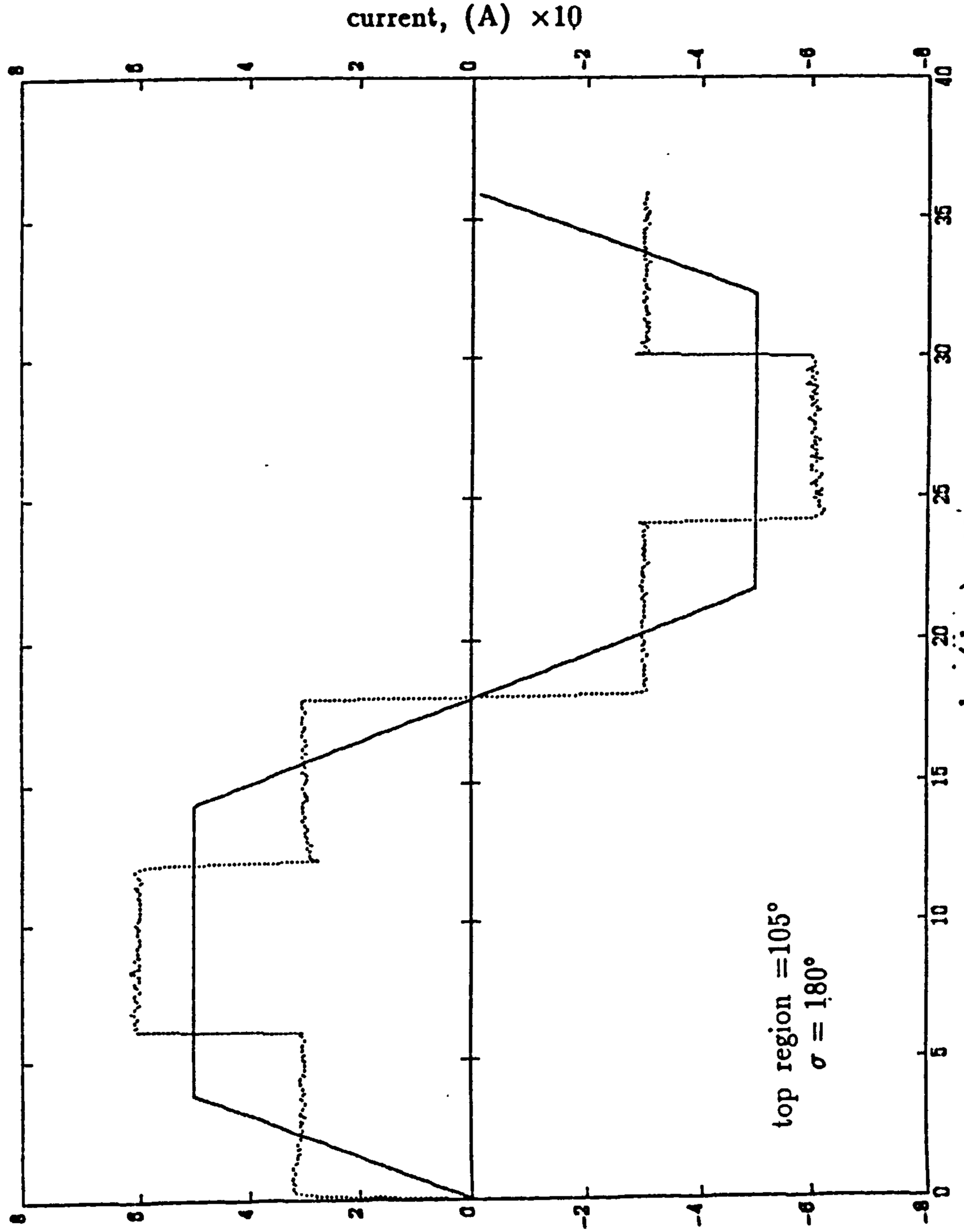
current, (A) ×10
back emf, (V) ×10
angle, (deg.) ×10
top region =105°
σ = 180°

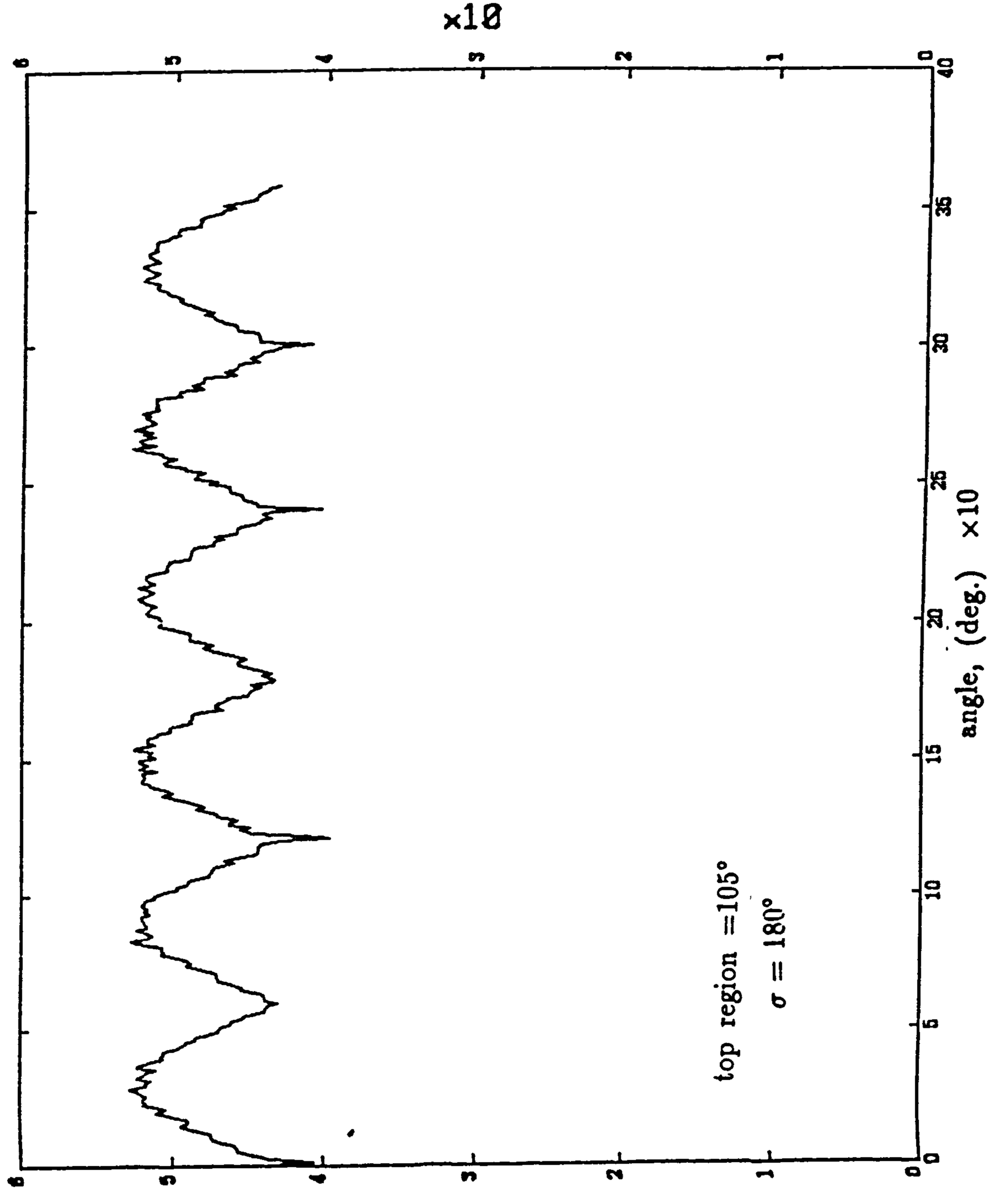
×10
torque, (Nm) ×10
angle, (deg.) ×10
top region =105°
σ = 180°

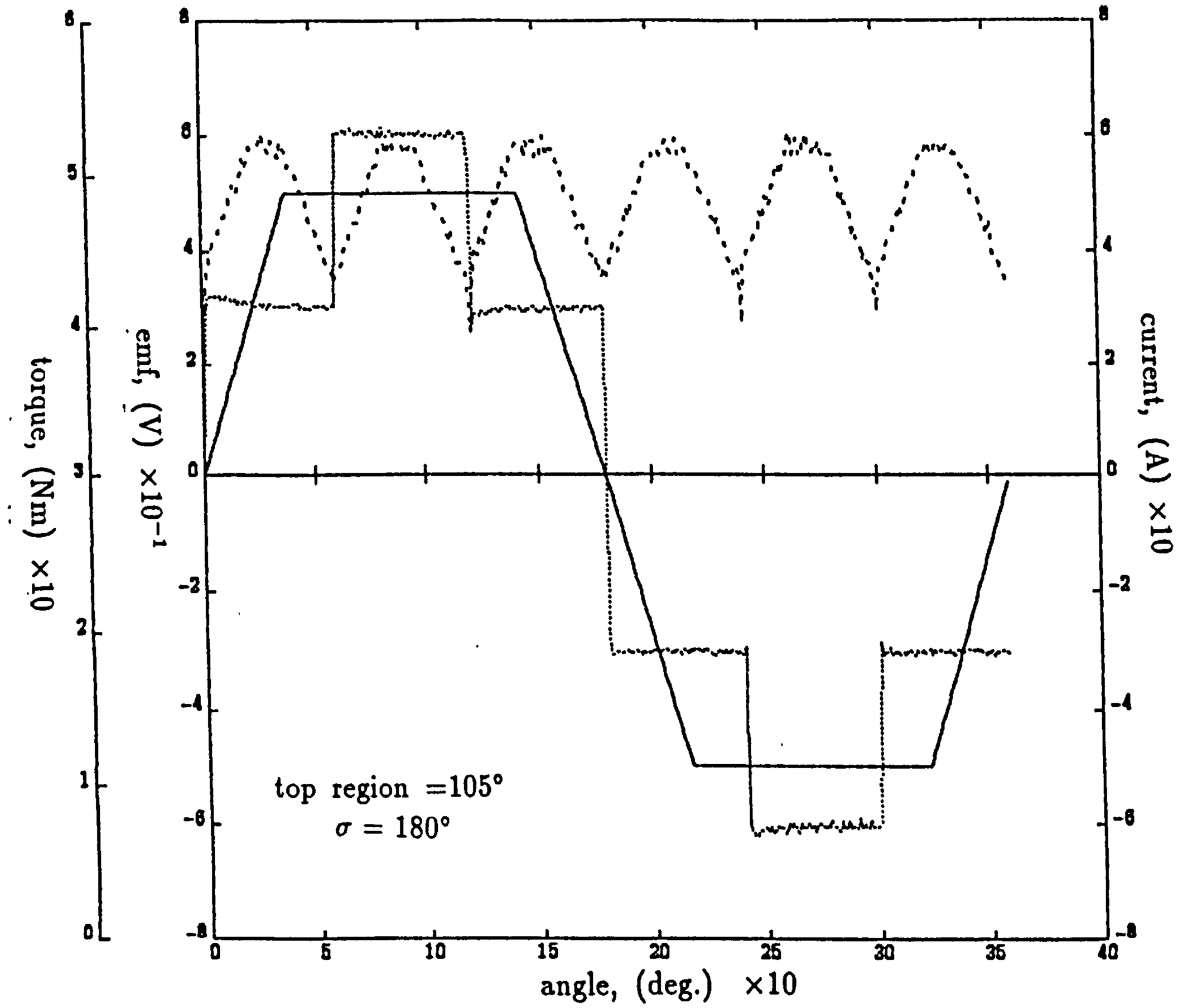

Figure 6.11 Current, back-emf and torque waveforms for 180° conduction angle at speed=100 rpm and constant top region=105°

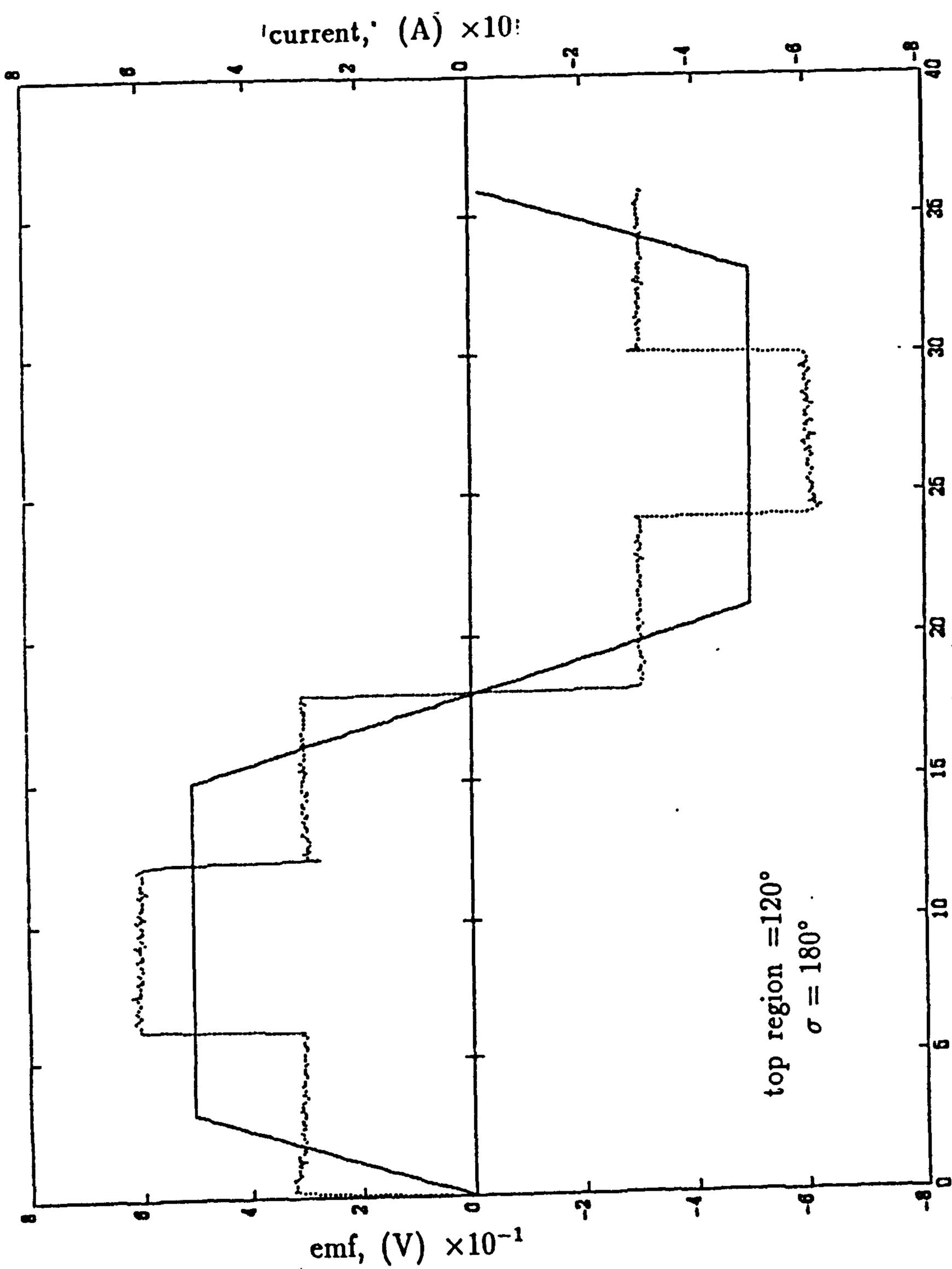
emf, (V) ×10⁻¹
angle, (deg.) ×10
top region =120°
σ = 180°

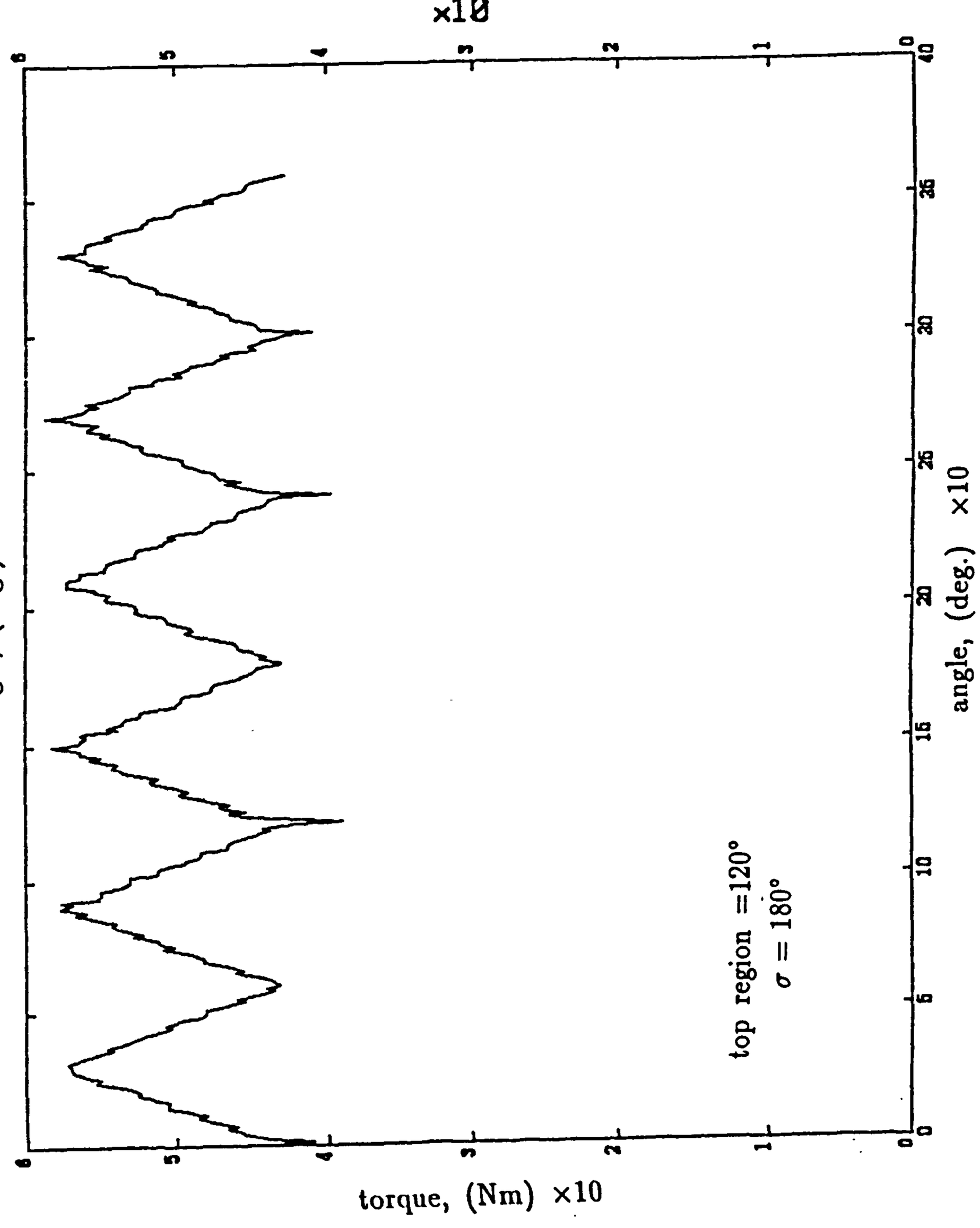
torque, (Nm) ×10
angle, (deg.) ×10
top region =120°
σ = 180°

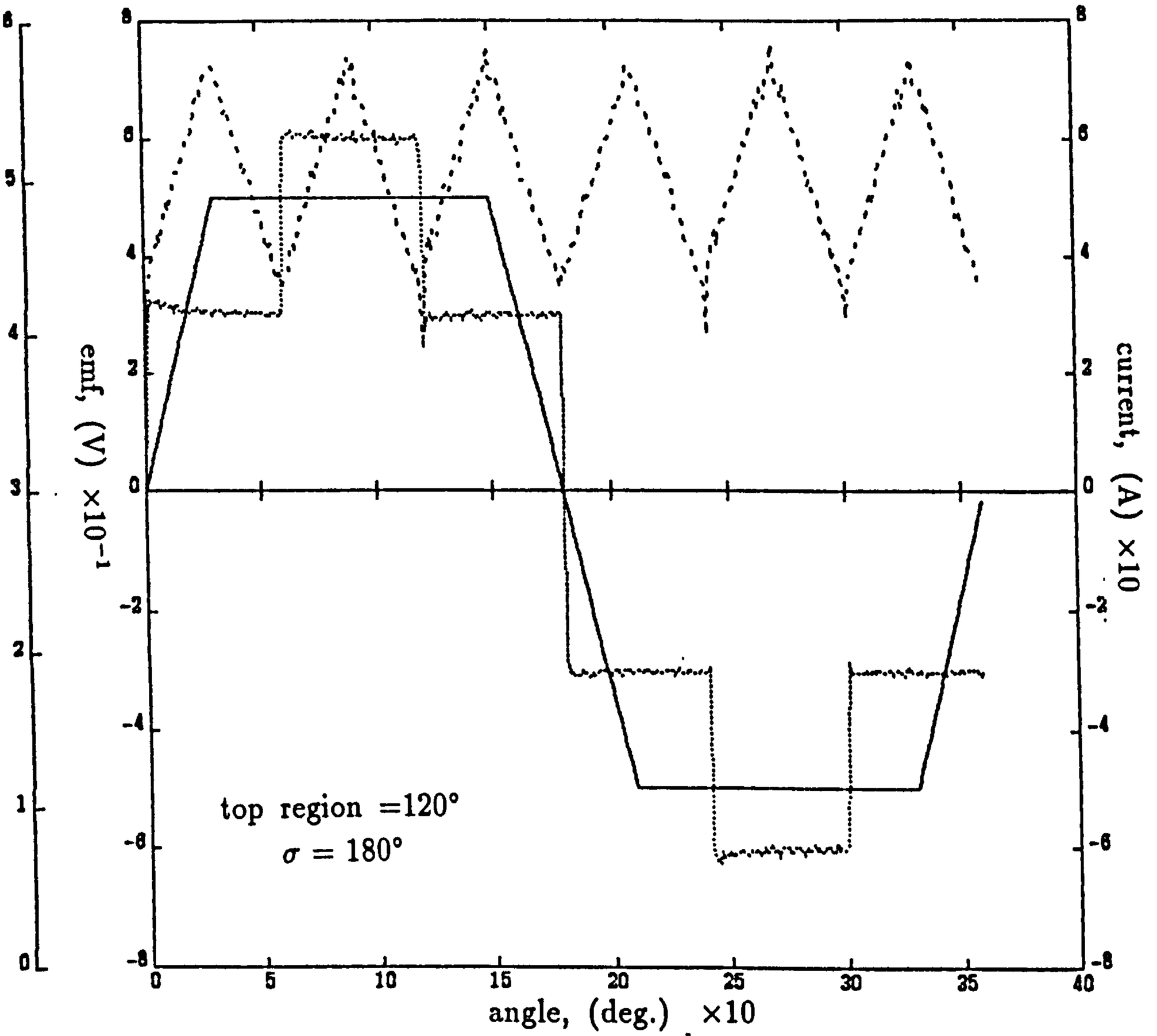

Figure 6.12 Current, back-emf and torque waveforms for 180° conduction angle at speed=100 rpm for Bosch drive.

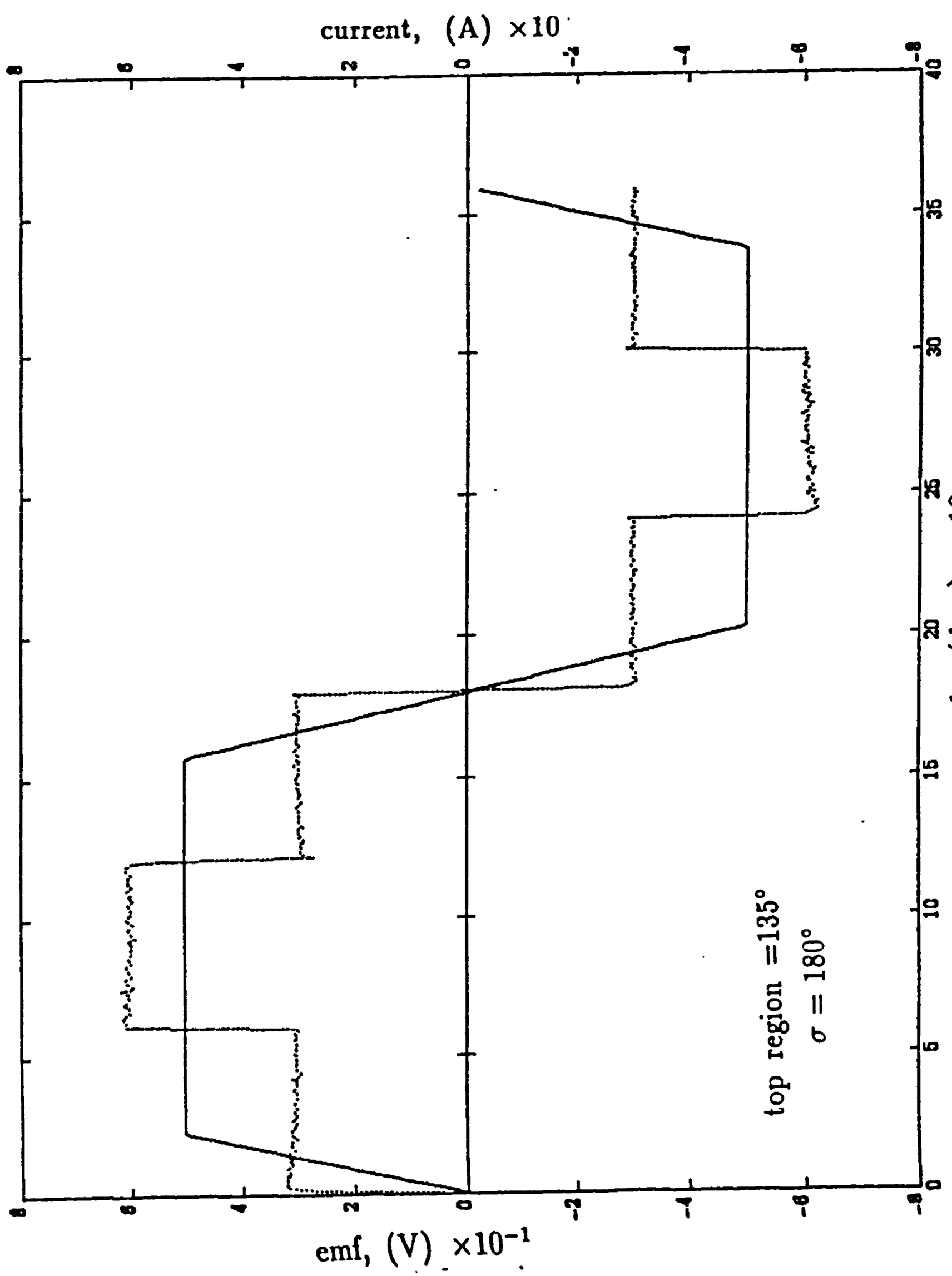
current, (A) ×10
emf, (V) ×10⁻¹
angle, (deg.) ×10
top region =135°
σ = 180°

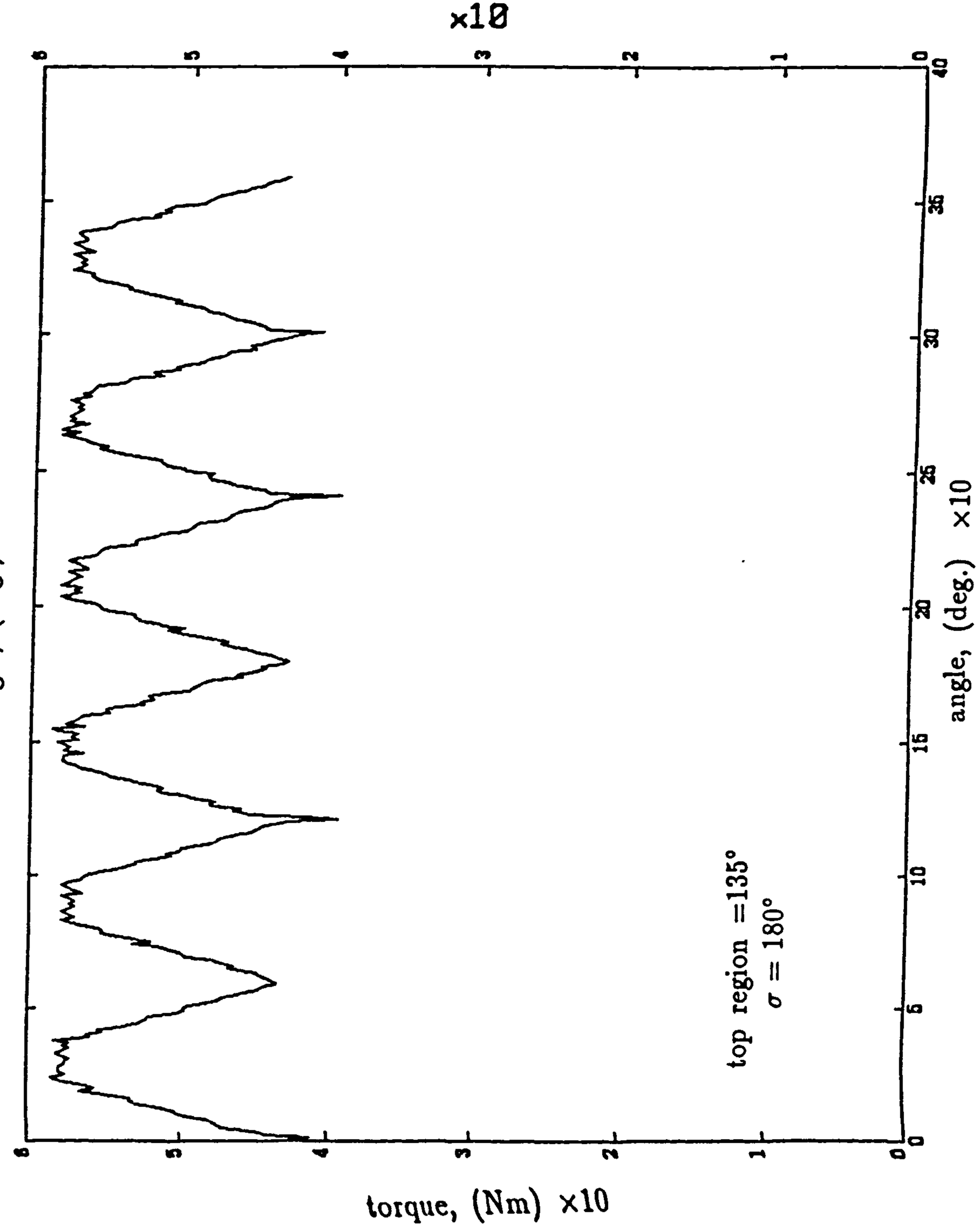
×10
torque, (Nm) ×10
angle, (deg.) ×10
top region =135°
σ = 180°

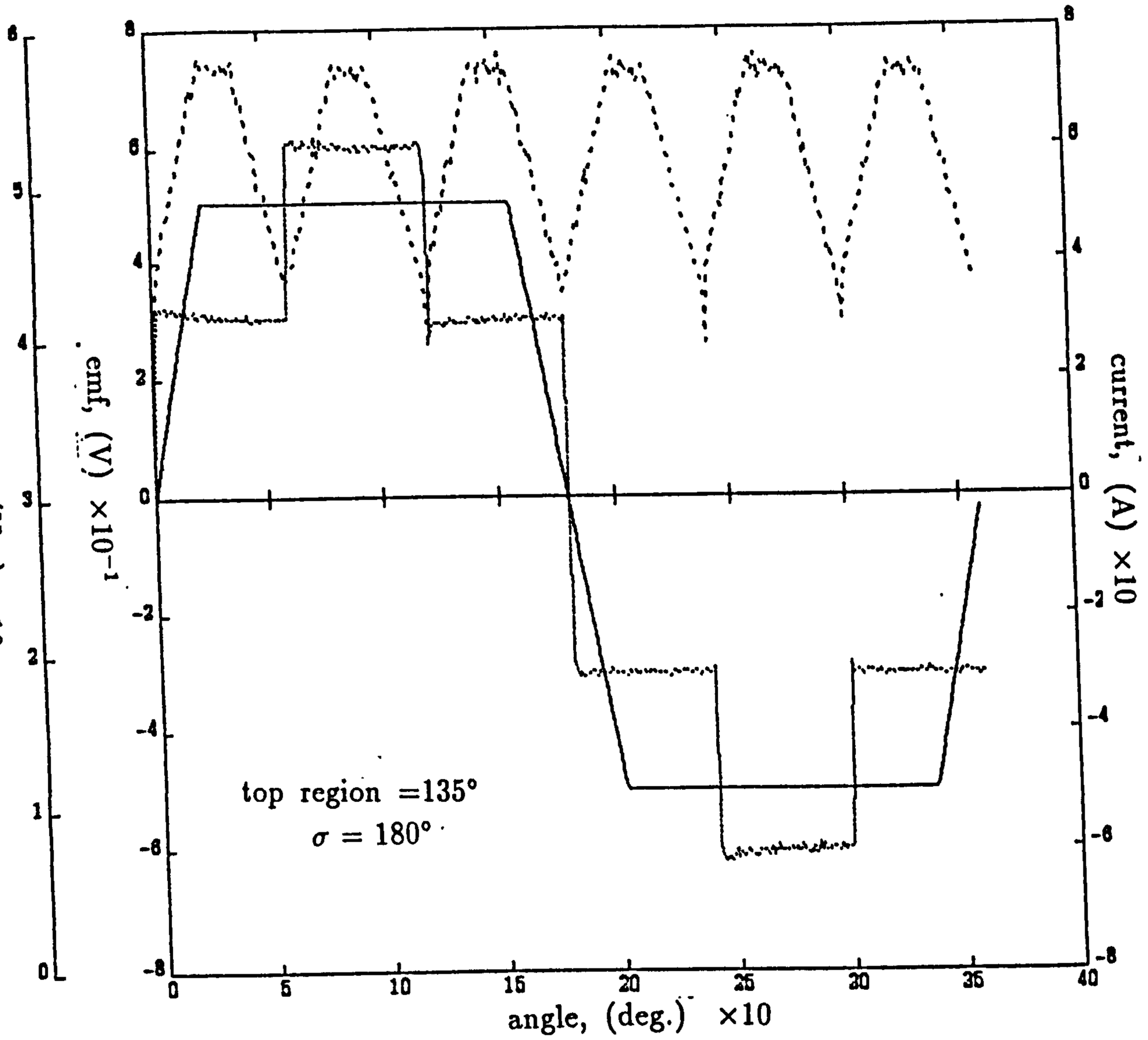

Figure 6.13 Current, back-emf and torque waveforms for 180° conduction angle at speed=100 rpm and constant top region=135°.

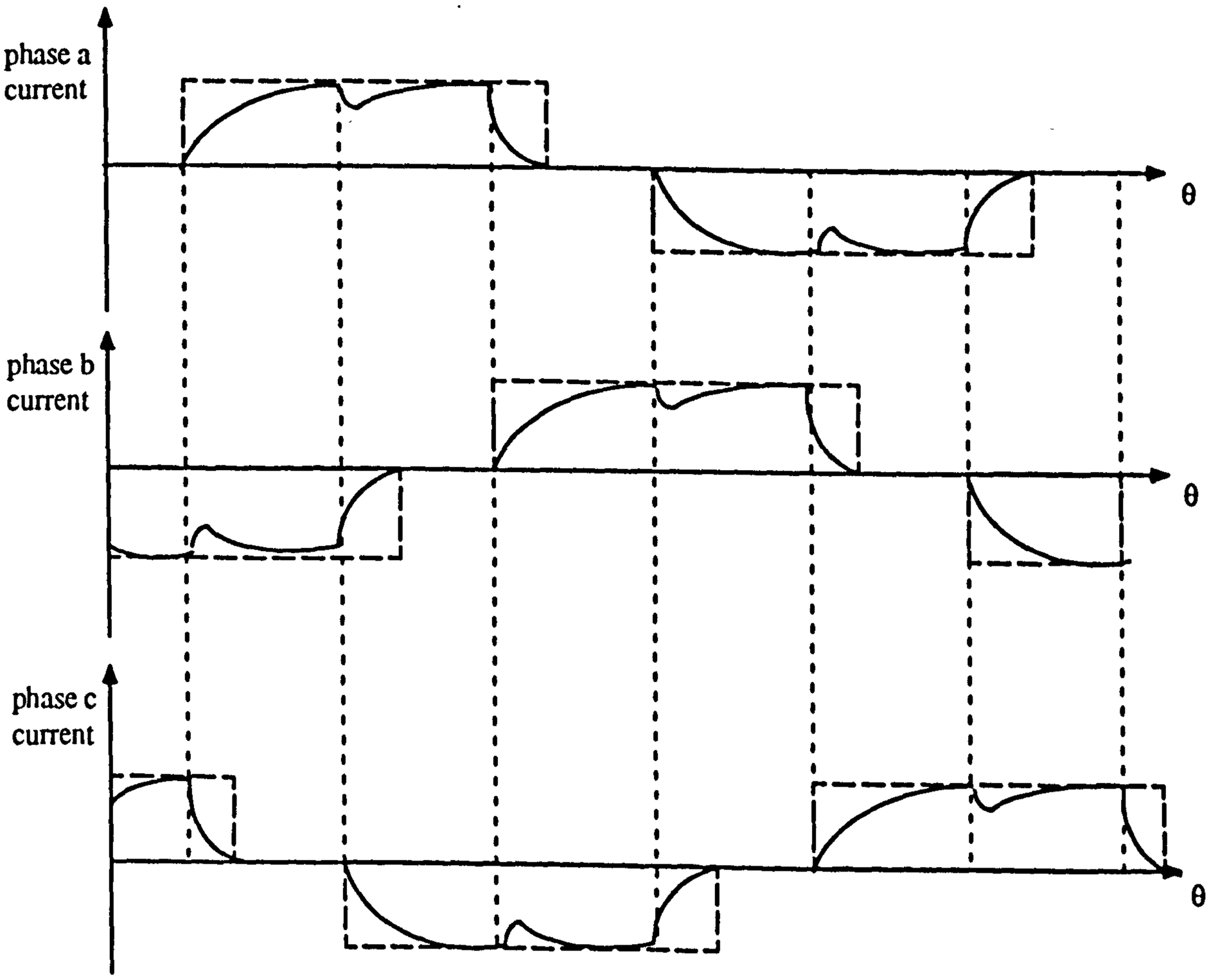

Figure 6.14 Current waveshapes

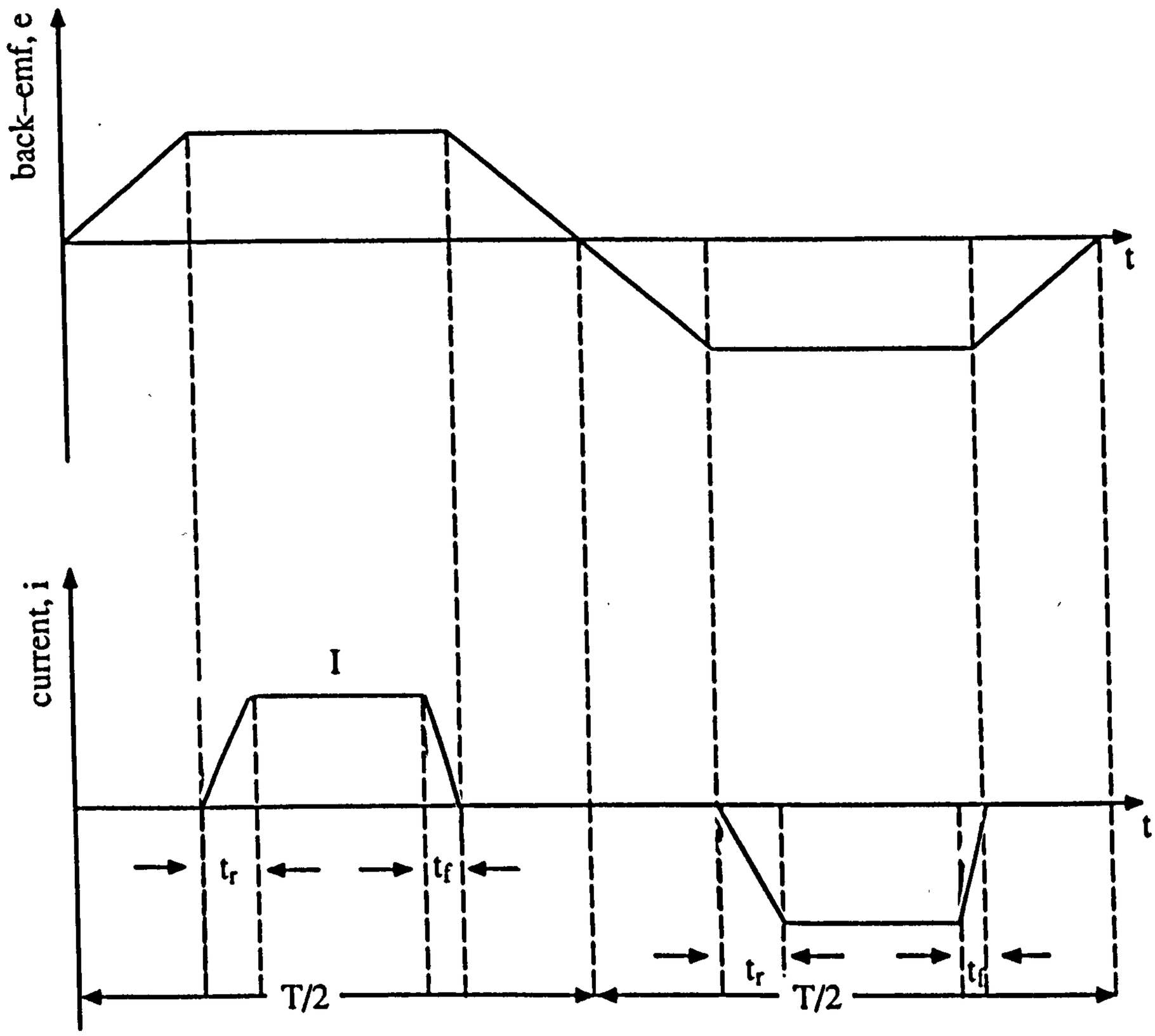

Figure 6.15 Analytical model for the phase advance

CHAPTER 7

EXPERIMENTAL TESTS AND MEASUREMENTS ON THE PROTOTYPE BRUSHLESS DC DRIVE

7.1 Introduction

It is intended that the high-speed torque control method based on the phase advance, which is investigated and analysed in the previous chapters, may be executed as far as possible by a microprocessor. Algorithm, software and hardware for designing and implementing the phase advance control using a digital signal processing (DSP) TMS320C30 are presented in this chapter. However, the control principle basically performs the task of the advance of the instant of the commutation with respect to the rotor position, in response to the motor speed and load conditions, allowing automatic operation of phase advance. The process occurs in "real time" and so if the microprocessor is used to implement phase advance control algorithms, it must likewise execute its software program in real time. It has been frequently claimed during recent years that a microprocessor can do anything providing it has the right software, and in general this is true, providing the microprocessor can execute the program in the available time. In motor control there is usually very little time available to perform the software routines and so the use of a microprocessor to implement the control algorithm is not necessarily straightforward.

It is briefly explained in chapter 2 how a microprocessor can perform the high speed torque control based on the phase advance control algorithm. This chapter contains some details of a digital signal processor TMS320C30 that is successfully used to implement the phase advance controller described

in the following sections.

This chapter consists of four major parts. The first part provides an overview of the tasks that a microprocessor can perform in a motor system and some of the problems that must be overcome are discussed. The reasons leading to the choice of the digital processing signal (DSP) TMS320C30 are explained and a description of the system. The second part presents the theoretical analysis of the variation of time advance to achieve the phase advance angle. The discussion on the development of the phase advance algorithms, leading to the derivation of the phase advance estimation algorithm is also given.

The third part details the system configuration and design of both hardware and software. Comments on the DSP system performance with a set-up of the proposed control system are given.

The fourth part presents experimental tests and measurements made upon the prototype brushless dc motor drive are presented and discussed. The experimental measurements enable the characteristics of the machine to be determined and also the validity of the proposed method is verified.

7.2 Microprocessor-Based Control

Microprocessors are relatively new devices and there are many applications in which they have yet to be used. However, they are now sufficiently common place that descriptions of their basic structure and operation can be found in many recent electronics textbooks. Nevertheless it is worthwhile stating that a typical microprocessor system consists of a microprocessor, a system clock, some Random Access Memory (RAM), some Read Only Memory (ROM), an Input/Output unit (I/O), and an interrupt handler. The system is interconnected by buses as shown schematically in figure 7.1. Data shifted around the system on the data bus. The address and control buses

ensure that the microprocessor only communicates with one location within the system at any time. The microprocessor deals with one instruction at a time and the rate at which it processes the program instructions is fixed by the system clock frequency.

A microprocessor can perform a variety of control commands in a brushless d.c. motor system. Fistly it can make the basic decision necessary to drive the motor. The microprocessor receives position information from the rotor position sensor and controls the inverter in a such a way as to maintain the motor in synchronism. In a high speed motor there are many inverter switchings per second and so the microprocessor must be able to respond very fast to the position information to avoid loss of synchronism. Secondly, the microprocessor can monitor variables in the motor system and attempt to regulate them within required limits. For example, it might be desired to control either the speed or torque in a motor system and the microprocessor can achieve this providing the necessary software is available. The response required to accurately control these motor variables is usually less than that needed to maintain synchronism. Therefore, these tasks can be given lower priorties within the program hierarchy. Thirdly the microprocessor can deal with the communication of data between it and the machine operator and vice-versa. Fourthly, the microprocessor can be used in supervisory role. For example it can arrange the successful starting of the motor system and can ensure that the motor runs in the required direction. Useful checks include the measurement of motor speed to detect dangerous overspeed condition; the measurement phase currents to detect short circuits on the inverter outputs; and the implementation of control algorithms to control and improve the system performance.

The control of the speed and torque of electrical machines, which had already considerably evolved with the adoption of power inverters, is now

undergoing an even more fundamental change towards less expensive though increasingly sophisticated systems owing to the introduction of microprocessors in the internal loops of the control system. A microprocessor based control system for industrial drives promises several distinct advantages. One of the most important is flexibility as the control procedure is implemented in the software. Therefore, to change the control procedure in order to obtain different drive characteristics, only the software needs to be modified with minimum or no change in hardware. The microprocessor control can be completely digitised, which will decrease its sensitivity to external influences. Discrete components and wiring can be reduced or eliminated, a factor which should improve reliability. Also as prices of microprocessor and associated peripherals continue to fall, the microprocessor-based control will become cost competitive. Continued developments in microprocessor technology leading to increase processing speeds will provide improved performance in speed, regulation, response time and resolution.

There have been various attempts to implement some of the above tasks by microprocessors. The references illustrate the principle advantage of a microprocessor with discrete logic circuits. A microprocessor is a very flexible device and it can be adapted into many applications. If changes in the operation of the motor system are required it is usually a simple matter of modifying the microprocessor software (that is, no hardware changes are necessary).

Unfortunately, the flexibility is not achieved without one significant disadvantage. The microprocessor is a sequential logic device which performs "one" instruction at a time, with each instruction taking a certain number of clock cycles to complete. Since even relatively simple tasks usually require several instructions, it follows that a microprocessor can take a significant number of clock cycles to complete one task. Hence there is a limit on the

number of times that a task can be performed per second, and this limit is essentially fixed by the clock cycle period which is typically of the order of $1\mu s$ in many common microprocessors. The execution of a task can be speeded up either by reducing the clock cycle period (e.g. by choosing a different microprocessor) and/or by reducing the number of software instructions in a given task.

In contrast a discrete logic circuit is much faster in its execution of a task, since the main limitations on its speed are the propagation delays through the logic gates. Such propagation delays are of the order of tens to hundreds of nanoseconds.

Microprocessor time spent on the automatic operation of the phase advance task can be minimised or eliminated completely by a suitable combination of a microprocessor and discrete logic. In this way it is possible to combine the flexibility of a microprocessor with the speed of discrete circuitry. For example, at any speed there is an optimum phase advance at which a brushless dc motor can operate to maximise its torque output as discussed in chapter 2. A microprocessor could be used to monitor the motor speed and calculate the optimum phase advance angle, and then instruct a discrete logic circuit to implement the required angle.

Critics may argue that the use of a microprocessor to implement the high-speed torque control algorithms can not be justified, but in general such an approach is attractive particularly because (i) the power of software can enable significant reduction in logic to be made, (ii) the microprocessor can be easily programmed, thus enabling changes to the control algorithms to be readily implemented. However the idea behind the microprocessor as part of this work is to investigate these potential benefits.

The subsequent sections describe the principle of a microprocessor-based high-speed torque control scheme for a brushless dc derive fed from a

dc source, which incorporates both PWM of motor currents at low speeds and field weakening by using phase advance control at high-speeds.

7.3 Control Algorithms for Microprocessor

7.3.1 Theoretical Analysis of Time Advance Control

Before describing the development of the high-speed control algorithms for the microprocessor based on the phase advance angle method, it is appropriate to describe briefly the variation of the time advance of the phase advance angle.

The principle of the phase advance control method is based on variation of the phase relationship between the winding current and rotor position and can be implemented using time shifting of the signals from the rotor position encoder, with time shift being a function of rotor speed.

The theoretical analysis of the preceding chapter has shown that the optimum position of the instant commutation of the phase current was found as follows

$$\theta_{opt} = \frac{\pi}{2} - \alpha_{opt} \tag{7.1}$$

where $\alpha_{opt} = tan^{-1}\frac{\omega_r L}{R}$. Equation (7.1) shows if $\omega_r = 0$, α_{opt} equals 0 indicating that the phase difference between the voltage (or current) and emf waveforms are coincident in time. However, as the speed increases the instant of current commutation should advance by position of $tan^{-1}\frac{\omega_r L}{R}$.

A variable phase advance angle can be implemented through the variation of the time advance or delay. The introduction of a time advance into position sensor signals represent the advance commutation of the current with respect to the back-emf. In effect, if time advance of Δt_a seconds is introduced into the position sensor signals the net effect is to cause the

position of the commutation angle or the current to be advanced. This is because at a motor speed n rpm the rotor moves through an angle $\Delta\theta_a$ during the advance time, Δt_a and the time advance required to achieve a particular phase advance angle can be described by the mathematical relation which is found in the following form;

$$\Delta t_a = \frac{\frac{\pi}{2} - \alpha_{opt}}{\omega_r} \tag{7.2}$$

This equation shows that the phase advance angle can vary as a result of introducing a time advance to the position signal. Also equation (7.2) shows that the required time advance, Δt_a is inversely proportional to the motor speed. The selection of the phase advance angle is determined automatically by closed loop which responds to the speed of the motor. Specifically the time advance variation of the angle α affects the performance of the motor drive and they are not constants. They need to be varied as a function of speed, magnitude of current and load desired for overall drive system.

This is a straightfoward problem when the drive is running at a constant speed, but more difficult during a speed transient, which is the very situation where the full benefit of enhanced torque from phase advance is needed. As the time-shift is in the backward direction it is necessary to anticipate the arrival of encoder signals.

Based on the above considerations, the phase advance control method must incorporate an algorithm for the microprocessor to predict and to select the time advance as a function of motor speed. The following section proposes an original microprocessor closed-loop system to estimate the time advance and improve the high-speed performance of the brushless dc motor drive.

7.3.2 Phase Advance Estimation Control Algorithm

Along with developing estimation algorithms for microprocessor and an understanding of the concept of the time advance variation the requirements, which are described earlier, demand the development of an improved control method for time advance, in order to predict accurately the performance characteristics of the machine. This section presents improved methods for estimating the time advance.

In these estimation methods, it is necessary to define a rapid predictive model for anticipatory determination of the times of encoder feedback pulses value based on previous disposable information. This predictive model included in the microprocessor time-controller structure is represented by "finite-difference equations".

To illustrate the principle of this method of estimation phase advance, consider the output waveforms of the encoder pulse shown figures 7.2-7.3, where θ_{k-2}, θ_{k-1}, θ_k, represent the position of the encoder pulses at the kth sampling points and t_1, t_2, t_3, represent the time intervals of the encoder signals. The method in which the estimated value of t_{k+1}, is presented in the following section.

7.3.3 First Order Estimation

Suppose the position $\theta(t)$ between three sampling points varies according to the following first-order function

$$\theta(t) = a(t) + b \tag{7.3}$$

using the equation (7.3) at kth sampling points and calculating the constants a and b in equation (7.3) for a given θ, the estimated value of t_{k+1} by first order estimation can be obtained using the following expression;

$$t_{k+1} = t_k + \Delta t \tag{7.4}$$

For example, for a given t_3 the estimation value of t_4 using the above equation can be obtained as

$$t_4 = t_3 + \Delta t \tag{7.5}$$

7.3.4 Second Order Estimation

Suppose the position $\theta(t)$ between three sampling points varies according to the following second-order function, (figure 7.2),

$$\theta(t) = a(t)^2 + b(t) + c \tag{7.6}$$

Using the values of time estimated in the previous three sampling instant, t_{k-2}, t_{k-1} and t_k, the predicted value of next sampling, t_{k+1}, may be calculated using the following procedure (difference equation)

$$\left.\begin{aligned} t_2 - t_1 &= \Delta t_1 \\ t_3 - t_2 &= \Delta t_2 \\ t_3 - t_1 &= \Delta t_3 \end{aligned}\right\} \tag{7.7}$$

and

$$\Delta t_2 - \Delta t_1 = t_3 - 2t_2 + t_1 \tag{7.8}$$

then

$$\left.\begin{aligned} t_4 &= t_3 + \Delta t_2 + \Delta t_2 - \Delta t_1 \\ t_4 &= t_3 + t_3 - t_2 + t_3 - 2t_2 + t_1 \end{aligned}\right\} \tag{7.9}$$

therefore

$$t_4 = 3t_3 - 3t_2 + t_1 \tag{7.10}$$

Equation (7.10) may also be written as

$$t_{(k+1)} = 3t_k - 3t_{(k-1)} + t_{(k-2)} \tag{7.11}$$

Therefore the time advance definition for t_4 value is given by

$$\Delta t_a = \frac{90° - \alpha}{60°} \times t_4 \tag{7.12}$$

7.4 Experimental System Control Components

This section describes briefly the practical system components, which are required to implement the control algorithms presented in the preceding section. The control system hardware consists of the following components (i) DSP TMS320C30 hardware (ii) Drive system hardware. A functional block diagram for the complete control system is shown in figure 7.4.

7.4.1 DSP TMS320C30 Processor Hardware

The system hardware consists of a XDS1000 development environment, which uses the TMS320C30 as its processor. A functional block diagram for the TMS320C30 is shown in figure 7.5. As is clear from examination of figure 7.5, the phase advance controller may be viewed as comprising of a set of software routines within TMS320, pulse associated external hardware to provide interfaces between the TMS320C30 and the incoming digital signals and a host CPU. The following discussion briefly describe the major hardware

and software features of the control system and some of the features of TMS320C30 which are of special benefit to this application.

The DSP TMS320C30 processor is ideally suited for the implementation of the control algorithm discussed above, since it has the capability and features to implement all required functions with full accuracy and speed. It possesses on-chip timers, hardware multiplier and 60 ns instruction. These last two features allow high-speed calculation of control algorithm. The TMS320C30 also provides multi-bus structure comparable to conventional processors. The TMS320C30 has two user accessible external buses that can operate at different speeds, and with the use of an integrated DMA can be accessed in parallel. The XDS1000 has the primary bus connected to SRAM for program and data storage, the secondary bus left for expansion. The TMS320C30 contains two 32-bit counter timers which are clocked at 33.33 MHz, one of them is used to provide the three time measurements required by control algorithm. The structure of the DSP hardware built is shown in figure 7.5.

The encoder signals are input through the digital input and the output of signals are output through the digital output. All system I/O is read from or written to the secondary bus by the DMA, while the control algorithm program runs in parallel on the primary bus. This structure reduces any delay in accessing slower I/O memory. These hardware aspects are briefly described in Appendix 2.

7.4.2 The Prototype Drive Components

The functional block of the prototype drive system with DSP hardware circuit is shown in figure 7.5. The inverter transforms the d.c. input power into a.c. power of variable frequency and voltage to drive the three phase permanent brushless d.c. motor. The phase advance controller circuit

generates advance signals to drive the inverter. These signals are based on the rotor position information from the encoder. These signals are connected to the inverter through an interface circuit. The dynamometer outputs variable torque on the motor shaft and give indication of the motor torque and speed.

Permanent Magnet Motor

The permanent magnet is a three phase, six pole, star connected, 550 volts 23 amperes, type SE-B4 210 motor+SM50/100-T inverter combination manufacture by Robert Bosch. This motor uses rare-earth material on its rotor. The motor parameters are given in Appendix 1.

Inverter

A three phase inverter with variable input voltage is used. The inverter which is a commercial SM50/100-T Bosch inverter and uses bipolar transistors on its bridge section.

Encoder

The encoder provides three digital signals. Each signal provides three TTL level pulses per mechanical revolution

Dynamometer

The motor, as shown in figure 7.4, is mechanically coupled to a dynamometer. This dynamometer is used to measure the output torque developed by the motor. The dynamometer applies variable torque to the motor shaft in order to measure the torque/speed characteristic of the brushless dc motor.

7.5 Position Detection and Commutation Control

To help in understanding the implementation of the phase advance in real time it is useful to explain briefly the relationship between sensors output states commutation control signals when the motor operates in the normal mode (zero phase advance).

The magnitude and commutation control circuit (or logic control circuit) consists of position sensors, control units, and logic gates. The logic gates are arranged to turn on the power on the power transistor in proper sequential order. The motor magnitude control unit provides the control of start/stop, direction, current and speed. As the permanent magnet rotates a position sensor senses the position of the rotating magnet and provides an on/off output.

The magnitude control unit provides control of the functions performed by the motor. By turning on and off the power transistors, it connects and disconnects the power to the motor windings. By reversing the sequence that the power transistors induced current into the windings. As explained in the previous chapter it also allows variable speed by using voltage method which achieves voltage control by pulse width modulation. The motor control unit also controls torque since torque increases as shaft speed decreases in the brushless motor.

Figure 7.6 illustrates the relation between the positions of the Hall elements, the back-emf, current distribution, the rotor position and the switching code.

In practice the way of encoding the Hall sensors output states is illustrated in figure 7.6. Also this figure shows the output of the sensors placed 60° electrical degrees apart in the brushless motor to provide the required 120° electrical degrees separation explained in the previous chapter.

Logic gates use the output of the three Hall effect sensors to turn on the power gates in proper sequential order. The logic values from the three sensors are shown in figure 7.6. Six different commutation logic combinations are provided by the sensors for each electrical revolution. These commutations proceed in sequential (100) $\longrightarrow$ (110) $\longrightarrow$ (111) $\longrightarrow$ (011) $\longrightarrow$ (001) $\longrightarrow$ (000). The combinations 010 and 101 are excluded since only six combinations are required. If the rotation proceeds in the reverse sequence, the motor will rotate in the opposite direction. Also by having one logic value different from the others allows for easier design of the gate arrangement. Since only two windings are required to be excited at a time, only two signals are needed from the gate logic and sensors.

7.6 Software Description

7.6.1 General

This section describes a software development which implements the high-speed torque control through the algorithm described earlier in real time on the DSP TMS320C30 processor. In this case when the processor receives data from the position sensor, the TMS320C30 system described earlier accomplishes basic functions of the control algorithm which are described in the following subsection.

7.6.2 Implementation Approach

The software of the control algorithm within the TMS320C30 may be conveniently split into the following procedures

(i) input signal processing which contain three tasks;

(a) Read the encoder signal: the digital encoder signals are connected to the input of the digital devices. The inputs are read during the program initialisation to determine the position of the switching signals. When the

machine operates at low speeds, the processor transmits these signals directly to the commutation control circuit since the optimum position for commutation between phases at these speeds is that detected by the position sensor. Once the speed of the motor exceeds the minimum value the processor changes the mode of operation from normal mode (zero advance) to phase advance control mode.

In this mode, after the timer has been initialised the program enters a loop which is normally executed repetitively for the remaining time that the control is switched-on. The first step in this loop is to wait for the processor to detect the transient pulse to happen. The next step is to read the time count after the transient happens. The timer is then reset to zero and the encoder time intervals updated.

(b) Identifies the direction of the motor,

(c) Filtered the input signals: the software filter procedure is responsible for rejecting noise on incoming encoder signals. The major task of the filter is to deal with short-duration noise pulses that cause the input logic level to momentarily change. The software filter procedure rejects these noise pulses by sampling the encoder signal logic levels and storing a time history in a memory. For each signal, if the input level has had the same value on four consecutive rising clock edges, that value becomes the new output of the filter; otherwise the output cannot change from high to low until the signal input has been low for four consecutive rising clock edges. This filtering procedure is done for each input encoder signal.

(ii) Pulse transition detector; in this procedure the processor used only to detect the transition and the timer of the TMS320C30 is then reset to zero after reading the value of pulse state. It is an easier way to achieve the time measurements required by the control algorithm, rather than including the additional complication of using the interrupt procedure of DSP and avoiding

other hardware techniques.

(iii) Update the time measurements and then the t_{k+1} or t_4 is predicted and this time is delayed by appropriate angle, α, which is stored in a look-up table, to produce the required advance encoder signals. Three consecutive feedback pulses, t_{k-2}, t_{k-1} and t_k are measured and the estimated t_{k+1} and corresponding predetermined Δt_a time delay are predicted. The time measurements are realised with one programmable timer 0 of the DSP system. This prediction of the time delay $t_{a_{k+1}}$ is based on the equations (7.11) and (7.12) and storing the value in the memory location.

(v) When the new signals have been latched the program then returns to the beginning of the main loop wait for the next transition pulse and the process is repeated again.

(vi) Output signal processing by applying the generated advance signals to the drive circuit. As the time shift is in the backward direction, it is necessary to anticipate the arrival of encoder signals. In this case, the processor generates the advance encoder signals from look-up table, as shown in figure 7.7, in order to advance the time of the encoder pulse. This procedure is very important to convert the time delay predicted by the control algorithm to time advance which corresponding to the speed of the motor. Finally the flow chart of the control software is shown in figure 7.8.

Conversion of the count into frequency or speed is carried out in software using the following procedure. If the count for timer value is C_v, and the frequency of the clock pulses is f_c (Hz), then the time for the motor to run by counter is

$$t_p = \frac{C_v}{f_c} \tag{7.13}$$

The rotor speed is determined by

$$f_r = \frac{1}{n_p t_p} \tag{7.14}$$

combining equations (7.13) and (7.14) yields

$$f_r = \frac{1}{n_p C_v / f_c} \tag{7.15}$$

or

$$f_r = \frac{f_c}{n_p C_v} \tag{7.16}$$

This results shows that the frequency (or speed) depends heavily on the accuracy of the timer.

7.6.3 Program Development

Most of the software for the control algorithms was written in the 'c' programming language. This choice was made as it has many inherent features accordant with the requirements of real-time control: Firstly, the richness of its operators and control structures yields a high enough programming level to facilitate an efficient transcription of algorithms into 'c' code. Secondly, robust software can be created because functions are afforded a high degree of modularity through their 'call by value' nature.

A further advantage is the processor TMS320C30 which is used to implement the control algorithm, is supported by a full set of software development tool. These software tools include an assembler, a linker, a simulator and a 'c' complier.

Although most of the software was writtern in 'c' and cross compiled to object code, so the procedures were writtern directly in assembl source code. In the first instance this is to manipulate registers in DSP interface chips, initially in order to configure them and then handle input/output signals.

7.7 Experimental Results and Discussion

7.7.1 General

A general discussion of the preliminary results obtained in the experiment is presented in this section. It is not intended to explain the results of the experiment through theoretical analysis. Instead a qualitative analysis that describes the predicted motor behaviour as a function of the control parameter is presented. More attention is given to the high-speed performance region, since the extension of the speed range is what this experiment attempts to accomplish. Appendix 1 shows the rating of the drive system used in this work. The drive is dynamometer tested under different load conditions. The drive is operating with closed-loop strategy, which uses phase advance control algorithms in conjunction with a pulse width modulation (PWM) current controller.

7.7.2 Experimental Performance Prediction

Two sets of experimental tests are presented here; one for the prototype brushless dc motor (Bosch drive) operating without phase advance and the other for this drive system operating with phase advance control. The experimental results consist of torque/speed and current measurement for various phase advance angles. In order to amplify the effect of the phase advance on the drive characteristics, the drive has been tested with a dc supply voltage of 120 V.

In addition, the high speed torque performance characteristic of the prototype brushless dc motor are represented, graphically, in terms of the torque/speed and current/speed characteristics. The procedure to collect the experimental results are described in the following subsection.

7.7.3 Experimental Data Acqauisition

The data collected consists of torque, speed and current measurements for each of the selected values of phase advance. The procedure to collect data is as follows

(a) Set the inverter input voltage to 120 V and adjust the dynamometer torque control to zero.

(b) Operate the motor with selected values of phase advance angle.

(c) Increase the torque in steps of certain value using the the dynamometer torque adjustment and record the values of speed and current.

(d) Continue the procedure in step d until the current exceeds 23 A.

Values of torque and speed are read directly from the display unit while values of current are also recorded.

7.7.4 Experimental Tests for High Torque-Speed Performance

A set of results, obtained from the experimental system are presented in this section together with predicted results for comparison. The results are shown in figure 7.9 which shows how torque varies with speed for two phase advance angles. The difference between the results of the predicted and the measured curves could be due to the windage and friction losses. Though saturation is generally small in the surface mounted machine (because it has large airgap), the field weakening characteristic is sensitive to the machine inductance and so the accurate and measured value should be used together with the saturated value.

To examine the effect of the phase advance control on the high speed drive performance, the torque was measured at many speeds as a function of the phase advance. The results are organised in the torque/speed plots of figure 7.10 which shows how torque varies with speed for different phase advance angles and loads.

The effect of phase advance on the torque/speed characteristics is demonstrated in Fig. 7.10 which shows the torque/speed characteristic of the machine as a function of speed with phase advance angle of $\alpha = 0°$, 15°, 30°, 45° and 60°. Torque-speed curves of figure 7.10f provide a useful summary of the motor's capacity to operate under closed-loop control, over the whole range of load conditions. The experimental torque/speed characteristics presented in figure 7.10 shows that the phase advance angle does affect the motor's high-speed performance to some extent. The changes in the torque/speed characteristics are a result of the changes in the phase current waveshape.

Figures 7.11-7.13 show a set of current measurements made using a load consisting of a dynamometer with variable armature load resistance at different speeds and operating at different phase advance angles of 0°, 15°, 45° and 60°. The results of these figures show that when the instant of commutating the is advanced by a reasonable phase advance angle, α, the phase current waveform rises steeply and their fall time at the end of each conduction period is also rapid.

Figures 7.11-7.13 also show how the phase current waveform square-up as the motor is loaded. For example, the current waveform in figure 7.11c is for operating conditions of 30° phase advance angle, 14.8 Nm torque and 1000 rpm. The current waveform has the desired shape and has almost constant on-value of about 14.0 A. However, the current waveform shown in figure 7.11e is close to the desired waveshape, although there is still a small switch on overshoot up to 25 A before the current settle down to an on-value of about

22 A. This improvement in current is due primarily to an increase in the voltage difference between the constant voltage supply and the corresponding back-emf. The phase advance control therefore enables a better waveshape current to be achieved with large phase currents than is possible with a 0° phase advance angle (i.e., compare figure 7.11a and 7.11e).

For completeness figure 7.14 shows how the current waveforms vary with phase advance at speed of 1000 rpm. This figure shows that the phase current peaks very sharply under load conditions.

However, the waveforms in figures 7.11-7.14 show that the ability to adjust the phase advance angle is a useful aid in achieving a better waveshape phase current over a range of operating speeds. Reference back to earlier graphs presented in figure 7.10 shows that there is some change in the torque/speed characteristic when the phase advance angle is changed under constant supply voltage conditions. For the range of the phase advance angle used in the tests (0° to 30°), the changes in the torque/speed characteristics are small, so the setting of the phase advance angle is not critical in this respect. However, the phase advance setting does affect the phase current waveform substantially. Hence it is possible to alter the phase advance angle so that the current waveform is essentially square in shape, whilst not affecting the motor torque to any great degree.

For further illustration, figures 7.15, 7.16, 7.17, 7.18 and 7.19 show the encoder signals when different phase advance angles are applied using the phase advance estimation control algorithm.

7.8 Summary and Conclusion

The advantage of incorporating a speed-dependent phase advance angle in a brushless dc drive system are clearly demonstrated by the experimental results. For this purpose phase advance estimation control algorithms which

are suited to microprocessor-based phase advance for brushless motor drives has been proposed.

The configuration and implementation of the control algorithms have been fully described. Experimental results on a drive system under consideration demonstrate the satisfactory performance of both the hardware and software of the control scheme and the ease with which the advance of the instant of the commutation angle is automatically adjusted to maintain the desired torque in response to the motor speed and load conditions.

It has been shown that if the drive is operating with closed loop strategy, which uses a phase advance control technique in conjunction with pulse width modulation (PWM) current controller, has distinct advantages when compared with a similar system which is operating without a phase advance technique. If the motor is operated over a wide speed range and delivers the maximum possible torque at all times, it is normally essential to have some form of phase advance angle control.

The advantage of the phase advance control in the operating speed range of the brushless dc drive has been well demonstrated in the context of using a microprocessor-based phase advance scheme. The configuration of the entire control method can be easily adopted for any brushless dc drive system. In addition the TMS320C30 digital signal processor offers many advantages for implementation of high-speed torque algorithms. Its 60 ns cycle time and special features, such as the signal cycle multiplication, allow high execution speed. Further, the availability of development tools such as c complier, assembler/linkers and in-circuit emulators that accelerate design time.

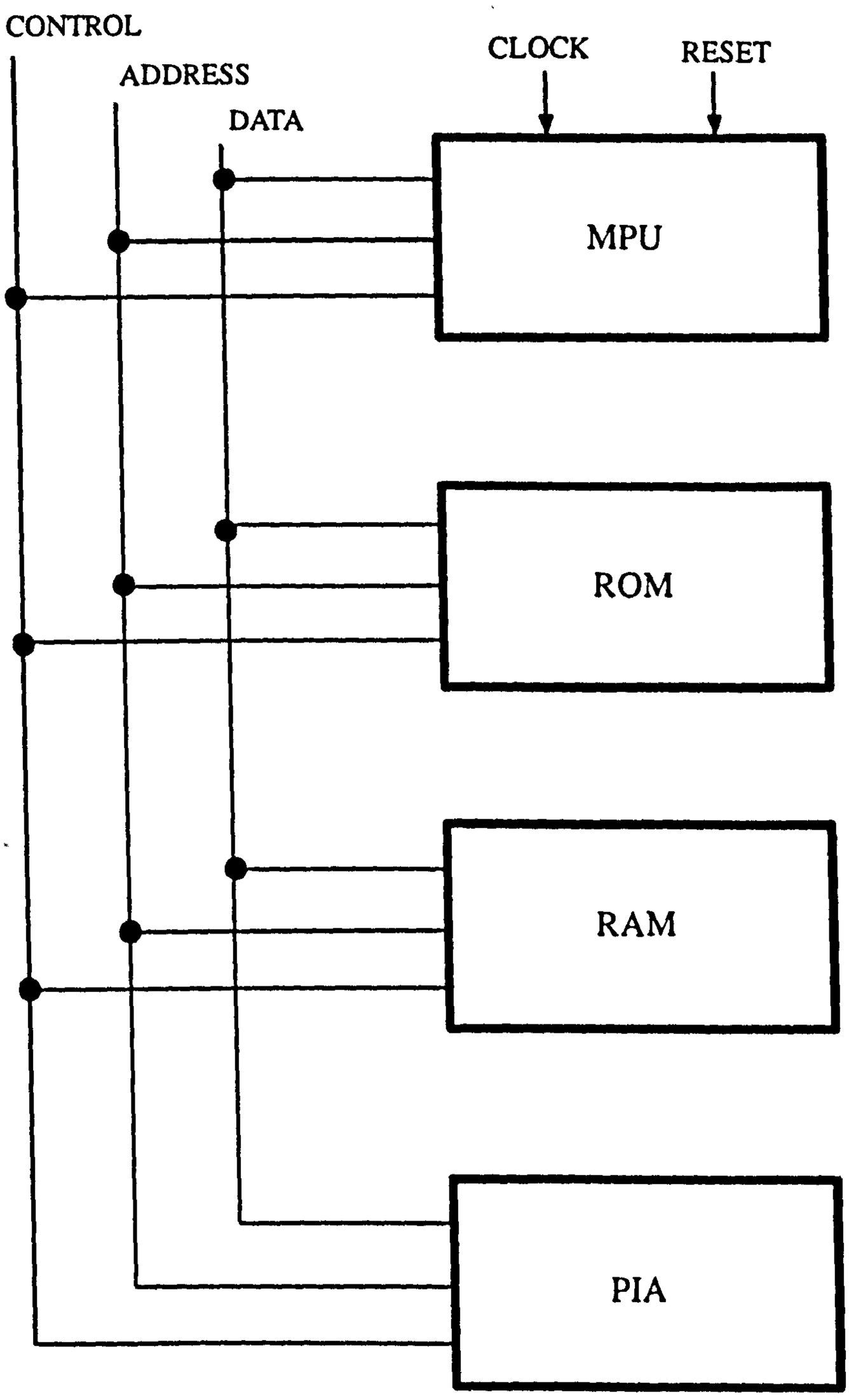

Figure 7.1 Basic hardware for the microprocessor

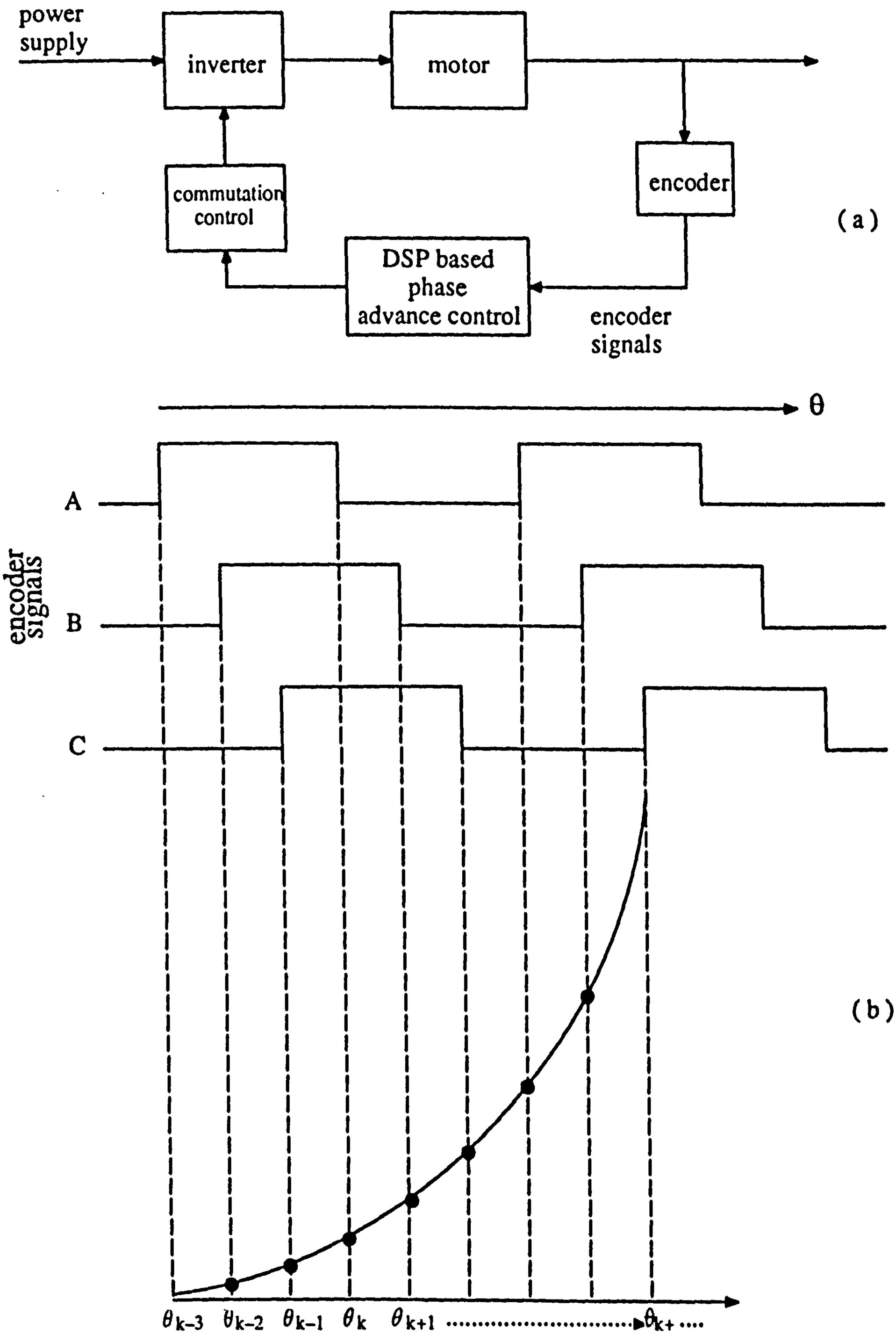

Figure 7.2 (a) Proposed control algorithm
(b) The time advance estimation model

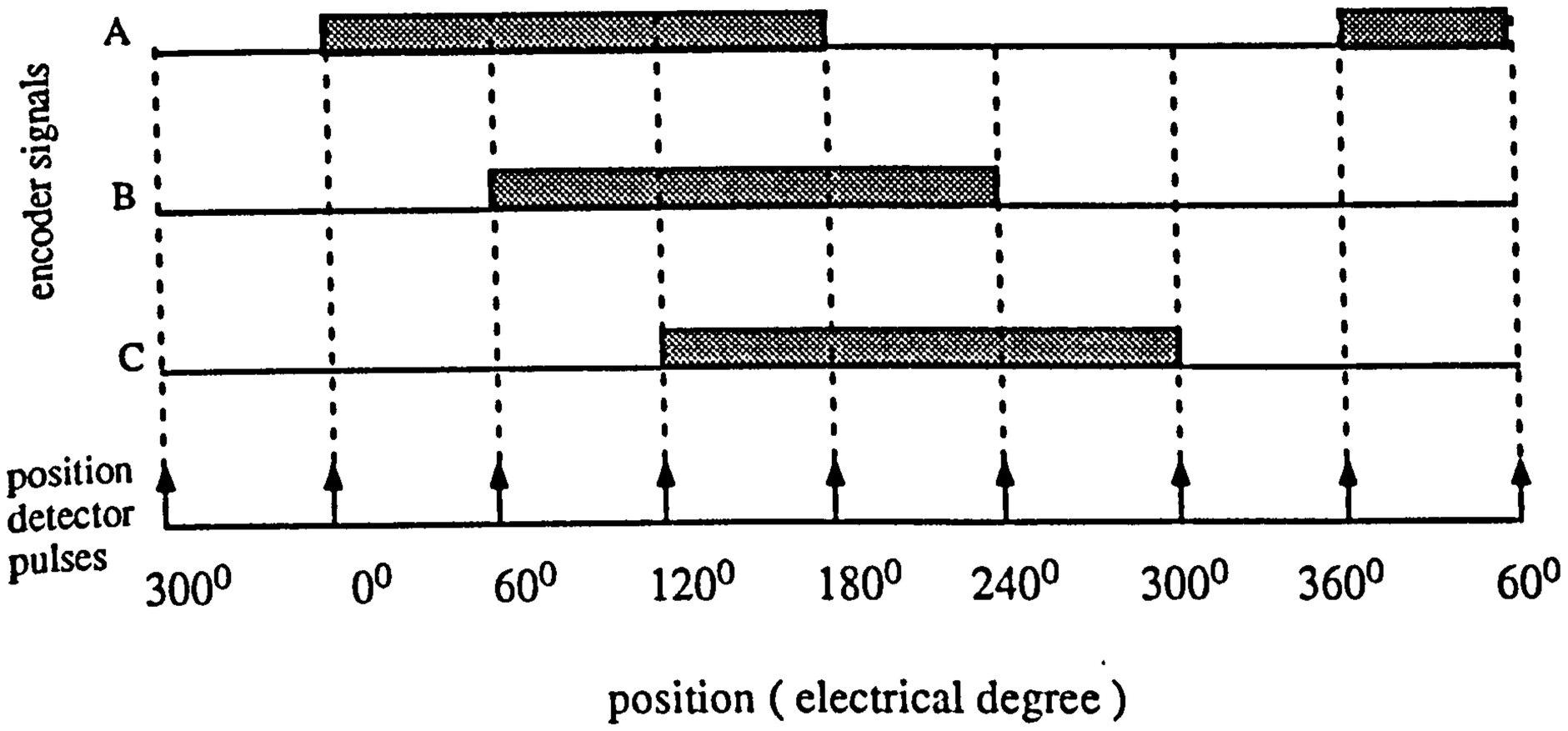

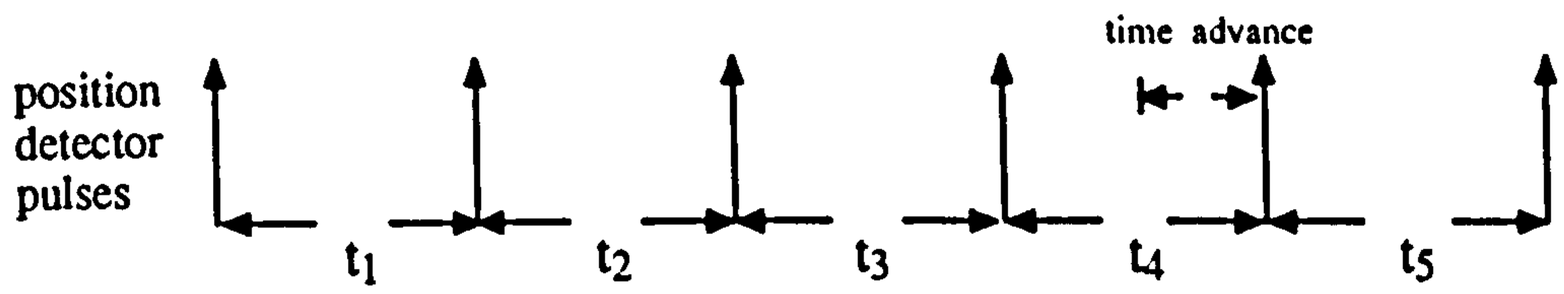

Figure 7.3 Microprocessor–based control of phase advance

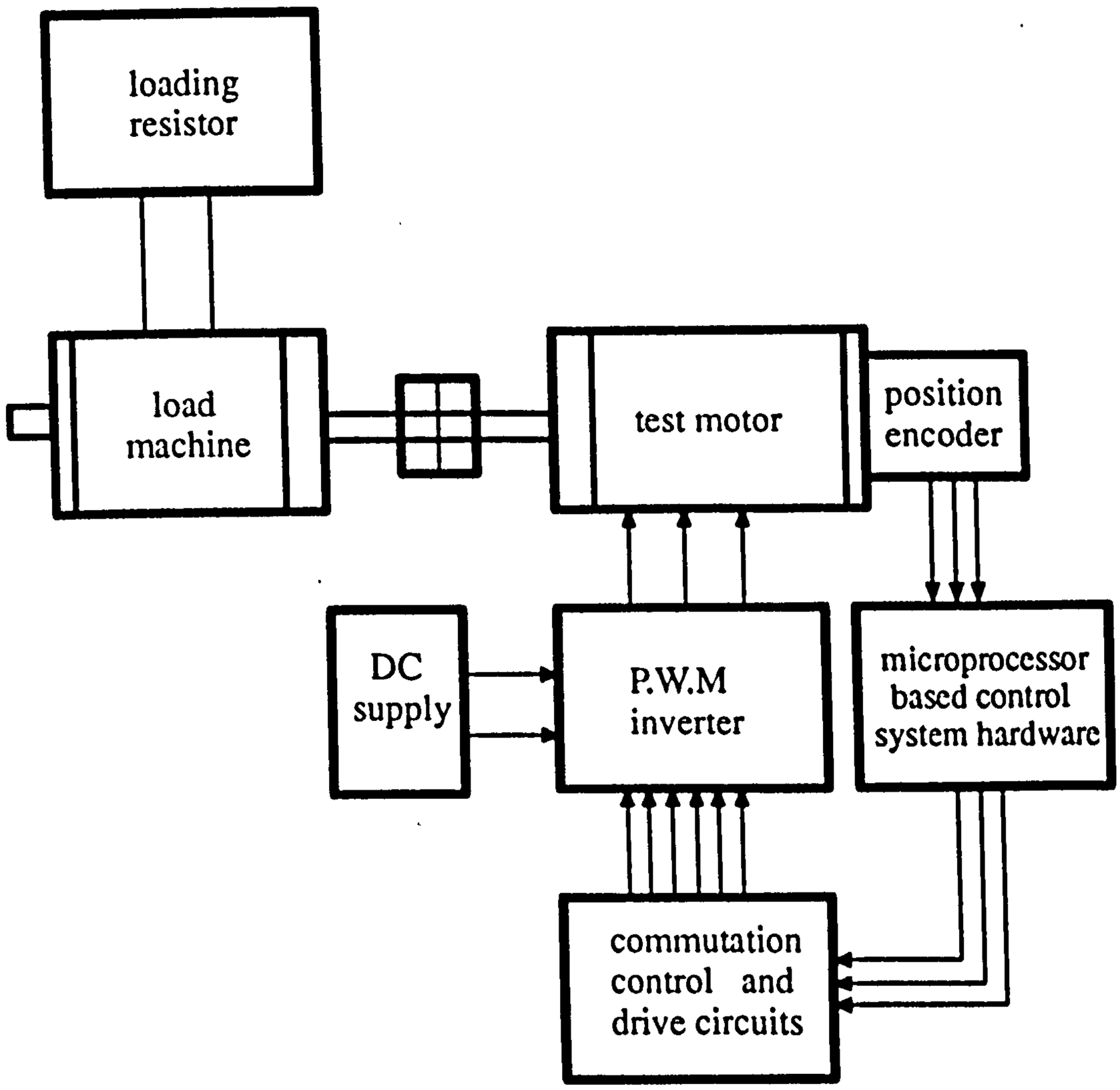

Figure 7.4 Experimental set–up

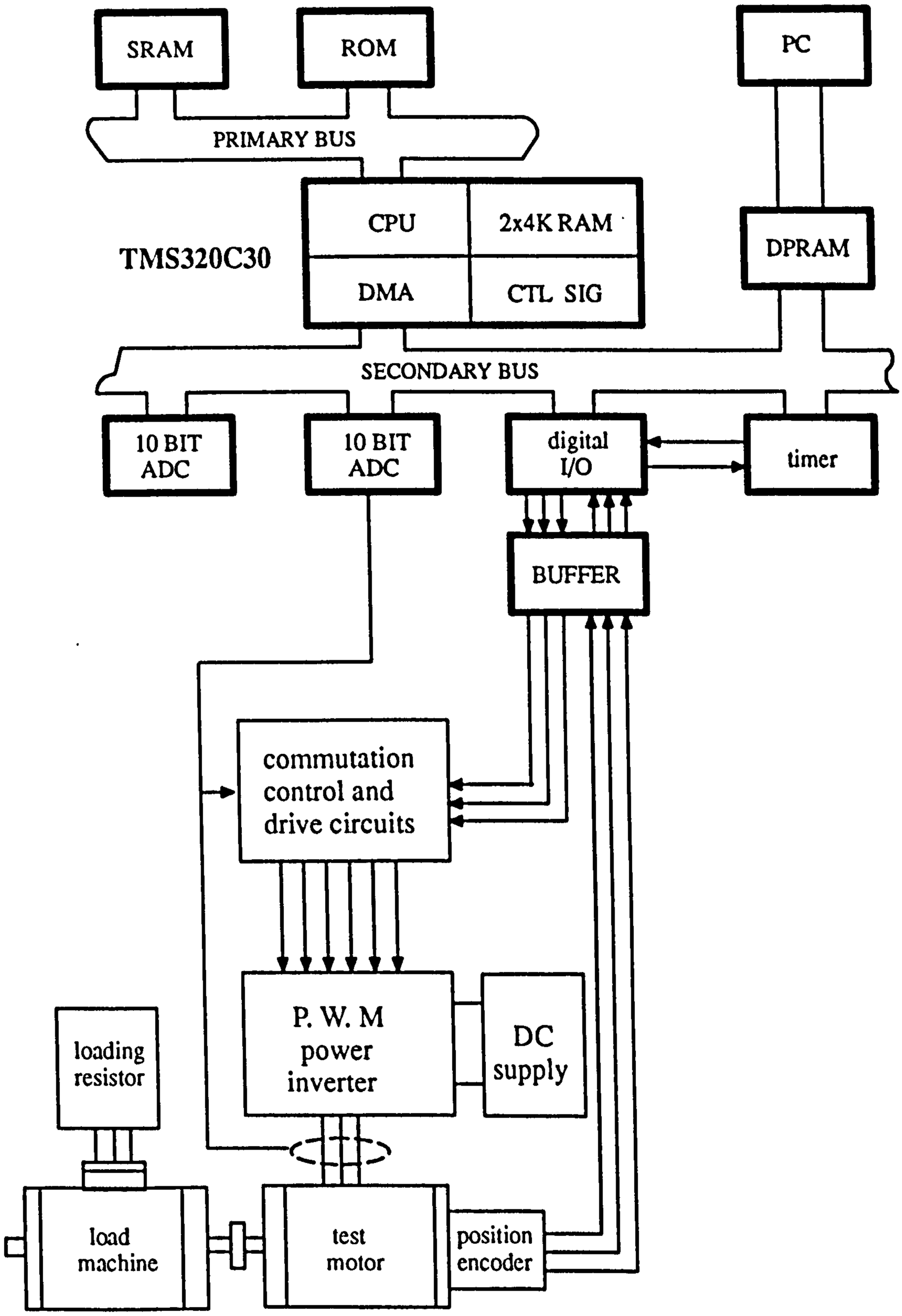

Figure 7.5 Experimental system hardware arrangement for the implementation of the control algorithm

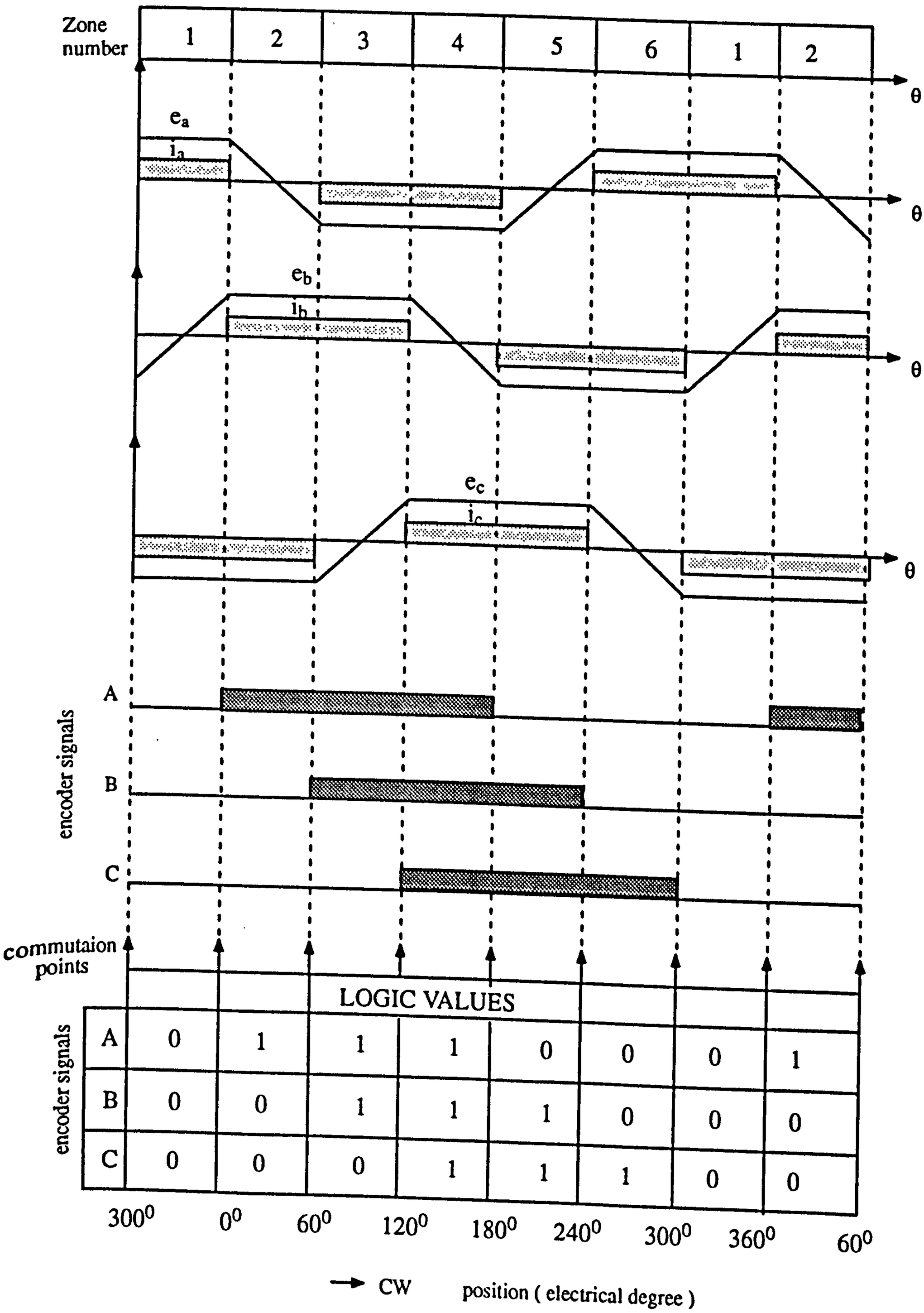

Figure 7.6 Relationship back–emf, currents and rotor positions

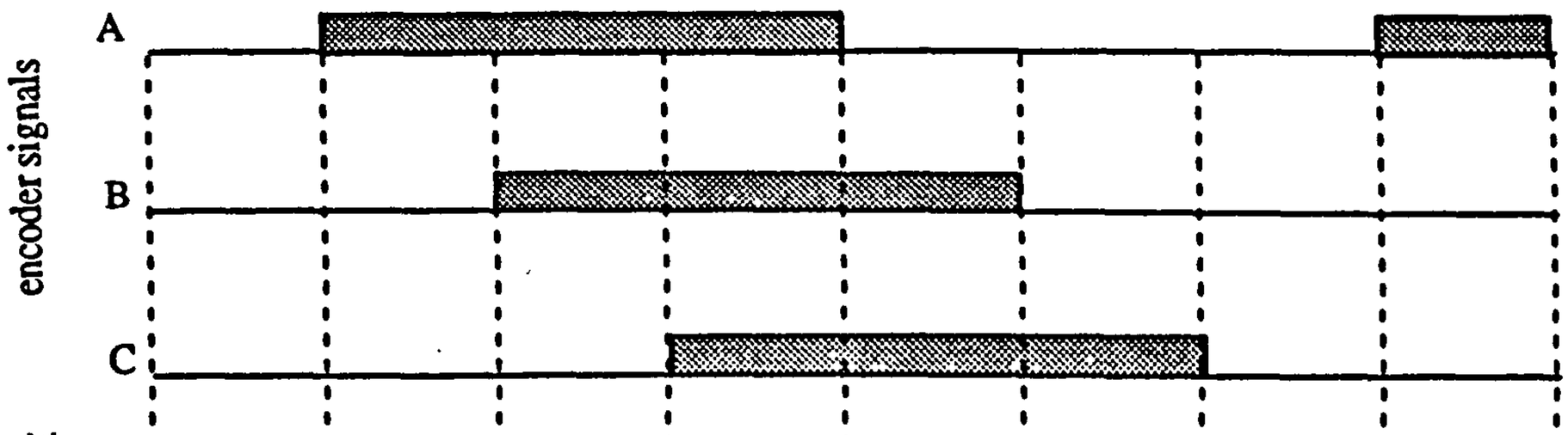

encoder signals	LOGIC VALUES							
A	0	1	1	1	0	0	0	1
B	0	0	1	1	1	0	0	0
C	0	0	0	1	1	1	0	0

300^0 0^0 60^0 120^0 180^0 240^0 300^0 360^0 60^0

→ CW position (electrical degree)

60^0 360^0 300^0 240^0 180^0 120^0 60^0 0^0

← CCW

CW Rotation

Index A	Index B	Index C	Generated I/O A	Generated I/O B	Generated I/O C
0	0	0	0	0	1
0	0	1	0	1	1
0	1	0	x	x	x
0	1	1	1	1	1
1	0	0	0	0	0
1	0	1	x	x	x
1	1	0	1	0	0
1	1	1	1	1	0

Index A	Index B	Index C	Generated I/O A	Generated I/O B	Generated I/O C
0	0	0	1	1	1
0	0	1	1	1	0
0	1	0	x	x	x
0	1	1	1	0	0
1	0	0	0	1	1
1	0	1	x	x	x
1	1	0	0	0	1
1	1	1	0	0	0

CCW Rotation

Figure 7.7 Generation of advanced output signals using microprocessor

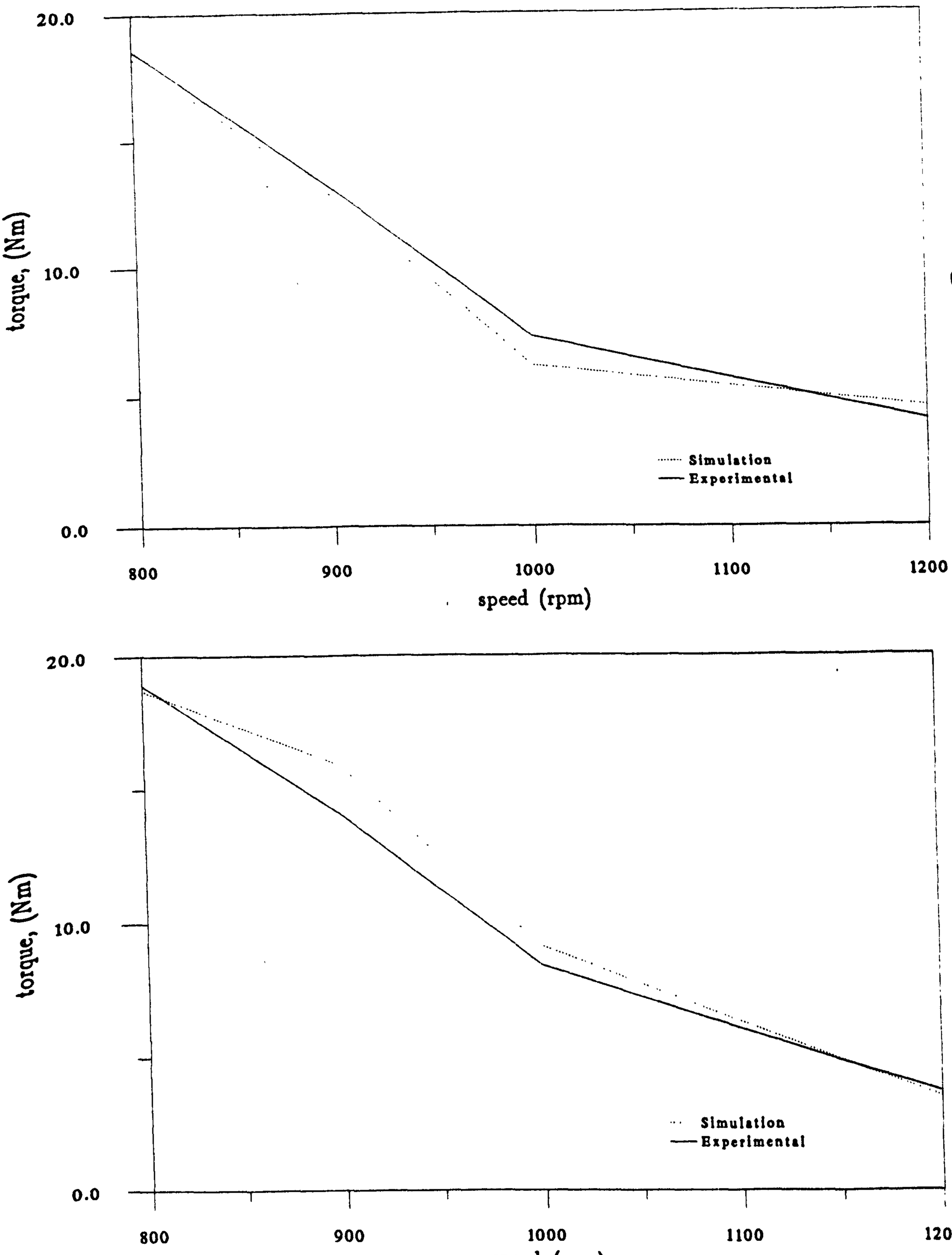

Figure 7.9 Torque/speed characteristics
(a) 0° electical phase advance
(b) 15° electical phase advance

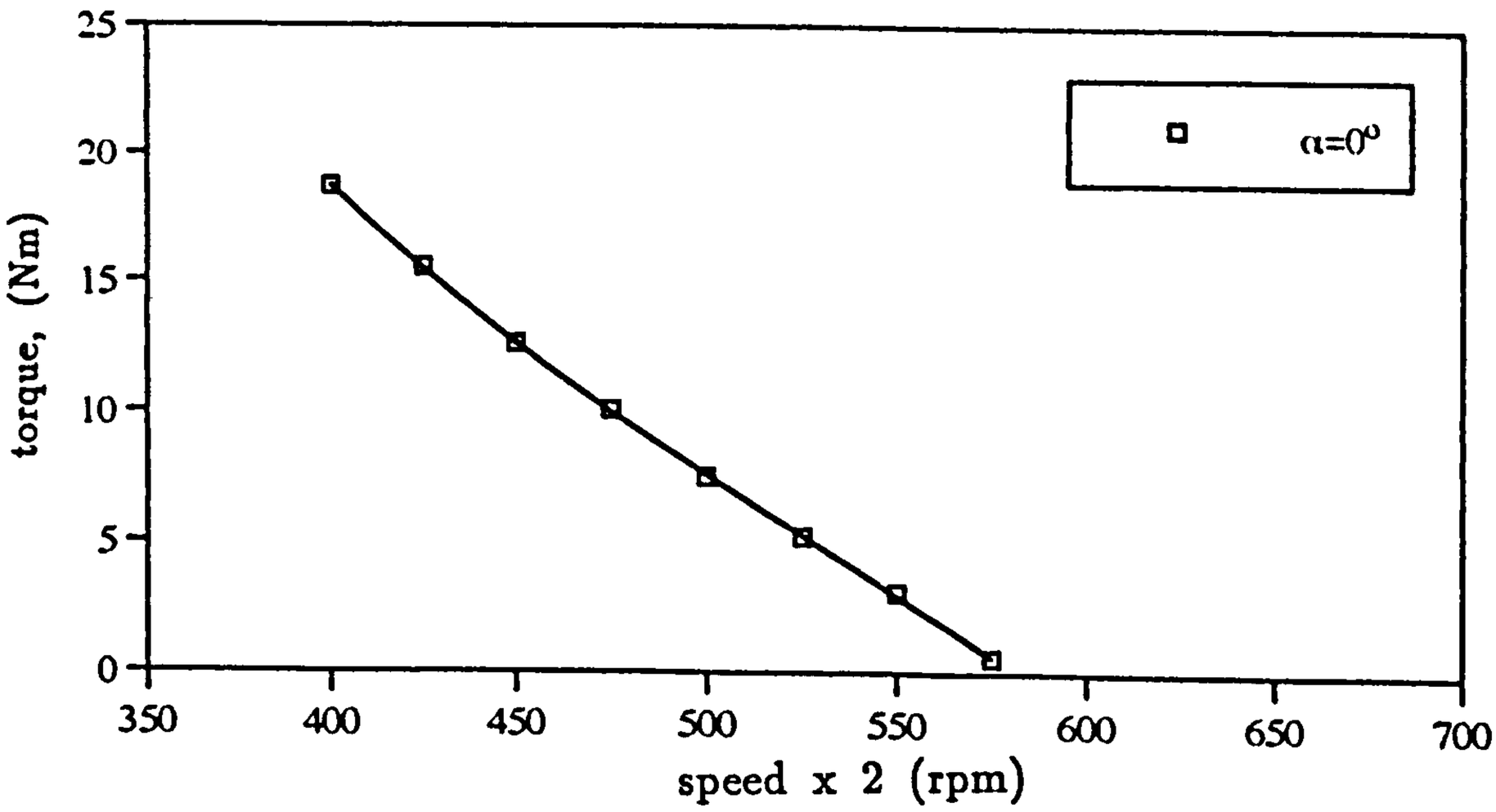
25
20
15
10
5
0
torque, (Nm)
350
400
450
500
550
600
650
700
speed x 2 (rpm)
α=0°

(a)

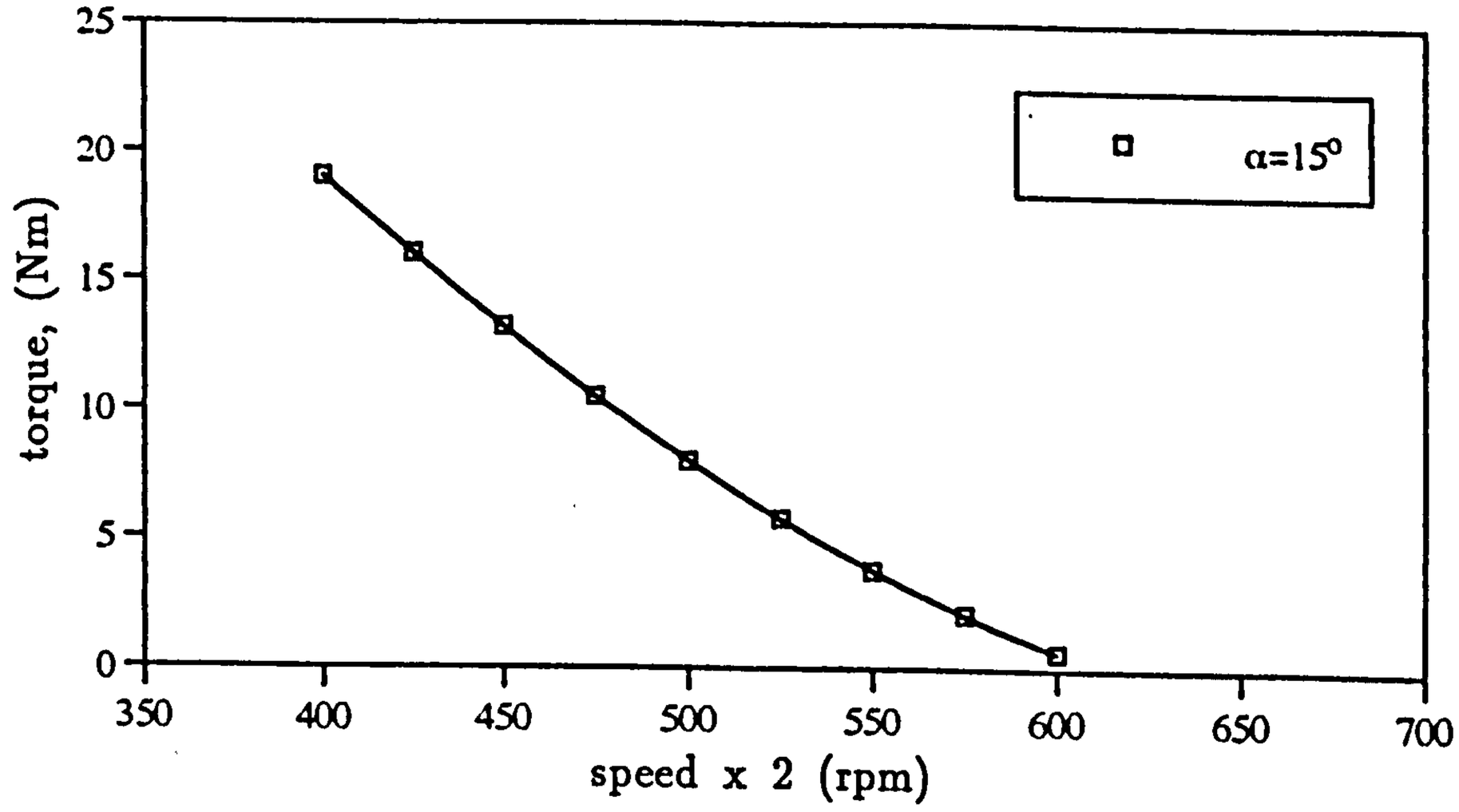
25
20
15
10
5
0
torque, (Nm)
350
400
450
500
550
600
650
700
speed x 2 (rpm)
α=15°

(b)

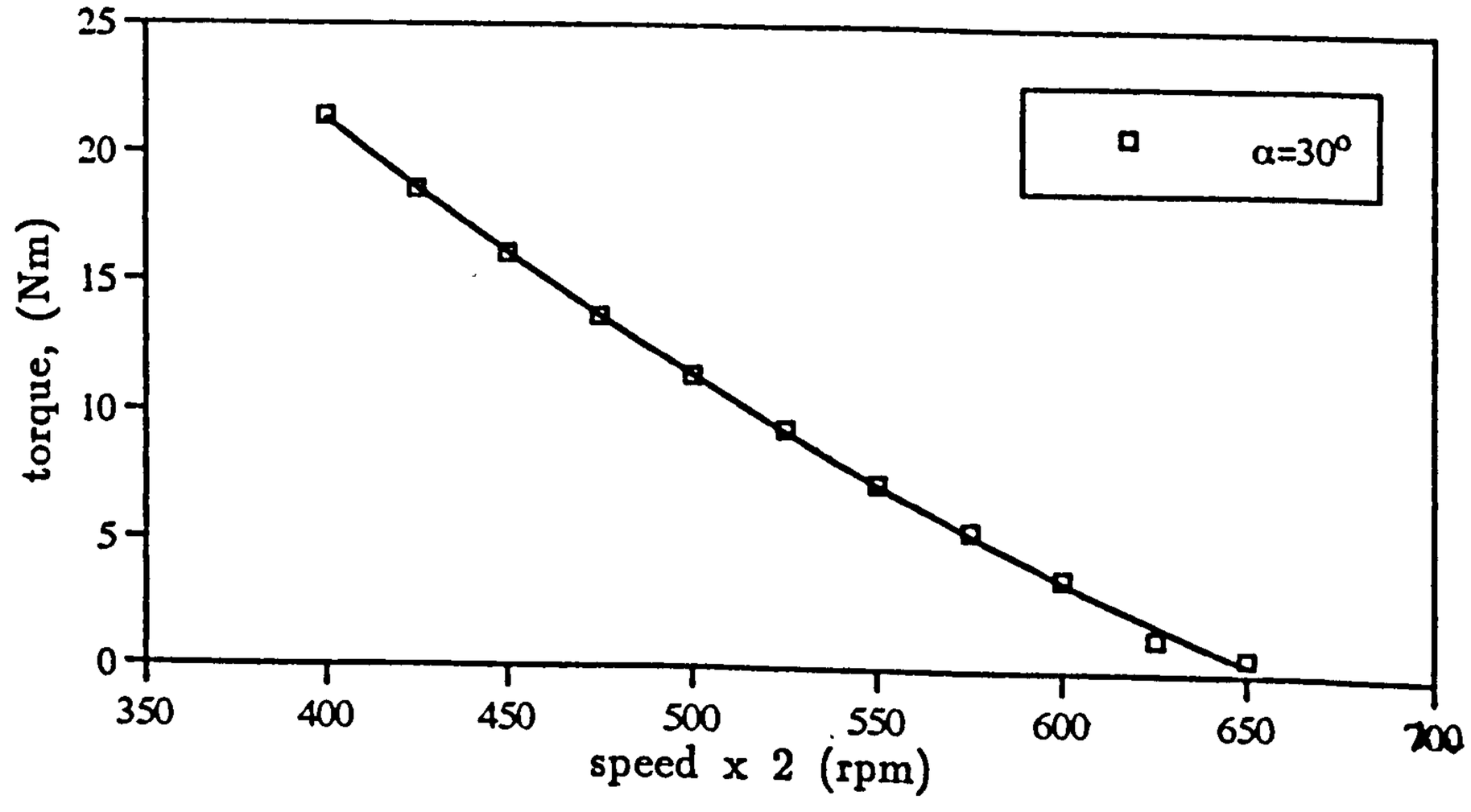
25
20
15
10
5
0
torque, (Nm)
350
400
450
500
550
600
650
700
speed x 2 (rpm)
α=30°

(c)

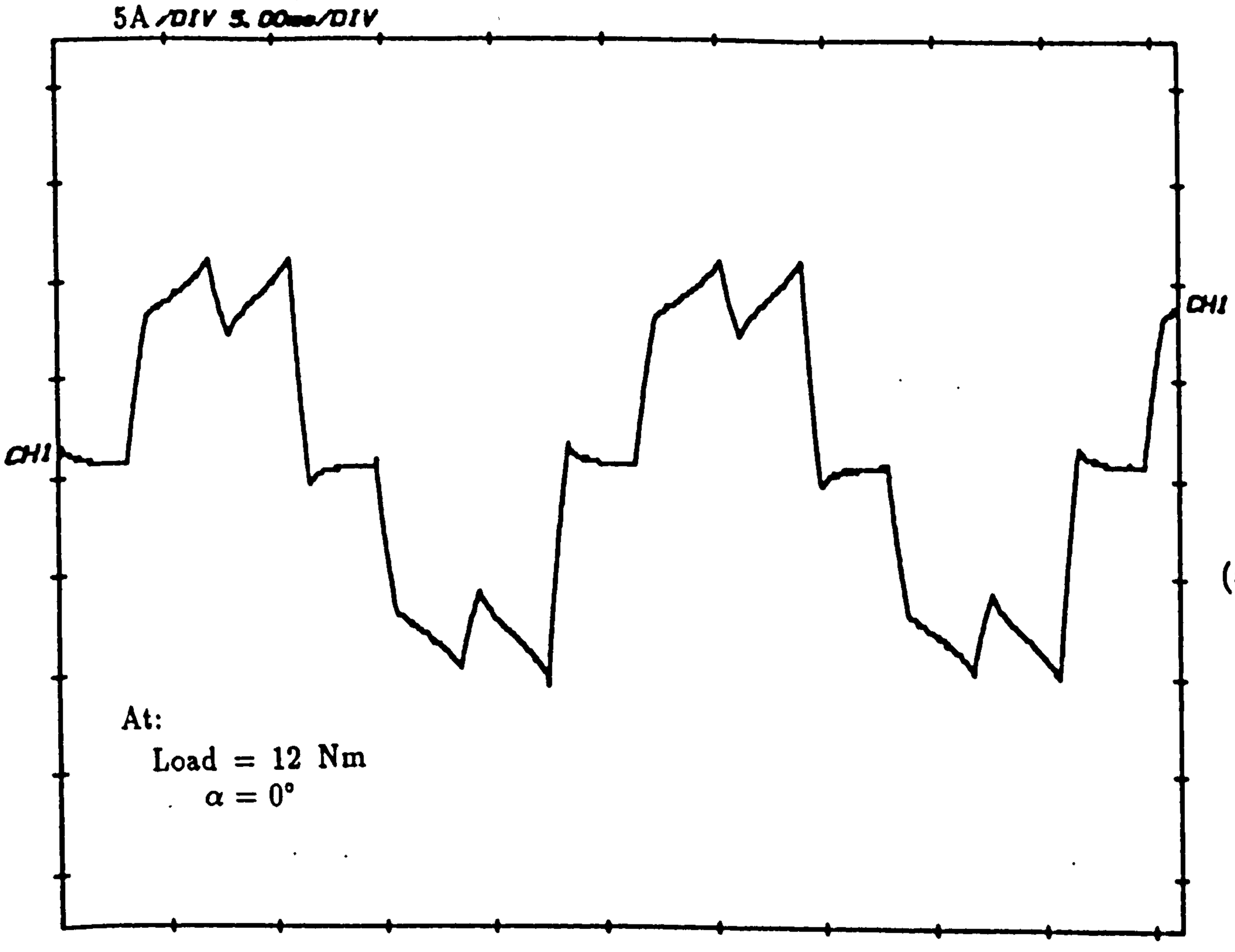

(a)

At:

Load = 12 Nm

$\alpha = 0°$

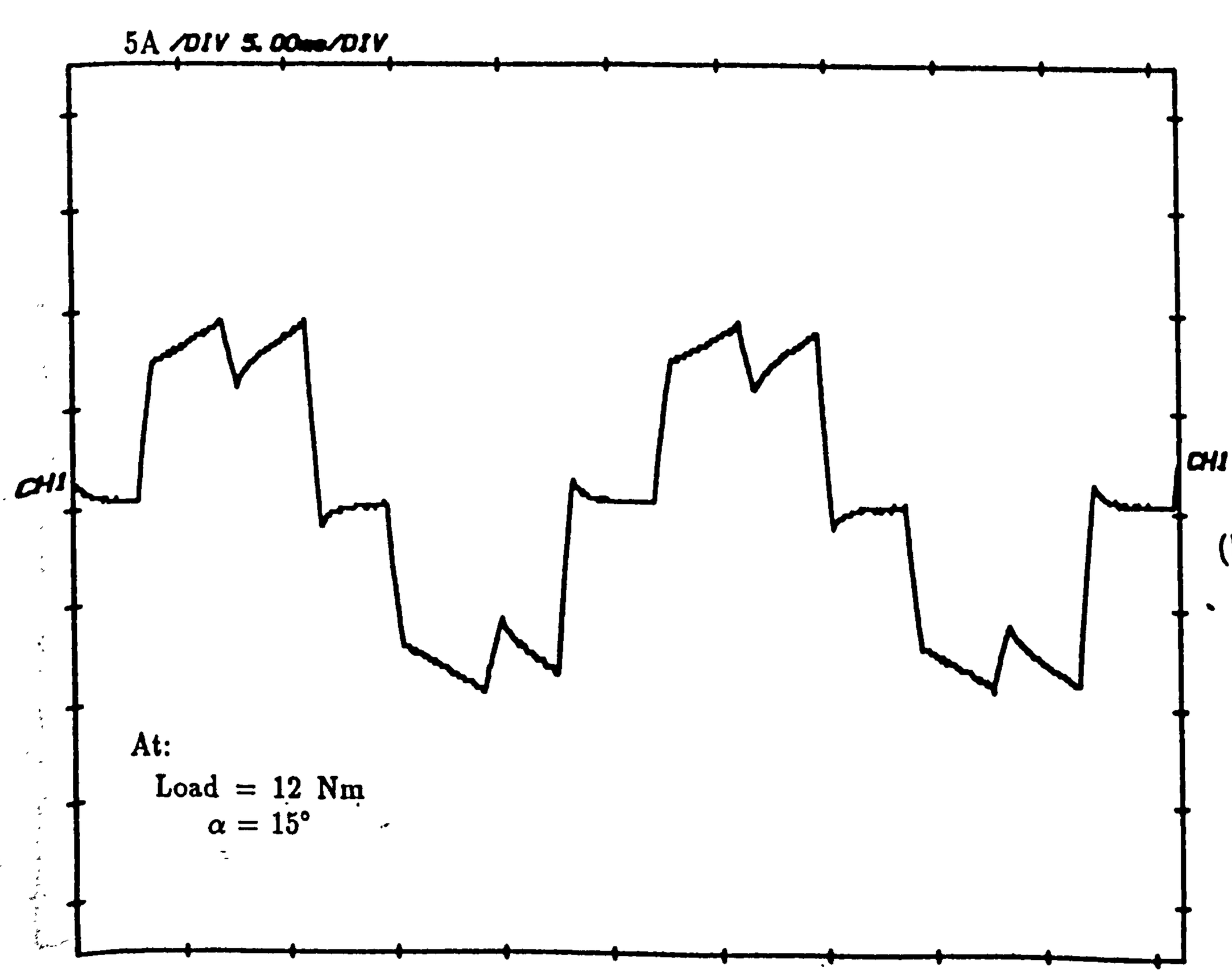

(b)

At:

Load = 12 Nm

$\alpha = 15°$

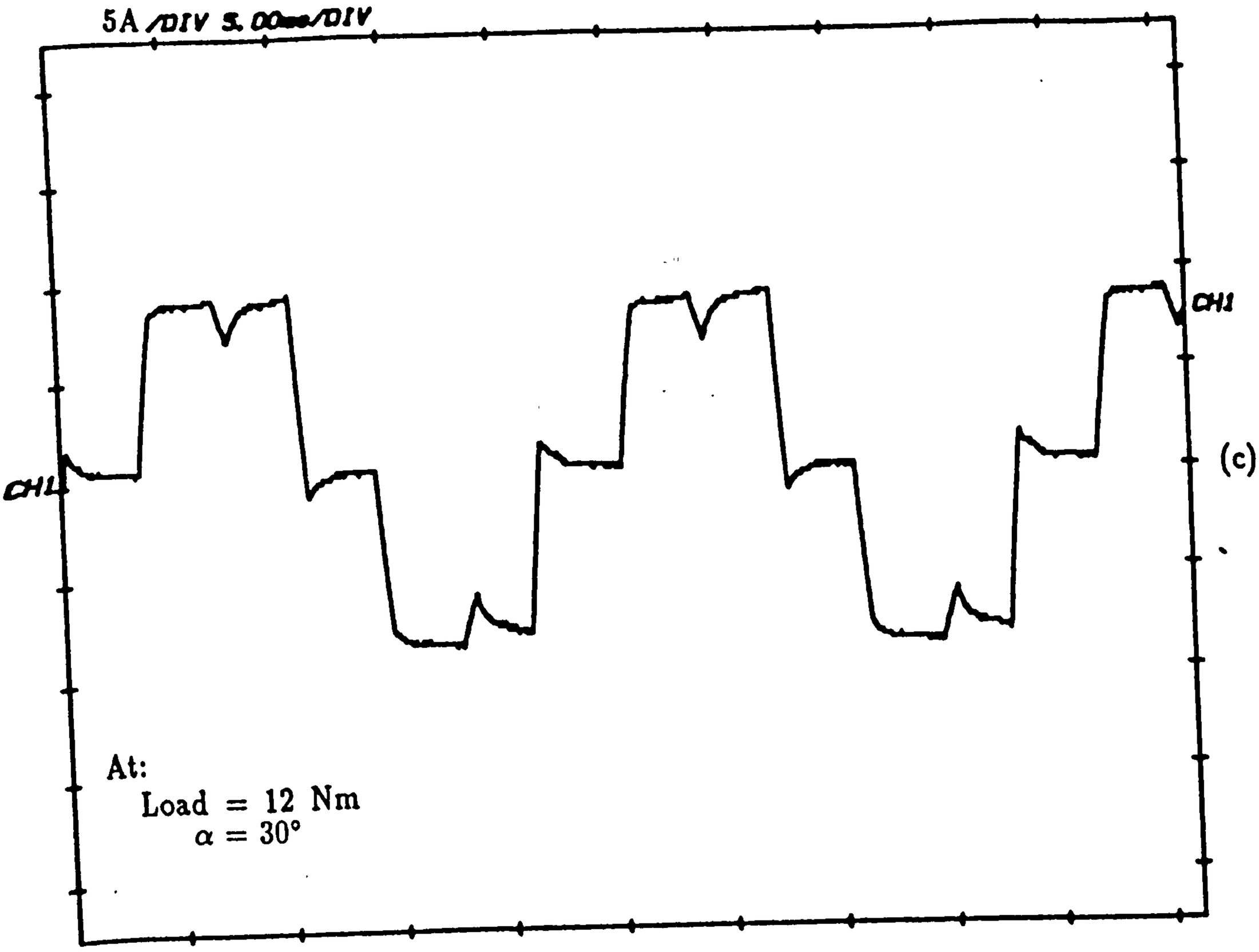
5A /DIV 5.00ms/DIV
CH1
CH1
At:
Load = 12 Nm
α = 30°

(c)

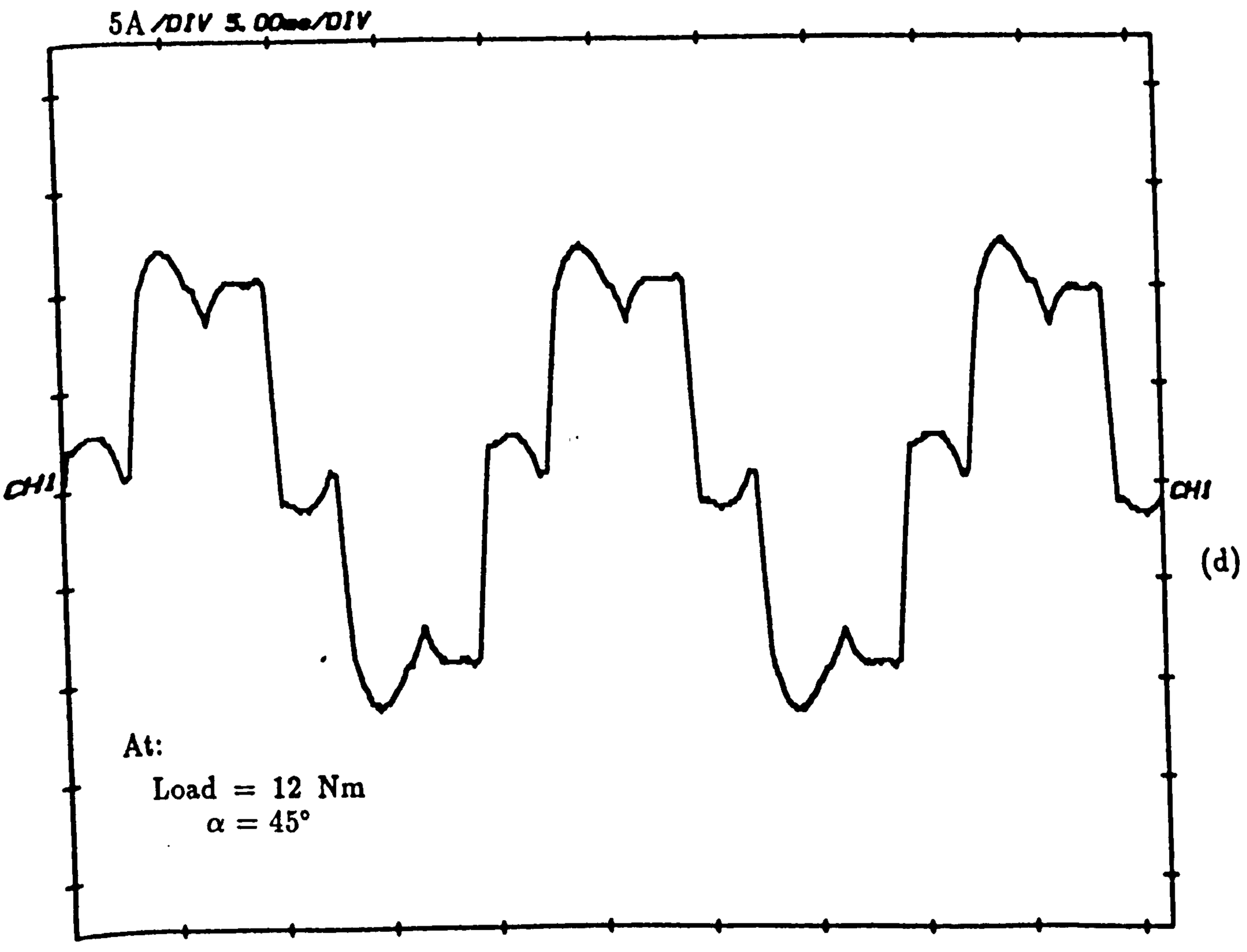
5A /DIV 5.00ms/DIV
CH1
CH1
At:
Load = 12 Nm
α = 45°

(d)

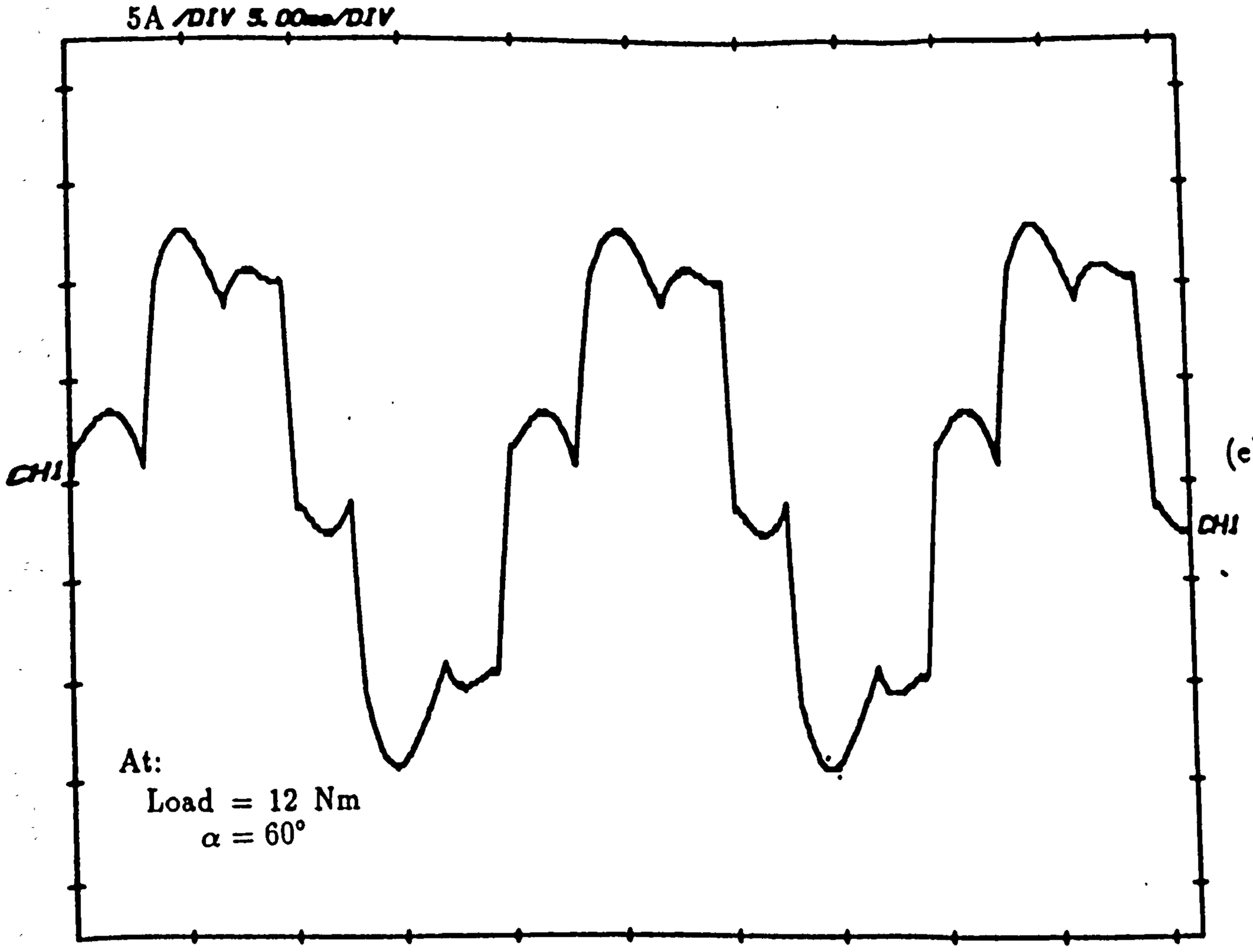

Figure 7.11 Measured current waveforms obtained for a prototype drive for different phase advance angles at load= 12 Nm.

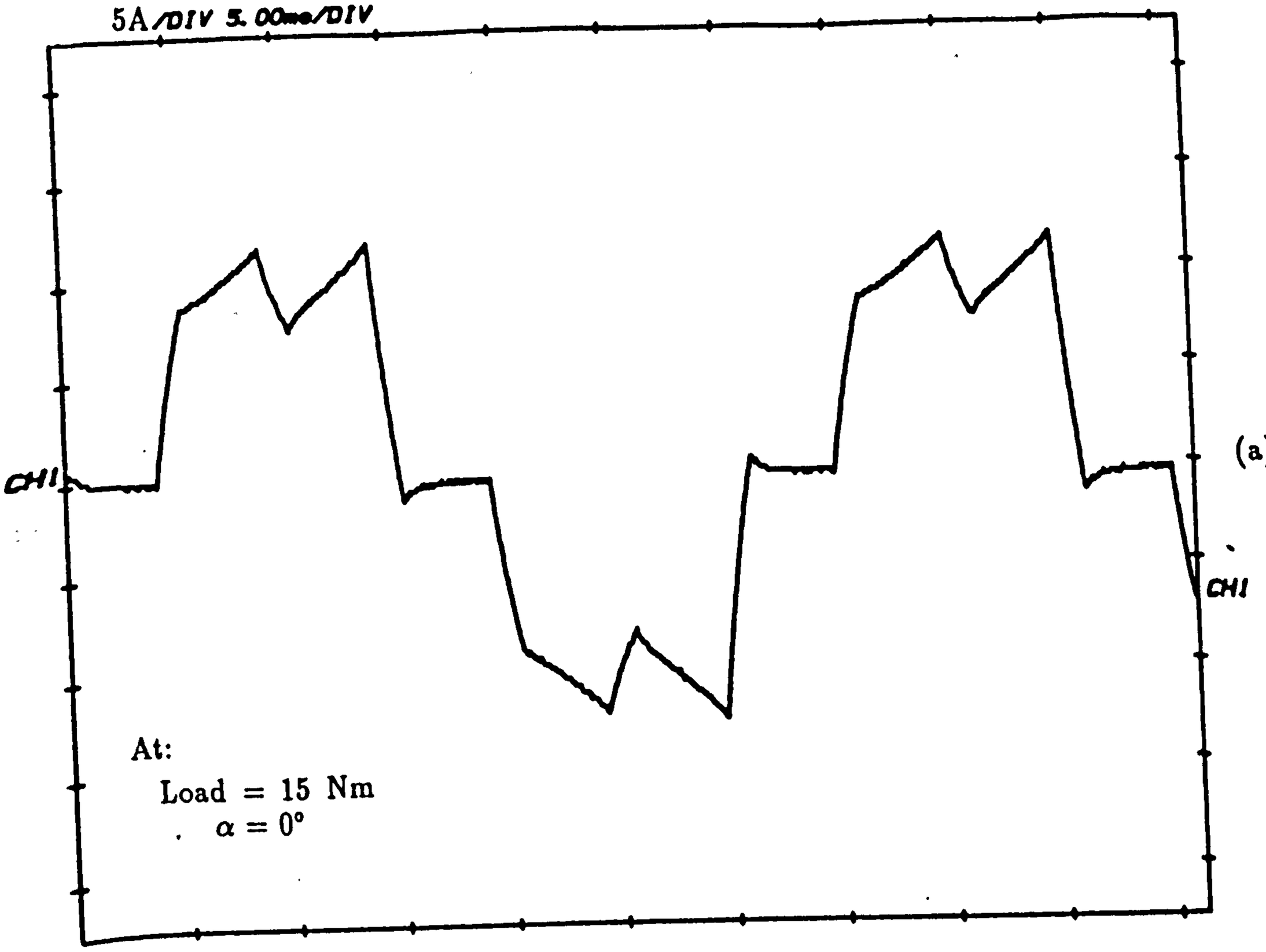
5A/DIV 5.00ms/DIV
CH1
CH1
(a)
At:
Load = 15 Nm
α = 0°

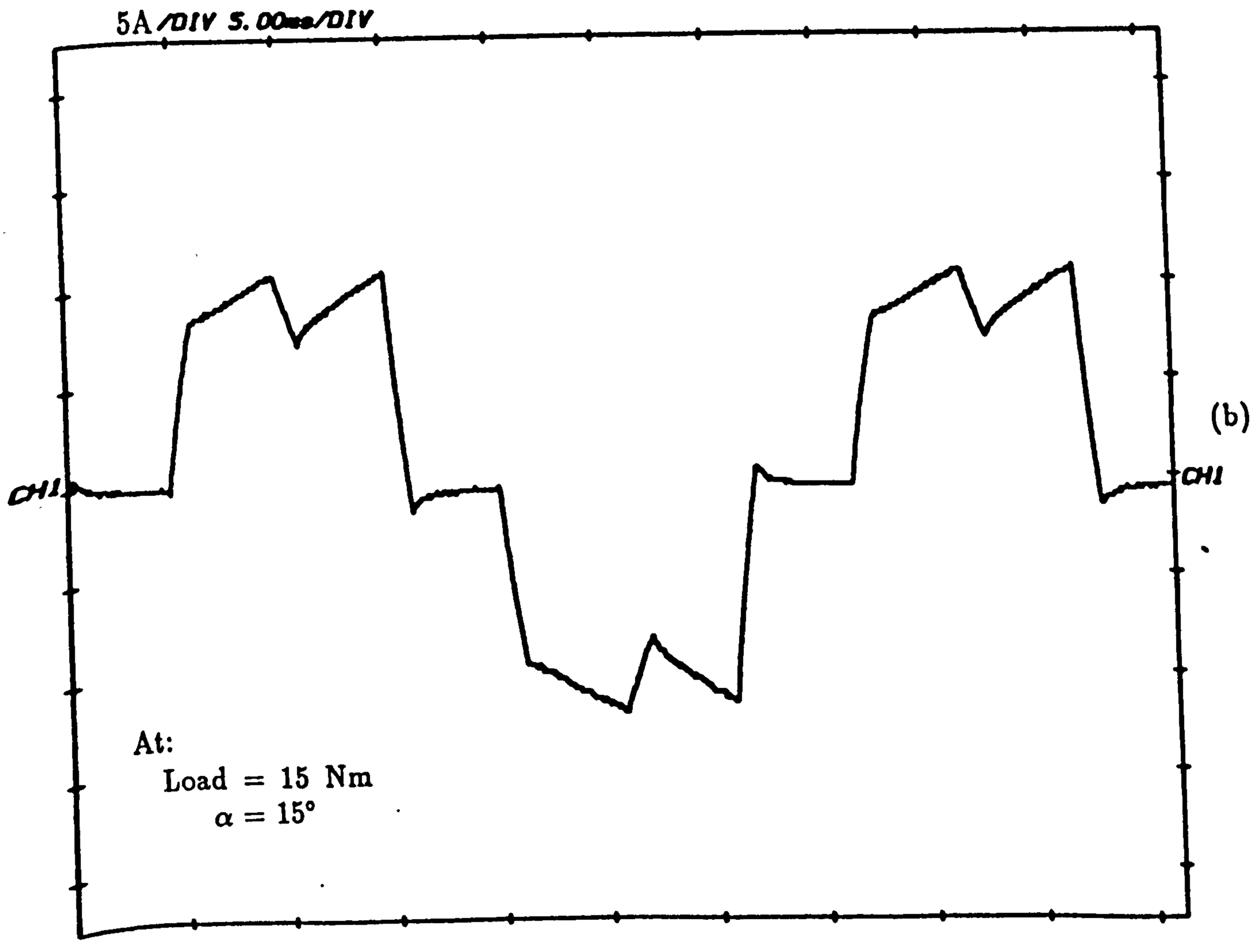
5A/DIV 5.00ms/DIV
CH1
CH1
(b)
At:
Load = 15 Nm
α = 15°

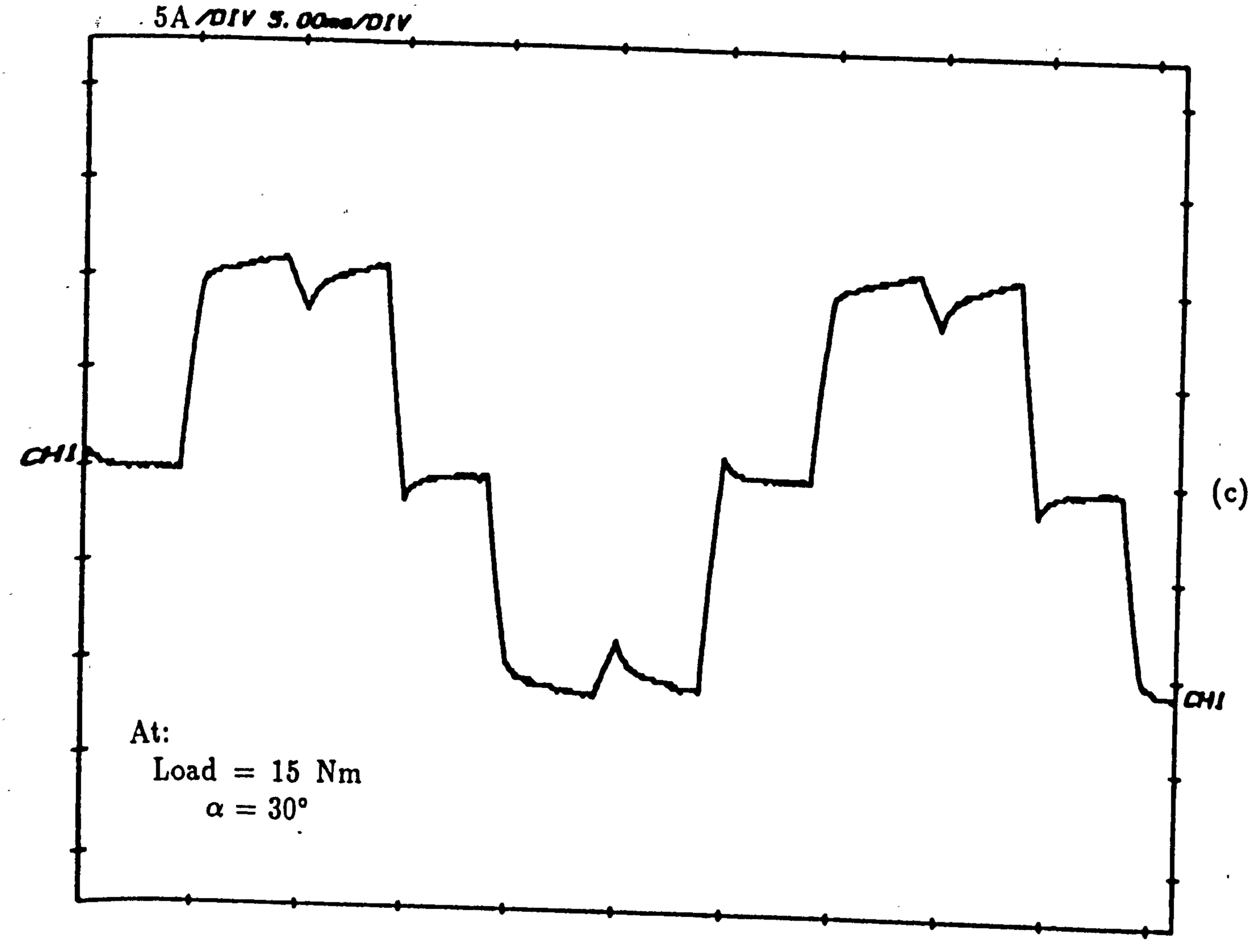
5A /DIV 5.00ms/DIV
CH1
(c)
CH1
At:
Load = 15 Nm
α = 30°

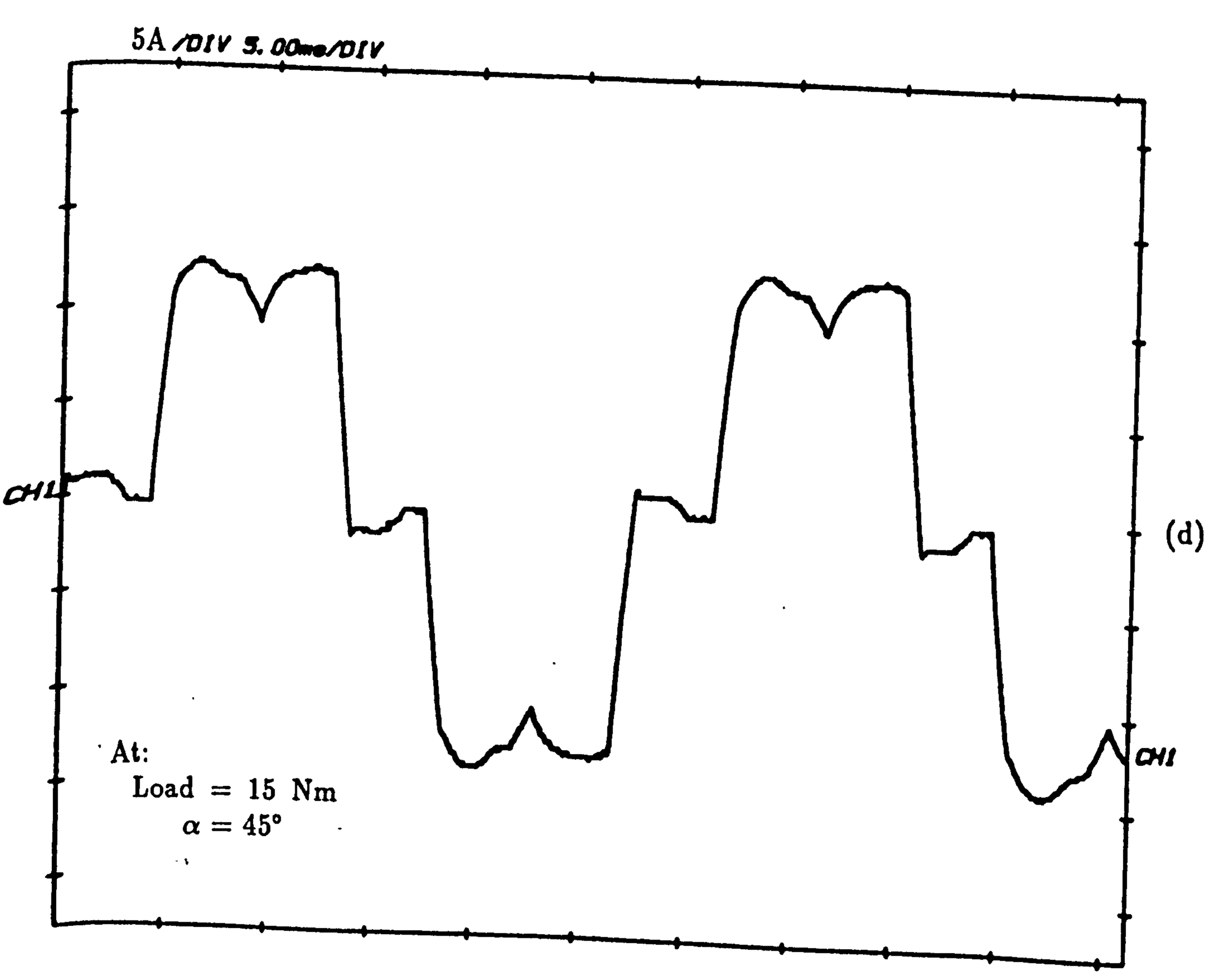
5A /DIV 5.00ms/DIV
CH1
(d)
CH1
At:
Load = 15 Nm
α = 45°

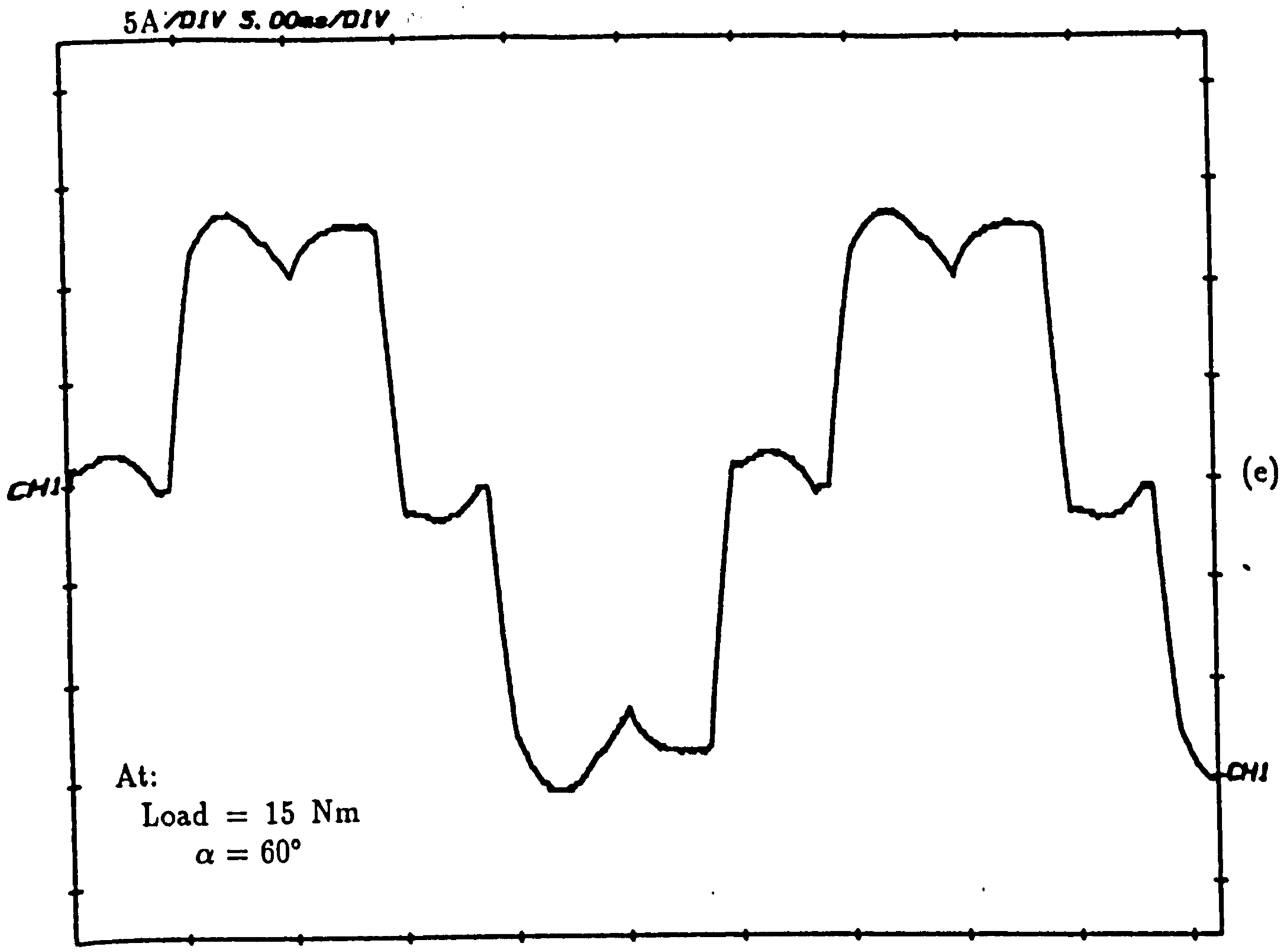

Figure 7.12 Measured current waveforms obtained for a prototype drive for different phase advance angles at load= 15 Nm.

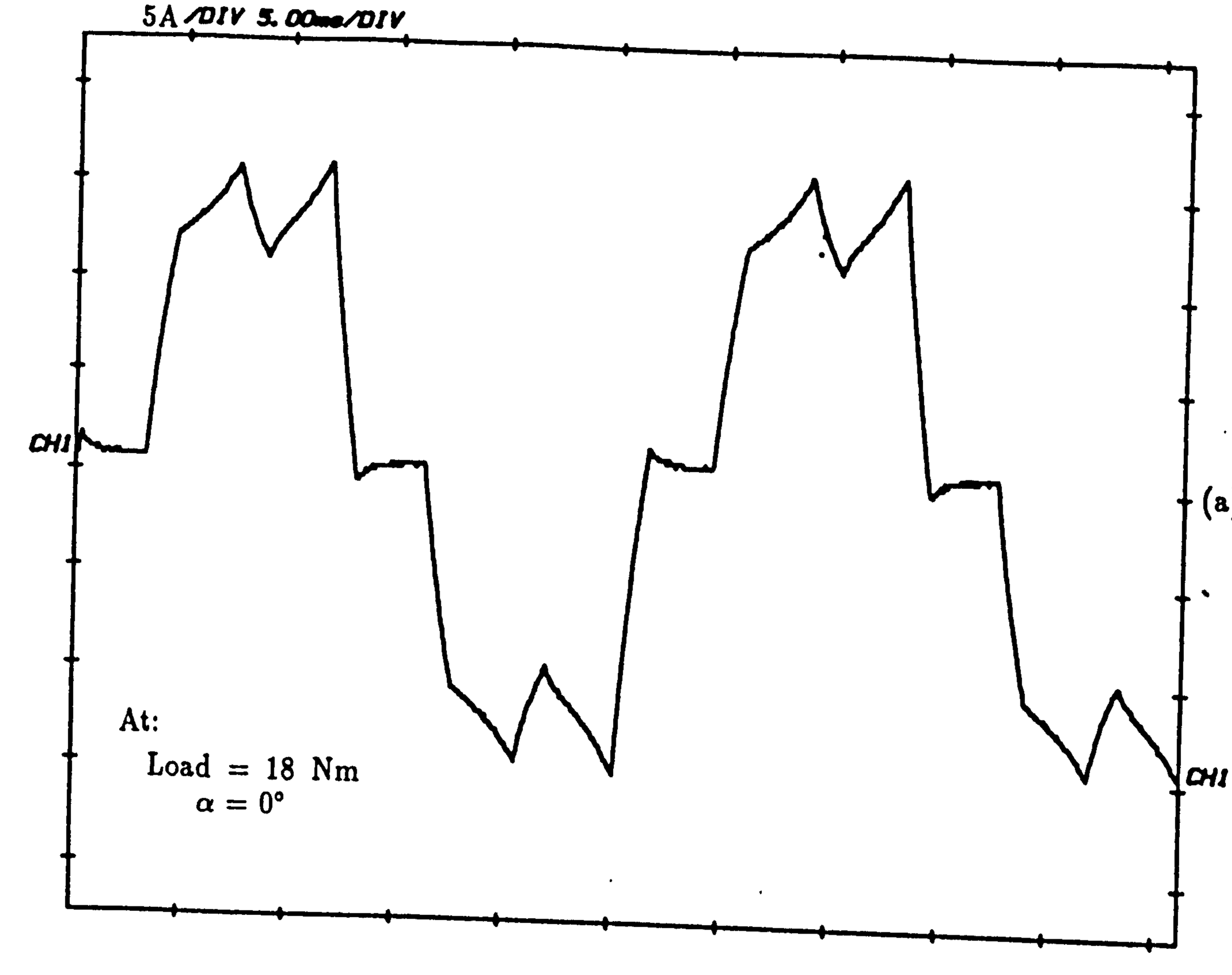
5A /DIV 5.00ms/DIV
CH1
(a)
At:
Load = 18 Nm
α = 0°
CH1

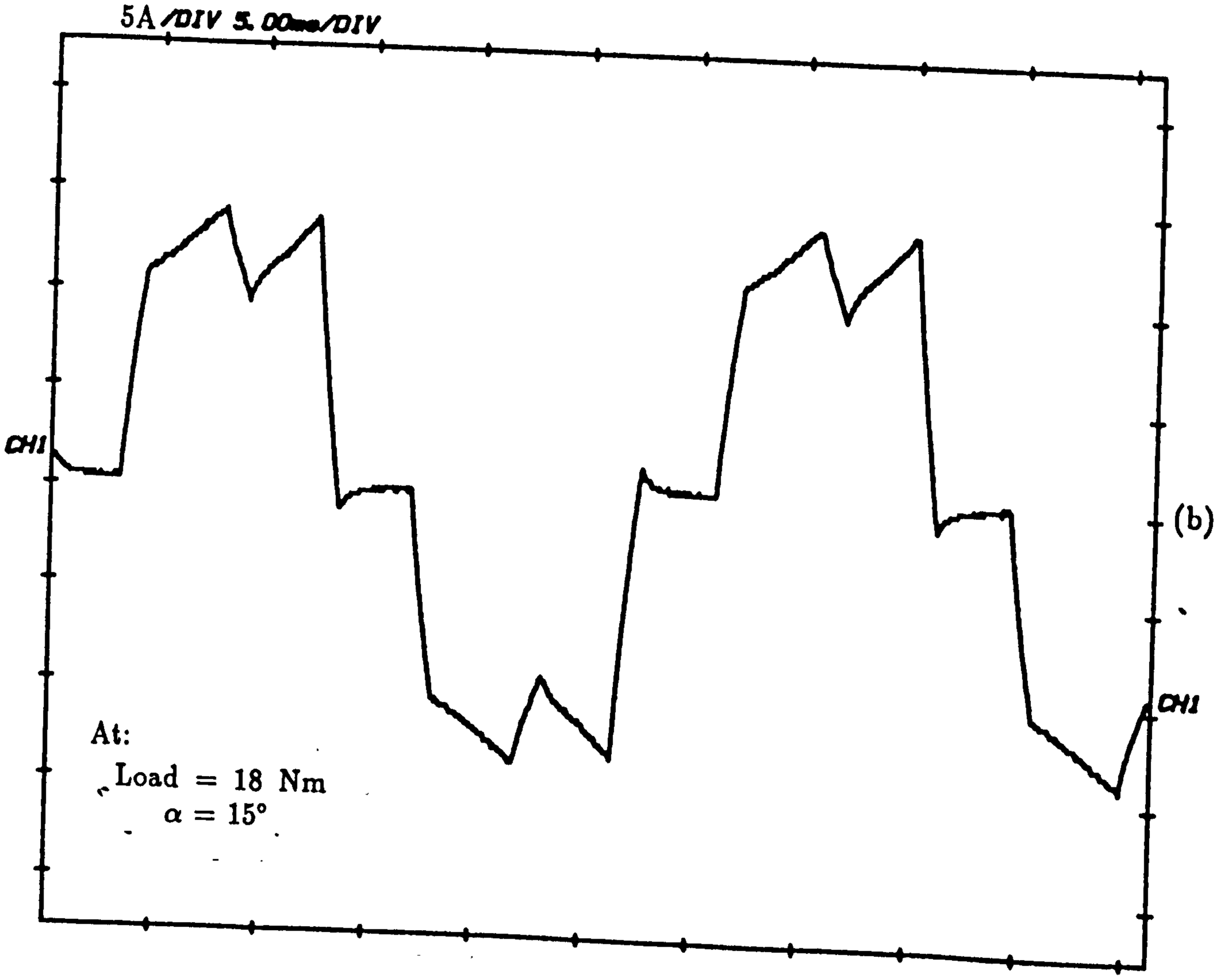
5A /DIV 5.00ms/DIV
CH1
(b)
At:
Load = 18 Nm
α = 15°
CH1

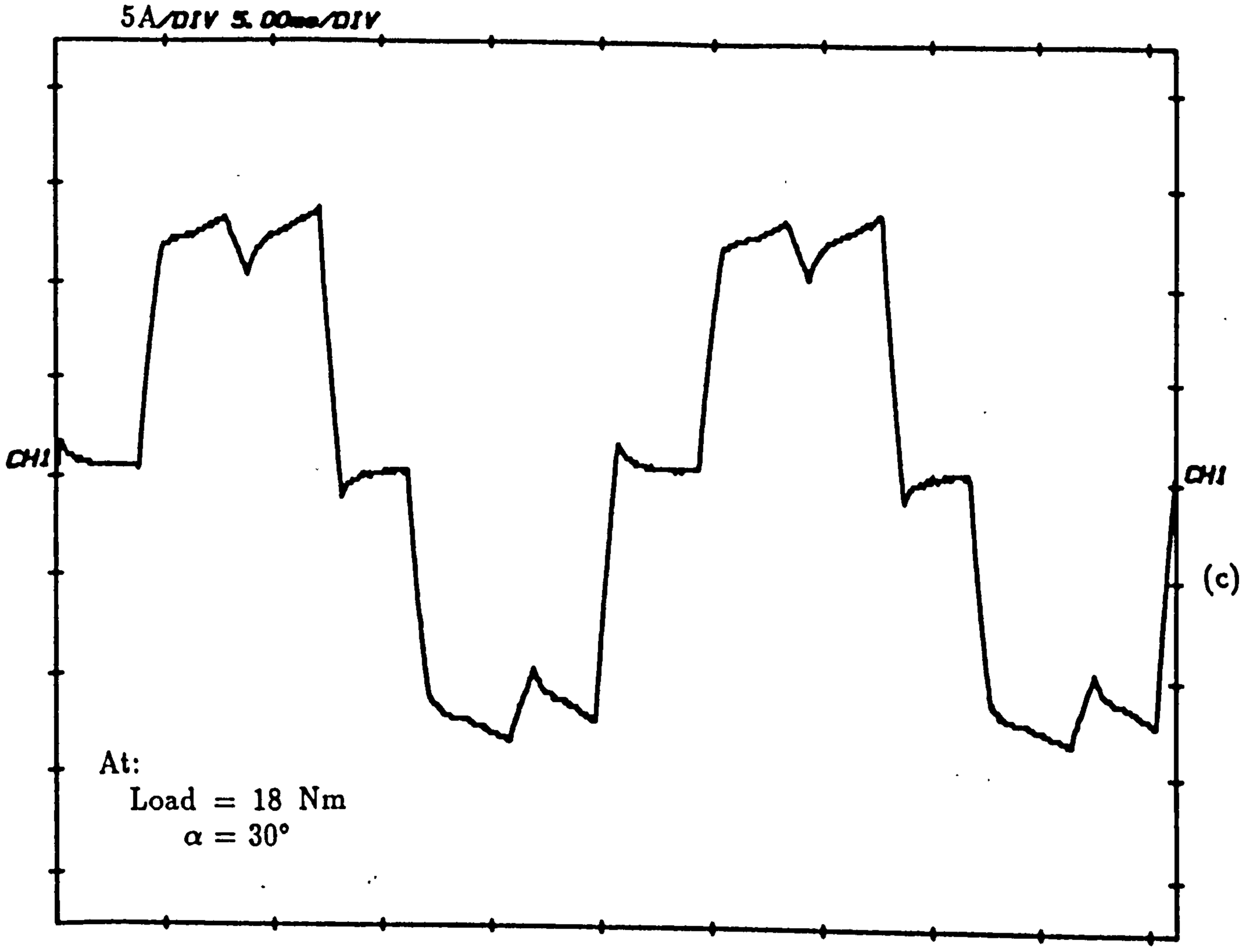
5A/DIV 5.00ms/DIV
CH1
CH1
(c)
At:
Load = 18 Nm
α = 30°

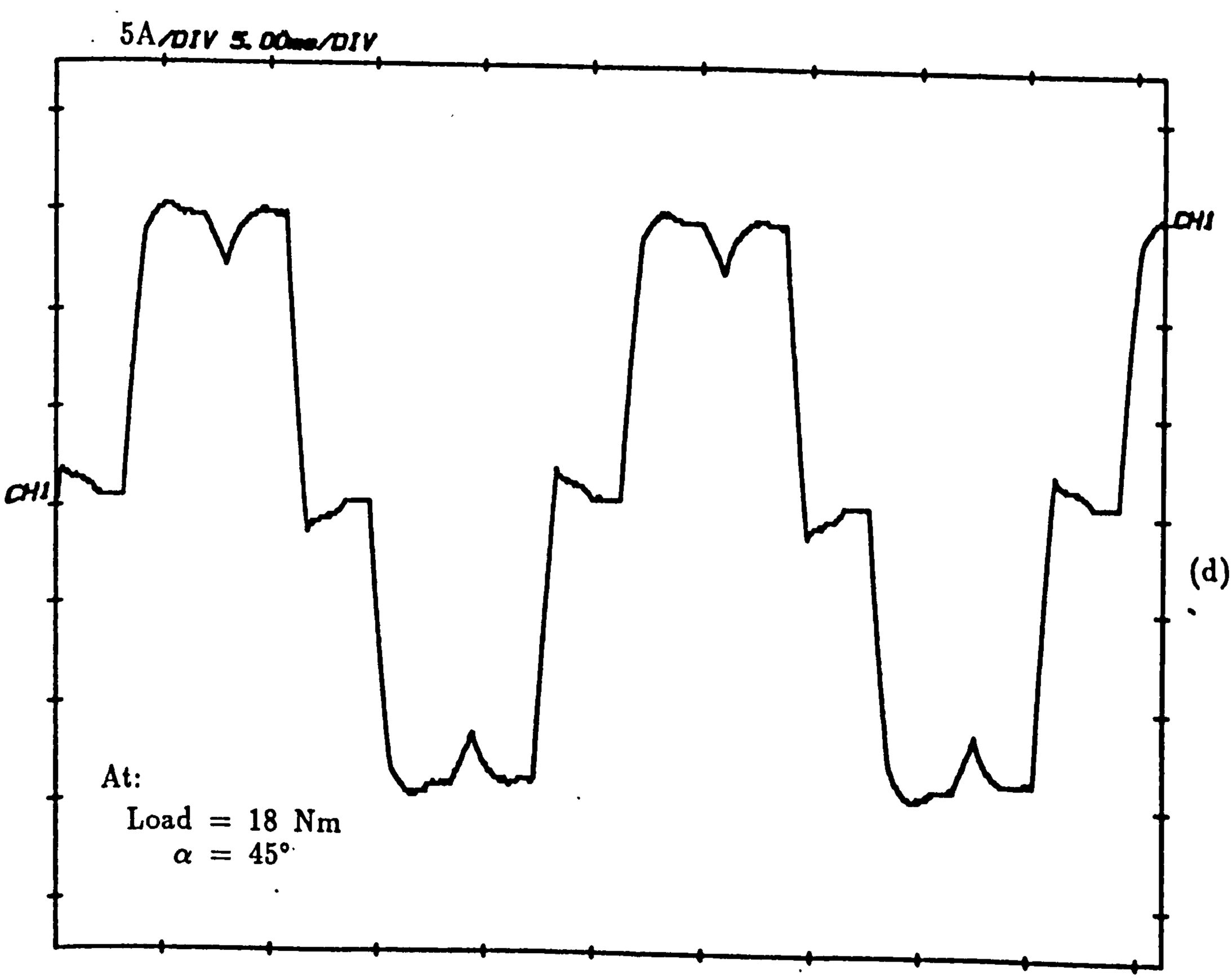
5A/DIV 5.00ms/DIV
CH1
CH1
(d)
At:
Load = 18 Nm
α = 45°

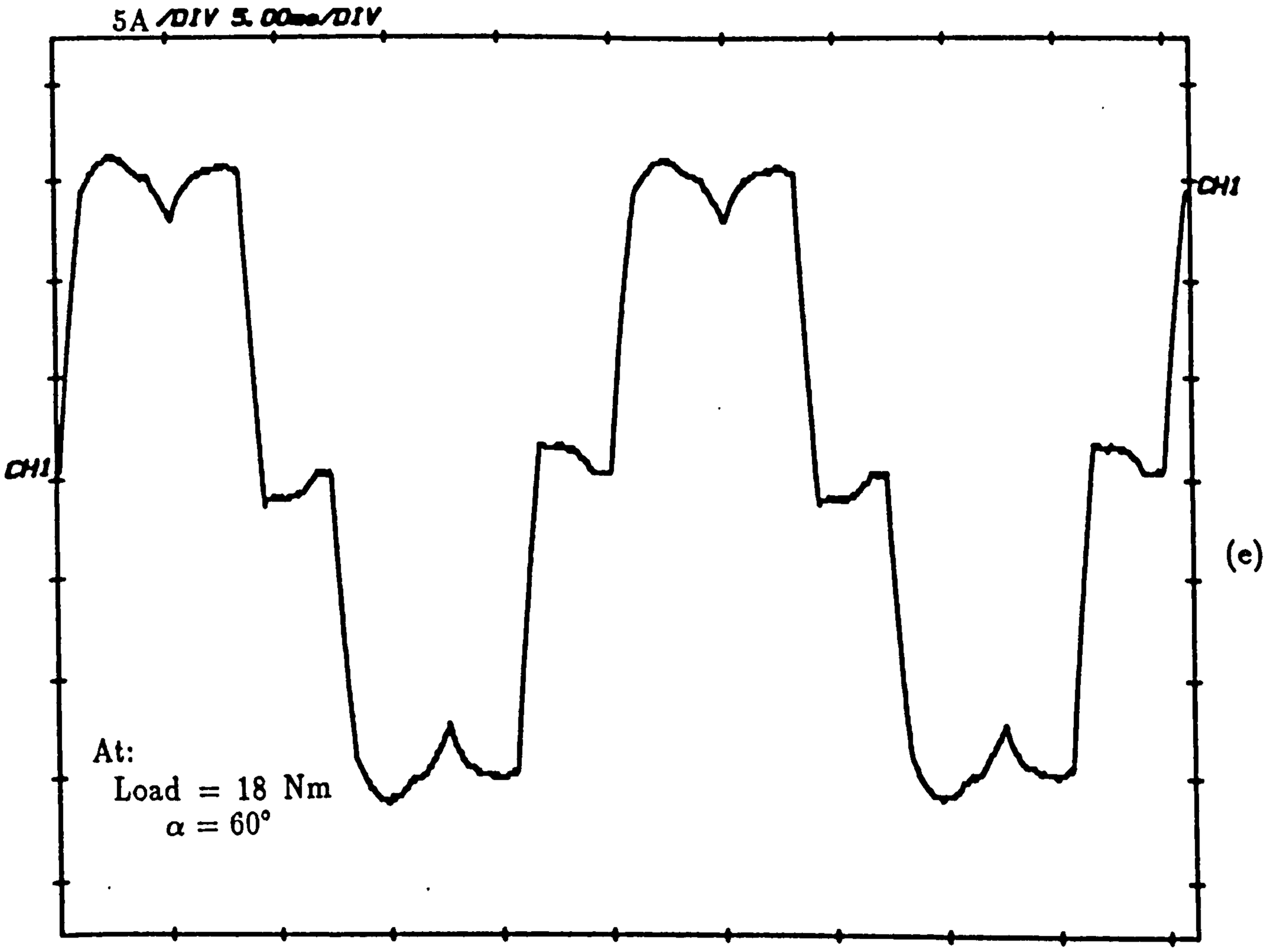

Figure 7.13 Measured current waveforms obtained for a prototype drive for different phase advance angles at load= 18 Nm.

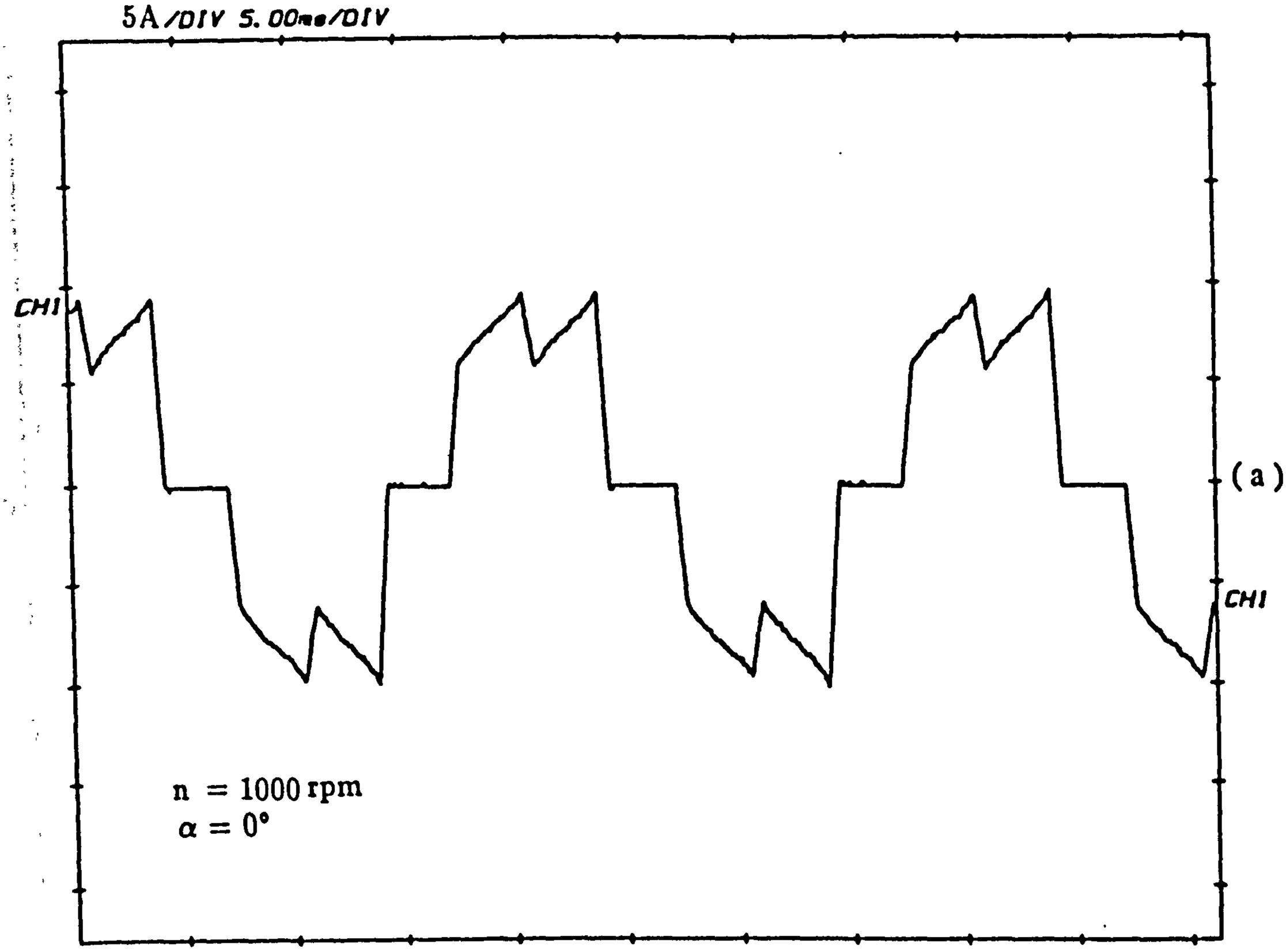
5A/DIV 5.00ms/DIV
CH1
(a)
CH1
n = 1000 rpm
α = 0°

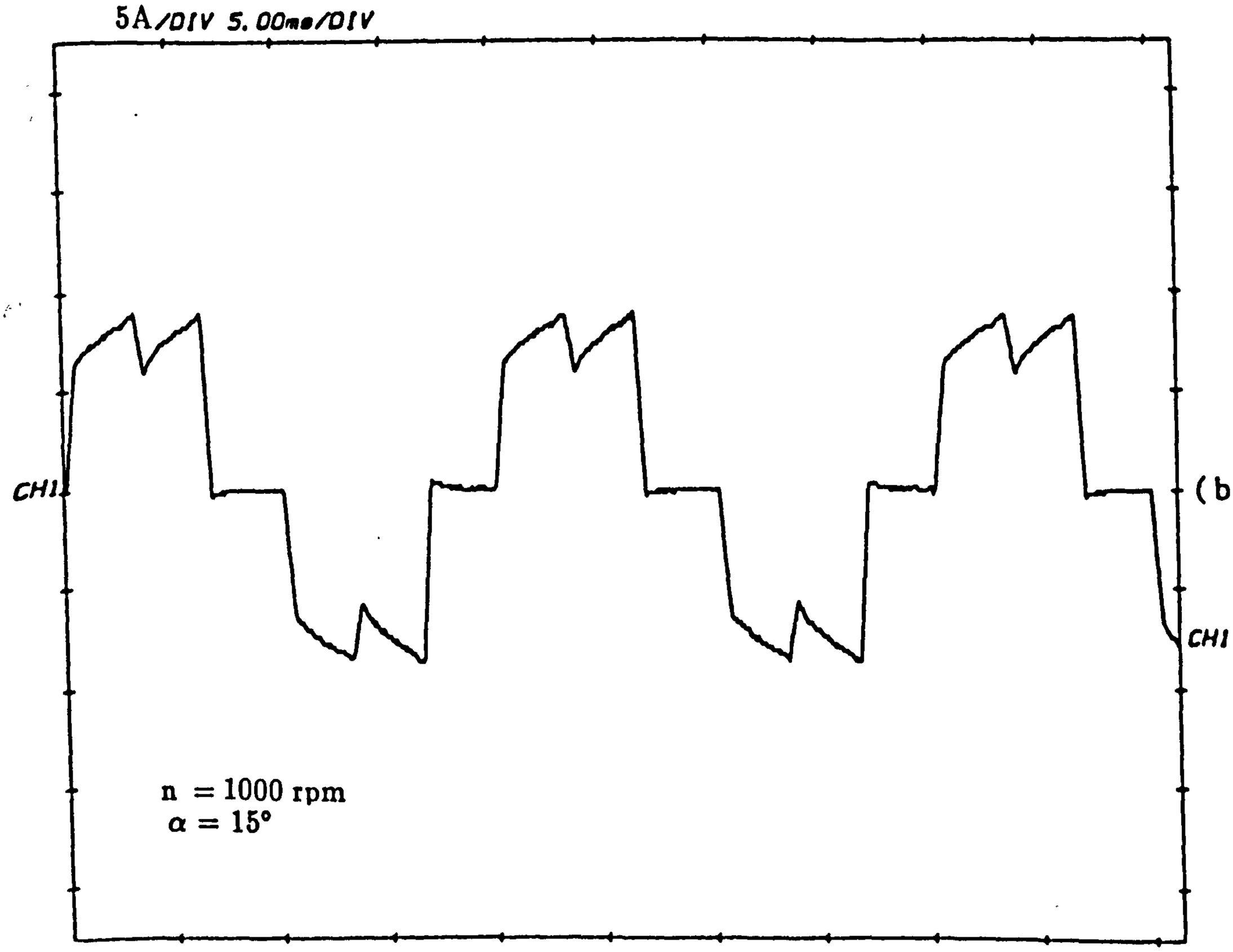
5A/DIV 5.00ms/DIV
CH1
(b)
CH1
n = 1000 rpm
α = 15°

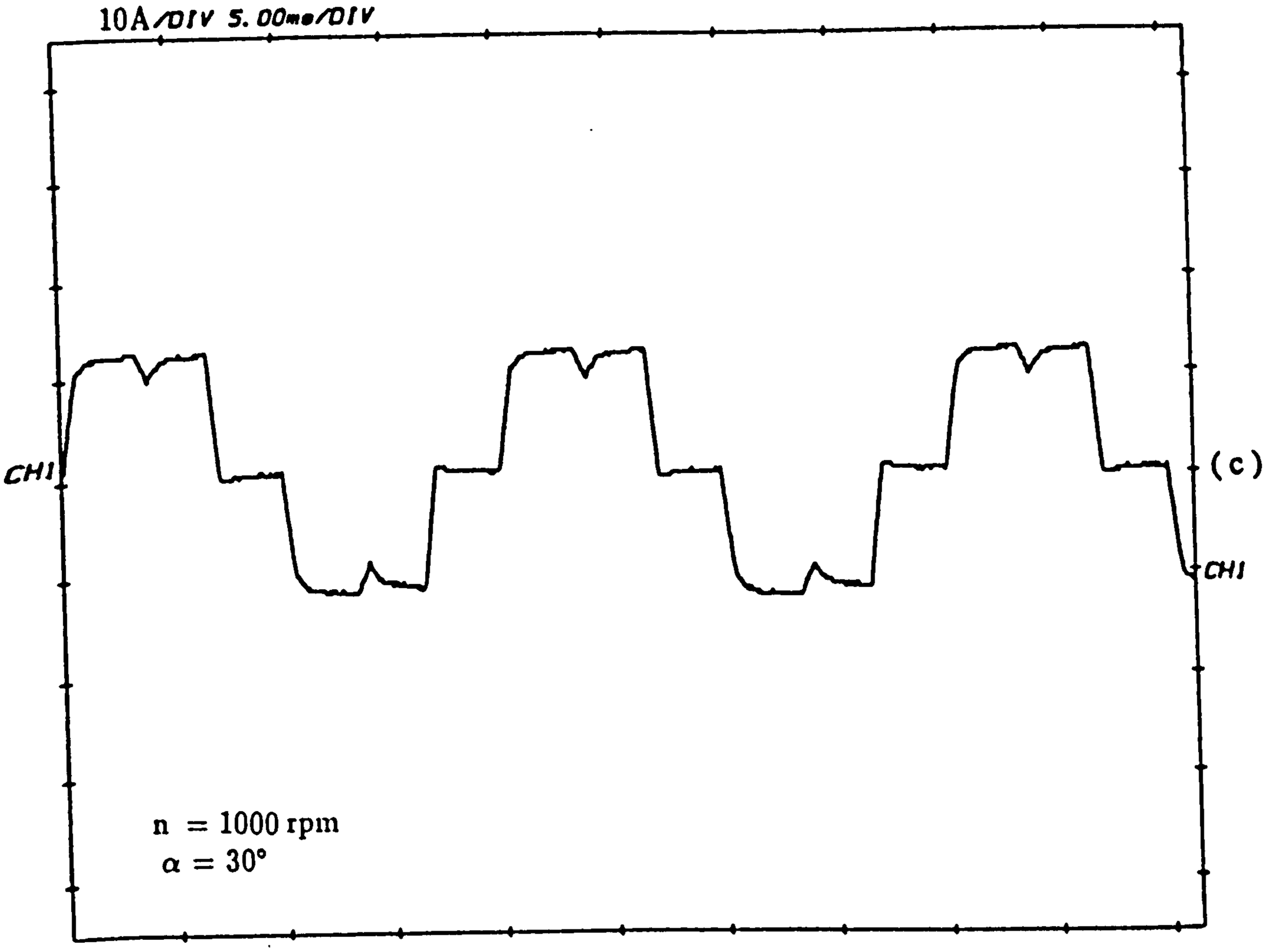
10A/DIV 5.00ms/DIV
CH1
(c)
CH1
n = 1000 rpm
α = 30°

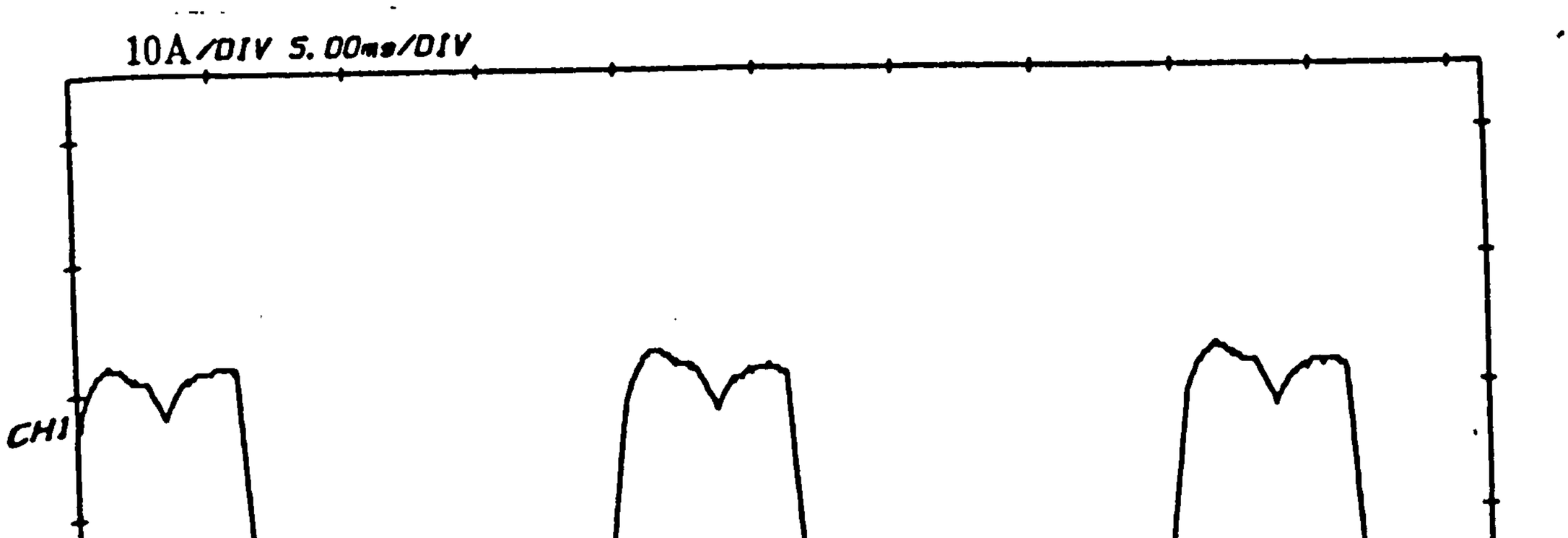
10A/DIV 5.00ms/DIV
CH1
(d)
CH1
n = 1000 rpm
α = 45°

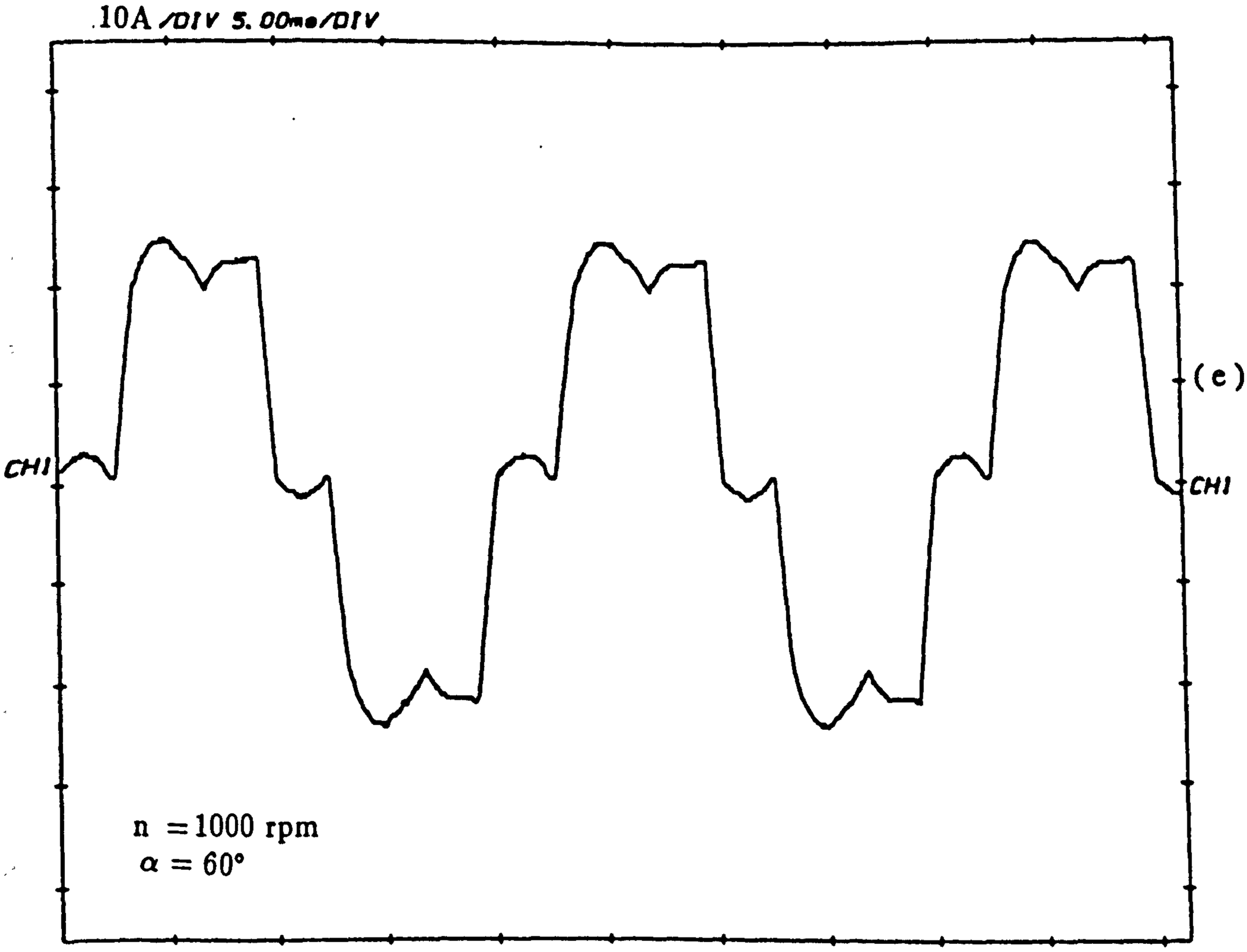

Figure 7.14 Measured current waveform for a brushless dc drive operating at speed= 1000 with five different advance angles of 0°, 15°, 30°, 45° and 60°.

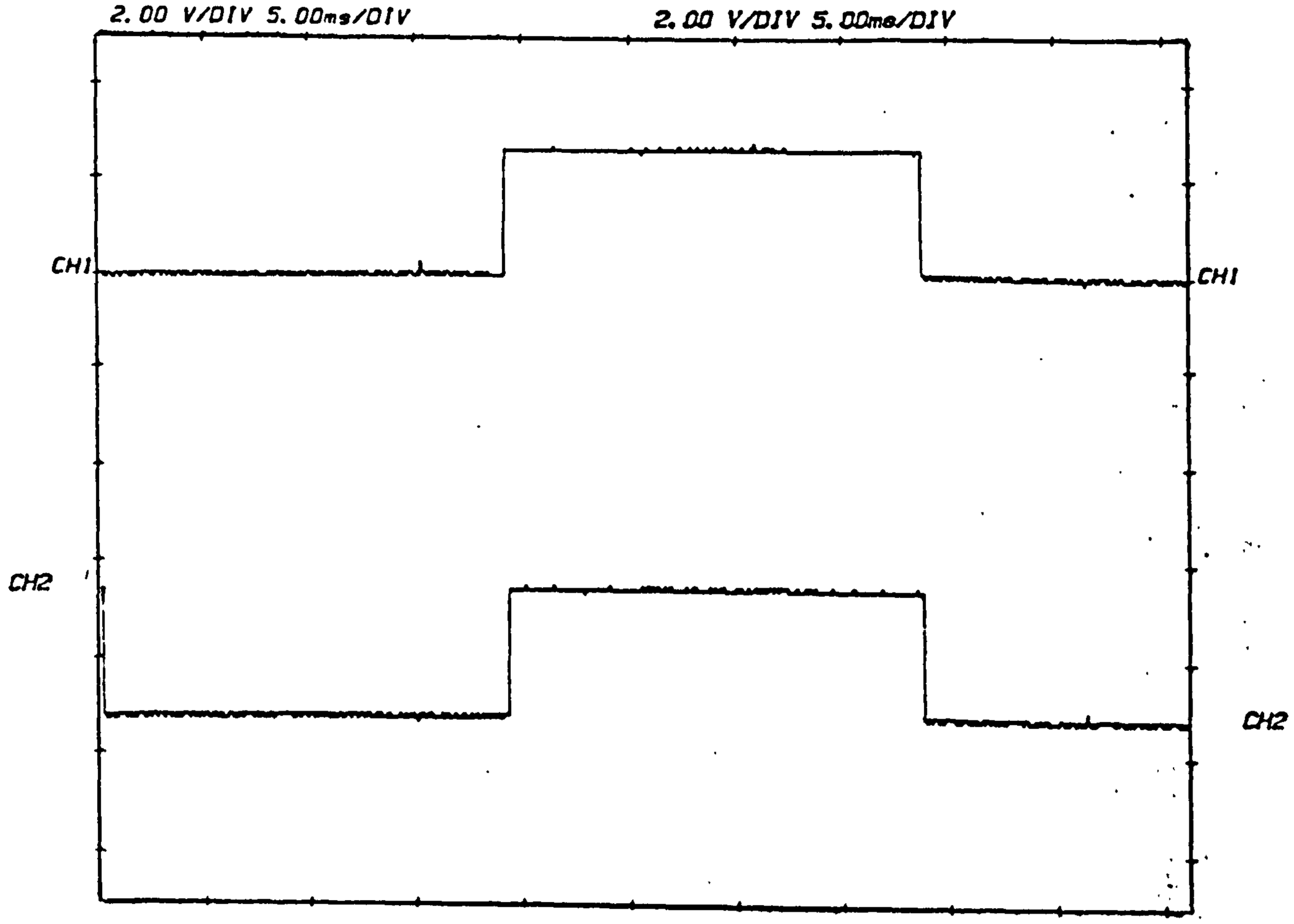

Figure 7.15 Encoder signals with phase advance angle=0°

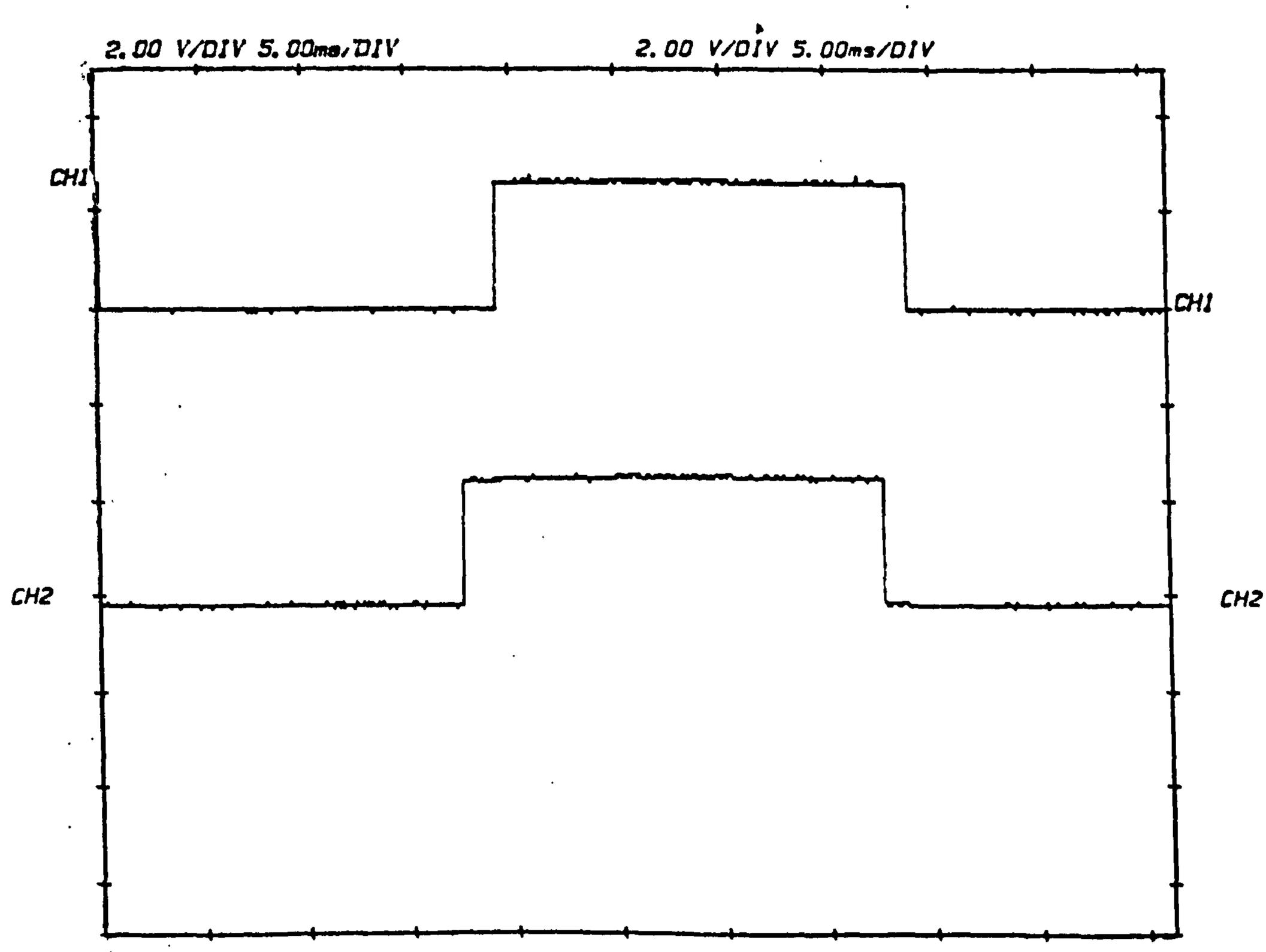

Figure 7.16 Encoder signals with phase advance angle=15°

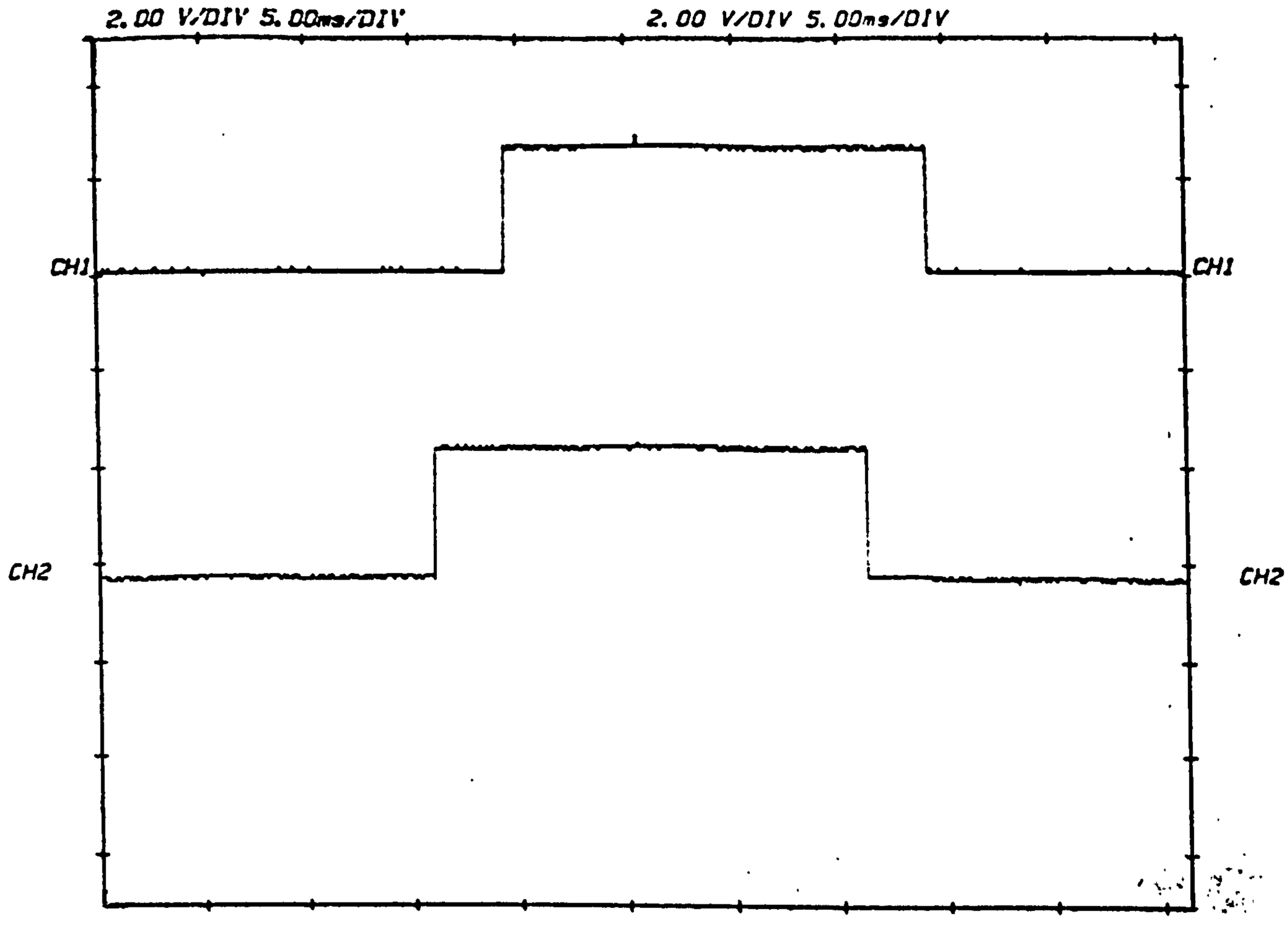

Figure 7.17 Encoder signals with phase advance angle=30°

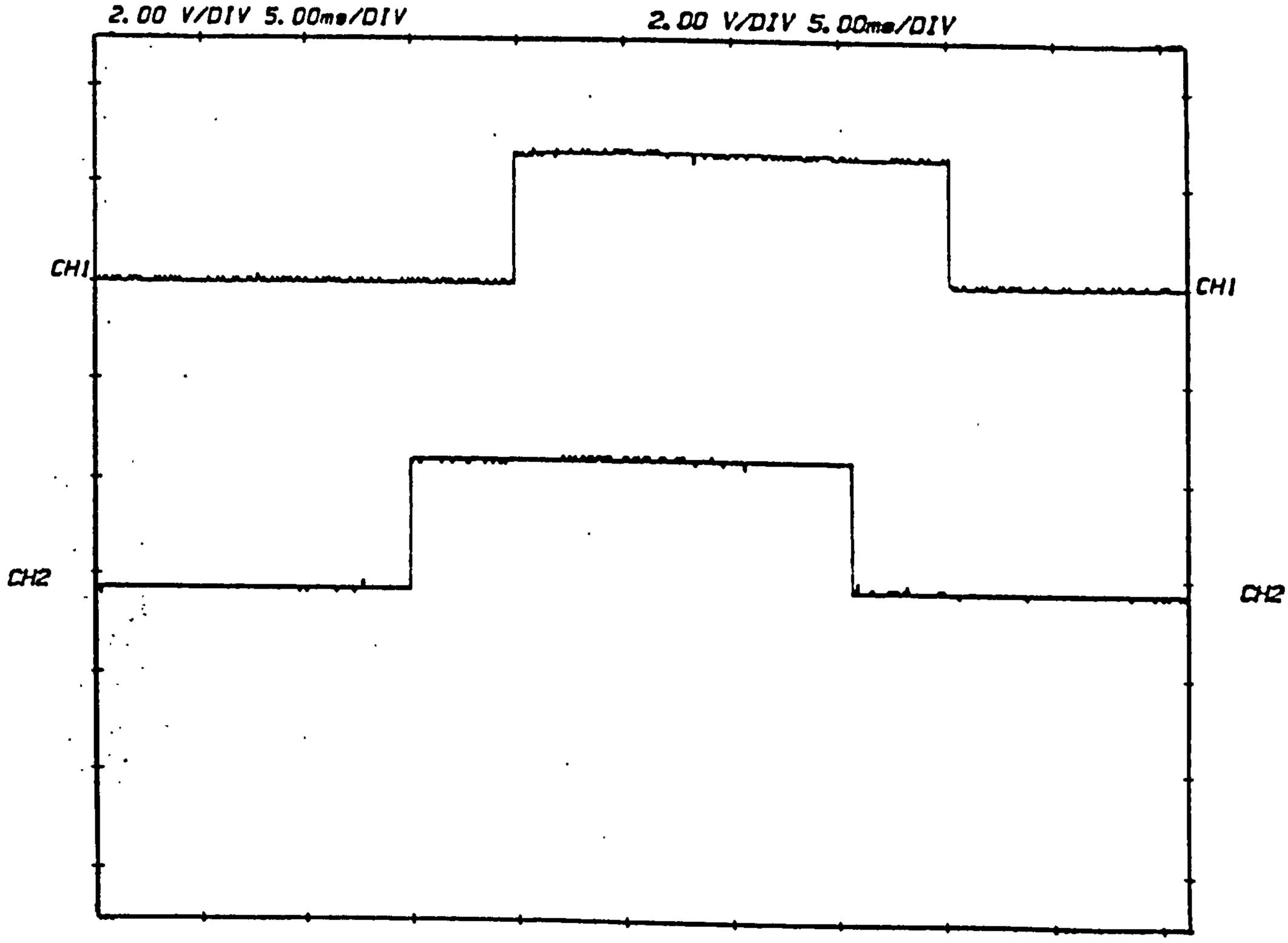

Figure 7.18 Encoder signals with phase advance angle=45°

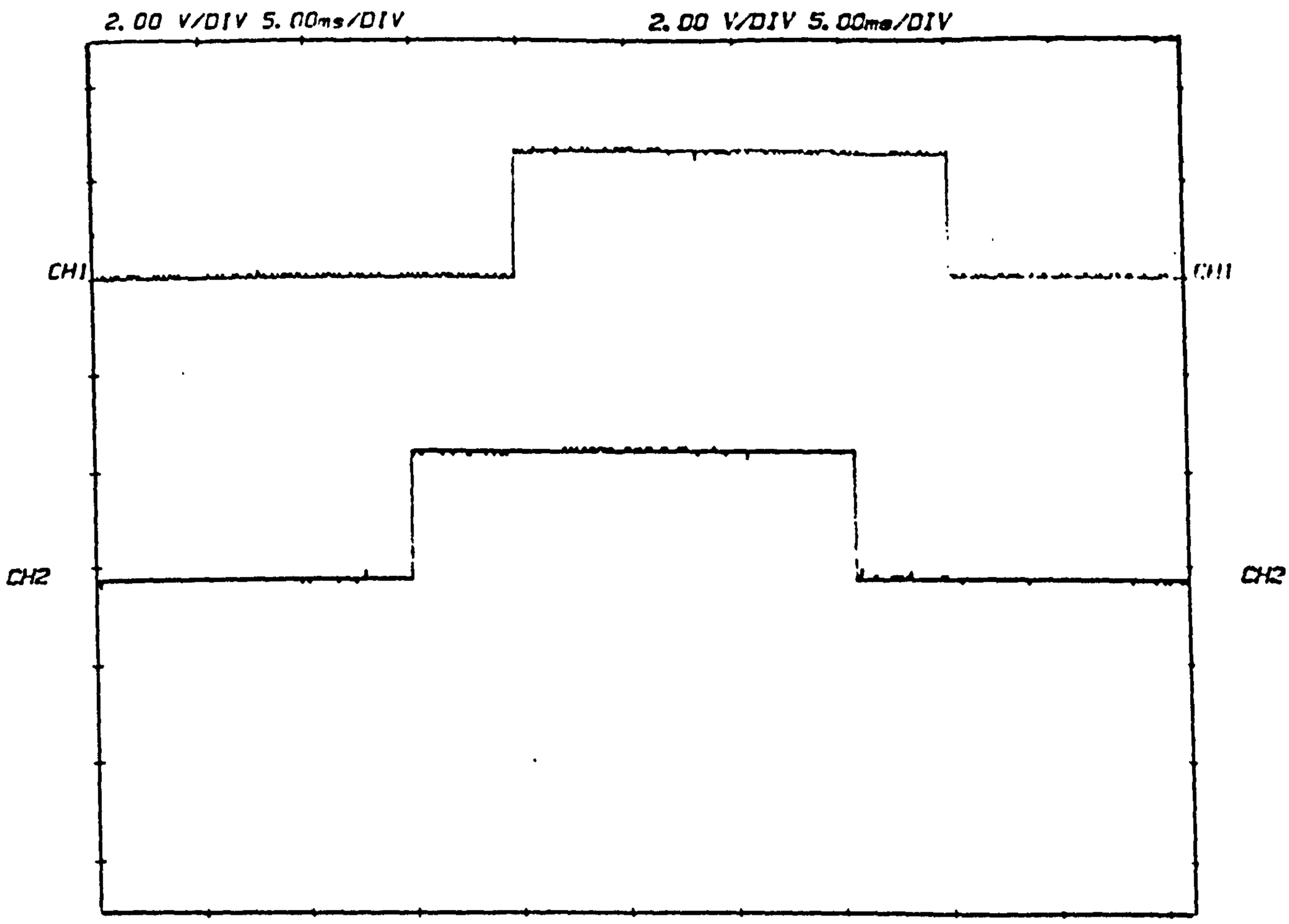

Figure 7.19 Encoder signals with phase advance angle=60°

CHAPTER 8

SUMMARY, GENERAL CONCLUSIONS, AND SUGGESTIONS FOR FURTHER WORK

8.1 Summary and General Conclusions

The work presented in this thesis has been concerned with the various aspects of the analysis, modelling, simulation and control of a surface mounted permanent magnet motor supply by a PWM inverter. Particular consideration has been given to a three phase motor with trapezoidal back-emf, although some of the analysis is applicable for all types of brushless dc drives. Detailed conclusions have been presented for each chapter but the overall conclusions from the work are summarised below.

In Chapter 1 an overall description of the design and construction of individual components of the brushless dc drive system is presented along with a review of the general concepts of the drive system. This type of machine is compared with other types of machine and the potential advantages of this new concept, both technical and economic, outlined.

In Chapter 2 the operation and the control aspects of the brushless dc motor are described, with particular emphasis placed on the basic requirements for the operation, torque production, performance characteristic and control. The high-speed torque control methods are also described and their merits are reviewed. In addition the effects of different parameters of machine design on the torque-speed characteristics is discussed.

Chapter 3 elaborates on the analysis and simulation work by presenting a comprehensive analysis which aims to show that direct three-phase representation can be used as an effective tool for performance assessement

of brushless dc drive systems operating over a wide speed range. During the course of the investigation, a mathematical model of the complete drive system based on the direct representation approach, has been presented. The model system includes representation of the motor, power inverter, and a PWM controller. The model incorporates a time stepping numerical technique, sets of differential equations which are used to describe the switching nature of the inverter devices under all its operating conditions and permits the motor neutral point to float. The simulation technique has been tested on the drive under consideration. The predicted and experimental results have been compared and discussed. Although the experiments agreed qualitatively with the theory, in order to get closer agreement between theory and practice, neglected effects should be considered.

An initial aim of the thesis is to analyse and to improve high-speed torque performance of a brushless dc drive. In Chapter 4 the performance of the brushless dc motor switched by a PWM inverter is investigated with a view to improving the high-speed torque performance. Simulation and analysis of the brushless dc motor is presented in which the actual parameters of the experimental machine are used. The aim of the analysis is to simulate a brushless d.c. drive system operating in closed-loop control modes, which uses phase advance control techniques in conjunction with a PWM control technique and also an investigation of this control on the dynamic behaviour of the system when account is taken of the load's mechanical dynamics. The investigation has included both 120° and 180° conduction angles of inverter operation, with provisions to select the phase advance angle for commutation. Performance characteristics, such as torque/speed, rms current, efficiency, current ripple, and torque ripple are obtained and compared for these control methods. Also the combined effects of the machine inductance and phase advance angle on the machine performance are assessed for conduction angles

of 120° and 180°. The effect of the variation of parameters such as the inductance on the high-speed torque performance of the drive has also been included in the study. The results of analysis has clearly shown that the high-speed torque characteristics of the brushless d.c. motor can be considerably improved simply by adjusting the chosen setting of the phase advance angle.

The results show that major improvements in torque output at high speed can be obtained by using appropriate conduction and phase advance angles. It has been shown that the torque available from a commercial drive above base speed can be improved by using phase advance control.

The analysis has clearly demonstrated that accurate phase advance angle selection is important if the optimum performance is to be obtained from a brushless dc drive. If the speed of the motor is kept constant, there is an optimum phase advance angle at which maximum torque occurs. The choice of $\alpha = \alpha_{opt}$ yields maximum torque and substantially improves the torque/speed characteristic above the rated speed.

In Chapter 4, numerical and analytical investigations to the operating range of the phase advance angle are presented. During this investigation a theoretical approach to demonstrate the operating range of the phase advance angle in permanent magnet brushless dc motors is presented. The results of the numerical and analytical analyses have shown that the phase advance should be within the range between 0° and 60° in order to provide a significant improvement in high-speed torque performance. A phase advance angle should be 0° for starting, the maximum value of 45° upto the base speed and a maximum value of 60° for speeds exceeding the base speed.

The simulated tests have also shown that in the high-speed region the current waveform becomes sinusoidal in shape because the current control capability of the drive is severely limited. The work has also shown that the electrical time constant of the winding is relatively large in comparison to the

excitation interval of each phase. Therefore the higher frequency components of excitation are heavily filtered and the major current component is at the fundamental frequency. As a consequence of this the current waveform becomes sinusoidal in shape. For these reasons and in order to predict the high-speed performance of the machine in term of the optimum phase advance angle quite reasonably, the sinusoidal analysis must be used. In the other words, sinusoidal analysis (machine theory) can be used to give a useful insight into the typical torque/speed curves that can be expected at high-speed operations.

In addition the phase advance angles affect the performance of the motor drive and they are not constants. They need to be varied as a function of speed, magnitude of current and load desired for overall drive system. The results of the analysis verify that the high speed torque characteristics of the brushless dc drive system are markedly influenced by controlling the phase advance angle.

A detailed analytical model which makes possible the use of machine theory for representing the performance of the brushless dc motor has been presented in Chapter 5. This model is used to derive the equations which describe the steady state characteristics of a drive system consisting of a permanent magnet machine supplied from a PWM voltage inverter operating in both 120° and 180° conduction angle modes and with provision to shift the phase of the stator voltages relative to the rotor position. The method utilizes the phasor diagram, where machine performance in terms of the main control variables (i.e. voltage and phase advance angle) is demonstrated.

Chapter 5 also presents an analytical expression for the phase-advance angle which yields maximum torque at a given motor speed. This expression is a very useful contribution for obtaining the machine performance in terms of optimum phase advance angle in higher speed operation. In addition the

quantitative effect of the phase advance angle on the torque/speed curve at high speed operation using sinusoidal analysis is presented.

Moreover, the brushless d.c. motor possesses a trapezoidal back-emf and a square wave current which are a major obstacle to any analysis based on sinusoidal assumptions. However, sinusoidal analysis of the brushless d.c. motor system gives a useful insight into the typical torque/speed curves that can be expected, particularly at high speed operations. Whilst the predictions are not necessarily quantitatively accurate, they do give a qualitative idea of the optimum operating conditions.

Although it would be possible to implement trail-and-error using the simulation, this approach is involved and requires a substantial amount of computation time to establish steady state operating points. Therefore it is desirable to establish simplified analytical representations which yield a more direct means of finding the optimum phase advance angle at the system operating limits in the high and extended speed ranges.

An analytical study concerning the optimum phase advance has been developed in chapter 6. In this work two analytical approaches to the problem of obtaining an optimum phase advance angle are presented. The first method is based on the controlled current waveform, where the phase current is effectively limited and therefore it assumes that the current must rise before back-emf in order that the current has attained the desired value at the start of the on-period. The second is based on the sinusoidal analysis where the stator current is effectively sinusoidal at high-speed operation and therefore it assumes sinusoidal inputs.

Chapter 6 also presents a detailed analysis of the shape of the current and back-emf waveforms in a trapeziodal brushless dc motor drive and their effects on the torque/speed performance. From this analysis, it has been shown that the current and back-emf waveform shapes have a direct effect

on the constant torque operation as well as the maximum torque that the brushless dc motor can deliver. During this investigation, a detailed analytical method for obtaining the required relationship between motor parameters in order to predict the desired shape of the current waveform is presented. This work in chapter 6 has also shown that the principle benefit of analytical solutions is that they make it much easier to predict the optimum phase advance angle and the shape of the current waveform and to see how the various motor and drive parameters affect the system performance.

Since research into high-speed control was directed at developing a robust method of implementing a speed dependent phase advance angle control, Chapter 7 presents the implementation of a microprocessor based system, which can set the phase advance angle to its optimum value at any motor speed. This implementation was done in real time on the prototype drive using a TMS320C30 digital signal processor. Features of the method proposed in this thesis include the estimation algorithms for predicting the time advance. It was found that the estimation algorithm is well suited for a microprocessor to predict the advance time and is effective.

The configuration and implementation of the control algorithms have been fully described. Experimental results on a drive system under consideration demonstrate the satisfactory performance of both the hardware and software of the control scheme and the ease with which the advance of the instant of the commutation angle is automatically adjusted to maintain the desired torque in response to the motor speed and load conditions.

The operation of the drive system was encouraging. The phase current waveform was advanced and the microprocessor successfully implemented the control method and the drive system operated reliably throughout the entire period of the tests reported in the thesis. This work on the brushless dc drive has clearly demonstrated that the estimation algorithms control can be

realised by the microprocessor. It has shown that a microprocessor is a very powerful logical unit with which it is possible to easily set up (and modify) logical tasks such as the starting sequence, direction and so forth.

The work on the effect of high-speed control based on the phase advance has clearly shown that this control can be used to modify the characteristic of the drive system in high-speed operations. In other words, it has been shown that if the drive is operating with closed loop strategy, which uses a phase advance control technique in conjunction with pulse width modulation (PWM) current controller, it has distinct advantages when compared with a similar system which is operating without a phase advance technique. If the motor is operated over a wide speed range and delivers the maximum possible torque at all times, it is normally essential to have some form of phase advance angle control. In addition, the cost of microprocessors are almost certain to fall as their usage in industry increases, and so a high-speed control method based on the phase advance algorithm described in this thesis should become commercially more viable in the future.

It is concluded from the microprocessor work carried on the brushless dc motor, that microprocessors do have a very important role to play in motor drive systems and should be used in any development or improvement of the drive system because it enables complex changes to the inverter control signals to be made simply by software modifications.

The advantage of applying phase advance control in the operating speed range of the brushless dc drive system has been well demonstrated in the context of using a microprocessor-based phase advance scheme. The configuration of the entire control method can be easily adopted for any brushless dc drive system.

8.2 Recommendations for Future Work

8.2.1 Recommendations for Control Aspects of the Drive System

Following the tests on the drive system there is no doubt that a microprocessor can be used very successfully in the control aspects of a brushless dc drive.

Future work on the control electronics of a brushless dc drive system should be aimed at minimising the number of integrated circuits required in order to reduce the size, cost and consumption of the control unit. There is, however, great scope for employing microprocessors in motor drive systems to perform tasks other than the high-speed control methods because there are ways in which the drive system could be simplified or modified to make it practical and cost effective. For example all of the control and monitoring tasks in the drive system can be achieved by conventional analogue and digital circuits, but it makes technical and economic sence to try to replace as many of the discrete circuits by a microprocessor, since such an approach reduces the component count and should improve reliability.

By careful design of both hardware and software it should be possible to evolve a basically simple control unit capable of operating the drive over the required speed range. There are several variations in the operation of the drive that are worthy of investigation in the future. One interesting variation in the control aspects of the system is to arrange the controlling logic by modifying the sequence of drive signals using the development program of this work so that it actively tries to minimise the torque ripple; to achieve this both phase advance and conduction angles must be varied as necessary to obtain the desired torque and this can also be set according to the machine parameters and to the requirements of the application. It is believed that the suggestions for future work are justified by successful implementation of

a microprocessor based system which automatically sets the phase advance angle to its optimum value at any speed.

The use of a one-chip microprocessor would enable a great reduction in the component count to be achieved and it is an advantage of using a signal microprocessor to replace control aspects of the drive. It is fair to say that in all other respects a TMS320C30 digital signal processor can perform reasonably these aspects. Because the TMS320C30 digital signal processor is a faster processor and also offers many advantages for implementation of these aspects. Its 60 ns cycle time and special features, such as the signal cycle multiplication, allow high execution speed. Further, the availability of development tools such as c complier, assembler/linkers and in-circuit emulators that accelerate design time.

8.2.2 Recommendations for High-speed Torque Control Methods

Undeniably, the use of estimation algorithms in the high-speed torque control of a brushless dc drive will continue to expand. It is worthwhile to guide this development in such a way that the experience gained is beneficial to the improvement of the high-speed performance of the brushless dc drive system. There does not appear to be any reason why phase advance adjustment facilities should not be a standard feature on a brushless drive system in the future.

It is suggested that in the future the phase advance control algorithms should be replaced by the higher-order algorithms such as third or fourth order-estimation algorithm in order to increase the accuracy of the their predictions.

REFERENCES

Acarnley, P.P., Hughes, A., 1981, 'Predicting the pullout torque/speed curve of variable-reluctance stepping motors', *Proc. IEE Pt B*, Vol., 128, No.2.

Acarnley, P.P., Hughes, A., 1988, 'Machine/drive circuit interactions in small variable-reluctance stepping and brushless dc motor systems', ', *Proc. IEEE Trans on Industrial Applications*, Vol., IA-35, pp 67-74.

Acarnley, P.P., Jack, A.G. and Jowett, P.T., 1988, 'Power circuits for a small permanent magnet brushless dc drives', *3rd International Conference, Power Electronics and Variable Speed Drives*, pp 237-240

Acarnley, P.P., 1982, 'Stepping motors: a guide to modern theory and practice', *IEE Control Engineering Series 19, Peter Peregrinus.*

Acarnley, P.P., Hill, R.J., Hooper, C.W., 1985, 'Detection of rotor position in stepping and switched motors by monitoring of current waveforms ', *Proc. IEEE Trans on Industrial Applications*, Vol., IA-32, pp 215-222.

Acarnley, P.P., Gibbons, P.A., 1982, 'Closed-loop control of stepping motors: prediction and realisation of optimum switching angle', *Proc. IEE Pt B*, Vol. 129 pp 211-216.

Adkins, B., 1957, 'The generalized theory of electrical machines', *Chapman and Hill, Ltd.*, London, England.

Adkins, B., 1957, 'The generalized theory of electrical machines', *Chapman and Hill, Ltd.*, London, England.

Baron, W., 1983, 'Position control of a brushless motor by microprocessor ', *Proc. of the Motor-Conference*, pp 123-128.

Binns, K.J., Barnard, W.R and Jabbar, M.A., 1978, 'Hybrid permanent-magnet synchronous motors', *Proc. IEE, Pt B*, Vol. 125, No. 3.

Bolton, H.R. and Ashen, R.A., 1984, 'Influence of motor design and feed-current waveform on torque ripple in brushless dc drives interior permanent magnet synchronous motor drive ', *Proc. IEE, Pt B*, Vol. 131, pp 82-90.

Bose, B.K., 1988, 'A high performance inverter fed drive system of an interior permanent magnet synchronous motor drive ',*Proc. IEEE Trans. on Industrial Applications*, Vol. IA-24, pp 987-997.

Boules, N., 1983, 'Two dimensional field analysis of cylindrical machines with permanent magnet excitation', *Proc. of the IEEE Industrial Applications Society Annual Meeting*, pp 446-454.

Bowes, S.R. and Clements, R.R., 1983, 'Digital computer simulation of variable-speed PWM inverter-machine drives', *Proc. IEE Pt B*, Vol. 130.

Bowes, S.R. and Clare, J.C., 1988, 'Computer-aided design of PWM power electronic variable speed drives', *Proc. IEE Pt B*, Vol. 135.

Brawn, M., 1982, 'Brushless dc or inverter motor drives; a comparison of attributes', *Proc. of the Motor Control Conference*, pp 111-123.

Brentani, G., 1985, 'Consideration on the locked rotor torque characteristics of brushless dc motors', *Proc. of the Motor Control Conference*, pp 107-114.

Brosnan, M.F. and Brown, B., 1984, 'Closed loop speed control using ac synchronous motor ', *Proc. of the IEE Conference on Power Electronics and Variable Speed Drives*, pp 373-376.

Carvajal, F.D., Hines, J.R., Lantzsch, T.P., 1985, 'A tutorial on the use of the Hall effect', *Proc. of the Motor-Control Conference*, pp 115-125.

Chalmer, B.J., Pacey, K. and Gibson, J.P., 1975, 'Brushless d.c. traction drive', *Proc. IEE Pt B*, Vol. 122, No.2.

Chalmer, B.J., Hamed, S. A. and Baines, G.D., 1985, 'Parameters and performance of a high-field permanent magnet synchronous motor for variable-frequency operation', *Proc. IEE Pt B*, Vol. 132, pp 117-124.

Davat, B., Rezine, H., Lajoie M.M., 1985, 'Modelling of a brushless dc motor with solid parts involving eddy currents, *Proc. of IEEE Trans. on Industrial Applications*, Vol. IA-21 pp 202-206.

Demerdash, W.A., Nehl, T.W., Overton, B.P., and Masklowski, E.A., 1982, 'Dynamic simulation of radially oriented permanent magnet-type electronically operated synchronous machines with parameters obtained from finite element field solution , *Proc. of IEEE Trans. on Industrial Applications*, Vol. IA-18, pp 172-181.

Demerdash, W.A., Miller, R.H., Nehl, T.W., Overton, B.P., and Ford, C.J., 1983, 'Comparison between features and performance characteristics of fifteen hp samarium cobalt and ferrite based brushless dc motors operated by the same power conditioner, *Proc. of IEEE Trans. on PAS*, Vol. PAS-102, pp 104-112.

El-sharkawi, M.A., Coleman, J.S., 1986, 'Microcomputer control of an electronically commutated dc motor, *Proc. of IEEE N.A.E Conference*, Vol. 1, pp 320-325.

Evans, P.D., and Brown, D., 1990, 'Simulation of brushless dc drives', *Proc. IEE, Pt B*, Vol. 137 pp 299-308.

Fouad, F.A., Nehl, T.W., 1981, 'Magnetic modelling of permanent magnet type electronically operated synchronous machines using finite elements', *Proc. IEEE Trans. on PAS*, Vol. PAS-100, pp 4125-4135.

Funabiki, S. and Himei, T., 1985, 'Estimation of torque pulsation due to the behaviour of a converter and an inverter in a brushless dc motor system', *Proc. IEE, Pt B*, Vol. 132 pp 215-222.

Goodman, E.D., 1982, 'Torque, Voltage and current harmonic of a synchronous machines ', *Proc. IEEE of Industrial Applications Society Annual Meeting*, pp 591-597.

Grandpierre, M., Faucher, J., Lajoie-Mazenc, M. and Brandao-Jacobina, C., 1984, 'Filtering of voltage signals for autopiloting without position sensor of converter fed synchronous machine', *Proc. of the Motor Control Conference*, pp 197-209.

Jahns, T.M., 1987, 'Flux-weakening of an interior permanent magnet synchronous motor drive ', *Proc. IEEE on Industrial Applications* Vol., IA-23, pp 681-689.

Jahns, T.M., 1984, 'Torque production in permanent magnet synchronous motor drives with rectangular current excitation', *Proc. IEEE Trans. on Industrial Applications*, Vol., IA-20, No. 4.

Jack, A.G., Acarnley, P.P., and Jowett, P.T., 1988, 'Design of small high-speed brushless d.c. machines', *ICEM, Pisa, Italy.*

Iizuka, K., Uzuhashi, H., Kano, M., Endo, T., and Mohri, K., 1985, 'Microcomputer control for sensorless brushless motor, *Proc. of IEEE Trans. on Industrial Applications*, Vol. IA-21 pp 595-601.

Le-Huy, H., Jakubowicz, A. and Perret, R., 1982 ' A self-controlled synchronous motor drive using terminal voltage system', *Proc. IEEE Trans. on Industrial Applications* Vol. IA-18, pp 46-53.

Le-Huy, H., Perret, R., and Feuillet, R., 1986 ' Minimisation of torque ripple in brushless dc motor drives', *Proc. IEEE Trans. on Industrial Applications* Vol. IA-22, pp 748-755.

Lipo, T.A., 1971 'The analysis of induction motors with voltage control by symmetrical triggered thyristors', *Proc. IEEE Trans. on PAS* Vol. PAS-90, pp 515-525.

Lipo, T.A., and Turnbull, F.G., 1975 'Analysis and comparison of two types of square-wave inverter drives', *Proc. IEEE Trans. on Industrial Applications* Vol. IA-11, pp 137-147.

Liu, Y.P., How, D., Birch, T.S. and Matthews, D.M.H., 1989 'Dynamic modelling and performance prediction of brushless permanent magnet drive system ', *Proc. IEE Conference on Power Electronics and Variable Speed Drives,* London.

Meshkat, S. and Persson, E.K., 1984, 'Optimum current vector control of a brushless servo amplifier using microprocessor ', *Proc. of the IEEE of Industrial Applications Society Annual Meeting,* pp 451-457.

Miller, T.J.E., Ilic-Spong, M., Macminn, S.R., Thorp, J.S., et al., 1987, 'Instantaneous torque control of electric motor drives',*Proc. IEEE trans. on the Power Electronic,* Vol. PE-2 pp 55-61.

Murty, B.V., 1984, 'Fast response reversible brushless dc drive with regenerative braking', *Proc. of the IEEE Industrial Applications Society Annual Meeting,* pp 445-450.

Nashiki, M. and Dote, Y., 1982, 'High performance current-controlled PWM transistor inverter-fed brushless servomotor ', *International semiconductor Power Converter Conference,* pp 349-356.

Naunin, D., 1983, 'The calculation of damper currents in synchronous machines at different wave forms ', *Proc. of the IFAC Conference on Control in Power electronic and Electrical Drives,* pp 399-405.

Novotny, D., and Fath, A. F., 1968, 'The analysis of induction machines controlled by series-connected semiconductor switches', *Proc. IEEE Trans. on PAS,* Vol. PAS-87, pp 597-605.

Nyamusa, T.A., and Demerdash, N.A., 1987, 'Transient analysis of partial armature short circuit in electronically commutated permanent magnet motor system using an integrated nonlinear magnetic field network model', *Proc. IEEE Trans. on Energy Conversion*, Vol. EC-2, pp 86-92.

Oudet, C. and Etteiman, D.J., 1985, 'An alternative to choosing between dc and stepper motors', *Proc. of the Motor-Control Conference*, pp 47-59.

Ogasawara, S.D, Nishimura, M., Akagi, H., Nabae, A., Nakanishi, Y., 1986, 'A high performance ac servo system with permanent magnet synchronous motors', *Proc. IEEE Trans. on Industrial Electronics*, Vol. IE-33, pp 87-91.

Krause, P. C. and Thomas, C. H., 1974, 'Simulation of symmetrical induction machinery', *Proc. IEEE Trans. on Power App. Syst.*, Vol. PAS-93, pp 1410-1418.

Krause, P.C., Voyles, R.M. and Wasynczvk., 1984, 'Analysis and simulation of a brushless dc servomotor', *Proc. of the Motor-Control Conference*, pp 86-93.

Krause, P.C., 1987, 'Analysis of Electrical Machinery', *McGraw Hill International.*

O'Kelly, D. and Simmons, S., 1968, 'Introduction to generalized electrical machine theory', *McGraw Hill,* New York.

Paraskeva, M. and Weison, M.J., 1984, 'Microprocessor control of a brushless d.c. motor', *Drives, Motors and Controls Conference*, pp 80-82.

Patrick, M., Charles, P. N., 1985, 'Pulsewidth modulation control of a brushless dc motors for robotic applications, *Proc. of IEEE Trans. on IE*, Vol. IE-32, pp 222-229.

Park, R.H., 1979, 'Two-reaction theory of synchronous machine- generalised method of analysis',*Part I, AIEE trans.*, Vol. 48, pp 716-727.

Persson, E.K. and Meshkat, S., 1985, 'Brushless servo system with expanded torque speed operating range', *Proc. of the Motor Control Conference*, pp 96-106.

Pfaff, G., Weschta, A., and Wick, A.F., 1983, 'Design and experimental results of a brushless ac servo-drive', *Proc. IEEE Trans. on Industrial Applications*, Vol. IA-20 pp 614-821.

Pillay, P., and Krishnan, R., 1989, 'Modelling, simulation and analysis of permanent magnet motor drives, Part II: The brushless dc motor drive ', *Proc. IEEE Trans. on Industrial Applications*, Vol. IA-25 pp 274-279.

Piriou, F., Razek, A., Perret, R. and Le-Huy, H., 1986, 'Torque characteristics of brushless dc motors with imposed current waveform ', *Proc. IEEE Conference IAS*, pp 176-181.

Piriou, F. and Razek, A.C., 1986, 'A model for inverter-fed synchronous motors considering control strategy ', *International Conference on Electrical Machines*, pp 752-755.

Safi, S.K., and Acarnley, P.P., 1992, 'High-Speed Control of permanent-magnet brushless d.c. drives', *27th Universities Power Engineering Conference, Bath, UK*, pp 209-212.

Safi, S.K., Acarnley, P.P., and Jack, A., 1992, 'Analysis and simulation of the high-speed torque performance of the brushless d.c. drives', *to be published in IEE Proceddings Pt B.*

Sebastian, T. and Slemon G.R., 1987, 'Transient modelling and performance of variable speed permanent magnet motors', *Proc. IEEE Conference, IAS*, pp 35-39.

Sebastian, T. and Slemon G.R., 1987, 'Operating limits of inverter-driven permanent magnet motor-drives', *Proc. IEEE Trans. on Industrial Applications*, Vol., IA-23, pp. 327-333.

Slemon, G.R. and Gumaste, A.V., 1983, 'Steady-state analysis of a permanent magnet synchronous motor drive with voltage source inverter permanent magnet motor-drives', *Proc. IEEE Trans. on Industrial Applications*, Vol., IA-19, pp. 190-197.

Sneyers, D.W., Novotny, and Lipo, T.A., 1987, 'Field weakening in buried permanent magnet motor-drives', *Proc. IEEE Trans. on Industrial Applications*, Vol., IA-21, pp. 398-407.

Stone, A.C. and Buckley, M.G., 1985, 'Novel design and control of a trapezoidal back-emf motor-the smooth transition from brush to brushless dc', *Proc. of the Motor-Control Conference*, pp 86-95.

TMS320C30 User's Guide, 1987, Houston, Tx: Texas Instruments Inc.

TMS320 Family Development Support Reference Guide, 1987, Houston, Tx: Texas Instruments Inc.

Tripathi, K.C., et al., 1980, 'A battery-run pulsed motor with inherent dynamic electronic switch control', *Proc. IEEE Trans. on IECI*, Vol. 27, pp 29-34.

Vagati, A. and Villata, F., 1983, 'A brushless system for position control ', *Proc. of the IEE Conference on Power Electronics and Variable Speed Drives*, pp 373-376.

Vagati, A. and Villata, F., 1985, 'Field-oriented ac motor: a particular implementation', *Proc. of the Motor Conference*, pp 160-172.

Walter, H.S., 1987, 'A brushless dc motor controlled by a microprocessor with examples for a three-phase motor', *Proc. of the IEEE on IE*, Vol. IE-34, pp 339-344.

Wallace, A.K. and Spee, R., 1987, 'The effects of motor parameters on the performance of brushless dc drives ', *Proc. of the IEEE Power Electronic Specialist Conference*, pp 591-597.

Weh, H., and Boules, N., 1980, 'Field analysis for a high-speed permanent magnet synchronous of the disc construction type', *Electric machine and Electromechanics*, Vol., 5, No. 1.

Williamson, A.C., Issa, N.A.H., and Makky, A.R.A.M. 1978, 'Variable-speed inverter-fed synchronous motor employing natural commutation', *Proc. IEE*, Vol. 125 pp 114-120.

Woodbury, J.R. 1974, 'The design of brushless dc motor systems ', *Proc. IEEE Trans. on IECI*, Vol. 21, pp 52-60.

Zimmerman, P., 1982, 'Electronically commutated dc feed drives for machine tools', *Drives and Control International*, pp 13-19.

APPENDIX 1

TEST MOTOR: Summary of Motor Design

1.2. Summary of Motor Design

The motor parameters were incorporated in the simulation package described in chapter 4 has an outline specification as given in table A1.1 below

Rated power	20 KW
Maximum speed at rated torque rated power	3000 rpm
No. of rotor poles	6
Continuous rated torque	57 Nm
Continuous static torque	21 Nm
Supply voltage	550 V
Continuous rated current	23 A
Maximum current	158 A
Electrical time constant	11.9 ms
Mechanical time constant	1.8 ms
Thermal time constant	35 min

Table A1.1 Specification of test motor

The permanent magnet motor is a three phase, six pole, star connected, type SE-B4 210 motor+SM50/100-T inverter combination manufactured by the Robert Bosch company. This motor uses rare-earth material on its rotor.

The stator was constructed using a slotted winding with one slot-per-pole per phase. Each stator slot was skewed by one stator slot pitch. As mentioned in the previous chapter this is necessary to eliminate the cogging torque which would be presented in an unskewed stator design.

The stator windings are the same and they are displayed by the number of the slots per phase per pole. It should be noted that this symmetry implies that there is an integral number of slots per phase. The arrangement of the winding starts with the number of coils and parallel paths per phase. Then for each parallel path the coils need go and return slots defining. It is assumed that each parallel path has the same number of coils (i.e. that coils per phase divided by parallel paths is an integral number). A summary of the principle features of the design is given in table A1.2

Magnet material	rare-earth
airgap flux density	0.505 T
No. of rotor poles	6
Pole arc	176.4° elec.
No. of stator slot	36
outer diameter	135.0 mm
inner diameter	00.0 mm
airgap depth	0.90 mm
magnet depth	2 mm
field core depth	41.60 mm
armature core depth	8.20 mm
slot depth	13.95 mm
tooth depth	4.20 mm
axial length	155.0 mm

Phase resistance	0.26 Ω
Phase self inductance	3.1 mH
Voltage constant (V/1000 rpm)	96.3

Table A1.2 Test motor: Design specification.

APPENDIX 2

HARDWARE OVERVIEW OF THE MICROPROCESSOR SYSTEM

A2.1. Introduction

The TMS320C30 [TMS320C30 User's Guide, 1987] is a texas instruments third generation member of the TMS320 family of compatible digital signal processors. With computation rate of 33 MFLOPS (millioon floating-point operations per second), the TMS320C30 far exceeds the perforrmance of any programable DSP available today. Total system cost is minimised with on-chip memory and on-chip peripherals such as timers and serial ports.

The TMS320C30 device offer the advantages of a floating-point processor and ease of use. This device is a higher speed and it delivers 33.3 MFLOPS (million floating-point operations per second) and runs at 33.33 $\times 10^6$ Hz. A functional block diagram of the TMS320 is shown in figure A2.1. Some key features of the TMS320C30 [TMS320C30 User's Guide, 1987] are listed below

(1) 60-ns signal cycle instruction executing time,

(2) 33.3 MFLOPS (million floating-point operations per second),

(3) 16.7 MIPS (million instructions per second),

(4) one 4K x 32-bit signal-cycle dual-access on-chip ROM block,

(5) two 1K x 32-bit signal-cycle dual-access on-chip RAM block,

(6) direct memory access (DAM) controller on-chip for cocurrent I/O and CPU operation,

(7) 32-bit instruction and data words, 24 bit addresses,

(8) two 32-bit data buses (24-and-13-bit address),

(9) two serial ports to support 8/16/24/32-bit transfers,

(10) two 32-bit timers,

A2.2. TMS320C30 Hardware

The architecture of the TMS320C30 is targeted at 60-ns and faster in cycle times. To achieve such high-performance goals while still providing low-cost system solutions, the TMS320C30 is designed using Texas instruments state of the art 1 μm CMOS process. The TMS320's high system performance is achieved through a high-degree of parallelism, the accuracy and precision of its floating-ponit unit, its on-chip DAM controller that supports concurrent I/O, and its general-purpose features. At a heart of the architecture is central processing unit (CPU).

Central Procssing Unit (CPU)

The CPU consists the floating-point/integer multiplier hardware, the Arithmetic Logic Unit (ALU) for performance floating-point, integer, and logical operation; auxiliary register arithmetic units; supporting register file, and associated buses. The units are shown in figure A2.2. The multiplier of the CPU performs floating-point and integer multiplication. When performing floating-point multiplication, the inputs are 32-bit floating-point numbers, and the result is a 40-bit floating point numbers. When performing integer multiplication, the input data is 24 bits and yields a 32-bit result. The ALU performs 32-bit integer, 32-bit logical, and 40-bit floating point operations. Results of the multiplier and the ALU are always maintained in 32-bit integer or 40-bit floating point formats. The TMS320C30 has the ability to perform, in a single cycle, parallel multiplies and adds (subtracts) in a single cycle which give the TMS320C30 its peak computational rate of 33 MFLOPS.

The register file contains 28 registers, which may be operated upon by the multiplier and ALU. The first eight of these register (R0-R8) are

the extended-precision registers, which support operations on 40-bit floating-point numbers and 32-bit integers. The next eight registers (AR0-AR8) are the auxiliary registers, whose primary function is related to the generation of addresses. However, they also may be used as general purpose 32-bit registers. Two auxiliary register arithmetic units (ARU0 and ARU1) can generate two addresses in a single cycle. The ARAUs operate in parallel with multiplier and ALU. They support addressing with displacements, index register (IR0 and IR1), and circular and bit-reversed addressing. The remaining registers support a variety of system functions: addressing, stack mangemen, processor status, block repeat, and interrupts.

Data Organization

Two integer formats are supported on the TMS320C30: a 16-bit format used for immediate integer operands and a 32-bit single-precision integer format. Two unsigned-integer formats are available: a 16 bit format for immediate unsigned-integer operands and a 32-bit single-precision unsigned-integer format.

The three floating-point formats are assumed to be normalised, thus providing an extra bit of precision. The first is a 16-bit short floating-point format for immediate floating-point operands, which consists of a 4-bit exponent, 1 sign bit, and an 11-bit fraction. The second is a single-precision format consisting of an 8-bit exponent, 1 sign bit, and a 23-bit fraction. The third is an extended-precision format consisting of an 8-bit exponent, 1 sign bit and a 31-bit fraction.

The total memory space of the TMS320C30 is 16 M (million) × 32 bits. A machine word is 32 bits, and all addressing is performed by word. Program, data, and I/O space are contained within the 16 M-word address space.

RAM blocks 0 and 1 are each 1K *times* 32 bits. The ROM block is 4K × 32 bits. Each RAM block and ROM block is capable of supporting two data accesses in a single cycle. For example, the user may, in a single cycle, access a program word and a data word from the ROM block.

The separate program data, and DMA buses allow for parallel program fetches, data reads and writes, and DMA operation. Mangement of memory resources and busing is handled by the memory controller. For example, a typical mode of operation could involve a program fetch from the on-chip program cache, two data fetches from RAM block 0, and the DMA moving data from off-chip memory to RAM block 1. All of this can be done in parallel with no impact on the performance of the CPU.

A 64 × 32-bit instruction cache allows for maximum system performance with minimal system cost. The instruction cache stores often repeated sections of code. The code may then be fetched from the cache, thus greatly reducing the number of off-chip access necessary. This allows for code to be stored off-chip in slower, lower cost memories. Also the external buses are freed, thus allowing for their use by the DMA or other devices in the system.

Direct Memory Access (DMA)

The TMS320C30 process an on-chip direct memory access (DMA) controller. The DMA controller is able to perform reads from and writes to any location in the memory map without interfering with operation of the CPU. As a consequence, it is possible to interface the TMS320C30 to slow external memories and peripherals (A/D's, timers, serial ports, etc.) without affecting the computional throughout of the CPU. The results in an improved system performance and decreased system cost.

The DMA controller contains its own address generators source and destination registers and transfer counter. Dedicated DMA address and data

buses allow for operation with no conflicts between the CPU and DMA controller. The DMA controller responds to interrupts in a similar way to the CPU. This ability allows the DMA to transfer data based upon the interrupts received. Thus I/O transfers that would normally be performed by the CPU may instead be performed by the DMA. Again the CPU may continue procssing data while the DMA receives or transmits data.

Peripherials

All peripheral modules are manipulated through memory-mapped resgisters loacted on a dedicated peripheral bus. This peripheral bus allow for the straightforward addition, removal and creation of peripheral modules. The initial TMS320C30 periheral will include timers and serial ports.

The Programmable Timer

The two timer modules (which are called timer 0 and timer 1) are general-purpose 32-bit timer/event counters with two signaling modes and internal or external clocking (see figure A2.3). Each timer has I/O pin that can be used as an input clock to the timer or as an ouput signal driven by the timer. The programmable timer modules can be employed as the basis for a variety of measurement circuits, including an event counter, frequency counter, or a pulse generator. For example the timer modules can be used to signal to the TMS320C30 or external word as specified intervals, or to count external events as used in present work.

Each timer can be programmed for specific applications by writing the mode of operation their control register. The control registers are designated global-control resgister, period register and counter register. The global-control register determines the operating mode of the timer, monitors the timer status, and controls the function of the I/O pin of the timer. The period register

specifies the timer's signaling frequency. The counter register contains the current value of the incrementing counter. The timer can be incremented on the rising edge or the falling edge of the input input clock. The counter is zeroed and can caused an interrupt whenever its value equals that in the period register. The memory map for the timer modules is given in the table A2.1 and shown below

Table A2.1 Memory-Mapped Timer Locations

Regester	Peripheral	Address
	Timer 0	Timer 1
Timer global control	808020h	808030h
Reserved	808021h	808031h
Reserved	808022h	808032h
Reserved	808023h	808033h
Timer counter	808024h	808034h
Reserved	808025h	808035h
Reserved	808026h	808036h
Reserved	808027h	808037h
Timer period	808028h	808038h
Reserved	808029h	808039h
Reserved	80802Ah	80803Ah
Reserved	80802Bh	80803Bh
Reserved	80802Ch	80803Ch
Reserved	80802Dh	80803Dh
Reserved	80802Eh	80803Eh
Reserved	80802Fh	80803Fh

The timer global control register is a 32-bit register that contain the global and port control bits for the timer module. Table A2.2 defines the register bits, names and functions. Bits 3-0 are the port control bits; bits 11-6 are the timer global control bits. Figure A2.4 shows the 32-bit register. Note that at reset, all bits are set to 0 except for DATIN (set to the value read on TCLK).

In this application one of the TMS320 timers is used to measure the times required by the phase advance algorithm (see chpater 7). In order to select this mode of operation the timers can be done by writing the mode of operation its control register. The control registers are designated global-control resgister, period register and counter register and these registers are configured to the time measurement mode.

The Serial Ports

The two serial ports are modular and totally independent. Each serial port can configured to transfer 8, 16, 24, or 32 bit data perform. The clock for each serial port can originate either internally or externally. An internally generated divide-down clock provided.

The Operation Units of the TMS320C30

The operation of the TMS320C30 is controlled by the following five major functional units;

(i) fetch unit which controls the program counter updates and fetches of the instruction words from memory,

(ii) decode unit which decodes the instruction word and control address generation,

(iii) read unit which controls the operand reads from memory.

(v) execute unit which reads operands from the register file, performs the

necessary operation and write results back to the register file and memory.

Finally the digital signal processor is essentially like any other microprocessor, no matter how impressive the performance of the processor or the ease of interfacing, without good development toolls and technical support, it is very difficult to design it into the system. In this respect the TMS320C30 has a wide range of development tools available [TMS320 Family Development Support Refence Guide, 1987].

Table A2.2 Timer global-control register bits summary

Bits	Name	Reset Value	Function
0	FUNC	0	FUNC controls the function of TCLK. If FUNC = 0, TCLK is configured as a general-purpose digital I/O port. If FUNC = 1, TCLK is configured as a timer pin (see Figure 2-4 for a description of the relationship between FUNC and CLKSRC).
1	I/O	0	If FUNC = 0 and CLKSRC = 0, TCLK is configured as a general-purpose I/O pin. In this case, if I/O = 0, TCLK is configured as a general-purpose input pin. If I/O = 1, TCLK is configured as a general-purpose output pin.
2	DATOUT	0	DATOUT drives TCLK when the TMS320C3x is in I/O port mode. DATOUT can also be used as an input to the timer.
3	DATIN	x †	Data input on TCLK or DATOUT. A write has no effect.
5—4	Reserved	0–0	Read as 0.
6	GO	0	The GO bit resets and starts the timer counter. When GO = 1 and the timer is not held, the counter is zeroed and begins incrementing on the next rising edge of the timer input clock. The GO bit is cleared on the same rising edge. GO = 0 has no effect on the timer.
7	$\overline{HLD}$	0	Counter hold signal. When this bit is zero, the counter is disabled and held in its current state. If the timer is driving TCLK, the state of TCLK is also held. The internal divide-by-two counter is also held so that the counter can continue where it left off when $\overline{HLD}$ is set to 1. The timer registers can be read and modified while the timer is being held. $\overline{RESET}$ has priority over $\overline{HLD}$. Table 2-3 shows the effect of writing to GO and $\overline{HLD}$.
8	C/$\overline{P}$	0	Clock/Pulse mode control. When C/$\overline{P}$ = 1, clock mode is chosen, and the signaling of the status flag and external output will have a 50 percent duty cycle. When C/$\overline{P}$ = 0, the status flag and external output will be active for one H1 cycle during each timer period.
9	CLKSRC	0	Specifies the source of the timer clock. When CLKSRC = 1, an internal clock with frequency equal to one-half the H1 frequency is used to increment the counter. The INV bit has no effect on the internal clock source. When CLKSRC = 0, an external signal from the TCLK pin can be used to increment the counter. The external clock is synchronized internally, thus allowing external asynchronous clock sources that do not exceed the specified maximum allowable external clock frequency. This will be less than f(H1)/2. (See Figure · for a description of the relationship between FUNC and CLKSRC).
10	INV	0	Inverter control bit. If an external clock source is used and INV = 1, the external clock is inverted as it goes into the counter. If the output of the pulse generator is routed to TCLK and INV = 1, the output is inverted before it goes to TCLK : If INV = 0, no inversion is performed on the input or output of the timer. The INV bit has no effect, regardless of its value, when TCLK is used in I/O port mode.
11	TSTAT	0	This bit indicates the status of the timer. It tracks the output of the uninverted TCLK pin. This flag sets a CPU interrupt on a transition from 0 to 1. A write has no effect
31—12	Reserved	0–0	Read as 0.

Table A2.2 Results of specified values of GO and HLD

GO	$\overline{HLD}$	Result
0	0	All timer operations are held. No reset is performed. (Reset value)
0	1	Timer proceeds from state before write.
1	0	All timer operations are held, including zeroing of the counter. The GO bit is not cleared until the timer is taken out of hold.
1	1	Timer resets and starts.

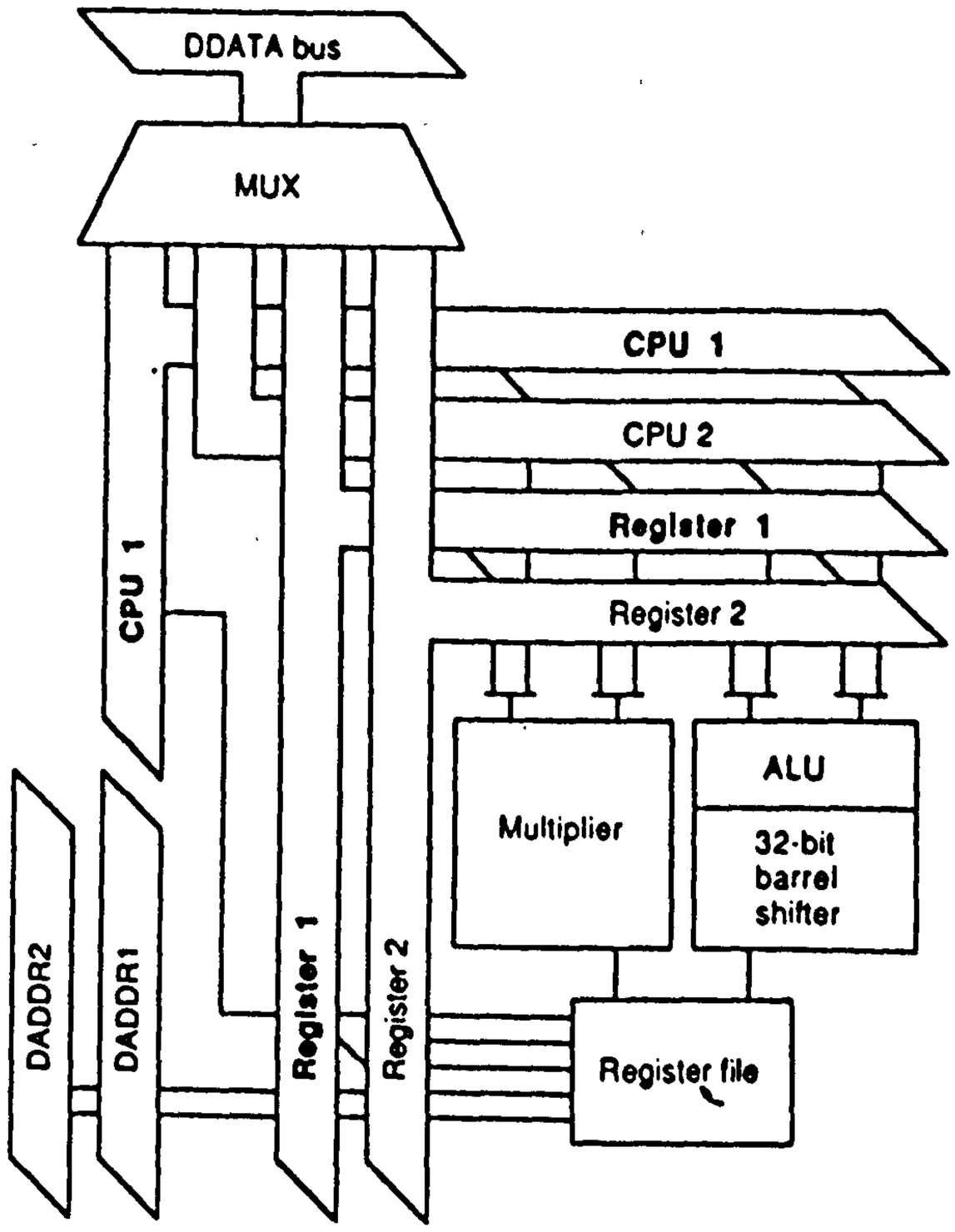

Figure A2.2 The central processing unit

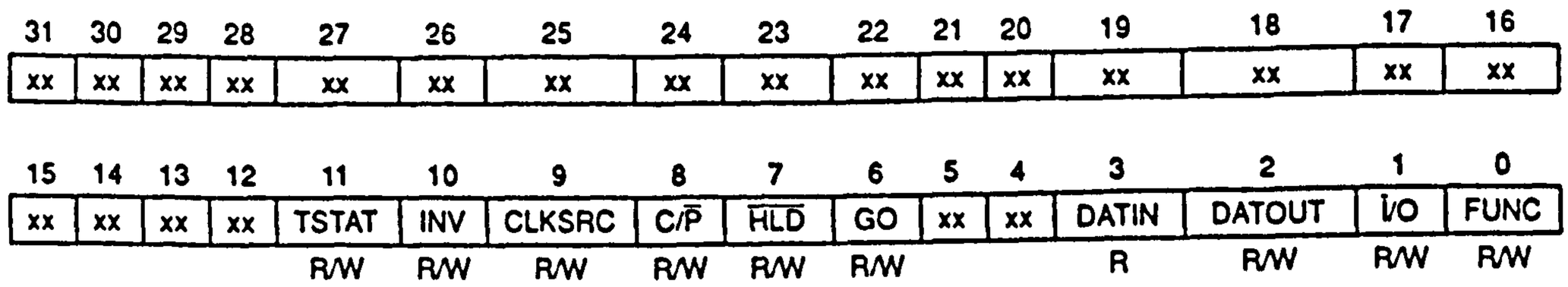

NOTE: xx = reserved bit, read as 0.
R = read, W = write.

Figure A2.4 Timer global-control register

APPENDIX 3

PUBLICATIONS

A3.1. Introduction

Three papers are published in connection with the research presented in this thesis. They are as follows,

Paper 1 : Safi, S.K. & Acarnley, P.P., *High-speed performance of brushless dc motor.*, UPEC Bath Unversity, 1992.

Paper 2 : Safi, S.K. & Jack, A. & Acarnley, P.P , *'Simulation of high-speed torque performance of brushless dc motor drive.*, to be published in IEE Proceedings Pt B.

Paper 3 : Safi, S.K. & Acarnley, P.P., *'Microprocessor optimisation of high-speed torque performance of brushless dc motor drive.*, in preparation to be published.